REPORT NO.
UCB/EERC-90/12
SEPTEMBER 1990

EARTHQUAKE ENGINEERING RESEARCH CENTER

EFFECTS OF TORSION ON THE LINEAR AND NONLINEAR SEISMIC RESPONSE OF STRUCTURES

by

HASSAN SEDARAT
VITELMO V. BERTERO

Report to the National Science Foundation

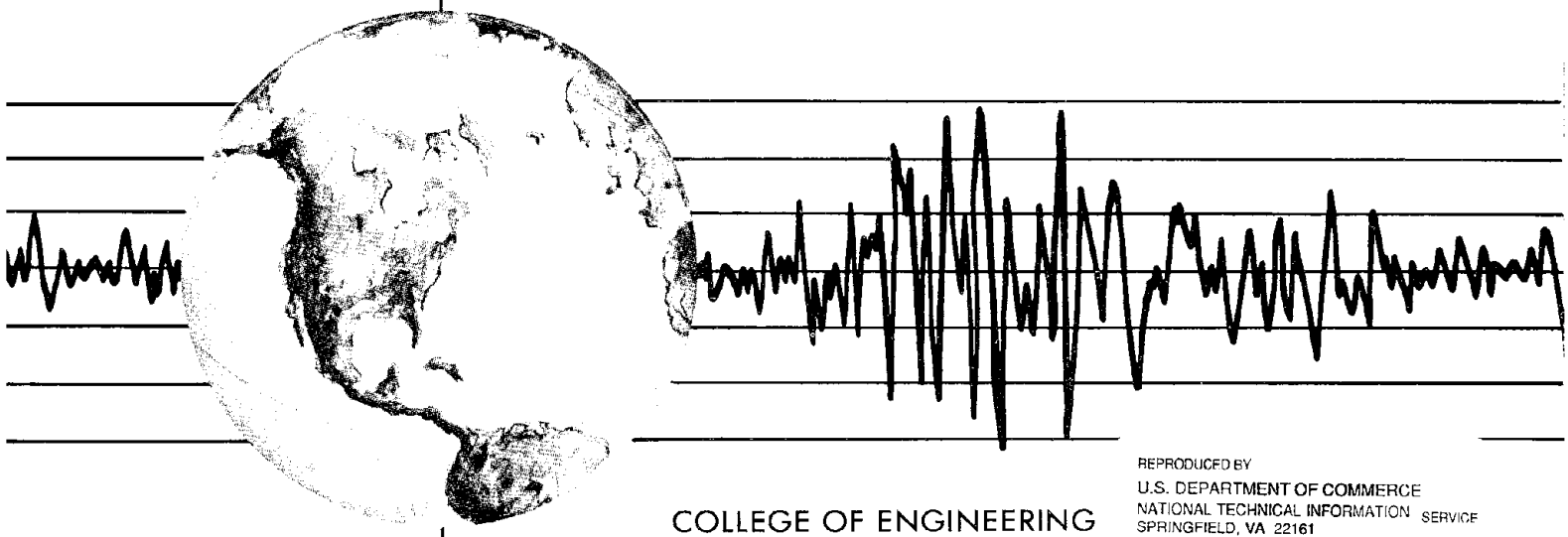

COLLEGE OF ENGINEERING

UNIVERSITY OF CALIFORNIA AT BERKELEY

i.b

For sale by the National Technical Information Service, U.S. Department of Commerce, Springfield, Virginia 22161

See back of report for up to date listing of EERC reports.

50272-101

REPORT DOCUMENTATION PAGE	1. REPORT NO. NSF/ENG-90006	2.	3. PB92-193002

4. Title and Subtitle
Effects of Torsion on the Linear and Nonlinear Seismic Response of Structures

5. Report Date
September 1990

6.

7. Author(s)
Hassan Sedarat and Vitelmo V. Bertero

8. Performing Organization Rept. No.
UCB/EERC- 90/12

9. Performing Organization Name and Address
Earthquake Engineering Research Center
University of California, Berkeley
1301 So. 46th Street
Richmond, Calif. 94804

10. Project/Task/Work Unit No.

11. Contract(C) or Grant(G) No.
(C)
(G) ECE 86-10870

12. Sponsoring Organization Name and Address
National Science Foundation
1800 G Street, N.W.
Washington, D.C. 20550

13. Type of Report & Period Covered

14.

15. Supplementary Notes

16. Abstract (Limit: 200 words)

To introduce parameters pertinent to the problem of torsion, the linear-elastic lateral-torsional response of an idealized single-story system to earthquake ground motion, characterized by flat and hyperbolic pseudo-acceleration response spectra is discussed. The way that major building codes handle torsion in their simplified regulations is described, illustrating clearly that torsional provisions of most present building codes are nonconservative. The results of linear-elastic static and dynamic analyses of a seven-story reinforced concrete frame-wall structure are presented and the importance of factors such as static lateral load profiles, static eccentricity ratio, and accidental eccentricity (as prescribed by the UBC) on the lateral-torsional response of structures is discussed. A discussion about mathematical modeling of structures for nonlinear analyses is presented. The computer program FACTS and its nonlinear three-dimensional reinforced concrete beam column element are employed in this research. Nonlinear static responses of the seven-story structure to two sets of monotonically increasing lateral loads, with triangular and uniform profiles, are studied. A realistic model of a seven-story structure, that represents typical frame-wall systems, is developed. The importance of such parameters as non-uniform distribution of mass, unsymmetrical distribution of yielding strength in the plan of the structure, and intensity of earthquake ground motion on the seismic response of a building is discussed in detail.

17. Document Analysis a. Descriptors

b. Identifiers/Open-Ended Terms

c. COSATI Field/Group

18. Availability Statement:	19. Security Class (This Report)	21. No. of Pages
Release Unlimited	unclassified	344
	20. Security Class (This Page) unclassified	22. Price

(See ANSI-Z39.18) *See Instructions on Reverse* OPTIONAL FORM 272 (4-77)
(Formerly NTIS-35)
Department of Commerce

EFFECTS OF TORSION ON THE LINEAR AND NONLINEAR SEISMIC RESPONSE OF STRUCTURES

by

Hassan Sedarat

and

Vitelmo V. Bertero

Report to the National Science Foundation

Report No. UCB/EERC-90/12
Earthquake Engineering Research Center
College of Engineering
University of California at Berkeley

September 1990

ABSTRACT

The studies reported herein focus on the effects of torsion on the three-dimensional linear-elastic and nonlinear inelastic seismic response of multi-story building structures. To introduce parameters pertinent to the problem of torsion, the linear-elastic lateral-torsional response of an idealized single-story system to earthquake ground motion, characterized by flat and hyperbolic pseudo-acceleration response spectra is discussed. The way that major building codes handle torsion in their simplified regulations is described, and it is clearly illustrated that torsional provisions of most present building codes are nonconservative.

The results of linear-elastic static and dynamic analyses of a seven-story reinforced concrete frame-wall structure are presented and the importance of factors such as static lateral load profiles, static eccentricity ratio, and accidental eccentricity (as prescribed by the UBC) on the lateral-torsional response of structures is discussed.

A discussion about mathematical modeling of structures for nonlinear analyses is presented. The computer program FACTS and its nonlinear three-dimensional reinforced concrete beam column element, which are employed in this research, are introduced. Nonlinear static responses of the seven-story structure to two sets of monotonically increasing lateral loads, with triangular and uniform profiles, are studied. On the basis of the results of this study a realistic model of a seven-story structure, that represents typical frame-wall systems, is developed.

The importance of such parameters as non-uniform distribution of mass (mass eccentricity); unsymmetrical distribution of yielding strength (resistance or strength eccentricity) in the plan of the structure; and intensity of earthquake ground motion on the three-dimensional nonlinear seismic response of a building is discussed in detail. Mass and resistance eccentricities are measured with respect to the geometrical centroid of the structure. It is shown that real nonlinear torsional response of structures may be significantly underestimated by a linear-elastic dynamic analysis, especially for large values of static

eccentricity ratio and intensity of ground motion. It is also shown that torsional effects on the nonlinear response of a structure can be reduced by proper distribution of yielding strength in the plan of the building.

Finally, a summary of the results, conclusions and a number of code-based recommendations are presented in addition to suggestions for future research regarding torsional effects.

ACKNOWLEDGMENTS

The research reported here was partially supported by the National Science Foundation, Grant Number ECE 86-10870. The authors are grateful for this support. Any opinions, discussions, findings, conclusions, and recommendations are those of the authors and do not necessarily reflect the views of the sponsor.

Many thanks to Professors Graham H. Powell and Stephen P. Diliberto, who reviewed this work. Special thanks to Professor Graham H. Powell, who made the computer program FACTS available to the Department of Civil Engineering at the University of California, Berkeley. His guidance in modifying this program is greatly appreciated. The authors also wish to acknowledge the invaluable assistance of Dr. Richard Sause in installing and debugging the computer program FACTS.

Special thanks to Dr. Beverley Bolt for editing this report.

TABLE OF CONTENTS

LIST OF TABLES

LIST OF FIGURES

CHAPTER ONE

INTRODUCTION

1.1 Introductory Remarks

Real structures, when subjected to earthquake ground motions, will, in general, undergo torsional vibrations in addition to lateral oscillations. Lateral-torsional response of structures arises from several sources. The most well-recognized source is unsymmetrical distribution of mass and/or unsymmetrical distribution of lateral load resisting elements in the plan of the structure, which induces eccentricity between the centers of mass and stiffness. This is usually referred to as real, static, mass, or stiffness eccentricity. However, even in symmetrical structures, torsional and translational motions may be coupled because of non-uniform ground motion along the foundation of the structure or because of the presence of torsional components of ground motions. Workmanship, and detailing of the "structural" components as well as of the "nonstructural" components of buildings may also be sources of unsymmetrical behavior of otherwise symmetrical structures. Owing to the uncertain nature of these sources it is difficult, if not impossible, to account for them with a direct deterministic approach. Therefore, in their regulations for torsion, most seismic building codes reflect these possible effects on the torsional response of structures by introducing the so-called accidental eccentricity.

The maximum value of story torque due to a dynamic excitation (such as earthquake ground motion) in an eccentric structure (a structure with static eccentricity) can be significantly larger than the static torque, calculated by the product of static eccentricity and story shear of the corresponding concentric structure (the same structure but with coincident centers of mass and stiffness). In order to account for this dynamic amplification of story torque, it is often convenient to employ the idea of "dynamic eccentricity". The concept is to define a torsional moment, which is to be applied as an external load to the corresponding concentric structure. This torsional moment is equal to that of the eccentric system. Therefore in a linear-elastic system, in which deformations are proportional to forces, the displacement of the concentric system due to this moment will be equal to that of the eccentric system. Hence, dynamic eccentricity may be defined to be the ratio

of the maximum dynamic story torque, about an axis passing through the center of stiffness of the floor, to the maximum dynamic base shear of the corresponding uncoupled system, in which centers of mass and stiffness are coincident. While U.S. building codes, with their equivalent static approach, require the static and the accidental eccentricities to be considered, there are other codes, such as the Mexico code, which have recognized that due to coupled lateral-torsional motions there is a dynamic amplification of the static eccentricity. This amplified eccentricity (dynamic eccentricity) can be much larger than the static eccentricity.

It is well recognized that in the case of extreme or even moderate earthquake ground motions most of the buildings will undergo inelastic behavior. However, it is not very well appreciated that, because of this inelastic behavior, the coupled lateral-torsional vibrations of the structure can be significantly higher than those predicted on the basis of linear-elastic analyses. As soon as one of the lateral load resisting elements yields, there is a change in the position of the center of stiffness and this change can induce significant change in the static eccentricity and therefore the dynamic eccentricity. Examples of coupled lateral-torsional vibrations have been observed for past earthquakes, particularly the September 1985 Mexico earthquake, for which large initial eccentricity was reported to be one of the major factors responsible for the severe damage or collapse of several structures [36,37]. Figures 1.1a and 1.1b show elevations and plan views of two adjacent buildings of different heights, located in Mexico city. They illustrate the torsional behavior of the taller building (Figure 1.1b), and the damage resulting from the 1985 Mexico earthquake (Figure 1.1a). The lateral-torsional response of the taller building (due to unsymmetrical distribution of stiffness in the plan) induced large lateral displacements, and consequently resulted in pounding of the two buildings and severe damage in both of them. Figure 1.2 shows a collapsed corner building after the 1985 Mexico earthquake. As can be observed from the Figure, the failure of the structure is due mainly to the excessively large torsional rotation.

Seismic lateral-torsional response of structures has been the subject of many studies [1 to 14]. A review of the literature, regarding both linear-elastic and nonlinear torsion, is presented in Chapter Two. Most of these studies reflect the linear-elastic torsional behavior of a typical idealized

single-story system [1 to 9]. Although there have been some studies regarding nonlinear torsion [6,10,11,12,13,14], opinions are different regarding the importance of different parameters on the inelastic torsional response of structures. Effects of torsion on the seismic response of structures become more complicated when nonlinear behavior is inevitable, because in addition to initial static eccentricity, translational frequency of the structure, ratio of torsional to translational frequencies, and damping, which influence the linear-elastic torsional response of structures, there are other parameters such as locations and force-deformation relationships of the resisting elements, that affect the nonlinear torsional response of buildings. Moreover, although yielding strengths of lateral load resisting elements and their distribution in the plan of a structure do not play any role in a linear-elastic analysis, they are important factors in evaluating the nonlinear torsional response of buildings to earthquake ground motions. Unsymmetrical distribution of yielding strength may be contemplated in the study of nonlinear torsion by introducing a newly defined "resistance eccentricity" (strength eccentricity). This eccentricity may be defined as the distance between the centroid of the yielding strength of lateral load resisting elements, in the direction perpendicular to the eccentricity, and the geometrical centroid of the story of interest.

Torsion provisions of most current seismic building codes are based on the results of studies conducted, using an idealized single-story system, hence their applicability to multi-story building structures is questionable, especially when nonlinear behavior of the system is of interest. Therefore, in order to improve the present knowledge of torsional response of real structures, and to offer practical recommendations to modify present regulations of torsion in the seismic building codes, it is important to study the effects of torsion on the nonlinear seismic response of multi-story building structures.

1.2 Objectives

The objective of the research reported herein is to study the effects of torsion on three-dimensional linear and nonlinear static and dynamic responses of multi-story building structures to unidirectional strong ground motions. In order to grasp the effects of the different eccentricities in the comparison of nonlinear torsion with linear torsion, and in an attempt to

improve state of the practice by recommending modifications to the present simplified code regulations, the linear and nonlinear responses are compared and the results are discussed. The main goals of this research can be summarized as:

1. to introduce parameters pertinent to the problem of torsion and to discuss their importance on the linear-elastic lateral-torsional response of structures by considering an idealized linear-elastic single-story system subjected to earthquake ground motions, characterized by their flat or hyperbolic acceleration spectra, and to compare state of the art with state of the practice;
2. to study the effects of different values of static eccentricity on the linear-elastic static and dynamic torsional responses of a multi-story building structure, and to assess torsion regulations of building codes by comparing the linear-elastic static and dynamic torsional responses of the structure;
3. to investigate the importance of static eccentricity and intensity of ground motion excitations on the linear and nonlinear coupled lateral-torsional response of multi-story building structures;
4. to assess the influence of an unsymmetrical distribution of yielding strength of lateral load resisting elements (resistance eccentricity) on the seismic response of multi-story building structures, and to discuss the possibility of reducing torsional effects on the nonlinear seismic response of structures by finding the proper location of the center of resistance, relative to the centers of mass and stiffness;
5. to recommend modifications to the torsion regulations of building codes, through comparison of the results obtained from three-dimensional linear-elastic and nonlinear seismic responses of multi-story building structures.

1.3 Scope

To achieve the objectives stated in Section 1.2, a seven-story reinforced concrete frame-wall structure with seven by three bays is considered. This structure consists of two reinforced concrete structural walls and six ductile moment resisting frames. Non-uniform distribution of mass (static

eccentricity), and unsymmetrical yielding strength distribution (resistance eccentricity) in the plan of the structure are assumed to be the sources of coupled lateral-torsional response of the structure. It is further assumed that the centers of mass of the floors all lie on one vertical axis.

In order to introduce parameters pertinent to the problem of torsion, response of a linear-elastic mono-symmetric single-story system to unidirectional earthquake ground motions characterized by a combined flat and hyperbolic pseudo acceleration design response spectrum, are studied in Chapter Two. The simplified regulations for torsion prescribed by major building codes, and a review of the literature regarding both linear-elastic and nonlinear torsion, are also presented in Chapter Two.

Differences between a linear-elastic static analysis (as is prescribed by building codes), and a three-dimensional linear-elastic dynamic time-history analysis, in estimating torsional responses of multi-story building structures are discussed in Chapter Three. In this chapter the importance of static eccentricity on linear-elastic static and dynamic responses of the structure is investigated. To assess the effects of lateral load distribution profile on torsional response of the system, two different static lateral load distributions are considered.

Chapter Four is dedicated to a discussion about mathematical modeling of structures for nonlinear analyses. The computer program FACTS [34], which is employed for nonlinear analyses in this research, and its nonlinear three-dimensional reinforced concrete beam column element are introduced. In this chapter a realistic model of the seven-story structure, which represents typical frame-wall systems, is developed.

Three-dimensional nonlinear seismic responses of the model developed in Chapter Four are investigated in Chapter Five. Effects of different values of static eccentricity and resistance eccentricity on the nonlinear torsional response of multi-story frame-wall systems are assessed in this chapter. In these studies different values of intensity level of the ground motion excitation are considered. In order to provide a better understanding of differences between linear and nonlinear torsion, comparison between linear-elastic and nonlinear inelastic responses are made.

Finally in Chapter Six a summary of the results of this research is presented. Conclusions are drawn and recommendations for future studies of the effects of torsion on seismic response of building structures are made.

CHAPTER TWO

LINEAR-ELASTIC SINGLE-STORY SYSTEMS

2.1 Introduction

In this chapter, the effects of torsion on the linear-elastic seismic response of single-story systems are investigated. Although the main objective of the report is to study the nonlinear torsional behavior of structures, it is necessary to consider the effects of the key parameters on the linear-elastic torsional response of single-story systems. It is important to note, however, that a comprehensive parametric study of the linear-elastic response of single-story systems is beyond the scope of this research and would be a repetition of previous studies [1 to 14]. This chapter is an introduction to the problem of torsion. A typical single-story system is defined first. Then, equations of motion are derived and the system is analyzed using a response spectra technique. The results from this analysis are used to assess the effectiveness of torsion regulations of building codes. A review of previous studies on torsional seismic response of structures concludes the chapter.

2.2 Systems and Earthquake Input

The system that is considered here is an idealized single-story building consisting of a rigid floor diaphragm with massless columns, and with shear walls or shear wall cores as lateral force resisting elements. The mass of the structure is lumped at the center of mass (CM). The resisting elements are assumed to be located symmetrically about one of the principal axes, which is an axis of symmetry for the building plan. Therefore the system is eccentric only in one direction. A typical single-story system, with one uncoupled (X-translational) and two coupled (Y-translational and torsional) degrees of freedom, is shown in Figure 2.1.

The earthquake ground motion is characterized by its pseudo-acceleration response spectrum which is idealized to a flat branch for the short-period range and a hyperbolic branch for the long-period range (Figure 2.2).

2.3 Equations of Motion

The single-story system shown in Figure 2.1 has three degrees of freedom. However, because of the rigid floor diaphragm assumption and symmetry of mass and stiffness distribution about the X-axis, only two of these degrees of freedom are coupled (Y-translational and torsional). These degrees of freedom are relative translational displacement of the center of mass (CM) of the floor along the Y-axis (u_y), and torsional rotation of the floor about a vertical axis passing through its center of mass (u_θ). Equations of motion of the system are developed in this section in terms of vector $U^T = (u_y \quad ru_\theta)$ where r is the radius of gyration of the floor about a vertical axis passing through its center of mass.

This system is subjected to a translational, unidirectional earthquake ground motion perpendicular to the eccentricity. Since the linear-elastic seismic response of the system is under consideration, and since the X-translational degree of freedom of the system is not coupled with the other two, the response of the system to the component of the translational earthquake ground motion in the X-direction can be treated separately. However, it must be noted that earthquake ground motions have, in general, three translational and three rotational components. The rotational components, as well as the vertical component of the ground motion are neglected here for simplicity. Therefore the undamped equations of motions of the system can be written as

$$\begin{pmatrix} m & 0 \\ 0 & m \end{pmatrix}\begin{pmatrix} \ddot{u}_y \\ r\ddot{u}_\theta \end{pmatrix}+\begin{pmatrix} K_y & \frac{e}{r}K_y \\ \frac{e}{r}K_y & \frac{1}{r^2}K_{\theta\theta} \end{pmatrix}\begin{pmatrix} u_y \\ ru_\theta \end{pmatrix}=\begin{pmatrix} -m\ddot{V}_g \\ 0 \end{pmatrix} \tag{2.1}$$

where

m = total translational mass of the system,

K_y = total lateral stiffness of the system in the Y-direction,

$K_{\theta\theta}$ = total rotational stiffness of the system around the center of mass.

$$K_{\theta\theta} = \Sigma(k_{\theta i} + x_i^2 k_{yi} + y_i^2 k_{xi}) \tag{2.2}$$

$\ddot{V}_g$ = ground motion acceleration (function of time),

e = static eccentricity, distance between centers of mass and stiffness,

r = radius of gyration about a vertical axis passing through the center of mass,

k_{xi} , k_{yi}= lateral stiffnesses of the element i along the two principal directions,

$k_{\theta i}$ = torsional stiffness of the element i about a vertical axis passing through its shear center, and

x_i , y_i= distance of the ith resisting element from the center of mass.

It is important to note that the rotational stiffness of the system about its center of stiffness (CS) is

$$K_{\theta S} = K_{\theta\theta} - e^2 K_y \tag{2.3}$$

and if static eccentricity is zero then $K_{\theta S} = K_{\theta\theta}$. The lateral and torsional vibration frequencies of the corresponding uncoupled system are

$$\omega_y = \sqrt{K_y/m} \tag{2.4a}$$

$$\omega_\theta = \sqrt{K_{\theta S}/mr^2} \tag{2.4b}$$

The corresponding uncoupled system is obtained from the actual system by shifting its mass so that center of mass coincides with the center of stiffness without modifying the locations of the resisting elements. With these definitions the undamped equations of motion can be written as

$$\begin{pmatrix} \ddot{u}_y \\ r\ddot{u}_\theta \end{pmatrix} + \omega_y^2 \begin{pmatrix} 1 & e/r \\ e/r & \Omega^2 + (e/r)^2 \end{pmatrix} \begin{pmatrix} u_y \\ r u_\theta \end{pmatrix} = \begin{pmatrix} -\ddot{V}_g \\ 0 \end{pmatrix} \tag{2.5}$$

where $\Omega = \omega_\theta/\omega_y$

is the ratio of uncoupled torsional frequency to translational frequency (uncoupled frequency ratio, UFR).

Thus from equations 2.1 to 2.5, the undamped lateral-torsional response of linear-elastic single-story systems (u_y and u_θ) to ground motion excitations ($\ddot{V}_g$) depends on three parameters;

static eccentricity ratio (e/r), uncoupled translational frequency (ω_y), and uncoupled frequency ratio ($\Omega = \omega_\theta/\omega_y$). Note that a damping ratio (ξ) should be added to these parameters for damped systems.

The system can now be analyzed using the modal superposition method. The coupled frequencies and mode shapes of the system can be calculated by solving the eigenvalue problem of equation 2.6 for the natural vibration frequencies and mode shapes of the system

$$\begin{pmatrix} 1-(\omega/\omega_y)^2 & e/r \\ e/r & \Omega^2+(e/r)^2-(\omega/\omega_y)^2 \end{pmatrix}\begin{pmatrix} \alpha_y \\ \alpha_\theta \end{pmatrix}=\begin{pmatrix} 0 \\ 0 \end{pmatrix} \tag{2.6}$$

These frequencies and mode shapes are

$$\frac{\omega_n}{\omega_y}=\left(\frac{1+(e/r)^2+\Omega^2}{2}\pm\sqrt{\left(\frac{1+(e/r)^2-\Omega^2}{2}\right)^2+(e/r)^2\Omega^2}\right)^{1/2} \tag{2.7a}$$

$$\begin{pmatrix} \alpha_{yn} \\ \alpha_{\theta n} \end{pmatrix}=\frac{1}{\sqrt{(e/r)^2+(1-(\omega_n/\omega_y)^2)^2}}\begin{pmatrix} -e/r \\ 1-(\omega_n/\omega_y)^2 \end{pmatrix} \tag{2.7b}$$

where ω_n and α_n are the nth (n = 1,2) frequency and mode shape, respectively, and ω_y is the translational frequency of the corresponding uncoupled system.

The natural coupled frequencies ω_n (n=1,2), which are computed from equation 2.7a, are normalized with respect to uncoupled translational frequency (ω_y) and plotted against uncoupled frequency ratio in Figure 2.3, for different values of static eccentricity ratio (e/r). The uncoupled translational and torsional frequencies, ω_y and ω_θ, are also normalized with respect to ω_y and shown in the same figure for comparison. It can be observed from Figure 2.3 that, the uncoupled translational and torsional frequencies, ω_y and ω_θ, are upper bounds of the first coupled frequency and lower bounds of the second coupled frequency. As e/r increases the first coupled frequency decreases below ω_y and ω_θ, whereas the second coupled frequency increases above ω_y and ω_θ. For values of uncoupled frequency ratio (UFR) less than one, ω_θ is the upper bound of the first coupled frequency and ω_y is the lower bound of the second coupled frequency. On the other hand, for values of UFR greater than one, ω_θ is the lower bound of ω_2 and ω_y is the upper bound of ω_1.

For values of UFR close to one the coupled frequencies are closest to one another, particularly when the static eccentricity ratio is smaller. It can be observed from Figure 2.3 that the variation of normalized coupled frequencies with UFR is not very sensitive to the value of e/r for small eccentricity ratios (less than 0.5).

2.4 Response Spectrum Analysis

The maximum response of individual modes of vibration is

$$\begin{pmatrix} u_{yn} \\ ru_{\theta n} \end{pmatrix} = \frac{\mathrm{L}_n}{\mathrm{M}_n \omega_n^2} \begin{pmatrix} \alpha_{yn} \\ \alpha_{\theta n} \end{pmatrix} S_{an} \qquad (2.8a)$$

Where

$$\mathrm{L}_n = (\alpha_{yn} \quad \alpha_{\theta n}) \begin{pmatrix} m & 0 \\ 0 & m \end{pmatrix} \begin{pmatrix} 1 \\ 0 \end{pmatrix}$$

$$\mathrm{M}_n = (\alpha_{yn} \quad \alpha_{\theta n}) \begin{pmatrix} m & 0 \\ 0 & m \end{pmatrix} \begin{pmatrix} \alpha_{yn} \\ \alpha_{\theta n} \end{pmatrix}$$

S_{an} is the pseudo-acceleration corresponding to the period T_n and damping ratio ξ_n. Note that mode shapes are normalized such that $\mathrm{M}_n = m$. Therefore the value of the modal participation factor for the nth mode shape becomes $(\mathrm{L}_n / \mathrm{M}_n) = \alpha_{yn}$, and equation 2.8a can be simplified to the following form

$$\begin{pmatrix} u_{yn} \\ ru_{\theta n} \end{pmatrix} = \frac{\alpha_{yn}}{\omega_n^2} \begin{pmatrix} \alpha_{yn} \\ \alpha_{\theta n} \end{pmatrix} S_{an} \qquad (2.8b)$$

The translational and torsional forces acting at the center of mass of the system (f_{yn} and $f_{\theta n}$) can be found for each mode of vibration from

$$\begin{pmatrix} f_{yn} \\ f_{\theta n} \end{pmatrix} = \begin{pmatrix} m & 0 \\ 0 & m \end{pmatrix} \begin{pmatrix} \ddot{u}_{yn} \\ r\ddot{u}_{\theta n} \end{pmatrix} \qquad (2.8c)$$

or from

$$\begin{pmatrix} f_{yn} \\ f_{\theta n} \end{pmatrix} = \begin{pmatrix} m & 0 \\ 0 & m \end{pmatrix} \begin{pmatrix} \omega_n^2 u_{yn} \\ \omega_n^2 r u_{\theta n} \end{pmatrix} \qquad (2.8d)$$

Using equations 2.8b and 2.8d Values of (f_{yn} and $f_{\theta n}$) can be written in the following form

$$\begin{pmatrix} f_{yn} \\ f_{\theta n} \end{pmatrix} = m\alpha_{yn}\begin{pmatrix} \alpha_{yn} \\ \alpha_{\theta n} \end{pmatrix} S_{an} \tag{2.8e}$$

Thus the total base shear (V_n), base torque around the center of mass (T_{Mn}) and base torque about center of stiffness (T_{Sn}) for each mode of vibration are

$$V_n = m\alpha_{yn}^2 S_{an} \tag{2.9a}$$

$$T_{Mn} = mr\alpha_{yn}\alpha_{\theta n} S_{an} \tag{2.9b}$$

$$T_{Sn} = T_{Mn} - eV_n \tag{2.9c}$$

Maximum base shear of the corresponding uncoupled system is obviously

$$V_0 = mS_{ay} \tag{2.10}$$

The dynamic eccentricity for each mode (e_{dn}) is defined as the ratio of T_{Sn} and V_0

$$e_{dn} = \frac{T_{Sn}}{V_0} = r\alpha_{yn}\left(\alpha_{\theta n} - \frac{e}{r}\alpha_{yn}\right)\frac{S_{an}}{S_{ay}} \tag{2.11}$$

Dynamic amplification of eccentricity for each mode is therefore

$$\frac{e_{dn}}{e} = \frac{T_{Sn}}{V_0 e} \tag{2.12}$$

From equation 2.12 it becomes clear that dynamic amplification of eccentricity is, in fact, equal to dynamic amplification of torque.

Dynamic eccentricity ratio (e_d/r), a dimensionless index for dynamic eccentricity, can be written for each mode as

$$\frac{e_{dn}}{r} = \frac{T_{Sn}}{rV_0} \tag{2.13}$$

In all the above relationships radius of gyration about the center of mass, r, was used because it comes naturally from the equations of motion (2.1). Although computation of this parameter is

rather easy, it does not carry a physical meaning. It might make more sense to utilize radius of gyration about the center of stiffness, the point about which the structure rotates. Radius of gyration about the center of stiffness, ρ, is related to r and e by

$$\rho^2 = r^2 + e^2 \tag{2.14}$$

Therefore eccentricities normalized with respect to r and ρ are related according to the following equation

$$\frac{e}{r} = \frac{e/\rho}{\sqrt{1-(e/\rho)^2}} \tag{2.15}$$

Now that the maximum response parameters for each mode of vibration have been calculated a combination rule is required to compute the total maximum response of the system. It is believed that the Complete Quadratic Combination (CQC) rule [15] is the most suitable rule, especially when the frequencies of the mode shapes are close. In this method the total maximum response, R, is given by

$$R = \left(\sum_{n=1}^{2} \sum_{m=1}^{2} \gamma_{nm} R_n R_m \right)^{1/2} \tag{2.16}$$

where γ_{nm} is the cross-correlation factor between modes n and m, R_n and R_m are the modal maxima of the response quantity in modes n and m, respectively. When the same modal damping ratio ($\xi_n = \xi$) is used for all the modes, then

$$\gamma_{nm} = \frac{8\xi^2(1+q_{nm})q_{nm}^{1.5}}{(1-q_{nm}^2)^2 + 4\xi^2 q_{nm}(1+q_{nm})^2} \tag{2.17a}$$

$$q_{nm} = \frac{\omega_n}{\omega_m} \tag{2.17b}$$

and equation 2.16 can be written as

$$R = (R_1^2 + R_2^2 + 2\gamma_{12} R_1 R_2)^{1/2} \tag{2.18}$$

2.5 Effects of Lateral-Torsional Coupling

In this section the response of the torsionally-coupled system to earthquake excitations is compared with that of the corresponding torsionally-uncoupled system, using an idealized (flat or hyperbolic) response spectrum.

Figures 2.4 and 2.5 show the variation of dynamic eccentricity ratio (e_d/ρ) and dynamic base shear, normalized with respect to maximum uncoupled base shear (V_y/V_0), against uncoupled torsional to translational frequency ratio (UFR), for different values of static eccentricity ratio (e/ρ), and for both flat and hyperbolic spectra. For the corresponding torsionally uncoupled system, e_d/ρ and V_y/V_0 are zero and one, respectively. Effects of torsion on the seismic response of the system are therefore measured by the deviation of e_d/ρ from zero and V_y/V_0 from one. Also note that the dynamic amplification of eccentricity is measured by the deviation of e_d/ρ from e/ρ. It can be observed from Figures 2.4 and 2.5 that lateral-torsional coupling has the effect of increasing eccentricity and decreasing maximum normalized base shear. For a system with small e/ρ the minimum value of V_y/V_0 and the maximum value of e_d/ρ occur when UFR is close to one; whereas for systems with larger e/ρ the amplification of eccentricity is significant over a wider ranger of UFR below and above unity for a flat spectrum, and in the range of UFR above unity in the case of a hyperbolic spectrum.

For torsionally stiff systems, i.e. UFR greater than one, the reduction in base shear is small and e_d/ρ approaches e/ρ implying no dynamic amplification of eccentricity. For torsionally flexible systems, i.e. UFR less than one, e_d/ρ is less than e/ρ in the case of a hyperbolic spectrum and approaches zero as UFR tends to zero, but e_d/ρ is almost equal to e/ρ in the case of a flat spectrum indicating no dynamic amplification.

It can be shown analytically [2] that the normalized shear forces and torque in a single-story structure due to earthquake ground motion in the Y-direction characterized by either a flat or hyperbolic acceleration spectrum satisfy the following interaction equation:

$$\left(\frac{V_x}{V_{y0}}\right)^2+\left(\frac{V_y}{V_{y0}}\right)^2+\left(\frac{T_M}{V_{y0}r}\right)^2=1 \qquad (2.19)$$

where V_x and V_y are base shears in the X and Y directions, respectively; V_{y0} is maximum base shear of the corresponding uncoupled system in the Y-direction; T_M is base torque around the center of mass; and r is radius of gyration about a vertical axis passing through the center of mass. For a system symmetric about the X-axis this interaction equation reduces to

$$\left(\frac{V_y}{V_{y0}}\right)^2+\left(\frac{T_M}{V_{y0}r}\right)^2=1 \tag{2.20}$$

It is obvious from the above interaction equation that the X- and Y-components of base shear as well as their vector sum, are less than the base shear computed by neglecting torsional coupling (Figure 2.5). However, the reduction of the base shear may not occur if a linear-elastic response spectrum (LERS), rather than an idealized design spectrum, is utilized or a time-history analysis is performed [5]. This is shown in Chapter Three with a time-history analysis approach.

The variations of dynamic amplification of eccentricity (equations 2.11 and 2.12) against UFR for different values of e/ρ for flat and hyperbolic spectra are shown in Figure 2.6, from which it can be observed that the dynamic amplification of eccentricity increases with decrease in e/ρ. For systems with small e/ρ, dynamic amplification is most pronounced when the uncoupled frequencies are closely spaced, but for systems with larger e/ρ dynamic amplification is practically equal to one for all values of UFR in the case of a flat spectrum, and equal to one for UFR greater than 1.4 in the case of a hyperbolic spectrum. However, the maximum dynamic amplification of static eccentricity is about the same for flat and hyperbolic spectra.

2.6 State of the Art and State of the Practice

In the simplified regulations for torsional effects in most seismic building codes, structures are required to be designed for the application of lateral loads and torsional moments at each story. The torsional moment at each story is defined as the product of story shear and a quantity named "design eccentricity" (e_x). In most seismic codes, the design eccentricity consists of two components. The first component is a function of distance between centers of mass and stiffness (e). This part counts for unsymmetrical distribution of both mass and lateral load resisting elements in the plan of the structure. The second component of the design eccentricity, which is usually

referred to as "accidental eccentricity", reflects effects of other factors such as non-uniform ground motion along the foundation of a structure; torsional components of ground motions; and the differences between actual and computed eccentricities. The design eccentricity of most seismic codes can be written as

$$e_x = \alpha e + \beta D \tag{2.21}$$

where D is a specified plan dimension of the structure; α and β are factors, which are given different values in different building codes. For example, in UBC [16] and ATC [17] their values are 1 and 0.05, respectively, whereas α is 1.5 in the Mexican [18] and Canadian [19] codes and β is 0.10 in the Mexican code and 0.05 in the Canadian code.

The factor α in equation 2.21 is to take into account the dynamic amplification of the static eccentricity. Therefore, dynamic eccentricity in the building codes is equal to αe. With a value of α equal to one, UBC and ATC do not consider any dynamic amplification for static eccentricity, while dynamic amplification of eccentricity in the Mexican and Canadian codes is 1.5. Although the values of these amplifications are different, all the above building codes assume a linear relationship between dynamic and static eccentricities. In order to assess the values of dynamic eccentricity given by the above building codes, a linear-elastic single-story system with a rectangular floor deck is considered. Dimensions of the floor are L and D, and the earthquake ground motion is assumed to be perpendicular to D. The variation of dynamic eccentricity against static eccentricity for different aspect ratios (L/D) for flat and hyperbolic spectra is illustrated in Figure 2.7. These plots are for the case that the UFR of the system is unity, which has already been shown to be the most critical case. Values of dynamic eccentricity given by the building codes are

UBC and ATC-3 [16,17]	$e_d = e$	(2.22*a*)
Mexican and Canadian [18,19]	$e_d = 1.5e$	(2.22*b*)

These values are also shown in Figure 2.7 for comparison. Note that values of dynamic eccentricity, given by the building codes, are not affected by the L/D aspect ratio, whereas the dynamic eccentricity ratio (e_d/D), which is computed from a response spectrum analysis attains different values for different L/D aspect ratios. It can be observed from Figure 2.7 that equation 2.22a underestimates the dynamic eccentricity ratio (e_d/D), due to a flat spectrum, for the whole range of static eccentricity ratio (e/D). Both equations 2.22a and 2.22b are nonconservative for small e/D for both flat and hyperbolic spectra. It is important to note that, according to Figure 2.7 static and dynamic eccentricities are not related linearly. Therefore equations 2.22a and 2.22b are not good representations of dynamic eccentricity. A bilinear relationship between static and dynamic eccentricities may be more suitable. An example of this type of relationship is suggested by Tso and Dempsey [5] as follows:

Flat spectrum:

$$\frac{e_d}{r} = \frac{6e}{r} \qquad \frac{e}{r} < 0.1 \qquad (2.23a)$$

$$\frac{e_d}{r} = 0.6 + 0.6\left(\frac{e}{r} - 0.1\right) \qquad \frac{e}{r} > 0.1 \qquad (2.23b)$$

Hyperbolic spectrum:

$$\frac{e_d}{r} = \frac{6e}{r} \qquad \frac{e}{r} < 0.1 \qquad (2.24a)$$

$$\frac{e_d}{r} = 0.6 + 0.4\left(\frac{e}{r} - 0.1\right) \qquad \frac{e}{r} > 0.1 \qquad (2.24b)$$

The above equations provide a better estimation of dynamic eccentricity than what is suggested by most building codes. Note that these values have to be added to the value of accidental eccentricity to obtain the design eccentricity.

Lateral and torsional motions of irregular building structures are strongly coupled. Irregularity has fortunately been addressed in the 1988 edition of UBC, and additional design requirements have been enforced for structures having irregular features. This is an important improvement from the 1985 edition of UBC, in which this issue was not clearly discussed.

According to the 1988 UBC, "irregular structures have significant physical discontinuities in configuration or in their lateral force-resisting systems". Irregular features include, but are not limited to, two main groups; namely, "vertical structural irregularities" and "plan structural irregularities" (1988 UBC). The first group includes

1. Stiffness irregularity-soft story
2. Weight (mass) irregularity
3. Vertical geometric irregularity
4. In-plane discontinuity in vertical lateral force-resisting element
5. Discontinuity in capacity-weak story;

and the second group includes

6. Torsional irregularity
7. Reentrant corners
8. Diaphragm discontinuity
9. Out-of-plane offsets
10. Nonparallel systems.

As mentioned earlier, the 1988 edition of UBC regulates additional requirements for each of the above irregularities: for example, dynamic analysis is required for structures with one of the first three types of irregularity; or where torsional irregularity, as defined in UBC, exists in buildings, the effects shall be accounted for by increasing the accidental eccentricity at each level by an amplification factor. A complete definition of each of the above irregularity features along with their corresponding additional requirements can be found in the 1988 edition of UBC, and further discussion regarding them is beyond the scope of this research.

Although the 1985 and 1988 editions of UBC recommend more or less similar static analysis procedures, the 1988 edition of UBC is more specific in its regulations for the dynamic analysis procedure. In this edition of UBC dynamic analysis is required for certain structures, besides

irregular buildings. These structures are specified as those "with 240 feet or more in height" and those "which are over five stories or 65 feet in height in seismic zones 3 and 4, not having the same structural system throughout their height".

An important issue, which has not been well appreciated by the seismic building codes, is torsional redundancy in buildings. When only linear-elastic behavior of a structure is considered or is of interest, the importance of providing a high degree of torsional redundancy to the structure does not become evident. However, most buildings undergo inelastic torsional behavior in the case of extreme or even moderate earthquake ground motions. As soon as one of the lateral load resisting elements yields, there is a change in the location of the center of stiffness and this change can induce a significant change in the static eccentricity and, therefore, in the dynamic eccentricity. This usually results in an increase in the torsional rotation of the structure and therefore can lead to serious damage in its members, or even to collapse of the building. In these cases, where inelastic torsional behavior is inevitable, it is important to provide as many lines of defence as possible to avoid a large increase in eccentricity between the centers of mass and stiffness and, as a result, to prevent partial or complete failure of the building due to large torsional rotations.

2.7 Review of Previous Studies

Effects of torsion on the seismic linear-elastic and nonlinear responses of structures have been investigated extensively in the past few years. In almost all of these studies an idealized single-story system has been considered, and the responses of buildings as influenced by the basic controlling parameters of the system, such as static eccentricity ratio (e/r), uncoupled translational frequency (ω_y), and uncoupled frequency ratio (UFR), have been evaluated.

Kan and Chopra [3] have shown that the linear-elastic torsional response of multi-story structures, which belong to a special class of buildings, can be determined by the study of a single-story torsionally coupled system together with an N-story torsionally uncoupled counterpart of the actual building. Therefore the use of an idealized asymmetrical single-story building model

with at least two independent degrees of freedom (one translational and one rotational) is sufficient to identify the more significant trends in the earthquake response of the special class of torsionally coupled systems [3].

Having analyzed a linear-elastic single-story system with an idealized (flat and hyperbolic) response spectra technique, Kan and Chopra [2] showed that base shears and torque in a torsionally coupled system are related to the base shear in the corresponding uncoupled system, through simple interaction equations (see equation 2.19). From this relationship, they proved that the value of total base shear in a torsionally coupled system is less than that in the corresponding uncoupled system, when an idealized design spectra technique is employed. In a study performed by Chandler and Hutchinson [8] with a linear-elastic time-history approach it was shown that, in the response to individual earthquakes, over some ranges of the parameters e/r and UFR, some small increase in dynamic shear may result from lateral-torsional coupling, and hence that ignoring the presence of the eccentricity in calculating the design story shear forces does not always provide a conservative estimate of response.

The importance of parameters e/r and UFR in the linear-elastic seismic response of torsionally coupled systems has been appreciated by many researchers [1,2,5,6,7,8]. It was shown, by both a time-history analysis approach and a response spectra approach, that for small static eccentricity ratios and values of UFR close to unity, the dynamic amplification of static eccentricity (e_d/e) is considerably large. Tso and Dempsey [5], in their assessment of the recommendations of five major building codes (Canada [19]; Mexico [18]; New Zealand [20]; ATC-3 [17]; and Germany [21]) for earthquake resistant design of torsionally coupled buildings, showed that all the codes except that of Germany, significantly underestimate the torsional moment and edge displacement of a typical linear-elastic single-story system, when the eccentricity ratio is small and UFR is close to unity. It was also found [5] that a bilinear relationship between the dynamic and static eccentricities is most suitable to represent the dynamic eccentricity in the building codes. The same results were obtained by Chandler and Hutchinson [8] through the use of a linear-elastic time-history analysis. They showed that the lateral seismic force, taking into account the accidental

eccentricity, is underestimated by ATC-3, and the Canadian, Mexican, and New Zealand codes, for small to moderate eccentricities and UFR in the range 0.8 to 1.7. All the above codes provide overly conservative estimates of lateral force response for UFR smaller than 0.8. However, the estimate of lateral force response, given by these building codes for UFR larger than 1.7 is reasonable. This confirms the earlier results of Kan and Chopra [6] that, for values of UFR larger than two, lateral deformation is essentially not affected by torsion, and torsional deformation is proportional to e/r, indicating no dynamic amplification.

The effect of torsion on the nonlinear seismic response of structures is complex and not well understood. Although there have been several studies on the inelastic seismic response of eccentric structures [6,10,11,12,13,14], opinions differ regarding the importance of different parameters on the inelastic torsional response of such structures. One reason for the diverse views is that only four parameters are needed to evaluate the elastic response of a single mass mono-symmetrical system, namely, uncoupled lateral frequency, system eccentricity ratio, uncoupled frequency ratio, and damping ratio, whereas for inelastic response studies, it is necessary to specify much more detailed data about the structural model, such as the locations and force-deformation characteristics of the resisting elements. It is possible to have different inelastic eccentric models having the same overall elastic responses [10]. Another reason is that some findings are based on one or two specific ground motion records [6,10], so that these results may be sensitive to the ground motion input.

Kan and Chopra [6], in their study of a nonlinear single-story system, stated that torsional coupling generally affects maximum deformations in inelastic systems to a lesser degree than in the corresponding linear-elastic systems, because after initial yielding the system has a tendency to yield further primarily in translation and behaves more and more like an inelastic single-degree-of-freedom system, responding primarily in translation. However, Tso and Sadek [10] showed that significant rotational motion is involved at the instant when peak ductility demand is reached. They also illustrated that an increase of over 100% in ductility demand is not uncommon for inelastic systems with large eccentricity, when compared with the response of the systems with small eccentricity.

It has been found [10,11] that, unlike elastic response studies, the coincidence of uncoupled torsional and translational frequencies does not lead to abnormally high inelastic peak responses. It was also found that effects of torsion on the element ductility and on the edge displacement are most pronounced for translationally stiff systems (with short lateral period) with yield strength considerably reduced from the elastic strength demand [11].

Unsymmetrical distribution of yielding strength of the lateral load resisting elements in the plan of a structure is an important source of lateral-torsional response in the structure, but unfortunately has been less appreciated than other sources. Resistance (or strength) eccentricity, e_r, (see Figure 2.1) is defined by Esteva [14] as "the distance between the centroid of the resistances in the direction perpendicular to the eccentricity and the line of action of the shear force (Y-axis) at the story of interest". Even in symmetrical structures with symmetrical distribution of mass and lateral load resisting elements in the plan, torsional and translational motion will be coupled if the yielding strengths of the lateral load resisting elements are not distributed symmetrically in the plan. Bruneau and Mahin [13] studied the effects of resistance eccentricity on the seismic response of different single-story systems, with and without static eccentricity. It has been shown that the element ductility demand will remain within reasonable bounds, compared with the ductility demand of the corresponding concentric structure, if

1. UFR is not excessively large (preferably 1.2 and lower). Larger UFR produces larger element ductility demand.

2. The yield level of the weaker element in the initially symmetric system is not less than the yield level of the system with synchronized yielding.

Esteva [14], in his paper regarding earthquake engineering research and practice in Mexico after the 1985 earthquake, defined resistance eccentricity and explained that if Q, which is the ratio between the maximum ordinates of the linear and of the corresponding reduced nonlinear acceleration response spectra, is taken as three, the restriction must be imposed that the yielding strengths of the structural members must be such that resistance eccentricity (e_r) and static eccentricity (e_s) have the same sign and e_r is at least as large as ($e_s - 0.20\,b$), where b is the

dimension of the story of interest in the direction parallel to the eccentricity. For Q larger than three the condition that e_r and e_s have the same sign is kept, but the lower bound to e_r is changed to $(e_s - 0.10\,b)$. These results must be investigated further. It is very important that rigorous studies be carried out on the effects of torsion on the nonlinear seismic response of structures, when both resistance eccentricity and static eccentricity exist in the system.

2.8 Summary and Conclusions

It is clear from the preceding discussions that the linear-elastic seismic response of a single-story system can be easily calculated. Although the torsion regulations of most building codes are based on the behavior of such systems, they underestimate the effects of torsion on the seismic response of structures and need to be improved. Factors such as uncoupled torsional frequency (UFR), and static eccentricity ratio (e/r) along with the other dynamic characteristics of structures, as well as dynamic characteristics of ground motions, have to be included in the building codes. The following are the main conclusions that can be drawn from this study:

1. Lateral-torsional linear-elastic response of single-story systems to an earthquake ground motion depends on the static eccentricity ratio (e/r), the uncoupled lateral vibration frequency (ω_y), the uncoupled frequency ratio (UFR), and for damped systems the damping ratio (ξ) of each mode of vibration of the structure.
2. The natural vibration frequencies of the system are influenced by lateral-torsional coupling. This influence decreases as the static eccentricity ratio decreases, and becomes smallest when the uncoupled frequency ratio is unity.
3. The maximum base torque and, therefore, the dynamic eccentricity of a linear-elastic single-story system increase as static eccentricity increases. This effect is most pronounced for systems with uncoupled frequency ratio (UFR) close to unity. Systems with closely spaced uncoupled torsional and translational frequencies exhibit maximum dynamic amplification of eccentricity. The dynamic amplification of eccentricity is larger when the static eccentricity ratio (e/r) is smaller. Most building codes, in their simplified regulations for torsion, do not account for the effects of different values of uncoupled frequency ratio

and static eccentricity ratio, and some of them do not even contemplate any dynamic amplification for static eccentricity. They provide nonconservative estimates of torsional seismic response of linear-elastic systems, when the static eccentricity ratio is small and the uncoupled frequency ratio is close to unity.

4. A linear relationship between dynamic and static eccentricities, as prescribed by most building codes, is not a good representation of the dynamic eccentricity (e_d), because it is nonconservative when the static eccentricity is small. A better estimation of the dynamic eccentricity can be obtained through bilinear relationships with the static eccentricity.

CHAPTER THREE

LINEAR-ELASTIC MULTI-STORY STRUCTURES

3.1 Introduction

Linear-elastic lateral-torsional seismic response of single-story systems was discussed in Chapter Two. In this chapter effects of torsion on the linear-elastic seismic response of a multi-story structure rather than a single-story system are discussed. A seven-story reinforced concrete frame-wall building is studied, the plan view and elevation of which are shown in Figures 3.1a and 3.1b. The primary structural system consists of two reinforced concrete frame-walls and six parallel reinforced concrete space frames. This structure is subjected to earthquake ground motion excitation in the direction of the shear walls. A similar structure was studied extensively as part of a U.S.-Japan Cooperative Research Program [25]. A full-scale model was tested in Japan under pseudo-dynamic loads. A 1/5 scale model was tested on the shaking table of the University of California at Berkeley. A 1/10 model was tested at the University of Illinois and a 1/15 scale model was tested at Stanford University. However, in all these studies the three-dimensional torsional effects have been practically eliminated by the design and construction of the models and the test program.

In this chapter the effects of different static lateral load distributions on the lateral-torsional response of this structure are investigated, then dynamic and static responses are compared. In these studies three cases are considered; namely, the concentric structure (no eccentricity between centers of mass and stiffness), and the eccentric structure with two different static eccentricities of 5 and 10 percent of the maximum dimension of the building plan, D=151 feet. These static eccentricities are about 96 and 192 inches, respectively. It is assumed that eccentricity between centers of mass and stiffness of the structure is due to asymmetrical variation in the distribution of mass throughout the floors of the structure. The effects of including accidental eccentricity in the design eccentricity (see Chapter Two), as prescribed by the building codes, are discussed at the end of this chapter.

3.2 Sectional Properties of Shear Walls, Columns and Beams

In this study, all dimensions and sizes, as well as the mechanical characteristics of the elements of the structure are taken to be the same as those in the U.S. Japan Cooperative Research Program [30]. Typical beam, column and structural wall cross sections are shown in Figure 3.2. The cracked transformed sectional properties and the uncracked moment of inertia and cross sectional area of a typical beam, column and wall are given in Table 3.1 [28,30]. Summaries of the properties of a typical beam, column and shear wall are given in Tables 3.2, 3.3 and 3.4, respectively [30]. Finally in Table 3.5 values of dead and live loads for each floor level and also the weight of reactive mass corresponding to each floor are given.

3.3 Mathematical Discretization

The computer program ETABS [24], which is an extended version of TABS [23], is used to analyze the structure of Figure 3.1. In this program, which has the ability to perform three-dimensional linear-elastic static and/or dynamic analyses of structures, buildings are idealized by a system of independent frames. The complete structure stiffness matrix is then formed under the assumption that all frames are connected at floor level by a diaphragm, which is rigid in its own plane. Although the assumption of a rigid floor diaphragm is usually made, its validity for certain types of reinforced concrete structures can be seriously questioned.

Each joint in the building has six degrees of freedom (displacement and rotation about each coordinate axis). Within each frame three of these degrees of freedom (the two translations and the rotation in the floor plane) can be transformed, using the assumption of a rigid floor diaphragm, to the frames' degrees of freedom at that level. The remaining three joint degrees of freedom are eliminated by static condensation [31] before each frame stiffness is added to the total structural stiffness matrix. The final structural degrees of freedom per floor correspond to one rotational and two translational degrees of freedom.

Shear walls are modeled by beam-column elements. However, beam-column element cannot represent the behavior of a shear wall properly. Some of the important aspects of the behavior of a shear wall are

1. Rocking of the shear wall.

2. Nonlinear shear deformation of the wall.

3. Variation in flexural and shear stiffness of the wall due to degree of cracking or variation of axial forces.

4. Fixed-end rotation of the shear wall due to deformation of the vertical bars along their foundation anchorage length.

Since these aspects cannot be modeled directly by a simple beam-column element, the most logical approach to take for modeling of the shear wall is to use finite element methods [29]. However, using this approach is beyond the scope of this research.

Although methods to incorporate the deformation of beam-column joints in frame analyses have been developed [32], ETABS assumes that there is no deformation within beam-column joints. The validity of this assumption has been questioned in the case of reinforced concrete joints. A number of experimental studies on the hysteretic behavior of reinforced concrete beam-column subassemblages [26,27] has shown that in moment-resisting frames, designed according to current practice, the most unfavorable bond conditions exist in interior beam-column joints leading to significant fixed-end rotations at the beam-column interfaces. Such fixed-end rotations due to bond deterioration and shear deformations in the joint can contribute up to 50% to overall deflections of beam-column subassemblages after yielding of the reinforcement [27]. The above fixed-end rotation has not been considered in the beam-column joints in this study, but as a compromise it is assumed that all beam-column joints in the structure have zero length.

3.4 Undamped Natural Frequencies and Mode Shapes

Natural mode shapes and periods of the structure were computed. The structure has been assumed to be completely symmetrical and therefore mode shapes and periods of vibration of the structure are uncoupled. Periods of the structure for each mode are listed in Table 3.6. The first three translational mode shapes in the direction of the shear walls (modes 2,6,9) are plotted in Figure 3.3. The torsional and X-translational (in the direction of shear walls) modes of vibration of the structure have very close periods. The uncoupled frequency ratio (UFR), which is the ratio

of uncoupled torsional frequency to uncoupled translational frequency, is about 0.93. Therefore, as was shown in Chapter Two, effects of torsion are expected to be significant on the linear-elastic seismic response of this structure. This will be discussed in more detail in the following sections. Uncracked sectional properties (Table 3.1) have been used to obtain the above periods and mode shapes. Therefore a lower bound of periods of the structure has been estimated.

3.5 Linear-Elastic Static Analysis

In this section responses of the structure of Figure 3.1 to static lateral loads have been studied. To assess the effects of lateral load distribution profile on the response of the structure, two different lateral load profiles, with triangular and uniform distributions, are employed. The total applied base shear force for each profile is 13.5% of the total reactive weight of the structure, which is the value that results from application of the force required by UBC [16] as the minimum total lateral seismic force. Values of lateral load acting at each floor for both triangular and uniform lateral load profiles are listed in Table 3.7.

For each lateral load profile three cases have been considered. In the first case, in which the lateral load resisting elements and mass are distributed uniformly in the plan of the structure, center of mass (CM) and center of stiffness (CS) of the structure are coincident, and therefore the structure is called concentric. In the second and the third cases CM and CS are not coincident, and therefore the structure is called eccentric. The amount of eccentricity between CM and CS in the eccentric cases is assumed to be 96 and 192 inches which are about 5% and 10%, respectively, of the maximum dimension of the building plan, D=151 feet.

In the following sections the responses of the structure of Figure 3.1 to the above lateral load profiles are grouped as follows:

1. Displacements and inter-story drift indices.
2. Bending moments and shear forces in shear walls and columns.
3. Bending moments in girders.

Displacements of the structure have been computed without any load factor, whereas in computing forces in beams, columns and shear walls a load factor of 1.4 has been utilized for dead loads, live loads and lateral loads to comply with the requirements of UBC [16].

3.5.1 Displacements and Inter-Story Drift Indices

Displacements of center of mass of each floor due to both triangular and uniform lateral load profiles in the concentric case are listed in Table 3.8. In the same table displacements of wall B, wall G and the corner of the structure, for 5% eccentricity, are listed for both triangular and uniform lateral load profiles. These values are illustrated in Figure 3.4. It can be observed from these results that displacements due to triangular lateral load are in general larger than those due to uniform lateral load. Torsional rotation of the building, in the eccentric case, has the effect of increasing the lateral displacement of the corner of the structure and wall G and decreasing that of wall B in comparison with the displacement of the CM of the concentric structure at each floor (Figure 3.4). Displacements of the corner of the structure and wall G for 5% eccentricity are, on average, 22% and 16% larger, respectively, than in the concentric case, for both triangular and uniform lateral load profiles. The displacements of wall B, wall G, and the corner of the structure for 10% eccentricity due to triangular and uniform lateral load profiles are listed in Table 3.9 and shown in Figure 3.5. Displacements of the corner of the structure and wall G for 5% eccentricity are, on average, 45% and 32% larger, respectively, than in the concentric case, for both triangular and uniform lateral load profiles.

Inter-story drift indices (IDI) at each story for 5% and 10% eccentricities are shown in Figures 3.6 and 3.7, respectively. These values along with the values of IDI for the concentric case are listed in Tables 3.10 and 3.11. In these figures, IDI of wall B, wall G and the corner of the structure for 5% and 10% eccentricities are illustrated as well as IDI of the center of mass in the concentric case. IDI of the corner of the structure and wall G for 5% eccentricity are, on average, 22% and 16% larger, respectively, than in the concentric case, for both triangular and uniform lateral load profiles, whereas these values for 10% eccentricity are 45% and 32%, respectively. It must be noted that the lateral displacements of walls are controlled by their flexural

type of deformation, whereas those of frames are governed by their shear type of deformation. Therefore when shear walls and frames are combined in a frame-wall structure, the interaction between walls and frames will control the lateral displacements of the system. Because of this frame-wall interaction the maximum IDI of the structure, as can be observed from Tables 3.10 and 3.11, occurs at the fourth story. It is important to note that, different lateral load profiles result in different lateral displacements and IDI, but the increases in these response parameters in the eccentric case compared with the concentric case are practically the same. From the above results it can be concluded that, lateral displacements and IDI in the structure increase with the increase in static eccentricity, but this increase is not a function of lateral load profile, in a linear-elastic static analysis.

3.5.2 Bending Moments and Shear Forces in the Shear Walls

Bending moments and shear forces at the base of walls B and G due to both triangular and uniform lateral load profiles for 5% and 10% eccentricities are listed in Table 3.12. It can be observed from this table that due to torsional rotation of the whole building, the bending moments and shear forces of wall G, for 5% and 10% eccentricities are increased, compared with the concentric case, by 16% and 32%, respectively, no matter which lateral load profile is utilized. However, as was expected, bending moments at the base of walls B and G due to uniform lateral load are smaller than those due to triangular lateral load, while shear forces at the base of walls B and G due to uniform lateral load are larger than those due to triangular lateral load.

Shear forces along the height of walls B and G for 5% and 10% eccentricities and for the concentric case due to both triangular and uniform lateral loads are shown in Figures 3.8 and 3.9, and listed in Tables 3.13 and 3.14. It is interesting to note that the increases of story shear of wall G for 5% and 10% eccentricities, compared with the concentric case, are about 16% and 32%, respectively, for all stories except for the roof: for the roof these increases are about 18% and 36%, respectively, for both triangular and uniform lateral load profiles. The total base shear carried

by each frame due to triangular and uniform lateral load is listed in Tables 3.15 and 3.16 in the concentric case, and the 5% and 10% eccentric cases. As expected, walls B and G carry most of the lateral load with 84.7% of the total triangular load and 85.2% of the total uniform load.

Although different lateral load profiles result in different shear forces and bending moments in the columns and walls of the structure, the percentage increases of these response parameters from the concentric case to the eccentric case are the same for both triangular and uniform profiles. This indicates that increasing the eccentricity in the structure has the effect of increasing shear forces and bending moments in the columns and walls but this effect is not a function of distribution of lateral load in a linear-elastic static analysis.

3.5.3 Bending Moments in Girders

Maximum bending moments occur in those girders which are adjacent to the shear walls at the fourth floor. The maximum positive and negative moments due to both triangular and uniform lateral load profiles for the concentric case and for 5% and 10% eccentricities are listed in Table 3.17. As can be observed from this table, the maximum positive moments for 5% and 10% eccentricities are greater than those of the concentric case, by 33% and 65%, respectively, when the triangular lateral load profile is imposed on the structure, while these increases are 49% and 97%, respectively, in the case of the uniform lateral load profile. The maximum negative moments, due to both triangular and uniform lateral loads, for 5% eccentricity are increased, over those of the concentric case, by about 10%, whereas for 10% eccentricity they are increased by about 19% for the triangular load profile, and 17% for the uniform lateral load profile. These results indicate that the bending moments in the girders increase with increase in static eccentricity.

The above results indicate that the percentage increases in the positive and negative moments in the eccentric cases, over those in the concentric case, are not the same. This is mainly due to the gravity loads which have the effect of increasing absolute value of the negative moment and decreasing that of the positive moment. Therefore the absolute values of the positive moments are smaller than those of the negative moments. However, it must be noted that the differences between moments in the eccentric case and moments in the concentric case are practically the

same for both positive and negative bending moments. This can be observed from Table 3.17. Compared with the concentric case, the positive and negative moments for 5% eccentricity are increased by about 323.7 in-kip and 343.6 in-kip, respectively, when the triangular lateral load profile is used, and by 246.8 in-kip and 262.6 in-kip, respectively, when the uniform lateral load profile is considered. For 10% eccentricity these differences are about 647.5 in-kip and 687.2 in-kip, respectively, when the triangular lateral load profile is used, and 493.5 in-kip and 525.3 in-kip, respectively, when the uniform lateral load profile is considered.

3.6 Linear-Elastic Dynamic Analysis

In the following sections three-dimensional linear-elastic dynamic time-history seismic responses of the structure of Figure 3.1 are discussed. An earthquake record is selected based on the dynamic characteristics of the structure. A series of linear-elastic analyses of the structure is conducted for the concentric and the eccentric cases. In the eccentric cases, two different static eccentricities of 96 inches and 192 inches are considered, which are about 5% and 10% of the maximum dimension of the building plan (151 feet), respectively. These eccentricities are obtained by non-uniform distribution of mass at each floor. The computer program ETABS [24] is employed in these studies; therefore the same mathematical discretization and assumptions, which were explained in Section 3.3, are valid.

3.6.1 Earthquake Input and Structural Damping Ratio

The earthquake excitation that is considered in this study is the N21E component of the 1952 Taft Kern County earthquake ground motion record [22], which is 54.4 seconds in length and the peak acceleration is 0.156g at the 9.1 seconds mark of the record, where g is the acceleration of gravity. The first 25 seconds of the acceleration time-history are presented in Figure 3.10a, its normalized Fourier amplitude spectrum (FAS) is shown in Figure 3.10b. The linear-elastic response spectra (LERS) of the first 25 seconds of the Taft record are shown in Figure 3.11. The first three uncoupled translational periods of vibration of the model in the direction of the shear walls, which were estimated in Section 3.4, are also shown in Figure 3.11. The FAS and LERS indicate that the dominant frequency content of the Taft record encompasses the fundamental

period of the model. It must be noted that the torsional component of ground motion is not considered here. However, it is important to mention that effects of torsion on the response of the structure may be increased if the period of the torsional motion of the ground is equal or close to the period of the first torsional mode of vibration of the structure.

The intensity level of the Taft ground motion used in the analyses is identified by the increased peak ground acceleration, PGA, of the record. The results from analyses with a PGA of 0.40g, which will be referred to as Taft-40, are presented and discussed herein. This normalized part of the Taft record has an effective peak acceleration EPA of 0.32g. This value was obtained using the procedure described by ATC [17]. This method may be summarized in 3 steps:

1. The 5% damped linear-elastic response spectrum, LERS, is evaluated.
2. The straight line (constant acceleration) of best fit to the spectral shape in the period range of 0.1 to 0.5 second is selected.
3. The acceleration ordinate of the line is divided by a factor of 2.5 to obtain the EPA.

The reduction factor of 2.5 is consistent with the spectrum amplification factor suggested by Newmark and Hall [33] for 5% damping and one sigma cumulative probability. The amplification factors suggested by Newmark and Hall were 2.71, 2.30 and 2.01 for the acceleration, velocity and displacement regions, respectively.

Mode shapes and periods of the structure were calculated in Section 3.4 (Figure 3.3, Table 3.6). The periods of the first three translational mode shapes in the direction of the shear walls are about 0.57, 0.15, and 0.07 second, respectively. Values of pseudo acceleration corresponding to these modes (see Figure 3.11) are 0.35g, 0.30g and 0.19g, considering 5% damping ratio, respectively. Pseudo velocities are 14, 5, and 0.5 inches per second, respectively. These values indicate that the contribution of the third and higher modes to the response of the structure to the Taft earthquake excitation (Figure 3.10) is practically negligible compared with that of the first mode. From these results, the damping ratio of the structure is assumed to be 5% for all modes because the values of damping ratio for higher modes cannot affect the total response of the structure significantly.

It should be noted that the mass of each floor of the building is based on the structural dead weight and the superimposed dead load such as partitions and mechanical equipment, but live load is not included.

Response of the structure of Figure 3.1 to Taft-40 is presented in the following sections. The value of each response parameter in the eccentric case is normalized by the corresponding response parameter in the concentric case. In order to study the differences between static torsion and dynamic torsion, these normalized response parameters are compared with their corresponding values in static analyses. This is a fair comparison, because the structure is assumed to remain elastic and therefore, in dynamic analyses these ratios are independent of the magnitude of peak ground acceleration of the record. Similarly, in static analyses the normalized response parameters are independent of the total value of applied lateral load.

3.6.2 Lateral Displacement and Inter-Story Drift Indices

The displacement time-histories of the structure due to Taft-40 in the concentric case are illustrated in Figure 3.12 for each floor. Since the floor diaphragm of the structure is assumed to be rigid in its plane, these time-histories represent the displacement of all the points in each floor. Shapes of the displacement time-histories at all floors are similar and their amplitudes increase with the height of the floors, indicating that higher modes have negligibly small effects on the response. The maximum displacement is 2.77 inches at the roof and 0.28 inch at the second floor. Because of torsional rotation of the whole building in the eccentric case, the maximum displacement of wall G and the corner of the structure are larger than those of the concentric case. This can be observed from their displacement time-histories in the eccentric cases. Displacement time-histories of wall B, wall G and the corner of the structure for 5% and 10% eccentricities are shown in Figures 3.13 to 3.18. The maximum values of roof displacement of wall B, wall G and the corner of the structure, for 5% eccentricity, are 3.06, 4.81, and 5.53 inches, respectively. The maximum displacements at the second floor, for 5% eccentricity, are 0.29, 0.47, and 0.54 inch,

respectively. For 10% eccentricity the maximum roof displacements of wall B, wall G, and the corner of the structure are 1.98, 5.68, and 6.53 inches, respectively. The maximum displacements at the second floor, for 10% eccentricity, are 0.18, 0.55, and 0.65 inch, respectively.

The maximum displacements of wall B, wall G, and the corner of the structure at each floor, in the concentric and the eccentric cases, are listed in Table 3.18 and shown in Figure 3.19. These values for wall G and the corner of the structure are larger than those for the concentric case. It can be observed from Table 3.18 that the values of maximum lateral displacement are increased with the increase in static eccentricity in the structure. This effect is most pronounced in higher floors. The maximum displacements of wall B, wall G, and the corner of the structure, for 5% eccentricity are, on the average, 10%, 73%, and 99% larger, respectively, than those in the concentric case. Maximum displacement of wall B for 10% eccentricity is, on the average, 31% smaller than that in the concentric case, whereas maximum displacements of wall G and the corner of the structure for 10% eccentricity are, on the average, 102% and 136% larger, respectively.

Inter-story drift indices (IDI) time-histories of the structure due to Taft-40 in the concentric case are illustrated in Figure 3.20 for each story. Since the floor diaphragm of the structure is assumed to be rigid in its plane, these time-histories represent the IDI of all the points in each story. Shapes of IDI time-histories at all stories are similar, indicating that the effects of higher modes on the response are practically negligible. The interaction between walls and frames controls the lateral displacements of the frame-wall system. This interaction, as explained earlier, is due to the different types of deformation of walls and frames; namely, flexural and shear deformation types, respectively. Because of this interaction between walls and frames the maximum IDI of the structure, as can be observed from Table 3.19, occurs at the fourth story. The maximum values of IDI are 0.32%, 0.39%, and 0.19% at the seventh, the fourth, and the first stories, respectively. Because of torsional rotation of the whole building in the eccentric cases, the maximum values of IDI of wall G and the corner of the structure are larger than those of the concentric case. IDI time-histories of wall B, wall G and the corner of the structure for 5% and 10% eccentricities are shown in Figures 3.21 to 3.26. The maximum values of IDI at the seventh story of wall B, wall

G and the corner of the structure, for 5% eccentricity, are 0.36%, 0.56%, and 0.64%, respectively. These maximum values of IDI at the fourth story are 0.43%, 0.67%, and 0.77%, respectively. The maximum values of IDI at the seventh story of wall B, wall G and the corner of the structure, for 10% eccentricity, are 0.24%, 0.66%, and 0.76%, respectively. These maximum values of IDI at the fourth story are 0.28%, 0.80%, and 0.91%, respectively.

The maximum values of IDI of wall B, wall G, and the corner of the structure at each story, in the concentric and the eccentric cases, are listed in Table 3.19 and shown in Figure 3.27. These values for wall G and the corner of the structure are larger than those for the concentric case. It can be observed from Table 3.19 that increasing eccentricity in the structure has the effect of increasing the values of maximum IDI. The maximum values of IDI of wall B, wall G, and the corner of the structure for 5% eccentricity are, on the average, 10%, 73%, and 99% larger, respectively, than those in the concentric case. Maximum IDI of wall B for 10% eccentricity is, on the average, 29% smaller than that in the concentric case, whereas maximum IDI of wall G and the corner of the structure for 10% eccentricity are, on the average, 104% and 136% larger, respectively. It is important to note that increasing the value of static eccentricity by a factor of 2 (from 5% to 10%) increases the maximum displacement and IDI by about 19% (see Tables 3.18 and 3.19). This indicates that the increases of displacement and IDI are not in direct proportion to the increase in static eccentricity.

The above results indicate the importance of torsional rotation of the structure and its frequency in conjunction with translational motion of the structure and its frequency. According to Table 3.6, translational and torsional periods of the structure are about 0.57, and 0.54 seconds, respectively. As was shown in Chapter Two large amplification of the response of a structure can be expected for a linear-elastic single-story system, when the uncoupled frequency ratio, UFR, is close to unity and the static eccentricity ratio is small. This, in fact, is the case for the structure of Figure 3.1 and, therefore, torsional and translational modes of vibration of the structure are excited in the eccentric case. This in effect, induces large displacements and IDI amplifications in the eccentric case compared with those of the concentric case.

In order to understand the linear-elastic torsional response of the structure better, and since most building codes prescribe static analysis in their simplified regulations of torsion, it is important to compare the static torsion with the dynamic torsion. To do so, each response parameter (such as displacement or IDI) in the eccentric case is normalized by its corresponding value in the concentric case for both the static and the dynamic analyses. In Table 3.20 the normalized values of displacement and IDI, for 5% and 10% eccentricities, due to triangular and uniform static lateral loads and Taft-40 are summarized. These values are computed based on the average values of maximum displacement and IDI of the structure along the height. The normalized values of displacement of wall B, wall G, and the corner of the structure, for 5% eccentricity, due to both static triangular and static uniform lateral load are 0.840, 1.160, and 1.224, respectively. These values, for 5% eccentricity, due to Taft-40 are 1.085, 1.716, and 1.972, respectively. The normalized values of displacement of wall B, wall G, and the corner of the structure, for 10% eccentricity, due to both static triangular and static uniform lateral load are 0.681, 1.320, and 1.446, respectively. These values, for 10% eccentricity, due to Taft-40 are 0.688, 2.022, and 2.360, respectively. Therefore the dynamic response of the structure is much larger than the static response, because torsional and translational frequencies are very close together (UFR = 0.93), and these frequencies are encompassed by the dominant frequency content of Taft-40. These results indicate that the static analyses significantly underestimate (by more than 62% for 5% eccentricity and 63% for 10% eccentricity) the effects of torsion on the seismic response of the structure, because in a static analysis the dynamic characteristics of the structure and their relation with the dynamic characteristics of the ground motion are not taken into account.

3.6.3 Bending Moments and Shear Forces

Bending moment time-histories at the base of wall B and wall G due to Taft-40 for 5% and 10% eccentricities and for the concentric case are shown in Figures 3.28 and 3.29. As can be observed from Table 3.21, the maximum base bending moments of walls B and G for 5% eccentricity are 7% and 70% larger, respectively, than those of walls B and G in the concentric case. The maximum bending moment of wall B for 10% eccentricity is 34% smaller than the

corresponding value in the concentric case, whereas the bending moment of wall G for 10% eccentricity is 100% larger than that in the concentric case. The above results are compared with the static responses of the structure in Table 3.26. As was discussed in the previous section, the static analyses greatly underestimate the linear-elastic torsional response of the structure. The normalized values of moment at the bases of walls B and G for 5% eccentricity due to both the static triangular and the static uniform lateral loads are 0.84 and 1.16, respectively, while these values for 5% eccentricity due to Taft-40 are 1.07 and 1.70, respectively. The normalized values of moment at the base of walls B and G for 10% eccentricity due to both the static triangular and the static uniform lateral loads are 0.67 and 1.32, respectively, while these values for 10% eccentricity due to Taft-40 are 0.66 and 2.00, respectively.

Base shear time-histories at the base of wall B and of wall G due to Taft-40 for 5% and 10% eccentricity and for the concentric case are shown in Figure 3.30. The maximum base shear forces of walls B and G for 5% eccentricity, which are listed in Table 3.21, are 0.97 and 1.57 times larger, respectively, than that of wall B (or G) in the concentric case. These values for 10% eccentricity are 0.57 and 1.89 (see Table 3.21). The maximum shear forces of walls B and G along the height of the structure, due to Taft-40, for the concentric and eccentric cases are listed in Tables 3.22 and 3.24 and shown in Figure 3.32. According to the values of Table 3.22, shear forces of wall B and wall G for 5% eccentricity are, on average, 1.03 and 1.62 times larger, respectively, than those of the concentric case. These values for 10% eccentricity (Table 3.24) are, on average, 0.66 and 1.97 times larger, respectively. It is important to note that increasing the value of static eccentricity by a factor of 2 (from 5% to 10%) increases the maximum shear forces of wall G by about 22% (see Tables 3.22 and 3.24).

The shear forces along the height of walls B and G, due to Taft-40, in the concentric and the eccentric cases at the time that total base shear reaches its maximum value (13.5 seconds for the concentric case, 14.2 seconds for 5% eccentricity, 14.6 seconds for 10% eccentricity) are shown in Figure 3.33 and listed in Tables 3.23 and 3.25. As can be observed from the results presented in these tables, the average values of shear forces of wall B along the height of the

structure for 5% and 10% eccentricities are 30% and 43% smaller, respectively, than that of the concentric case, whereas those of wall G for 5% and 10% eccentricities are increased by 63% and 115%, respectively, compared with the concentric case.

Dynamic and static responses of the structure are compared in Table 3.26. The normalized values of average maximum story shear of walls B and G along the height of the structure, for 5% eccentricity, due to both the static triangular and the static uniform lateral loads are 0.84 and 1.16, respectively, while these values due to Taft-40 are 1.027 and 1.619, respectively. The normalized values of average maximum story shear of walls B and G, for 10% eccentricity, due to both the static triangular and the static uniform lateral loads are 0.68 and 1.32, respectively, while these values due to Taft-40 are 0.66 and 1.973, respectively. Therefore dynamic response of the structure is much larger than the static response, because torsional and translational frequencies are very close together (UFR = 0.93), and these frequencies are encompassed by the dominant frequency content of Taft-40. These results indicate, as explained earlier, that static analyses significantly underestimate (by more than 39% for 5% eccentricity and 49% for 10% eccentricity) the effects of torsion on the maximum value of the shear forces of wall G. It should be noted that the underestimation of the response by static analyses (as compared with dynamic analyses) increases monotonically, but not proportionally, with the increase in static eccentricity.

The maximum total story shears of the structure at each floor, due to Taft-40, for 5% and 10% eccentricities and the concentric case are listed in Table 3.27 and are shown in Figure 3.34. According to the results presented in this table, the maximum total story shears for 5% and 10% eccentricities are, on average, 14% and 28% larger, respectively, than that in the concentric case. This result supports our discussion in Chapter Two, which stated that "total story shear of a linear-elastic system, which is analyzed using a flat or hyperbolic ground acceleration spectrum, will, in general, be lower in the eccentric case than in the concentric case. However, this may not be true if a linear-elastic response spectrum (LERS), rather than an idealized design spectrum, is utilized in the analysis of the structure or when a time-history analysis is performed".

Total story shears of the structure, due to Taft-40, for 5% and 10% eccentricities and the concentric case when total base shear reaches its maximum value (13.5 seconds for the concentric case, 14.2 seconds for 5% eccentricity, 14.6 seconds for 10% eccentricity) are shown in Figure 3.35 and listed in Table 3.28. As can be observed from the results presented in this table, the average values of total story shear for 5% and 10% eccentricities are 20% and 42%, respectively, larger than that of the concentric case. The maximum base shear forces that are carried by each frame in the concentric and eccentric cases are listed in Tables 3.29 and 3.30. According to the values of Table 3.29, the normalized base shear for 5% eccentricity, that is carried by each frame, varies from 0.970 (for frame B) to 1.861 (for frame H), whereas these values for the static triangular and static uniform lateral load vary from 0.773 (for frame A) to 1.227 (for frame H) (see Table 3.15). For 10% eccentricity (Table 3.30), the normalized value of the base shear, that is carried by each frame, varies from 0.573 (for frame B) to 2.274 (for frame H), whereas these values for the static triangular and static uniform lateral load vary from 0.546 (for frame A) to 1.454 (for frame H) (see Table 3.16). As mentioned earlier, static analyses (as compared with dynamic analyses) underestimate (by more than 51% for 5% eccentricity and 56% for 10% eccentricity) the total base shear carried by each frame.

3.6.4 Dynamic Eccentricity

Dynamic eccentricity in a single-story system is the ratio of the maximum dynamic base torque around an axis passing through the center of stiffness, CS, of the floor to the maximum dynamic base shear of the corresponding uncoupled system, in which centers of mass and stiffness are coincident. For a multi-story system the dynamic eccentricity at each story may be defined as the ratio of the maximum dynamic torque about CS at that story to the maximum dynamic uncoupled shear force at the same story. According to this definition the dynamic eccentricity, e_d, is computed as

$$e_d = \frac{T_d}{V_0} \tag{3.1}$$

where T_d is the maximum story torque and V_0 is the maximum dynamic total story shear of the corresponding uncoupled system. The dynamic amplification of eccentricity is defined as

$$\frac{e_d}{e} = \frac{T_d}{V_0 e} \tag{3.2}$$

It must be noted that the concept of dynamic eccentricity is to define a torsional moment, which is to be applied as an external load to the corresponding concentric system. This torsional moment is equal to that of the eccentric system. Therefore in a linear-elastic system, in which deformations are proportional to forces, the displacements of the concentric system due to this torsional moment will be equal to those of the eccentric system.

Dynamic eccentricities of each story, for 5% and 10% eccentricities, are listed in Table 3.31. In the same table the values of dynamic amplification of eccentricity are given. These values are variable along the height of the structure. For 5% eccentricity, the amplification of eccentricity reaches a maximum value of 4.25 at the sixth story and a minimum of 3.75 at the first story, while for 10% eccentricity these values are 3.04 and 2.59 at the sixth and the first stories, respectively. The value of amplification of eccentricity, which is computed from equation 3.2, is larger at upper stories, because the maximum values of total story shear are smaller at upper stories. Average values of dynamic amplification of eccentricity along the height of the structure for 5% and 10% eccentricities are about 4.1 and 2.8, respectively. Therefore the amplification of eccentricity decreases with the increase in the static eccentricity. This result is in complete agreement with that obtained in Chapter Two for an idealized single-story system (see Figure 2.6). Dynamic amplification of eccentricity of a linear-elastic single-story system with the same values of UFR is about 3.8 for 5% eccentricity and about 2.2 for 10% eccentricity, when a flat or hyperbolic pseudo acceleration spectra is utilized to characterize the earthquake ground motion (see Chapter Two). Practically these values are good estimates of the average dynamic amplification of the structure of Figure 3.1, when it is subjected to Taft-40. Therefore the value of dynamic amplification of eccentricity for a multi-story structure may be estimated, for preliminary design, by the dynamic amplification of eccentricity obtained from analyzing an idealized linear-elastic

single-story system with the same values of eccentricity ratio (e/D) and uncoupled frequency ratio (UFR) as those of the multi-story structure (see Figure 2.7), using idealized flat or hyperbolic pseudo acceleration spectra to characterize the earthquake ground motion.

3.6.5 Bending Moment in Girders

The maximum positive and negative bending moments in girders, due to Taft-40 and the gravity loads (no load factor), take place in those girders which are adjacent to the shear walls at the fourth floor. These bending moments for 5% and 10% eccentricities and the concentric case are listed in Table 3.32. According to this table the maximum positive and negative bending moments of girders for 5% eccentricity are 91% and 62% larger, respectively, than those in the concentric case. These values, for 10% eccentricity, are 131% and 89%, respectively. These results are compared with the static responses of the structure in Table 3.33. The normalized values of the positive bending moments of girders, for 5% eccentricity, are 1.326 for the static triangular load; 1.486 for the static uniform load; and 1.91 for Taft-40. These values for 10% eccentricity are 1.652 for the static triangular load; 1.971 for the static uniform load; and 2.313 for Taft-40. The normalized values of the negative bending moments, for 5% eccentricity, are 1.094 for the static triangular load; 1.083 for the static uniform load; and 1.62 for Taft-40. These values for 10% eccentricity are 1.188 for the static triangular load; 1.167 for the static uniform load; and 1.89 for Taft-40. These results indicates that static analyses significantly underestimate the effects of torsion on the seismic response of the structure.

3.6.6 State of the Art and State of the Practice

In the simplified regulations for torsional effects of most building codes, the concept of "design eccentricity" (see Section 2.6) is employed. As described in Chapter Two, design eccentricity consists of two components (see equation 2.21). The first component, dynamic eccentricity, is the product of static eccentricity and an amplification factor. In UBC this factor is unity so that the dynamic and static eccentricities are assumed to be equal. The second component is the accidental eccentricity. In UBC the accidental eccentricity is equal to 5% of the building plan dimension perpendicular to the direction of ground motion excitation. Not only does the

accidental eccentricity reflect the effects of unforeseen factors such as non-uniform ground motion along the foundation of a structure; torsional components of ground motions; and the differences between actual and computed eccentricities, but it is also meant to compensate for the nonconservative torsional regulations of UBC in estimating dynamic eccentricity, especially for small values of static eccentricity. The effect of including accidental eccentricity in the design eccentricity on the static and dynamic torsional responses of structures is assessed in this section by considering the structure of Figure 3.1 with 5% eccentricity. According to UBC an accidental eccentricity of 5% is to be added to the static eccentricity, and therefore the structure has to be analyzed for 10% design eccentricity. The maximum normalized value of displacements for 10% eccentricity, due to a static analysis, is 1.447, while this value due to Taft-40 is 2.359 (see Table 3.20(b)). Therefore UBC underestimates the maximum displacement of the structure by 63%. Similarly it can be concluded from Table 3.26(b) and 3.33(b) that UBC underestimates bending moments at the bases of walls, shear forces of walls, and positive and negative bending moments of girders by 52%, 49%, 40%, and 59%, respectively.

If the accidental eccentricity is not included in the design eccentricity, the static analysis underestimates the values of maximum displacement of the structure, bending moments at the bases of walls, shear forces of walls, and positive and negative bending moments of girders by 61%, 47%, 39%, 44%, and 48% respectively. These values are smaller (except for the positive bending moment in girders) than those obtained after including accidental eccentricity in the design eccentricity. Therefore including accidental eccentricity in the design eccentricity does not compensate for the nonconservative torsional regulations of UBC in estimating the seismic response of structures, unless the real accidental eccentricity is known to be smaller than the one given by UBC. In this case the dynamic analysis can be conducted using the actual eccentricity (static eccentricity plus the real accidental eccentricity) rather than the design eccentricity given by UBC.

3.7 Summary and Conclusions

From the studies described in this chapter it is clear that the presence of an eccentricity between centers of mass and stiffness of the structure subjected to translational, unidirectional earthquake ground motion perpendicular to the eccentricity, results in coupling of lateral and torsional responses. These responses are generally larger than those which result in a concentric system, in which centers of mass and stiffness are coincident. These studies clearly indicate that a static analysis underestimates the effects of torsion on the seismic response of structures. The following are the main conclusions that can be drawn from these studies:

1. Lateral-torsional coupling in a structure has the effect of increasing lateral displacements, inter-story drift indices (IDI), shear forces of walls and bending moments in girders in both static and dynamic analyses. The maximum values of these response parameters due to Taft-40 ground motion increased with the increase in the static eccentricity ratio (e/D). However, this increase was not in direct proportion to the increase in static eccentricity.
2. Effects of torsion on the seismic response of structures can be highly underestimated if a static analysis is utilized. The underestimation of maximum displacements, bending moments at the base of a wall, and shear forces of walls from static analyses, as compared with dynamic analyses, increases monotonically, but not proportionally, with increase in static eccentricity. Building codes should consider the importance of dynamic characteristics of structures and of the ground motion on the torsional response of structures. Moreover, they have to include such factors as eccentricity ratio (e/D), translational period of the structure, and uncoupled frequency ratio (UFR) in their simplified regulations for torsional effects.
3. Dynamic amplification of eccentricity of the structure for 5% and 10% eccentricities are, on average, 4.1 and 2.8, respectively, whereas UBC in its regulations for torsion considers an amplification of eccentricity equal to one. Therefore there is a need to increase the value of amplification of eccentricity in the present code, especially when the uncoupled frequency ratio (UFR) is close to unity and static eccentricity ratio (e/D) is small (5%). It

must be noted that including accidental eccentricity in the design eccentricity reduces the amplification of eccentricity but it cannot compensate for the nonconservative torsional regulations of UBC in estimating dynamic eccentricity, unless the accidental eccentricity, required by the code, is larger than what can really be expected.

4. The value of dynamic amplification of eccentricity for a linear-elastic multi-story structure may be approximated, for preliminary design, by that obtained from analyzing an idealized linear-elastic single-story system with the same values of eccentricity ratio (e/D) and uncoupled frequency ratio (UFR) as those of the multi-story structure (see Figure 2.7), using idealized flat or hyperbolic pseudo acceleration spectra to characterize the earthquake ground motion.
5. Lateral load distribution profile does not play an important role in amplifying lateral displacements, inter-story drift indices (IDI), and shear forces of walls in the eccentric case compared with the concentric case, in a static analysis.
6. The seven-story structure was assumed to have a uniform 5% static eccentricity ratio (e/D) over the height. The linear-elastic response of this structure to Taft-40 ground motion produced a total story shear force that was, on average, 14% larger than that developed in the corresponding concentric structure. When the static eccentricity was increased to 10% of the maximum dimension of building plan, total story shear was increased, on average, to a level 28% larger than that for the concentric case. This indicates that total story shear does not always reduce in lateral-torsional coupled systems. Therefore, ignoring the effects of torsional coupling on the total story shear does not always provide a conservative estimate of the value of the total story shear.
7. The presence of an eccentricity between the centers of mass and stiffness in the structure has the effect of inducing the greatest increase in the shear forces and bending moments of those beams, columns, and shear walls which are at the furthest distance from the center of stiffness. The static analysis underestimates the above effects.

CHAPTER FOUR

STRUCTURAL MODELING FOR NONLINEAR ANALYSES

4.1 Introduction

The key ingredients in any structural analysis, linear-elastic or nonlinear, are the same. Real structure is specified first. Then, through certain idealization or modeling, which depends on engineering judgement, a mathematical model of this structure is developed. The model is then analyzed with a special computational strategy, which depends on the type of problem (linear-elastic or nonlinear). This analysis is almost always conducted by a computer program. The results of the analysis of the model have to be interpreted, with engineering judgement, to obtain results of the analysis for the real structure.

The computational strategy in linear-elastic structural analyses is quite different from that in nonlinear analyses. Linear-elastic analysis of structures is a standard procedure, and is straightforward. There are many computer programs, which perform linear-elastic static and/or dynamic analyses. These programs are generally reliable and ready-to-use. However, nonlinear computer programs are not usually ready-to-use, and modification and/or correction of their source code are usually needed for nonlinear analysis of structures. There are several reasons for this diversity between linear and nonlinear analyses. A nonlinear analysis is not a standard procedure and solution algorithms are problem dependent. This means that a given algorithm may work effectively for one type of nonlinearity, but not for other types, unlike a linear-elastic analysis. Besides, nonlinear analyses are much slower and more elaborate input data need to be provided by the user, therefore the cost for a nonlinear analysis is significantly higher compared with a linear-elastic one. As a result, mathematical modeling of structures for nonlinear analyses needs special attentions.

Three-dimensional nonlinear analysis of the structure of Figure 3.1, with the present computer technology, is very expensive, because of the size of the structure. However, because of certain characteristics of frame-wall systems, which are explained in this chapter, it is possible to localize the nonlinearity in the structure and to reduce the number of nonlinear elements, and

hence reduce the cost of the analysis. This chapter is dedicated to a discussion of the modeling procedure (idealization) of the structure of Figure 3.1, and starts with a description of the computer program "FACTS" [34], which is used for nonlinear static and dynamic analyses in this research. It must be noted that the model, which is developed in this chapter, may not simulate the exact response of the real structure of Figure 3.1. However, it is a practical model, which can be analyzed with the present computer technology within reasonable cost and, more important, it represents typical frame-wall systems realistically.

4.2 Description of the Computer Program FACTS

FACTS [34] is a finite element program for three-dimensional linear and/or nonlinear static and dynamic analyses. The advantage of a general purpose program, such as FACTS, is its capability of analyzing different structures with almost no limitation in their configurations. In this computer program many different types of elements, with diverse action-deformation relations, may be combined to model the structure. This is an important feature of FACTS, because in many nonlinear structures certain elements are expected to remain linear-elastic during the analysis. Therefore in these cases linear-elastic and nonlinear elements may be combined to model the structure more efficiently. Different sources of nonlinearity may be introduced and several methods of solving nonlinear problems are available.

4.2.1 Solution Strategy

FACTS performs a step-by-step analysis, accounting for material and geometric nonlinearity as well as boundary nonlinearity (such as contact problem or friction problem). The structural analysis is based on the direct stiffness method. Two solution strategies are available:

1. Step-by-step analysis with the Newton-Raphson (NR) equilibrium equation, using tangent or constant stiffness.

2. Step-by-step analysis with event-to-event solution.

The first strategy is a mathematical iteration scheme, whereas the second one is a physical approach, and hence is more reliable and stable. The latter approach, event-to-event, is used throughout this study for both static and dynamic analyses, although the Newton-Raphson iteration scheme is usually faster.

Loading is applied to the model by means of nodal static forces or nodal dynamic load functions. The analysis of nonlinear dynamic response is achieved by direct integration, performing a series of linear incremental analyses in essentially the same manner as for static nonlinear analysis. All structural masses are assumed to be lumped at nodes, thereby producing a diagonal mass matrix. Translational mass as well as rotational mass may be specified for each node. Damping can be proportional to mass, initial and/or tangential stiffnesses of the structure.

Both static and dynamic FACTS analyses are executed in double precision (64 bytes) on a Micro-Vax workstation at the University of California at Berkeley. The nonlinear three-dimensional reinforced concrete beam-column element, which is employed in this research, is introduced in the next section. During the use of the computer program FACTS, the original source code of this element was modified and corrected. These modifications and corrections range from changing input/output operations to debugging complex state determination and factor calculation routines.

4.2.2 Nonlinear 3-D Reinforced Concrete Beam-Column Element

This element, which is shown in Figure 4.1 [35], is intended to model inelastic reinforced concrete beams and columns with particular emphasis on the three-dimensional behavior. Yielding is assumed to take place only in concentrated, zero-length plastic hinges located at the element ends (lumped plasticity model [35]). The part of the element between the hinge is assumed to remain linearly-elastic. This elastic part is defined by an axial stiffness, two flexural stiffnesses, a torsional stiffness, and an effective shear rigidity. The hinges are assumed to have elastic-plastic-strain-hardening behavior. All plastic deformation effects are defined by means of

trilinear moment-rotation, trilinear torque-torsional twist, and trilinear force-axial extension relationships for hinges (Figure 4.2 [35]). The stiffnesses of hinges may degrade when reversed loading is applied. The degradation is controlled by user specified coefficients [35].

Different yielding strengths can be specified at the hinges at each end, if desired. Different yielding strengths can be specified for axial tension and axial compression. The source code of this element was modified so that different yielding strengths for positive and negative bending moments can also be specified. Therefore, not only reinforced concrete columns and rectangular beams can be modeled, but also reinforced concrete beams with T-cross sections, for example, may be specified.

Interaction between bending moments, torque, and axial force are considered by means of four-dimensional yield surfaces. Five different types of yield surface are available as shown in Figure 4.3 [35]. A kinematic hardening rule is assumed for post-yield behavior, which allows for translation of yield surface without change of size or shape.

4.3 Modeling of the Elements Sectional Properties

Moment-rotation and axial force-extension relationships of beams, columns, and shear walls are defined in this section. According to Figure 4.2, values of the first and the second yielding, as well as the stiffness values have to be specified. For simplicity, it is assumed that the action-deformation relationships are bilinear, although trilinear relationships as shown in Figure 4.2 can also be utilized. For bilinear action-deformation models, it is necessary to define F_{y1}, F_{y3}, Y_{s1}, Y_{s3}, K_1, and K_2 (see Figure 4.2). Values of EI, EA, and GA (where E and G are modulus of elasticity and shear modulus, respectively, I and A are moment of inertia and area of the cross section, respectively) for typical beam, column, and shear wall are summarized in Table 4.1 [30]. Since axial forces in beams are usually small, their moment-axial force interaction curve need not be specified. The values of positive and negative yielding bending moments of a typical beam are 3750 k-in and 937.5 k-in, respectively [30]. Based on reference [30] a 10% hardening (value of K_2 in moment-rotation relation) is considered for beams. This value is about 1% for columns and walls [30].

Moment-axial force interaction curves of a typical column and shear wall are shown in Figure 4.4. The dashed curves in these graphs are those given by reference [30], and the solid curves are the interaction relations that are used in this study. It must be noted that the portion of dashed moment-axial force interaction curves located above the balance point, as can be observed from Figure 4.4, is simply a straight line, which connects the balance point to the maximum axial force capacity of typical columns or walls. This part is an upper bound to the real moment-axial force interaction curve. The yield surface type two (see Figure 4.3) is employed to model the moment-axial force interaction curves of columns and walls (solid curves in Figure 4.4). As can be observed from Figure 4.4, yield surface curves of columns and walls follow the real curves (dashed curve) very closely for axial forces smaller than the balance point, whereas for larger values of axial forces they are not good approximations of the real moment-axial force interaction curves. However, this discrepancy of the model and real moment-axial force interaction is not important here, because it was observed from the results of studies, performed in Chapter Three, that the maximum axial forces of columns and shear walls are well below the balance value. Therefore, the yield surface curves (solid curves) shown in Figure 4.4 are acceptable models of the real ones (dashed curves), because they follow the real curve quite closely for axial forces smaller than the balance point.

4.4 Nonlinear Static Analysis

As was discussed earlier, nonlinear analysis of a structure is generally a slower process, and therefore more costly, than linear-elastic analysis of the same structure. The cost of a nonlinear analysis depends not only on the number of joints (as for a linear-elastic analysis), but what is more important it depends on the number of nonlinear elements. Since in many structures, nonlinearity is localized, which means only certain elements undergo nonlinear behavior and the rest of the structure remain linear-elastic, it is of great importance to study the possibility of localizing the nonlinearity in the structure before performing any complex expensive three-dimensional nonlinear dynamic analysis.

To investigate the possibility of localizing nonlinearity in the structure of Figure 3.1, its nonlinear static responses, assuming that centers of mass and stiffness are coincident, to two sets of monotonically increasing lateral loads are discussed here. The first set has a triangular profile, while the lateral distribution of the second set along the height of the structure is uniform. The structure is modeled as two-dimensional planner frames, which are connected to each other by rigid links as shown in Figure 4.5. The total base shear of the system against the inter-story drift index (IDI) of the first story due to both the triangular and uniform lateral loads is shown in Figure 4.6. The total base shear of the structure, the total base shear of frames (excluding walls), and the total base shear of walls are plotted against the IDI of the first story for the triangular and uniform lateral loads in Figures 4.7(a) and 4.7(b), respectively. It can be observed from these Figures that the nonlinear behavior of the structure is initiated by yielding of shear walls at the base. The IDI of the first story at the first yielding is about 0.09% and the total base shear of the structure due to the triangular and uniform loads are 1217 and 1408 kips, respectively.

Values of base shear carried by shear walls, frames (excluding walls), and the whole structure, corresponding to the first yielding and the incipient collapse for both triangular and uniform lateral loads, are listed in Table 4.2. It can be observed from the values of this table that about 88% of the total base shear of the structure, at the first yielding, is carried by the shear walls. This value at the incipient collapse is 52% for the triangular load and 60% for the uniform load. This result shows that shear walls dominate the response of the structure up to the first yielding. Thereafter, as can be observed from Figure 4.7, the frames start taking more and more shear force. However, the frames never carry more shear force than the walls and, at incipient collapse, they carry only 49% and 40% of the total base shear of the structure for the triangular and uniform loads, respectively. It is of great importance to note that response of frames (excluding walls) is practically linear-elastic up to an IDI of the first story equal to 0.54%, which is about 6 times larger than that of the first yielding. It can therefore be concluded that frames A,C,D,E,F, and H

can be considered to remain linear-elastic, while frames B and G are nonlinear. This realistic assumption reduces the total number of nonlinear elements from 560 to 70, and localize the nonlinearity in frames B and G.

The values of total strength of the structure under triangular and uniform lateral load are 2241 kips and 2773 kips, respectively. These values are about 26.5% and 32.8%, respectively, of the total reactive weight of the structure (8462.1 kips), while the UBC strength demand is about 13% of the total reactive weight.

4.5 Further Simplification of the Model

The number of nonlinear elements was reduced, by a factor of 8, by localizing nonlinearity in the structure. However, three-dimensional nonlinear dynamic analysis of this model is still impractical, because the model is too big. Further simplification of the model is possible. As discussed earlier and from Table 4.2, it can be easily observed that the total base shear of the structure is predominantly resisted by the shear walls. This is an important characteristic of frame-wall systems, and because of that the nonlinear response of the model very much depends on the behavior of frames B and G. Hence, to simplify the model further, it was decided to combine frames A,C,D,E,F, and H in two linear-elastic frames C′ and F′ as shown in Figure 4.8. The sectional properties of the frame C′ are nothing but the summation of those of the frames A,C, and D. Similarly, the sectional properties of the frame F′ are defined as the combination of those of the frames E,F, and H. The sectional properties of the longitudinal beams (L1) in the model are twice as much as those of a longitudinal beam in the structure, therefore the outriggering action of the frames on the shear walls is simulated properly in the model. Sectional properties of the longitudinal beams (L2) are yet to be specified.

In Chapter Two it was shown that two linear-elastic single-story systems will have the same response if they have the same mass, damping, translational frequency and uncoupled frequency ratio. Since the mass and damping of the model are the same as those of the real structure, the model will simulate the response of the real structure if their frequencies are equal. Therefore sectional properties of beams L2 can be best calculated by matching the frequencies of the real

structure and those of the model. To achieve this, the frequencies of the model for different sectional properties of beam L2 were computed and compared with those of the real structure. From this study, it was found out that the frequencies of the model and structure are practically the same, when the stiffness of beams L2 is 9 times larger than that of a longitudinal beam of the real structure. Figure 4.9 shows the periods of each vibrational mode of the model; these values are listed in Table 4.3. Natural periods of the real structure are also given in this table and shown by dots in Figure 4.9, for comparison.

It must be noted that the model, which has been developed in this chapter, may not simulate the exact response of the real structure of Figure 3.1. However, it is a practical model, which can be analyzed with the present computer technology within reasonable cost and, more important, it represents typical reinforced concrete frame-wall systems realistically.

4.6 Mass and Damping

The translational mass of each floor is listed in Table 4.4. Damping is assumed to be in the form of Rayleigh damping, which is proportional to mass and initial stiffness, and computed by

$$\mathrm{C} = a_0 \mathrm{M} + a_1 \mathrm{K} \tag{4.1}$$

where C, M, and K are the damping, the mass, and the stiffness matrices of the structure, respectively. Factors a_0 and a_1 can be calculated by

$$\begin{pmatrix} a_0 \\ a_1 \end{pmatrix} = \frac{2\omega_i\omega_j}{\omega_i^2 - \omega_j^2} \begin{pmatrix} \omega_i & -\omega_j \\ \dfrac{-1}{\omega_i} & \dfrac{1}{\omega_j} \end{pmatrix} \begin{pmatrix} \xi_i \\ \xi_j \end{pmatrix} \tag{4.2}$$

Where ω_i and ξ_i are frequency and damping ratio of the ith mode, respectively. The natural frequencies of the model with cracked sectional properties are listed in Table 4.3. It is assumed that the second and the sixth modes, which are the first two translational mode shapes in the direction of shear walls, have 5% damping ratio. Therefore from the above formula a_0 and a_1 are computed to be 0.67133 and 0.00238, respectively. The modal damping ratios for each mode can be calculated by

$$\xi_i = \frac{1}{2}\left(\frac{a_0}{\omega_i} + a_1\omega_i\right) \tag{4.3}$$

These values are shown in Figure 4.10 for each mode shape.

4.7 Summary and Conclusions

The model of the structure of Figure 3.1 developed in this chapter has the following features:

1. Nonlinear three-dimensional reinforced concrete beam-column elements are used to model the beams, columns, and shear walls.
2. Yielding is assumed to take place only in concentrated, zero-length plastic hinges located at the element ends (lumped plasticity model).
3. All plastic deformation effects are defined by means of bilinear action-deformation relationships for hinges.
4. Interaction between bending moments, torque, and axial force are considered by means of a four-dimensional yield surface.
5. A kinematic hardening rule is assumed for post-yield behavior, which allows for translation of yield surface without change of size or shape.
6. The solution strategy is based on a step-by-step analysis with the event-to-event algorithm.

It has been shown that the model represents typical frame-wall systems realistically, and therefore, in the next chapter the effects of torsion on its linear and nonlinear seismic responses will be assessed.

CHAPTER FIVE

NONLINEAR INELASTIC MULTI-STORY STRUCTURES

5.1 Introduction

As was discussed in Chapter Two, there have been some studies regarding inelastic seismic response of eccentric systems. In most of them the response of an idealized single-story system has been evaluated. However, there are diverse opinions regarding the importance of different parameters on the torsional response of structures, indicating that nonlinear torsion is not yet well understood. Therefore, in order to improve present knowledge about the nonlinear torsional behavior of real buildings, it is necessary to study the effects of torsion on the seismic nonlinear response of multi-story structures. In this chapter three-dimensional nonlinear response of reinforced concrete frame-wall structures to ground motion excitations is discussed. The mathematical model of Figure 5.1 is used in these studies. This model, which represents typical frame-wall structures, was developed in Chapter Four. The computer program FACTS [34] is employed in these studies.

An earthquake record is selected on the basis of the dynamic characteristics of the structure. A series of nonlinear analyses of the model, subjecting it to different excitation levels of this record, is conducted. For each excitation level three cases are studied; namely, the concentric model, and the eccentric model with two different initial static eccentricities of 5 and 25 percent of the maximum dimension of building plan, D=151 feet. These initial static eccentricities are 96 and 453 inches, respectively. It is assumed that eccentricity between centers of mass and stiffness of the structure is due to asymmetrical variation in the distribution of mass throughout the floors of the model and therefore the location, stiffness, and yielding strength of the lateral resisting elements remain unchanged. In this case it is assumed that the center of stiffness (CS) and the center of resistance (CR) are both located on the geometric centroid of the structure.

The effect of introducing unsymmetrical distribution of yielding strength of lateral load resisting elements on the seismic response of the structure is discussed next. In these studies the resistance eccentricity, as shown in Figure 5.1, is measured with respect to the geometric centroid

of the structure, which in this case is coincident with the initial location of the center of stiffness. Therefore no resistance eccentricity means that yielding strength of the lateral load resisting elements is distributed symmetrically in each story. It is important to note that if it is desired to keep the distribution of stiffness unchanged, the logical approach to reduce torsional effects on the seismic response of the structure (by having the shear walls yield at the same time) would be to design the yielding strength of the walls such that the center of resistance (CR) coincides with the center of mass (CM) and not with the center of stiffness (CS).

In all the above studies, the nonlinear dynamic response of the structure is compared with that of the linear-elastic structure. This is particularly important in revealing the error that can be made when the real elastic-inelastic seismic response of a structure is to be estimated just by its linear-elastic dynamic behavior.

5.2 Earthquake Input

The earthquake excitation that is considered in this study is the N21E component of the 1952 Taft Kern County earthquake ground motion record [22], which is 54.4 seconds in length and the peak acceleration is 0.156g at the 9.1 seconds mark of the record, where g is the acceleration of gravity. The first 25 seconds of the acceleration time-history are presented in Figure 3.10a, its normalized Fourier amplitude spectrum (FAS) is shown in Figure 3.10b. The linear-elastic response spectra (LERS) of the first 25 seconds of the Taft record are shown in Figure 3.11.

Limitation of available computer memory storage and also the fact that the available version of FACTS is a slow program, are the two main reasons for using a truncated record for this research. In this study only 8 seconds of the above record, from the 2.74 second to the 10.74 second mark of the record, have been used in the nonlinear dynamic analyses. This part of the ground motion, which is shown in Figure 5.2a contains important features of the record such as long duration pulses and the peak ground acceleration. The FAS and LERS of this acceleration time-history are shown in Figures 5.2b and 5.2c, respectively. The first three uncoupled translational periods of vibration of the model in the direction of the walls, which were estimated in Chapter Four, are also shown in this figure. The FAS and LERS indicate that the dominant frequency content of the

Taft record encompasses the fundamental period of the model. From the comparison of the LERS of the whole record (Figure 3.11) with the LERS of the truncated record (Figure 5.2c), it can be observed that the latter obtains smaller values of pseudo velocity, indicating that the truncated record is not as critical as the whole record.

It must be noted that the torsional ground motion is not considered here. However, it is important to mention that effects of torsion on the response of the structure may be increased if the period of the torsional ground motion is equal or close to the period of the first torsional mode of vibration of the structure.

The different intensity levels of the Taft ground motion used in the analyses are identified by the increased peak ground acceleration, PGA, of the record. The results from analyses with three PGA (0.18g, 0.40g, and 0.60g, referred to as Taft-18, Taft-40, and Taft-60, respectively) are presented and discussed herein. These normalized parts of the Taft record have an effective peak acceleration EPA of 0.14g, 0.32g, and 0.48g, respectively. These values were obtained using the procedure described by ATC [17], and summarized in Section 3.6.1 in Chapter Three.

5.3 Nonlinear Dynamic Response of the Model to Taft-40

5.3.1 Displacements

The displacement time-histories of the model due to Taft-40 in the concentric case are illustrated in Figure 5.3 for each floor. Since the floor diaphragm of the structure is assumed to be rigid in its plane, these time-histories represent the displacement of all the points in each floor. As expected, shapes of the displacement time-histories at all floors are similar and their amplitudes increase with the height of the floor. The maximum displacement at all floors occurred at about 4.15 seconds of the response. These values, which are listed in Table 5.1, are about 4 inches at the roof and 0.6 inch at the second floor.

The displacement time-histories of walls G and B due to Taft-40 for 5% eccentricity are illustrated in Figures 5.4 and 5.7 respectively. It can be observed from these plots that the shapes of displacement time-histories of wall G are similar at all floors, while they attain larger values at upper floors. This is also true for the displacement time-histories of wall B.

The maximum displacements of wall G in this case, which are presented in Table 5.1, occur at about 4.2 seconds of the response at all floors. These values are almost equal to those in the concentric case. It is important to note that displacement time-histories of wall G, as shown in Figure 5.4, attain a very large value at about 1.2 seconds of the response. The value of this large displacement is very close to the maximum displacement of wall G, which occurred at 4.2 seconds, and is about 34% larger, on average, than the peak displacement of the concentric case at about 1.17 seconds. The displacement time-histories of wall G becomes similar to those in the concentric case after about 2 seconds. The reason for this behavior in the eccentric structure will become clear when time-histories of plastic hinge rotation at the bases of walls discussed later.

The maximum displacements of wall B in this case, which are presented in Table 5.1, occurred at 4.4 seconds of the response, except at the second and the third floors. At these floors the maximum displacements occur after 6.6 seconds. It can be observed from the values of Table 5.1 that displacements of wall B are 18% smaller, on average, than those in the concentric case. It is important to note that between 4 and 6 seconds of the response, the displacement time-histories of wall B do not oscillate about the zero displacement axis. This is due to permanent inelastic displacement of wall B that occurred at about 4.4 seconds. This is also true in the case of wall G.

Floor displacement time-histories of wall G due to Taft-40 for 25% eccentricity are illustrated in Figure 5.5. It can be observed from these plots that shapes of displacement time-histories at all floors are similar while they attain larger values as the height of floor increases. The displacement time-histories of wall G in this case are quite different from those of the concentric and 5% eccentric structures. To explain this difference it is necessary to study the response of the model to a static lateral load as shown schematically in Figure 5.6. In this figure lateral load V is applied statically to the center of mass of the model. The effect of this lateral load, which generates a story shear and a story torque, is lateral translation and torsional rotation of the model. This latter component of motion increases the lateral displacement of wall G and decreases the lateral displacement of

wall B. The larger the eccentricity, the more torsional rotation can be experienced by the model and this in effect, leads to larger displacement of wall G and smaller lateral displacement of wall B.

Once one of the lateral load resisting elements yields the location of the current center of stiffness changes. This will increase the eccentricity between the centers of mass and stiffness and therefore, increase the torque. The increment of applied lateral force has an increasing effect on the value of base shear of wall B, whereas the increment of applied torque has a decreasing effect on the value of base shear of wall B. For 5% eccentricity the increasing effect of lateral force increment is larger than the decreasing effect of torque increment, as will be shown numerically later. Therefore wall B yields immediately after wall G. However, for 25% eccentricity the increasing effect of lateral force increment cannot overcome the decreasing effect of torque increment, therefore wall B, which never yields in this case, has a shear force much smaller than that of wall G. Therefore the response of the 25% eccentric model is different from those of the concentric and 5% eccentric models.

From analysis of the displacement time-histories of wall G due to Taft-40 for 25% eccentricity shown in Figure 5.5, three distinct displacement peaks can be easily observed. These peaks occur at about 1.3, 3.7 and 6.6 seconds of the response. The first distinct peak, which occurs during the first two seconds of the response, is also the maximum displacement value. This was not observed for 5% eccentricity, because torsional rotation and translational motion of the model are practically in phase, whereas for 25% eccentricity these motions are out of phase due to large initial eccentricity.

The maximum values of the displacements of wall G due to Taft-40 and 25% static eccentricity are presented in Table 5.1. In this table ratios of wall G maximum displacements to those of the concentric case at each floor are also given. According to these ratios, the maximum values of displacements of wall G for 25% eccentricity are 58% larger, on average, than those in the concentric case.

The displacement time-histories of wall B due to Taft-40 for 25% eccentricity are illustrated in Figure 5.8. It can be observed from these plots that the shapes of the displacement time-histories at all floors are similar, while they attain larger values at upper floors. The displacement time-histories of wall B are quite different from those of the concentric and 5% eccentric structures. The difference of the response of wall B in this case from those of the concentric and 5% eccentric structures becomes more clear by comparing Figure 5.8 with Figures 5.3 and 5.7. Referring to Figure 5.6, it becomes clear why the displacement of wall B is smaller in this case than for the concentric and 5% eccentric models.

As explained earlier and shown in Figure 5.6, the total shear force of the wall is a combination of shear due to lateral force, induced by translational inertia forces, and shear due to story torque, induced by torsional inertia. The contribution of torque to the total shear of the wall is larger for 25% eccentricity and therefore the total shear force of wall B becomes so small that it does not even yield during Taft-40 and basically responds elastically. Therefore, the period of vibration of wall B, which not only depends on mass but also depends on its current stiffness, is shorter in this case than that of the concentric and 5% eccentric models. The maximum displacements of wall B at all floors occur at 4 seconds of the response in this case. These maximum values are listed in Table 5.1. The smaller values of displacement of wall B, compared with those of wall G, are obvious from this table. The maximum displacements of wall B in this case are, on average, of 69% lower than those of the concentric case.

In order to grasp the effects of different eccentricities in the comparison of nonlinear torsion with linear torsion, and in an attempt to clarify the above discussion further, the linear and nonlinear responses of the structure are compared next. The linear-elastic displacement time-histories of walls B and G due to Taft-40 for the concentric case, 5% eccentricity, and 25% eccentricity are shown in Figures 5.9 to 5.13. The maximum displacements of the walls for these cases are listed in Table 5.2. The following observations can be made.

1. The period of the structure is modified by introducing eccentricity in the system even in the linear-elastic range. This is due to coupling of lateral and torsional motions in the structure for the eccentric cases. This results in an increase in period of the response of wall G and a decrease in period of the response of wall B compared with the concentric case. Note that, in all the previous cases the nonlinear responses of the structure, as shown in Figures 5.3 to 5.8, have larger periods than those of the linear-elastic responses, which are shown in Figures 5.9 to 5.13.
2. The linear-elastic displacement time-histories of wall G due to Taft-40 for the concentric case, 5% and 25% eccentricities are very similar in shape (not in order of magnitude), whereas the nonlinear displacement time-histories of wall G for 25% eccentricity, as pointed out earlier, are quite different from those for the concentric case and 5% eccentricity. This observation indicates that the modification of the response of the structure due to change in location of the center of stiffness for 25% eccentricity continues up to the end of the response, whereas for 5% eccentricity this modification is minor because wall B, as explained earlier, yields immediately after wall G and the center of stiffness returns almost to its initial location.
3. The linear-elastic and nonlinear displacement time-histories of wall B for 25% eccentricity are very similar in shape (not in order of magnitude). This confirms that wall B, as mentioned earlier, behaves elastically in the 25% eccentric nonlinear structure.
4. The values of maximum linear-elastic displacements of wall G for 5% eccentricity are larger than those for 25% eccentricity, because, as discussed in Chapter Two, the smaller the eccentricity ratio in a linear-elastic system, the larger is the dynamic amplification of the response.
5. The values of maximum linear-elastic and nonlinear displacements of wall G for 5% eccentricity are very close at lower floors. However, linear-elastic displacements of wall G at upper floors are larger than the nonlinear ones, because plastic rotations at the base of walls modify the behavior of the structure from a cantilever type of building to a shear type of building. In other words, when the shear walls yield the frame-wall behavior of the structure

is controlled by frame action rather than wall action. For the same reason, the values of maximum linear-elastic displacement of wall G for 25% eccentricity are smaller than the nonlinear ones at all floors except at the seventh floor and at the roof.

Envelopes of the maximum nonlinear floor displacement of walls B and G for the concentric, 5% and 25% eccentric structures are presented in Figure 5.14. It is obvious from Figure 5.14a that maximum displacements of wall B along the height of the structure decrease with increase of the initial eccentricity. For 5% eccentricity the maximum displacement of wall B decreases by a maximum value of 20% at the fourth floor and a minimum value of 15% at the roof. For 25% eccentricity, however, the maximum decrease is 78% at the second floor and the minimum decrease is 64% at the roof. From the results shown in Figure 5.14b, it is clear that the maximum displacements of wall G along the height of the structure for 5% eccentricity are practically the same as those for the concentric case, while these values for 25% eccentricity are larger than those for the concentric case. The maximum displacement of wall G increases by a maximum of 71% at the second floor. This was not the case when the static eccentricity was 5%. In the latter case the maximum displacement ratio was at the roof. For 5% eccentricity, where the amount of plastic rotation at the base of the wall is smaller, wall G behaves more like a cantilever beam with maximum displacement at the roof, whereas for 25% eccentricity the amount of yielding in wall G increases and wall G behaves more like a shear beam with large displacement at the second floor.

From the envelope of displacements shown in Figure 5.14 it becomes clear that the displacements of wall B for 25% eccentricity are so small that wall B responds elastically. However, the displacements of wall G are significantly larger than those for the concentric case because of the large initial static eccentricity in this case, which results in very early yielding of this wall. However, it is not clear why the maximum displacements for 5% eccentricity are practically the same as those in the concentric case. To find an explanation for these results, the plastic hinge rotation time-histories at the bases of walls B and G in the concentric and eccentric structures, shown in Figure 5.15, must be studied. Zero plastic hinge rotation at the base of a wall indicates that the response of the wall is linear-elastic.

The plastic hinge rotations at the base of wall G for the concentric and 5% eccentric structures are compared in Figure 5.15a. In Figure 5.15b the concentric and 25% eccentric models are compared and Figure 5.15c illustrates the plastic hinge rotation at the base of wall B in the concentric and 5% eccentric models. Wall B for the 25% eccentric model, subjected to Taft-40, does not show any inelastic behavior. The maximum values of plastic hinge rotation at the bases of walls B and G during the first 2 seconds and the 8 seconds of the response are listed in Table 5.3. In the first two seconds of the response the plastic hinge rotation at the base of wall G for 5% eccentricity attains a peak value which is 60% larger than that in the concentric case, whereas the maximum plastic hinge rotation at the base of wall G during the whole 8 seconds of response is almost the same as that in the concentric case. Moreover, Figure 5.15c indicates that for 5% eccentricity wall B yields right after wall G. Once both walls yield the current eccentricity between centers of mass and stiffness decreases to about the initial static eccentricity of the structure, and therefore the response of the structure becomes very similar to that of the concentric case because the initial eccentricity is small.

The above results can be explained by analyzing Figures 5.6 and 5.16. It has already been mentioned that, in the eccentric models shear forces of the walls are due to a combination of the effect of lateral translational inertia force (lateral force), and the effect of torsional inertia (torque). The contributions from each of these are shown in Figure 5.6. It is a reasonable approximation to assume that the increment of shear force of a wall due to incremental lateral force and due to incremental torque are

$$\Delta V_{GS} = \Delta V_{BS} = \frac{\Delta V}{2} \tag{5.1}$$

$$\Delta V_{GT} = \Delta V_{BT} = \frac{(\Delta V)\, e_c}{D} \tag{5.2}$$

where

ΔV_{BS} is increment of shear force of wall B due to increment of applied lateral force,

ΔV_{GS} is increment of shear force of wall G due to increment of applied lateral force,

ΔV_{BT} is increment of shear force of wall B due to increment of applied torque,

ΔV_{GT} is increment of shear force of wall G due to increment of applied torque,

ΔV is increment of applied lateral load,

e_c is current eccentricity between CM and CS, and

D is distance between walls B and G (shown in Figure 5.1).

Therefore values of total increment of shear forces of walls B and G are

$$\Delta V_B = \frac{\Delta V}{2} - \frac{(\Delta V) e_c}{D} \tag{5.3}$$

$$\Delta V_G = \frac{\Delta V}{2} + \frac{(\Delta V) e_c}{D} \tag{5.4}$$

Base shear of walls B and G, for 5% eccentricity, right before yielding of wall G are 658 kips and 757 kips, respectively. In the next step these values increase to 711 kips and 986 kips, respectively. Substituting these values in the above equation leads to

$$\frac{(\Delta V) e_c}{D} = 0.624 \frac{\Delta V}{2} \tag{5.5}$$

Therefore, the decreasing effect of torque on the base shear of wall B cannot overcome the increasing effect of lateral force. Hence wall B yields immediately after wall G. On the other hand, for 25% eccentricity the same calculations lead to

$$\frac{(\Delta V) e_c}{D} = 1.766 \frac{\Delta V}{2} \tag{5.6}$$

Therefore, the decreasing effect of torque on the base shear of wall B is larger than the increasing effect of lateral force. Hence wall B never yields even after wall G experienced large plastic hinge rotation at its base.

In Figure 5.16 total base shear forces of each wall against inter-story drift index (IDI) of the first story at the time that wall G has just yielded are shown schematically. For 5% eccentricity shear forces produced by torque are small enough that the total shear force of wall B is close to that of wall G. Therefore wall B yields right after wall G. However, for 25% eccentricity shear

forces produced by torque are so large that the total shear force of wall B is significantly smaller than that of wall G. In this case wall B does not yield even after wall G experienced large plastic hinge rotations at its base.

For 25% eccentricity the maximum plastic hinge rotation at the base of wall G occurs between the 1.34 and the 1.48 second marks of the response and is 1.93 times larger than that in the concentric case during the whole 8 seconds of the response (see Table 5.3). This maximum value is 3.55 times larger than the peak value in the concentric case during the first two seconds of the response. In this case with 25% eccentricity, wall B never yields and this is mainly due to large initial eccentricity of the structure.

From the above discussion it now becomes clear that when the initial eccentricity of a structure is small enough (5%) that the main lateral resisting elements yield one after the other, the lateral and torsional motions of the system may not be significantly coupled and therefore response of the structure is similar to that of the concentric case. However, for larger (25%) initial eccentricities the lateral-torsional coupling affects significantly the response of the structure when compared with the concentric case.

5.3.2 Inter-Story Drift Indices

Inter-story drift indices (IDI) time-histories of the model due to Taft-40 in the concentric case are illustrated in Figure 5.17 for each story. It can be observed from these plots that shapes of the IDI time-histories are similar at all stories. The maximum values of IDI at all stories occur between 4.15 and 4.20 seconds of the response. These values, which are listed in Table 5.4, attain a maximum of 0.52% at the fourth story and a minimum of 0.38% at the first story.

The IDI time-histories of walls G and B due to Taft-40 for 5% eccentricity are illustrated in Figures 5.18 and 5.19, respectively. The maximum IDI of wall G at all stories occurred at the 4.195 seconds mark of the response, except at the seventh story, in which it occurred at the 4.245 seconds mark of the response. The maximum values of IDI of wall G are almost equal to those of the concentric case. These values, which are presented in Table 5.4, attain a maximum of 0.53% at the fourth story and a minimum of 0.36% at the first story. It must be noted that the IDI

time-histories of wall G, shown in Figure 5.18, attain a peak value within the first two seconds, which on average is about 33% larger than that in the concentric case. However, IDI time-histories of wall G become similar to those in the concentric case after 2 seconds. The reason, as explained in the previous section and illustrated in Figures 5.6 and 5.16, is due to immediate yielding of wall B after wall G in this case.

The maximum IDI of wall B at all stories occurred at about the 6.5 seconds mark of the response, except for the third story. These values, which are given in Table 5.4, attain a maximum of 0.46% at the seventh story and a minimum of 0.31% at the first story. It can be observed from this table that the maximum IDI of wall B are 13% smaller, on average, than those for the concentric case. It is important to note that, between 4 and 6 seconds of the response, the IDI time-histories of wall B (Figure 5.19) do not show oscillation about the axis of zero displacement, and this is due to permanent plastic rotation locked in at the base of wall B during this period.

The IDI time-histories of wall G due to Taft-40 for 25% eccentricity are illustrated in Figure 5.20. The shapes of IDI time-histories at all stories are similar. There are 3 distinct peaks at about 1.3, 3.7, and 6.6 seconds of the response. The first distinct peak, which occurs during the first two seconds, is also the maximum IDI of wall G. The IDI time-histories in this case are quite different from those for the concentric and 5% eccentric models (Figures 5.17 and 5.18).

The maximum values of IDI of wall G along the height of the structure, which are presented in Table 5.4, have a maximum of 0.79% at the fifth story and a minimum of 0.65% at the first story. In this table ratios of the maximum values of IDI for wall G for the eccentric structure to that for the concentric case are also given. According to these ratios, the maximum values of IDI of wall G are generally larger than those for the concentric case. The average increase of maximum IDI of wall G with respect to the concentric case is 57%.

The IDI time-histories of wall B for the 25% eccentric model, subjected to Taft-40, are illustrated in Figure 5.21. The shapes of IDI time-histories at all stories are similar. However, the IDI time-histories of wall B are quite different from those of the concentric and 5% eccentric structures, as can be observed by comparing Figure 5.21 with Figures 5.17 and 5.19. The initial

eccentricity in this case is so large that the torsional effects reduce the value of shear force acting on the wall B significantly, and therefore wall B responds elastically, as discussed in the previous section. The maximum values of IDI of wall B occur between 1.24 and 1.34 seconds at all stories. These maximum values, which are given in Table 5.4, are obviously smaller than the concentric case and have a maximum of 0.20% at the fifth story and a minimum of 0.08% at the first story. The maximum IDI of wall B in this case is 64% smaller, on average, than that for the concentric case.

Envelopes of IDI profiles of walls B and G for 5% and 25% eccentricities are presented in Figure 5.22. It is obvious from Figure 5.22a that the maximum values of IDI of wall B decrease with the increase of initial static eccentricity. These values decrease by a maximum of 20% at the second story and a minimum of 7% at the seventh story for 5% eccentricity. However, for 25% eccentricity the maximum decrease is 78% at the first story and the minimum decrease is 59% at the seventh story.

The maximum values of IDI of wall G along the height of the structure for 5% eccentricity are shown in Figure 5.22b. These values, as expected after the discussion of the previous section, are practically the same as those in the concentric case, whereas the maximum values of IDI of wall G for 25% eccentricity are larger than those in the concentric case and increase by a maximum of 71% at the first story and a minimum of 49% at the fourth story compared with the concentric case.

5.3.3 Story Shear Forces

Story shear time-histories of wall B (or G) for the concentric model, subjected to Taft-40, are shown in Figure 5.23 for each story. The maximum values of story shear of a wall in this case, which are listed in Table 5.5, are larger, as expected, at lower stories.

Story shear time-histories of walls G and B due to Taft-40 for 5% eccentricity are presented in Figures 5.24 and 5.25, respectively. The maximum values of story shear of walls B and G, which are listed in Table 5.5, are larger at lower stories. From the values of this table it can be observed that the maximum story shear of walls for 5% eccentricity are practically the same as

those for the concentric case. The maximum story shear value for wall G for 5% eccentricity is only 3% larger, on average, than those for the concentric case, while the maximum shear for wall B is only 2% smaller, on average. From the values of Table 5.5, it can be observed that shear forces of walls B and G for 5% eccentricity are very close. This, as was already discussed and illustrated in Figures 5.6 and 5.16, is the main reason that wall B yields right after wall G for 5% eccentricity. Therefore its response in this case is similar to that of the concentric model.

Story shear time-histories of walls G and B due to Taft-40 for 25% eccentricity are illustrated in Figures 5.26 and 5.27, respectively. The story shear time-histories of walls in this case are completely different from those for the concentric and 5% eccentric models, shown in Figures 5.23 to 5.25. The maximum values of story shear of wall B, which basically responds elastically, occur at 4 seconds of the response, at all stories. These values, which are listed in Table 5.5, are generally smaller than those in the concentric case. The average reduction of wall B shear in this case is 51% compared with the concentric case.

The maximum story shears of wall G, which are given in Table 5.5, are larger than those in the concentric case. The average increase of wall G shear for 25% eccentricity is 58% above the corresponding value in the concentric case. The maximum base shear of wall G for 25% eccentricity is 1.713 times larger than that for the concentric case. This is a large increase considering the fact that wall G yields in the concentric case (see Figure 5.15). Increase of the base shear of wall G after yielding of the wall can be due to strain hardening of the wall. However, strain hardening of the wall cannot be the only reason for this large increase. To explain this important observation, story shear and distribution of lateral force profiles acting on wall G (due to Taft-40) at the time of maximum base shear of wall G are illustrated in Figure 5.28a for 25% eccentricity and the concentric case.

It can be observed from Figure 5.28a that, lateral forces acting on wall G for 25% eccentricity, compared with the concentric case, are redistributed along the height of the wall. The resultant of the lateral forces acts at 24.25 feet from the base of wall G for the concentric case, whereas for 25% eccentricity the resultant is at 17.53 feet from the base of the wall (see Figure 5.28a). Therefore

the contribution of the redistribution of lateral forces along the height of the wall in increasing the value of maximum base shear of the wall in the eccentric case can be approximated by the ratio of the lever arms of the resultants and is 1.383 (=24.25/17.53). This is about 81% of the total increase (1.713), indicating that only 19% of the increase of the maximum base shear of the wall in the eccentric case results from strain hardening of the wall.

From the values of Table 5.5, it can be observed that for 25% eccentricity maximum shear forces of wall B are much smaller than those of wall G. This is basically due to large torsional rotation of the model which results from large initial eccentricity in this case. Therefore, as illustrated in Figures 5.6 and 5.16, total story shear of wall G increases and that of wall B decreases because of induced story torque. The decrease in the total shear forces of wall B, due to induced story torque, is such that wall B responds elastically during the whole 8 seconds of the response of the 25% eccentric model, subjected to Taft-40.

Envelopes of story shear along the height of walls B and G for the concentric, 5% and 25% eccentric models are presented in Figure 5.28b. It is obvious from these plots that maximum story shear of wall B at all stories decreases with the increase of initial eccentricity. However, maximum story shear of wall B for 5% eccentricity at all stories is practically the same as those in the concentric case. These values for 25% eccentricity decrease by a maximum of 71% at the seventh story and a minimum of 36% at the first story when compared with the concentric case. The large reduction of story shear of wall B for 25% eccentricity when compared with the concentric case is basically due to large initial eccentricity in the structure, which in effect leads to large torsional rotation of the model in this case.

Total story shear time-histories of the concentric, 5% and 25% eccentric models due to Taft-40 are presented in Figures 5.29 to 5.31, respectively. The maximum values of total story shear of the model, which are listed in Table 5.6, are larger, as expected, at lower stories. The envelope values of total story shear of the model are shown in Figure 5.35.

The maximum values of total story shear for 5% eccentricity are 12% smaller, on average, than those of the concentric model, whereas these values for 25% eccentricity are 25% smaller, on average, than those for the corresponding concentric model. These results clearly indicate that the maximum values of total story shear of the eccentric models are smaller than those of the concentric one.

To explain the above observations, the values of base shear carried by each frame of the concentric and eccentric models, at the time that total base shear is maximum, are shown in Figure 5.32. Values of IDI of each frame of the model, at the time of maximum total base shear are also shown in this figure.

As explained in detail, in Chapter Four, frames C′ and F′ are assumed to behave elastically. Therefore shear forces, carried by each of these frames, are directly proportional to the lateral displacement of these frames. The sum of IDI of the first story of frame C′ and F′, when total base shear reaches its maximum value, is 0.69% for the concentric case. This value for 5% eccentricity is 0.39% and for 25% eccentricity is 0.41%. These values for the eccentric models are smaller than that for the concentric one, because of torsional rotation of the whole structure in the eccentric models, as shown in Figure 5.32. Therefore the total base shear of frames C′ and F′ for the eccentric models is smaller than that for the concentric case. This in effect, leads to smaller maximum total base shear for the eccentric models compared with the concentric one.

Although the maximum values of total base shear in the eccentric models are smaller than in the concentric case, shear forces of walls B and G for 5% eccentricity and those of wall G for 25% eccentricity attain larger values than those for the corresponding concentric models, because of strain hardening of the walls and also as a result of redistribution of lateral forces acting on the wall along its height. Therefore the designer must be aware that reduction of total story shear in the eccentric structure from that of the concentric one, is not, necessarily, synonymous to the reduction of shear force of the walls. Therefore total story shear is not a good index to estimate the effects of torsion on the seismic response of structures, particularly when realistic nonlinear (inelastic) behavior is considered.

It is important to note that the above discussion does not guarantee a reduction of total story shear in all eccentric structures compared with that of their corresponding concentric ones. As shown in Chapter Three, the total story shear forces of the eccentric structure were larger than those of the concentric one in the linear-elastic range.

5.3.4 Story Torque

The total story torque at a story is the sum of the torsional moments, about a reference axis, induced by the X- and Y-components of shear forces of each column and shear wall of that story. Having the total story torque about a fixed point, one can easily compute the total story torque about any other point at each story. In these studies the total story torque at each story is computed about the initial location of center of stiffness. Story torque time histories for the 5% and 25% eccentric models, subjected to Taft-40, are presented in Figures 5.33 and 5.34. A positive torque acts clockwise in the plan of the structure at each story and therefore produces negative displacement at wall G and positive displacement at wall B (see Figure 5.1 for sign convention).

Values of total story torque, as shown in Figures 5.33 and 5.34, are smaller at higher stories and their maximum values, as shown in Figure 5.36 and listed in Table 5.7, increase with the increase in initial eccentricity. To explain these results it is necessary to study the maximum values of story torque resisted by the shear walls, which are listed in Table 5.8.

Ratios of maximum story torque resisted by walls to the maximum total story torque, as presented in Table 5.8, indicate that shear walls contribute significantly to resisting total story torque. According to the values of this table, an average of 72% and 67% of the total torque are resisted by walls for 5% and 25% eccentricity, respectively. Torque resisted by walls is larger at lower stories because of larger shear forces of walls.

Therefore it can be concluded that the total story torque depends on the story torque resisted by the shear walls and this, in turn, depends on the values of shear forces of walls. The shear forces developed at the walls, as discussed earlier, are larger at lower stories, therefore the values of total story torque are larger at lower stories. On the other hand, the maximum values of shear forces of wall G, as shown in Figure 5.28b, increase with the increase in initial eccentricity. Therefore

the values of total story torque of the model also increase with the increase in the initial eccentricity. From this discussion it now becomes clear that the shape and values of total story torque time-histories for 5% and 25% eccentricity, which are shown in Figures 5.33 and 5.34, are quite different, because shear forces developed at the walls for 5% and 25% eccentricities, as discussed earlier in Section 5.3.3, are different.

The evaluations of torsional provisions in many building codes [2,4,7,8], as explained in Chapter Two, have been carried out by a common approach based on the "dynamic eccentricity" concept. Dynamic eccentricity is defined as distance measured from center of stiffness to be multiplied by the uncoupled dynamic story shear in order to produce the same torsional moment as computed by dynamic analysis. According to this definition the dynamic eccentricity, e_d is computed by

$$e_d = \frac{T_d}{V_0} \tag{5.7}$$

where T_d is the maximum story torque and V_0 is the maximum dynamic total story shear of the corresponding uncoupled system. The above definition, however, is not clear for a nonlinear system, because the location of CS is not fixed once yielding initiates in the system. To get around this problem, T_d may be calculated about a fixed reference point, such as initial location of CS. Therefore values of e_d will be given with respect to initial location of center stiffness.

The dynamic amplification of eccentricity is defined as

$$\frac{e_d}{e} = \frac{T_d}{V_0 e} \tag{5.8}$$

The values of dynamic amplification of eccentricity are presented in Table 5.7. These values for 5% eccentricity have a maximum of 3.29 at the first story and a minimum of 2.45 at the third story. However, for 25% eccentricity the dynamic amplification of eccentricity is less than one, except for the sixth story with a value of 1.16 and for the seventh story with a value of 1.25. These results are expected, because as was discussed in Chapter Two the larger the static eccentricity, the smaller the dynamic amplification of eccentricity.

It is important to note that the maximum values of total story torque and total story shear in an eccentric structure do not necessarily occur at the same time. The values of total story shear and story shear forces of walls B and G, at the time that total story torque reaches its maximum value, are presented in Table 5.9. Ratios of total story shear to the maximum total story shear at each story and ratios of story torque resisted by the shear walls to the maximum total story torque at each story are also listed in this table, from which it can be observed that total story shear at the time of maximum story torque for 5% eccentricity is very small compared with the maximum total story shear.

As shown in Table 5.9 the shear forces of walls B and G are acting in opposite directions at all stories except at the seventh one for 5% eccentricity. This naturally leads to small total shear force and large story torque, resisted by the shear walls, which in effect leads to large total story torque for the 5% eccentric model. Even at the seventh story, in which shear forces of walls are acting in the same direction, the value of shear force of wall B is so small, compared with that of wall G, that practically it does not increase the total story shear of that story. For 25% eccentricity, however, the values of total story shear, as can be observed from Table 5.9, are not small compared with the maximum values of total story shear. This is mainly because the initial eccentricity in this case is large enough that the shear forces of wall B, as already discussed in previous sections, are much smaller than those of wall G. Therefore, practically, the values of total story shear are not decreased by shear forces of wall B, which act in opposite direction to the shear forces of wall G at all stories except at the seventh and the first ones.

It must be noted that the concept of dynamic eccentricity is based on defining a torsional moment, which is to be applied as an external load to the concentric system. This torsional moment is equal to that of the eccentric system. Therefore in a linear-elastic system, in which deformations are proportional to forces, the values of displacement of the concentric system due to this torsional moment will be equal to that of the corresponding eccentric system. This is not the case for a nonlinear system, in which forces and deformations are not proportionally related, and the principle of superposition is not valid. Therefore values of dynamic eccentricity computed by equation 5.7

cannot be used in nonlinear concentric systems to estimate the maximum values of deformation of the corresponding structure with eccentricity. Moreover, total shear resistance in the concentric system (V_0 in equation 5.8) can be considerably higher than the shear that is developed in the eccentric systems. Therefore the dynamic eccentricity concept is not suitable for estimating the effect of torsion on the seismic nonlinear response of structures, and more reliable indices have to be used to measure these effects on the values of displacements, IDI, and hinge rotations. A reliable method is the one which estimates the value of dynamic amplification of displacements or IDI of the structure.

Tso and Bozorgnia [12] tried to find an alternative to the dynamic eccentricity. They extended the concept of "effective eccentricity", which was originally introduced for linear-elastic systems, to nonlinear single-story structures. Their idea is "to match the maximum dynamic displacement at the edge of the building to the edge displacement of the same system subjected to an equivalent static lateral load applied at a distance equal to the effective eccentricity value from the center of stiffness. The equivalent static lateral load is the maximum shear force that would be developed in the corresponding symmetrical system under dynamic excitation".

5.3.5 Response at Maximum Displacement, Shear, Torque

In the previous sections the time-histories of displacement, IDI, story shear, and story torque and their envelope values were compared for the concentric, 5% and 25% eccentric models. The effect of torsion on the seismic response of the model can be clarified further by investigating the variation of each of the remaining response parameters at the time that one of the parameters reaches its maximum value.

Figures 5.37 to 5.39 illustrate displacement profiles at the time of maximum displacement, at the time of maximum total base shear, and at the time of maximum total base torque, respectively. In these figures the displacement profiles of the concentric case as well as the displacement profiles of walls B and G for 5% and 25% eccentricities are shown. Deviation of displacement profiles of wall B from those of wall G is an indication of the amount of torsional rotation in the eccentric models. The larger the deviation, the larger the torsional rotation is. From Figure 5.37 to 5.39 it

becomes clear that torsional rotation of the 25% eccentric model is larger at the time of maximum displacement, whereas torsional rotation for the 5% eccentric model is larger at the time of maximum total base torque.

This can be explained by studying Figure 5.43. For 5% eccentricity the torque profile at the time of maximum base torque is larger, on average, than those at the time of maximum total base shear and at the time of maximum displacement. Therefore larger torsional rotation occurs when base torque is maximum. On the other hand for 25% eccentricity, torque profiles at the time of maximum displacement are larger, except for the first story, than those at the time of maximum total base shear and at the time of maximum total base torque. Therefore, in this case, larger torsional rotation occurs when the roof displacement of wall G is maximum.

Although shear forces of the walls, as shown in Figures 5.40 to 5.42, are generally larger at the time of maximum total base shear, the displacement profiles of walls are not larger at this time. Therefore total base shear does not constitute a reliable index for identifying the largest displacement in the structure, and hence it is not a proper index to evaluate the effects of torsion on seismic response of structures.

5.4 Effects of Excitation Level and Initial Eccentricity on the Response

5.4.1 Introduction

To obtain a better understanding of the problem of torsion and its effect on the response of structures, it is necessary to study the importance of intensity of the ground motion and value of static eccentricity on the linear-elastic and nonlinear torsional responses of structures. In previous sections it was pointed out that the lateral and torsional motions of the model are strongly coupled in the first two seconds of the response to Taft-40, particularly for 5% eccentricity. Therefore parametric studies during these two seconds of response are of great importance.

In the following sections the first two seconds of the response of the model to the Taft record of Figure 5.2c, with three different intensity levels (0.18g, 0.40g, 0.60g) are examined. Taft-18 with a PGA of 0.18g, but an EPA of 0.14g, is chosen because it induces practically no yielding in the concentric case during the first two seconds. In other words, this is the case in which the

structure has such a high yielding strength that will not yield when there is no eccentricity between centers of mass and stiffness, and therefore responses of the eccentric structures in this case are of great importance when they are compared with the corresponding concentric one. Taft-40 with a PGA of 0.40g, but an EPA of 0.32g, represents a possible severe earthquake ground motion and Taft-60 with a PGA of 0.60g, but an EPA of 0.48g, represents an extreme rare earthquake ground motion. These two cases also represent structures with lower yielding strength levels, in which significant inelastic responses are expected even in the concentric case. As before, for each level of excitation three cases are studied; namely, the concentric model, and the eccentric models with two different initial static eccentricities of 5 and 25 percent of the maximum dimension of the building plan (96 and 453 inches, respectively).

5.4.2 Response of the Model to Taft-18, 40, and 60

5.4.2.1 Displacements

Envelopes of lateral displacements of walls B and G along the height of the structure due to Taft-18, Taft-40 and Taft-60, are presented in Figures 5.44 to 5.46 and listed in Tables 5.10 to 5.12. The maximum displacements of wall B for the eccentric structures, as discussed earlier in the previous sections, are generally smaller than those for the concentric case, while the maximum displacements of wall G are larger. The maximum displacements of wall B decrease with the increase of initial eccentricity and the maximum displacements of wall G increase with the increase of initial eccentricity.

The maximum displacement of wall B for 5% eccentricity due to Taft-18, Taft-40 and Taft-60 are, on average, 17%, 24%, and 27% smaller, respectively, than those in the corresponding concentric cases, while these values for 25% eccentricity are, on average, 74%, 66%, and 71% smaller, respectively. The maximum displacement of wall G for 5% eccentricity due to Taft-18, Taft-40 and Taft-60 are, on average, 12%, 34%, and 32% larger, respectively, than those in the corresponding concentric cases, while these values for 25% eccentricity are, on average, 67%, 140%, and 114% larger, respectively. In contrast to what may be expected, these values due to Taft-60 are smaller than those due to Taft-40. This shows that the maximum values of displacement

of wall G for the concentric model due to Taft-60 are large enough (due to large plastic hinge rotation at the base of wall G in this case) that the ratios of the maximum values of displacement of wall G for the eccentric models to those for the concentric model are smaller than these ratios due to Taft-40. However, it must be noted that the absolute values of displacement of wall G increase, as expected, with the increase in PGA. This is clearly shown in Figure 5.47. In this figure the variation of maximum displacements of wall G at each floor against PGA of the record are presented for different initial eccentricities. The average differences between values of displacement of wall G for the 5% eccentric and the concentric models due to Taft-18, Taft-40 and Taft-60 are 0.091, 0.510, and 0.836 inch, respectively, while these values for 25% eccentricity are 0.476, 2.071, and 2.949 inches, respectively.

According to these results, and as can be observed from Figure 5.47, the increase in displacement of wall G due to eccentricity is not significant, practically, for the 5% eccentric model, subjected to Taft-18, whereas this increase in displacement becomes more significant as the PGA and initial eccentricity increase. However, as mentioned earlier, increasing the intensity level of an earthquake is synonymous to decreasing yielding strength of the structure. Therefore effects of torsion on the maximum displacement of structures, subjected to earthquake excitations, can be minimized by increasing the yielding strength of structures and decreasing initial static eccentricity.

To understand the real torsional response of the structure, and to assess the validity of a linear-elastic analysis in predicting the behavior of the building, it is important to compare maximum values of linear-elastic and nonlinear displacements of the walls. Maximum values of linear-elastic displacements of walls B and G along the height of the structure due to Taft-18, Taft-40, and Taft-60 are listed in Tables 5.13 to 5.15. The envelope values of linear-elastic and nonlinear displacements of wall G due to Taft-18, Taft-40, and Taft-60 are compared in Figures 5.48 and 5.49. From these figures it can be observed that the envelope values of displacements due to Taft-18 in linear-elastic and nonlinear cases are practically identical. However, as the PGA increases to 0.40g and 0.60g the nonlinear response of the structure deviates from the linear-elastic

behavior. Plastic rotation at the base of the shear wall modifies the behavior of the structure from a cantilever type of building to a shear type of building. In other words, when the shear walls yield the frame-wall behavior of the structure is controlled by the frame action. Therefore nonlinear displacement of the structure is larger than its linear-elastic displacement at lower stories. It can be observed from Tables 5.13 to 5.15 that for 5% eccentricity the nonlinear displacements of the second floor due to Taft-40 and Taft-60 are 39% and 79%, respectively, larger than their linear-elastic displacements. When the eccentricity increases to 25% the nonlinear displacements of the second floor due to Taft-18, Taft-40, and Taft-60 are 24%, 92%, and 134%, respectively, larger than their linear-elastic displacements. These important results indicate how a linear-elastic dynamic analysis can underestimate the real nonlinear response of the structure particularly when the initial eccentricity is large. Therefore, it is necessary to restrict the amount of acceptable initial eccentricity, if the present simplified regulations for torsional effects of the building codes are used.

5.4.2.2 Inter-Story Drift Indices

The envelopes of IDI of walls B and G along the height of the structure due to Taft-18, Taft-40, and Taft-60 are presented in Figures 5.50 to 5.52 and listed in Tables 5.16 to 5.18. As already discussed, the maximum values of IDI of wall B in the eccentric structures are, in general, smaller than those in the concentric case and decrease with the increase of initial eccentricity. However, the maximum values of IDI of wall G in the eccentric structures are generally larger than those in the concentric case and increase with the increase of initial eccentricity.

The lateral displacements of walls are controlled by their flexural type of deformation, whereas those of frames are governed by shear type of deformation. Therefore, when shear walls and frames are combined in a frame-wall structure, the interaction between walls and frames will control the lateral displacements of the system. Because of this interaction between walls and frames the maximum IDI of walls for the concentric and eccentric models subjected to Taft-18, Taft-40 and Taft-60 are largest at the third, the fourth, or the fifth story, except for wall G for the 25% eccentric model subjected to Taft-60. In the latter case the maximum IDI of wall G is largest

at the first story. This is mainly due to large plastic hinge rotation at the base of wall G, which will be discussed later, and also due to formation of a plastic hinge at the top of the first story of wall G because of high intensity of excitation (Taft-60) and large initial eccentricity (25%).

The maximum IDI of wall B for 5% eccentricity due to Taft-18, Taft-40, and Taft-60 are, on average, 15%, 17%, and 21% smaller, respectively, than those in the corresponding concentric cases, while these values for 25% eccentricity are, on average, 74%, 61%, and 64% smaller, respectively. The maximum IDI of wall G for 5% eccentricity due to Taft-18, Taft-40, and Taft-60 are, on average, 13%, 33%, and 32% larger, respectively, than those in the corresponding concentric cases, while these values for 25% eccentricity are, on average, 60%, 131%, and 106% larger, respectively. In contrast to what may be expected, the relative increases in IDI with respect to the concentric case due to Taft-60 are smaller than those due to Taft-40. This shows that the maximum values of IDI of wall G for the concentric model, subjected to Taft-60, are already sufficiently large that ratios of the maximum values of IDI of wall G for the eccentric models to those for the concentric model are smaller than these ratios due to Taft-40. However, it must be noted that the absolute values of IDI of wall G increase, as expected, with the increase of PGA. This is clearly shown in Figure 5.53. In this figure the variation of maximum values of IDI of wall G at each floor against PGA of the record is presented for different initial eccentricities. The average differences between values of IDI of wall G for the 5% eccentric and the concentric models due to Taft-18, Taft-40, and Taft-60 are about 0.02%, 0.11%, and 0.18%, respectively, while these values for 25% eccentricity are about 0.11%, 0.42%, and 0.59%, respectively.

According to these results, and as can be observed from Figure 5.53, the increase in IDI of wall G due to eccentricity is not significant practically for the 5% eccentric model subjected to Taft-18, whereas this increase in IDI becomes more significant as the PGA and the initial eccentricity increase. However, as mentioned earlier, increasing the intensity of an earthquake is synonymous to decreasing yielding strength of the structure. Therefore, effects of torsion on the maximum IDI of structures that are subjected to earthquake excitations, can be minimized by increasing the yielding strength of the structure and decreasing the initial static eccentricity.

To understand the real torsional response of structures and to assess the validity of a linear-elastic analysis in predicting the behavior of the building, it is important to compare maximum values of linear-elastic and nonlinear IDI of the walls. Maximum values of linear-elastic IDI of walls B and G along the height of the structure due to Taft-18, Taft-40, and Taft-60 are listed in Tables 5.19 to 5.21. The envelope values of linear-elastic and nonlinear IDI of wall G due to Taft-18, Taft-40, and Taft-60 are compared in Figures 5.54 and 5.55. From these figures it can be observed that the envelope values of IDI due to Taft-18 in the linear-elastic and nonlinear cases are practically identical. However, as the PGA increases to 0.40g and 0.60g the nonlinear response of the structure deviates from the linear-elastic behavior. Plastic rotation at the base of a shear wall modifies the behavior of the structure from a cantilever type of building to a shear type of building. In other words, when the shear walls yield the frame-wall behavior of the structure is controlled by the frame action. Therefore nonlinear IDI of the structure are larger than its linear-elastic IDI at lower stories. It can be observed from Tables 5.19 to 5.21 that for 5% eccentricity the nonlinear IDI of the first story due to Taft-40 and Taft-60 are 39% and 79%, respectively, larger than their linear-elastic IDI. When the eccentricity increases to 25% the nonlinear IDI of the first story due to Taft-18, Taft-40, and Taft-60 are 24%, 92%, and 134%, respectively, larger than their linear-elastic IDI. These important results indicate how a linear-elastic dynamic analysis can underestimate the real nonlinear response of the structure particularly when the initial eccentricity is large. Therefore, it is necessary to restrict the amount of acceptable initial eccentricity, if the present simplified regulations for torsional effects of building codes are used.

5.4.2.3 Plastic Hinge Rotations

The time-histories of plastic hinge rotation at the base of wall G in the concentric and eccentric structures due to Taft-18, Taft-40 and Taft-60 are shown in Figures 5.56 and 5.57. Time-histories of plastic hinge rotation at the base of wall B due to Taft-40 and Taft-60 for 5%

eccentricity compared with the corresponding concentric cases, and due to Taft-60 for 25% eccentricity compared with the corresponding concentric case, are also shown in Figure 5.58. Wall B does not show any inelastic behavior in other cases.

The maximum values of the plastic hinge rotation at the bases of walls B and G during the first two seconds of the response are listed in Table 5.22, from which it can be observed that wall B remains elastic during Taft-18 for both 5% and 25% eccentricities and during Taft-40 for 25% eccentricity. There is, however, minor yielding at the base of wall B during Taft-60 for 5% and 25% eccentricities. The maximum plastic hinge rotations at the base of wall G for 5% eccentricity due to Taft-18, Taft-40, and Taft-60 are 218%, 60%, and 46%, respectively, larger than those in the corresponding concentric cases, while these values for 25% eccentricity are 1422%, 255%, and 178%, respectively, larger. These values decrease with the increase in PGA, because the plastic hinge rotation at the bases of the walls for the concentric model is smaller when PGA is smaller, and this is obviously because a small PGA can be interpreted as representing a structure with higher yielding strength and therefore with less inelastic rotation at the bases of the walls. However, it must be noted that absolute values of plastic hinge rotation at the bases of the walls increase, as expected, with the increase in PGA, as clearly shown in Figure 5.59. In this figure the variation of maximum values of plastic hinge rotation at the base of wall G against PGA of the record is presented for different initial eccentricities. The differences between values of plastic hinge rotation at the base of wall G for the 5% eccentric and the concentric models due to Taft-18, Taft-40, and Taft-60 are about 0.0001, 0.0009, and 0.0018 radian, respectively, while these values for 25% eccentricity are about 0.0009, 0.0039, and 0.0068 radian, respectively.

According to these results, and as can be observed from Figure 5.59, the increase in the plastic hinge rotation at the base of wall G due to eccentricity is practically negligible for the 5% eccentric model subjected to Taft-18, whereas this increase becomes more significant as the PGA and the initial eccentricity increase. Therefore torsional effects on the maximum plastic hinge rotation at the bases of the walls can be reduced and eliminated by increasing the yielding strength of the structure and decreasing the initial static eccentricity.

The maximum plastic hinge rotation capacity at the base of a wall was found to be about 0.01 radian [30]. As can be observed from Table 5.22, the maximum plastic hinge rotation at the base of wall G for 25% eccentricity due to Taft-60 is somewhat larger than this capacity. This indicates the failure of wall G in this case. The maximum plastic hinge rotation at the base of wall G, in this case, is about 2 times larger than that for the 25% eccentric model, subjected to Taft-40, and more than 11 times when it is subjected to Taft-18. Therefore, decreasing the intensity level from Taft-60 by factors of 1.5 and 3.3 will decrease the maximum plastic hinge rotation demand at the base of the walls by factors of 2 and 11, respectively. This clearly indicates that the plastic hinge rotation demand at the base of a wall decreases rapidly with the decrease of the intensity of the earthquake ground motion or similarly with the increase of the yielding strength of the structure. Therefore it is very important to increase the yielding strength of structures to reduce the effects of torsion on their seismic responses, or if this is not possible the acceptable value of eccentricity should be restricted.

5.4.2.4 Story Shear

The maximum values of story shear of walls B and G due to Taft-18, Taft-40 and Taft-60 in the concentric and eccentric structures are shown in Figures 5.60 to 5.62 and listed in Tables 5.23 to 5.25. It can be observed from these results that the maximum values of shear forces of wall G increase with the increase of initial eccentricity, while the maximum values of wall B decrease with the increase of initial eccentricity.

As was discussed in Section 5.3.3 and illustrated in Figures 5.6 and 5.16, total shear forces of walls for the eccentric models due to earthquake excitations are composed of shear due to lateral translational inertia forces (lateral forces), and shear due to torsional inertia forces (torque). Therefore, as shown in Figures 5.6 and 5.16, the maximum values of shear of wall B for the eccentric models are smaller than those of wall G. This is clearly shown in Figures 5.60 to 5.62. The maximum values of shear forces of wall G for 5% eccentricity due to Taft-18, Taft-40 and Taft-60 are, on average, 16%, 4%, and 8% larger, respectively, than those for the corresponding concentric cases, while these values for 25% eccentricity are, on average, 40%, 50%, and 44%

larger, respectively. The maximum values of shear forces of wall B for 5% eccentricity due to Taft-18, Taft-40 and Taft-60 are, on average, 12%, 7%, and 11% smaller, respectively, than those for the corresponding concentric cases, while these values for 25% eccentricity are, on average, 74%, 57%, and 50% smaller, respectively.

It can be observed from these results that base shear forces of wall G for the eccentric models are larger than those for the corresponding concentric models. Because the walls in the concentric model experienced inelastic rotation at their bases, the increase in base shear of wall G in the eccentric models is partly due to strain hardening of the walls and, as was discussed in Section 5.3.3, is mainly a result of the redistribution of lateral forces acting on the wall along the height. To clarify this, story shear and distribution of lateral force profiles acting on wall G (due to Taft-18, Taft-40, and Taft-60) at the time of maximum base shear of wall G are illustrated in Figures 5.63 to 5.65 for 25% eccentricity and the concentric case.

It can be observed from Figures 5.63 to 5.65 that lateral forces acting on wall G for 25% eccentricity, compared with the concentric case, are redistributed along the height of the wall. Resultants of the lateral forces due to Taft-18, Taft-40, and Taft-60 act at 34.15, 24.25, and 21.68 feet, respectively, from the base of wall G for the concentric case, whereas for 25% eccentricity the resultants are at 24.44, 23.55, and 20.74 feet, respectively, from the base of the wall (see Figures 5.63 to 5.65). Therefore the contributions of the redistribution of lateral forces along the height of the wall in increasing the maximum values of base shear of the wall in the eccentric case can be approximated by the ratio of the lever arms of the resultants and are 1.397 (=34.15/24.44), 1.030 (=24.25/23.55), and 1.045 (=21.68/20.74) for Taft-18, Taft-40, and Taft-60, respectively. These are about 99.6%, 81.5%, and 86.3% of the total increases of maximum base shear forces of wall G, respectively. These results show that the contribution of strain hardening in increasing maximum base shear of wall G is a practically negligible for Taft-18. It must be noted that there is practically negligible amount of yielding at the base of wall G due to Taft-18 for the concentric case, whereas wall G experiences nonlinear behavior due to Taft-18 for 25% eccentricity (see

Figure 5.57). Therefore it can be concluded that immediately after the first yielding at the base of a wall, the base shear of the wall increases mainly on account of the redistribution of lateral forces along the height of the wall.

The variations of the maximum values of story shear of walls G and B against PGA of the record for different initial eccentricities are presented in Figures 5.66 and 5.67. Maximum values of shear forces of wall G, as shown in Figure 5.66, increase with the increase in initial eccentricity and PGA. At the first story the maximum base shears of wall G for 5% and 25% eccentricities are larger than those for the concentric model, because plastic hinge rotations at the base of wall G in the eccentric models are larger than that in the concentric model and, consequently, large strain hardening, as well as redistribution of lateral forces along the height of the wall, is developed in wall G in the eccentric cases. However, wall G does not experience any inelastic rotation at upper stories and therefore the story shear at these stories is proportional to the displacement of wall G. Since the maximum values of displacement of wall G for 5% eccentricity, as explained earlier, are not much larger than those for the concentric model, the story shears of wall G at the second story and higher are close to those for the concentric model, as shown in Figure 5.66.

On the other hand, for 25% eccentricity the plastic hinge rotation at the base of wall G and its lateral displacements are significantly larger than the corresponding concentric model (Figures 5.47 and 5.59). Therefore the maximum values of story shear of wall G for 25% eccentricity are larger than those for the corresponding concentric model at all stories, as shown in Figure 5.66. Maximum values of shear forces of wall B, as shown in Figure 5.67, decrease with the increase in initial eccentricity but increase with the increase in PGA. These values for 5% eccentricity, as expected, are very close to those for the concentric case in the second story and higher, whereas for 25% eccentricity the maximum values of wall B shear are smaller than those for the concentric and 5% eccentric structures at all stories.

The maximum values of total story shear of the structure due to Taft-18, Taft-40, and Taft-60 in the concentric and eccentric structures are shown in Figure 5.68 and listed in Table 5.26. The maximum values of total story shear forces for the eccentric models are generally smaller than

those for the concentric model. However, for 5% eccentricity the maximum total shears due to Taft-18 at the first and the second stories are slightly larger than the corresponding values for the concentric case. To explain these results, values of base shear, when total base shear reaches its maximum value, carried by each frame due to Taft-18, Taft-40, and Taft-60 are shown in Figures 5.69 to 5.71. The values of IDI of the first story, for each frame, at the time that total base shear is maximum, are also illustrated in these figures.

As shown in Figure 5.69, the values of IDI of walls B and G for the 5% eccentric model, subjected to Taft-18, are very close to those for the concentric model. Therefore base shear of wall B for 5% eccentricity is very close to that for the concentric model. However, base shear of wall G for 5% eccentricity is larger than that for the concentric case, because of strain hardening of the wall and because of the redistribution of lateral forces along the height of the wall. Therefore, the total base shear of the 5% eccentric model is slightly larger than for the corresponding concentric model. For 25% eccentricity, however, the torsional rotation of the model is so large, as shown by the values of IDI in Figure 5.69, that base shear of wall B is 78% smaller than that for the concentric model. Therefore the total base shear in this case is smaller than that for the concentric model; that is, the increase in the shear resistance developed at wall G due to strain hardening and in frame F′ due to larger elastic displacement cannot overcome the elastic decrease in resistance of frame C′ and in wall B.

As shown in Figure 5.70, the values of base shear of frames for the 5% eccentric model, subjected to Taft-40, are so close to those for the concentric model that total base shear is practically the same as that for the concentric model. This is mainly because of small torsional rotation of the 5% eccentric model, as shown by the values of the IDI of each frame. On the other hand, the torsional rotation of the 25% eccentric model, as shown by the values of IDI in Figure 5.70, is so large that wall B does not yield at all and therefore the base shear of frame B is much smaller than that for the concentric case. Therefore the total base shear of the 25% eccentric model due to Taft-40 is smaller than that for the concentric one.

As shown in Figure 5.71 the IDI of wall B for the 5% eccentric model, subjected to Taft-60, is smaller than that for the concentric case. Therefore wall B, and consequently frame B, carry smaller base shear in this case. For the 25% eccentric model, the torsional rotation at the time of maximum total base shear of the structure, is so large that wall B does not yield. Therefore base shear of frame B in this case is so small that the total base shear of the 25% eccentric model is smaller than that for the concentric model. It is interesting to mention that wall B in this case experiences a small amount of yielding only after 1.52 seconds of the response as shown in Figure 5.58, however, maximum total base shear in the model occurs at 1.38 seconds of the response. Note that shear the forces of walls B and G shown in Figures 5.69 to 5.71 should not be mistaken for the maximum base shear of walls B and G, because the values shown in these figures are shear forces of walls B and G when total base shear of the structure reaches its maximum value.

According to the above discussion, the reduction of maximum values of total story shear for 25% eccentricity compared with the concentric model is more than that for 5% eccentricity. The maximum values of total story shear for 25% eccentricity due to Taft-18, Taft-40 and Taft-60 are, on average, 32%, 22%, and 21% smaller, respectively, than those for the corresponding concentric case, while these values for 5% eccentricity decrease by less than 10%. The above results are summarized in Figure 5.72. The maximum values of total story shear, as shown in this figure increase with the increase of PGA. However, this increase, as shown earlier, is not proportional to the increase in PGA. Since torsional rotation of the 5% eccentric model is small, the values of total story shear for this model, as already discussed, are about the same as those for the concentric model. This is clearly shown in Figure 5.72.

5.4.2.5 Story Torque

The maximum values of total story torque of the eccentric models, subjected to Taft-18, Taft-40, and Taft-60, are shown in Figure 5.73 and listed in Table 5.27. Variations of maximum total story torque against PGA for different values of initial static eccentricity are presented in Figure 5.74. From these results it can be observed that the maximum values of total story torque increase with the increase in PGA and initial eccentricity. From a quick inspection of the results

presented in Figure 5.74, it can be concluded that the total story torque does not increase proportionally with the value of static eccentricity ratio (e/D). While this is correct, it also points out that total story torque is not a good index to measure torsional effects. The values of the total story torque are limited by the total story shear resistance of the structure, which in turn is controlled by the yielding strength of the structure (mainly yielding strength of the shear walls in this case).

The study of the maximum values of story torque resisted by the shear walls, which are listed in Table 5.28 and shown in Figure 5.75, will provide better insight to the effect of torsion on the total story torque. The ratio of maximum story torque resisted by the walls to the maximum total story torque, as presented in Table 5.28, indicates the amount of contribution of the shear walls in resisting the maximum total story torque. This contribution for the 5% eccentric model, subjected to Taft-18, Taft-40, and Taft-60 is, on average, 69%, 71%, and 74%, respectively. These values increase with the increase in PGA, because as already discussed, the values of shear forces of walls B and G for 5% eccentricity increase with the increase in PGA.

The contribution of the shear walls in resisting the maximum total story torque for the 25% eccentric model, subjected to Taft-18, Taft-40, and Taft-60, is, on average, 70%, 63%, and 59% respectively. The large torsional rotation of the 25% eccentric model leads to an increase in torque resisted by the frames, compared with that resisted by the walls. Therefore torque resisted by the shear walls contributes less to the total story torque as torsional rotation of the model increases. On the other hand, torsional rotation of the model increases with the increase in PGA. Hence, the contribution of the shear walls in resisting the maximum total story torque for the 25% eccentric model decreases with the increase in PGA.

It must be noted that small shear force of wall B compared with that of wall G for 25% eccentricity, is another reason for the smaller contribution of the walls in resisting total story torque, compared with the 5% eccentric model. This can be specifically observed in Figure 5.75. In this figure the maximum torque resisted by the walls for the 25% eccentric model, subjected to Taft-60, is slightly smaller than that for the 5% eccentric model at the first story. When the torque resisted by the shear walls reaches its maximum value, the shear force of wall G are 981

and 378 kips for 25% and for 5% eccentricities, respectively, whereas shear forces of wall B are 57 and 636 kips for 25% and for 5% eccentricities. Although the shear force of wall G at its base for 25% eccentricity is more than 2.5 times larger than that for the 5% eccentricity, the shear force of wall B for 5% eccentricity is about 11 times larger than that for 25% eccentricity. Therefore the maximum torque resisted by the walls for the 25% eccentric model, subjected to Taft-60, is smaller than that for the 5% eccentric model, at the first story.

From these results it can be concluded that a major part of the total story torque of the model is resisted by the shear walls. Therefore variation of total story torque with initial eccentricity and PGA can be explained by the values of the shear forces of the walls. Shear forces of the walls, as discussed earlier, are larger at lower stories, and therefore total story torque is larger at lower stories, as illustrated in Figures 5.33 and 5.34. On the other hand the shear forces of wall G increase with the increase in initial eccentricity, therefore the total story torque of the model increases with the increase in initial eccentricity, as shown in Figure 5.34. It must be noted, however, that this increase is not in direct proportion to the increase in eccentricity ratio (e/D).

From Table 5.28 it can be concluded that shear walls in dual systems with small eccentricity ratio (e/D=0.05) resist the major part of the total story torque. Therefore shear walls may be designed to resist the total story torque, for preliminary design. However, design of the walls according to this concept can be quite conservative when the initial static eccentricity ratio (e/D) and intensity of the ground motion (PGA) are large (e/D=0.25 and Taft-60).

The values of dynamic amplification of eccentricity, defined by equation 5.8, are presented in Table 5.27. It is clearly shown in Table 5.27 and Figure 5.76 that the larger the static eccentricity, the smaller the dynamic amplification of eccentricity. The dynamic amplification of eccentricity for the 5% eccentric model, subjected to Taft-18, Taft-40, and Taft-60, is, on average, 2.06, 2.83, and 2.63, respectively, while these values for 25% eccentricity are less than or equal to unity. Variations of dynamic amplification of eccentricity against PGA for different values of initial eccentricity are shown in Figure 5.76. It can be observed from this figure that for 5% eccentricity

the eccentricity amplification due to Taft-40 is larger than that due to Taft-18, because the maximum total torque due to Taft-18 is smaller. This value due to Taft-40 is also larger than that due to Taft-60, because the maximum total story shear due to Taft-60 is larger.

Values of linear-elastic dynamic amplification of eccentricity are also shown in Figure 5.76. These values are compared with nonlinear dynamic amplification of eccentricity in Table 5.29. It is obvious that linear-elastic dynamic amplification of eccentricity does not vary with the change of PGA, therefore it attains the same value for Taft-18, Taft-40, and Taft-60. From Figure 5.76 and Table 5.29, it can be observed that for 25% eccentricity the values of nonlinear dynamic amplification of eccentricity are smaller than the linear-elastic ones at the first four stories, and for 5% eccentricity the values of nonlinear dynamic amplification of eccentricity at the first story are smaller than the linear-elastic ones. However, Figures 5.48 and 5.49 indicate that for 25% eccentricity, values of maximum nonlinear displacements due to Taft-40 and Taft-60 are larger than the linear-elastic ones at the first five stories. Similarly for 5% eccentricity, values of maximum nonlinear displacements due to Taft-40 at the first two stories, and those due to Taft-60 at the first four stories, are larger than their corresponding linear-elastic ones. These results, which clearly contradict what is expected from the comparison of values of linear and nonlinear dynamic amplification of eccentricity, show that the dynamic amplification of eccentricity, as defined by equation 5.8, is not a good index to measure the effects of torsion on the nonlinear seismic response of structures.

5.5 Resistance Eccentricity

5.5.1 Introduction

In the following sections the effect of yielding resistance eccentricity on the seismic response of the structure is studied. Resistance eccentricity (or strength eccentricity) results from unsymmetrical distribution of yielding strength of lateral load resisting elements in the plan of the structure. Therefore, the presence of this eccentricity has no effect on the response of the structure in the linear-elastic range. However, the nonlinear response of the structure can be affected significantly by introducing resistance eccentricity in the structure. The designer, in order

to reduce torsional effects, may increase yielding strength of some lateral load resisting elements (wall G) in comparison with others (wall B) such that the center of resistance (CR) comes as close as possible to the center of mass (CM) as shown in Figure 5.1. Note that if it is desirable to keep symmetry of stiffness, the logical approach would be to design the yielding resistance of the walls such that CR and CM coincide. This seems to be a good way to reduce the effects of torsion on the seismic response of the structure. To assess this design methodology, and to evaluate the effects of resistance eccentricity on the torsional response of structures, two cases are considered in the following sections.

In the first case the structure is assumed to have 5% static eccentricity and 4% resistance eccentricity (referred to as resistance/mass eccentric structure hereinafter). The response of this structure to the Taft ground motion is compared with that of the structure with 5% static eccentricity (referred to as corresponding mass eccentric structure hereinafter). In the second case the static and resistance eccentricities are assumed to be 25% and 11%, respectively. The seismic response of this structure is compared with that of the structure with 25% static eccentricity. The values of resistance eccentricity in these cases have been chosen such that walls B and G do not yield under the UBC lateral loads in the following cases:

1. When static eccentricity is zero.
2. When static eccentricity is 5% of the maximum dimension of the building plan (resulting in 4% resistance eccentricity).
3. When static eccentricity is 25% of the maximum dimension of the building plan (resulting in 11% resistance eccentricity).

The first constraint simply satisfies the building code requirement that torsion shall not be included where its inclusion results in lower stresses in the member under investigation. To satisfy the second and the third constraints it is necessary to increase the yielding strength of wall G by about 29% and 101%, respectively. To compensate for the increase in the yielding strength of the structure (due to the second and the third constraints), Taft-60 ground motion is utilized in the following studies. It is important to note that, the value of resistance eccentricity, as shown in Figure 5.1, is

measured from the geometric centroid of the structure. Therefore the value of resistance eccentricity of a system with symmetrical distribution of yielding strength of the lateral load resisting elements in the plan, is zero and the center of resistance in this system coincides with the geometric centroid of the structure.

5.5.2 Displacements

Envelopes of lateral displacements of walls B and G along the height of the structure due to Taft-60, are presented in Table 5.30. In this table maximum values of displacements of walls B and G in the resistance/mass eccentric case are compared with those of the concentric case and the mass eccentric case. These values are illustrated in Figures 5.77 and 5.78. It can be observed from these figures that introducing resistance eccentricity, with the same sign as mass eccentricity, in the structure will not change the maximum response of the system qualitatively. However, as it was expected the maximum displacements of walls B and G are decreased to smaller values. The maximum displacements of wall G for the 4% resistance eccentric case are, on average, 11% smaller than those in the corresponding 5% mass eccentric case, and the maximum displacements of wall G for the 11% resistance eccentric case are, on average, 14% smaller than those in the corresponding 25% mass eccentric case.

The linear-elastic and nonlinear values of maximum displacement of wall G due to Taft-60 are shown in Figure 5.79 and listed in Table 5.31. In this figure, displacements for the 5% and 25% mass eccentric linear-elastic cases, the nonlinear 4% and 11% resistance/mass eccentric cases, and their corresponding 5% and 25% mass eccentric cases are compared. From the results presented in Table 5.31, it can be observed that the maximum displacement for the resistance/mass eccentric case at lower floors is still larger than the linear-elastic displacement. For 4% resistance eccentricity the nonlinear displacement of the second floor due to Taft-60 is 48% larger than its linear-elastic displacement. When static eccentricity increases to 25% and the resistance eccentricity is 11% the nonlinear displacement of the second floor due to Taft-60 is 60% larger than its linear-elastic displacement. The results of Table 5.31 show how a linear-elastic dynamic analysis can underestimate the real nonlinear response of the structure. From the values of Table

5.30 it can be concluded that introducing resistance eccentricity, with the same sign as mass eccentricity, in a building that is already mass eccentric, will reduce the torsional effects on the nonlinear seismic response of the structure.

5.5.3 Inter-Story Drift Indices

Envelopes of inter-story drift indices (IDI) of walls B and G along the height of the structure due to Taft-60, are presented in Table 5.32. In this table maximum values of IDI of walls B and G in the resistance/mass eccentric case are compared with those for the concentric case and the mass eccentric case. These values are illustrated in Figures 5.80 and 5.81, which show that introducing resistance eccentricity, with the same sign as mass eccentricity, in the structure will not change the maximum response of the system qualitatively. However, as was expected the maximum IDI of walls B and G reduce to smaller values at the lower stories. Note that the values of IDI for the resistance/mass eccentric cases are practically the same as those for the corresponding mass eccentric cases at upper stories. This is due to the fact that shear walls do not show any nonlinear behavior at upper stories, therefore the presence of resistance eccentricity at these levels cannot play an important role in modifying the response of the structure at these stories. As can be observed from Table 5.32, the value of maximum IDI of wall G at the first story for the 4% resistance eccentric case is 17% smaller than that in the corresponding 5% mass eccentric structure. The value of maximum IDI of wall G at the first story for the 11% resistance eccentric case is 31% smaller than that in the corresponding 25% mass eccentric structure.

The linear-elastic and nonlinear values of maximum IDI of wall G due to Taft-60 are shown in Figure 5.82 and listed in Table 5.33. In this figure, the IDI of the 5% and 25% mass eccentric linear-elastic cases, the 4% and 11% nonlinear resistance/mass eccentric cases, and their corresponding 5% and 25% mass eccentric cases are compared. From Table 5.33, it can be observed that the maximum IDI of the resistance/mass eccentric case at the lower floors are still larger than the linear-elastic IDI. For 4% resistance eccentricity the nonlinear IDI of the first story due to Taft-60 is 48% larger than its linear-elastic IDI. When static eccentricity increases to 25% and the resistance eccentricity is 11% the nonlinear IDI of the first story due to Taft-60 is 60% larger than

its linear-elastic IDI. These results show that a linear-elastic dynamic analysis can underestimate the real nonlinear response of the structure. They also indicate that introducing resistance eccentricity, with the same sign as mass eccentricity, in an already mass eccentric system, will reduce the torsional effects on the nonlinear seismic response of the structure.

5.5.4 Plastic Hinge Rotations

The maximum values of plastic hinge rotation at the bases of walls B and G during the first two seconds of the response of the model to Taft-60 are listed in Table 5.34. In this table the resistance/mass eccentric case is compared with the mass eccentric case and the concentric case. It can be observed from this table that introducing resistance eccentricity, with the same sign as mass eccentricity, reduces the plastic rotation at the base of the walls. This reduction is particularly pronounced for the case that static eccentricity is 25% and resistance eccentricity is 11%. In this case the maximum value of plastic rotation at the base of wall G is about 0.0057 radian, which is 46% smaller than the 0.0106 radian of plastic rotation in the corresponding 25% mass eccentric system, whereas for 4% resistance eccentricity plastic rotation at the base of wall G is about 0.0041 radian, which is 27% smaller than the 0.0056 radian of plastic rotation in the corresponding 5% mass eccentric system.

It was mentioned earlier that the maximum plastic hinge rotation at the base of wall G for 25% static eccentricity due to Taft-60 is somewhat larger (about 6%) than its capacity. This indicates the failure of wall G in this case. However, introducing resistance eccentricity, with the same sign as the mass eccentricity, in the system not only reduced the values of plastic hinge rotation of walls, but it also prevented failure of wall G. These results clearly indicate that in order to reduce the effects of torsion, the designer must intelligently distribute the yielding strength in the structure so that the center of resistance and the center of mass of the structure come as close as possible.

5.6 Summary and Conclusions

In this chapter non-uniform distribution of mass (static eccentricity), and unsymmetrical yielding strength distribution (resistance eccentricity) in the plan of the structure were assumed

to be the sources of lateral-torsional coupling in the seven-story reinforced concrete frame-wall structure. The different levels of intensity, used in the analyses, were identified by the increased peak ground acceleration, PGA, values 0.18g, 0.40g, and 0.60g of the record.

The nonlinear responses of the concentric, mass eccentric, and resistance/mass eccentric structures to the above intensity levels were compared. The conventional earthquake resistant design of structures is based on the total story shear forces, but this study clearly showed that the total story shears did not constitute a reliable index for identifying the maximum nonlinear response of the structure. In the studies presented in this chapter, where period of the structure and the uncoupled frequency ratio (UFR) were fixed values, it was shown that the initial static eccentricity, resistance eccentricity, yielding strength of the whole structure, and torsional redundancy were four important parameters, by which the effects of torsion on the seismic response of the structure could be controlled. The following are the main conclusions that can be drawn from these studies:

1. Linear-elastic dynamic analyses underestimate the nonlinear dynamic response of the structure. The seven-story reinforced concrete frame-wall structure was assumed to have a uniform 5% static eccentricity ratio (e/D) over the height. The nonlinear response of this structure to the Taft-40 and Taft-60 ground motions produced maximum lateral displacements at the second floor that were 40% and 80%, respectively, larger than those predicted by linear-elastic analyses. When the static eccentricity was increased to 25% of the maximum building plan dimension, these displacements increased to a level 92% and 134%, respectively, larger than those predicted by linear-elastic analyses.
2. The maximum response values of the structure with large static eccentricity ratio (e/D = 0.25) are significantly affected by the torsional motion of the structure, as well as by its translational motion.
3. The plastic rotation demand at the bases of the walls for the structure with 25% static eccentricity, subjected to Taft-60, exceeds its plastic rotation capacity by about 6%. However, these values for the structure with 5% static eccentricity and the concentric

structure are 44% and 62%, respectively, smaller than the plastic rotation capacity at the bases of the walls. Therefore to avoid significant torsional effects on the response of structures, the amount of static eccentricity has to be restricted.

4. Torsional effects on the maximum displacements, inter-story drift indices, shear forces of the walls, and plastic rotation at the bases of the walls can be significantly reduced by increasing the yielding strength of the structure. Decreasing the intensity level (which can be interpreted as increasing the yielding strength of the structure) from Taft-60 by factors of 1.5 and 3.3 will decrease the maximum plastic rotation demand at the bases of the walls by factors of 2 and 11, respectively. Therefore to prevent significantly large torsional response in the structure, excessively large reduction of yielding strength compared with linear-elastic strength demands has to be avoided.
5. The maximum values of displacements, inter-story drift indices, plastic rotations at the bases of walls, and story torque increase with increase in static eccentricity and peak ground acceleration (PGA). The increases of these parameters are monotonic (but not proportional) functions of the intensity level.
6. The maximum values of total story torque, which are limited by the value of yielding strength of the structure (mainly yielding strength of the shear walls in this study), do not increase in direct proportion to static eccentricity ratio (e/D). Consequently, values of dynamic amplification of eccentricity, which are not good factors in identifying maximum displacement of the structure, are not suitable indices to measure the effects of torsion on the seismic nonlinear response of the structure. Amplifications of displacement and inter-story drift index, rather than the amplification of eccentricity, are more reliable indices in identifying torsional effects, when nonlinear response of structures is of interest.
7. The nonlinear seismic response of the seven-story structure with a uniform mass eccentricity over the height, produced a maximum value of total story shear that was smaller than that of the corresponding concentric case. Maximum values of total shear forces in the mass eccentric structures decreased with the increase in the initial static eccentricity

and decrease in the peak ground acceleration (PGA). Moreover, total base shear did not constitute a reliable index for identifying the largest displacement in the structure. Therefore, this parameter cannot be used to measure torsional effects.

8. Maximum values of displacements, inter-story drift indices, and shear forces of wall G and B increase and decrease, respectively, with the increase in initial static eccentricity. These response parameters increase with the increase in peak ground acceleration (PGA) but not proportionally.

9. The use of multi-story buildings with a dual structural system (frame-wall) allowed significant redistribution of the lateral inertia forces after the first yielding of the most critically excited wall. The yielding of the first story of the wall led to change in the lateral deformation pattern and this resulted in a different distribution of the lateral forces along the height of the walls and frames as well as different horizontal distribution at each floor level. All this resulted in some significant increase in the story shear that the critical wall could resist.

10. The seven-story structure was assumed to have a uniform eccentricity between the center of mass (CM) and the center of stiffness (CS) over the height. If it is desired to keep the stiffness distribution of the structure unchanged, the logical approach to reduce the effects of torsion on the seismic response of the structure is to design the yielding strength of the walls such that the center of resistance (CR) coincides with the center of mass.

11. Effects of torsion on the seismic response of a structure with static eccentricity may be reduced by introducing resistance eccentricity, with the same sign as mass eccentricity, in the structure. This reduction is most pronounced at story levels, where most of the nonlinear behavior is concentrated. In the case of the seven-story frame-wall structure studied here, the major part of the nonlinear behavior was concentrated at the bases of the walls, therefore values of displacements and inter-story drift indices at the first story level were particularly reduced by introducing resistance eccentricity properly.

12. The amount of acceptable initial static eccentricity should be restricted, if torsional regulations of present building codes are used. In cases where nonlinear behavior of the structure is inevitable, the importance of torsional redundancy and resistance eccentricity on the lateral-torsional response must be taken into account by the building codes. They must lead designers to distribute, intelligently, the largest possible number of lateral load resisting structural elements and to select their yielding strength such that the center of resistance comes as close as possible to the center of mass of the structure at each floor. Moreover, to avoid large torsional response in structures, building codes should not prescribe excessively large reduction of yielding strength, compared with the linear-elastic strength demands.

CHAPTER SIX

SUMMARY, CONCLUSIONS AND RECOMMENDATIONS

6.1 Summary

The real response of a structure to ground motion excitations is, in general, affected by a combination of lateral translational vibration and torsional rotational oscillation of the system. These motions may be coupled due to several sources such as presence of static eccentricity (due to unsymmetrical distribution of mass and/or stiffness in the plan), and/or accidental eccentricity (due to unforeseen factors such as non-uniform ground motion along the foundation of structures, presence of torsional components in ground motions, workmanship, detailing of the structural components as well as the nonstructural elements). Although the effects of torsion due to static eccentricity on the linear-elastic seismic response of structures have been the subject of many studies, there have been few studies regarding nonlinear torsion.

The linear-elastic response of single-story structures depends on eccentricity ratio (e/r), uncoupled translational frequency (ω_y), ratio of uncoupled torsional frequency to uncoupled translational frequency (uncoupled frequency ratio, UFR), and damping (ξ). When nonlinear inelastic lateral-torsional behavior of structures is of interest, factors such as locations and force-deformation relations of the resisting elements, and torsional redundancy in the structure, which have no influence on the linear-elastic response of the system, become very important. Moreover, unsymmetrical distribution of yielding strength of lateral load resisting elements in the plan of a structure is quite possible, and therefore to study nonlinear torsion it is necessary to account for resistance eccentricity (as a measure of unsymmetrical distribution of yielding strength) in addition to static and accidental eccentricities. Consequently, much more detailed information is necessary to conduct a nonlinear analysis, compared with a linear-elastic analysis, and this has limited the number of studies on nonlinear torsion. In almost all the previous studies on linear-elastic torsion and nonlinear inelastic torsion, a typical single-story system was used, and

most of the linear-elastic analyses were performed by using idealized response spectra techniques. In this research the effects of torsion on the linear-elastic and nonlinear seismic responses of multi-story structures were studied.

An important issue, which has not been well appreciated by the seismic building codes, is torsional redundancy in buildings. When only linear-elastic behavior of structures is considered or is of interest, the importance of providing a high degree of torsional redundancy to the structure is not evident. However, most buildings undergo inelastic torsional behavior in the case of extreme, or even moderate, earthquake ground motions. As soon as one of the lateral load resisting elements yields, there is a change in the location of the center of stiffness and this change can induce a significant change in the static eccentricity and therefore in the dynamic eccentricity. This usually results in an increase in torsional rotation of the structure and therefore can lead to serious damage in the members of the structure or even collapse of the building. In these cases, where inelastic torsional behavior of the structure is inevitable, it is important to provide as many lines of defense as possible in the structure to avoid a large increase in eccentricity between the centers of mass and stiffness and, as a result, to prevent partial or complete failure of the building due to large torsional rotations.

A review of the literature, regarding both linear-elastic and nonlinear torsion clearly illustrated that torsional provisions of most building codes are nonconservative and they need to be modified. It was clearly pointed out that a realistic simplified regulation for torsion must account for the effects of e/r, ω_y, UFR, along with torsional redundancy, irregularity, and the other dynamic characteristics of the structure. It was pointed out that opinions differ regarding the importance of different parameters on the inelastic torsional response of structures. A reason for these diverse views is that for inelastic response studies much more detailed specifications of the structural model such as locations and force-deformation characteristics of the resisting elements are needed, as compared with a linear-elastic analysis. This indicates that effects of torsion on the nonlinear seismic response of structures are complex, and are yet to be understood.

Torsional provisions of building codes are based on the results of studies conducted, using an idealized single-story system, hence their applicability to multi-story structures, especially when nonlinear behavior of the system is of interest, is questionable. Therefore, it is very important to understand torsional response of multi-story structures. This study of the seven-story reinforced concrete frame-wall building underlines the differences between a linear-elastic static analysis (as is prescribed by the building codes), and a linear-elastic dynamic analysis in evaluating torsional response of multi-story systems.

The effects of lateral load distribution profile on the torsional response of the structure were assessed for two different static lateral load distributions, with triangular and uniform profiles. The total applied base shear for each profile was equal to the value that results from application of the force required by UBC as the minimum total lateral seismic force. In the dynamic analyses, the three-dimensional linear-elastic response of the structure to the N21E component of 1952 Kern County, Taft Lincoln School Tunnel earthquake record was investigated by a time-history approach. For both static and dynamic analyses two different static eccentricity were considered.

The results of these studies indicate that a linear-elastic static analysis underestimates the linear-elastic dynamic torsional response of structures. When the static eccentricity was 5% the values of maximum displacement of the structure, bending moment at the base of walls, and shear force of walls were underestimated by more than 61%, 47%, and 39%, respectively, by the static analysis. When static eccentricity was increased to 10% these response parameters were underestimated by more than 63%, 52%, and 49%, respectively, indicating that the underestimation of the response by static analyses increases monotonically, but not proportionally, with increase in static eccentricity. It was also recognized that, for preliminary design, the value of dynamic amplification of eccentricity for a linear-elastic multi-story structure may be approximated by the dynamic amplification of eccentricity computed from an idealized linear-elastic single-story system with the same values of eccentricity ratio (e/D) and uncoupled frequency ratio (UFR) as those of the multi-story structure (see Figure 2.7), using idealized flat or hyperbolic pseudo acceleration spectra to characterize the earthquake ground motion.

It is well recognized that in the case of extreme, or even moderate, earthquake ground motion excitations most buildings will undergo inelastic behavior. However, the fact that because of this inelastic behavior the torsional responses of the structure can be significantly higher than those predicted on the basis of linear-elastic analyses, is not very well appreciated. Almost all of the previous studies on the inelastic seismic responses of eccentric structures examined the torsional responses of idealized single-story systems. In order to understand the lateral-torsional response of real buildings to seismic excitations, it is important to investigate the effects of torsion on the nonlinear response of multi-story structures. However, three-dimensional nonlinear static and dynamic analyses of a structure are not standard procedures, and the solution algorithms are problem dependent.

Nonlinear computer programs are not usually ready-to-use, and modification or correction or both of their source code is usually needed. This means that, unlike a linear-elastic analysis, a given algorithm may work effectively for one type of nonlinearity, but not for other types. Besides, nonlinear analyses are much slower and more elaborate input data need to be provided by the user, therefore the cost for a nonlinear analysis is significantly higher than for a linear-elastic one. These problems become more serious when a multi-story structure is under investigation. Nonetheless, nonlinearity in structures can be localized intelligently, depending on the type of structure, so that the best simulation of the real response can be achieved.

The computer program FACTS [34] and its nonlinear three-dimensional reinforced concrete beam column element were used to study the nonlinear static responses of the real structure (of Figure 3.1) to two sets of monotonically increasing lateral loads, with triangular and uniform profiles. Based on these results a realistic model of the seven-story structure, which represents typical frame-wall systems, was developed. It was shown that total strength of the structure (at incipient collapse) under triangular and uniform lateral load were 2241 kips and 2773 kips, respectively. These values were about 26.5% and 32.8%, respectively, of the total reactive weight of the structure (8462.1 kips), while the UBC strength demand was about 13% of the total reactive weight.

In the study of three-dimensional nonlinear seismic response of the model it was assumed that non-uniform distribution of mass (mass eccentricity), and unsymmetrical distribution of yielding strength (resistance eccentricity) in the plan of the structure were the sources of lateral-torsional coupling in the structure. Three different levels of intensity of ground motion and five different eccentricities (mass and strength eccentricities) were considered.

It was pointed out that to introduce 4% resistance eccentricity in the model it was necessary to increase the yielding strength of wall G by about 29%, whereas for 11% resistance eccentricity the yielding strength of wall G was increased by 101%. It was shown that, if it is desired to keep the stiffness distribution in the structure unchanged, effects of torsion on the seismic response of the structure can be reduced by proper distribution of yielding strength of major lateral load resisting elements in the plan. The ideal solution to this type of problem is to locate the center of resistance on the center of mass. In all these studies comparisons were made between the linear-elastic and nonlinear responses in order to provide a better understanding of the differences between the two cases.

6.2 Conclusions

The main conclusions, regarding the effects of torsion on the seismic response of structures, are presented here. These conclusions, strictly speaking, are only valid for the structure and the model described in this research and for the types of earthquake excitation used to analyze them.

1. A linear-elastic static analysis cannot provide a reliable estimate of torsional effects on the linear-elastic dynamic responses of structures, no matter what static lateral load profile is selected, unless proper amplification of eccentricity is considered in the static analysis. The linear-elastic dynamic response of the seven-story building to the Taft earthquake ground motion, with 5% and 10% uniform static eccentricity ratios (e/D) over the height, produced maximum inter-story drift indices that were underestimated, by more than 62% and 63%, respectively, by linear-elastic static analyses (using no amplification of eccentricity). Note that this underestimation is not in direct proportion to the increase in static eccentricity. For a linear-elastic multi-story building, where distributions of mass

and stiffness do not vary from story to story, the amplification of eccentricity may be approximated, for preliminary design, by that obtained from analyzing an idealized linear-elastic single-story system, having the same values of static eccentricity ratio (e/D), and uncoupled torsional to translational frequency ratio (UFR) as the original building, using idealized flat or hyperbolic pseudo acceleration spectra to characterize the earthquake ground motion.

2. Linear-elastic dynamic analyses, may significantly underestimate effects of torsion on the nonlinear inelastic dynamic response of structures. The nonlinear response of the seven-story building, with 5% uniform static eccentricity ratio (e/D) over the height, to the Taft-40 and Taft-60 ground motions produced maximum lateral displacements at the second floor that were 40% and 80%, respectively, larger than those predicted by linear-elastic analyses. When the static eccentricity was increased to 25% of the maximum building plan dimension, these displacements increased to 92% and 134%, respectively, larger than those predicted by linear-elastic analyses. Since most buildings undergo nonlinear behavior in the case of extreme, or even moderate, earthquake ground motions, and in order to understand the true behavior of a structure, it is important to pay more attention to nonlinear inelastic analysis of a structure.

3. Maximum values of response of the structure with large static eccentricity ratio (e/D=25%) are significantly affected by the torsional motion of the structure, as well as by its translational motion. Maximum values of displacements, inter-story-drift indices, shear forces carried by lateral load resisting elements, and plastic rotations at the bases of walls increase with the increase in static eccentricity ratio and intensity of the ground motion excitation. This increase is a monotonic, but not proportional, function of intensity level.

4. Yielding strength of lateral load resisting elements can be wisely distributed unsymmetrically in the plan of an eccentric (with static eccentricity) structure to reduce the torsional effects. This reduction is most pronounced at the stories where most of the nonlinearity is concentrated. If it is desired to keep the stiffness distribution of the structure

unchanged, seismic torsional responses of structures can be effectively controlled by proper design of yielding strength of major lateral load resisting elements such that the center of resistance (strength) comes as close as possible to the center of mass.

5. Yielding strength of the whole structure is an important factor in controlling torsional behavior of a structure. Effects of torsion on the maximum values of displacements, inter-story drift indices, shear forces carried by lateral load resisting elements, and their plastic rotations can be significantly reduced by increasing the yielding strength of the whole structure.

6. Most of the seismic building codes, in their simplified regulations for torsional effects, underestimate the linear-elastic dynamic torsional response of a structure. They are also nonconservative when nonlinear behavior of structures is of interest. Therefore there is a need to improve the codes.

6(a) The concept of dynamic eccentricity may be used to estimate the linear-elastic response of building structures for preliminary design. However, the value of dynamic eccentricity prescribed by UBC is nonconservative, especially for small values of static eccentricity ratio. Including the accidental eccentricity, prescribed by UBC, in the design eccentricity cannot compensate for the nonconservative torsional regulations of UBC in estimating dynamic eccentricity, although it reduces the value of amplification of eccentricity. Dynamic amplification of eccentricity for a linear-elastic multi-story structure may be approximated, for preliminary design, by that obtained from analyzing an idealized linear-elastic single-story system with the same values of eccentricity ratio (e/D) and uncoupled frequency ratio (UFR) as those of the multi-story structure (see Figure 2.7), using idealized flat or hyperbolic pseudo acceleration spectra to characterize the earthquake ground motion. It must be noted that the concept of dynamic eccentricity, which has been developed for single-story systems, may not be used to estimate the linear-elastic response

of multi-story buildings, when distributions of mass and/or stiffness of the lateral load resisting elements in the plan of the structure vary from story to story. In such cases a dynamic analysis must be performed.

6(b) Total story torque and total story shear forces in a nonlinear structure are insensitive to the value of initial static eccentricity. Moreover, dynamic eccentricity is not a good index in identifying the maximum displacement of a structure. Therefore they are not good indices to measure nonlinear torsional response of a structure. For preliminary design, dynamic amplification of total displacements and inter-story drift indices are more reliable indices to estimate torsional effects for the cases where nonlinear behavior of the structure is of interest. Note that a three-dimensional nonlinear dynamic analysis should be performed for the final design.

6(c) In both linear-elastic and nonlinear inelastic ranges the amount of acceptable initial static eccentricity should be restricted if the torsional regulations of present building codes are used. It is recommended that maximum static eccentricity be limited to 20% of the maximum building plan dimension.

6(d) In cases where nonlinear behavior of structures is inevitable, the importance of torsional redundancy and resistance eccentricity on the lateral-torsional response must be taken into account by the building codes. They must lead designers to distribute, intelligently, the largest possible number of lateral load resisting structural elements and to select their yielding strengths such that the center of resistance comes as close as possible to the center of mass of the structure at each floor.

6(e) In order to avoid large torsional response in structures, building codes should not prescribe an excessively large reduction of the yielding strength compared with the linear-elastic strength demands.

7. The use of multi-story buildings with a dual structural system (frame-wall) allowed significant redistribution of the lateral inertia forces after the first yielding of the most critically excited wall. The yielding of the first story of the wall led to a change in the

lateral deformation pattern and this resulted in a different distribution of the lateral forces along the height of the walls and frames, as well as a different horizontal distribution at each floor level. All this resulted in some significant increase in the story shear that the critical wall could resist.

8. Three-dimensional nonlinear static and dynamic analyses of structures are, in general, very costly and in some cases, because of the size of the structure, are impractical. However, in some cases, it is possible to take advantage of the actual behavior of the system, and to localize nonlinearity in the structure. This will, in effect, reduce the cost of nonlinear analyses, without losing generality. The reinforced concrete frame-wall system in the structure studied in this research, is a system with special properties that allow localization of nonlinearity. Systems of this type can be effectively modeled for nonlinear analyses so that the computer cost decreases to a reasonable level. Therefore as long as present computer technology is used, the selection of systems that can be efficiently analyzed by nonlinear computer programs is of great importance.

6.3 Recommendations for Future Studies

Most of the previous researches have focussed on the torsional response of an idealized single-story system, and only some of them considered nonlinear behavior of structures. This research, to the best knowledge of the authors, is the first to study the effects of torsion on the linear-elastic and nonlinear seismic responses of multi-story structures. Because of the complexity of the problem of torsion, especially when dealing with multi-story structures, it has not been possible to consider the effects of all the parameters, pertinent to the problem of torsion, in this study. Therefore it is necessary to conduct further rigorous and comprehensive studies. Some recommendations for future research regarding the effects of torsion on the seismic response of structures, follow:

1. Although it is recognized that torsional redundancy is an important issue in earthquake resistant design of structures, its effects on the nonlinear torsional response of dual systems have not been thoroughly studied yet. Building codes have not considered this issue in

their current seismic regulations for torsion. Therefore it is necessary to investigate the effects of torsional redundancy on the nonlinear response of structures and to suggest the minimum lines of defense in a torsionally coupled system.

2. In multi-story structures, it is quite possible that centers of mass of different floors do not lie on a vertical line. Similarly, distributions of stiffness and yielding strength of the lateral load resisting elements, in the plan of the structure, may vary from story to story. These possibilities, along with other irregularity features, were not considered in this research and they need to be addressed in future studies.

3. Nonlinear responses of structures are model dependent. Therefore the findings of this research, which studied the torsional response of a multi-story frame-wall building, may not be applicable to a ductile moment resisting space frame or some other structural system. Similarly, the response of a structure to an earthquake ground motion may be quite different if another type of ground motion excitation is selected. Therefore it is important to study the effects of torsion on the seismic response of different types of structures, and to reflect the effects of different types of ground motions on the torsional response of structures, in future investigations.

4. In order to obtain a better understanding of the effects of various parameters such as static and resistance eccentricity ratios, uncoupled translational frequency, and ratio of uncoupled torsional frequency to translational frequency, on the torsional response of structures, it is necessary to extend the parametric studies conducted in this investigation, to systems with different values of the parameters.

5. More studies are needed for to improve the torsional regulations of the building codes. For linear-elastic structures, the value of dynamic eccentricity can be approximated using bilinear relation with static eccentricity, rather than a linear relation. In a more direct way an idealized single-story system may be used to estimate the value of dynamic eccentricity. For nonlinear inelastic structures more reliable indices, such as amplifications of displacements and inter-story drift index, have to be substituted for dynamic eccentricity.

Moreover, a lower bound has to be established for the value of resistance eccentricity, relative to static eccentricity, so that it leads the designer to distribute the yielding strength of resisting elements in the plan of the structure so that the centers of mass and resistance are as close as possible.

6. In order to assess the validity of mathematical models, used in studies of linear-elastic torsion and nonlinear inelastic torsion, it is necessary to correlate the analytical evaluations and experimental studies of the torsional response of structures.

REFERENCES

REFERENCES

[1]. C.L. Kan and A.K. Chopra, "Coupled Lateral Torsional Response Of Buildings To Ground Shaking", Report No. UCB/EERC-76/13, Earthquake Engineering Research Center, University Of California, Berkeley May 1976.

[2]. C.L. Kan and A.K. Chopra, "Effects Of Torsional Coupling On Earthquake Forces In Buildings", Journal Of The Structural Division, Vol. 103, No. ST4 April 1977, pp. 805-819.

[3]. C.L. Kan and A.K. Chopra, "Elastic Earthquake Analysis Of A Class Of Torsionally Coupled Buildings", Journal Of The Structural Division, Vol. 103, No. ST4 April 1977, pp. 821-838.

[4]. C.L. Kan and A.K. Chopra, "Linear And Non-linear Earthquake Responses Of Simple Torsionally Coupled Systems", Earthquake Engineering Research Center, Report No. UCB/EERC-79/03, University Of California, Berkeley, 1979.

[5]. W.K. Tso and Dempsey, "Seismic Torsional Provisions For Dynamic Eccentricity", Earthquake Engineering And Structural Dynamics, Vol. 8, pp. 275-289 (1980).

[6]. C.L. Kan and A.K. Chopra, "Torsional Coupling And Earthquake Response Of Simple Elastic And Inelastic Systems", Journal Of Structural Division, Proceedings Of American Society Of Civil Engineers, Vol. 107, No. ST8, August,1981.

[7]. A.M. Chandler and G.L. Hutchinson, "Torsional Coupling Effects In The Earthquake Response Of Asymmetric Buildings", Engineering Structure, Vol. 8, October 1986, Butterworth & Co. Ltd., pp. 222-236.

[8]. A.M. Chandler and G.L. Hutchinson, "Evaluation Of Code Torsional Provisions By A Time-History Approach", Earthquake Engineering And Structural Dynamics, Vol. 15, pp. 491-516, 1987.

[9]. R. Hejal and A.K. Chopra, "Earthquake Response Of Torsionally-Coupled Buildings", Report No. UCB/EERC-87/20, Earthquake Engineering Research Center, University Of California, Berkeley 1987.

[10]. W.K. Tso and A.W. Sadek, "Inelastic Seismic Response Of Simple Eccentric Structures", Earthquake Engineering And Structural Dynamic, Vol. 13, pp. 255-269 (1985).

[11]. Y. Bozorgnia and W.K. Tso, "Inelastic Earthquake Response Of Asymmetric Structures", Journal Of Structural Engineering, Vol. 112, No. 2, February, 1986.

[12]. W.K. Tso and Y. Bozorgnia, "Effective Eccentricity For Inelastic Seismic Response Of Buildings", Earthquake Engineering And Structural Dynamics, Vol. 14, pp. 413-427 (1986).

[13]. M. Bruneau and S. Mahin, "Inelastic Seismic Response Of Structures With Mass Or Stiffness Eccentricities In Plan", Report No. UCB/EERC-87/12, Earthquake Engineering Research Center, University Of California, Berkeley 1987.

[14]. L. Esteva, "Earthquake Engineering Research And Practice In Mexico After The 1985 Earthquakes", Bulletin Of The New Zealand National Society For Earthquake Engineering, Vol. 20, No. 3, pp. 159-200, September 1987.

[15]. E.L. Wilson, A. Der Kiureghian and E. Bayo, "A Replacement For The SRSS Method In Seismic Analysis", Earthquake Engineering And Structural Dynamics, Vol. 9, pp. 187-192, 1981.

[16]. Uniform Building Code, 1985 edition.

[17]. Applied Technology Council, "Tentative Provisions For The Development Of Seismic Regulations For Buildings", ATC 3-06, National Bureau Of Standards, U.S. Department Of Commerce, Washington, D.C., 1984.

[18]. E. Rosenblueth, "Seismic Design Requirements In A Mexican 1976 Code", Earthquake Engineering And Structural Dynamics, Vol. 7, pp. 49-61, 1979.

[19]. National Building Code Of Canada, 1985, subsection 4.1.9.1.

[20]. New Zealand Standard NZS 4203: 1976, "Code Of Practice For General Structural Design And Design Loadings For Buildings".

[21]. DIN 4149, "Bauten In Deutschen Erdbebengebieten Entwurf", December 1976.

[22]. Analysis Of Strong Motion Earthquake Accelerograms, Volume III-Response Spectra, EERL 72-80, California Institute Of Technology, Pasadena, California, August 1972.

[23]. E.L. Wilson and H.H. Dovey, "Three-Dimensional Analysis Of Building Systems-TABS", Report No. UCB/EERC-72/08, Earthquake Engineering Research Center, University Of California, Berkeley 1972.

[24]. E.L. Wilson , J.P. Hollings , H.H. Dovey, "ETABS, Three Dimensional Analysis Of The Building Systems (Extended Version)", Report No. UCB/EERC-75/13 , Earthquake Engineering Research Center, University Of California , Berkeley. April 1975.

[25]. U.S.-Japan Planning Group, Cooperative Research Program Utilizing Large-Scale Testing Facilities, "Recommendation For a U.S.-Japan Cooperative Research Program Utilizing Large-Scale Testing Facilities", Report No. UCB/EERC-79/26, Earthquake Engineering Research Center, University of California, Berkeley 1979.

[26]. S. Viwathanatepa, E.P. Popov, and V.V. Bertero, "Seismic Behavior Of Reinforced Concrete Interior Beam-Column Subassemblages", Earthquake Engineering Research Center, Report No. UCB/EERC-79/14, University Of California, Berkeley, June 1979.

[27]. D. Soleimani, E.P. Popov, and V.V. Bertero, "Hysteretic Behavior Of Reinforced Concrete Subassemblages", ACI Journal, Vol. 76, No. 11, Nov. 1979.

[28]. F.A. Charney and V.V. Bertero, "An Evaluation Of The Design And Analytical Seismic Response Of A Seven-Story Reinforced Concrete Frame-Wall Structure", Report No. UCB/EERC-82/08, Earthquake Engineering Research Center, University Of California, Berkeley, 1982.

[29]. S. Moazzami and V.V. Bertero, "Three Dimensional Inelastic Analysis Of Reinforced Concrete Frame-Wall Structures", Report No. UCB/EERC-87/05, Earthquake Engineering Research Center, University Of California, Berkeley, May 1987.

[30]. V.V. Bertero, A.E. Aktan, F.A. Charney, R. Sause, "U.S.-Japan Cooperative Earthquake Research Program : Earthquake Simulation Tests And Associated Studies Of A 1/5th-Scale Model Of A 7-Story Reinforced Concrete Test Structure", Report No. UCB/EERC-84/05, Earthquake Engineering Research Center, University of California , Berkeley, June 1984.

[31]. E.L. Wilson, "The Static Condensation Algorithm", University Of California, Berkeley.

[32]. F.C. Filippou and A. Issa, "Analysis Of Non-linear Response Of Reinforced Concrete Frames To Cyclic Loads Reversals", Report No. UCB/EERC-88/12, Earthquake Engineering Research Center, University Of California, Berkeley, September 1988.

[33]. N.M. Newmark and W.J. Hall, "Earthquake Spectra And Design", Earthquake Engineering Research Institute, 1982.

[34]. FACTS, "Finite-element Analysis of Complex Three-dimensional Systems", Version 87.1, Developed by SSD, Inc., 1930 Shattuck Avenue, Berkeley, California 94704, April 1987.

[35]. P.F. Chen and G.H. Powell, "Generalized Plastic Hinge Concepts For 3D Beam-Column Elements", Report No. UCB/EERC-82/20, Earthquake Engineering Research Center, University Of California, Berkeley, 1982.

[36]. R. Meli, "Evaluation Of Performance Of Concrete Buildings Damaged By The September 19, 1985 Mexico Earthquake", The Mexico Earthquakes 1985-Proceedings Of The International Conference (ASCE), Mexico City, 1986, pp. 308-327.

[37]. D. Mitchell, J. Adams, R.H. DeVall, R.C. Lo, D. Weicert, "Lessons Learned From The 1985 Mexican Earthquake", Canadian Journal Of Civil Engineering, Vol. 13, No. 5, October 1986, pp. 535-557.

[38]. V.V. Bertero, "Observations On Structural Pounding", "The Mexico Earthquakes 1985, Factors Involved And Lessons Learned", Special Meeting, American Society Of Civil Engineers (ASCE), pp.264-278, ISBN 0-87262-579-6.

[39]. Corner Building In Mexico City On Nuevo Leon Street After 1985 Mexico Earthquake (Picture Courtesy Eduardo Miranda).

TABLES

Type of Member	E* (ksi)	A* (Gross) (in^2)	I* (Uncracked) (in^4)	I* (Cracked) (in^4)
Typical Column	3537.0	387.50	12510.0	3424.0
Typical Beam	3537.0	----	14370.0	2711.0
Typical Shear Wall				
Level G-1	3537.0	2170.0	11181680.0	2940000.0
Level 1-2	3537.0	2170.0	11181680.0	2800000.0
Level 2-3	3537.0	2170.0	11181680.0	2650000.0
Level 3-4	3537.0	2170.0	11181680.0	2490000.0
Level 4-5	3537.0	2170.0	11181680.0	2320000.0
Level 5-6	3537.0	2170.0	11181680.0	2150000.0
Level 6-7	3537.0	2170.0	11181680.0	1970000.0

* Note :
E Is Modulus of Elasticity.
A Is Cross Sectional Area.
I Is Cross Sectional Moment of Inertia.

TABLE 3.1 : SECTIONAL PROPERTIES [30]

Location	Width* (in)	Sign	MCR* (k-in)	MY* (k-in)	MU* (k-in)
Support	196.9	-	3855	5146	5831
		+	1010	1300	1900
	118.1	-	2918	3524	3950
		+	953	1106	1595
	59.1	-	1883	2226	2700
		+	874	970	1386
Mid-Span	196.9	-	3916	4104	4755
		+	1049	1705	2421
	118.1	-	2941	2549	2961
		+	989	1540	2125
	59.1	-	1885	1633	2121
		+	908	1380	1921

* Note :
Width Width of Contributing Slab.
MCR Cracking Moment.
MY First Yield Moment.
MU Ultimate Moment.

TABLE 3.2 : FLEXURAL AND SHEAR STRENGTH OF A TYPICAL BEAM [30]

Axial Load (kips)	MCR* (k-in)	MY* (k-in)	MMAX* (k-in)
-250.0	231.25	---	715.0
-125.0	656.25	795.00	1691.25
0.0	1077.50	1768.75	2625.00
50.0	1240.00	2136.25	2875.00
100.0	1406.25	2446.25	3141.25
150.0	1567.50	2750.00	3500.00
200.0	1728.75	3098.75	3812.50
250.0	1887.50	3418.75	4116.25
375.0	2280.00	4165.00	4885.00
500.0	2663.75	4878.75	5400.00
625.0	3033.75	5300.00	5852.50

* Note :
MCR Cracking Moment.
MY First Yield Moment.
MMAX Maximum Moment.

TABLE 3.3 SECTION PROPERTIES OF A TYPICAL COLUMN [30]

Axial Load (kips)	MCR* (k-in)	MY* (k-in)	MMAX* (k-in)
0	82625.0	70125.0	113375.0
250.0	94375.0	93125.0	136250.0
500.0	105875.0	115625.0	159375.0
750.0	117500.0	138375.0	181625.0
1000.0	129000.0	157125.0	203000.0
1250.0	140500.0	178875.0	223125.0
1500.0	151750.0	196625.0	242750.0
2500.0	212500.0	270000.0	318500.0

* Note :
MCR Cracking Moment.
MY First Yield Moment.
MMAX Maximum Moment.

TABLE 3.4 : SECTION PROPERTIES OF A TYPICAL SHEAR WALL [30]

	Floor (psf)	Roof (psf)
5 inches Reinforced Concrete Slab	62.5	62.5
Ceiling And Roofing		16.0
Ceiling and Floor finishes	12.0	
Beams	20.0	20.0
Partitions	20.0	
Miscellaneous	2.0	2.0
Total	116.5	100.50

(a) DEAD LOAD

	Reactive Weight (psf)	Live Load (psf)
Roof	125.0	20.0
Floors 7 To 3	146.0	40.0
Floor 2	150.0	40.0
Total	1005.0	260.0

(b) WEIGHT OF REACTIVE MASS AND LIVE LOAD

TABLE 3.5 : DESIGN LOADS

Mode	Direction*	Period (sec)
1	Y-Translation	0.906
2	X-Translation	0.574
3	Torsional Rotation	0.536
4	Y-Translation	0.293
5	Y-Translation	0.167
6	X-Translation	0.152
7	Torsional Rotation	0.143
8	Y-Translation	0.112
9	Y-Translation	0.083
10	X-Translation	0.074
11	Torsional Rotation	0.070
12	Y-Translation	0.066
13	Y-Translation	0.057
14	X-Translation	0.049
15	Torsional Rotation	0.046
16	X-Translation	0.037
17	Torsional Rotation	0.035
18	X-Translation	0.031
19	Torsional Rotation	0.029
20	X-Translation	0.028
21	Torsional Rotation	0.027

* Note :
X-Translation is translational mode in the direction of walls.
Y-Translation is translational mode perpendicular to the walls.
Torsional Rotation is rotational mode about the center of mass at each floor.

TABLE 3.6 : UNDAMPED NATURAL PERIOD OF THE UNCOUPLED STRUCTURE USING UNCRACKED SECTIONAL PROPERTIES

Story Level	Reactive Weight (kips)	Height (inch)	Triang.* (kips)	Uniform* (kips)
7	1052.50	856.08	247.29	163.56
6	1229.32	738.00	248.99	163.56
5	1229.32	619.92	209.15	163.56
4	1229.32	501.84	169.31	163.56
3	1229.32	383.76	129.48	163.56
2	1229.32	265.68	89.63	163.56
1	1263.00	147.60	51.16	163.56
Total	8462.10	----	1145.00	1145.00

* Note :
Triang. Is Triangular Lateral Load Distribution.
Uniform Is Uniform Lateral Load Distribution.

TABLE 3.7 : REACTIVE WEIGHT AND LATERAL LOAD DISTRIBUTION ALONG THE HEIGHT OF THE STRUCTURE

Floor	1.CCM* (in)	2.ECO* (in)	3.EWG* (in)	4.EWB* (in)	(2)/(1)	(3)/(1)	(4)/(1)
7	0.7722	0.9439	0.8949	0.6495	1.222	1.159	0.841
6	0.6669	0.8155	0.7730	0.5608	1.223	1.159	0.841
5	0.5495	0.6721	0.6370	0.4619	1.223	1.159	0.841
4	0.4244	0.5193	0.4922	0.3567	1.224	1.160	0.840
3	0.2973	0.3639	0.3448	0.2497	1.224	1.160	0.840
2	0.1772	0.2169	0.2056	0.1488	1.224	1.160	0.840
1	0.0761	0.0932	0.0883	0.0639	1.225	1.161	0.839

(a) DUE TO TRIANGULAR LOAD

Floor	1.CCM* (in)	2.ECO* (in)	3.EWG* (in)	4.EWB* (in)	(2)/(1)	(3)/(1)	(4)/(1)
7	0.6083	0.7437	0.7050	0.5117	1.222	1.159	0.841
6	0.5305	0.6488	0.6150	0.4460	1.223	1.159	0.841
5	0.4437	0.5428	0.5145	0.3730	1.223	1.159	0.841
4	0.3500	0.4282	0.4059	0.2941	1.224	1.160	0.840
3	0.2520	0.3085	0.2923	0.2117	1.224	1.160	0.840
2	0.1557	0.1907	0.1807	0.1307	1.225	1.160	0.840
1	0.0702	0.0860	0.0815	0.0589	1.226	1.161	0.839

(b) DUE TO UNIFORM LOAD

* Note :
  - CCM Is Displacement of CM in Concentric.
  - ECO Is Displacement of Corner of Structure for 5% Eccentricity.
  - EWG Is Displacement of Wall G for 5% Eccentricity.
  - EWB Is Displacement of Wall B for 5% Eccentricity.

TABLE 3.8 : LATERAL DISPLACEMENTS OF EACH FLOOR FOR 5% ECCENTRICITY FROM STATIC ANALYSIS

Floor	1.CCM* (in)	2.ECO* (in)	3.EWG* (in)	4.EWB* (in)	(2)/(1)	(3)/(1)	(4)/(1)
7	0.7722	1.1156	1.0175	0.5269	1.445	1.318	0.682
6	0.6669	0.9640	0.8791	0.4547	1.445	1.318	0.682
5	0.5495	0.7947	0.7246	0.3744	1.446	1.319	0.681
4	0.4244	0.6141	0.5599	0.2889	1.447	1.319	0.681
3	0.2973	0.4304	0.3924	0.2022	1.448	1.320	0.680
2	0.1772	0.2567	0.2340	0.1204	1.449	1.321	0.679
1	0.0761	0.1104	0.1006	0.0516	1.450	1.322	0.678

(a) DUE TO TRIANGULAR LOAD

Floor	1.CCM* (in)	2.ECO* (in)	3.EWG* (in)	4.EWB* (in)	(2)/(1)	(3)/(1)	(4)/(1)
7	0.6083	0.8791	0.8017	0.4150	1.445	1.318	0.682
6	0.5305	0.7670	0.6994	0.3616	1.446	1.318	0.682
5	0.4437	0.6419	0.5852	0.3022	1.446	1.319	0.681
4	0.3500	0.5066	0.4618	0.2381	1.447	1.320	0.680
3	0.2520	0.3650	0.3327	0.1713	1.448	1.320	0.680
2	0.1557	0.2257	0.2057	0.1057	1.450	1.321	0.679
1	0.0702	0.1019	0.0928	0.0476	1.451	1.322	0.678

(b) DUE TO UNIFORM LOAD

* Note :
  - CCM Is Displacement of CM in Concentric.
  - ECO Is Displacement of Corner of Structure for 10% Eccentricity.
  - EWG Is Displacement of Wall G for 10% Eccentricity.
  - EWB Is Displacement of Wall B for 10% Eccentricity.

TABLE 3.9 : LATERAL DISPLACEMENTS OF EACH FLOOR FOR 10% ECCENTRICITY FROM STATIC ANALYSIS

Story	1.CCM* (%)	2.ECO* (%)	3.EWG* (%)	4.EWB* (%)	(2)/(1)	(3)/(1)	(4)/(1)
7	0.0891	0.1088	0.1032	0.0751	1.220	1.157	0.843
6	0.0995	0.1215	0.1152	0.0837	1.221	1.158	0.842
5	0.1059	0.1294	0.1227	0.0892	1.221	1.158	0.842
4	0.1077	0.1316	0.1248	0.0905	1.223	1.159	0.841
3	0.1017	0.1244	0.1179	0.0855	1.223	1.160	0.841
2	0.0856	0.1048	0.0993	0.0719	1.224	1.160	0.840
1	0.0516	0.0632	0.0598	0.0433	1.225	1.161	0.839

(a) DUE TO TRIANGULAR LOAD

Story	1.CCM* (%)	2.ECO* (%)	3.EWG* (%)	4.EWB* (%)	(2)/(1)	(3)/(1)	(4)/(1)
7	0.0659	0.0804	0.0762	0.0556	1.219	1.157	0.843
6	0.0735	0.0897	0.0851	0.0619	1.221	1.158	0.842
5	0.0794	0.0970	0.0920	0.0668	1.222	1.158	0.842
4	0.0830	0.1014	0.0962	0.0698	1.222	1.159	0.841
3	0.0815	0.0997	0.0945	0.0685	1.223	1.160	0.840
2	0.0724	0.0886	0.0840	0.0608	1.224	1.160	0.840
1	0.0476	0.0583	0.0552	0.0399	1.225	1.161	0.839

(b) DUE TO UNIFORM LOAD

* Note :
  - CCM Is IDI of Center of Mass in Concentric Case.
  - ECO Is IDI of Corner of Structure for 5% Eccentricity.
  - EWG Is IDI of Wall G for 5% Eccentricity.
  - EWB Is IDI of Wall B for 5% Eccentricity.

TABLE 3.10 : INTER-STORY DRIFT INDEX OF EACH STORY FOR 5% ECCENTRICITY FROM STATIC ANALYSIS

Story	1.CCM* (%)	2.ECO* (%)	3.EWG* (%)	4.EWB* (%)	(2)/(1)	(3)/(1)	(4)/(1)
7	0.0891	0.1284	0.1172	0.0611	1.441	1.315	0.685
6	0.0995	0.1434	0.1308	0.0681	1.442	1.315	0.685
5	0.1059	0.1530	0.1395	0.0723	1.444	1.317	0.683
4	0.1077	0.1555	0.1419	0.0735	1.445	1.318	0.682
3	0.1017	0.1471	0.1342	0.0693	1.447	1.319	0.681
2	0.0856	0.1239	0.1130	0.0582	1.448	1.320	0.680
1	0.0516	0.0748	0.0681	0.0350	1.450	1.322	0.678

(a) DUE TO TRIANGULAR LOAD

Story	1.CCM* (%)	2.ECO* (%)	3.EWG* (%)	4.EWB* (%)	(2)/(1)	(3)/(1)	(4)/(1)
7	0.0659	0.0949	0.0866	0.0452	1.440	1.314	0.686
6	0.0735	0.1060	0.0967	0.0503	1.442	1.316	0.684
5	0.0794	0.1146	0.1045	0.0543	1.443	1.316	0.684
4	0.0830	0.1199	0.1093	0.0566	1.445	1.318	0.682
3	0.0815	0.1180	0.1076	0.0555	1.447	1.319	0.681
2	0.0724	0.1049	0.0956	0.0492	1.448	1.320	0.680
1	0.0476	0.0690	0.0629	0.0322	1.451	1.322	0.678

(b) DUE TO UNIFORM LOAD

* Note :
  CCM Is IDI of Center of Mass in Concentric Case.
  ECO Is IDI of Corner of Structure for 10% Eccentricity.
  EWG Is IDI of Wall G for 10% Eccentricity.
  EWB Is IDI of Wall B for 10% Eccentricity.

TABLE 3.11 : INTER-STORY DRIFT INDEX OF EACH STORY FOR 10% ECCENTRICITY FROM STATIC ANALYSIS

Case	Triangular Load		Uniform Load	
Location	Moment (k-in)	Shear (kips)	Moment (k-in)	Shear (kips)
1. Wall B (or G) Concentric Case	246538.9	678.6	215654.5	683.0
2. Wall B 5% Eccentricity	207034.9	568.7	181053.8	572.5
3. Wall G 5% Eccentricity	286042.3	788.4	250254.7	793.6
4. Wall B 10% Eccentricity	167531.4	458.9	146453.5	461.9
5. Wall G 10% Eccentricity	325546.1	898.2	284855.3	904.2
Ratio of (2) to (1)	0.84	0.84	0.84	0.84
Ratio of (3) to (1)	1.16	1.16	1.16	1.16
Ratio of (4) to (1)	0.67	0.68	0.68	0.67
Ratio of (5) to (1)	1.32	1.32	1.32	1.32

TABLE 3.12 : BENDING MOMENT AND SHEAR FORCE AT THE BASE OF SHEAR WALLS FROM STATIC ANALYSES

Story	1.CSW*	2.ESWG*	3.ESWB*	Ratio 2/1	Ratio 3/1
7	-65.56	-77.268	-53.861	1.179	0.822
6	136.617	157.759	115.470	1.155	0.845
5	258.963	299.931	217.990	1.158	0.842
4	371.770	431.052	312.492	1.159	0.841
3	472.530	548.247	396.811	1.160	0.840
2	569.255	660.826	477.680	1.161	0.839
1	678.556	788.372	568.737	1.162	0.838

(a) TRIANGULAR LOAD

Story	1.CSW*	2.ESWG*	3.ESWB*	Ratio 2/1	Ratio 3/1
7	-61.908	-72.744	-51.071	1.175	0.825
6	74.350	85.651	63.044	1.152	0.848
5	168.310	194.827	141.786	1.158	0.842
4	273.165	316.681	229.644	1.159	0.841
3	387.749	449.901	325.592	1.160	0.840
2	521.460	605.409	437.514	1.161	0.839
1	683.046	793.619	572.470	1.162	0.838

(b) UNIFORM LOAD

* Note :
CSW Story Shear of One Wall in Concentric Case.
ESWG Story Shear of Wall G for 5% Eccentricity.
ESWB Story Shear of Wall B for 5% Eccentricity.

TABLE 3.13 : STORY SHEAR OF WALLS FOR 5% ECCENTRICITY DUE TO STATIC LOAD

Story	1.CSW*	2.ESWG*	3.ESWB*	Ratio 2/1	Ratio 3/1
7	-65.56	-88.969	-42.151	1.357	0.643
6	136.617	178.896	94.327	1.309	0.690
5	258.963	340.899	177.020	1.316	0.684
4	371.770	490.329	253.212	1.319	0.681
3	472.530	623.964	321.094	1.320	0.680
2	569.255	752.400	386.108	1.322	0.678
1	678.556	898.189	458.921	1.324	0.676

(a) TRIANGULAR LOAD

Story	1.CSW*	2.ESWG*	3.ESWB*	Ratio 2/1	Ratio 3/1
7	-61.908	-83.584	-40.236	1.350	0.650
6	74.350	96.950	51.744	1.304	0.696
5	168.310	221.346	115.268	1.315	0.685
4	273.165	360.199	186.129	1.319	0.681
3	387.749	512.056	263.439	1.321	0.679
2	521.460	689.357	353.567	1.322	0.678
1	683.046	904.193	461.897	1.324	0.676

(b) UNIFORM LOAD

* Note :
CSW Story Shear of One Wall in Concentric Case.
ESWG Story Shear of Wall G for 10% Eccentricity.
ESWB Story Shear of Wall B for 10% Eccentricity.

TABLE 3.14 : STORY SHEAR OF WALLS FOR 10% ECCENTRICITY DUE TO STATIC LOAD

	Concentric Triangular (kips)	Concentric Uniform (kips)	Eccentric Triangular (kips)	Eccentric Uniform (kips)
Frame A	35.281	34.026	27.279	26.307
Frame B	695.615	699.379	583.050	586.170
Frame C	35.279	34.024	31.868	30.730
Frame D	35.329	34.063	34.187	32.963
Frame E	35.329	34.063	36.469	35.163
Frame F	35.279	34.024	38.690	37.318
Frame G	695.615	699.382	808.186	812.591
Frame H	35.281	34.026	43.283	41.745
Wall B	678.552	683.043	568.737	572.470
Wall G	678.556	683.043	788.372	793.619
Total	1603.0	1603.0	1603.0	1603.0

TABLE 3.15 : TOTAL BASE SHEAR CARRIED BY EACH FRAME FOR 5% ECCENTRICITY DUE TO STATIC LOAD

	Concentric Triangular (kips)	Concentric Uniform (kips)	Eccentric Triangular (kips)	Eccentric Uniform (kips)
Frame A	35.281	34.026	19.277	18.589
Frame B	695.615	699.379	470.483	472.961
Frame C	35.279	34.024	28.456	27.436
Frame D	35.329	34.063	33.047	31.863
Frame E	35.329	34.063	37.608	36.263
Frame F	35.279	34.024	42.102	40.612
Frame G	695.615	699.382	920.753	925.801
Frame H	35.281	34.026	51.285	49.462
Wall B	678.552	683.043	458.921	461.897
Wall G	678.556	683.043	898.189	904.193
Total	1603.0	1603.0	1603.0	1603.0

TABLE 3.16 : TOTAL BASE SHEAR CARRIED BY EACH FRAME FOR 10% ECCENTRICITY DUE TO STATIC LOAD

Case	Triangular Load		Uniform Load	
Location	Pos. Moment (k-in)	Neg. Moment (k-in)	Pos. Moment (k-in)	Neg. Moment (k-in)
1. Frame B (or G) Concentric Case	993.55	3660.65	508.23	3149.89
2. Frame B 5% Eccentricity	669.84	3317.05	261.47	2887.25
3. Frame G 5% Eccentricity	1317.25	4004.24	754.98	3412.52
4. Frame B 10% Eccentricity	346.14	2973.45	14.71	2624.62
5. Frame G 10% Eccentricity	1641.00	4347.84	1001.74	3675.16
Ratio (2)/(1)	0.674	0.906	0.514	0.917
Ratio (3)/(1)	1.326	1.094	1.486	1.083
Ratio (4)/(1)	0.348	0.812	0.029	0.833
Ratio (5)/(1)	1.652	1.188	1.971	1.167

TABLE 3.17 : MAXIMUM POSITIVE AND NEGATIVE MOMENTS IN GIRDERS DUE TO STATIC LOAD

Floor	1	2	3	4	5	6	7
1. CCM*	0.28	0.65	1.07	1.52	1.97	2.39	2.77
Time (sec)	13.5	13.5	13.5	14.8	14.8	14.8	14.8
2. ECO*	0.54	1.25	2.11	3.03	3.93	4.77	5.53
Time (sec)	14.9	14.9	14.9	14.9	14.9	14.9	14.9
3. EWB*	0.29	0.69	1.16	1.67	2.17	2.64	3.06
Time (sec)	7.3	7.3	7.3	7.3	7.3	7.3	7.3
4. EWG*	0.47	1.09	1.84	2.63	3.41	4.15	4.81
Time (sec)	14.9	14.9	14.9	14.9	14.9	14.9	14.9
(2)/(1)	1.929	1.923	1.972	1.993	1.995	1.996	1.996
(3)/(1)	1.036	1.062	1.084	1.099	1.102	1.105	1.105
(4)/(1)	1.679	1.677	1.720	1.730	1.731	1.736	1.736

(a) 5% Eccentricity

Floor	1	2	3	4	5	6	7
1. CCM*	0.28	0.65	1.07	1.52	1.97	2.39	2.77
Time (sec)	13.5	13.5	13.5	14.8	14.8	14.8	14.8
2. ECO*	0.65	1.52	2.54	3.62	4.68	5.66	6.53
Time (sec)	14.9	14.9	14.9	14.9	14.9	14.9	14.9
3. EWB*	0.18	0.43	0.73	1.06	1.39	1.70	1.98
Time (sec)	7.3	7.3	7.3	7.3	7.3	7.3	7.3
4. EWG*	0.55	1.29	2.16	3.10	4.03	4.90	5.68
Time (sec)	14.9	14.9	14.9	14.6	14.6	14.6	14.6
(2)/(1)	2.321	2.338	2.374	2.382	2.376	2.368	2.357
(3)/(1)	0.643	0.662	0.682	0.697	0.706	0.711	0.715
(4)/(1)	1.964	1.985	2.019	2.039	2.046	2.050	2.051

(b) 10% Eccentricity

* Note :
  - CCM Max. Displacement of CM in Concentric Case (in).
  - ECO Max. Displacement of Corner of Structure in Eccentric Case (in).
  - EWB Max. Displacement of Wall B in Eccentric Case (in).
  - EWG Max. Displacement of Wall G in Eccentric Case (in).

TABLE 3.18 : MAXIMUM LATERAL DISPLACEMENT FOR 5% AND 10% ECCENTRICITIES DUE TO TAFT-40

Story	1	2	3	4	5	6	7
1. CCM* Time (sec)	0.1912 13.5	0.3078 13.5	0.3648 14.8	0.3866 14.8	0.3806 14.8	0.3570 14.8	0.3198 14.8
2. ECO* Time (sec)	0.3629 14.9	0.6083 14.9	0.7271 14.9	0.7729 14.9	0.7621 14.9	0.7155 14.9	0.6400 14.9
3. EWB* Time (sec)	0.1967 7.3	0.3348 7.3	0.4030 7.3	0.4299 7.3	0.4246 7.3	0.3989 7.3	0.3571 7.3
4. EWG* Time (sec)	0.3158 14.9	0.5293 14.9	0.6326 14.9	0.6722 14.9	0.6626 14.9	0.6220 14.9	0.5565 14.9
(2)/(1)	1.898	1.976	1.993	1.999	2.002	2.004	2.001
(3)/(1)	1.029	1.088	1.105	1.112	1.116	1.117	1.117
(4)/(1)	1.652	1.720	1.734	1.739	1.741	1.742	1.740

(a) 5% Eccentricity

Story	1	2	3	4	5	6	7
1. CCM* Time (sec)	0.1912 13.5	0.3078 13.5	0.3648 14.8	0.3866 14.8	0.3805 14.8	0.3570 14.8	0.3198 14.8
2. ECO* Time (sec)	0.4412 14.9	0.7329 14.9	0.8685 14.9	0.9143 14.9	0.9007 14.6	0.8450 14.6	0.7551 14.6
3. EWB* Time (sec)	0.1205 7.3	0.2096 7.3	0.2569 7.3	0.2787 7.3	0.2794 7.3	0.2651 7.3	0.2378 7.3
4. EWG* Time (sec)	0.3748 14.9	0.6226 14.9	0.7474 14.6	0.7970 14.6	0.7866 14.6	0.7382 14.6	0.6599 14.6
(2)/(1)	2.308	2.381	2.381	2.365	2.367	2.367	2.361
(3)/(1)	0.630	0.681	0.704	0.721	0.734	0.743	0.744
(4)/(1)	1.960	2.023	2.049	2.062	2.067	2.068	2.063

(b) 10% Eccentricity

* Note :
  CCM Max. IDI of CM in Concentric Case (%).
  ECO Max. IDI of Corner of Structure in Eccentric Case (%).
  EWB Max. IDI of Wall B in Eccentric Case (%).
  EWG Max. IDI of Wall G in Eccentric Case (%).

TABLE 3.19 : MAXIMUM INTER-STORY DRIFT INDEX FOR 5% AND 10% ECCENTRICITIES DUE TO TAFT-40

Case	Location	Dis.[1]	IDI[2]
Triangular[3]	Corner	1.224	1.222
	Wall G	1.160	1.159
	Wall B	0.840	0.841
Uniform[4]	Corner	1.224	1.222
	Wall G	1.160	1.159
	Wall B	0.840	0.841
Taft-40[5]	Corner	1.972	1.982
	Wall G	1.716	1.724
	Wall B	1.085	1.098

(a) 5% Eccentricity

Case	Location	Dis.[1]	IDI[2]
Triangular[3]	Corner	1.447	1.445
	Wall G	1.320	1.318
	Wall B	0.680	0.682
Uniform[4]	Corner	1.448	1.445
	Wall G	1.320	1.318
	Wall B	0.680	0.682
Taft-40[5]	Corner	2.359	2.361
	Wall G	2.022	2.042
	Wall B	0.688	0.708

(b) 10% Eccentricity

Notes:

1. Lateral Displacement Normalized With the Corresponding Value in the Concentric Case.
2. Inter-Story Drift Index Normalized With the Corresponding Value in the Concentric Case.
3. Triangular Static Analysis.
4. Uniform Static Analysis.
5. Taft Earthquake with PGA = 0.40g.

TABLE 3.20 : NORMALIZED VALUES OF DISPLACEMENTS AND INTER-STORY DRIFT INDICES IN STATIC AND DYNAMIC ANALYSES

	Moment (in-k)	Shear (kips)
1. Wall B (or G) Concentric Case	638669.9	1868.53
2. Wall B 5% Eccentricity	682073.8	1812.05
3. Wall G 5% Eccentricity	1085170.0	2938.60
4. Wall B 10% Eccentricity	424662.5	1069.33
5. Wall G 10% Eccentricity	1278642.8	3532.08
Ratio of (2) to (1)	1.07	0.97
Ratio of (3) to (1)	1.70	1.57
Ratio of (4) to (1)	0.66	0.57
Ratio of (5) to (1)	2.00	1.89

TABLE 3.21 : MAXIMUM BENDING MOMENT AND SHEAR FORCE AT THE BASE OF WALLS DUE TO TAFT-40

Story	1. CSW*	2. ESWB*	3. ESWG*	(2)/(1)	(3)/(1)
7 (Time)	-215.61 (13.5)	-187.04 (7.1)	-303.73 (10.0)	0.87	1.41
6 (Time)	407.80 (11.7)	-404.94 (7.3)	622.43 (14.9)	0.99	1.53
5 (Time)	668.65 (14.8)	-762.19 (7.3)	1176.31 (14.9)	1.14	1.76
4 (Time)	958.19 (14.8)	-1078.10 (7.3)	1671.99 (14.9)	1.13	1.74
3 (Time)	1235.02 (13.5)	-1337.55 (7.3)	2097.24 (14.9)	1.08	1.70
2 (Time)	1540.96 (13.5)	-1559.47 (7.3)	2490.15 (14.9)	1.01	1.62
1 (Time)	1868.53 (13.5)	1812.06 (7.1)	2938.60 (14.9)	0.97	1.57

* Note :
CSW Story Shear of One Wall in Concentric Case (kips).
ESWG Story Shear of Wall G for 5% Eccentricity (kips).
ESWB Story Shear of Wall B for 5% Eccentricity (kips).

TABLE 3.22 : MAXIMUM STORY SHEAR OF WALLS FOR 5% ECCENTRICITY DUE TO TAFT-40

Story	1. CSW*	2. ESWB*	3. ESWG*	(2)/(1)	(3)/(1)
7	-215.61	-126.51	-299.64	0.59	1.39
6	245.38	206.89	503.39	0.84	2.05
5	573.52	426.45	1013.81	0.74	1.77
4	914.00	642.12	1492.77	0.70	1.63
3	1235.02	844.21	1920.62	0.68	1.56
2	1540.96	1045.73	2334.11	0.68	1.51
1	1868.53	1272.57	2810.30	0.68	1.50

* Note :
CSW Story Shear of One Wall in Concentric Case (kips).
ESWG Story Shear of Wall G for 5% Eccentricity (kips).
ESWB Story Shear of Wall B for 5% Eccentricity (kips).

TABLE 3.23 : STORY SHEAR OF WALLS WHEN TOTAL BASE SHEAR IS MAXIMUM FOR 5% ECCENTRICITY DUE TO TAFT-40

Story	1. CSW*	2. ESWB*	3. ESWG*	(2)/(1)	(3)/(1)
7 (Time)	-215.61 (13.5)	-112.08 (10)	-414.71 (7.1)	0.52	1.92
6 (Time)	407.80 (11.7)	-302.16 (7.3)	-746.16 (14.6)	0.74	1.83
5 (Time)	668.65 (14.8)	-523.28 (7.3)	-1415.06 (14.6)	0.78	2.12
4 (Time)	958.19 (14.8)	-698.48 (7.3)	-2002.14 (14.6)	0.73	2.09
3 (Time)	1235.02 (13.5)	-828.89 (7.3)	2491.36 (14.9)	0.67	2.02
2 (Time)	1540.96 (13.5)	-937.09 (7.3)	2988.71 (14.9)	0.61	1.94
1 (Time)	1868.53 (13.5)	-1069.33 (7.3)	3532.08 (14.9)	0.57	1.89

* Note :
CSW Story Shear of One Wall in Concentric Case (kips).
ESWG Story Shear of Wall G for 10% Eccentricity (kips).
ESWB Story Shear of Wall B for 10% Eccentricity (kips).

TABLE 3.24 : MAXIMUM STORY SHEAR OF WALLS FOR 10% ECCENTRICITY DUE TO TAFT-40

Story	1. CSW*	2. ESWB*	3. ESWG*	(2)/(1)	(3)/(1)
7	-215.61	-73.11	-359.08	0.34	1.67
6	245.38	215.39	746.16	0.88	3.04
5	573.52	389.38	1415.06	0.68	2.47
4	914.00	541.44	2002.14	0.59	2.19
3	1235.02	663.37	2481.26	0.54	2.01
2	1540.96	765.61	2896.59	0.50	1.88
1	1868.53	874.56	3368.54	0.47	1.80

* Note :
CSW Story Shear of One Wall in Concentric Case (kips).
ESWG Story Shear of Wall G for 10% Eccentricity (kips).
ESWB Story Shear of Wall B for 10% Eccentricity (kips).

TABLE 3.25 : STORY SHEAR OF WALLS WHEN TOTAL BASE SHEAR IS MAXIMUM FOR 10% ECCENTRICITY DUE TO TAFT-40

	Moment[1]		Shear[2]	
Case	Wall B	Wall G	Wall B	Wall G
Triangular[3]	0.84	1.16	0.838	1.162
Uniform[4]	0.84	1.16	0.839	1.161
Taft-40[5]	1.07	1.70	1.027	1.619

(a) 5% Eccentricity

	Moment[1]		Shear[2]	
Case	Wall B	Wall G	Wall B	Wall G
Triangular[3]	0.67	1.32	0.676	1.324
Uniform[4]	0.68	1.32	0.678	1.322
Taft-40[5]	0.66	2.00	0.660	1.973

(b) 10% Eccentricity

Notes:

1. Moment at the Base of Walls Normalized With the Corresponding Value in the Concentric Case.
2. Average Shear Force of Walls Normalized With the Corresponding Value in the Concentric Case.
3. Triangular Static Analysis.
4. Uniform Static Analysis.
5. Taft Earthquake With PGA = 0.40g.

TABLE 3.26 : NORMALIZED VALUES OF BENDING MOMENTS AND SHEAR FORCES OF WALLS IN STATIC AND DYNAMIC ANALYSES

Story	1.Concentric (kips)	2.Eccentric (5%) (kips)	3. Eccentric (10%) (kips)	Ratio of (2)/(1)	Ratio of (3)/(1)
7 (Time)	903.95 (11.7)	1049.53 (10.1)	-1181.33 (14.6)	1.16	1.31
6 (Time)	1782.02 (14.8)	-2046.14 (13.9)	-2388.99 (14.6)	1.15	1.34
5 (Time)	2542.71 (14.8)	-2936.14 (13.9)	-3393.57 (14.6)	1.15	1.33
4 (Time)	3150.98 (14.8)	-3659.14 (13.9)	-4163.90 (14.6)	1.16	1.32
3 (Time)	3627.13 (13.5)	-4207.57 (13.9)	-4681.75 (14.6)	1.16	1.29
2 (Time)	4092.53 (13.5)	-4578.89 (13.9)	-4954.64 (14.6)	1.12	1.21
1 (Time)	4399.08 (13.5)	4815.86 (14.2)	-5022.70 (14.6)	1.09	1.14

TABLE 3.27 : MAXIMUM TOTAL STORY SHEAR OF THE STRUCTURE FOR 5% AND 10% ECCENTRICITIES DUE TO TAFT-40

Story	1.Concentric (kips)	2.Eccentric (5%) (kips)	3.Eccentric (10%) (kips)	Ratio of (2)/(1)	Ratio of (3)/(1)
7	672.67	913.90	1181.33	1.36	1.76
6	1468.20	1895.79	2388.99	1.29	1.63
5	2260.67	2772.11	3393.57	1.23	1.50
4	3001.68	3512.02	4163.90	1.17	1.39
3	3627.13	4096.32	4681.75	1.13	1.29
2	4092.53	4524.66	4954.64	1.11	1.21
1	4399.08	4815.86	5022.70	1.09	1.14

TABLE 3.28 : TOTAL STORY SHEAR OF THE STRUCTURE WHEN TOTAL BASE SHEAR IS MAXIMUM FOR 5% AND 10% ECCENTRICITIES DUE TO TAFT-40

	1.Concentric	2.Eccentric	(2)/(1)
Frame A (kips) Time (sec)	95.03 13.5	97.21 7.3	1.023
Frame B (kips) Time (sec)	1914.26 13.5	1857.60 7.1	0.970
Frame C (kips) Time (sec)	95.03 13.5	96.92 7.1	1.020
Frame D (kips) Time (sec)	95.03 13.5	99.82 7.1	1.050
Frame E (kips) Time (sec)	95.03 13.5	113.33 14.2	1.193
Frame F (kips) Time (sec)	95.03 13.5	130.70 14.9	1.375
Frame G (kips) Time (sec)	1914.32 13.5	3012.96 14.9	1.574
Frame H (kips) Time (sec)	95.03 13.5	176.86 14.9	1.861
Wall B (kips) Time (sec)	1868.50 13.5	1812.05 7.1	0.970
Wall G (kips) Time (sec)	1868.50 13.5	2938.60 14.9	1.573
Total Max. (kips) Ratio To Total Weight Time (sec)	4399.08 0.517 13.5	4815.86 0.566 14.2	1.095

TABLE 3.29 : MAXIMUM BASE SHEAR OF EACH FRAME FOR 5% ECCENTRICITY DUE TO TAFT-40

	1.Concentric	2.Eccentric	(2)/(1)
Frame A (kips) Time (sec)	95.03 13.5	75.99 7.5	0.800
Frame B (kips) Time (sec)	1914.26 13.5	1097.24 7.3	0.573
Frame C (kips) Time (sec)	95.03 13.5	73.14 7.1	0.770
Frame D (kips) Time (sec)	95.03 13.5	98.88 14.6	1.041
Frame E (kips) Time (sec)	95.03 13.5	125.07 14.6	1.316
Frame F (kips) Time (sec)	95.03 13.5	151.00 14.6	1.589
Frame G (kips) Time (sec)	1914.32 13.5	3620.63 14.9	1.891
Frame H (kips) Time (sec)	95.03 13.5	216.13 14.9	2.274
Wall B (kips) Time (sec)	1868.50 13.5	1069.33 7.3	0.572
Wall G (kips) Time (sec)	1868.50 13.5	3532.08 14.9	1.890
Total Max. (kips) Ratio To Total Weight Time (sec)	4399.08 0.517 13.5	5022.70 0.591 14.6	1.142

TABLE 3.30 : MAXIMUM BASE SHEAR OF EACH FRAME FOR 10% ECCENTRICITY DUE TO TAFT-40

	5% Eccentricity		10% Eccentricity	
Floor	DE*	DEA*	DE*	DEA*
7	403.45	4.203	576.75	3.004
6	407.91	4.249	583.48	3.039
5	406.94	4.239	565.74	2.947
4	404.13	4.210	545.70	2.842
3	396.74	4.133	540.21	2.814
2	375.54	3.912	517.41	2.695
1	359.59	3.746	497.68	2.592

* Note :
DE Is Dynamic Eccentricity (inch).
DEA Is Dynamic Amplification of Eccentricity (Ratio of Dynamic Eccentricity to Static Eccentricity).

TABLE 3.31 : DYNAMIC ECCENTRICITY AND DYNAMIC AMPLIFICATION OF ECCENTRICITY DUE TO TAFT-40

	Pos. Moment (in-k)	Neg. Moment (in-k)
1. Frame B (or G) Concentric Case	4493.53	6626.13
2. Frame B 5% Eccentricity	5118.95	7251.55
3. Frame G 5% Eccentricity	8599.96	10732.56
4. Frame B 10% Eccentricity	3057.14	5101.29
5. Frame G 10% Eccentricity	10393.31	12525.91
(2) To (1)	1.139	1.094
(3) To (1)	1.914	1.620
(4) To (1)	0.680	0.770
(5) To (1)	2.313	1.890

TABLE 3.32 : MAXIMUM MOMENT IN GIRDERS FOR 5% AND 10% ECCENTRICITIES DUE TO TAFT-40

	Pos. M[1]	Neg. M[2]
Case	Girder	Girder
Triangular[3]	1.326	1.094
Uniform[4]	1.486	1.083
Taft-40[5]	1.914	1.620

(a) 5% Eccentricity

	Pos. M[1]	Neg. M[2]
Case	Girder	Girder
Triangular[3]	1.652	1.188
Uniform[4]	1.971	1.167
Taft-40[5]	2.313	1.890

(b) 10% Eccentricity

Notes:

1. Positive Moment in Girders Normalized With the Corresponding Value in the Concentric Case.
2. Negative Moment in Girders Normalized With the Corresponding Value in the Concentric Case.
3. Triangular Static Analysis.
4. Uniform Static Analysis.
5. Taft Earthquake With PGA = 0.40g.

TABLE 3.33 : NORMALIZED VALUES OF BENDING MOMENTS IN GIRDERS IN STATIC AND DYNAMIC ANALYSES

	Columns	Shear Walls	Beams
EI* ($k\text{-}in^2$)	26195906	2.23×10^{10}	25413345
EA* (kips)	1370588	7675290	1627020
GA* (kips)	--	1970388	--

* Notes :
- E Modulus of Elasticity (ksi).
- G Shear Modulus of Elasticity (ksi).
- I Sectional Moment of Inertia (in^4).
- A Area of Cross Section (in^2).

TABLE 4.1: Sectional Properties [30]

LOAD	CASE	1.IDI*	2.TS*	3.WS*	4.FS*	(3)/(2)	(4)/(2)
Triangular Profile	F.Y.*	0.085	1217	1065	152	0.875	0.125
	I.C.*	0.705	2241	1153	1088	0.515	0.485
Uniform Profile	F.Y.*	0.088	1408	1242	166	0.882	0.118
	I.C.*	0.807	2773	1672	1101	0.603	0.397

* Notes :
- F.Y. First Yield.
- I.C. Incipient Collapse.
- IDI Inter-Story Drift Index.
- TS Total Base Shear of the Structure (kips).
- WS Shear at the Base of Walls (kips).
- FS Shear at the Base of Frames (excluding walls) (kips).

TABLE 4.2: BASE SHEAR AT THE FIRST YIELDING AND AT INCIPIENT COLLAPSE

	REAL STRUCTURE		MODEL	
Mode	Direction*	Period (sec)	Direction*	Period (sec)
1	Y-Translation	1.204	Y-Translation	1.202
2	X-Translation	0.749	X-Translation	0.749
3	Torsional Rotation	0.701	Torsional Rotation	0.747
4	Y-Translation	0.387	Y-Translation	0.386
5	Y-Translation	0.218	Y-Translation	0.217
6	X-Translation	0.187	X-Translation	0.187
7	Torsional Rotation	0.176	Torsional Rotation	0.181
8	Y-Translation	0.144	Y-Translation	0.144
9	Y-Translation	0.105	Y-Translation	0.104
10	X-Translation	0.086	X-Translation	0.086
11	Y-Translation	0.082	Torsional Rotation	0.083
12	Torsional Rotation	0.081	Y-Translation	0.082
13	Y-Translation	0.070	Y-Translation	0.070
14	X-Translation	0.055	X-Translation	0.055
15	Torsional Rotation	0.051	Torsional Rotation	0.052
16	X-Translation	0.041	X-Translation	0.041
17	Torsional Rotation	0.038	Torsional Rotation	0.039
18	X-Translation	0.034	X-Translation	0.034
19	Torsional Rotation	0.032	Torsional Rotation	0.032
20	X-Translation	0.030	X-Translation	0.030
21	Torsional Rotation	0.029	Torsional Rotation	0.029

* Note :
X-Translation is translational mode in the direction of walls.
Y-Translation is translational mode perpendicular to the walls.
Torsional Rotation is rotational mode about the center of mass at each floor.

TABLE 4.3: UNDAMPED NATURAL PERIOD OF THE REAL STRUCTURE AND THE MODEL USING CRACKED SECTIONAL PROPERTIES

FLOOR	MASS (kips-sec^2/in)
ROOF	2.72
3 TO 7	3.18
2	3.27

TABLE 4.4: TRANSLATIONAL MASS

Floor	1.CCM* (in)	2.ECM* (in)	3.EWB* (in)	4.EWG* (in)	Ratio (3)/(1)	Ratio (4)/(1)
TAFT-40 ; Static Eccentricity = 5 %						
Roof (Time)	-4.034 (4.15)	-3.397 (4.145)	3.425 (4.445)	-4.056 (4.195)	0.849	1.005
7 (Time)	-3.516 (4.15)	-2.947 (4.145)	2.952 (4.445)	-3.512 (4.195)	0.840	0.999
6 (Time)	-2.957 (4.15)	-2.462 (4.145)	2.447 (4.445)	-2.930 (4.195)	0.828	0.991
5 (Time)	-2.361 (4.15)	-1.950 (4.145)	1.920 (4.445)	-2.317 (4.195)	0.813	0.981
4 (Time)	-1.742 (4.15)	-1.424 (4.145)	1.391 (4.445)	-1.693 (4.195)	0.799	0.972
3 (Time)	-1.130 (4.15)	-.9104 (4.145)	0.9137 (6.60)	-1.087 (4.195)	0.809	0.962
2 (Time)	-0.5630 (4.15)	-.4448 (4.145)	0.4589 (6.60)	-0.5368 (4.195)	0.815	0.953
TAFT-40 ; Static Eccentricity = 25 %						
Roof (Time)	-4.034 (4.15)	5.437 (1.30)	-1.461 (4.00)	6.210 (1.28)	0.362	1.539
7 (Time)	-3.516 (4.15)	4.724 (1.32)	-1.239 (4.00)	5.383 (1.30)	0.352	1.531
6 (Time)	-2.957 (4.15)	3.999 (1.32)	-1.005 (4.00)	4.535 (1.32)	0.340	1.534
5 (Time)	-2.361 (4.15)	3.234 (1.32)	-0.7633 (4.00)	3.666 (1.32)	0.323	1.553
4 (Time)	-1.742 (4.15)	2.441 (1.34)	-0.5239 (4.00)	2.759 (1.34)	0.301	1.584
3 (Time)	-1.130 (4.15)	1.636 (1.34)	-0.3033 (4.00)	1.849 (1.34)	0.268	1.636
2 (Time)	-0.5630 (4.15)	0.8532 (1.34)	-0.1239 (4.00)	0.9648 (1.34)	0.220	1.714

* Note :
CCM Displacement of CM in Concentric Case.
ECM Displacement of CM in Eccentric Case.
EWB Displacement of Wall B in Eccentric Case.
EWG Displacement of Wall G in Eccentric Case.

TABLE 5.1 : MAXIMUM LATERAL DISPLACEMENTS FOR THE NONLINEAR INELASTIC CASE (TAFT-40, 0-8 Seconds)

Floor	1.LCM* (in)	2.LEWB* (in)	3.LEWG* (in)	Ratio (3)/(1)	Ratio (4)/(1)
TAFT-40 ; Static Eccentricity = 5 %					
Roof (Time)	5.786 (7.40)	4.303 (4.40)	7.426 (4.45)	0.744	1.283
7 (Time)	4.826 (7.40)	3.651 (4.40)	6.285 (4.45)	0.757	1.302
6 (Time)	-3.859 (7.75)	2.945 (4.40)	5.056 (4.45)	0.763	1.310
5 (Time)	-2.960 (7.75)	2.214 (4.40)	3.787 (4.45)	0.748	1.279
4 (Time)	-2.047 (7.75)	1.496 (4.40)	2.546 (4.45)	0.731	1.244
3 (Time)	-1.188 (7.75)	0.8459 (4.40)	1.430 (4.45)	0.712	1.204
2 (Time)	-0.4812 (7.75)	0.3320 (4.40)	0.5547 (4.45)	0.690	1.153
TAFT-40 ; Static Eccentricity = 25 %					
Roof (Time)	5.786 (7.40)	-1.117 (4.00)	-6.459 (1.70)	0.193	1.116
7 (Time)	4.826 (7.40)	-0.9487 (4.00)	-5.480 (1.70)	0.197	1.136
6 (Time)	-3.859 (7.75)	-0.7694 (4.00)	-4.428 (1.70)	0.199	1.147
5 (Time)	-2.960 (7.75)	-0.5837 (4.00)	-3.336 (1.70)	0.197	1.127
4 (Time)	-2.047 (7.75)	-0.3995 (4.00)	-2.259 (1.70)	0.195	1.104
3 (Time)	-1.188 (7.75)	-0.2299 (4.00)	-1.280 (1.70)	0.194	1.077
2 (Time)	-0.4812 (7.75)	-0.0923 (4.00)	-0.5022 (1.70)	0.192	1.044

* Note :
LCM Displacement of CM in Linear Elastic Concentric Case.
EWB Displacement of Wall B in Linear Elastic Eccentric Case.
EWG Displacement of Wall G in Linear Elastic Eccentric Case.

TABLE 5.2 : MAXIMUM LATERAL DISPLACEMENTS FOR THE LINEAR ELASTIC CASE (TAFT-40, 0-8 Seconds)

Location	e/D*[1]	Maximum Values of Plastic Rotation (radians)	
		TAFT-40 (0-2 Sec.)*[2]	TAFT-40 (0-8 Sec.)*[3]
1.One Wall	0.00	0.00153	-0.00281
2.Wall B	0.05	-0.00087	0.00202
3.Wall B	0.25	0.00	0.00
4.Wall G	0.05	0.00245	-0.00267
5.Wall G	0.25	0.00543	0.00543
Ratio (2)/(1)		0.57	0.72
Ratio (3)/(1)		0.00	0.00
Ratio (4)/(1)		1.60	0.95
Ratio (5)/(1)		3.55	1.93

* Note :
1. e/D Initial (Static) Eccentricity Ratio.
2. During 0 to 2 seconds of the response.
3. During 0 to 8 seconds of the response.

TABLE 5.3 : MAXIMUM PLASTIC HINGE ROTATION (Radians) AT BASE OF WALLS (TAFT-40)

Story	1.CCM* (%)	2.EWB* (%)	3.EWG* (%)	Ratio (2)/(1)	Ratio (3)/(1)
TAFT-40 ; Static Eccentricity = 5 %					
7 (Time)	-0.4609 (4.20)	0.4310 (6.50)	-0.4615 (4.245)	0.935	1.001
6 (Time)	-0.4903 (4.20)	0.4562 (6.50)	-0.4935 (4.195)	0.930	1.007
5 (Time)	-0.5047 (4.15)	0.4635 (6.55)	-0.5185 (4.195)	0.918	1.027
4 (Time)	-0.5241 (4.15)	0.4524 (6.55)	-0.5290 (4.195)	0.863	1.009
3 (Time)	-0.5183 (4.15)	0.4295 (4.445)	-0.5131 (4.195)	0.829	0.990
2 (Time)	-0.4799 (4.15)	0.3851 (6.60)	-0.4659 (4.195)	0.802	0.971
1 (Time)	-0.3814 (4.15)	0.3109 (6.60)	-0.3637 (4.195)	0.815	0.954
TAFT-40 ; Static Eccentricity = 25 %					
7 (Time)	-0.4609 (4.20)	-0.1875 (4.00)	0.7375 (1.24)	0.407	1.600
6 (Time)	-0.4903 (4.20)	-0.1985 (4.00)	0.7739 (1.24)	0.405	1.578
5 (Time)	-0.5047 (4.15)	-0.2047 (4.00)	0.7902 (1.26)	0.406	1.566
4 (Time)	-0.5241 (4.15)	-0.2027 (4.00)	0.7829 (1.26)	0.387	1.494
3 (Time)	-0.5183 (4.15)	-0.1869 (4.00)	0.7761 (1.32)	0.361	1.497
2 (Time)	-0.4799 (4.15)	-0.1519 (4.00)	0.7493 (1.32)	0.317	1.561
1 (Time)	-0.3814 (4.15)	-0.0839 (4.00)	0.6537 (1.34)	0.220	1.714

* Note :
CCM IDI of CM in Concentric Case.
EWB IDI of Wall B in Eccentric Case.
EWG IDI of Wall G in Eccentric Case.

TABLE 5.4 : MAXIMUM INTER-STORY DRIFT INDICES FOR THE NONLINEAR INELASTIC CASE (TAFT-40, 0-8 Seconds)

Story	1.CSW* (kips)	2.ESWG* (kips)	3.ESWB* (kips)	Ratio (2)/(1)	Ratio (3)/(1)
TAFT-40 ; Static Eccentricity = 5 %					
7 (Time)	244.05 (4.15)	207.92 (4.145)	-210.56 (6.60)	0.85	0.86
6 (Time)	-283.54 (7.15)	-325.29 (6.35)	285.16 (7.395)	1.15	1.01
5 (Time)	404.25 (7.40)	420.82 (4.445)	422.87 (6.50)	1.04	1.05
4 (Time)	475.90 (7.40)	-498.84 (7.095)	483.72 (6.50)	1.05	1.02
3 (Time)	-617.10 (7.05)	-601.56 (4.145)	564.85 (4.395)	0.97	0.92
2 (Time)	-753.03 (7.05)	-735.15 (4.145)	731.72 (6.60)	0.98	0.97
1 (Time)	852.70 (1.00)	985.58 (1.00)	893.81 (7.295)	1.16	1.05
TAFT-40 ; Static Eccentricity = 25 %					
7 (Time)	244.05 (4.15)	-368.36 (1.34)	-69.88 (1.38)	1.51	0.29
6 (Time)	-283.54 (7.15)	706.89 (6.55)	-104.38 (4.00)	2.49	0.37
5 (Time)	404.25 (7.40)	683.40 (6.55)	-187.80 (4.00)	1.69	0.46
4 (Time)	475.90 (7.40)	-596.13 (4.10)	-271.11 (4.00)	1.25	0.57
3 (Time)	-617.10 (7.05)	661.22 (1.34)	-351.13 (4.00)	1.07	0.57
2 (Time)	-753.03 (7.05)	1002.5 (3.81)	-424.75 (4.00)	1.33	0.56
1 (Time)	852.70 (1.00)	1460.7 (6.70)	-548.68 (4.00)	1.71	0.64

* Note :
CSW Story Shear of One Wall in Concentric Case.
ESWB Story Shear of Wall B in Eccentric Case.
ESWG Story Shear of Wall G in Eccentric Case.

TABLE 5.5 : MAXIMUM STORY SHEAR FORCES OF WALLS FOR THE NONLINEAR INELASTIC CASE (TAFT-40, 0-8 Seconds)

Story	7	6	5	4	3	2	1
TAFT-40							
1.CN* Time	-750.35 7.15	-1240.3 4.20	-1524.4 4.20	-1748.5 4.15	-2032.0 4.15	-2189.8 4.10	-2231.2 4.10
2.E05* Time	642.3 6.50	1119.1 6.50	-1367.0 7.095	-1533.1 4.095	-1736.2 4.145	1870.9 6.60	2074.9 6.60
3.E25* Time	663.53 6.55	1005.9 6.55	934.51 6.55	1065.4 1.34	1323.5 1.34	1647.7 3.81	2081.5 6.70
(2)/(1)	0.86	0.90	0.90	0.88	0.85	0.85	0.93
(3)/(1)	0.88	0.81	0.61	0.61	0.65	0.75	0.93

* Note :
CN Total Story Shear Force (kips) in Concentric Case.
E05 Total Story Shear Force (kips) for 5% eccentricity.
E25 Total Story Shear Force (kips) for 25% eccentricity.

TABLE 5.6 : MAXIMUM TOTAL STORY SHEAR FORCES FOR THE NONLINEAR INELASTIC CASE (TAFT-40, 0-8 Seconds)

Story	7	6	5	4	3	2	1
TAFT-40							
TE05* Time	-230499 7.645	-383396 7.645	476299 4.295	497946 4.295	478013 5.85	616978 5.85	705708 5.85
TE25* Time	-423488 3.96	-649941 3.96	-633125 6.55	-680598 1.24	-678555 1.24	-713708 1.30	-860076 6.70
Td05*	3.20	3.22	3.25	2.97	2.45	2.93	3.29
Td25*	1.25	1.16	0.92	0.86	0.74	0.72	0.85

* Note :
TE05 Story Torque (k-in) for 5% eccentricity.
TE25 Story Torque (k-in) for 25% eccentricity.
Td05 Dynamic Amplification of Eccentricity for 5% Eccentricity.
Td25 Dynamic Amplification of Eccentricity for 25% Eccentricity.

TABLE 5.7 : MAXIMUM TOTAL STORY TORQUES AND VALUES OF DYNAMIC AMPLIFICATION OF ECCENTRICITY FOR THE NONLINEAR INELASTIC CASE (TAFT-40, 0-8 Seconds)

Story	7	6	5	4	3	2	1
TAFT-40							
WT05* Time	-137360 4.395	-267764 7.645	302793 4.295	335323 4.295	359051 2.55	504570 5.85	587628 5.85
WT25* Time	178031 1.34	-447816 6.55	-449320 6.55	461904 4.15	477888 4.20	-500053 1.30	-733017 6.70
R1*	0.60	0.70	0.64	0.67	0.75	0.82	0.83
R2*	0.42	0.67	0.71	0.67	0.70	0.70	0.85

* Note :

WT05 Story Torque (k-in) Resisted by Walls for 5% eccentricity.
WT25 Story Torque (k-in) Resisted by Walls for 25% eccentricity.
R1 Ratio of WT05 to Maximum Story Torque.
R2 Ratio of WT25 to Maximum Story Torque.

TABLE 5.8 : MAXIMUM STORY TORQUES RESISTED BY WALLS FOR THE NONLINEAR INELASTIC CASE (TAFT-40, 0-8 Seconds)

Story	Time (sec)	TV* (kips)	SWG* (kips)	SWB* (kips)	R1*	R2*
TAFT-40 ; Static Eccentricity = 5 %						
7	7.645	45.60	138.75	4.27	0.35	0.07
6	7.645	-46.41	245.97	-207.33	0.70	0.04
5	4.295	-15.10	-202.77	309.83	0.64	0.01
4	4.295	-8.72	-221.09	346.58	0.67	0.01
3	5.85	100.96	-296.76	304.84	0.74	0.06
2	5.85	-165.15	-535.63	318.56	0.82	0.09
1	5.85	-449.85	-732.50	262.30	0.83	0.22
TAFT-40 ; Static Eccentricity = 25 %						
7	3.96	584.17	246.62	1.30	0.34	0.88
6	3.96	799.37	630.83	-97.71	0.66	0.79
5	6.55	934.51	683.40	-77.26	0.71	1.00
4	1.24	902.89	548.49	-149.60	0.61	0.85
3	1.24	865.16	543.38	-170.90	0.62	0.65
2	1.30	1252.86	794.23	-52.31	0.70	0.76
1	6.70	2081.50	1460.70	219.77	0.85	1.00

* Note:
- TV Total Story Shear in Eccentric Case.
- SWB Story Shear of Wall B in Eccentric Case.
- SWG Story Shear of Wall G in Eccentric Case.
- R1 Ratio of Torque Resisted by the Walls to Maximum Total Torque.
- R2 Ratio of (TV) to Maximum Total Story Shear in Eccentric Case.

TABLE 5.9 : SHEAR FORCES AND TORQUES RESISTED BY THE WALLS WHEN THE TOTAL STORY TORQUE IS MAXIMUM FOR THE NONLINEAR INELASTIC CASE (TAFT-40, 0-8 Seconds)

Floor	1.CCM* (in)	2.ECM* (in)	3.EWB* (in)	4.EWG* (in)	Ratio (3)/(1)	Ratio (4)/(1)
TAFT-18 ; Static Eccentricity = 5 %						
Roof (Time)	1.600 (1.95)	-1.431 (1.60)	1.381 (1.88)	-1.788 (1.62)	0.863	1.117
7 (Time)	1.358 (1.95)	-1.203 (1.58)	1.160 (1.88)	-1.503 (1.62)	0.854	1.107
6 (Time)	1.097 (1.95)	-0.9708 (1.58)	0.9258 (1.90)	-1.199 (1.60)	0.844	1.093
5 (Time)	0.8275 (1.95)	-0.7444 (1.56)	0.6883 (1.90)	-0.8969 (1.60)	0.832	1.084
4 (Time)	0.5623 (1.95)	-0.5212 (1.54)	0.4590 (1.90)	-0.6186 (1.56)	0.816	1.100
3 (Time)	0.3210 (1.95)	-0.3122 (1.54)	0.2590 (1.92)	-0.3686 (1.56)	0.807	1.148
2 (Time)	0.1300 (2.00)	-0.1323 (1.54)	-0.1049 (1.52)	-0.1577 (1.56)	0.807	1.214
TAFT-18 ; Static Eccentricity = 25 %						
Roof (Time)	1.600 (1.95)	2.124 (1.20)	0.4160 (1.70)	2.447 (1.22)	0.260	1.529
7 (Time)	1.358 (1.95)	1.795 (1.22)	-0.3493 (1.54)	2.067 (1.22)	0.257	1.522
6 (Time)	1.097 (1.95)	1.446 (1.22)	-0.2840 (1.54)	1.665 (1.22)	0.259	1.518
5 (Time)	0.8275 (1.95)	1.114 (1.28)	-0.2158 (1.54)	1.277 (1.26)	0.261	1.543
4 (Time)	0.5623 (1.95)	0.8057 (1.28)	-0.1479 (1.54)	0.9202 (1.28)	0.263	1.636
3 (Time)	0.3210 (1.95)	0.5096 (1.30)	-0.0853 (1.54)	0.5787 (1.30)	0.266	1.803
2 (Time)	0.1300 (2.00)	0.2417 (1.30)	-0.0347 (1.54)	0.2743 (1.30)	0.267	2.110

* Note :
CCM Displacement of CM in Concentric Case.
ECM Displacement of CM in Eccentric Case.
EWB Displacement of Wall B in Eccentric Case.
EWG Displacement of Wall G in Eccentric Case.

TABLE 5.10 : MAXIMUM LATERAL DISPLACEMENTS FOR THE NONLINEAR INELASTIC CASE (TAFT-18, 0-2 Seconds)

Floor	1.CCM* (in)	2.ECM* (in)	3.EWB* (in)	4.EWG* (in)	Ratio (3)/(1)	Ratio (4)/(1)
TAFT-40 ; Static Eccentricity = 5 %						
Roof (Time)	2.731 (1.15)	2.894 (1.15)	-2.128 (1.60)	3.596 (1.20)	0.779	1.317
7 (Time)	2.366 (1.15)	2.493 (1.15)	-1.820 (1.60)	3.123 (1.20)	0.769	1.320
6 (Time)	1.972 (1.15)	2.063 (1.15)	-1.490 (1.60)	2.615 (1.20)	0.756	1.326
5 (Time)	1.554 (1.15)	1.634 (1.20)	-1.186 (1.545)	2.081 (1.20)	0.763	1.339
4 (Time)	1.146 (1.20)	1.195 (1.20)	-0.8808 (1.545)	1.531 (1.20)	0.769	1.336
3 (Time)	0.7396 (1.20)	0.7657 (1.20)	-0.5653 (1.545)	0.9930 (1.25)	0.764	1.343
2 (Time)	0.3628 (1.20)	0.3747 (1.20)	-0.2699 (1.545)	0.5052 (1.25)	0.744	1.393
TAFT-40 ; Static Eccentricity = 25 %						
Roof (Time)	2.731 (1.15)	5.437 (1.30)	-1.083 (1.54)	6.210 (1.28)	0.397	2.274
7 (Time)	2.366 (1.15)	4.724 (1.32)	-0.9126 (1.54)	5.383 (1.30)	0.386	2.275
6 (Time)	1.972 (1.15)	3.999 (1.32)	-0.7343 (1.54)	4.535 (1.32)	0.372	2.300
5 (Time)	1.554 (1.15)	3.234 (1.32)	-0.5524 (1.54)	3.666 (1.32)	0.355	2.359
4 (Time)	1.146 (1.20)	2.441 (1.34)	-0.3748 (1.54)	2.759 (1.34)	0.327	2.408
3 (Time)	0.7396 (1.20)	1.636 (1.34)	-0.2140 (1.54)	1.849 (1.34)	0.289	2.500
2 (Time)	0.3628 (1.20)	0.8532 (1.34)	-0.0866 (1.54)	0.9648 (1.34)	0.239	2.659

* Note :
CCM Displacement of CM in Concentric Case.
ECM Displacement of CM in Eccentric Case.
EWB Displacement of Wall B in Eccentric Case.
EWG Displacement of Wall G in Eccentric Case.

TABLE 5.11 : MAXIMUM LATERAL DISPLACEMENTS FOR THE NONLINEAR INELASTIC CASE (TAFT-40, 0-2 Seconds)

Floor	1.CCM* (in)	2.ECM* (in)	3.EWB* (in)	4.EWG* (in)	Ratio (3)/(1)	Ratio (4)/(1)
TAFT-60 ; Static Eccentricity = 5 %						
Roof (Time)	4.710 (1.20)	4.972 (1.195)	-3.671 (1.645)	6.096 (1.195)	0.779	1.294
7 (Time)	4.117 (1.20)	4.315 (1.195)	-3.134 (1.645)	5.302 (1.245)	0.761	1.288
6 (Time)	3.480 (1.20)	3.614 (1.195)	-2.565 (1.645)	4.506 (1.245)	0.737	1.295
5 (Time)	2.805 (1.20)	2.880 (1.195)	2.030 (1.145)	3.660 (1.245)	0.724	1.305
4 (Time)	2.102 (1.20)	2.146 (1.245)	1.502 (1.145)	2.771 (1.245)	0.715	1.318
3 (Time)	1.394 (1.20)	1.439 (1.245)	0.9767 (1.145)	1.865 (1.245)	0.701	1.338
2 (Time)	0.7153 (1.20)	0.7515 (1.245)	0.4874 (1.195)	0.9782 (1.245)	0.681	1.368
TAFT-60 ; Static Eccentricity = 25 %						
Roof (Time)	4.710 (1.20)	8.357 (1.34)	-1.690 (1.54)	9.464 (1.32)	0.359	2.009
7 (Time)	4.117 (1.20)	7.331 (1.34)	-1.421 (1.54)	8.293 (1.34)	0.345	2.014
6 (Time)	3.480 (1.20)	6.255 (1.36)	-1.142 (1.54)	7.061 (1.36)	0.328	2.029
5 (Time)	2.805 (1.20)	5.130 (1.36)	-0.8597 (1.54)	5.792 (1.36)	0.306	2.065
4 (Time)	2.102 (1.20)	3.964 (1.38)	-0.5863 (1.54)	4.474 (1.38)	0.279	2.128
3 (Time)	1.394 (1.20)	2.765 (1.38)	-0.3396 (1.54)	3.122 (1.38)	0.244	2.240
2 (Time)	0.7153 (1.20)	1.558 (1.38)	-0.1434 (1.54)	1.760 (1.38)	0.200	2.461

* Note :
CCM Displacement of CM in Concentric Case.
ECM Displacement of CM in Eccentric Case.
EWB Displacement of Wall B in Eccentric Case.
EWG Displacement of Wall G in Eccentric Case.

TABLE 5.12 : MAXIMUM LATERAL DISPLACEMENTS FOR THE NONLINEAR INELASTIC CASE (TAFT-60, 0-2 Seconds)

Floor	1.LEB* (in)	2.LEG* (in)	3.EWB* (in)	4.EWG* (in)	Ratio (3)/(1)	Ratio (4)/(2)
TAFT-18 ; Static Eccentricity = 5 %						
Roof (Time)	1.275 (1.90)	1.819 (1.95)	1.381 (1.88)	-1.788 (1.62)	1.083	0.983
7 (Time)	1.080 (1.90)	1.534 (2.00)	1.160 (1.88)	-1.503 (1.62)	1.074	0.980
6 (Time)	0.8693 (1.90)	1.268 (2.00)	0.9258 (1.90)	-1.199 (1.60)	1.065	0.946
5 (Time)	0.6511 (1.90)	0.9805 (2.00)	0.6883 (1.90)	-0.8969 (1.60)	1.057	0.915
4 (Time)	0.4376 (1.90)	0.6825 (2.00)	0.4590 (1.90)	-0.6186 (1.56)	1.049	0.906
3 (Time)	0.2459 (1.90)	0.3977 (2.00)	0.2590 (1.92)	-0.3686 (1.56)	1.053	0.927
2 (Time)	-0.0971 (1.50)	0.1610 (2.00)	-0.1049 (1.52)	-0.1577 (1.56)	1.080	0.980
TAFT-18 ; Static Eccentricity = 25 %						
Roof (Time)	0.3243 (1.70)	-2.855 (1.70)	0.4160 (1.70)	2.447 (1.22)	1.283	0.857
7 (Time)	-0.2691 (1.55)	-2.423 (1.70)	-0.3493 (1.54)	2.067 (1.22)	1.298	0.853
6 (Time)	-0.2204 (1.55)	-1.957 (1.70)	-0.2840 (1.54)	1.665 (1.22)	1.289	0.851
5 (Time)	-0.1685 (1.55)	-1.475 (1.70)	-0.2158 (1.54)	1.277 (1.26)	1.281	0.866
4 (Time)	-0.1160 (1.55)	-0.9985 (1.70)	-0.1479 (1.54)	0.9202 (1.28)	1.275	0.922
3 (Time)	-0.0671 (1.55)	-0.5656 (1.70)	-0.0853 (1.54)	0.5787 (1.30)	1.271	1.023
2 (Time)	-0.0271 (1.55)	-0.2220 (1.70)	-0.0347 (1.54)	0.2743 (1.30)	1.280	1.236

* Note :

LEB Displacement of Wall B in Linear Elastic Eccentric Case.
LEG Displacement of Wall G in Linear Elastic Eccentric Case.
EWB Displacement of Wall B in Nonlinear Eccentric Case.
EWG Displacement of Wall G in Nonlinear Eccentric Case.

TABLE 5.13 : MAXIMUM LATERAL DISPLACEMENTS (Linear vs. Nonlinear, TAFT-18, 0-2 Seconds)

Floor	1.LEB* (in)	2.LEG* (in)	3.EWB* (in)	4.EWG* (in)	Ratio (3)/(1)	Ratio (4)/(2)
TAFT-40 ; Static Eccentricity = 5 %						
Roof (Time)	2.885 (1.90)	4.117 (1.95)	-2.128 (1.60)	3.596 (1.20)	0.738	0.873
7 (Time)	2.444 (1.90)	3.470 (2.00)	-1.820 (1.60)	3.123 (1.20)	0.745	0.900
6 (Time)	1.967 (1.90)	2.868 (2.00)	-1.490 (1.60)	2.615 (1.20)	0.757	0.912
5 (Time)	1.473 (1.90)	2.218 (2.00)	-1.186 (1.545)	2.081 (1.20)	0.805	0.938
4 (Time)	0.9901 (1.90)	1.544 (2.00)	-0.8808 (1.545)	1.531 (1.20)	0.890	0.992
3 (Time)	0.5563 (1.90)	0.8997 (2.00)	-0.5653 (1.545)	0.9930 (1.25)	1.016	1.104
2 (Time)	-0.2196 (1.50)	0.3641 (2.00)	-0.2699 (1.545)	0.5052 (1.25)	1.229	1.388
TAFT-40 ; Static Eccentricity = 25 %						
Roof (Time)	0.7337 (1.70)	-6.459 (1.70)	-1.083 (1.54)	6.210 (1.28)	1.476	0.961
7 (Time)	-0.6087 (1.55)	-5.480 (1.70)	-0.9126 (1.54)	5.383 (1.30)	1.499	0.982
6 (Time)	-0.4987 (1.55)	-4.428 (1.70)	-0.7343 (1.54)	4.535 (1.32)	1.472	1.024
5 (Time)	-0.3813 (1.55)	-3.336 (1.70)	-0.5524 (1.54)	3.666 (1.32)	1.449	1.099
4 (Time)	-0.2625 (1.55)	-2.259 (1.70)	-0.3748 (1.54)	2.759 (1.34)	1.428	1.221
3 (Time)	-0.1517 (1.55)	-1.280 (1.70)	-0.2140 (1.54)	1.849 (1.34)	1.411	1.445
2 (Time)	-0.0614 (1.55)	-0.5022 (1.70)	-0.0866 (1.54)	0.9648 (1.34)	1.410	1.921

* Note :

LEB Displacement of Wall B in Linear Elastic Eccentric Case.
LEG Displacement of Wall G in Linear Elastic Eccentric Case.
EWB Displacement of Wall B in Nonlinear Eccentric Case.
EWG Displacement of Wall G in Nonlinear Eccentric Case.

TABLE 5.14 : MAXIMUM LATERAL DISPLACEMENTS (Linear vs. Nonlinear, TAFT-40, 0-2 Seconds)

Floor	1.LEB* (in)	2.LEG* (in)	3.EWB* (in)	4.EWG* (in)	Ratio (3)/(1)	Ratio (4)/(2)
TAFT-60 ; Static Eccentricity = 5 %						
Roof (Time)	4.328 (1.90)	6.174 (1.95)	-3.671 (1.645)	6.096 (1.195)	0.848	0.987
7 (Time)	3.666 (1.90)	5.206 (2.00)	-3.134 (1.645)	5.302 (1.245)	0.855	1.018
6 (Time)	2.950 (1.90)	4.302 (2.00)	-2.565 (1.645)	4.506 (1.245)	0.869	1.047
5 (Time)	2.210 (1.90)	3.328 (2.00)	2.030 (1.145)	3.660 (1.245)	0.919	1.100
4 (Time)	1.485 (1.90)	2.316 (2.00)	1.502 (1.145)	2.771 (1.245)	1.011	1.196
3 (Time)	0.8345 (1.90)	1.350 (2.00)	0.9767 (1.145)	1.865 (1.245)	1.170	1.381
2 (Time)	-0.3294 (1.50)	0.5462 (2.00)	0.4874 (1.195)	0.9782 (1.245)	1.480	1.791
TAFT-60 ; Static Eccentricity = 25 %						
Roof (Time)	1.101 (1.70)	-9.689 (1.70)	-1.690 (1.54)	9.464 (1.32)	1.535	0.977
7 (Time)	-0.9131 (1.55)	-8.220 (1.70)	-1.421 (1.54)	8.293 (1.34)	1.556	1.009
6 (Time)	-0.7481 (1.55)	-6.642 (1.70)	-1.142 (1.54)	7.061 (1.36)	1.527	1.063
5 (Time)	-0.5720 (1.55)	-5.004 (1.70)	-0.8597 (1.54)	5.792 (1.36)	1.503	1.157
4 (Time)	-0.3938 (1.55)	-3.389 (1.70)	-0.5863 (1.54)	4.474 (1.38)	1.489	1.320
3 (Time)	-0.2276 (1.55)	-1.919 (1.70)	-0.3396 (1.54)	3.122 (1.38)	1.492	1.627
2 (Time)	-0.0921 (1.55)	-0.7533 (1.70)	-0.1434 (1.54)	1.760 (1.38)	1.557	2.336

* Note :
LEB Displacement of Wall B in Linear Elastic Eccentric Case.
LEG Displacement of Wall G in Linear Elastic Eccentric Case.
EWB Displacement of Wall B in Nonlinear Eccentric Case.
EWG Displacement of Wall G in Nonlinear Eccentric Case.

TABLE 5.15 : MAXIMUM LATERAL DISPLACEMENTS (Linear vs. Nonlinear, TAFT-60, 0-2 Seconds)

Story	1.CCM* (%)	2.EWB* (%)	3.EWG* (%)	Ratio (2)/(1)	Ratio (3)/(1)
TAFT-18 ; Static Eccentricity = 5 %					
7 (Time)	0.2133 (1.90)	0.1876 (1.88)	-0.2413 (1.62)	0.880	1.131
6 (Time)	0.2284 (1.90)	0.2008 (1.88)	-0.2579 (1.62)	0.879	1.129
5 (Time)	0.2313 (1.90)	0.2038 (1.88)	-0.2612 (1.62)	0.881	1.129
4 (Time)	0.2246 (1.95)	0.1949 (1.88)	-0.2488 (1.62)	0.868	1.108
3 (Time)	0.2044 (1.95)	0.1721 (1.90)	-0.2185 (1.60)	0.842	1.069
2 (Time)	0.1635 (1.95)	0.1330 (1.90)	-0.1786 (1.56)	0.813	1.092
1 (Time)	0.0880 (2.00)	-0.0711 (1.52)	-0.1068 (1.56)	0.808	1.214
TAFT-18 ; Static Eccentricity = 25 %					
7 (Time)	0.2133 (1.90)	0.0579 (1.70)	0.3245 (1.20)	0.271	1.521
6 (Time)	0.2284 (1.90)	0.0599 (1.70)	0.3437 (1.20)	0.262	1.505
5 (Time)	0.2313 (1.90)	0.0602 (1.70)	0.3479 (1.20)	0.260	1.504
4 (Time)	0.2246 (1.95)	0.0577 (1.70)	0.3340 (1.20)	0.257	1.487
3 (Time)	0.2044 (1.95)	-0.0530 (1.54)	0.2981 (1.22)	0.259	1.458
2 (Time)	0.1635 (1.95)	-0.0429 (1.54)	0.2589 (1.28)	0.262	1.583
1 (Time)	0.0880 (2.00)	-0.0235 (1.54)	0.1859 (1.30)	0.267	2.113

* Note :
CCM IDI of CM in Concentric Case.
EWB IDI of Wall B in Eccentric Case.
EWG IDI of Wall G in Eccentric Case.

TABLE 5.16 : MAXIMUM INTER-STORY DRIFT INDICES FOR THE NONLINEAR INELASTIC CASE (TAFT-18, 0-2 Seconds)

Story	1.CCM* (%)	2.EWB* (%)	3.EWG* (%)	Ratio (2)/(1)	Ratio (3)/(1)
TAFT-40 ; Static Eccentricity = 5 %					
7 (Time)	-0.3195 (1.65)	0.2885 (1.90)	0.4293 (1.15)	0.903	1.344
6 (Time)	-0.3438 (1.65)	0.3081 (1.90)	0.4565 (1.15)	0.896	1.328
5 (Time)	-0.3550 (1.65)	0.3131 (1.90)	0.4689 (1.15)	0.882	1.321
4 (Time)	0.3618 (1.15)	0.2988 (1.90)	0.4656 (1.20)	0.826	1.287
3 (Time)	0.3508 (1.15)	-0.2671 (1.545)	0.4575 (1.20)	0.761	1.304
2 (Time)	0.3192 (1.20)	-0.2502 (1.545)	0.4220 (1.20)	0.784	1.322
1 (Time)	0.2458 (1.20)	-0.1829 (1.545)	0.3423 (1.25)	0.744	1.393
TAFT-40 ; Static Eccentricity = 25 %					
7 (Time)	-0.3195 (1.65)	-0.1439 (1.54)	0.7375 (1.24)	0.450	2.308
6 (Time)	-0.3438 (1.65)	-0.1510 (1.54)	0.7739 (1.24)	0.439	2.251
5 (Time)	-0.3550 (1.65)	-0.1541 (1.54)	0.7902 (1.26)	0.434	2.226
4 (Time)	0.3618 (1.15)	-0.1504 (1.54)	0.7829 (1.26)	0.416	2.164
3 (Time)	0.3508 (1.15)	-0.1362 (1.54)	0.7761 (1.32)	0.388	2.212
2 (Time)	0.3192 (1.20)	-0.1079 (1.54)	0.7493 (1.32)	0.338	2.347
1 (Time)	0.2458 (1.20)	-0.0586 (1.54)	0.6537 (1.34)	0.238	2.659

* Note :
CCM IDI of CM in Concentric Case.
EWB IDI of Wall B in Eccentric Case.
EWG IDI of Wall G in Eccentric Case.

TABLE 5.17 : MAXIMUM INTER-STORY DRIFT INDICES FOR THE NONLINEAR INELASTIC CASE (TAFT-40, 0-2 Seconds)

Story	1.CCM* (%)	2.EWB* (%)	3.EWG* (%)	Ratio (2)/(1)	Ratio (3)/(1)
TAFT-60 ; Static Eccentricity = 5 %					
7 (Time)	0.5202 (1.15)	-0.4542 (1.645)	0.6945 (1.195)	0.873	1.335
6 (Time)	0.5577 (1.15)	-0.4826 (1.645)	0.7360 (1.195)	0.865	1.320
5 (Time)	0.5840 (1.15)	-0.4931 (1.645)	0.7631 (1.195)	0.844	1.307
4 (Time)	0.5958 (1.20)	-0.4833 (1.645)	0.7725 (1.195)	0.811	1.297
3 (Time)	0.5996 (1.20)	-0.4483 (1.645)	0.7672 (1.245)	0.748	1.280
2 (Time)	0.5745 (1.20)	0.4147 (1.145)	0.7514 (1.245)	0.722	1.308
1 (Time)	0.4846 (1.20)	0.3302 (1.195)	0.6627 (1.245)	0.681	1.368
TAFT-60 ; Static Eccentricity = 25 %					
7 (Time)	0.5202 (1.15)	-0.2280 (1.54)	1.083 (1.26)	0.438	2.082
6 (Time)	0.5577 (1.15)	-0.2364 (1.54)	1.132 (1.26)	0.424	2.030
5 (Time)	0.5840 (1.15)	-0.2391 (1.54)	1.153 (1.28)	0.409	1.974
4 (Time)	0.5958 (1.20)	-0.2315 (1.54)	1.160 (1.30)	0.389	1.947
3 (Time)	0.5996 (1.20)	-0.2089 (1.54)	1.161 (1.34)	0.348	1.936
2 (Time)	0.5745 (1.20)	-0.1662 (1.54)	1.153 (1.38)	0.289	2.007
1 (Time)	0.4846 (1.20)	-0.0972 (1.54)	1.193 (1.38)	0.201	2.462

* Note :
CCM IDI of CM in Concentric Case.
EWB IDI of Wall B in Eccentric Case.
EWG IDI of Wall G in Eccentric Case.

TABLE 5.18 : MAXIMUM INTER-STORY DRIFT INDICES FOR THE NONLINEAR INELASTIC CASE (TAFT-60, 0-2 Seconds)

Story	1.LEB* (%)	2.LEG* (%)	3.EWB* (%)	4.EWG* (%)	Ratio (3)/(1)	Ratio (4)/(2)
TAFT-18 ; Static Eccentricity = 5 %						
7 (Time)	0.1652 (1.90)	0.2461 (1.95)	0.1876 (1.88)	-0.2413 (1.62)	1.136	0.980
6 (Time)	0.1787 (1.90)	0.2629 (1.95)	0.2008 (1.88)	-0.2579 (1.62)	1.124	0.981
5 (Time)	0.1848 (1.90)	0.2665 (1.95)	0.2038 (1.88)	-0.2612 (1.62)	1.103	0.980
4 (Time)	0.1808 (1.90)	0.2549 (1.95)	0.1949 (1.88)	-0.2488 (1.62)	1.078	0.976
3 (Time)	0.1624 (1.90)	0.2412 (2.00)	0.1721 (1.90)	-0.2185 (1.60)	1.060	0.906
2 (Time)	0.1272 (1.90)	0.2005 (2.00)	0.1330 (1.90)	-0.1786 (1.56)	1.046	0.891
1 (Time)	-0.0658 (1.50)	0.1090 (2.00)	-0.0711 (1.52)	-0.1068 (1.56)	1.081	0.980
TAFT-18 ; Static Eccentricity = 25 %						
7 (Time)	0.0469 (1.70)	-0.3665 (1.70)	0.0579 (1.70)	0.3245 (1.20)	1.235	0.885
6 (Time)	0.0478 (1.70)	-0.3939 (1.70)	0.0599 (1.70)	0.3437 (1.20)	1.253	0.873
5 (Time)	0.0474 (1.70)	-0.4086 (1.70)	0.0602 (1.70)	0.3479 (1.20)	1.270	0.851
4 (Time)	0.0449 (1.70)	-0.4032 (1.70)	0.0577 (1.70)	0.3340 (1.20)	1.285	0.828
3 (Time)	-0.0415 (1.55)	-0.3666 (1.70)	-0.0530 (1.54)	0.2981 (1.22)	1.277	0.813
2 (Time)	-0.0338 (1.55)	-0.2910 (1.70)	-0.0429 (1.54)	0.2589 (1.28)	1.269	0.890
1 (Time)	-0.0184 (1.55)	-0.1504 (1.70)	-0.0235 (1.54)	0.1859 (1.30)	1.277	1.236

* Note :
LEB IDI of Wall B in Linear Elastic Eccentric Case.
LEG IDI of Wall G in Linear Elastic Eccentric Case.
EWB IDI of Wall B in Nonlinear Eccentric Case.
EWG IDI of Wall G in Nonlinear Eccentric Case.

TABLE 5.19 : MAXIMUM INTER-STORY DRIFT INDICES
(Linear vs. Nonlinear, TAFT-18, 0-2 Seconds)

Story	1.LEB* (%)	2.LEG* (%)	3.EWB* (%)	4.EWG* (%)	Ratio (3)/(1)	Ratio (4)/(2)
TAFT-40 ; Static Eccentricity = 5 %						
7 (Time)	0.3737 (1.90)	0.5569 (1.95)	0.2885 (1.90)	0.4293 (1.15)	0.772	0.771
6 (Time)	0.4042 (1.90)	0.5949 (1.95)	0.3081 (1.90)	0.4565 (1.15)	0.762	0.767
5 (Time)	0.4181 (1.90)	0.6029 (1.95)	0.3131 (1.90)	0.4689 (1.15)	0.749	0.778
4 (Time)	0.4090 (1.90)	0.5768 (1.95)	0.2988 (1.90)	0.4656 (1.20)	0.731	0.807
3 (Time)	0.3674 (1.90)	0.5458 (2.00)	-0.2671 (1.545)	0.4575 (1.20)	0.727	0.838
2 (Time)	0.2878 (1.90)	0.4536 (2.00)	-0.2502 (1.545)	0.4220 (1.20)	0.869	0.930
1 (Time)	-0.1488 (1.50)	0.2467 (2.00)	-0.1829 (1.545)	0.3423 (1.25)	1.229	1.388
TAFT-40 ; Static Eccentricity = 25 %						
7 (Time)	0.1060 (1.70)	-0.8292 (1.70)	-0.1439 (1.54)	0.7375 (1.24)	1.358	0.889
6 (Time)	0.1081 (1.70)	-0.8912 (1.70)	-0.1510 (1.54)	0.7739 (1.24)	1.397	0.868
5 (Time)	0.1073 (1.70)	-0.9244 (1.70)	-0.1541 (1.54)	0.7902 (1.26)	1.436	0.885
4 (Time)	0.1016 (1.70)	-0.9122 (1.70)	-0.1504 (1.54)	0.7829 (1.26)	1.480	0.858
3 (Time)	-0.0938 (1.55)	-0.8295 (1.70)	-0.1362 (1.54)	0.7761 (1.32)	1.452	0.936
2 (Time)	-0.0765 (1.55)	-0.6583 (1.70)	-0.1079 (1.54)	0.7493 (1.32)	1.410	1.138
1 (Time)	-0.0416 (1.55)	-0.3402 (1.70)	-0.0586 (1.54)	0.6537 (1.34)	1.409	1.922

* Note :
LEB IDI of Wall B in Linear Elastic Eccentric Case.
LEG IDI of Wall G in Linear Elastic Eccentric Case.
EWB IDI of Wall B in Nonlinear Eccentric Case.
EWG IDI of Wall G in Nonlinear Eccentric Case.

TABLE 5.20 : MAXIMUM INTER-STORY DRIFT INDICES (Linear vs. Nonlinear, TAFT-40, 0-2 Seconds)

Story	1.LEB* (%)	2.LEG* (%)	3.EWB* (%)	4.EWG* (%)	Ratio (3)/(1)	Ratio (4)/(2)
TAFT-60 ; Static Eccentricity = 5 %						
7 (Time)	0.5606 (1.90)	0.8354 (1.95)	-0.4542 (1.645)	0.6945 (1.195)	0.810	0.831
6 (Time)	0.6063 (1.90)	0.8924 (1.95)	-0.4826 (1.645)	0.7360 (1.195)	0.796	0.825
5 (Time)	0.6272 (1.90)	0.9044 (1.95)	-0.4931 (1.645)	0.7631 (1.195)	0.786	0.844
4 (Time)	0.6135 (1.90)	0.8652 (1.95)	-0.4833 (1.645)	0.7725 (1.195)	0.788	0.893
3 (Time)	0.5511 (1.90)	0.8187 (2.00)	-0.4483 (1.645)	0.7672 (1.245)	0.813	0.937
2 (Time)	0.4317 (1.90)	0.6804 (2.00)	0.4147 (1.145)	0.7514 (1.245)	0.961	1.104
1 (Time)	-0.2232 (1.50)	0.3701 (2.00)	0.3302 (1.195)	0.6627 (1.245)	1.479	1.791
TAFT-60 ; Static Eccentricity = 25 %						
7 (Time)	0.1590 (1.70)	-1.244 (1.70)	-0.2280 (1.54)	1.083 (1.26)	1.434	0.871
6 (Time)	0.1622 (1.70)	-1.337 (1.70)	-0.2364 (1.54)	1.132 (1.26)	1.457	0.847
5 (Time)	0.1610 (1.70)	-1.387 (1.70)	-0.2391 (1.54)	1.153 (1.28)	1.485	0.831
4 (Time)	0.1524 (1.70)	-1.368 (1.70)	-0.2315 (1.54)	1.160 (1.30)	1.519	0.848
3 (Time)	-0.1407 (1.55)	-1.244 (1.70)	-0.2089 (1.54)	1.161 (1.34)	1.485	0.933
2 (Time)	-0.1148 (1.55)	-0.9875 (1.70)	-0.1662 (1.54)	1.153 (1.38)	1.448	1.168
1 (Time)	-0.0624 (1.55)	-0.5103 (1.70)	-0.0972 (1.54)	1.193 (1.38)	1.558	2.338

* Note :
LEB IDI of Wall B in Linear Elastic Eccentric Case.
LEG IDI of Wall G in Linear Elastic Eccentric Case.
EWB IDI of Wall B in Nonlinear Eccentric Case.
EWG IDI of Wall G in Nonlinear Eccentric Case.

TABLE 5.21 : MAXIMUM INTER-STORY DRIFT INDICES (Linear vs. Nonlinear, TAFT-60, 0-2 Seconds)

Location	e/D*	Maximum Values of Plastic Rotation (radians)		
		TAFT-18	TAFT-40	TAFT-60
1.One Wall	0.00	0.000062	0.001532	0.003819
2.Wall B	0.05	0.00	-0.000874	0.002415
3.Wall B	0.25	0.00	0.00	-0.000101
4.Wall G	0.05	-0.000196	0.002456	0.005585
5.Wall G	0.25	0.000940	0.005433	0.010608
Ratio (2)/(1)		0.00	0.57	0.63
Ratio (3)/(1)		0.00	0.00	0.03
Ratio (4)/(1)		3.18	1.60	1.46
Ratio (5)/(1)		15.22	3.55	2.78

* Note :
e/D Initial Static Eccentricity Ratio.

TABLE 5.22 : MAXIMUM PLASTIC HINGE ROTATION (Radians) AT BASE OF WALLS (0-2 Seconds)

Story	1.CSW* (kips)	2.ESWG* (kips)	3.ESWB* (kips)	Ratio (2)/(1)	Ratio (3)/(1)
TAFT-18 ; Static Eccentricity = 5 %					
7 (Time)	-87.46 (2.00)	112.07 (1.54)	84.59 (1.52)	1.28	0.97
6 (Time)	178.44 (1.90)	209.48 (1.94)	149.81 (1.88)	1.17	0.84
5 (Time)	264.31 (1.90)	289.03 (1.94)	226.00 (1.88)	1.09	0.86
4 (Time)	310.82 (1.90)	342.17 (1.98)	275.59 (1.90)	1.10	0.89
3 (Time)	378.43 (1.95)	-426.83 (1.54)	311.38 (1.92)	1.13	0.82
2 (Time)	469.84 (2.00)	-550.61 (1.52)	-415.21 (1.52)	1.17	0.88
1 (Time)	554.33 (2.00)	-652.84 (1.52)	-517.57 (1.52)	1.18	0.93
TAFT-18 ; Static Eccentricity = 25 %					
7 (Time)	-87.46 (2.00)	-152.85 (1.06)	-27.51 (1.12)	1.75	0.31
6 (Time)	178.44 (1.90)	-266.48 (1.64)	39.79 (1.70)	1.49	0.22
5 (Time)	264.31 (1.90)	-343.19 (1.64)	59.38 (1.70)	1.30	0.22
4 (Time)	310.82 (1.90)	412.82 (1.18)	-80.53 (1.54)	1.33	0.26
3 (Time)	378.43 (1.95)	450.36 (1.06)	-101.42 (1.54)	1.19	0.27
2 (Time)	469.84 (2.00)	628.27 (1.04)	-118.60 (1.54)	1.34	0.25
1 (Time)	554.33 (2.00)	777.49 (1.02)	-151.64 (1.54)	1.40	0.27

* Note :
CSW Story Shear of One Wall in Concentric Case.
ESWB Story Shear of Wall B in Eccentric Case.
ESWG Story Shear of Wall G in Eccentric Case.

TABLE 5.23 : MAXIMUM STORY SHEAR FORCES OF WALLS FOR THE NONLINEAR INELASTIC CASE (TAFT-18, 0-2 Seconds)

Story	1.CSW* (kips)	2.ESWG* (kips)	3.ESWB* (kips)	Ratio (2)/(1)	Ratio (3)/(1)
TAFT-40 ; Static Eccentricity = 5 %					
7 (Time)	164.50 (1.55)	-190.46 (1.25)	147.53 (1.545)	1.16	0.90
6 (Time)	262.64 (1.90)	230.95 (1.95)	221.2 (1.90)	0.88	0.84
5 (Time)	369.89 (1.90)	-344.79 (1.70)	347.17 (1.90)	0.93	0.94
4 (Time)	406.08 (1.90)	-432.39 (1.70)	417.17 (1.90)	1.06	1.03
3 (Time)	-501.37 (1.55)	517.68 (1.20)	-464.47 (1.545)	1.03	0.93
2 (Time)	-662.61 (1.55)	723.7 (1.00)	-640.12 (1.545)	1.09	0.97
1 (Time)	852.70 (1.00)	985.58 (1.00)	-746.66 (1.545)	1.16	0.88
TAFT-40 ; Static Eccentricity = 25 %					
7 (Time)	164.50 (1.55)	-368.36 (1.34)	-69.88 (1.38)	2.24	0.42
6 (Time)	262.64 (1.90)	-444.39 (1.62)	-88.21 (1.24)	1.69	0.34
5 (Time)	369.89 (1.90)	-493.06 (1.66)	-148.21 (1.54)	1.33	0.40
4 (Time)	406.08 (1.90)	548.49 (1.24)	-203.17 (1.54)	1.35	0.50
3 (Time)	-501.37 (1.55)	661.22 (1.34)	-249.55 (1.54)	1.32	0.50
2 (Time)	-662.61 (1.55)	878.81 (1.06)	-280.02 (1.54)	1.33	0.42
1 (Time)	852.70 (1.00)	1078.0 (1.06)	-377.86 (1.52)	1.26	0.44

* Note :
CSW Story Shear of One Wall in Concentric Case.
ESWB Story Shear of Wall B in Eccentric Case.
ESWG Story Shear of Wall G in Eccentric Case.

TABLE 5.24 : MAXIMUM STORY SHEAR FORCES OF WALLS FOR THE NONLINEAR INELASTIC CASE (TAFT-40, 0-2 Seconds)

Story	1.CSW* (kips)	2.ESWG* (kips)	3.ESWB* (kips)	Ratio (2)/(1)	Ratio (3)/(1)
TAFT-60 ; Static Eccentricity = 5 %					
7 (Time)	-272.39 (1.20)	-359.63 (1.295)	-223.98 (1.145)	1.32	0.82
6 (Time)	394.68 (1.945)	353.68 (0.895)	333.01 (1.895)	0.90	0.84
5 (Time)	450.40 (1.945)	-436.36 (1.695)	440.26 (1.895)	0.97	0.98
4 (Time)	-484.51 (1.645)	534.98 (1.145)	462.6 (1.895)	1.10	0.95
3 (Time)	-585.58 (1.545)	611.02 (1.245)	-552.87 (1.545)	1.04	0.94
2 (Time)	-848.13 (1.545)	904.60 (0.995)	-775.81 (1.545)	1.07	0.91
1 (Time)	1079.4 (1.00)	1217.5 (0.995)	-870.63 (1.545)	1.13	0.81
TAFT-60 ; Static Eccentricity = 25 %					
7 (Time)	-272.39 (1.20)	-520.58 (1.42)	-108.66 (1.38)	1.91	0.40
6 (Time)	394.68 (1.945)	-538.28 (1.64)	-140.6 (1.54)	1.36	0.36
5 (Time)	450.40 (1.945)	-622.31 (1.66)	-222.97 (1.54)	1.38	0.50
4 (Time)	-484.51 (1.645)	685.48 (1.24)	-295.3 (1.54)	1.41	0.61
3 (Time)	-585.58 (1.545)	808.34 (1.34)	-360.59 (1.52)	1.38	0.62
2 (Time)	-848.13 (1.545)	1222.7 (1.38)	-398.45 (1.52)	1.44	0.47
1 (Time)	1079.4 (1.00)	1307.6 (1.06)	-588.71 (1.52)	1.21	0.55

* Note :
CSW Story Shear of One Wall in Concentric Case.
ESWB Story Shear of Wall B in Eccentric Case.
ESWG Story Shear of Wall G in Eccentric Case.

TABLE 5.25 : MAXIMUM STORY SHEAR FORCES OF WALLS FOR THE NONLINEAR INELASTIC CASE (TAFT-60, 0-2 Seconds)

Story	7	6	5	4	3	2	1
TAFT-18							
1.CN* Time	397.54 1.90	731.16 1.90	928.06 1.90	1006.7 1.95	1113.1 1.95	1217.1 2.00	1271.7 2.00
2.E05* Time	-361.60 1.60	648.94 1.92	828.39 1.92	901.46 1.92	-1040.4 1.54	-1222.9 1.52	-1329.3 1.52
3.E25* Time	-264.47 1.62	-456.63 1.62	580.21 1.16	638.66 1.18	737.05 1.06	897.55 1.04	1006.3 1.04
(2)/(1)	0.91	0.89	0.89	0.90	0.93	1.00	1.05
(3)/(1)	0.67	0.62	0.63	0.63	0.66	0.74	0.79
TAFT-40							
1.CN* Time	546.63 1.95	970.75 1.95	-1230.9 1.65	-1392.5 1.65	1540.6 1.15	-1749.6 1.55	2015.1 1.00
2.E05* Time	-434.47 1.65	-804.14 1.65	1100.9 1.15	1331.4 1.15	1492.0 1.15	-1669.0 1.545	2002.6 1.00
3.E25* Time	386.64 1.22	684.46 1.22	846.21 1.24	1065.4 1.34	1323.5 1.34	1473.6 1.08	1729.8 1.06
(2)/(1)	0.79	0.83	0.89	0.96	0.97	0.95	0.99
(3)/(1)	0.71	0.71	0.69	0.77	0.86	0.84	0.86
TAFT-60							
1.CN* Time	755.34 1.945	-1339.6 1.645	-1680.2 1.645	1895.8 1.15	2103.6 1.20	2375.8 1.20	2753.5 1.00
2.E05* Time	609.45 1.145	1177.0 1.145	1590.1 1.145	1852.8 1.145	2063.8 1.195	2193.1 1.195	2590.3 0.995
3.E25* Time	553.25 1.52	917.51 1.26	1148.0 1.32	1505.7 1.34	1783.0 1.34	2155.3 1.38	2380.7 1.38
(2)/(1)	0.81	0.88	0.95	0.98	0.98	0.92	0.94
(3)/(1)	0.73	0.68	0.68	0.79	0.85	0.91	0.86

* Note :
CN Total Story Shear Force (kips) for Concentric Case.
E05 Total Story Shear Force (kips) for 5% eccentricity.
E25 Total Story Shear Force (kips) for 25% eccentricity.

TABLE 5.26 : MAXIMUM TOTAL STORY SHEAR FORCES FOR THE NONLINEAR INELASTIC CASE (0-2 Seconds)

Story	7	6	5	4	3	2	1
TAFT-18							
TE05* Time	75901 1.66	132540 1.66	163115 1.68	185596 1.72	233120 1.74	269194 1.74	283375 1.74
TE25* Time	152191 1.64	268553 1.64	-347243 1.20	388668 1.68	422190 1.70	452369 1.74	466763 1.74
Td05*	1.99	1.89	1.83	1.92	2.18	2.30	2.32
Td25*	0.845	0.811	0.826	0.852	0.837	0.820	0.810
TAFT-40							
TE05* Time	150249 1.85	257540 1.85	298699 1.85	388690 1.80	467159 1.80	504897 1.80	498475 1.80
TE25* Time	-260632 1.22	-478514 1.24	-618762 1.24	-680598 1.24	-678555 1.24	-713708 1.30	-728861 1.30
Td05*	2.86	2.76	2.53	2.91	3.16	3.01	2.58
Td25*	1.05	1.09	1.11	1.08	0.97	0.90	0.80
TAFT-60							
TE05* Time	181363 1.845	337098 1.845	427729 1.845	461829 1.845	560916 1.795	642501 1.795	664538 1.795
TE25* Time	-407681 1.52	-666145 1.24	-850788 1.24	-911698 1.24	-874811 1.24	-895622 1.38	-1014778 1.40
Td05*	2.50	2.62	2.65	2.54	2.78	2.82	2.51
Td25*	1.19	1.10	1.12	1.06	0.92	0.83	0.81

* Note :
TE05 Story Torque (k-in) for 5% eccentricity.
TE25 Story Torque (k-in) for 25% eccentricity.
Td05 Dynamic Amplification of Eccentricity for 5% Eccentricity.
Td25 Dynamic Amplification of Eccentricity for 25% Eccentricity.

TABLE 5.27 : MAXIMUM TOTAL STORY TORQUES AND VALUES OF DYNAMIC AMPLIFICATION OF ECCENTRICITY FOR THE NONLINEAR INELASTIC CASE (0-2 Seconds)

Story	7	6	5	4	3	2	1
TAFT-18							
WT05* Time	-33243 1.74	81003 1.84	104493 1.68	128793 1.72	177982 1.74	221383 1.74	251810 1.74
WT25* Time	75851 1.06	169564 1.64	221953 1.66	275983 1.68	317543 1.70	366089 1.74	407168 1.74
R1*	0.44	0.61	0.64	0.69	0.76	0.82	0.89
R2*	0.50	0.63	0.64	0.71	0.75	0.81	0.87
TAFT-40							
WT05* Time	87085 1.25	148832 1.85	185498 1.85	274020 1.80	356381 1.80	408262 1.80	441660 1.80
WT25* Time	178031 1.34	267432 1.64	-342470 1.24	-411771 1.24	-421925 1.24	-500053 1.30	-482531 1.06
R1*	0.58	0.58	0.62	0.70	0.76	0.81	0.89
R2*	0.68	0.56	0.55	0.61	0.62	0.70	0.66
TAFT-60							
WT05* Time	140520 1.495	190696 1.845	271279 1.845	313106 1.845	442180 1.795	543474 1.795	599472 1.795
WT25* Time	253012 1.44	350666 1.68	-464119 1.24	-536681 1.24	-524359 1.22	-628446 1.38	-545716 1.40
R1*	0.77	0.57	0.63	0.68	0.79	0.85	0.90
R2*	0.62	0.53	0.55	0.59	0.60	0.70	0.54

* Note :

WT05 Story Torque (k-in) Resisted by Walls for 5% eccentricity.
WT25 Story Torque (k-in) Resisted by Walls for 25% eccentricity.
R1 Ratio of WT05 to Maximum Story Torque.
R2 Ratio of WT25 to Maximum Story Torque.

TABLE 5.28 : MAXIMUM STORY TORQUES RESISTED BY WALLS FOR THE NONLINEAR INELASTIC CASE (0-2 Seconds)

Story	7	6	5	4	3	2	1
LINEAR ELASTIC							
e05*	2.21	2.02	1.97	2.19	2.60	2.77	2.82
e25*	0.99	0.97	1.06	1.19	1.21	1.18	1.14
NONLINEAR INELASTIC ; TAFT-18							
e05*	1.99	1.89	1.83	1.92	2.18	2.30	2.32
e25*	0.845	0.811	0.826	0.852	0.837	0.82	0.81
NONLINEAR INELASTIC ; TAFT-40							
e05*	2.86	2.76	2.53	2.91	3.16	3.01	2.58
e25*	1.05	1.09	1.11	1.08	0.97	0.90	0.80
NONLINEAR INELASTIC ; TAFT-60							
e05*	2.50	2.62	2.65	2.54	2.78	2.82	2.51
e25*	1.19	1.10	1.12	1.06	0.92	0.83	0.81

* Note :
e05 Dynamic Amplification of Eccentricity for 5% Eccentricity.
e25 Dynamic Amplification of Eccentricity for 25% Eccentricity.

TABLE 5.29 : DYNAMIC AMPLIFICATION OF ECCENTRICITY
(Linear vs. Nonlinear, 0-2 Seconds)

Floor	1.CCM* (in)	2.EWG* (in)	3.RWB* (in)	4.RWG* (in)	Ratio (4)/(1)	Ratio (4)/(2)
TAFT-60 ; Static Eccentricity = 5% ; Resistance Eccentricity = 4%						
Roof (Time)	4.710 (1.20)	6.096 (1.195)	-3.517 (1.635)	5.664 (1.195)	1.203	0.929
7 (Time)	4.117 (1.20)	5.302 (1.245)	3.052 (1.175)	4.897 (1.195)	1.189	0.924
6 (Time)	3.480 (1.20)	4.506 (1.245)	2.575 (1.175)	4.085 (1.215)	1.174	0.907
5 (Time)	2.805 (1.20)	3.660 (1.245)	2.066 (1.175)	3.261 (1.215)	1.163	0.891
4 (Time)	2.102 (1.20)	2.771 (1.245)	1.535 (1.175)	2.418 (1.235)	1.150	0.873
3 (Time)	1.394 (1.20)	1.865 (1.245)	1.004 (1.175)	1.593 (1.235)	1.143	0.854
2 (Time)	0.7153 (1.20)	0.9782 (1.245)	0.5047 (1.175)	0.8105 (1.255)	1.133	0.829
TAFT-60 ; Static Eccentricity = 25% ; Resistance Eccentricity = 11%						
Roof (Time)	4.710 (1.20)	9.464 (1.32)	-1.594 (1.535)	9.114 (1.26)	1.935	0.963
7 (Time)	4.117 (1.20)	8.293 (1.34)	-1.347 (1.535)	7.775 (1.26)	1.889	0.938
6 (Time)	3.480 (1.20)	7.061 (1.36)	-1.086 (1.535)	6.425 (1.28)	1.846	0.910
5 (Time)	2.805 (1.20)	5.792 (1.36)	-0.8200 (1.535)	5.096 (1.30)	1.817	0.880
4 (Time)	2.102 (1.20)	4.474 (1.38)	-0.5587 (1.535)	3.743 (1.32)	1.781	0.837
3 (Time)	1.394 (1.20)	3.122 (1.38)	-0.3209 (1.535)	2.430 (1.32)	1.743	0.778
2 (Time)	0.7153 (1.20)	1.760 (1.38)	-0.1307 (1.535)	1.208 (1.32)	1.689	0.686

* Note:
CCM Displacement of CM in Concentric Case.
EWG Displacement of Wall G in Mass Eccentric Case.
RWB Displacement of Wall B in Resistance/Mass Eccentric Case.
RWG Displacement of Wall G in Resistance/Mass Eccentric Case.

TABLE 5.30 : MAXIMUM LATERAL DISPLACEMENTS
Mass Eccentricity vs. Resistance/Mass Eccentricity
(TAFT-60, 0-2 Seconds)

Floor	1.LEB* (in)	2.LEG* (in)	3.RWB* (in)	4.RWG* (in)	Ratio (3)/(1)	Ratio (4)/(2)
TAFT-60 ; Static Eccentricity = 5% ; Resistance Eccentricity = 4%						
Roof (Time)	4.328 (1.90)	6.174 (1.95)	-3.517 (1.635)	5.664 (1.195)	0.813	0.917
7 (Time)	3.666 (1.90)	5.206 (2.00)	-3.052 (1.175)	4.897 (1.195)	0.833	0.941
6 (Time)	2.950 (1.90)	4.302 (2.00)	2.575 (1.175)	4.085 (1.215)	0.873	0.950
5 (Time)	2.210 (1.90)	3.328 (2.00)	2.066 (1.175)	3.261 (1.215)	0.935	0.980
4 (Time)	1.485 (1.90)	2.316 (2.00)	1.535 (1.175)	2.418 (1.235)	1.034	1.044
3 (Time)	0.8345 (1.90)	1.350 (2.00)	1.004 (1.175)	1.593 (1.235)	1.203	1.180
2 (Time)	-0.3294 (1.50)	0.5462 (2.00)	0.5047 (1.175)	0.8105 (1.255)	1.532	1.484
TAFT-60 ; Static Eccentricity = 25% ; Resistance Eccentricity = 11%						
Roof (Time)	1.101 (1.70)	-9.689 (1.70)	-1.594 (1.535)	9.114 (1.26)	1.448	0.941
7 (Time)	-0.9131 (1.55)	-8.220 (1.70)	-1.347 (1.535)	7.775 (1.26)	1.475	0.946
6 (Time)	-0.7481 (1.55)	-6.642 (1.70)	-1.086 (1.535)	6.425 (1.28)	1.452	0.967
5 (Time)	-0.5720 (1.55)	-5.004 (1.70)	-0.8200 (1.535)	5.096 (1.30)	1.434	1.018
4 (Time)	-0.3938 (1.55)	-3.389 (1.70)	-0.5587 (1.535)	3.743 (1.32)	1.419	1.104
3 (Time)	-0.2276 (1.55)	-1.919 (1.70)	-0.3209 (1.535)	2.430 (1.32)	1.410	1.266
2 (Time)	-0.0921 (1.55)	-0.7533 (1.70)	-0.1307 (1.535)	1.208 (1.32)	1.419	1.604

* Note :

LEB Displacement of Wall B in Linear Elastic Eccentric Case.
LEG Displacement of Wall G in Linear Elastic Eccentric Case.
RWB Displacement of Wall B in Resistance/Mass Eccentric Case.
RWG Displacement of Wall G in Resistance/Mass Eccentric Case.

TABLE 5.31 : MAXIMUM LATERAL DISPLACEMENTS (Linear vs. Nonlinear, TAFT-60, 0-2 Seconds)

Story	1.CCM* (%)	2.EWG* (%)	3.RWB* (%)	4.RWG* (%)	Ratio (4)/(1)	Ratio (4)/(2)
TAFT-60 ; Static Eccentricity = 5% ; Resistance Eccentricity = 4%						
7 (Time)	0.5202 (1.15)	0.6945 (1.195)	-0.4413 (1.635)	0.6693 (1.155)	1.287	0.964
6 (Time)	0.5577 (1.15)	0.7360 (1.195)	-0.4693 (1.635)	0.7093 (1.155)	1.272	0.964
5 (Time)	0.5840 (1.15)	0.7631 (1.195)	-0.4773 (1.635)	0.7319 (1.175)	1.253	0.959
4 (Time)	0.5958 (1.20)	0.7725 (1.195)	-0.4638 (1.635)	0.7339 (1.175)	1.232	0.950
3 (Time)	0.5996 (1.20)	0.7672 (1.245)	0.4495 (1.175)	0.7101 (1.195)	1.184	0.926
2 (Time)	0.5745 (1.20)	0.7514 (1.245)	0.4230 (1.175)	0.6628 (1.235)	1.154	0.882
1 (Time)	0.4846 (1.20)	0.6627 (1.245)	0.3419 (1.175)	0.5492 (1.255)	1.133	0.829
TAFT-60 ; Static Eccentricity = 25% ; Resistance Eccentricity = 11%						
7 (Time)	0.5202 (1.15)	1.083 (1.26)	-0.2096 (1.535)	1.179 (1.22)	2.266	1.089
6 (Time)	0.5577 (1.15)	1.132 (1.26)	-0.2205 (1.535)	1.228 (1.22)	2.202	1.085
5 (Time)	0.5840 (1.15)	1.153 (1.28)	-0.2257 (1.535)	1.229 (1.22)	2.104	1.066
4 (Time)	0.5958 (1.20)	1.160 (1.30)	-0.2213 (1.535)	1.189 (1.24)	1.996	1.025
3 (Time)	0.5996 (1.20)	1.161 (1.34)	-0.2014 (1.535)	1.125 (1.30)	1.876	0.969
2 (Time)	0.5745 (1.20)	1.153 (1.38)	-0.1611 (1.535)	1.035 (1.30)	1.802	0.898
1 (Time)	0.4846 (1.20)	1.193 (1.38)	-0.0886 (1.535)	0.8187 (1.32)	1.689	0.686

* Note:
CCM IDI of CM in Concentric Case.
EWG IDI of Wall G in Mass Eccentric Case.
RWB IDI of Wall B in Resistance/Mass Eccentric Case.
RWG IDI of Wall G in Resistance/Mass Eccentric Case.

TABLE 5.32 : MAXIMUM INTER-STORY DRIFT INDICES
Mass Eccentricity vs. Resistance/Mass Eccentricity
(TAFT-60, 0-2 Seconds)

Story	1.LEB* (%)	2.LEG* (%)	3.RWB* (%)	4.RWG* (%)	Ratio (3)/(1)	Ratio (4)/(2)
TAFT-60 ; Static Eccentricity = 5% ; Resistance Eccentricity = 4%						
7 (Time)	0.5606 (1.90)	0.8354 (1.95)	-0.4413 (1.635)	0.6693 (1.155)	0.787	0.801
6 (Time)	0.6063 (1.90)	0.8924 (1.95)	-0.4693 (1.635)	0.7093 (1.155)	0.774	0.795
5 (Time)	0.6272 (1.90)	0.9044 (1.95)	-0.4773 (1.635)	0.7319 (1.175)	0.761	0.809
4 (Time)	0.6135 (1.90)	0.8652 (1.95)	-0.4638 (1.635)	0.7339 (1.175)	0.756	0.848
3 (Time)	0.5511 (1.90)	0.8187 (2.00)	-0.4495 (1.175)	0.7101 (1.195)	0.816	0.867
2 (Time)	0.4317 (1.90)	0.6804 (2.00)	0.4230 (1.175)	0.6628 (1.235)	0.980	0.974
1 (Time)	-0.2232 (1.50)	0.3701 (2.00)	0.3419 (1.175)	0.5492 (1.255)	1.532	1.484
TAFT-60 ; Static Eccentricity = 25% ; Resistance Eccentricity = 11%						
7 (Time)	0.1590 (1.70)	-1.244 (1.70)	-0.2096 (1.535)	1.179 (1.22)	1.318	0.948
6 (Time)	0.1622 (1.70)	-1.337 (1.70)	-0.2205 (1.535)	1.228 (1.22)	1.359	0.918
5 (Time)	0.1610 (1.70)	-1.387 (1.70)	-0.2257 (1.535)	1.229 (1.22)	1.402	0.886
4 (Time)	0.1524 (1.70)	-1.368 (1.70)	-0.2213 (1.535)	1.189 (1.24)	1.452	0.869
3 (Time)	-0.1407 (1.55)	-1.244 (1.70)	-0.2014 (1.535)	1.125 (1.30)	1.431	0.904
2 (Time)	-0.1148 (1.55)	-0.9875 (1.70)	-0.1611 (1.535)	1.035 (1.30)	1.403	1.048
1 (Time)	-0.0624 (1.55)	-0.5103 (1.70)	-0.0886 (1.535)	0.8187 (1.32)	1.420	1.604

* Note :

LEB	IDI of Wall B in Linear Elastic Eccentric Case.
LEG	IDI of Wall G in Linear Elastic Eccentric Case.
RWB	IDI of Wall B in Resistance/Mass Eccentric Case.
RWG	IDI of Wall G in Resistance/Mass Eccentric Case.

TABLE 5.33 : MAXIMUM INTER-STORY DRIFT INDICES
(Linear vs. Nonlinear, TAFT-60, 0-2 Seconds)

Location	e_s*	TAFT-60	e_s*	e_r*	TAFT-60
1.One Wall	0.00	0.003819	0.00	0.00	0.003819
2.Wall B	0.05	0.002416	0.05	0.04	0.002438
3.Wall B	0.25	-0.000101	0.25	0.11	0.000031
4.Wall G	0.05	0.005585	0.05	0.04	0.004106
5.Wall G	0.25	0.010608	0.25	0.11	0.005722
Ratio (2)/(1)		0.63	(2)/(1)		0.64
Ratio (3)/(1)		0.03	(3)/(1)		0.01
Ratio (4)/(1)		1.46	(4)/(1)		1.08
Ratio (5)/(1)		2.78	(5)/(1)		1.50

* Note :
e_s Initial Static Eccentricity Ratio.
e_r Initial Resistance Eccentricity Ratio.

TABLE 5.34 : MAXIMUM PLASTIC HINGE ROTATION (Radians) AT BASE OF WALLS (TAFT-60, 0-2 Seconds) Mass Eccentricity vs. Resistance/Mass Eccentricity

FIGURES

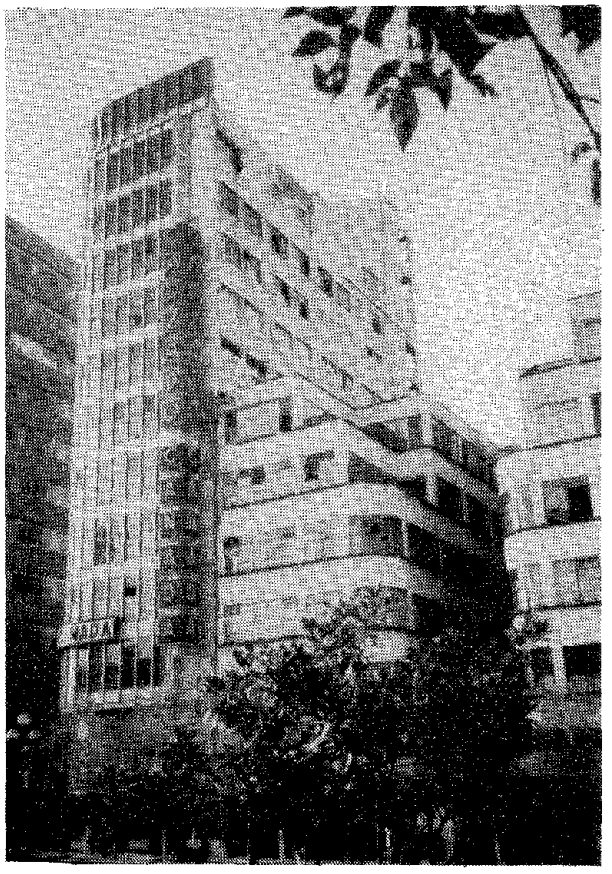

Figure 1.1(a): TWO ADJACENT BUILDINGS WITH DIFFERENT HEIGHTS AFTER 1985 MEXICO EARTHQUAKE [38]

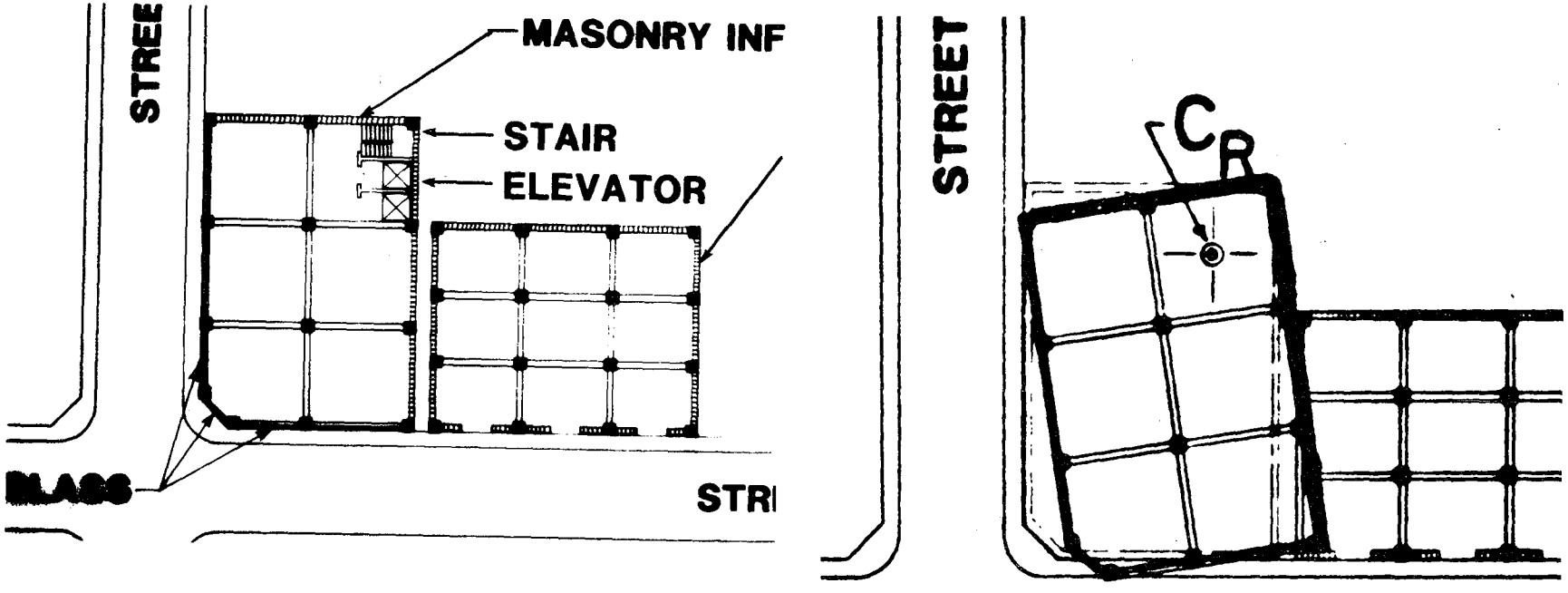

BEFORE EARTHQUAKE

AFTER EARTHQUAKE

Figure 1.1(b): PLAN VIEWS OF TWO ADJACENT BUILDINGS BEFORE AND AFTER 1985 MEXICO EARTHQUAKE [38]

Figure 1.2: A CORNER BUILDING IN MEXICO CITY COLLAPSED DUE TO LARGE TORSIONAL RESPONSE AFTER 1985 MEXICO EARTHQUAKE [39]

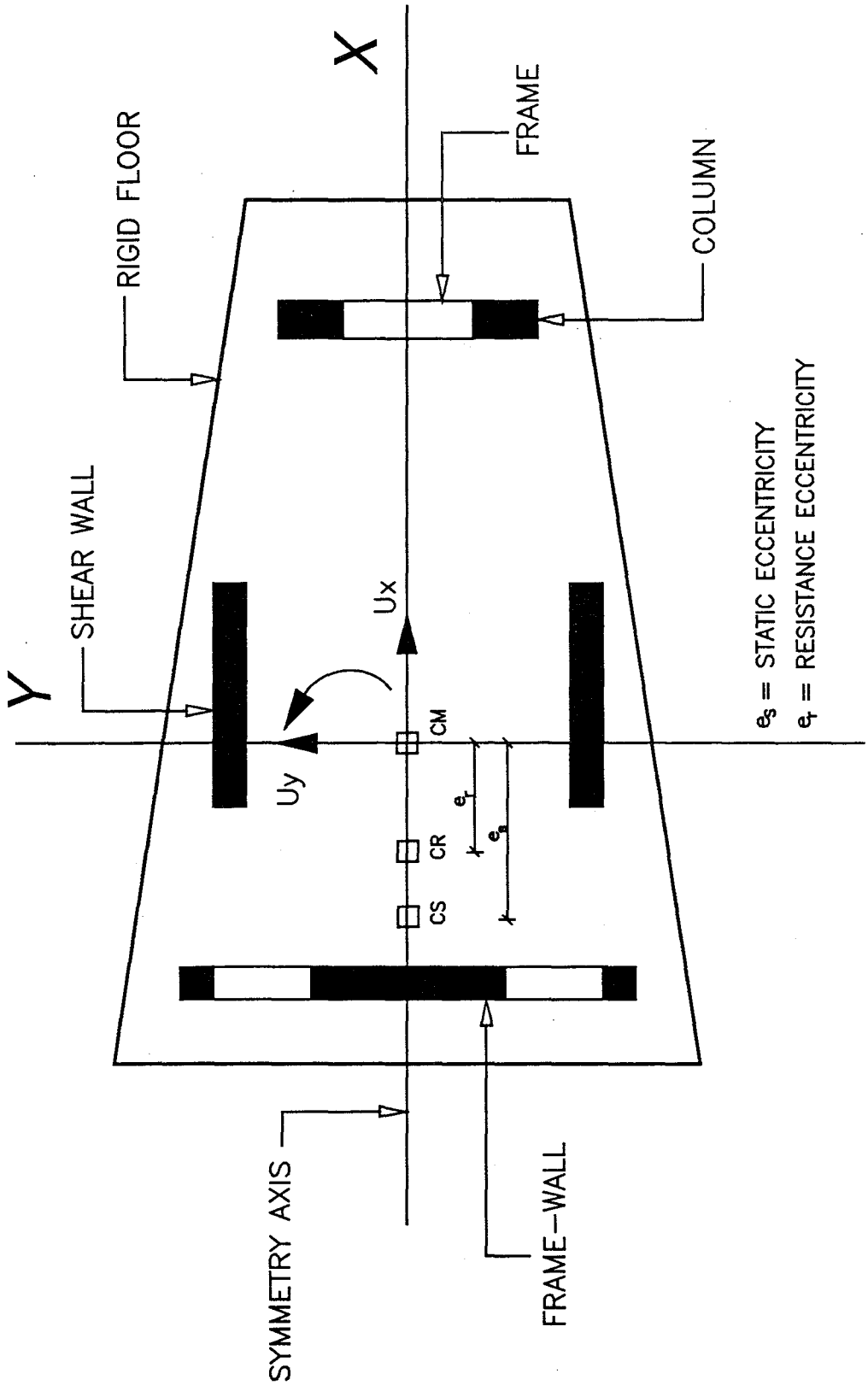

Figure 2.1: PLAN VIEW OF A TYPICAL SINGLE STORY SYSTEM

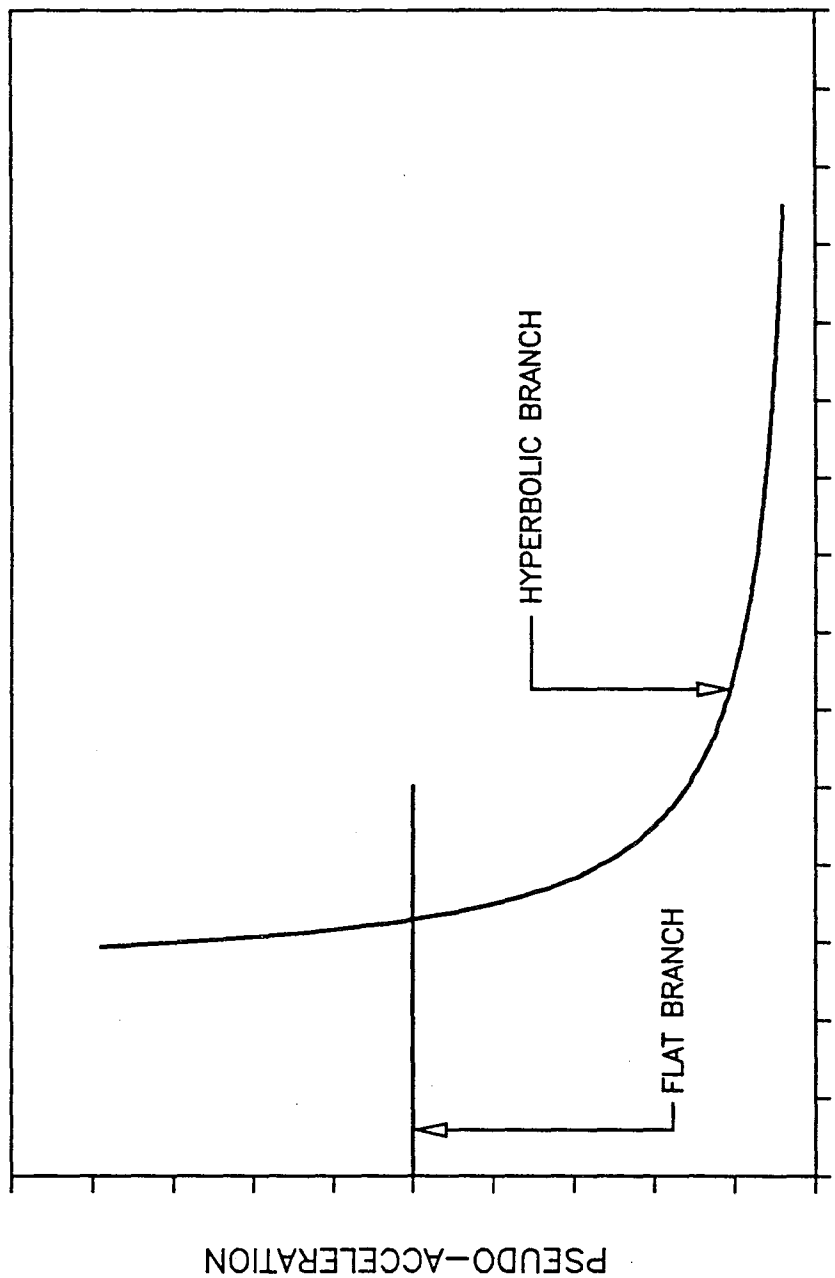

Figure 2.2: FLAT AND HYPERBOLIC SPECTRA

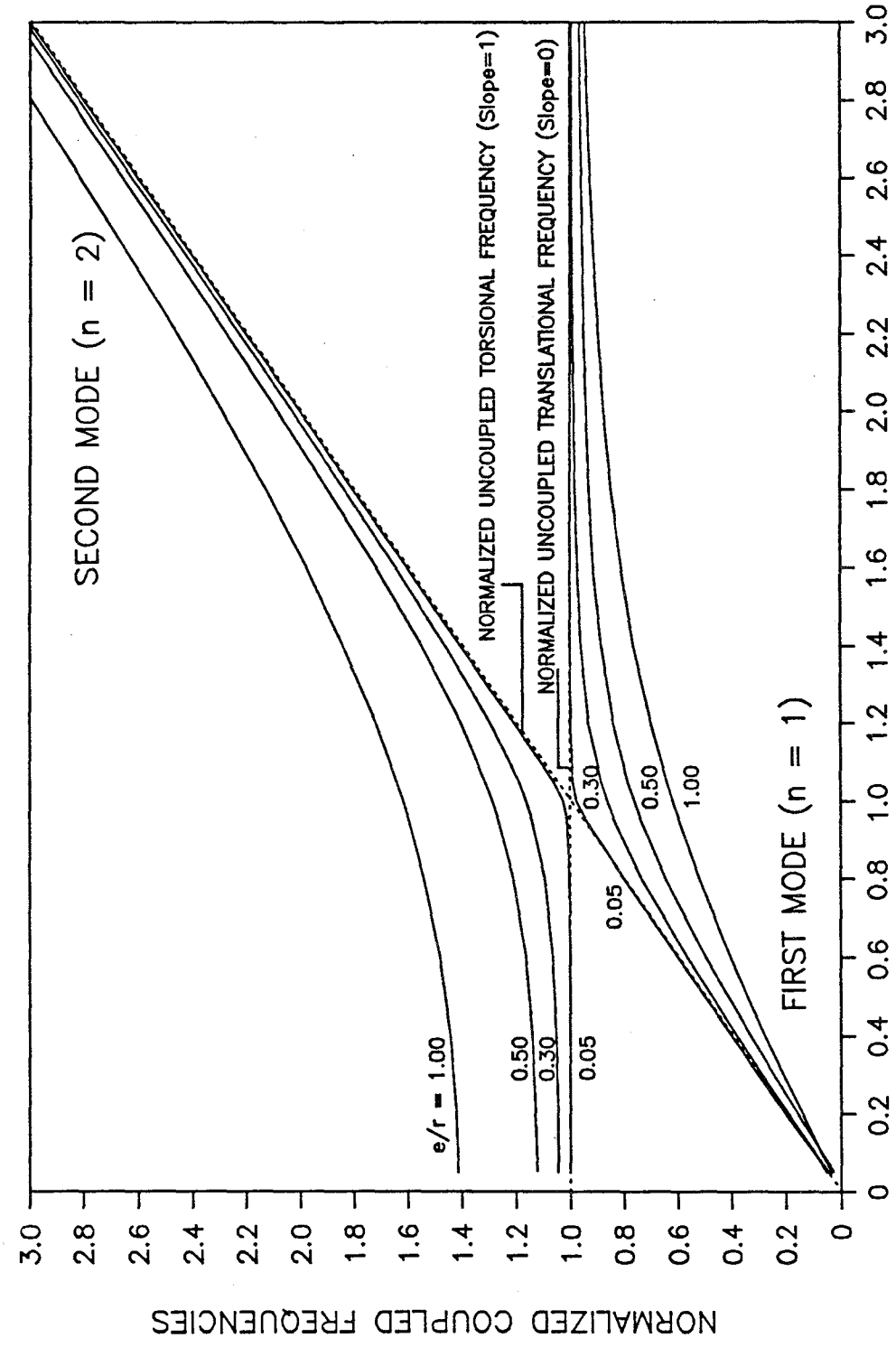

Figure 2.3: VARIATION OF COUPLED FREQUENCIES WITH UNCOUPLED FREQUENCY RATIO

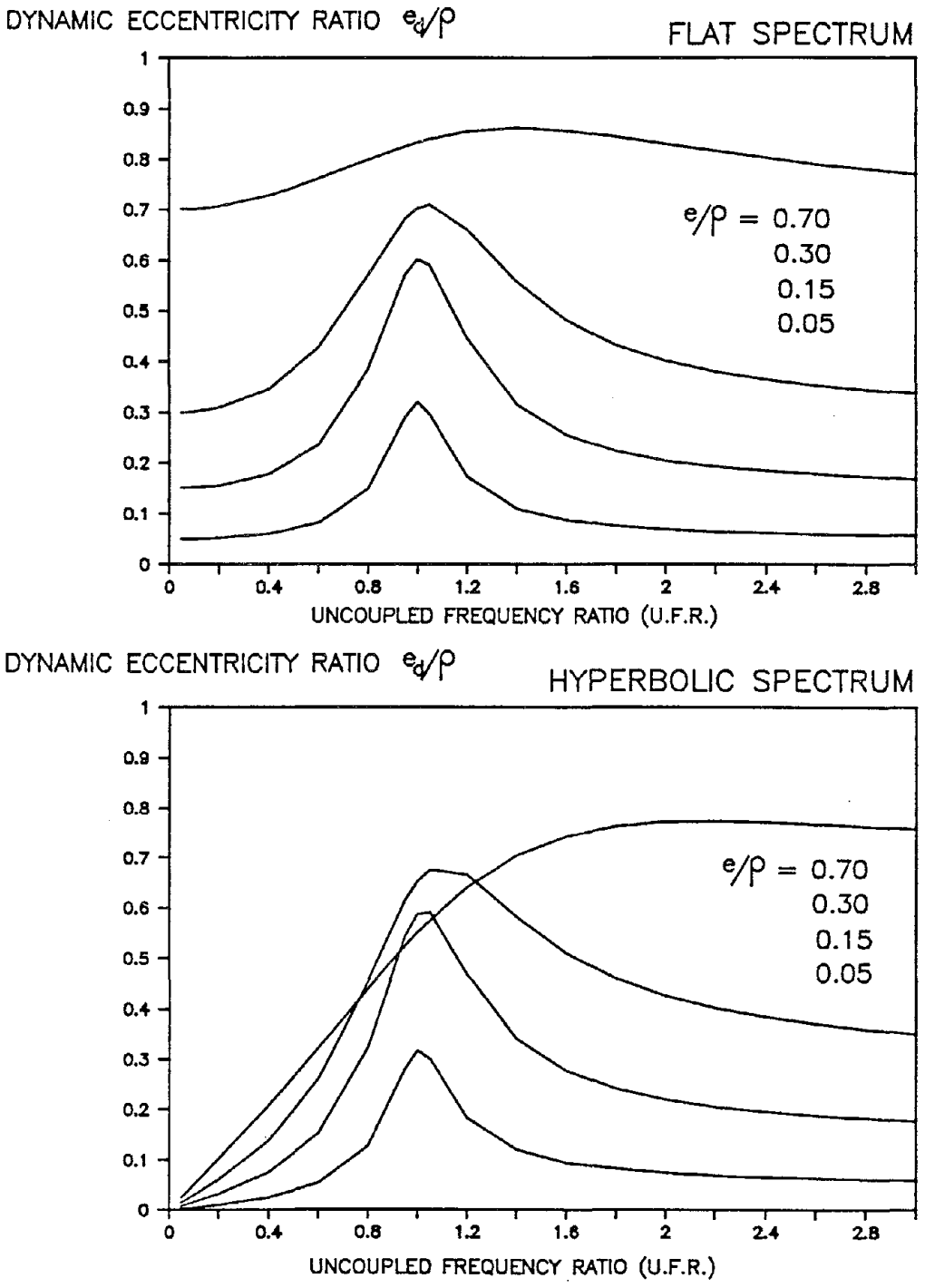

Figure 2.4: VARIATION OF DYNAMIC ECCENTRICITY WITH UNCOUPLED FREQUENCY RATIO

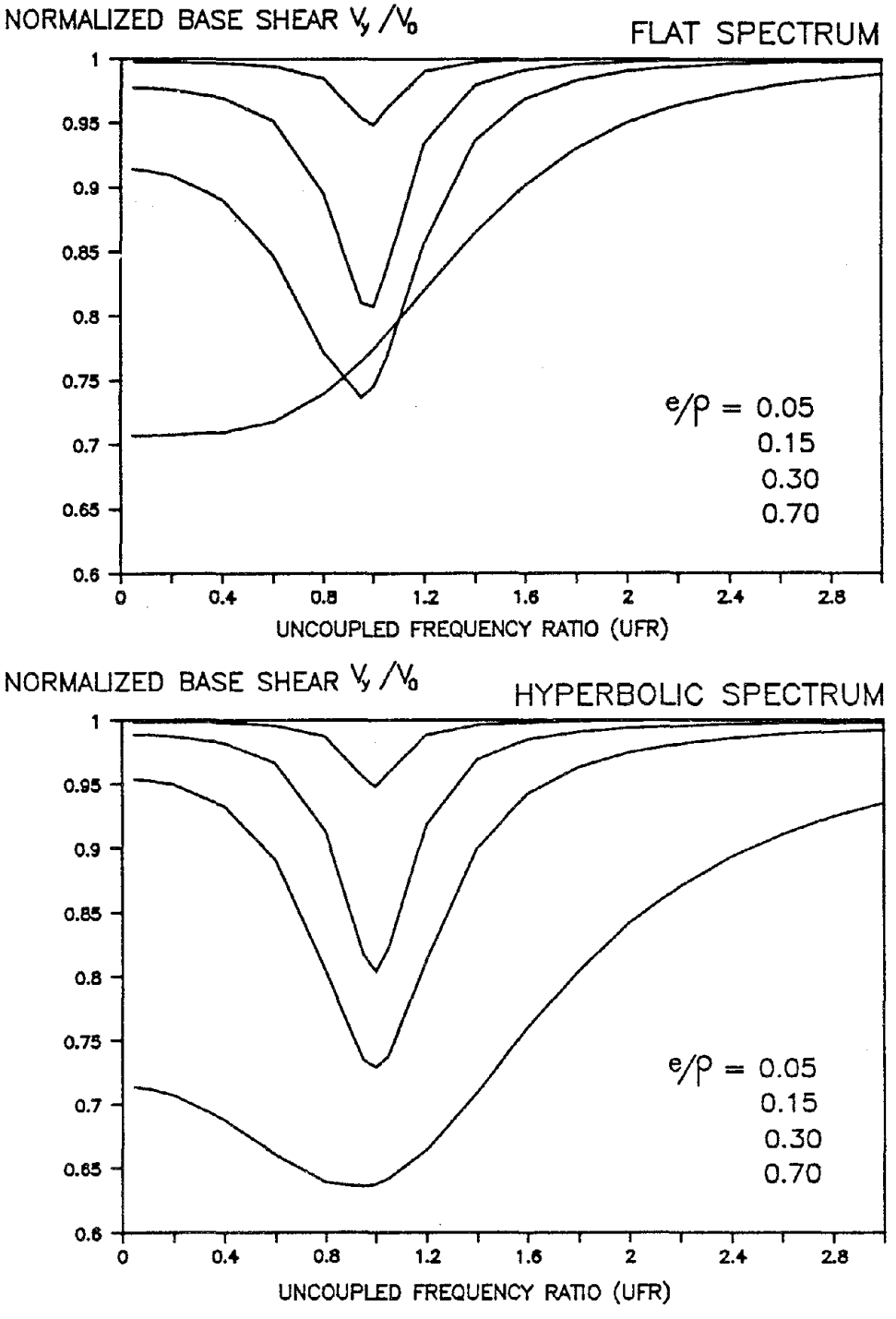

Figure 2.5: REDUCTION OF BASE SHEAR WITH UNCOUPLED FREQUENCY RATIO

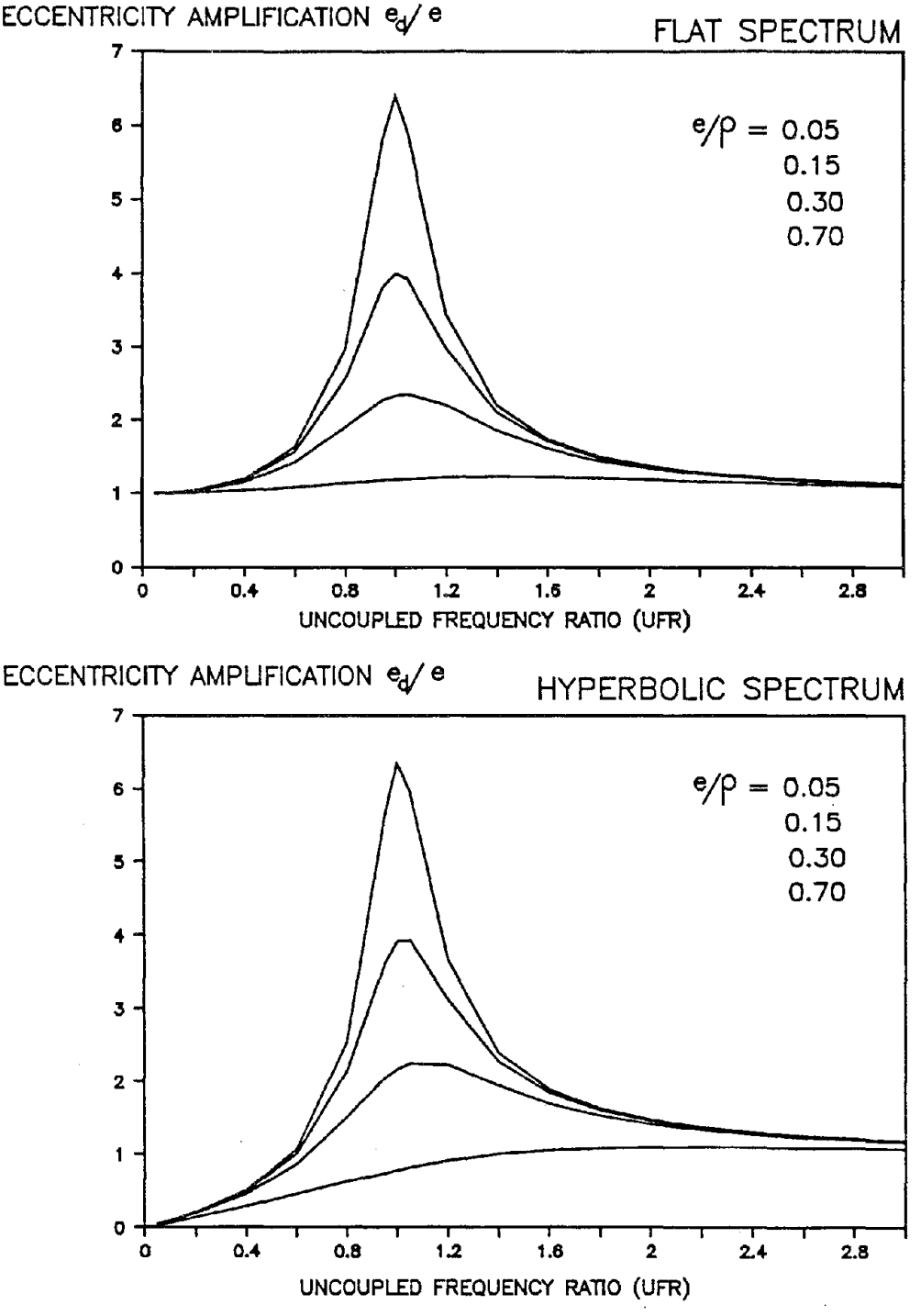

Figure 2.6: VARIATION OF DYNAMIC AMPLIFICATION OF ECCENTRICITY WITH UNCOUPLED FREQUENCY RATIO

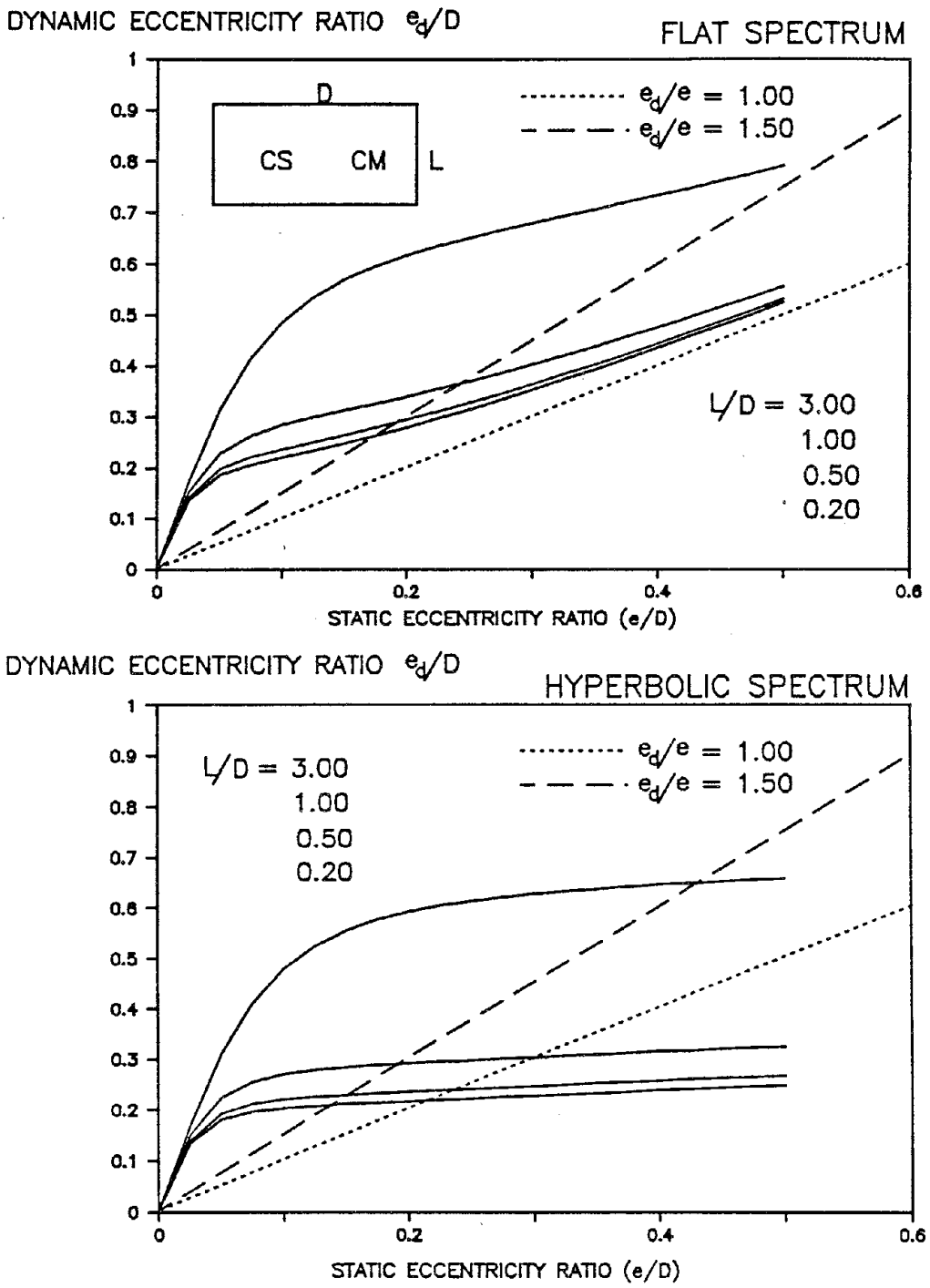

Figure 2.7: VARIATION OF DYNAMIC ECCENTRICITY WITH STATIC ECCENTRICITY

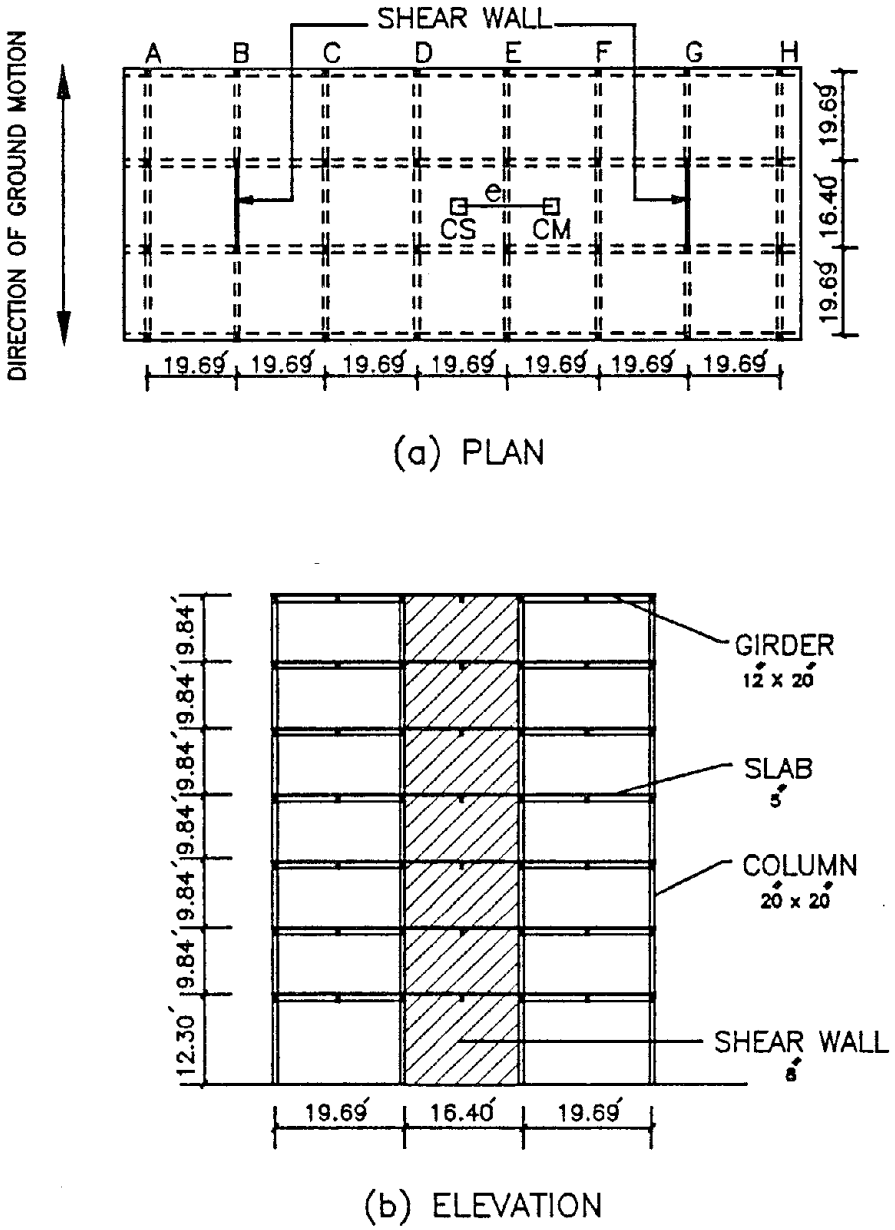

Figure 3.1: PLAN VIEW AND ELEVATION OF THE STRUCTURE

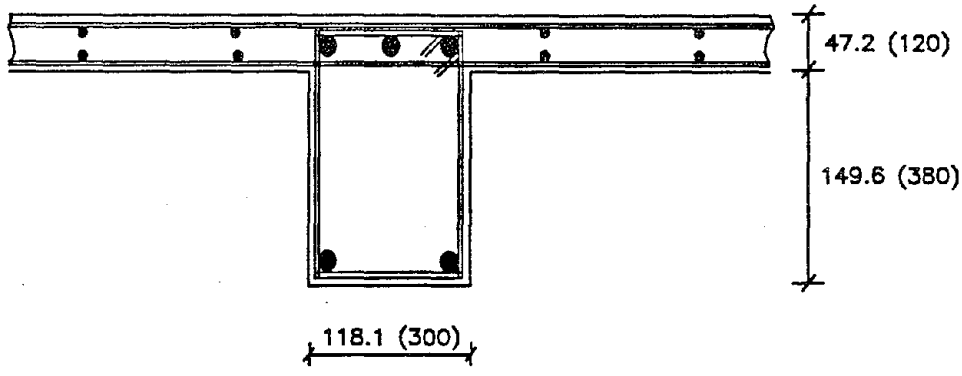

(a) TYPICAL BEAM CROSS SECTION

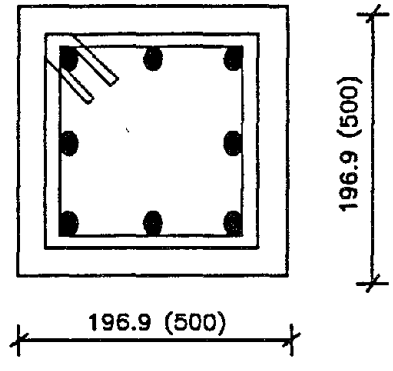

(b) TYPICAL COLUMN CROSS SECTION

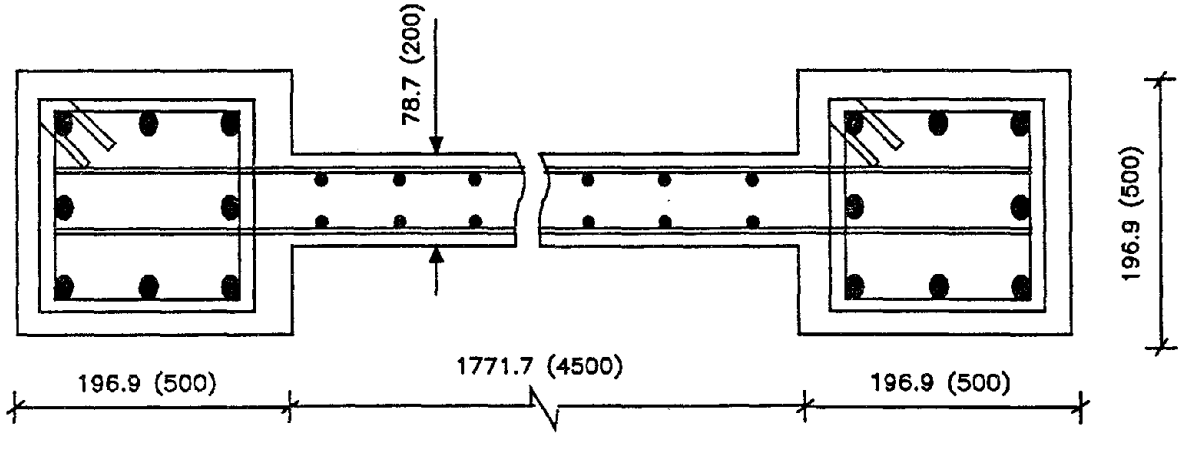

(c) TYPICAL SHEAR WALL CROSS SECTION

Figure 3.2: TYPICAL CROSS SECTIONS OF BEAMS, COLUMNS, AND SHEAR WALLS
All Units Are In Inches (Millimeters)

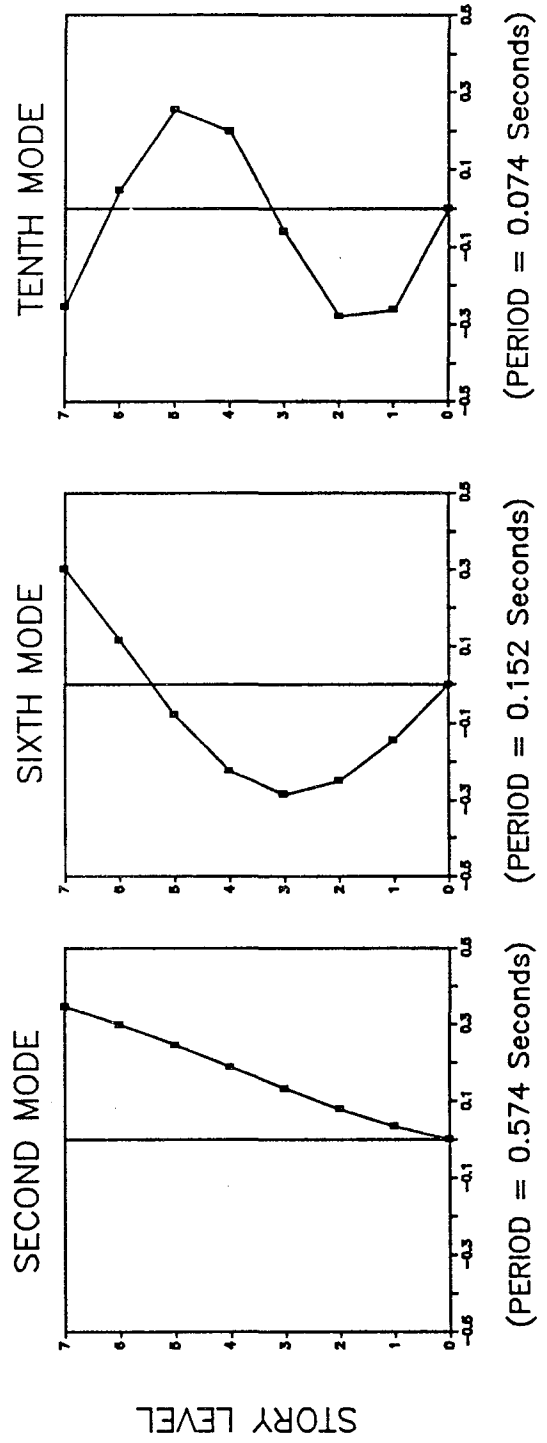

Figure 3.3: THE FIRST THREE TRANSLATIONAL MODE SHAPES

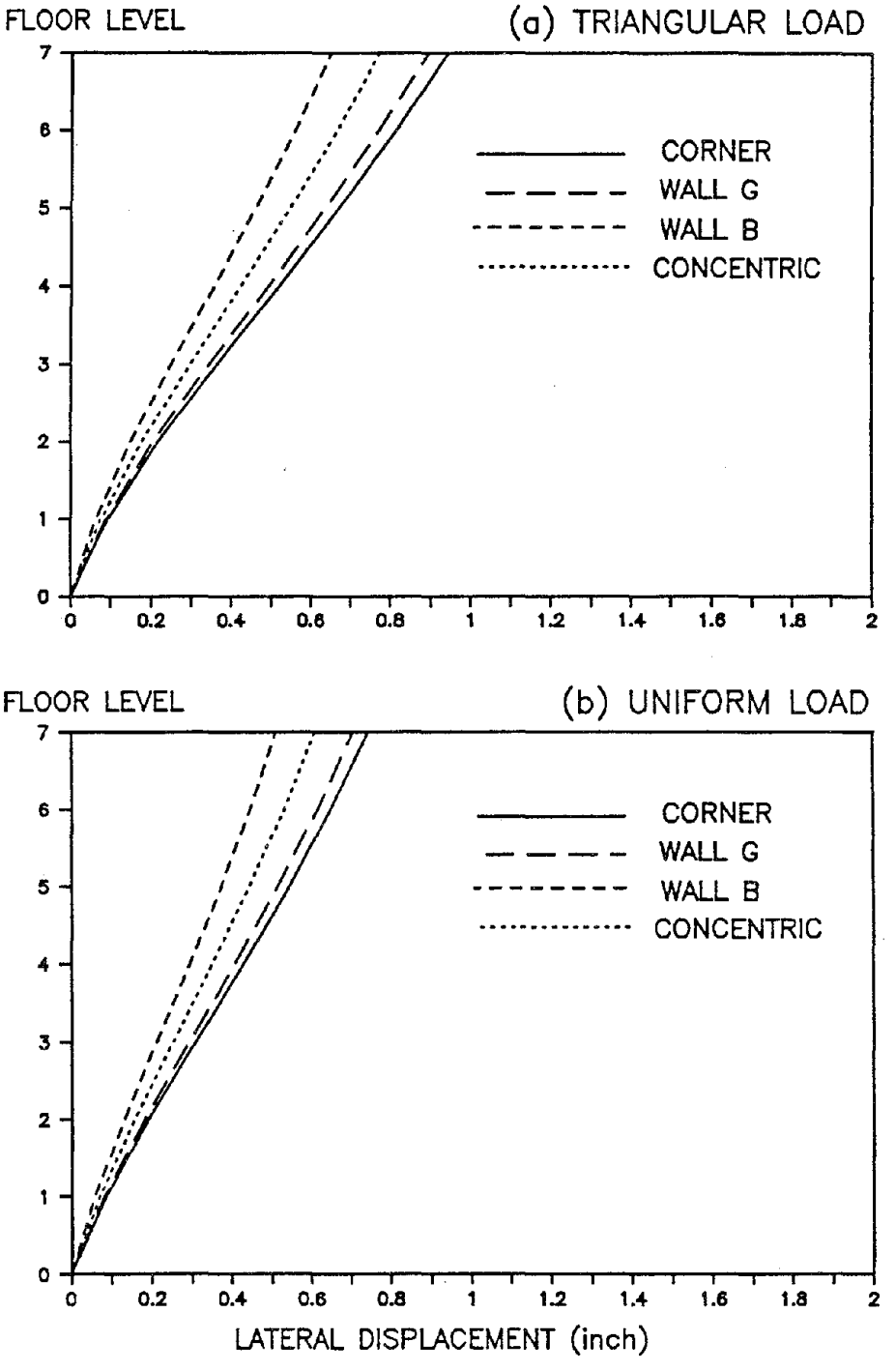

Figure 3.4: LATERAL DISPLACEMENT PROFILE (e/D = 0.05 , STATIC LOAD)

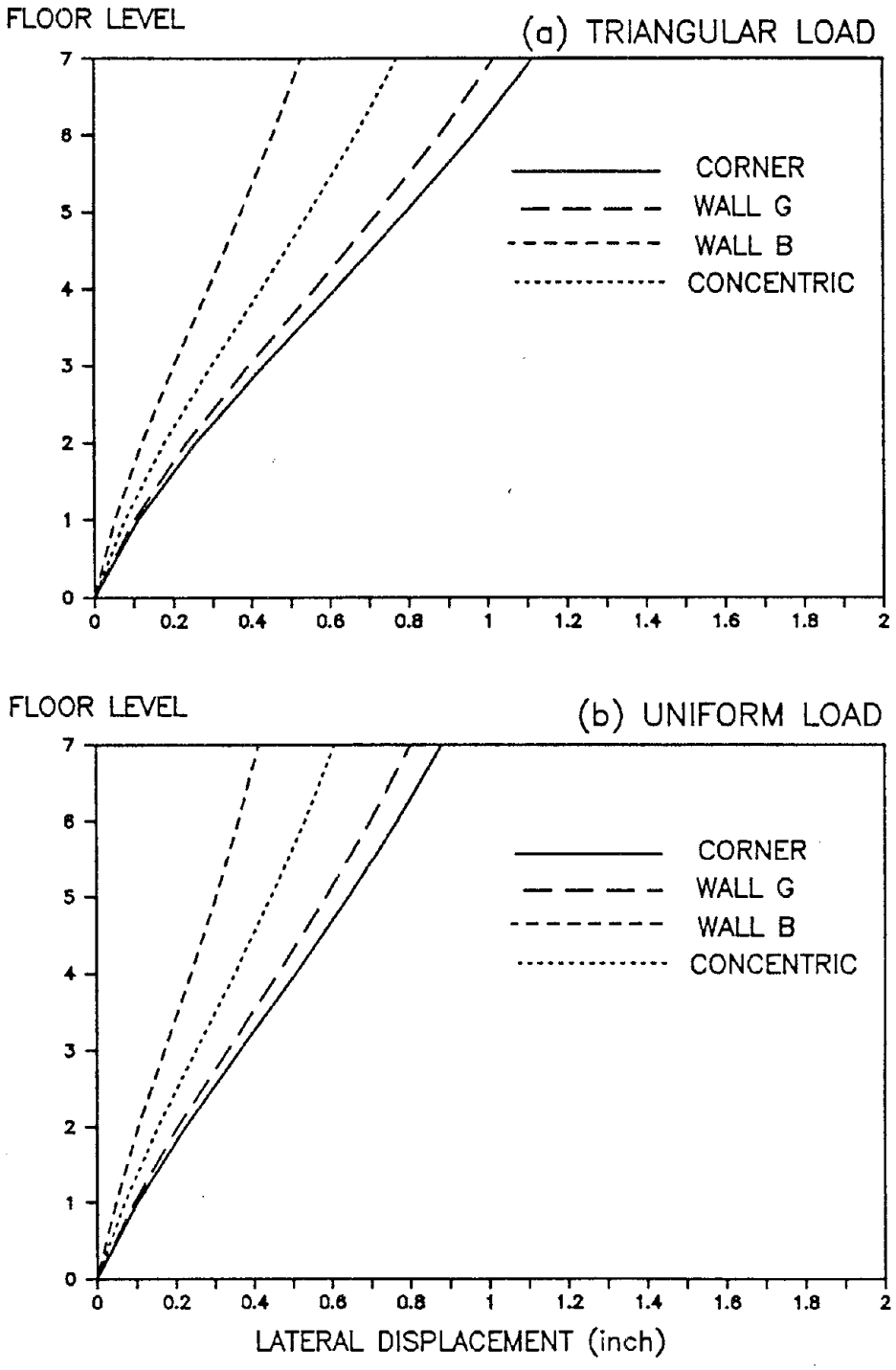

Figure 3.5: LATERAL DISPLACEMENT PROFILE (e/D = 0.10 , STATIC LOAD)

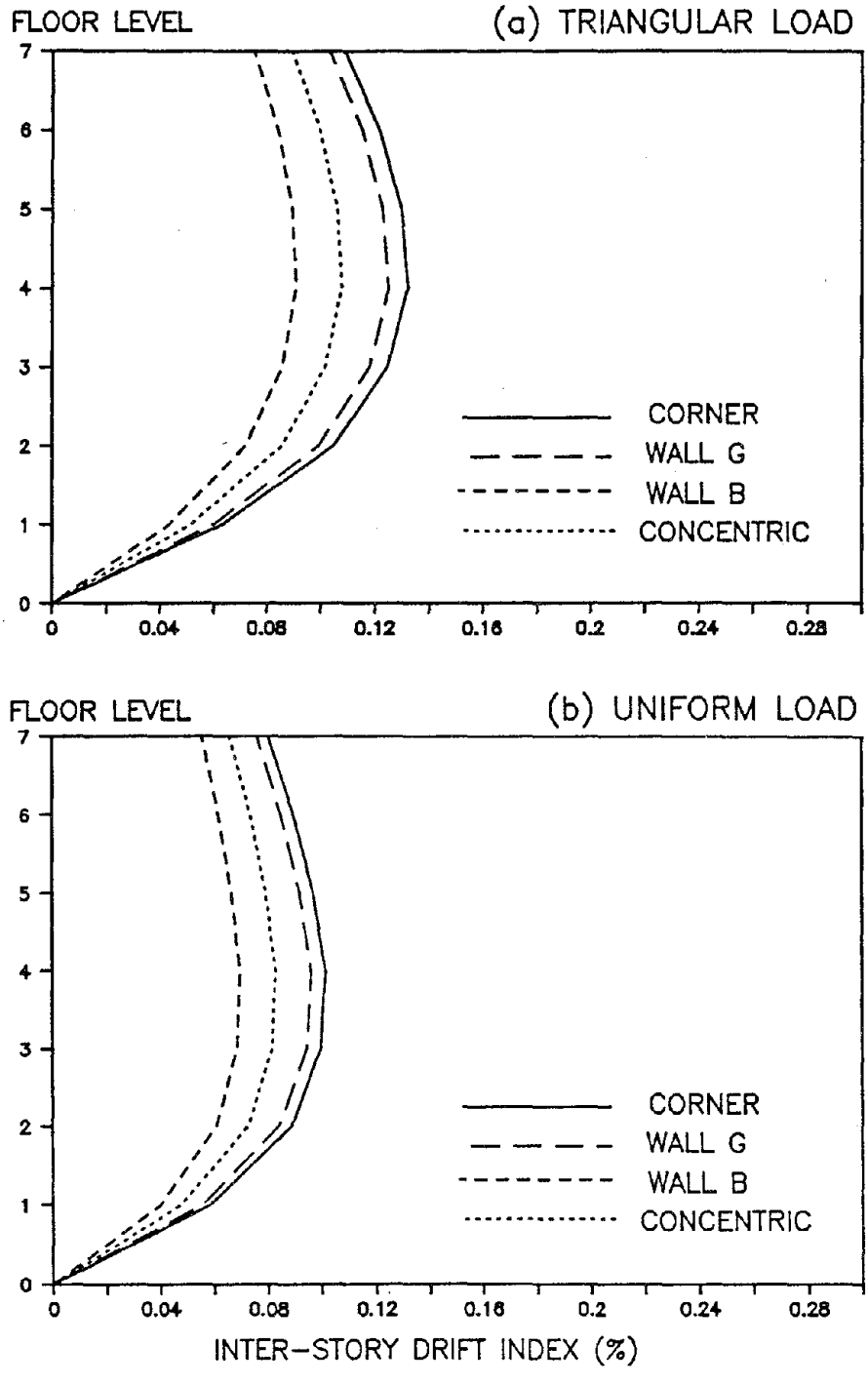

Figure 3.6: INTER-STORY DRIFT INDEX
(e/D = 0.05 , STATIC LOAD)

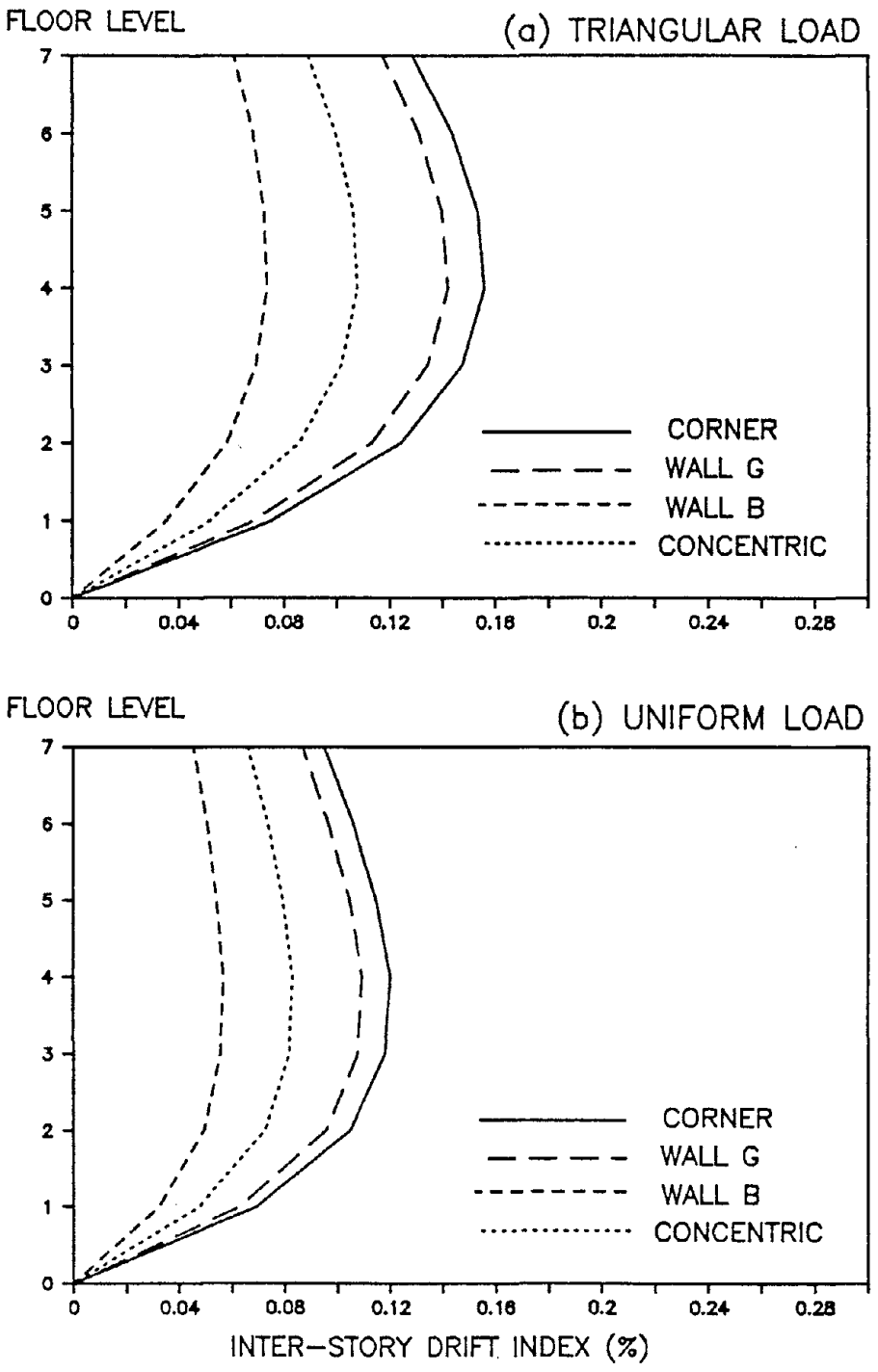

Figure 3.7: INTER-STORY DRIFT INDEX (e/D = 0.10 , STATIC LOAD)

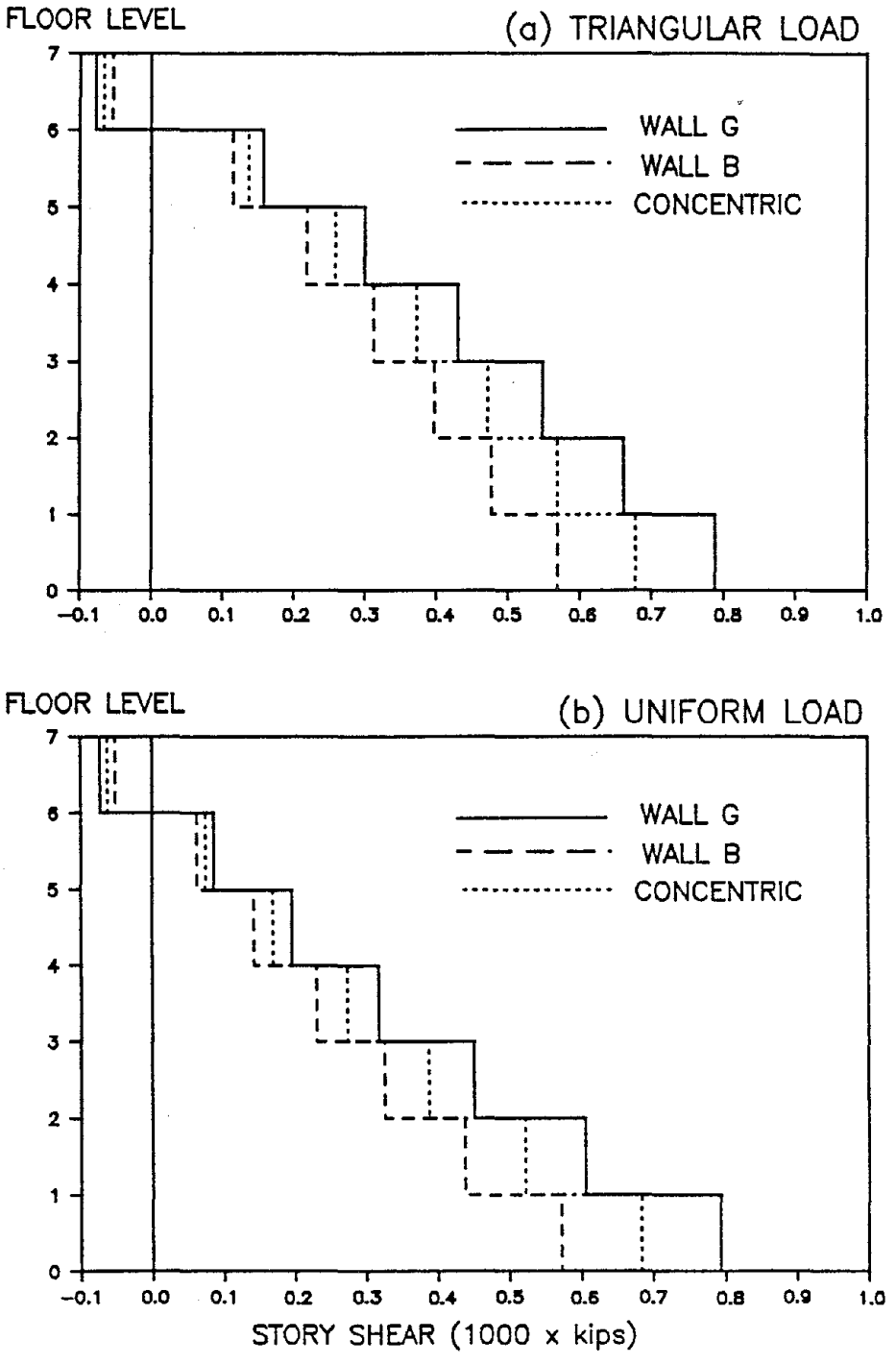

Figure 3.8: WALLS SHEAR FORCE
(e/D = 0.05 , STATIC LOAD)

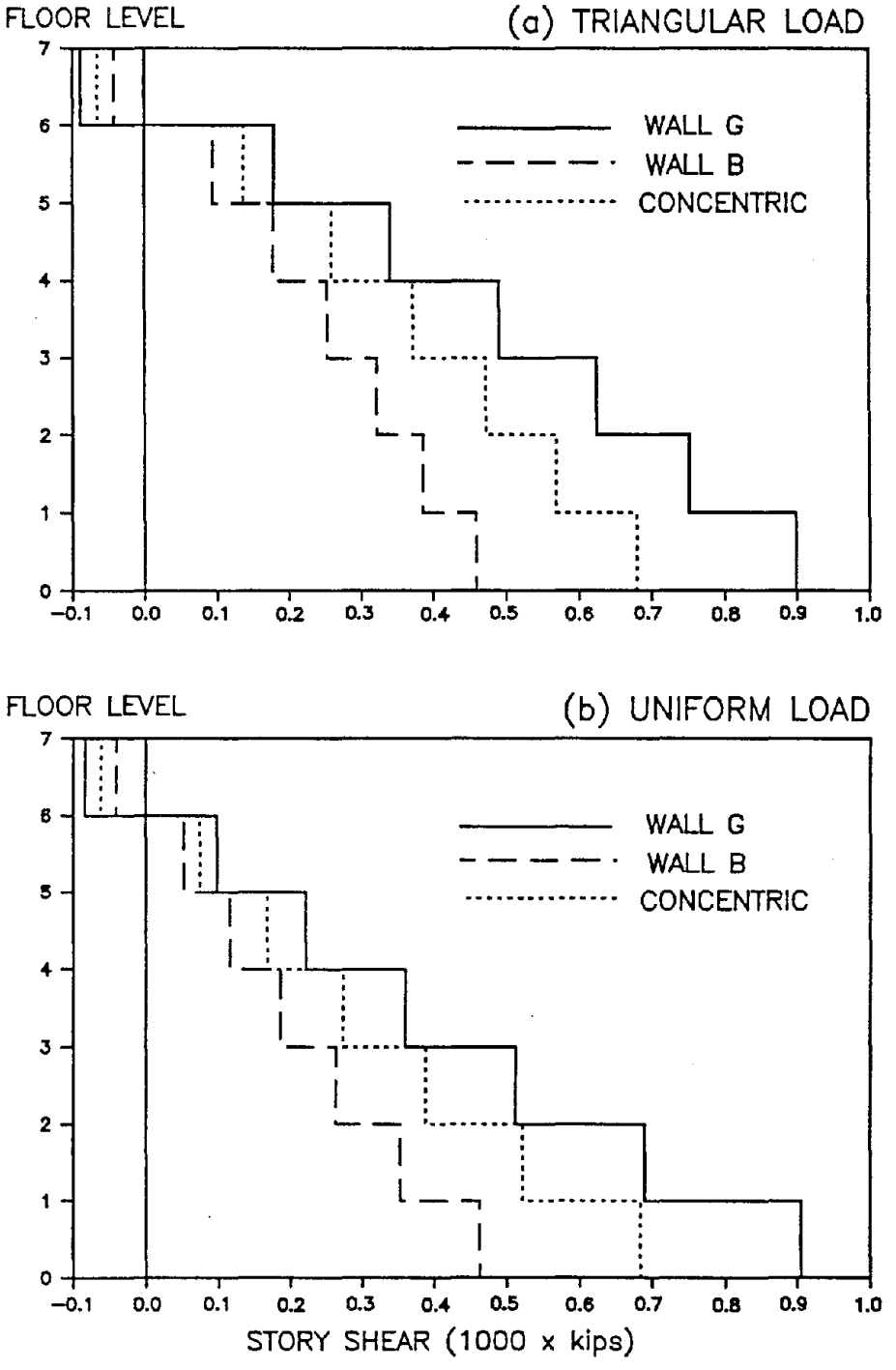

Figure 3.9: WALLS SHEAR FORCE
(e/D = 0.10 , STATIC LOAD)

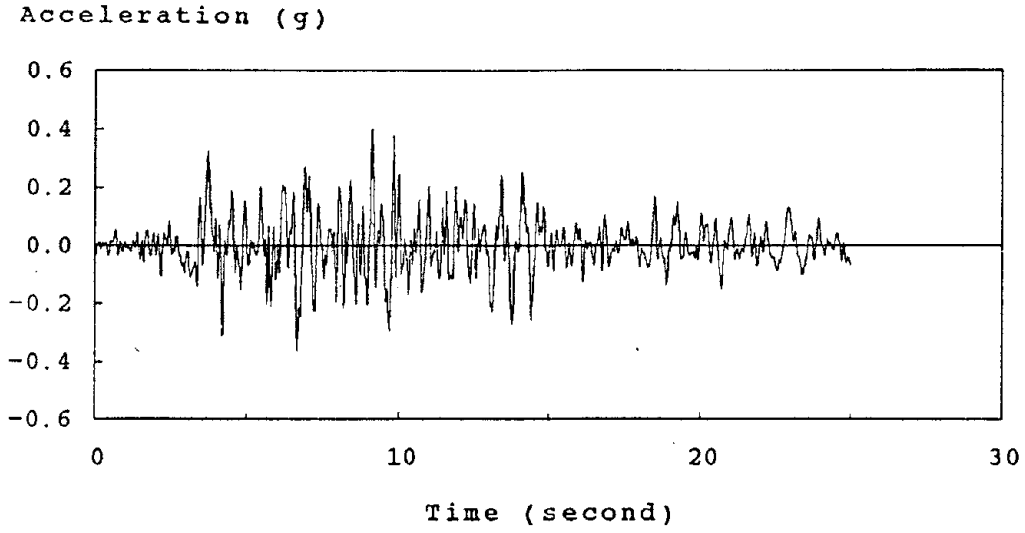

Figure 3.10(a): ACCELERATION TIME-HISTORY OF N21E 1952 TAFT KERN COUNTY RECORD; NORMALIZED TO A MAXIMUM PEAK GROUND ACCELERATION OF 0.40g

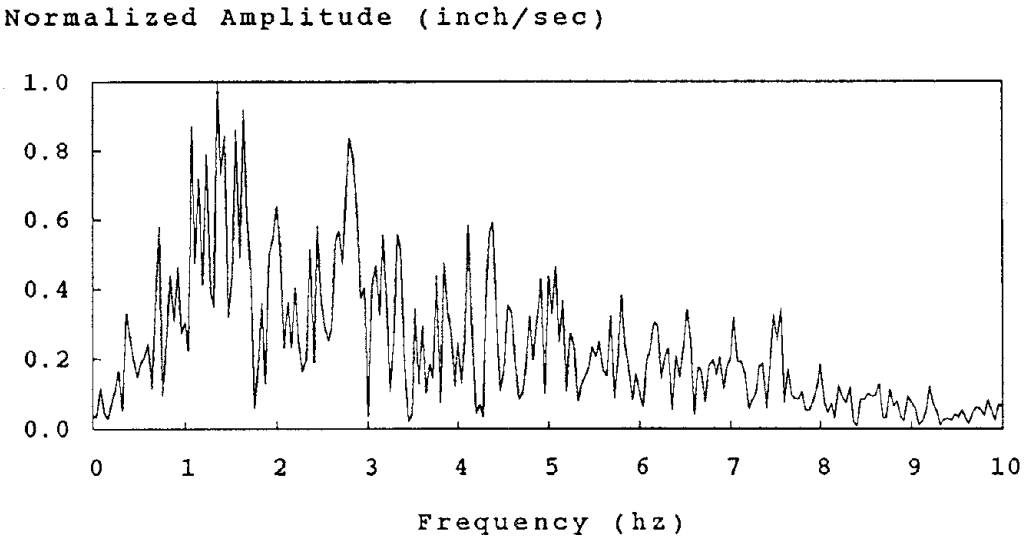

Figure 3.10(b): NORMALIZED FOURIER AMPLITUDE SPECTRUM

THE FIRST THREE TRANSLATIONAL PERIODS:

T_1 = 0.57 Seconds
T_6 = 0.15 Seconds
T_{10} = 0.07 Seconds

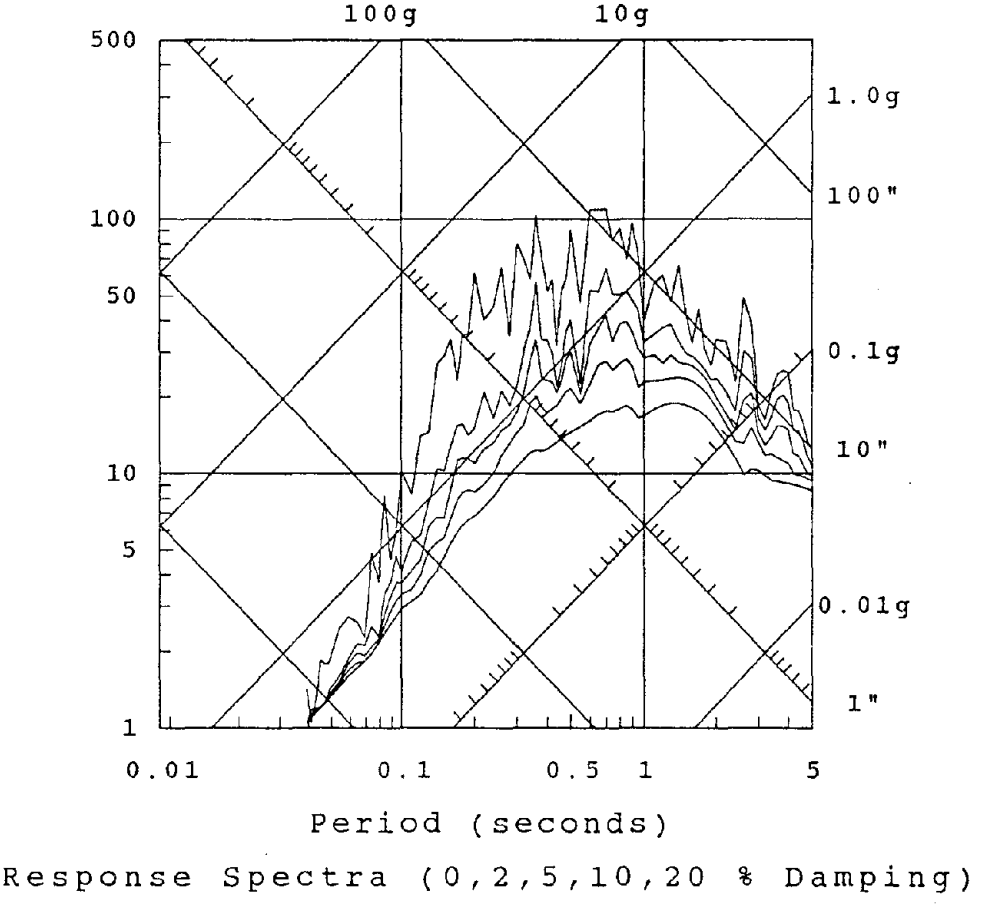

Figure 3.11: LINEAR-ELASTIC RESPONSE SPECTRA OF 1952 TAFT KERN COUNTY

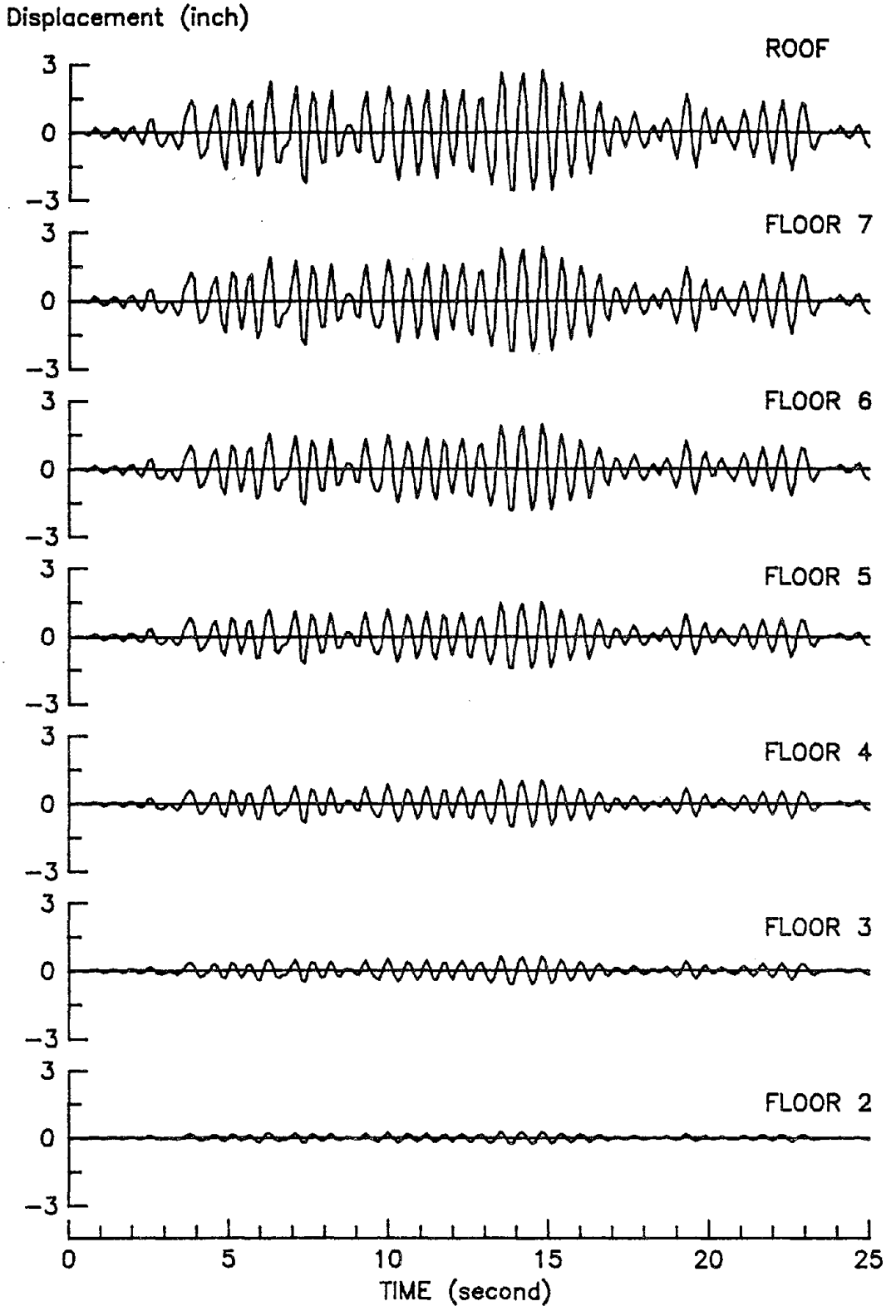

Figure 3.12: DISPLACEMENT TIME-HISTORIES OF THE CONCENTRIC STRUCTURE DUE TO TAFT-40

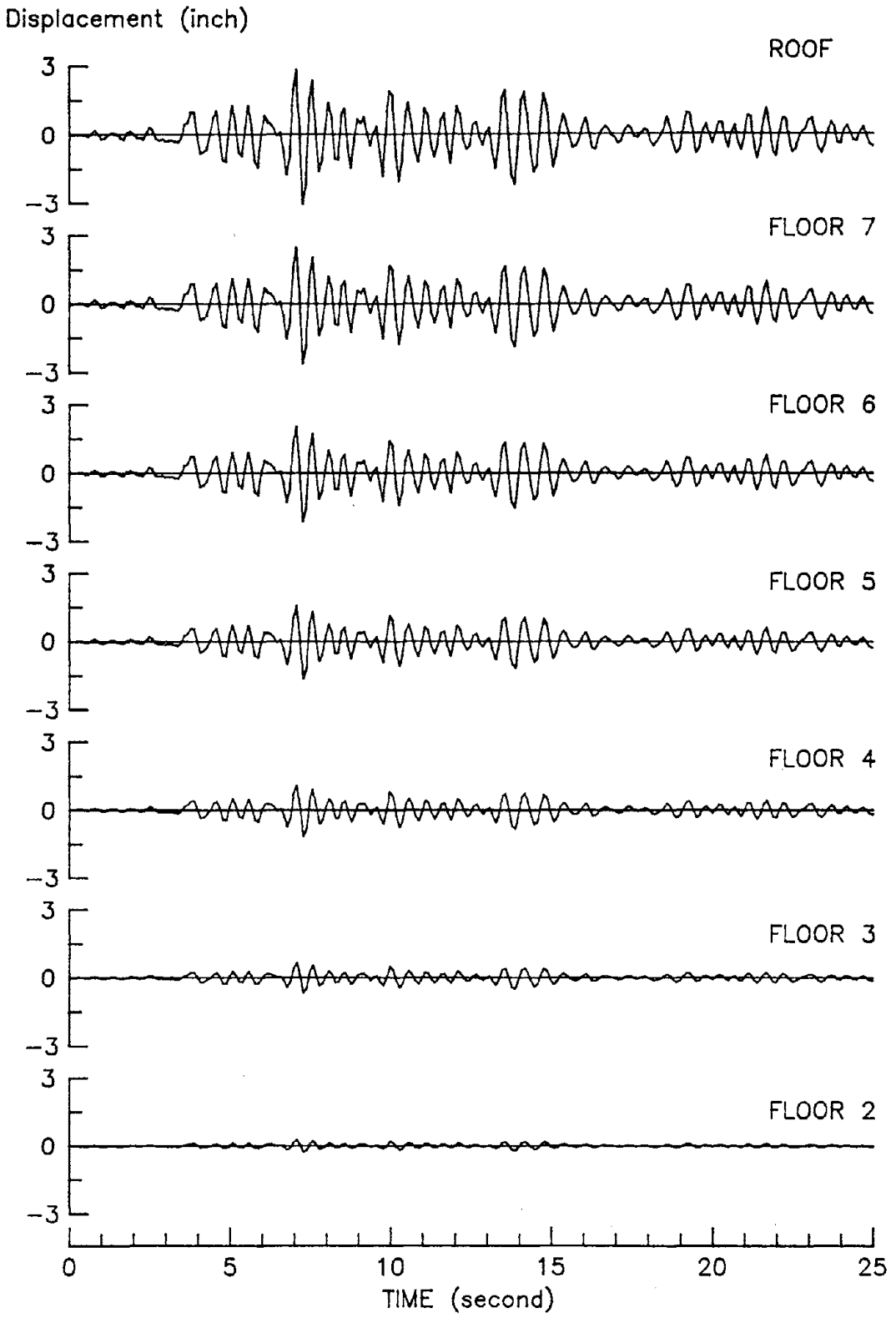

Figure 3.13: DISPLACEMENT TIME-HISTORIES OF WALL B DUE TO TAFT-40 (e/D = 0.05)

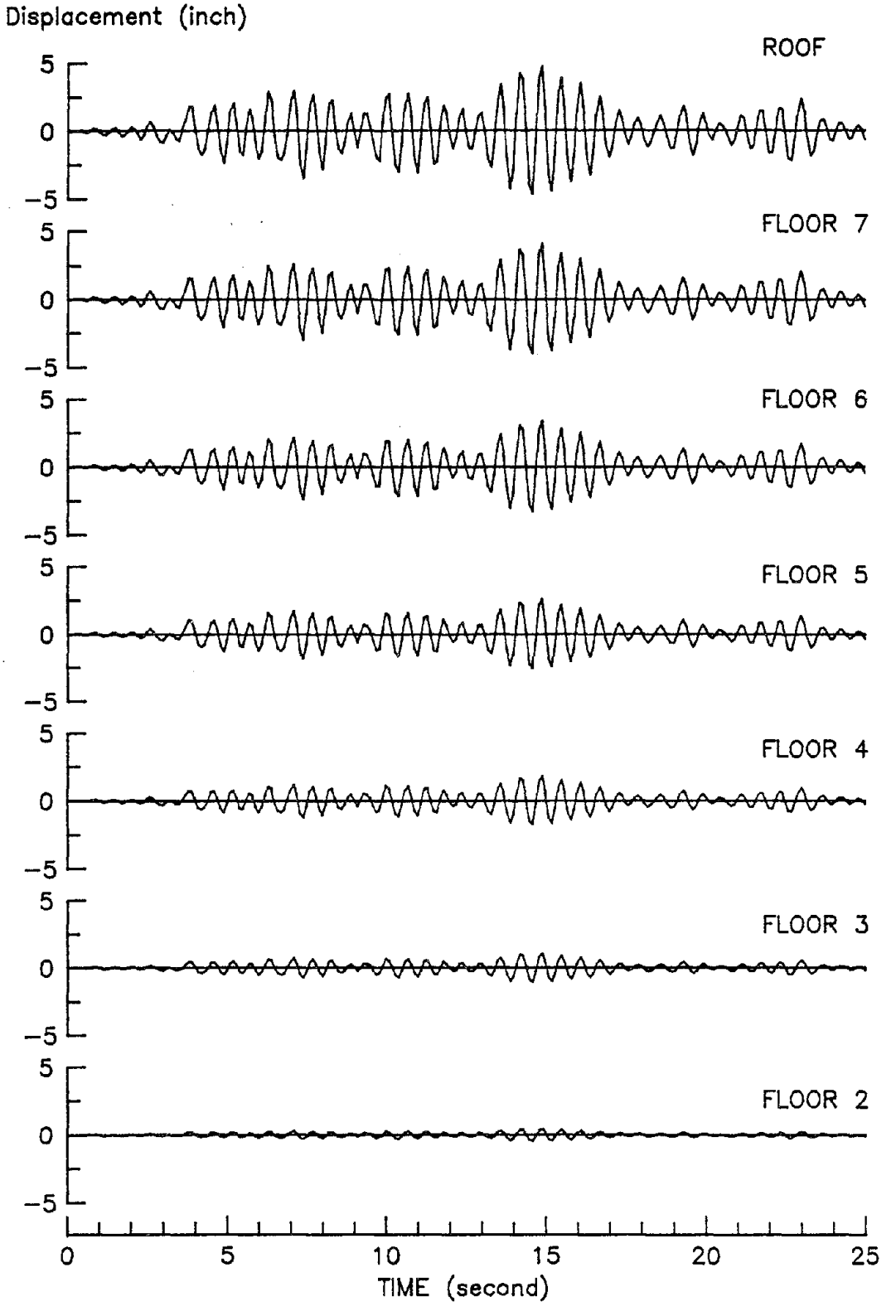

Figure 3.14: DISPLACEMENT TIME-HISTORIES OF WALL G DUE TO TAFT-40 (e/D = 0.05)

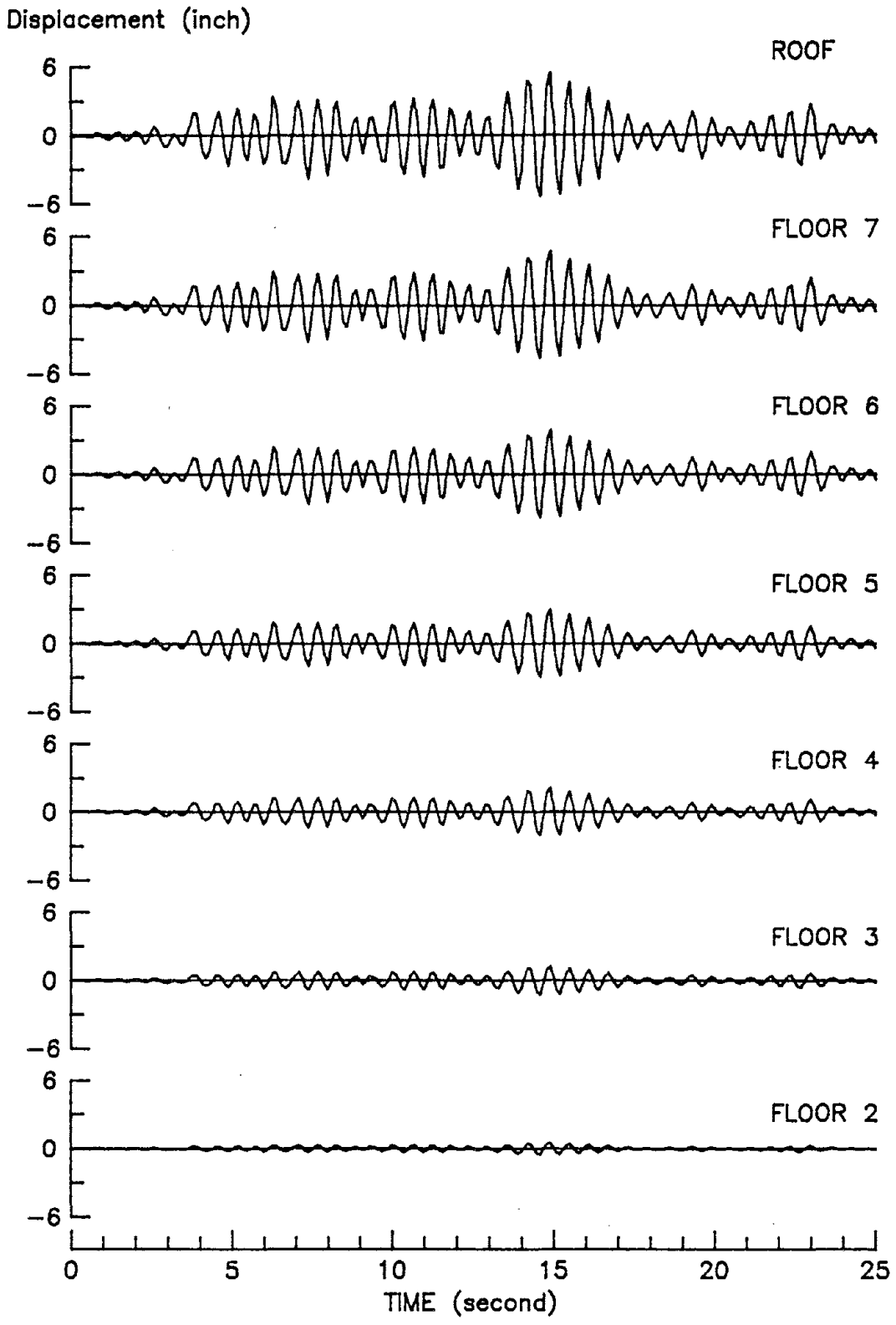

Figure 3.15: DISPLACEMENT TIME-HISTORIES OF THE CORNER OF THE STRUCTURE DUE TO TAFT-40 (e/D = 0.05)

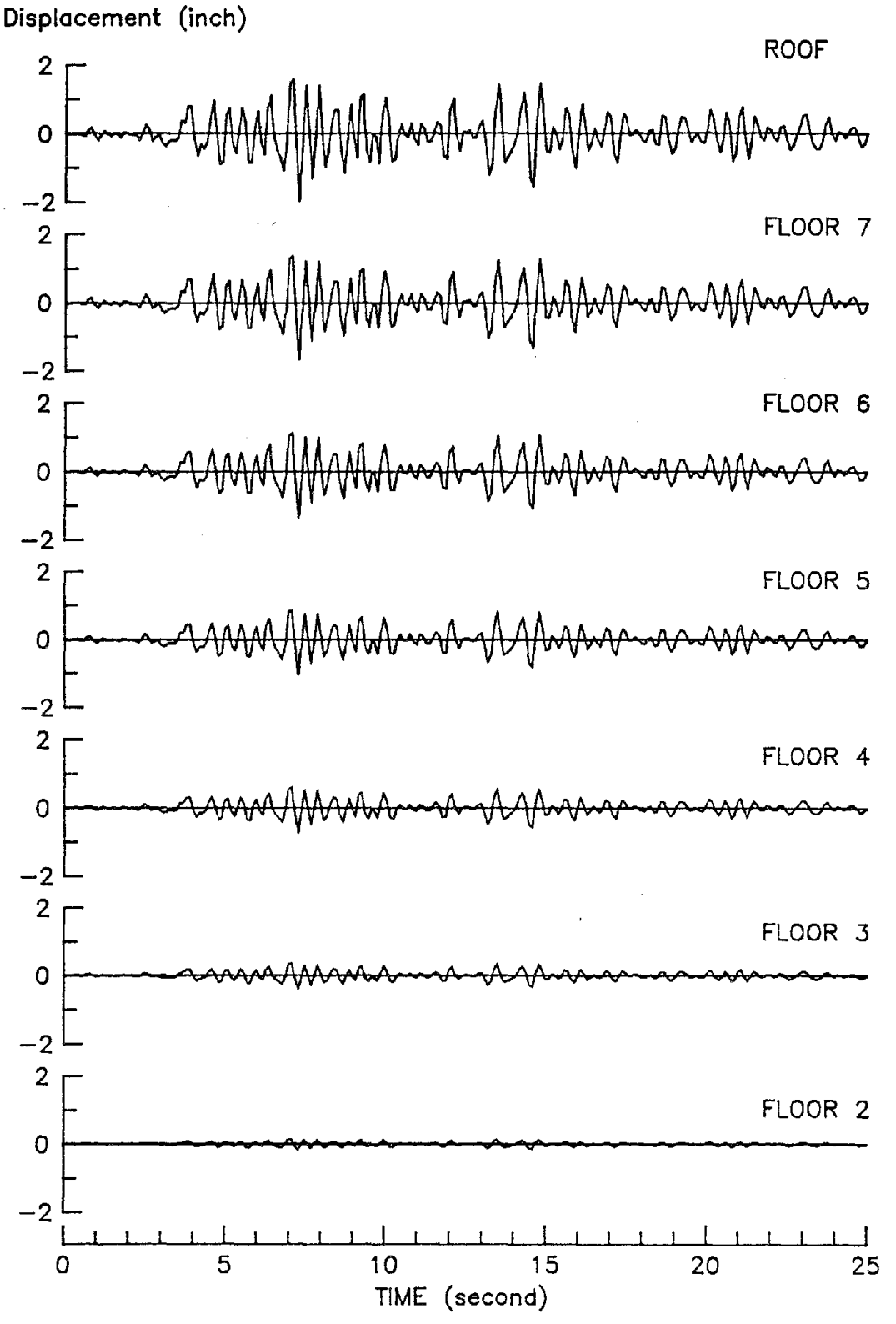

Figure 3.16: DISPLACEMENT TIME-HISTORIES OF WALL B DUE TO TAFT-40 (e/D = 0.10)

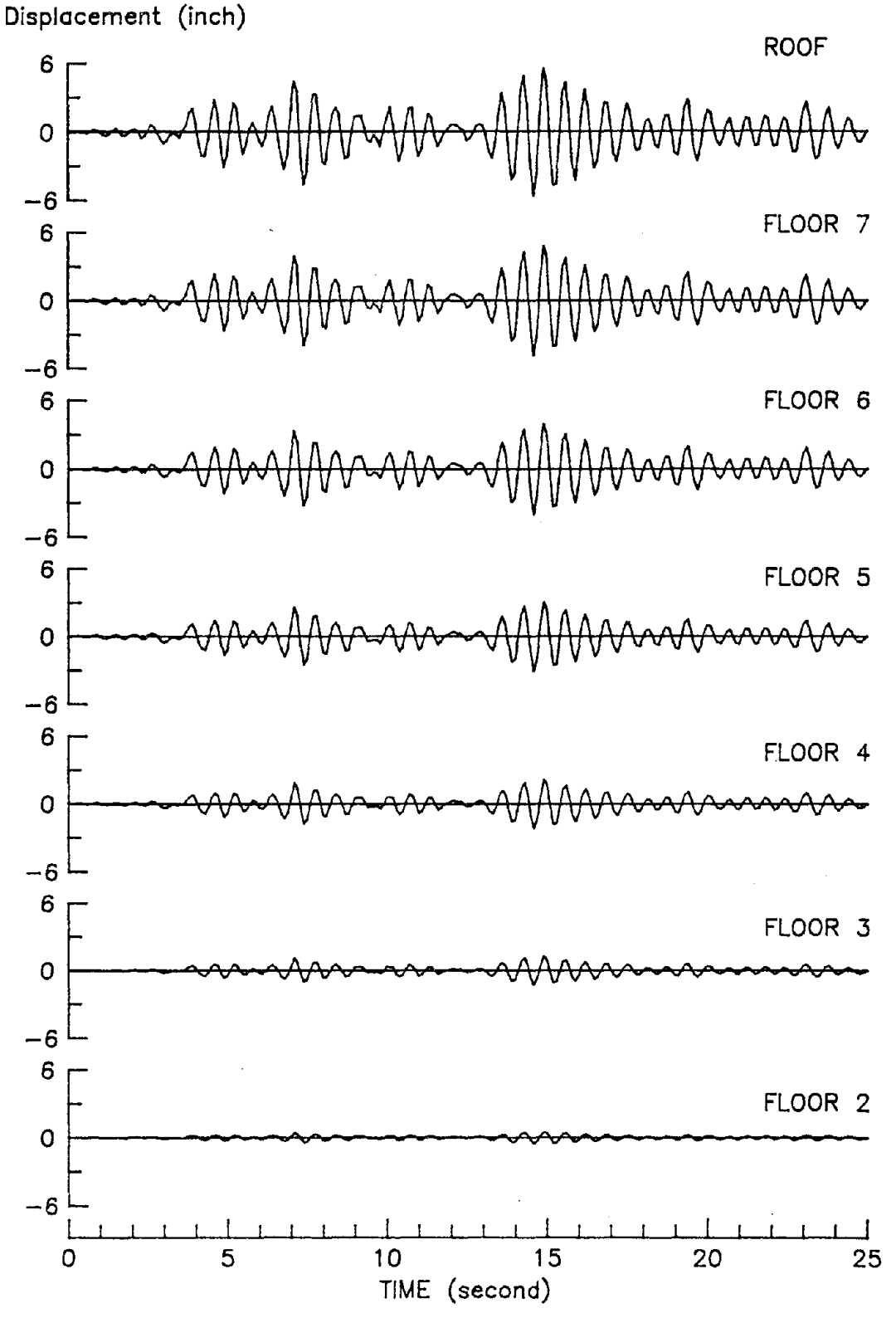

Figure 3.17: DISPLACEMENT TIME-HISTORIES OF WALL G DUE TO TAFT-40 (e/D = 0.10)

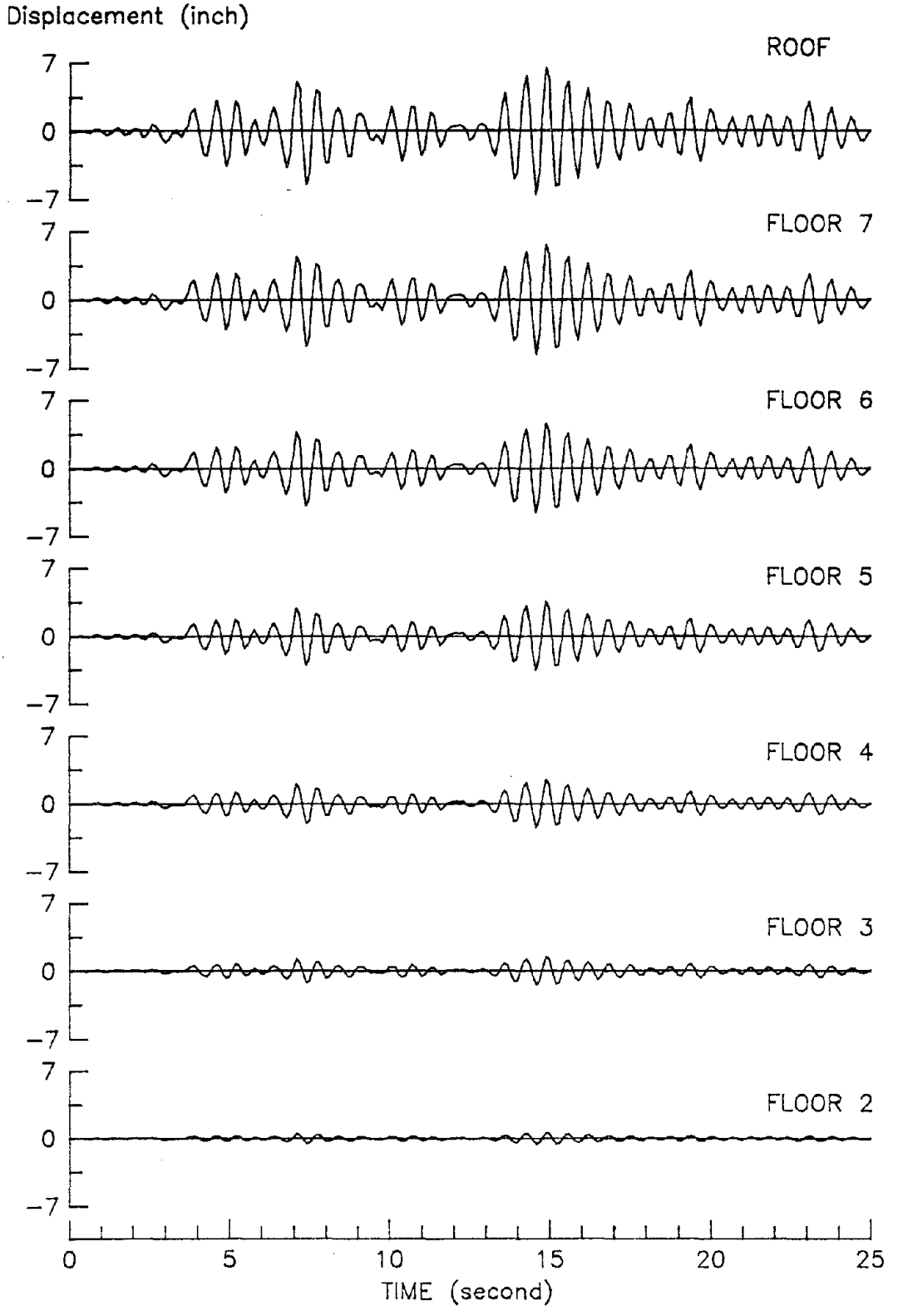

Figure 3.18: DISPLACEMENT TIME-HISTORIES OF THE CORNER OF THE STRUCTURE DUE TO TAFT-40 (e/D = 0.10)

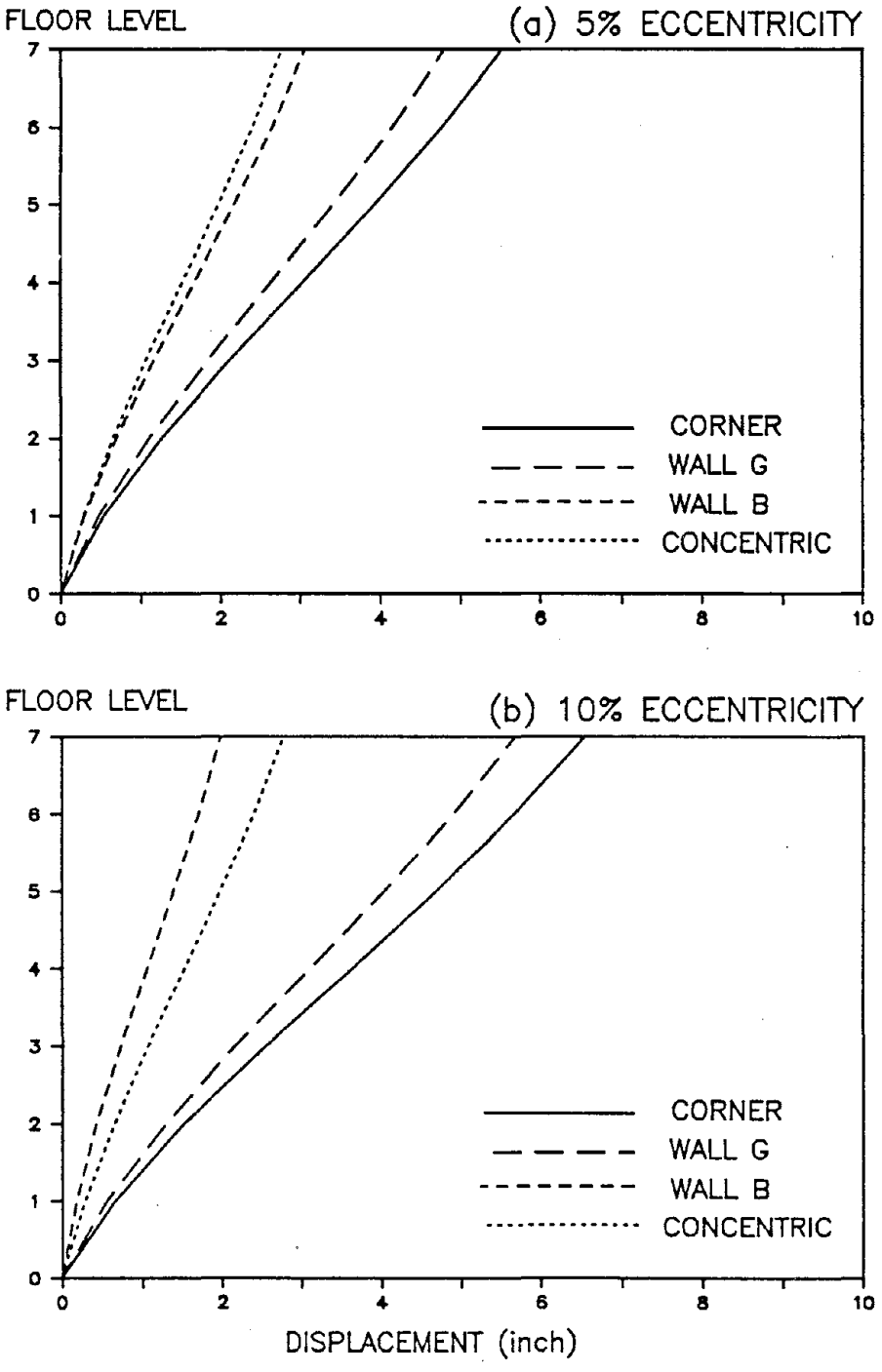

Figure 3.19: DISPLACEMENT ENVELOPES DUE TO TAFT-40

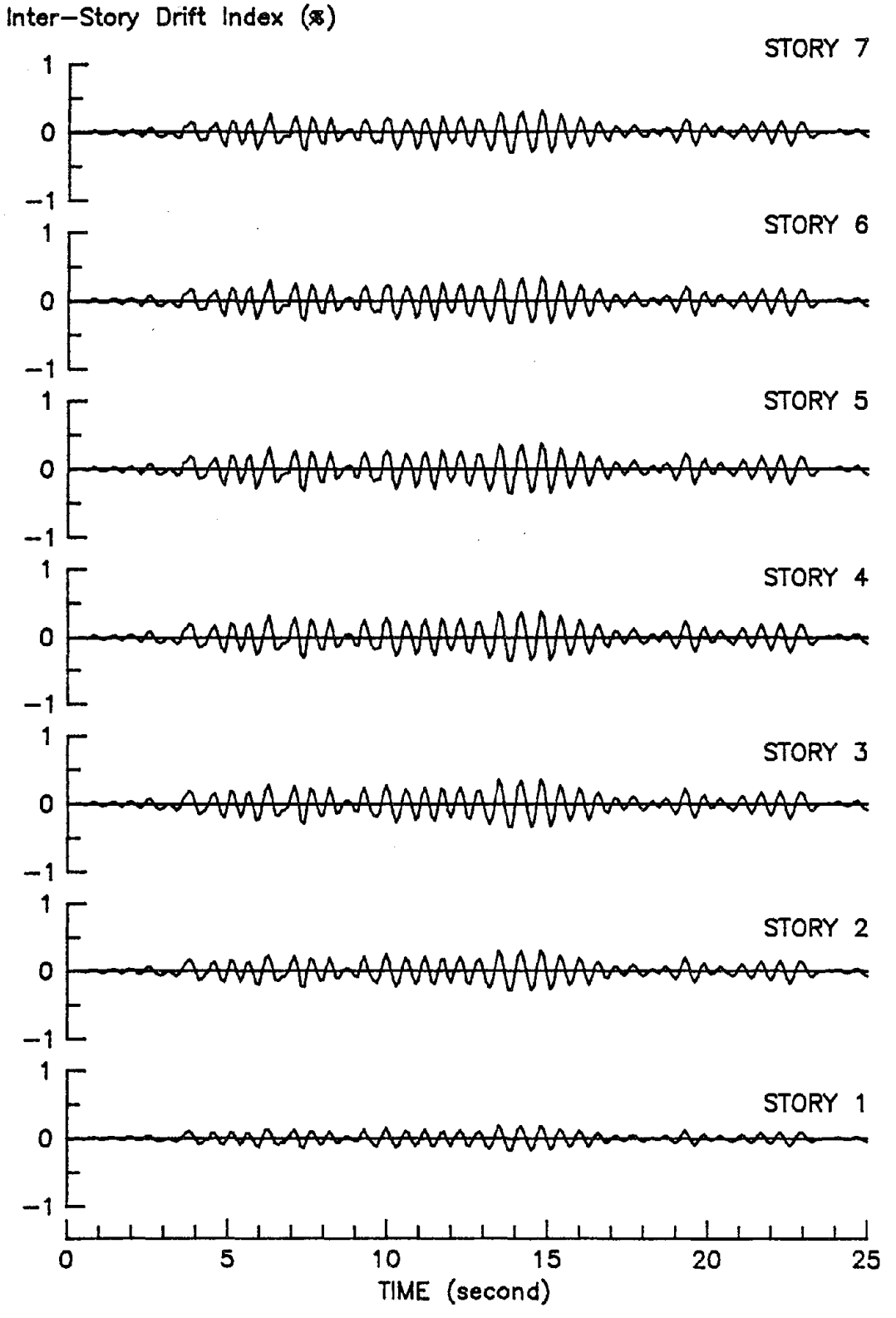

Figure 3.20: INTER-STORY DRIFT INDEX TIME-HISTORIES OF THE CONCENTRIC STRUCTURE DUE TO TAFT-40

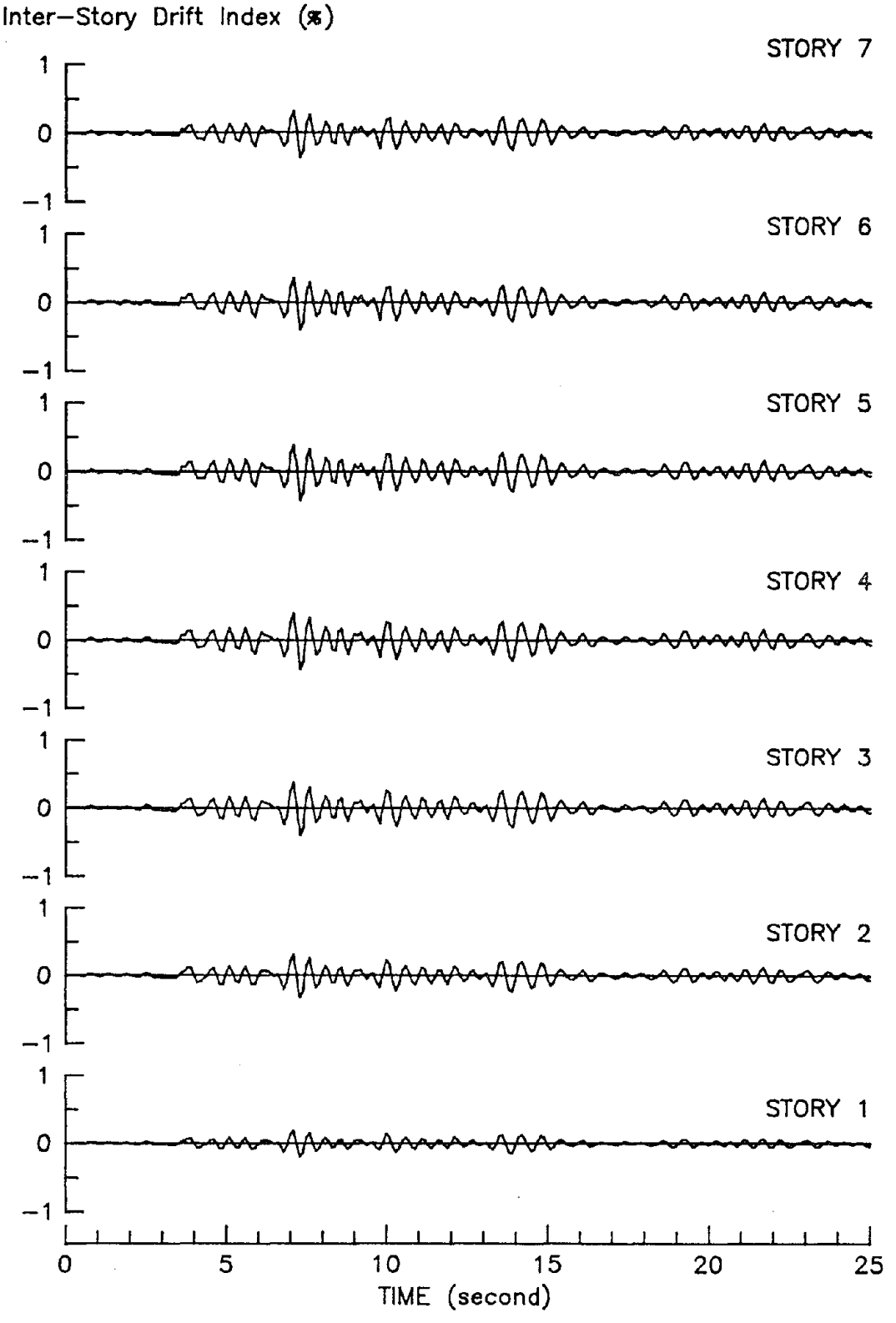

Figure 3.21: INTER-STORY DRIFT INDEX TIME-HISTORIES OF WALL B DUE TO TAFT-40 (e/D = 0.05)

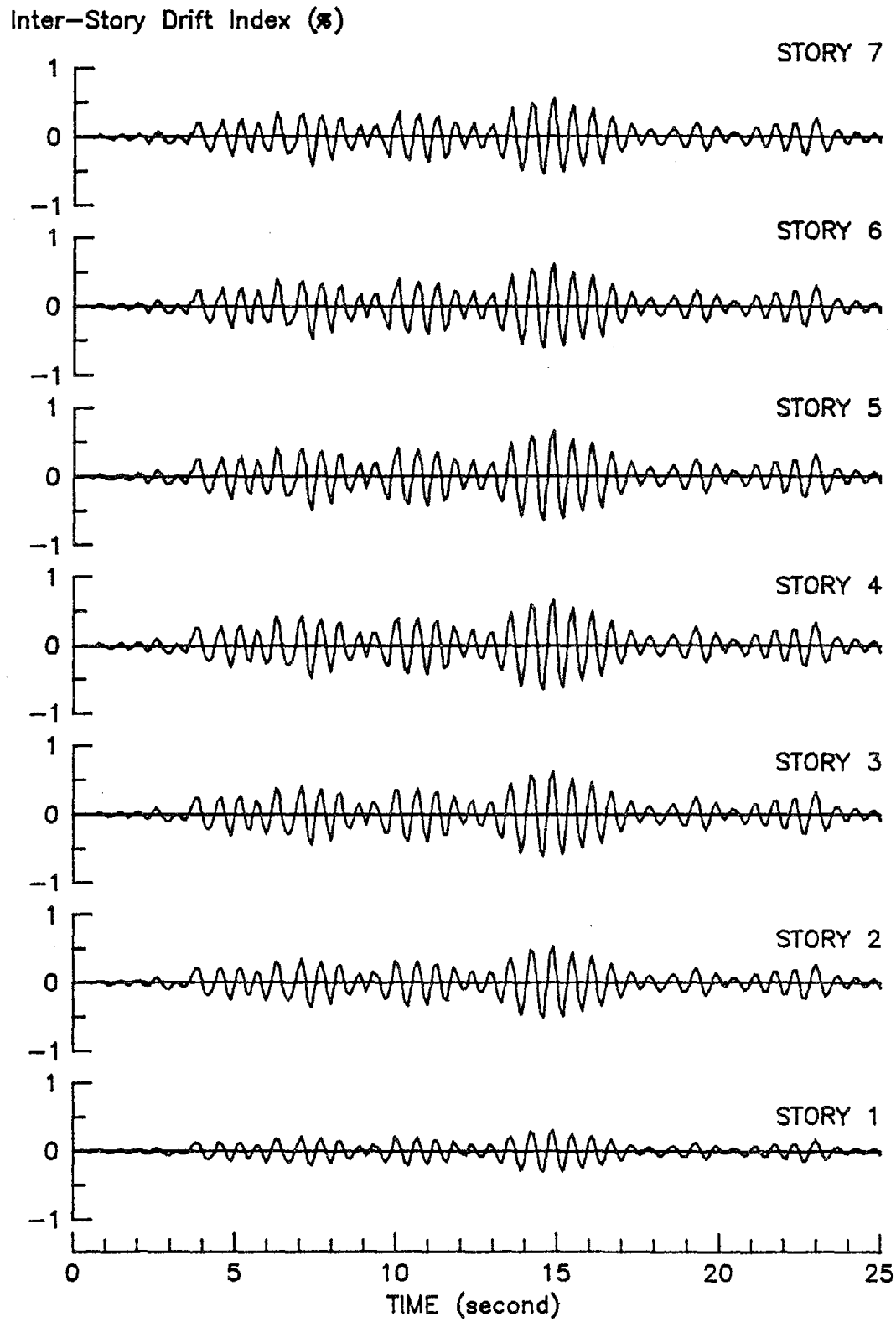

Figure 3.22: INTER-STORY DRIFT INDEX TIME-HISTORIES OF WALL G DUE TO TAFT-40 (e/D = 0.05)

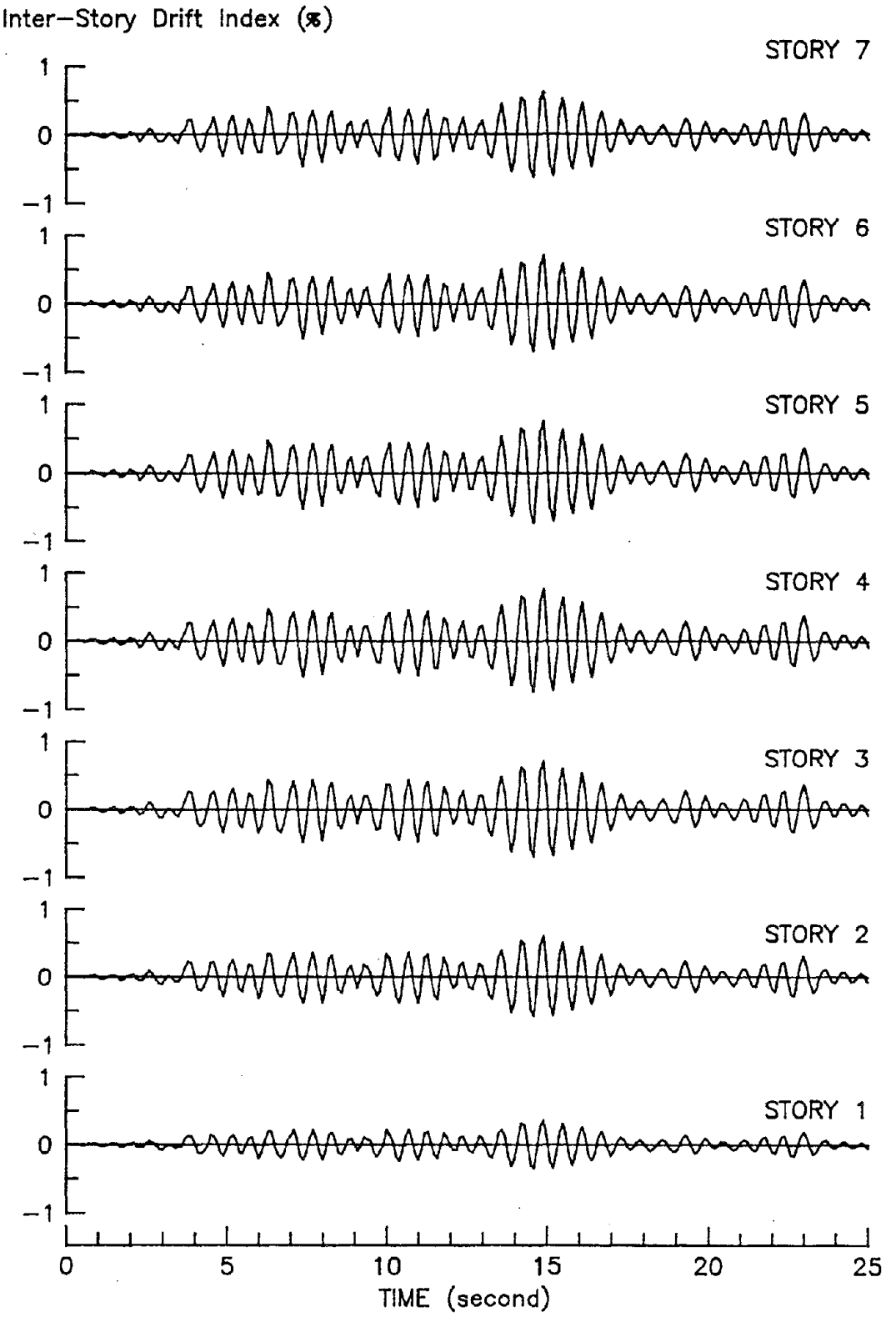

Figure 3.23: INTER-STORY DRIFT INDEX TIME-HISTORIES OF THE CORNER OF THE STRUCTURE DUE TO TAFT-40 (e/D = 0.05)

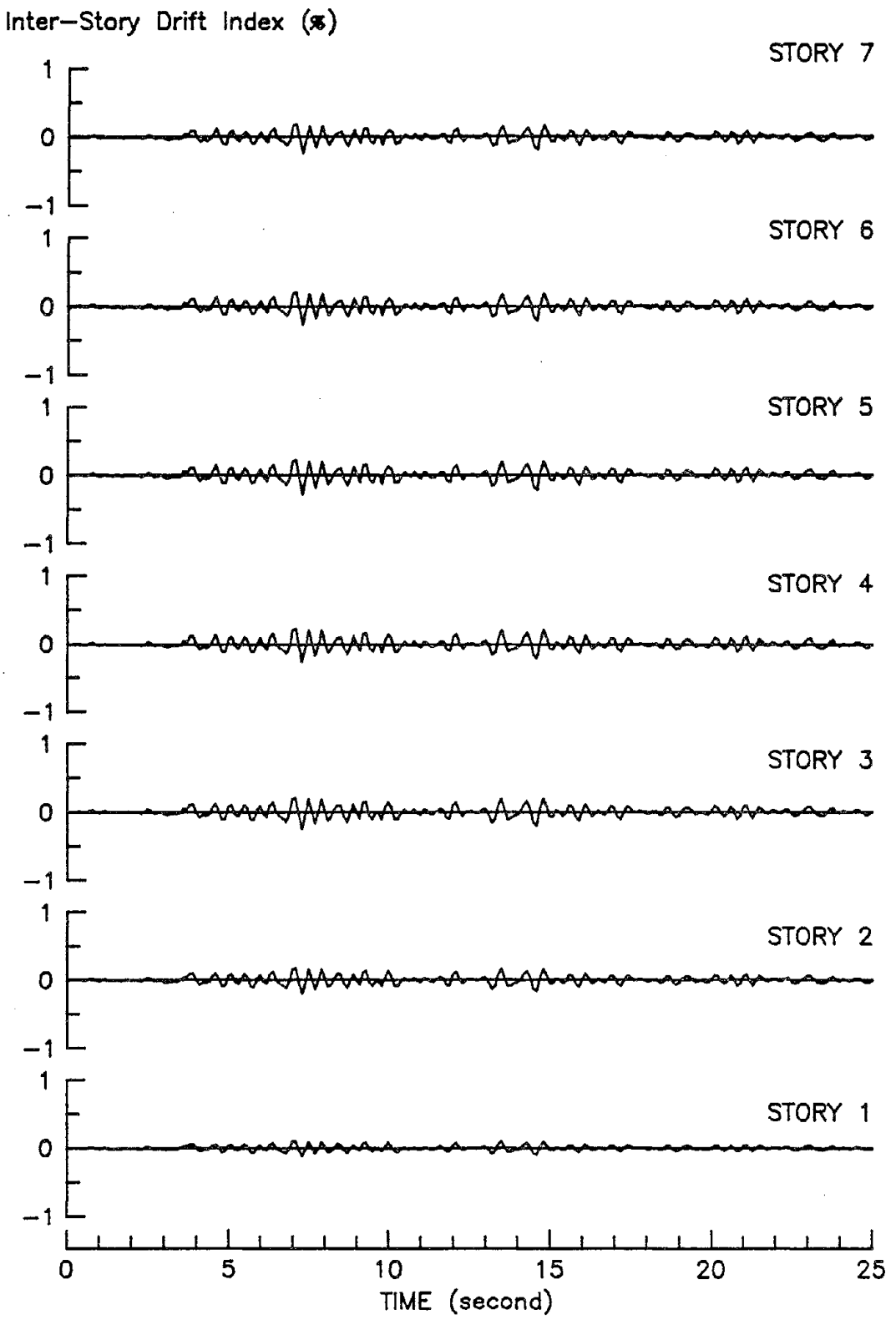

Figure 3.24: INTER-STORY DRIFT INDEX TIME-HISTORIES OF WALL B DUE TO TAFT-40 (e/D = 0.10)

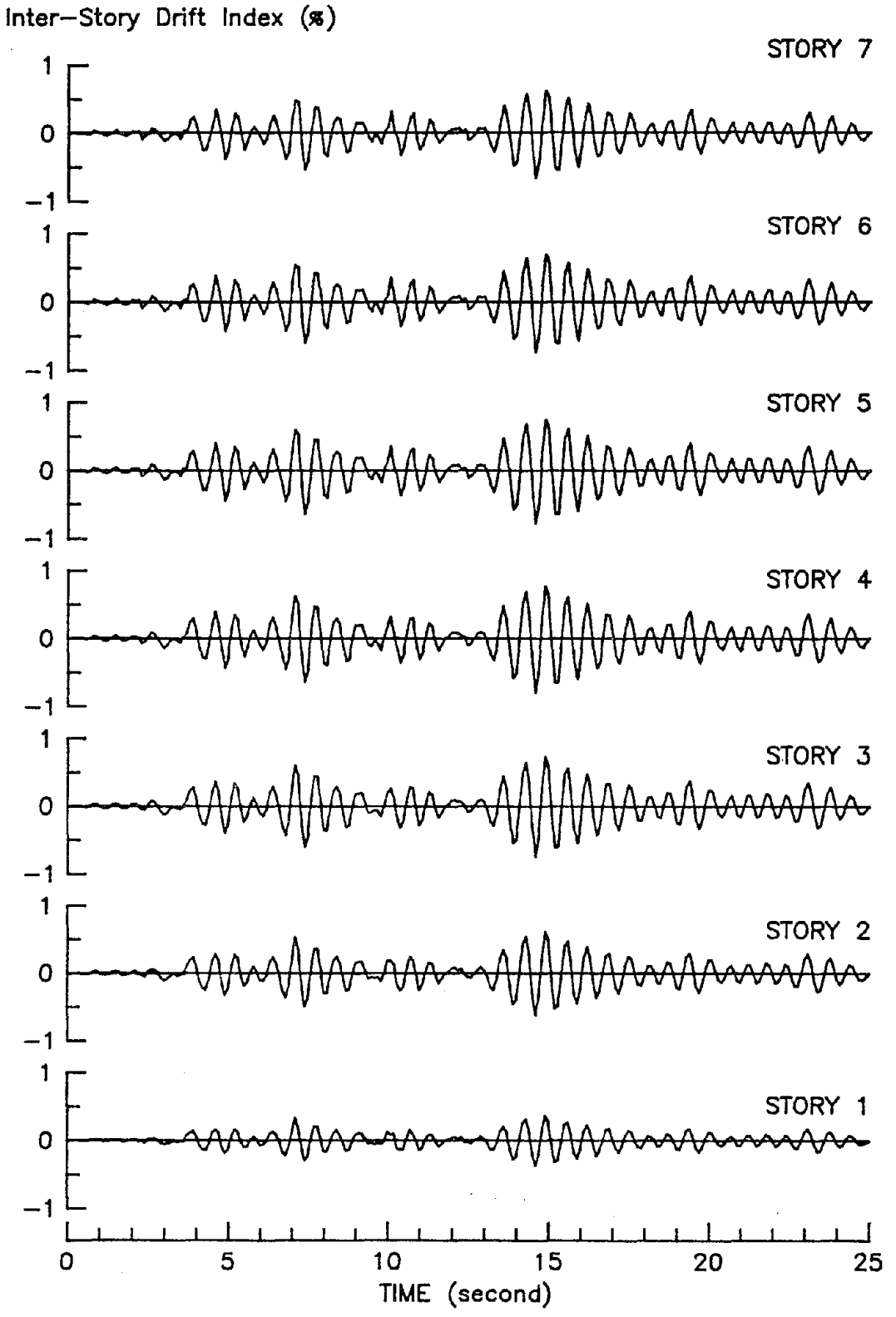

Figure 3.25: INTER-STORY DRIFT INDEX TIME-HISTORIES OF WALL G DUE TO TAFT-40 (e/D = 0.10)

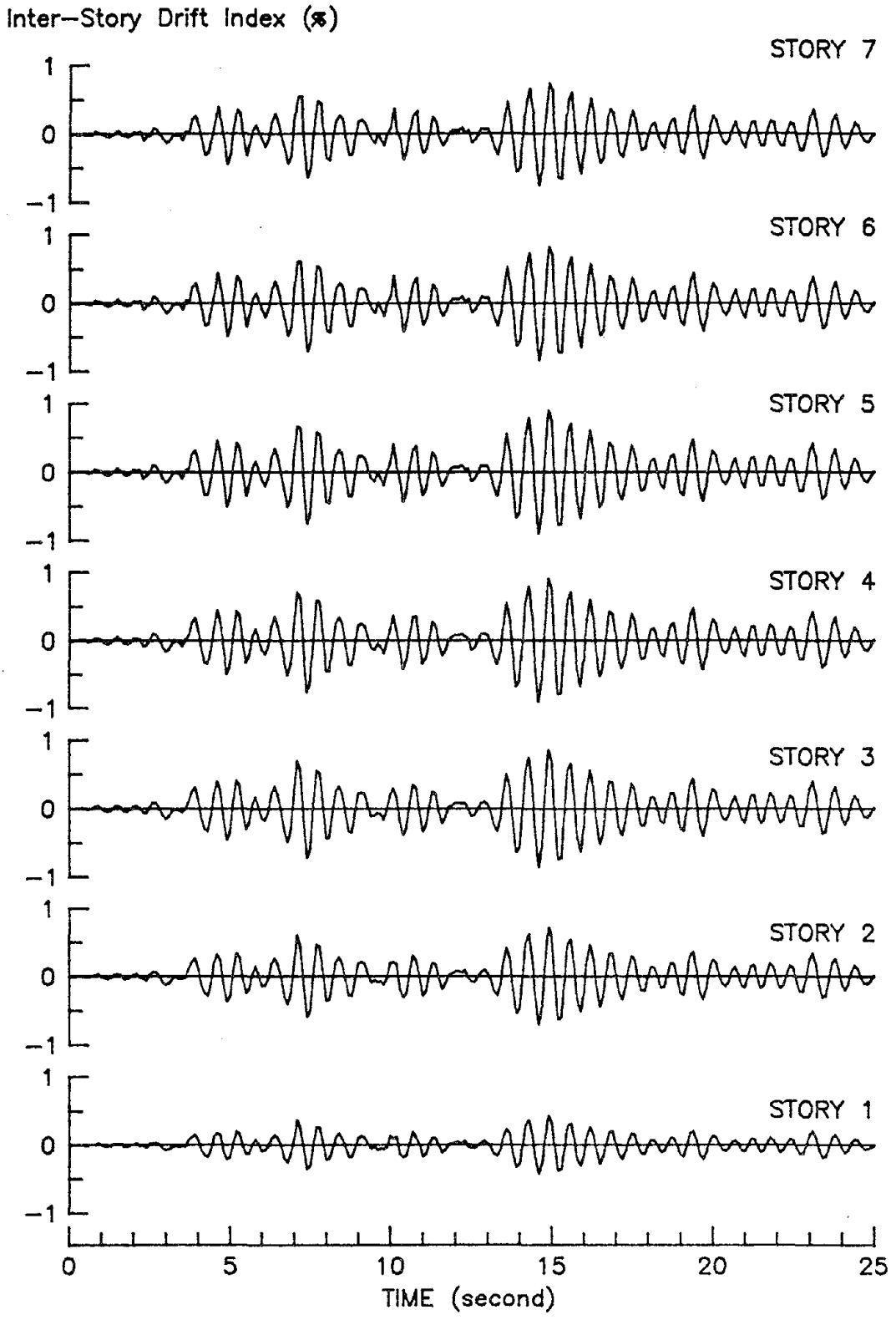

Figure 3.26: INTER-STORY DRIFT INDEX TIME-HISTORIES OF THE CORNER OF THE STRUCTURE DUE TO TAFT-40 (e/D = 0.10)

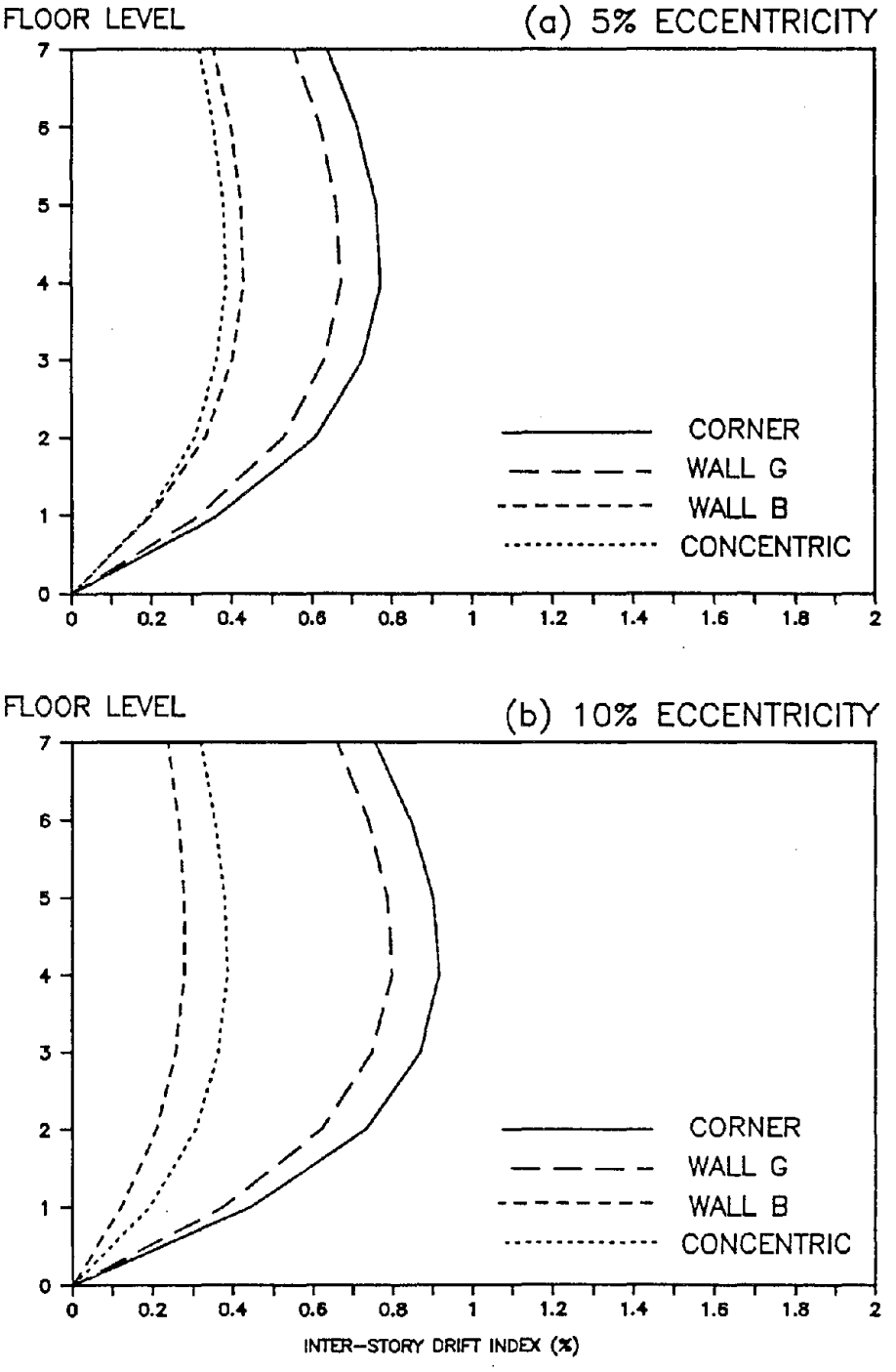

Figure 3.27: INTER-STORY DRIFT INDEX ENVELOPES DUE TO TAFT-40

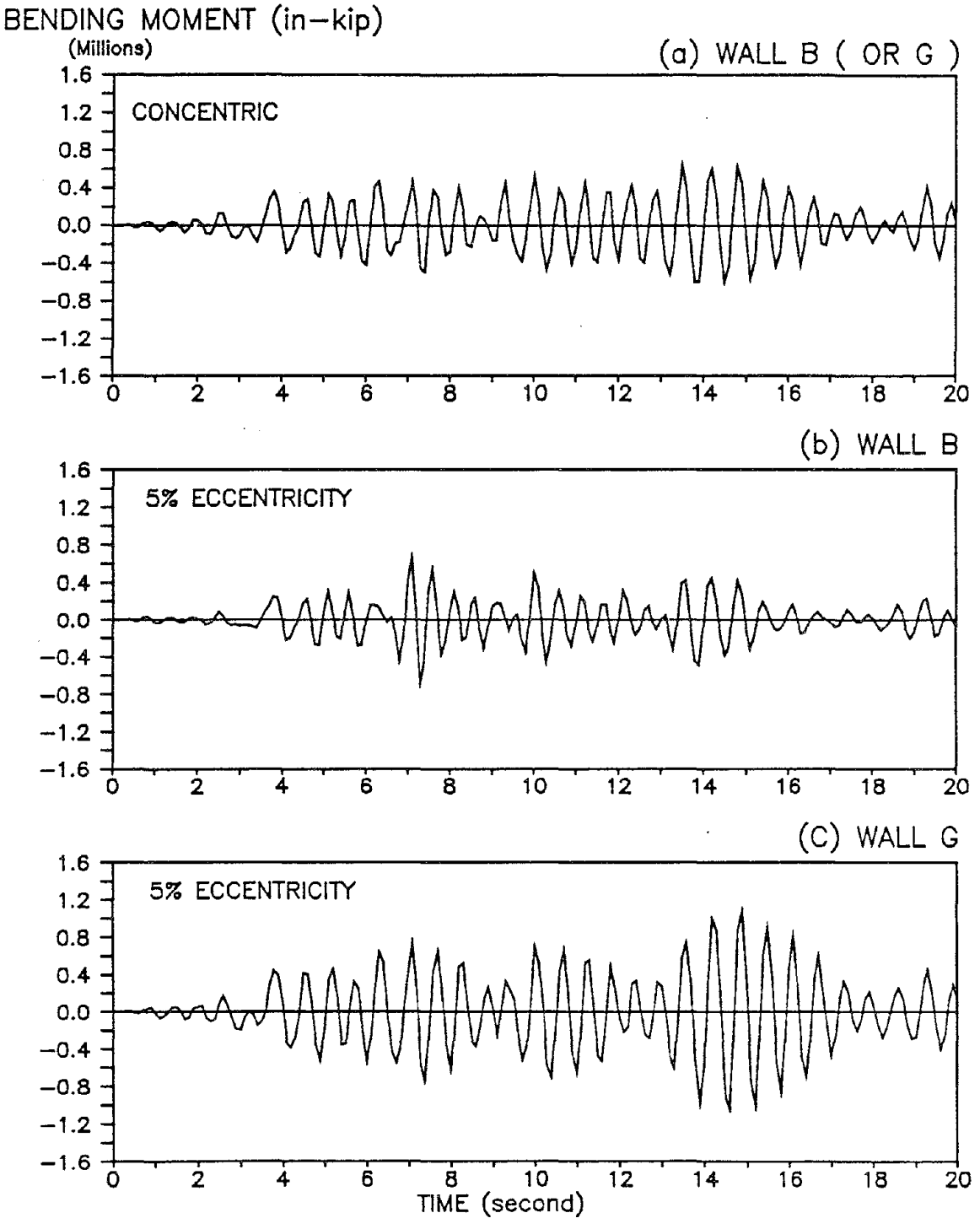

Figure 3.28: TIME-HISTORIES OF BASE MOMENT OF WALLS (e/D = 0.05 , TAFT-40)

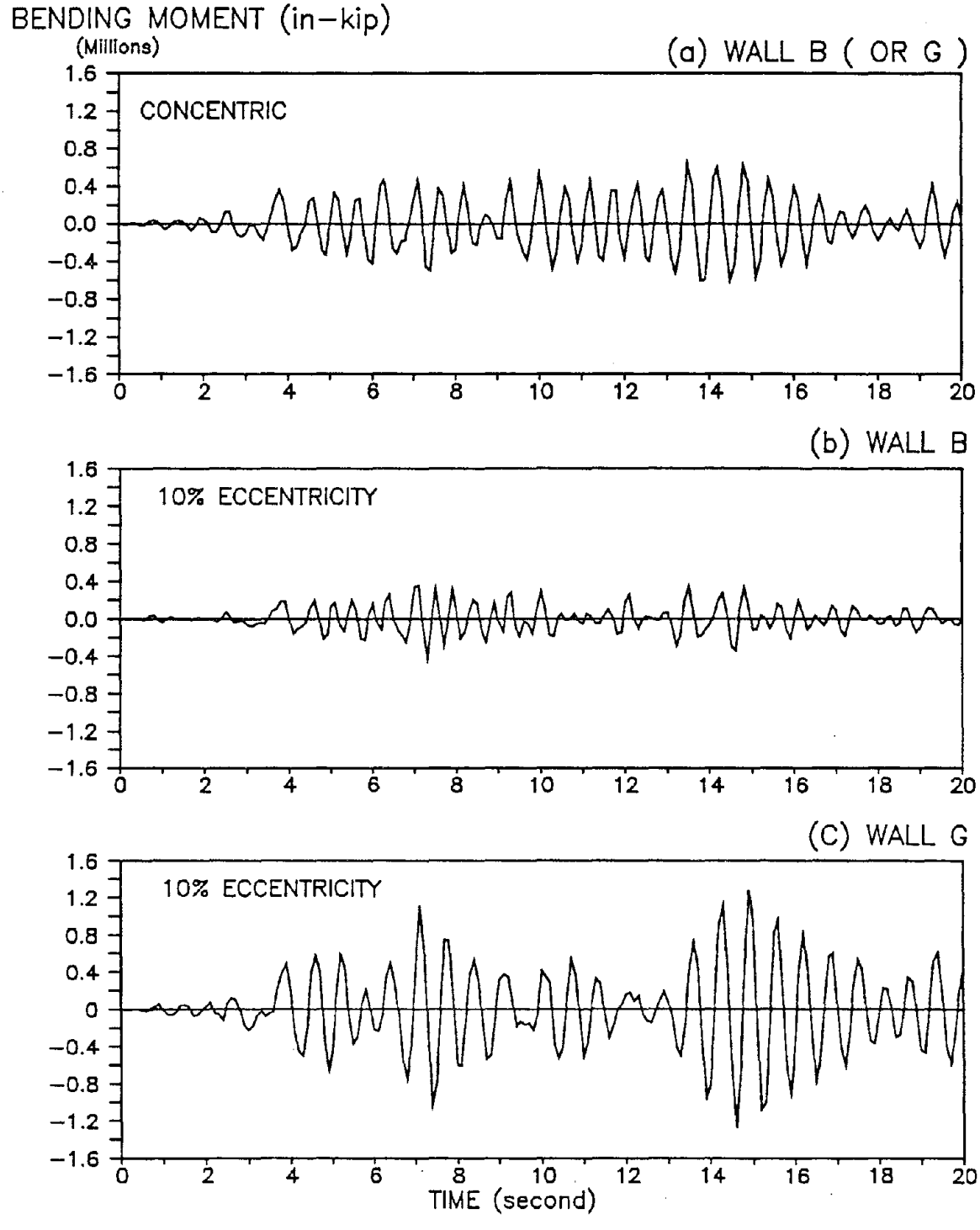

Figure 3.29: TIME-HISTORIES OF BASE MOMENT OF WALLS (e/D = 0.10 , TAFT-40)

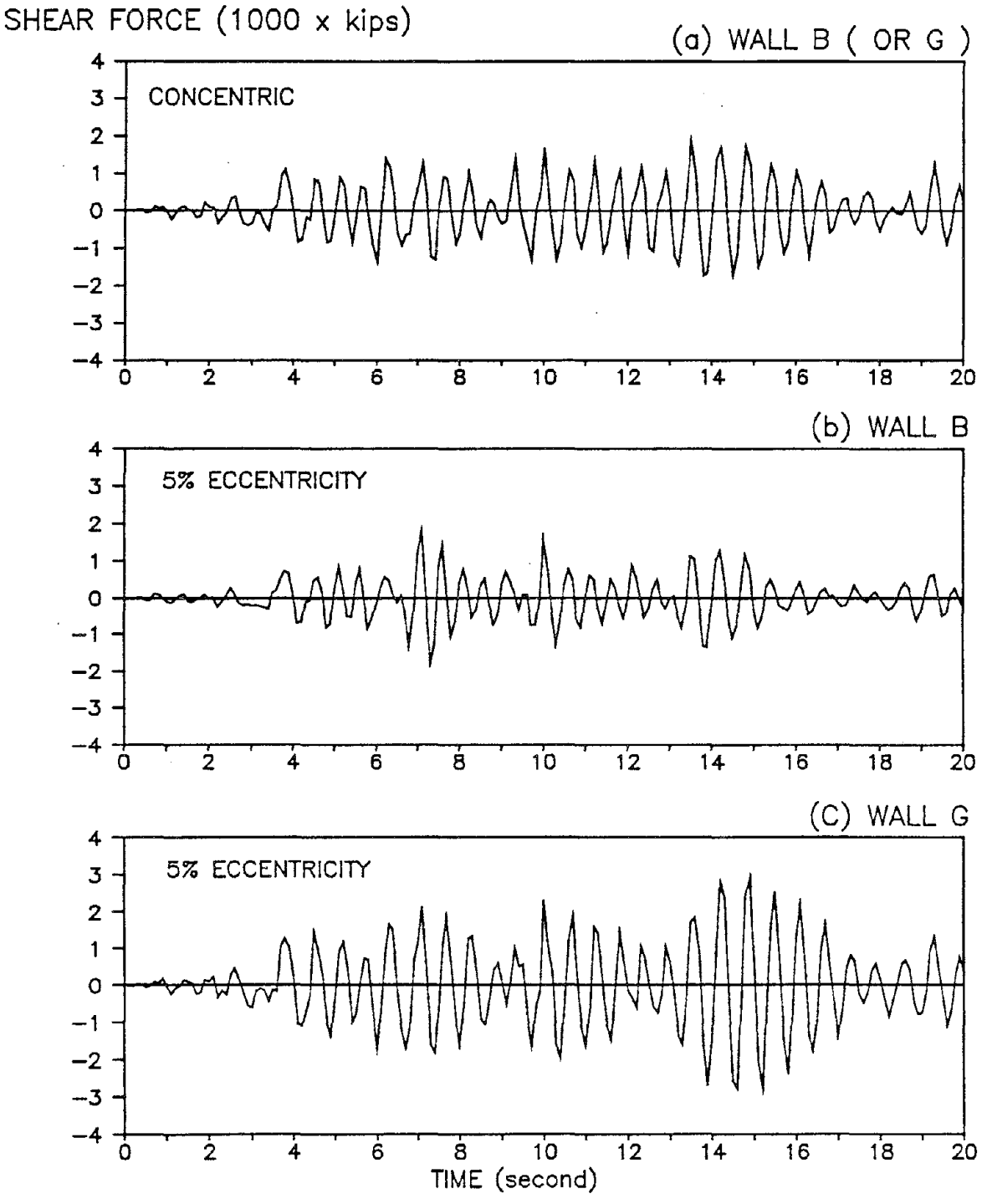

Figure 3.30: TIME-HISTORIES OF BASE SHEAR OF WALLS (e/D = 0.05 , TAFT-40)

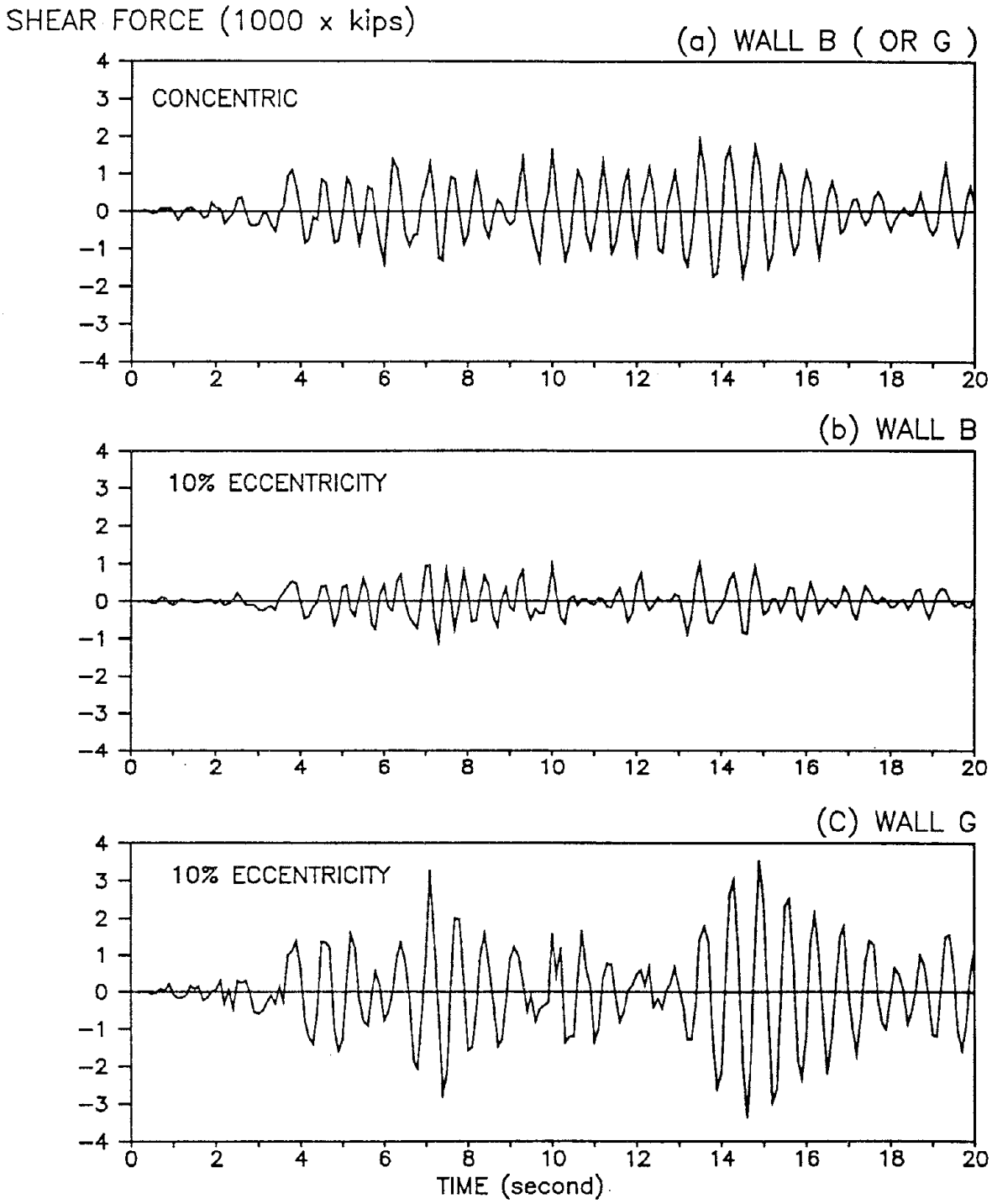

Figure 3.31: TIME-HISTORIES OF BASE SHEAR OF WALLS (e/D = 0.10 , TAFT-40)

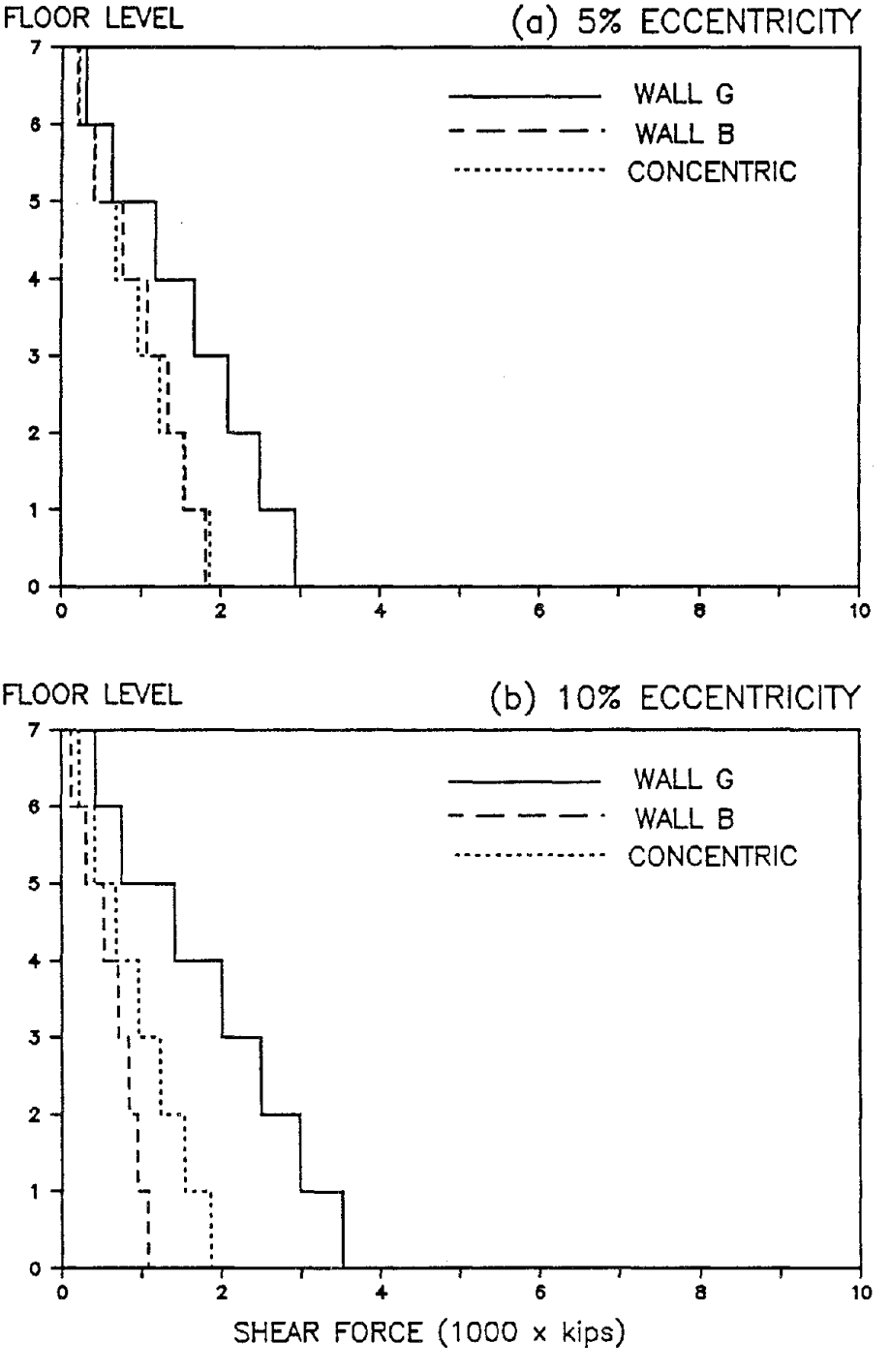

Figure 3.32: SHEAR FORCE ENVELOPES DUE TO TAFT-40

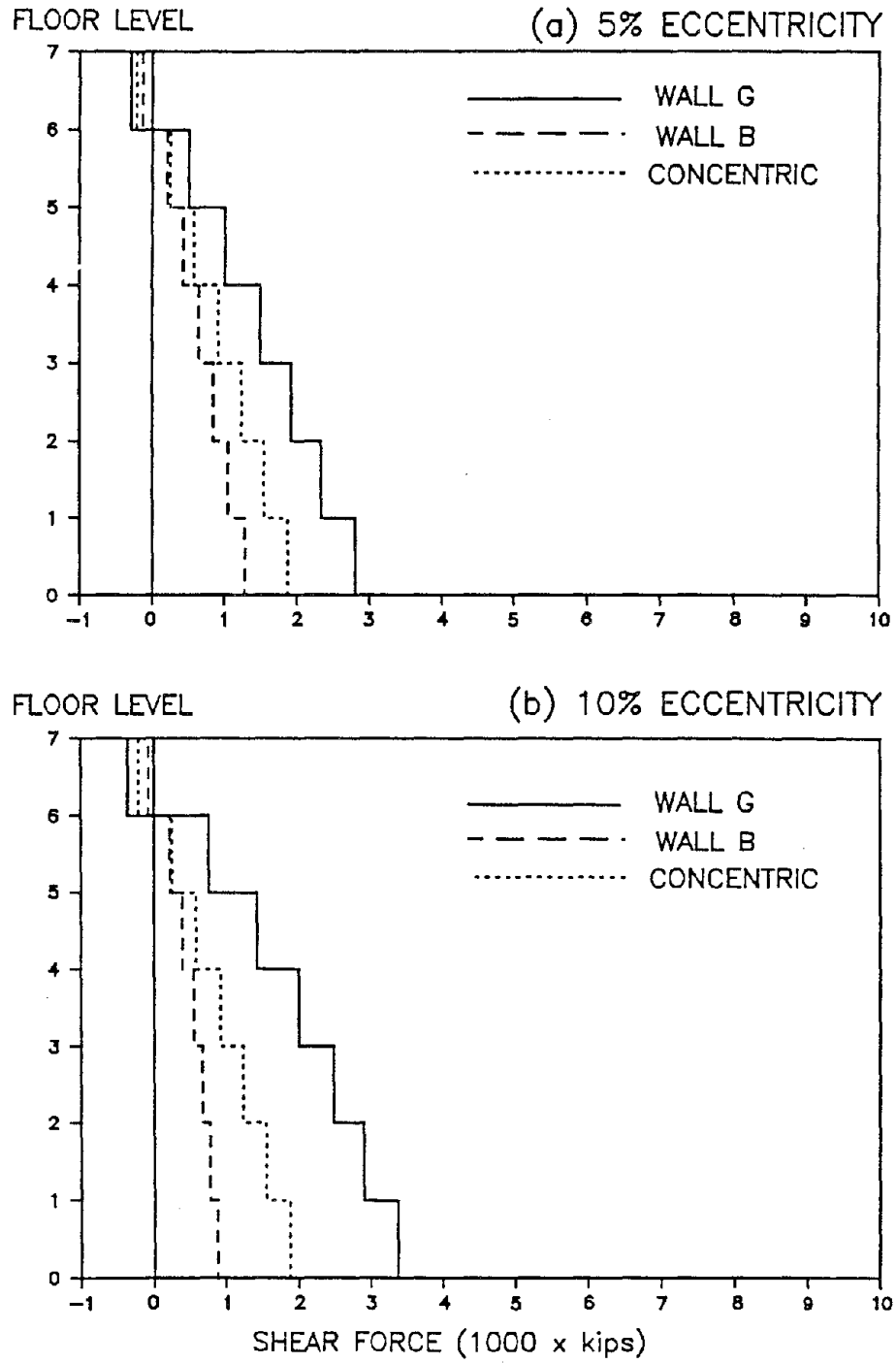

Figure 3.33: SHEAR FORCE PROFILES WHEN TOTAL BASE SHEAR IS MAXIMUM

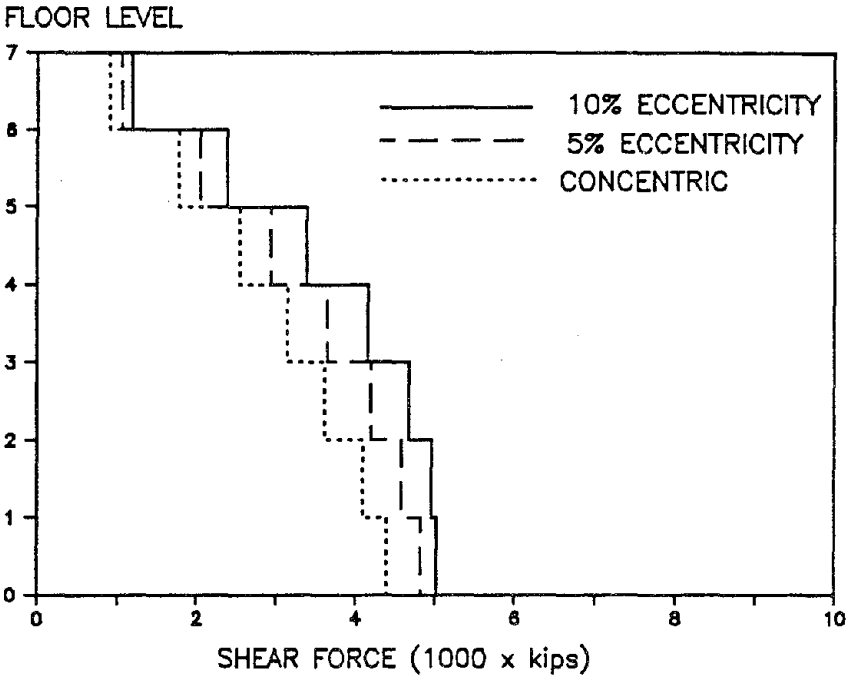

Figure 3.34: TOTAL STORY SHEAR ENVELOPES

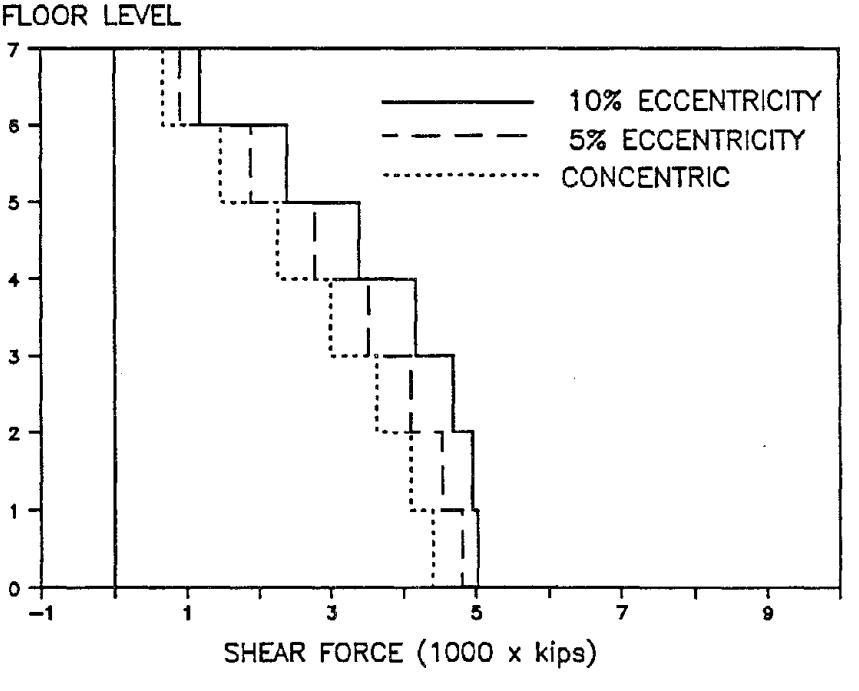

Figure 3.35: TOTAL STORY SHEAR FORCE PROFILES WHEN TOTAL BASE SHEAR IS MAXIMUM

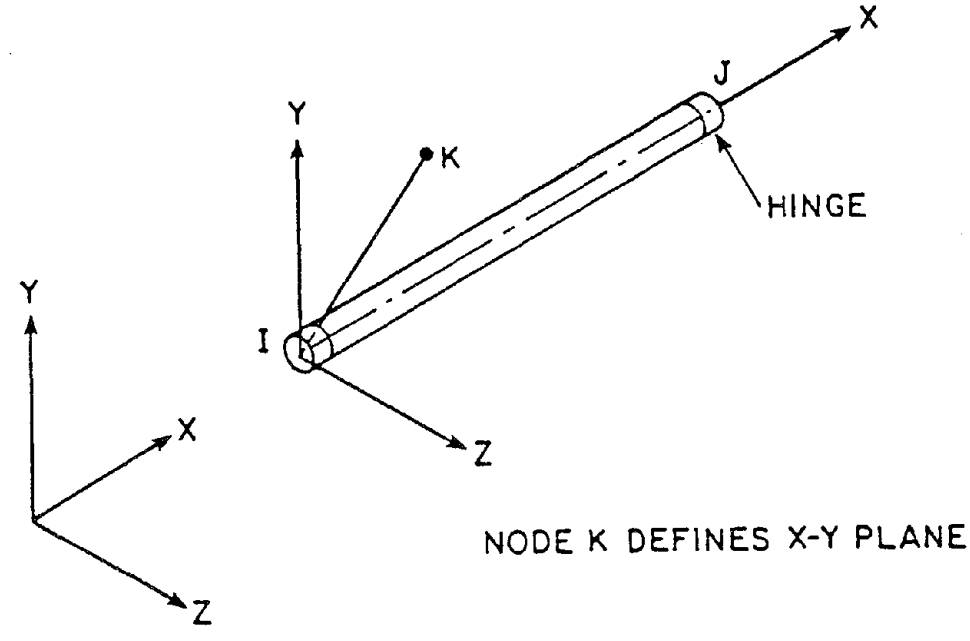

(a) ELEMENT AXES

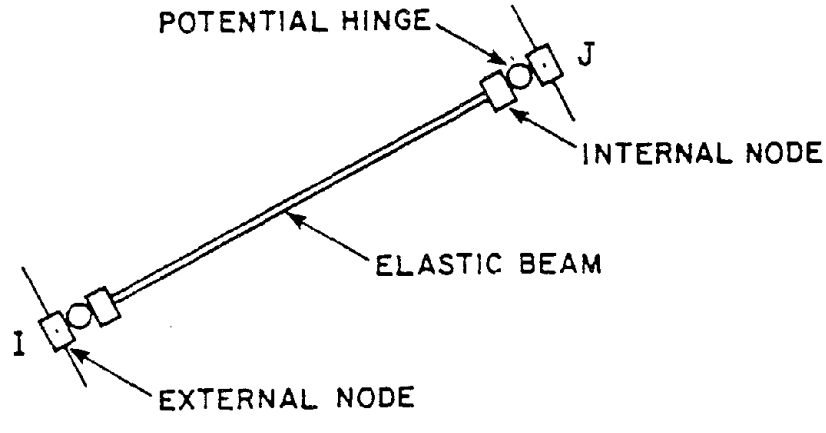

(b) ELEMENT IDEALIZATION

Figure 4.1: THREE-DIMENSIONAL BEAM-COLUMN ELEMENT AND ITS IDEALIZATIONS [34,35]

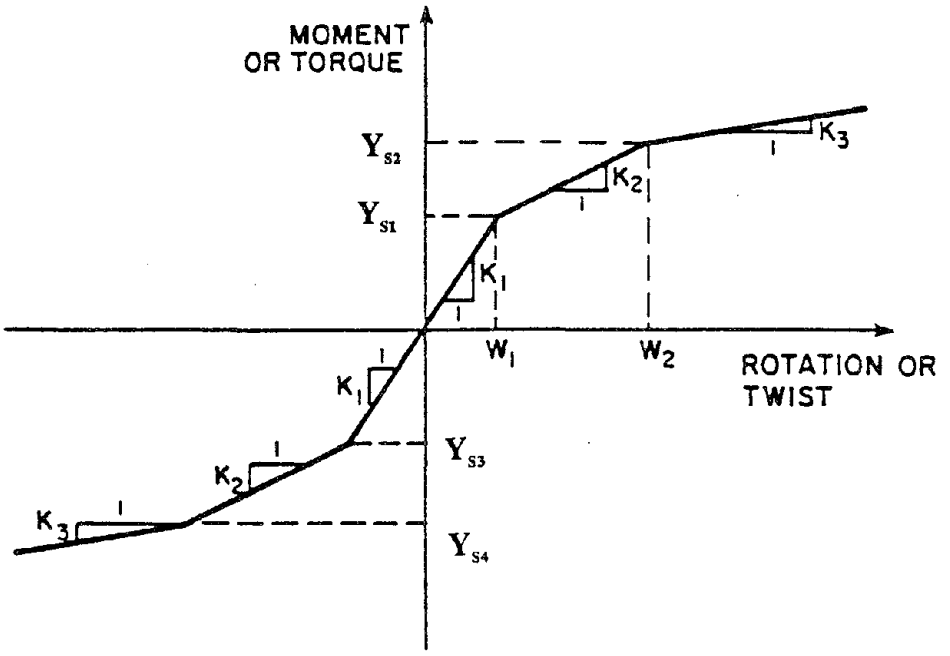

$W_1 : W_2$ MUST BE SAME FOR ALL RELATIONSHIPS

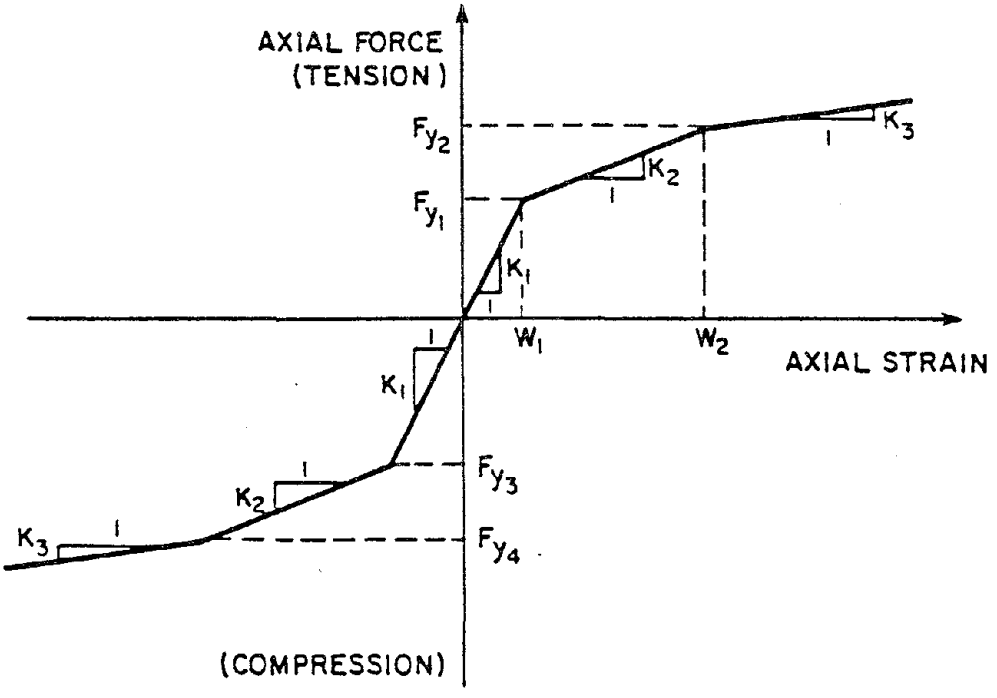

Figure 4.2: ACTION-DEFORMATION RELATIONSHIPS [34,35]

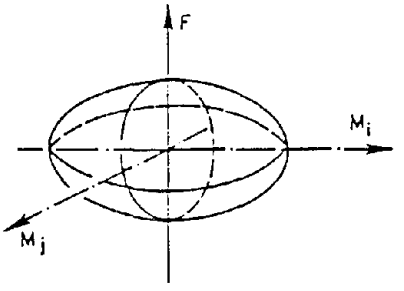

$$\phi = \left(\frac{M_y}{M_{yu}}\right)^2 + \left(\frac{M_z}{M_{zu}}\right)^2 + \left(\frac{M_x}{M_{xu}}\right)^2 + \left(\frac{F}{F_u}\right)^2 - 1$$

(A) SURFACE TYPE 1

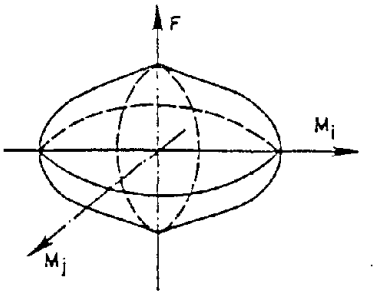

$$\phi = \left[\left(\frac{M_y}{M_{yu}}\right)^2 + \left(\frac{M_z}{M_{zu}}\right)^2 + \left(\frac{M_x}{M_{xu}}\right)^{2/3}\right]^{3/4} + \left(\frac{F}{F_u}\right)^2 - 1$$

(B) SURFACE TYPE 2

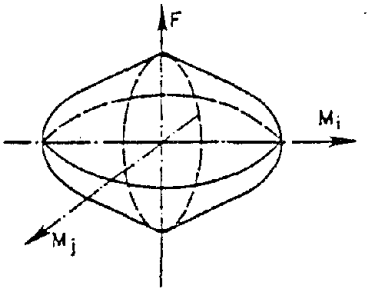

$$\phi = \left[\left(\frac{M_y}{M_{yu}}\right)^2 + \left(\frac{M_z}{M_{zu}}\right)^2 + \left(\frac{M_x}{M_{xu}}\right)^{2/3}\right]^{3/4} + \left(\frac{F}{F_u}\right)^{a_1} - 1$$

(C) SURFACE TYPE 3

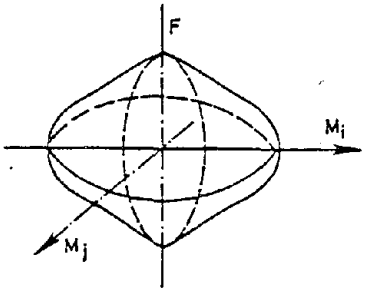

$$\phi = \left[\left(\frac{M_y}{M_{yu}}\right)^2 + \left(\frac{M_z}{M_{zu}}\right)^2 + \left(\frac{M_x}{M_{xu}}\right)^{a_2}\right]^{a_1} + \left(\frac{F}{F_u}\right)^{a_3} - 1$$

(D) SURFACE TYPE 4

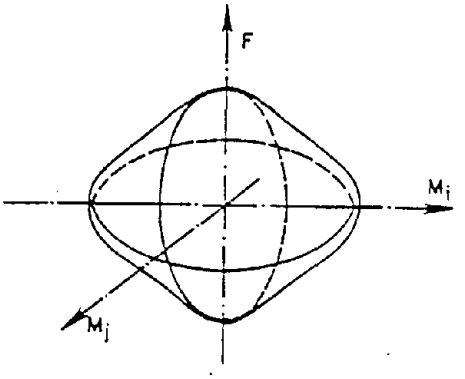

$$\phi = \left(\frac{M_x}{M_{xu}}\right)^{a_1} + \left(\frac{M_z}{M_{zu}}\right)^{a_2} + \left(\frac{T}{T_u}\right)^{a_3} + \left(\frac{F}{F_u}\right)^{a_4} - 1$$

Figure 4.3: YIELD SURFACES [34,35]

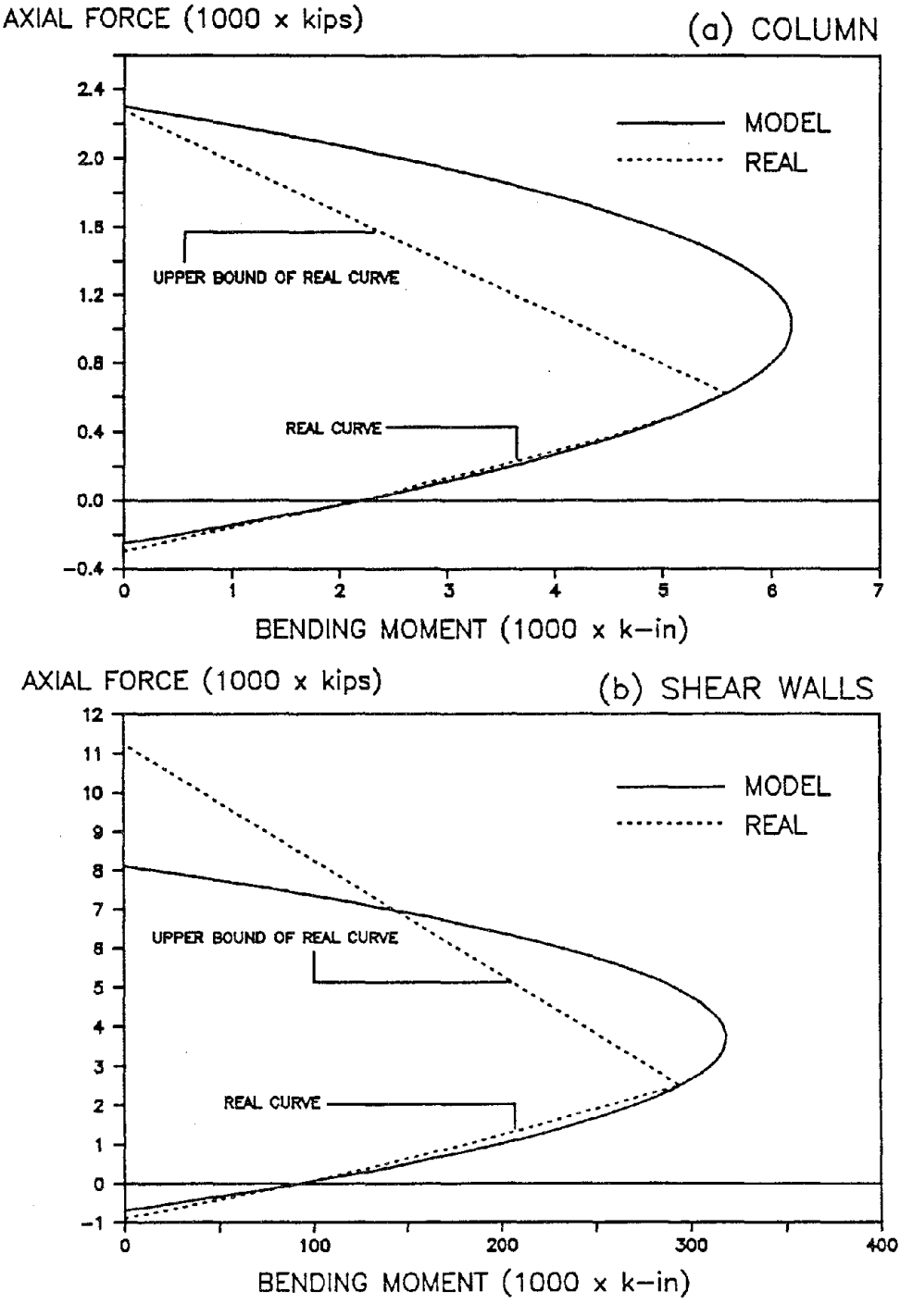

Figure 4.4: MOMENT-AXIAL FORCE INTERACTIONS OF COLUMNS AND SHEAR WALLS

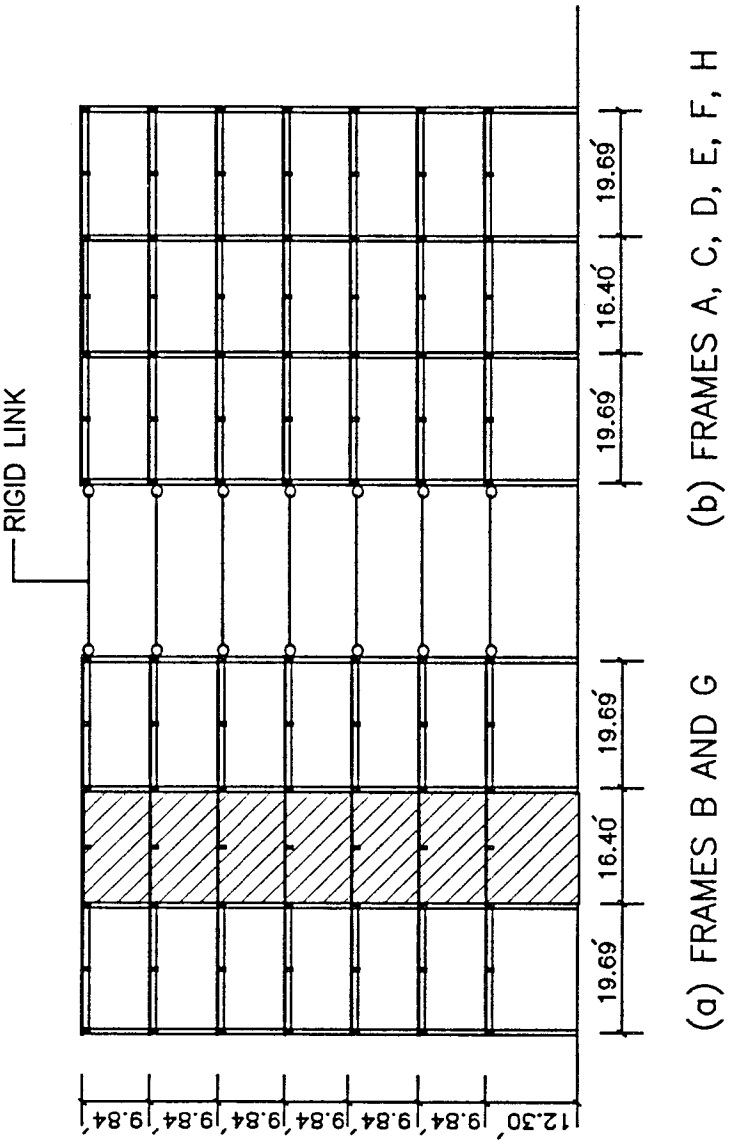

Figure 4.5: TWO-DIMENSIONAL MODEL OF THE STRUCTURE

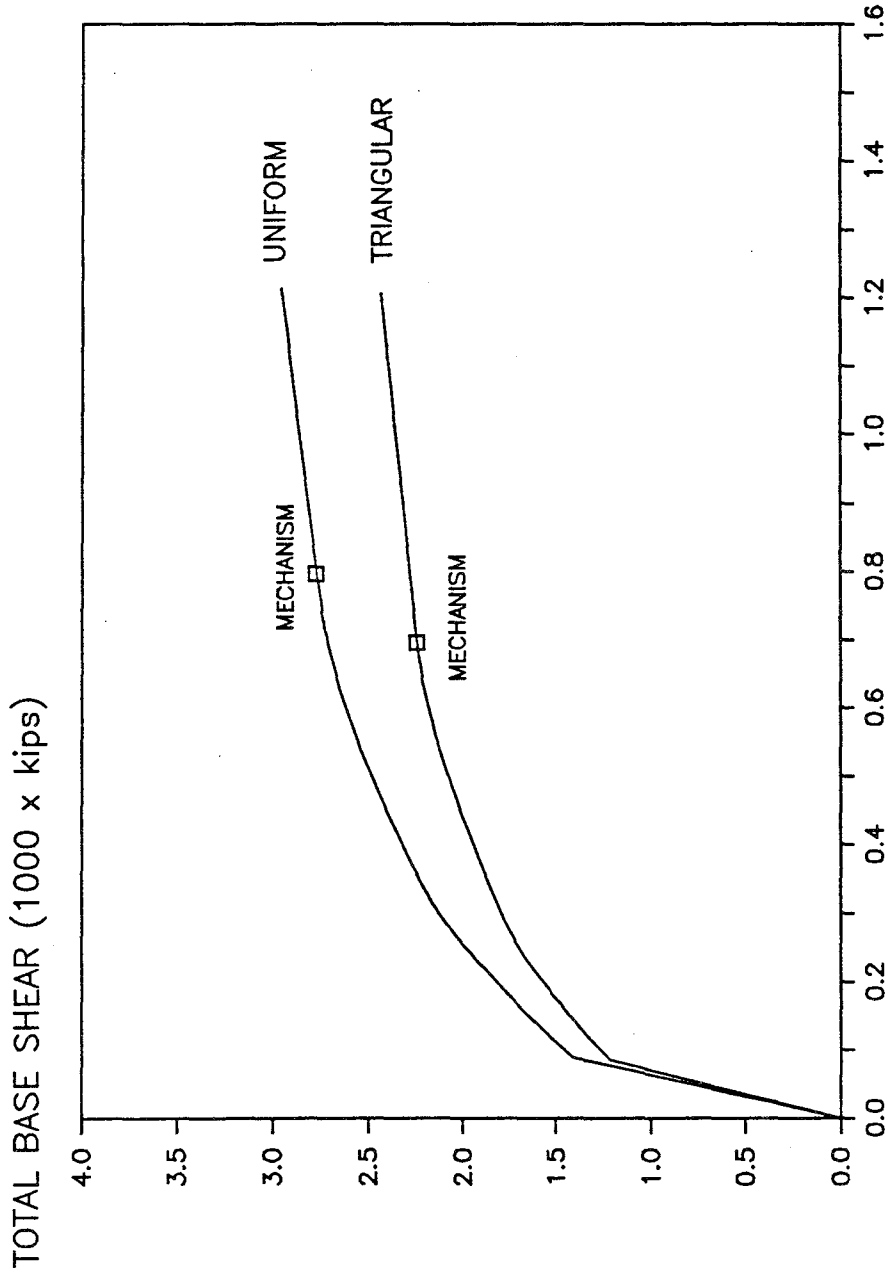

Figure 4.6: TOTAL BASE SHEAR VERSUS FIRST STORY INTER-STORY DRIFT INDEX FOR THE 2-D MATHEMATICAL MODEL

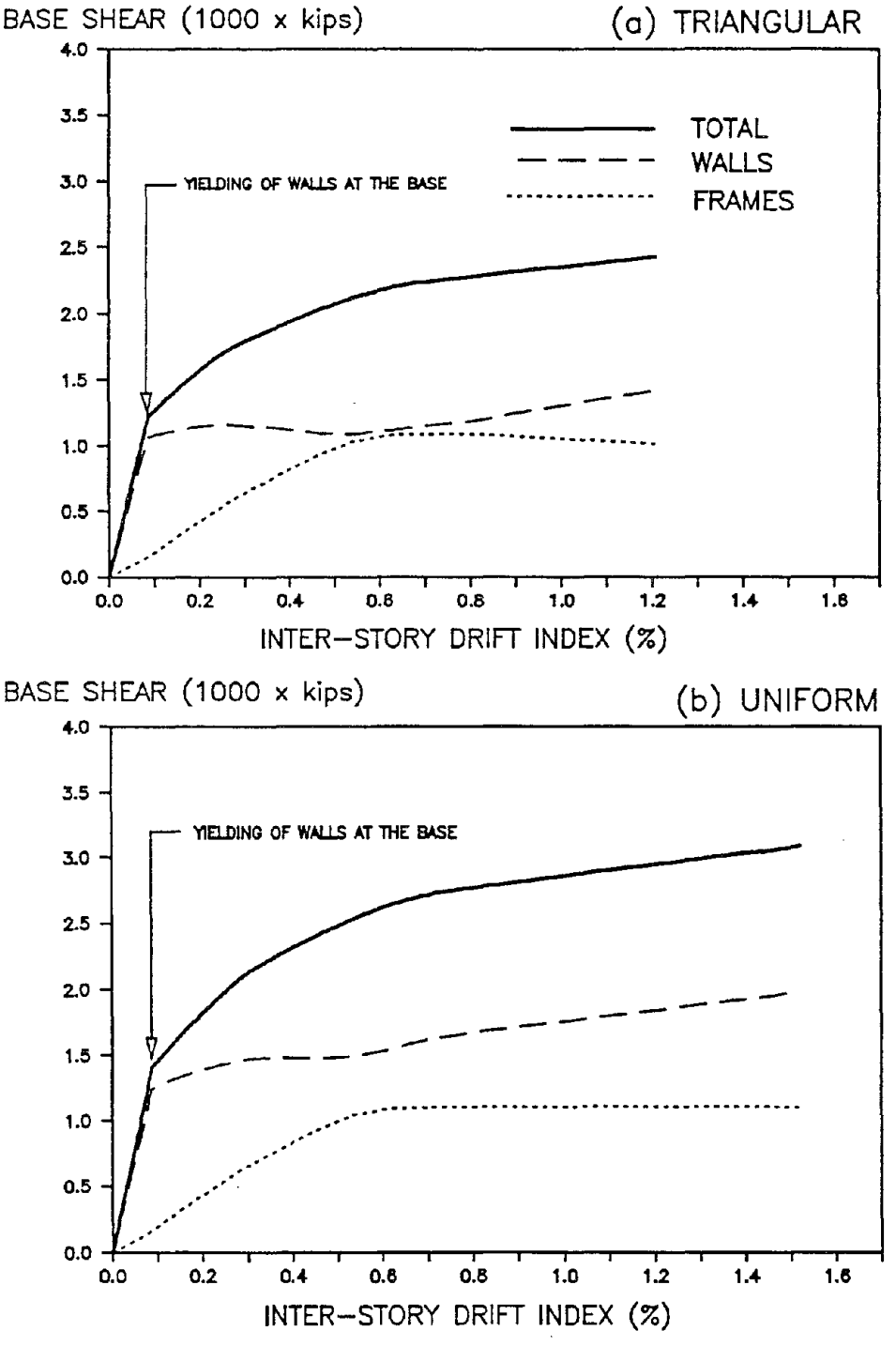

Figure 4.7: SHEAR VERSUS INTER-STORY DRIFT INDEX OF THE FIRST STORY

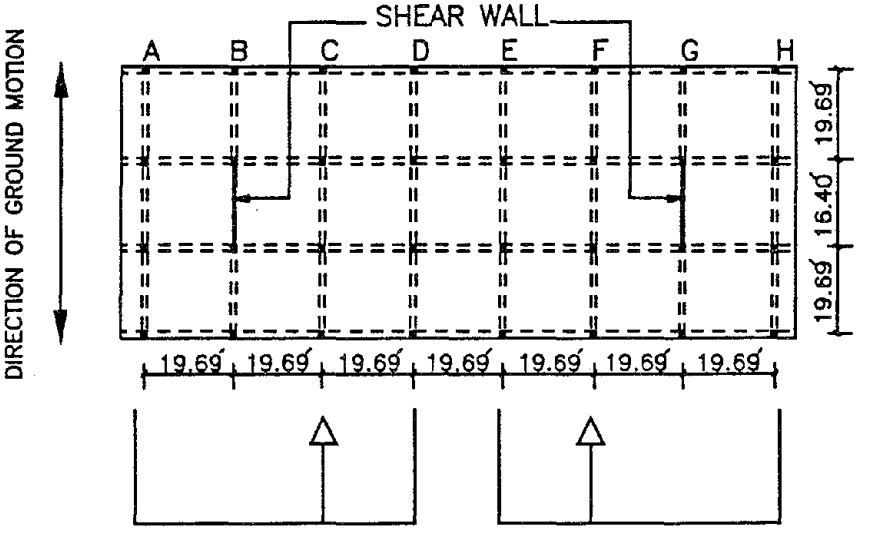

(a) PLAN OF THE REAL STRUCTURE

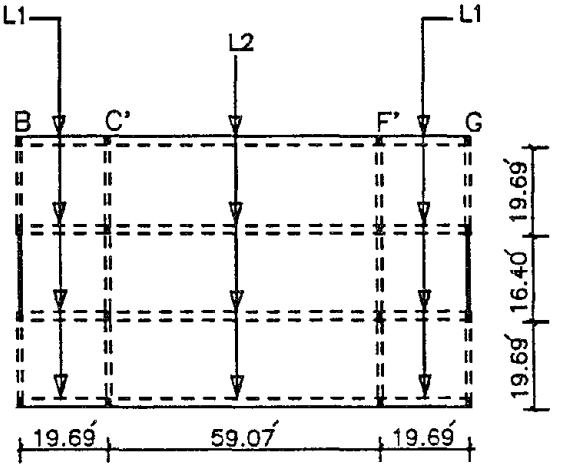

(b) PLAN OF THE MODEL

Figure 4.8: PLANS OF THE REAL AND MODEL STRUCTURES

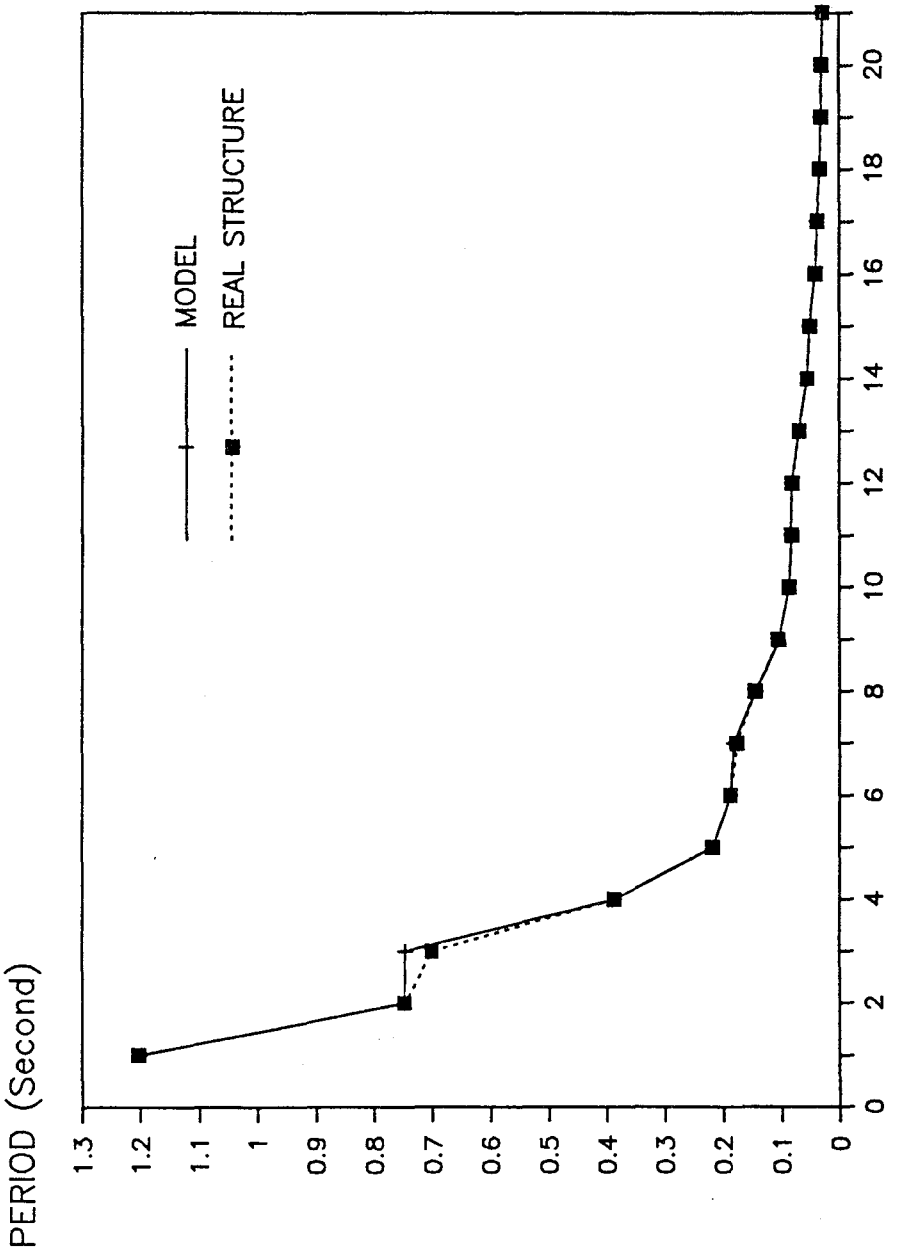

Figure 4.9: PERIODS OF REAL STRUCTURE AND MODEL

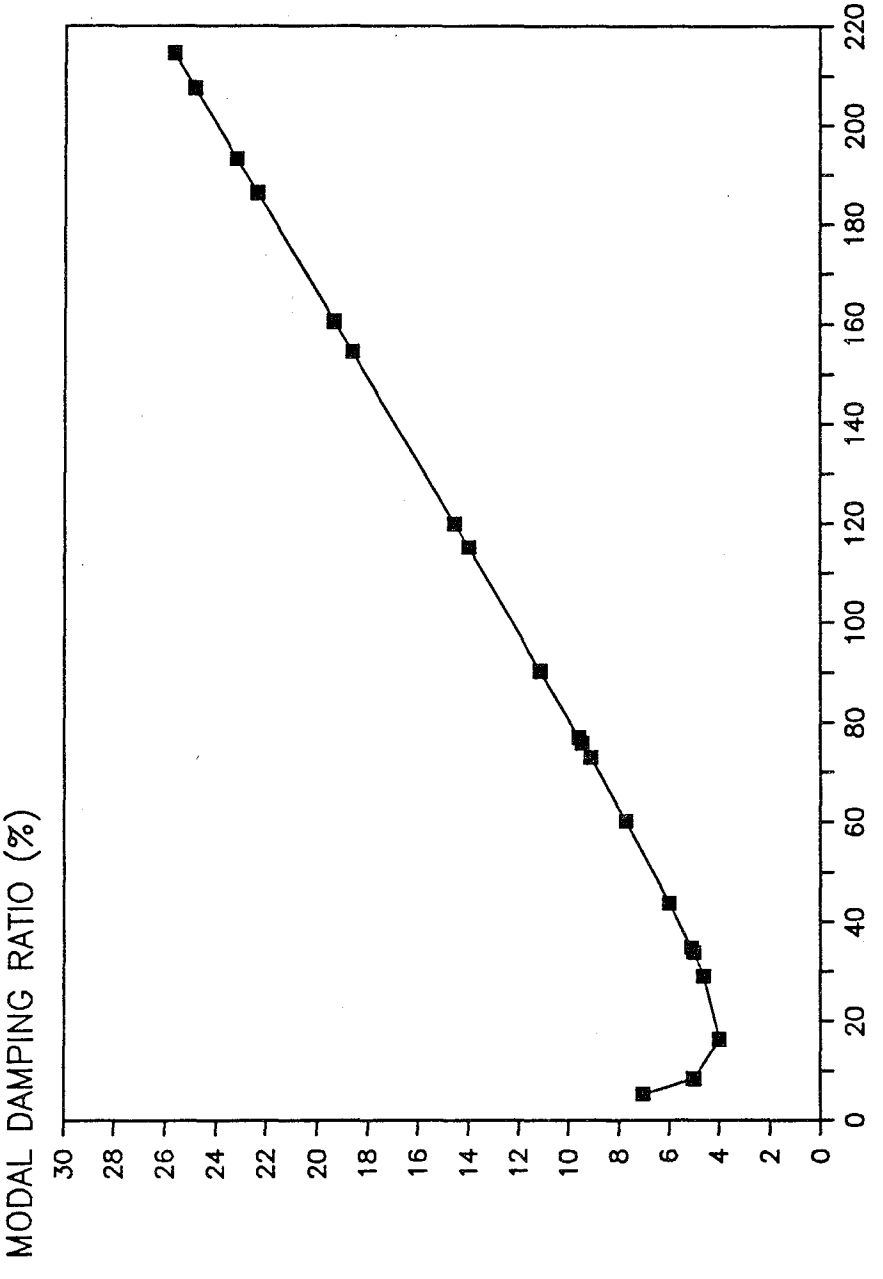

Figure 4.10: DAMPING RATIO VERSUS FREQUENCY FOR THE MODEL

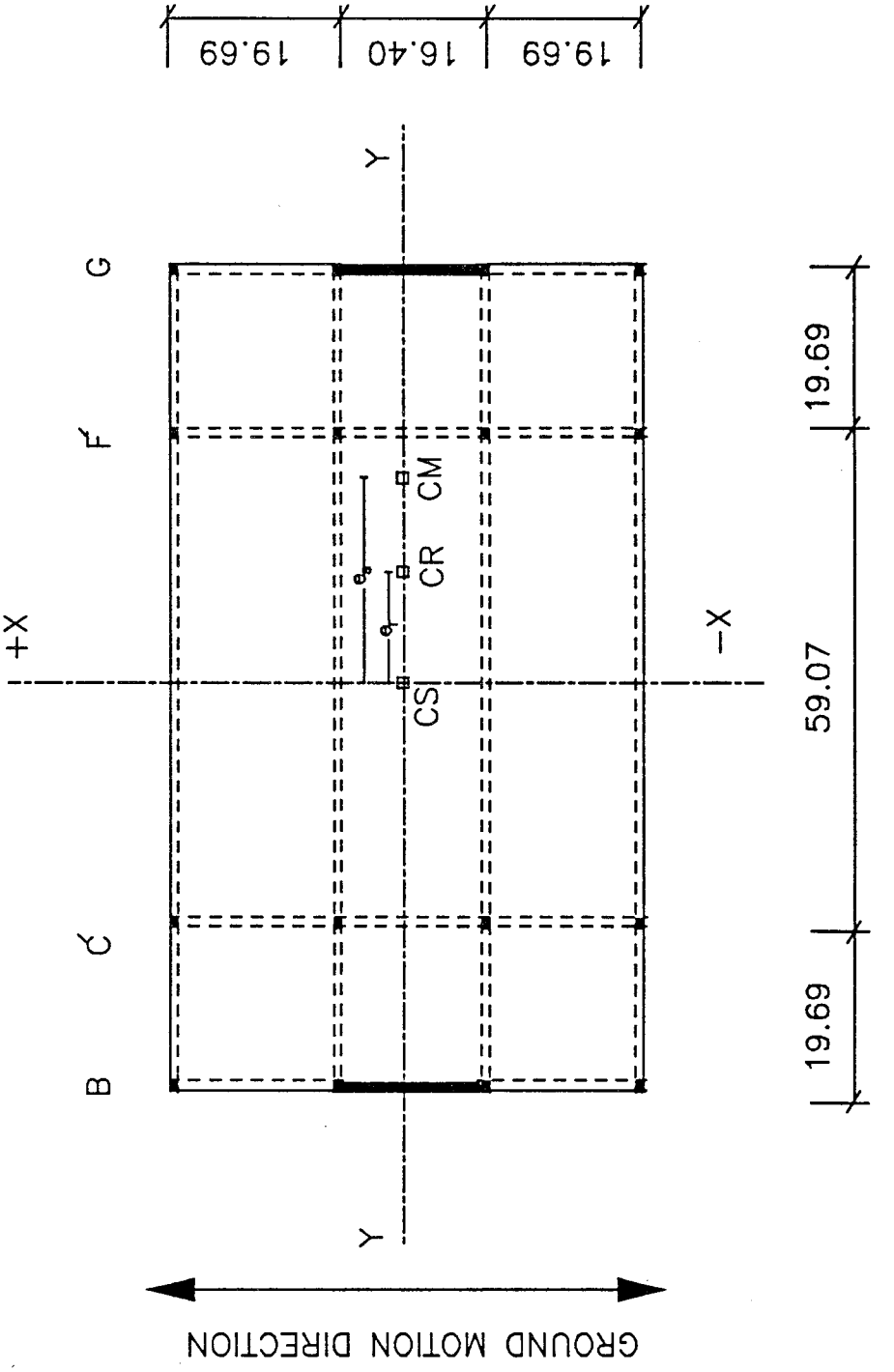

Figure 5.1: PLAN VIEW OF THE MODEL STRUCTURE
(All Units Are In Feet)

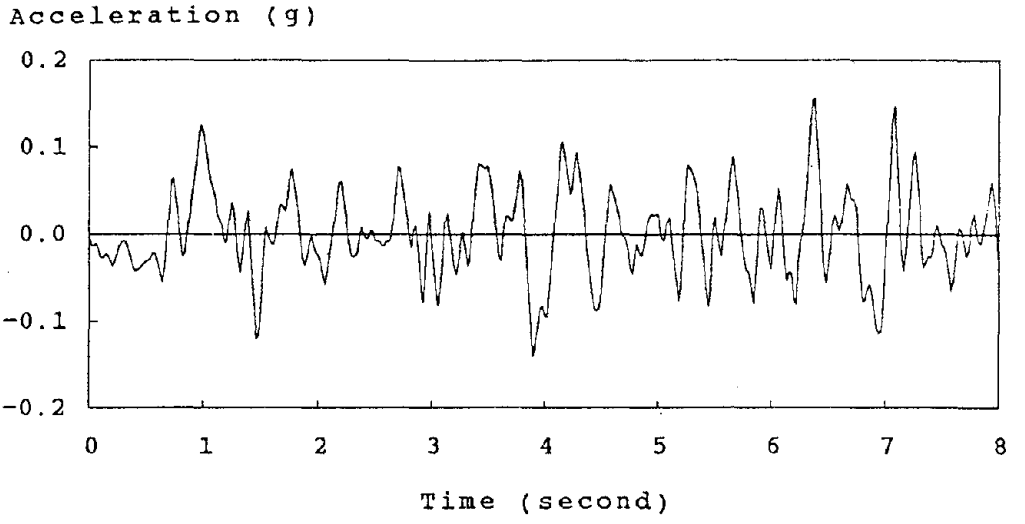

Figure 5.2(a): EIGHT SECONDS OF N21E 1952 TAFT KERN COUNTY RECORD

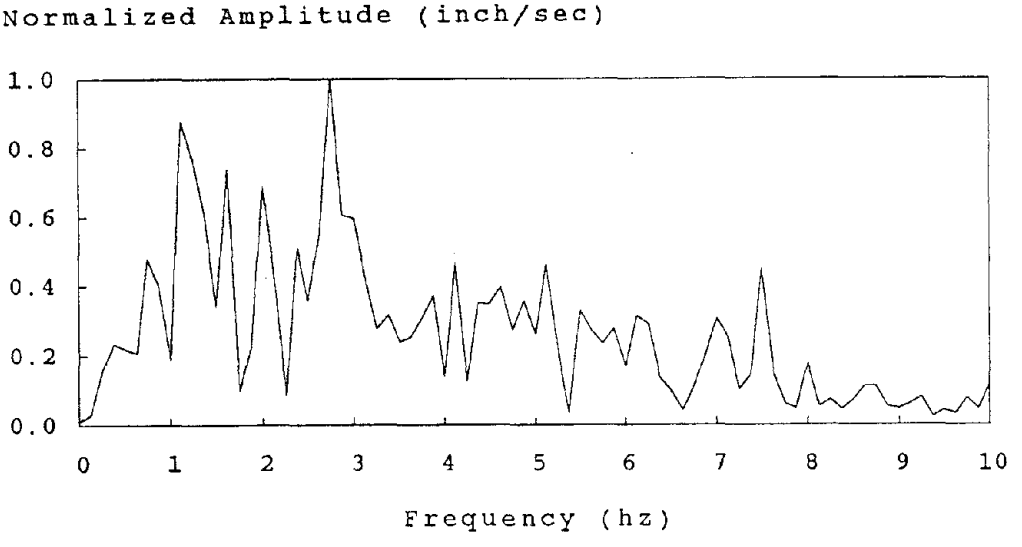

Figure 5.2(b): NORMALIZED FOURIER AMPLITUDE SPECTRUM

THE FIRST THREE TRANSLATIONAL PERIODS:

T_2 = 0.75 Seconds
T_6 = 0.19 Seconds
T_{10} = 0.09 Seconds

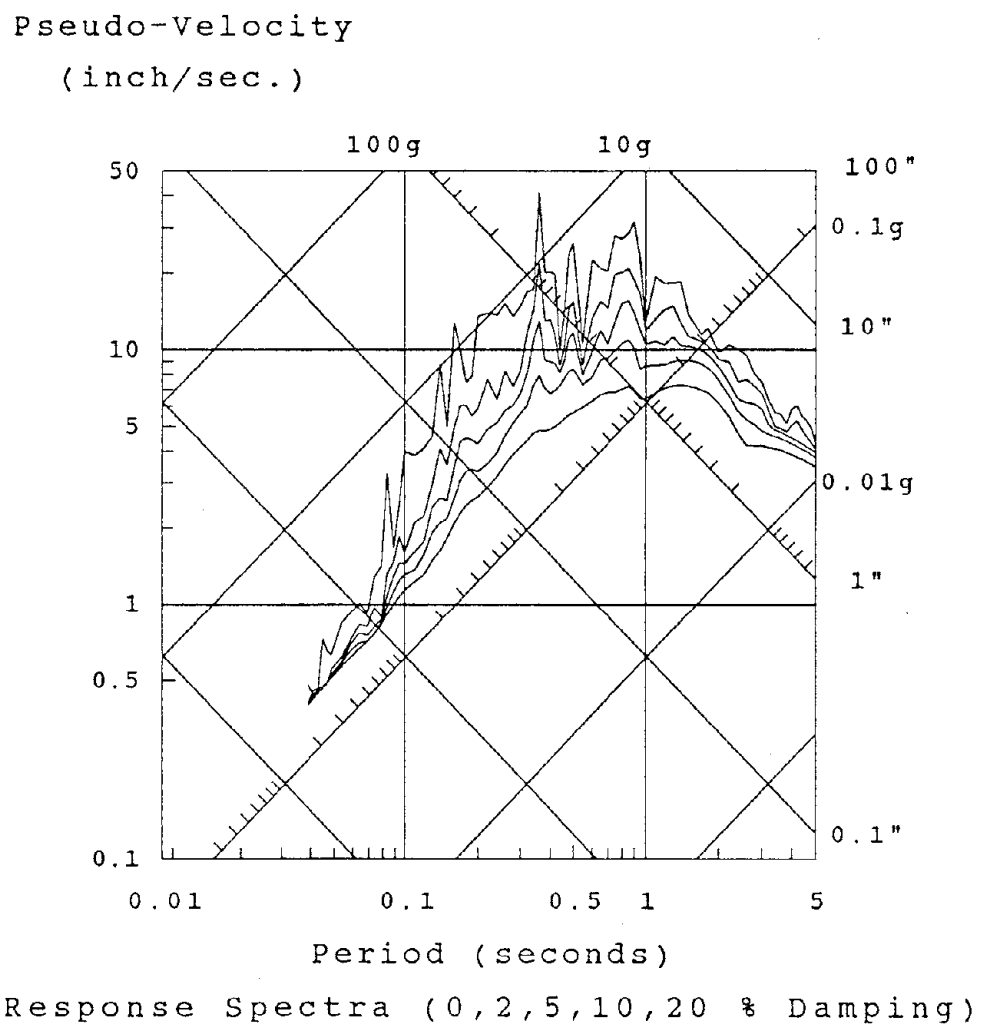

Figure 5.2(c): LINEAR-ELASTIC RESPONSE SPECTRA OF EIGHT SECONDS OF TAFT RECORD

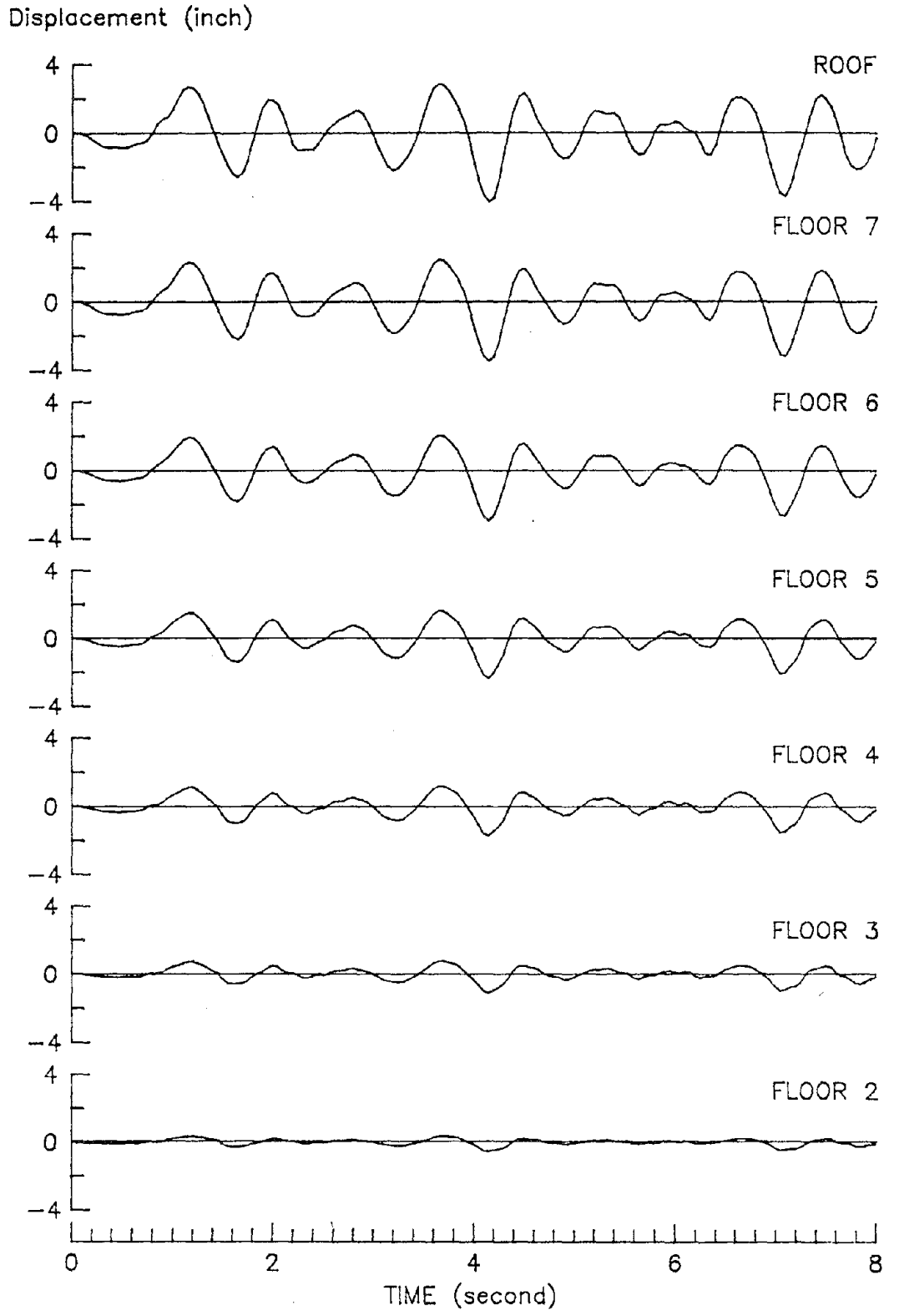

Figure 5.3: DISPLACEMENT TIME-HISTORIES OF THE CONCENTRIC STRUCTURE DUE TO TAFT-40

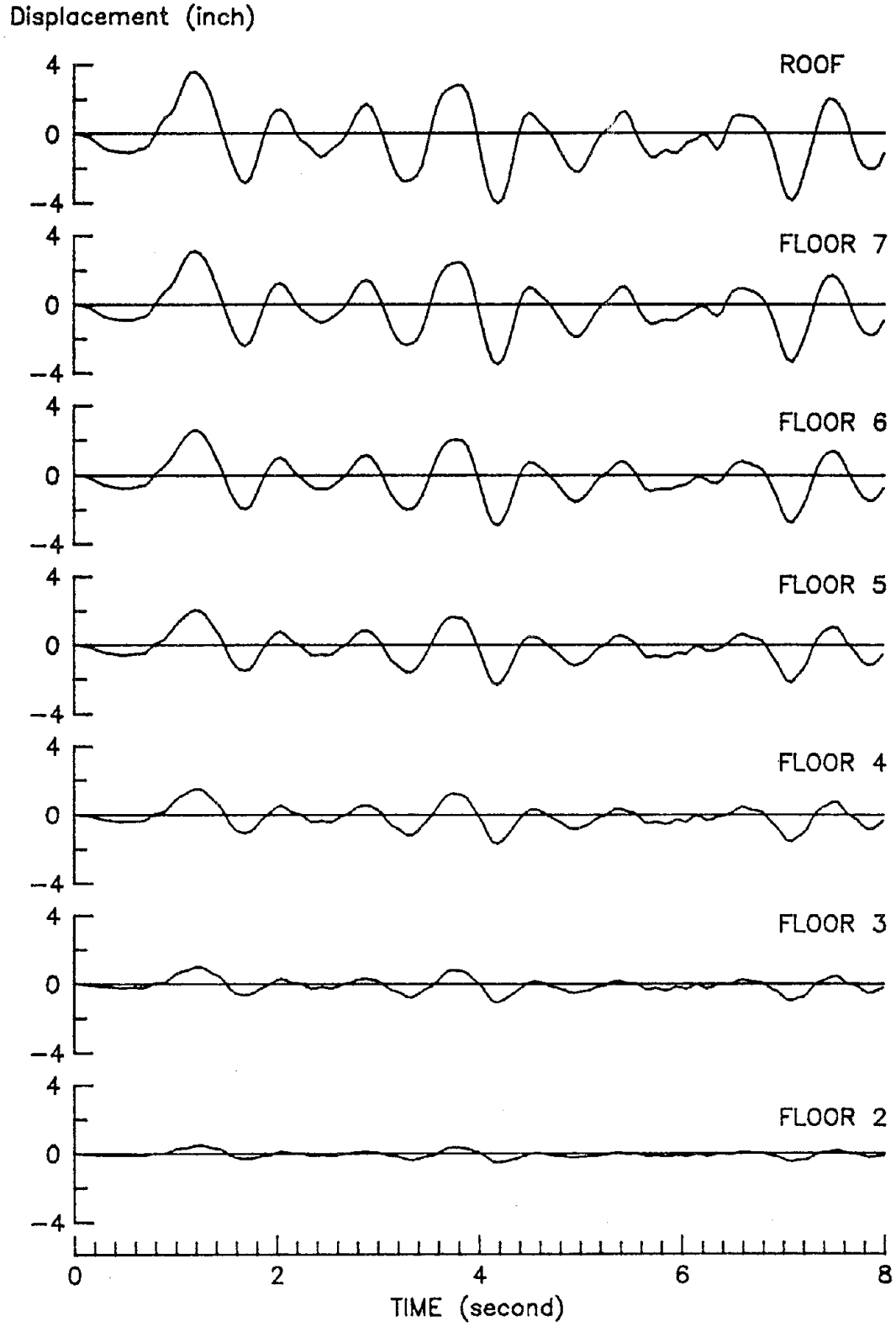

Figure 5.4: DISPLACEMENT TIME-HISTORIES OF WALL G DUE TO TAFT-40 (e/D = 0.05)

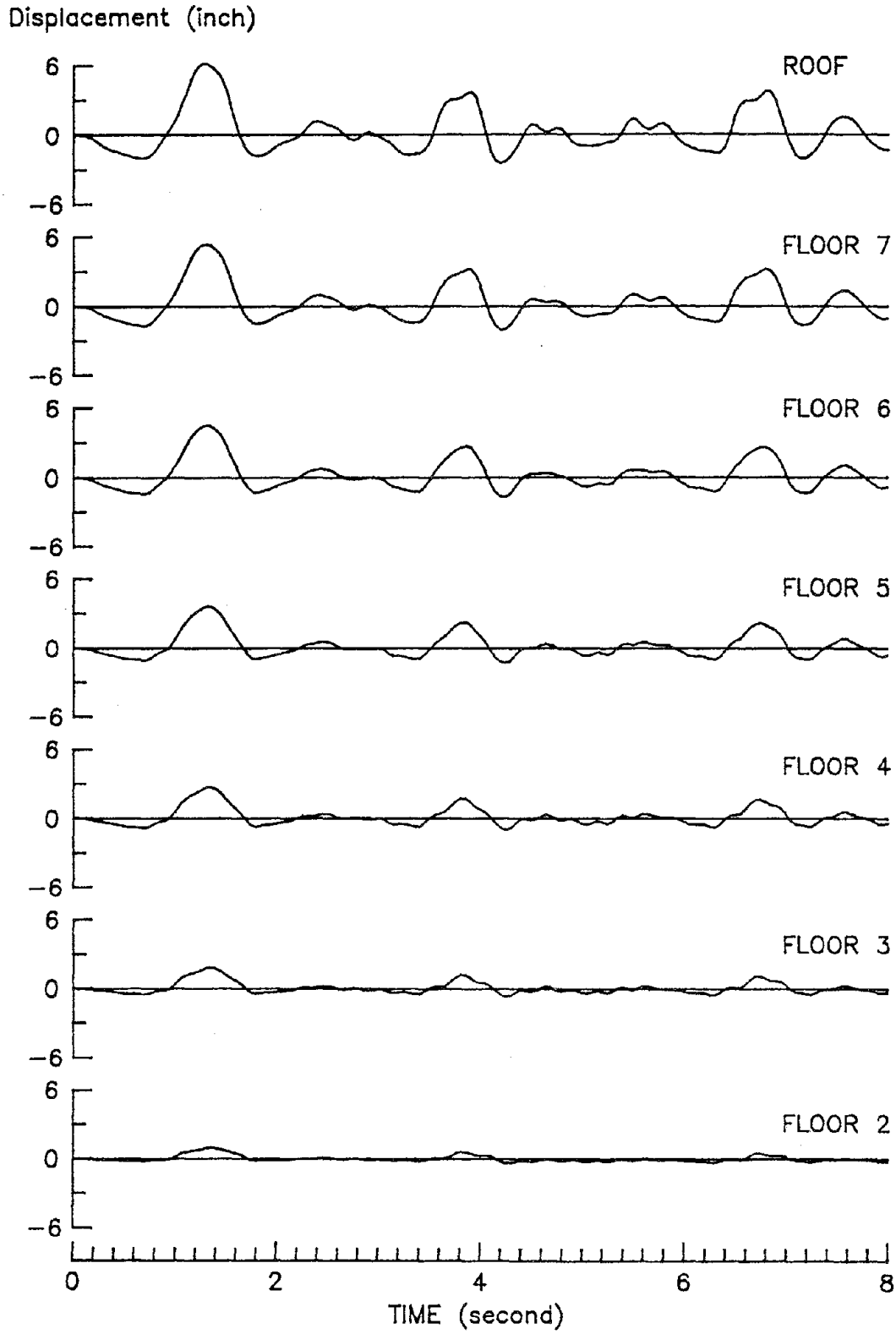

Figure 5.5: DISPLACEMENT TIME-HISTORIES OF WALL G DUE TO TAFT-40 (e/D = 0.25)

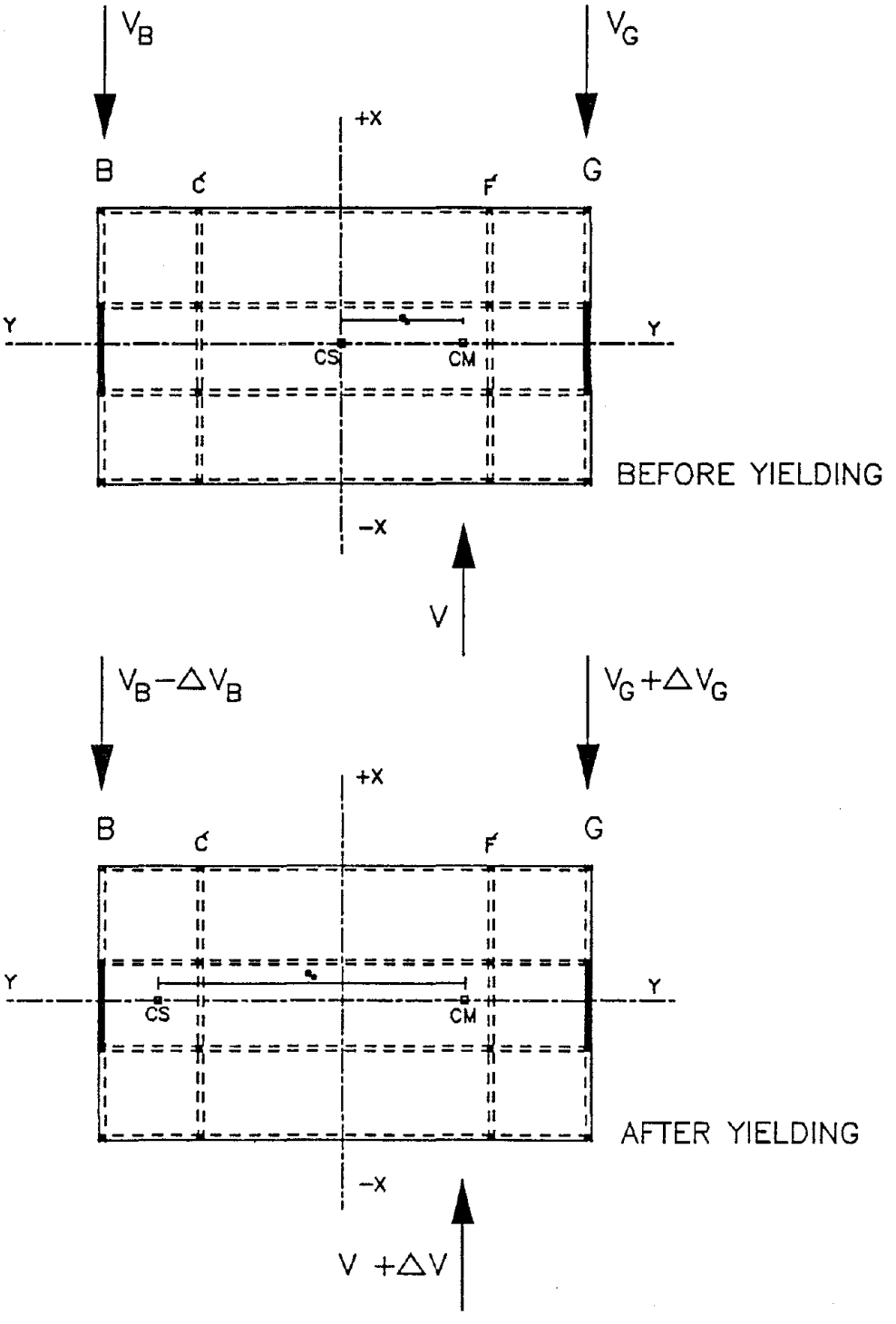

Figure 5.6: EFFECTS OF STATIC LATERAL LOAD ON THE ECCENTRIC MODEL

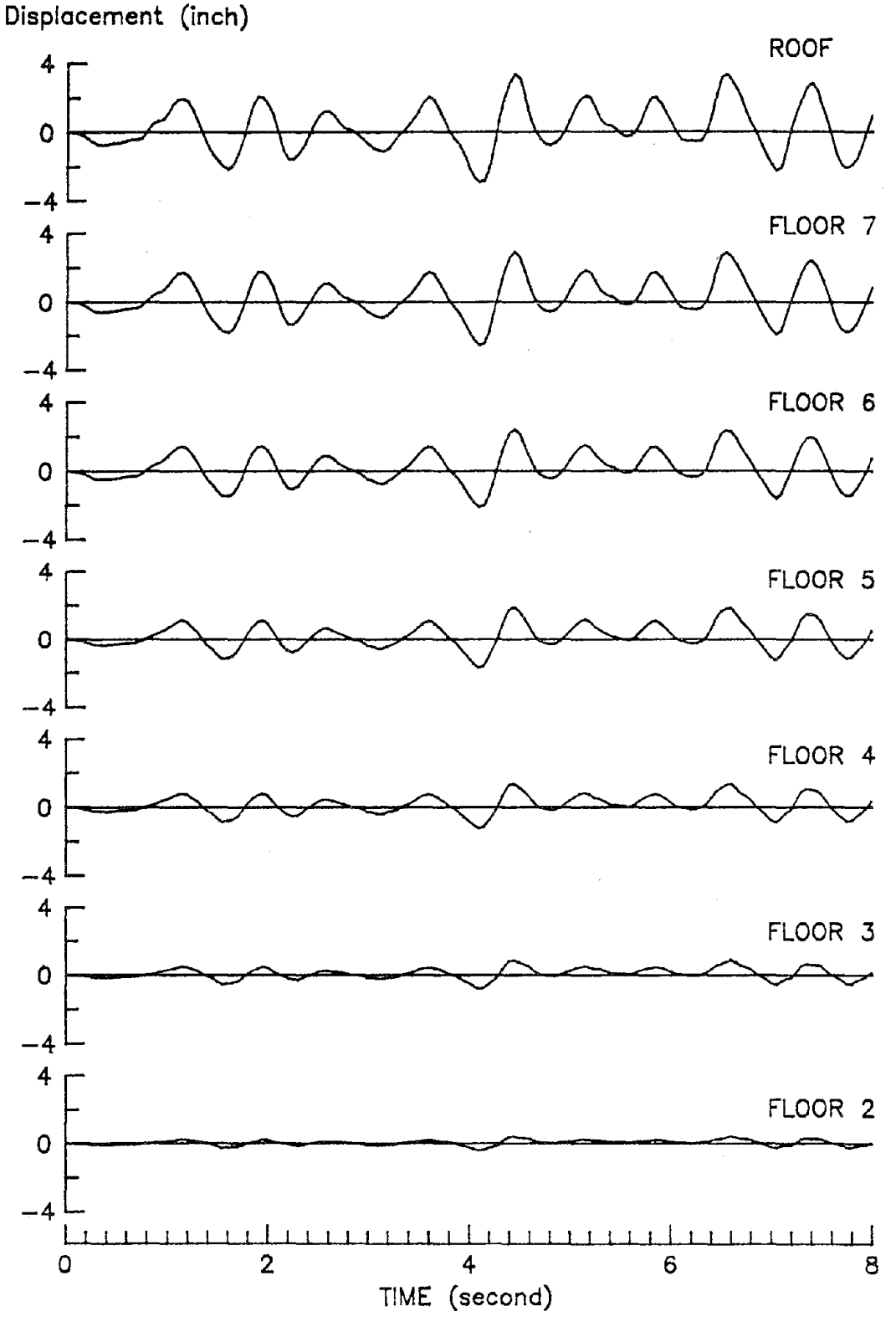

Figure 5.7: DISPLACEMENT TIME-HISTORIES OF WALL B DUE TO TAFT-40 (e/D = 0.05)

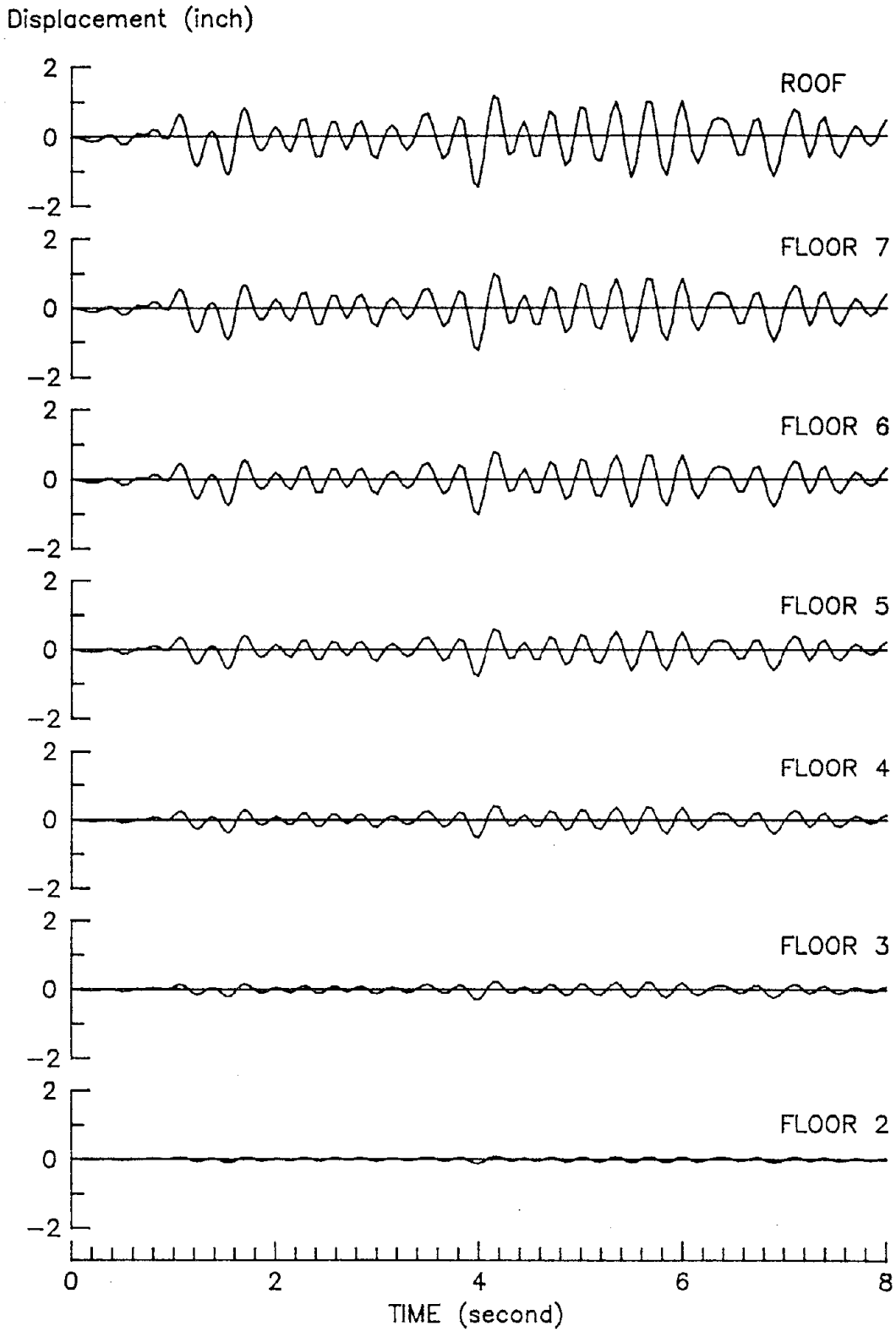

Figure 5.8: DISPLACEMENT TIME-HISTORIES OF WALL B DUE TO TAFT-40 (e/D = 0.25)

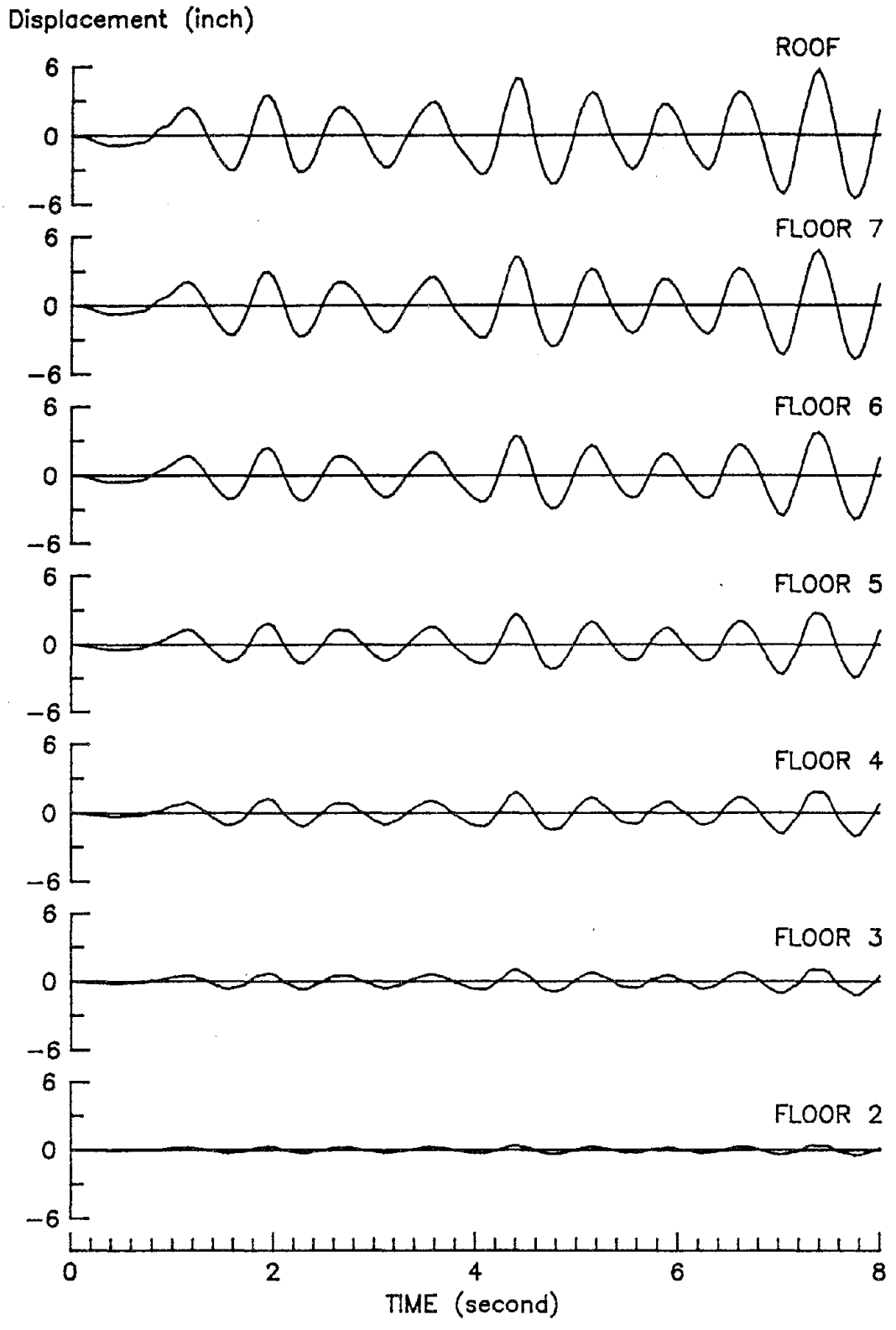

Figure 5.9: LINEAR-ELASTIC DISPLACEMENT TIME-HISTORIES OF THE CONCENTRIC STRUCTURE DUE TO TAFT-40

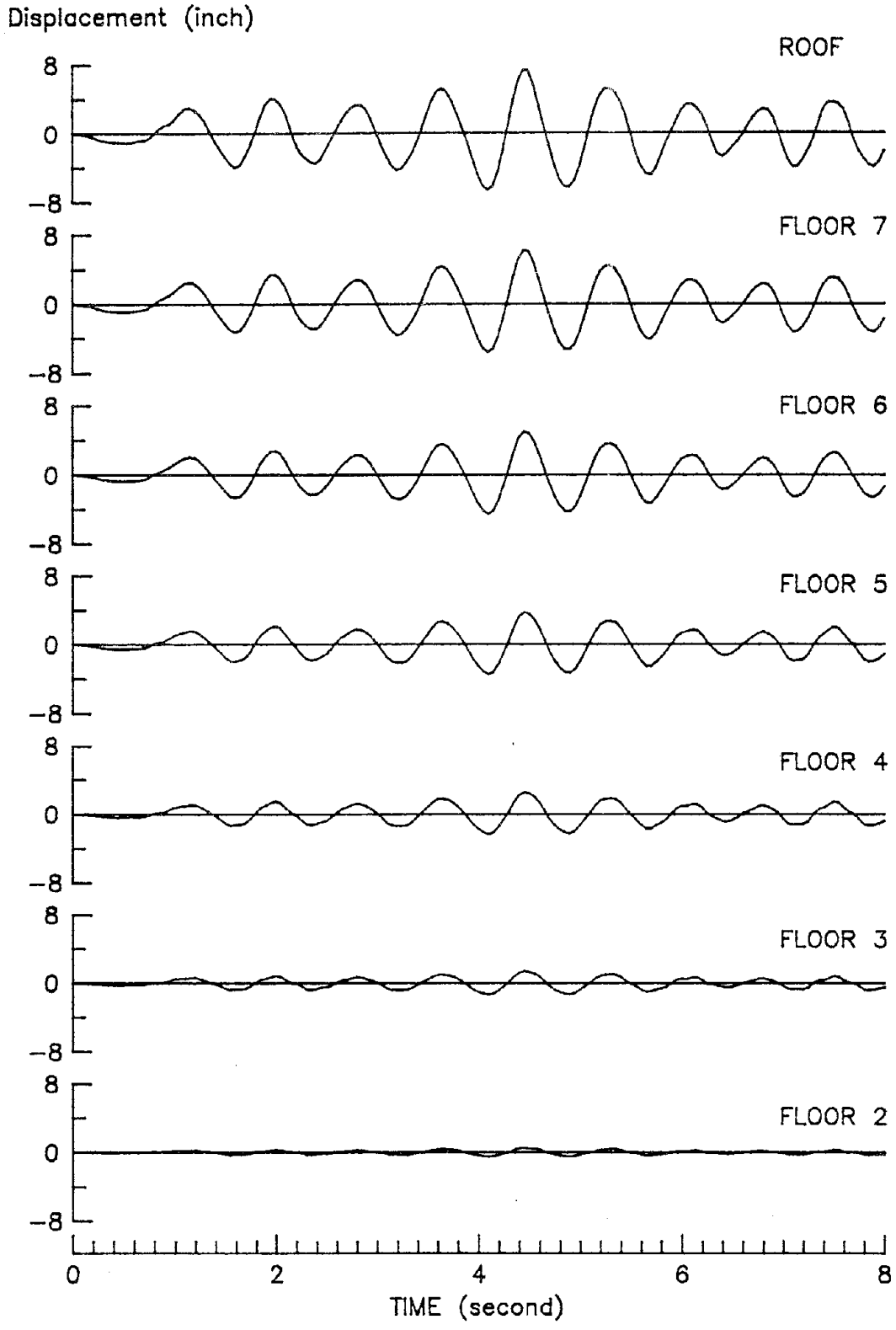

Figure 5.10: LINEAR-ELASTIC DISPLACEMENT TIME-HISTORIES OF WALL G DUE TO TAFT-40 (e/D = 0.05)

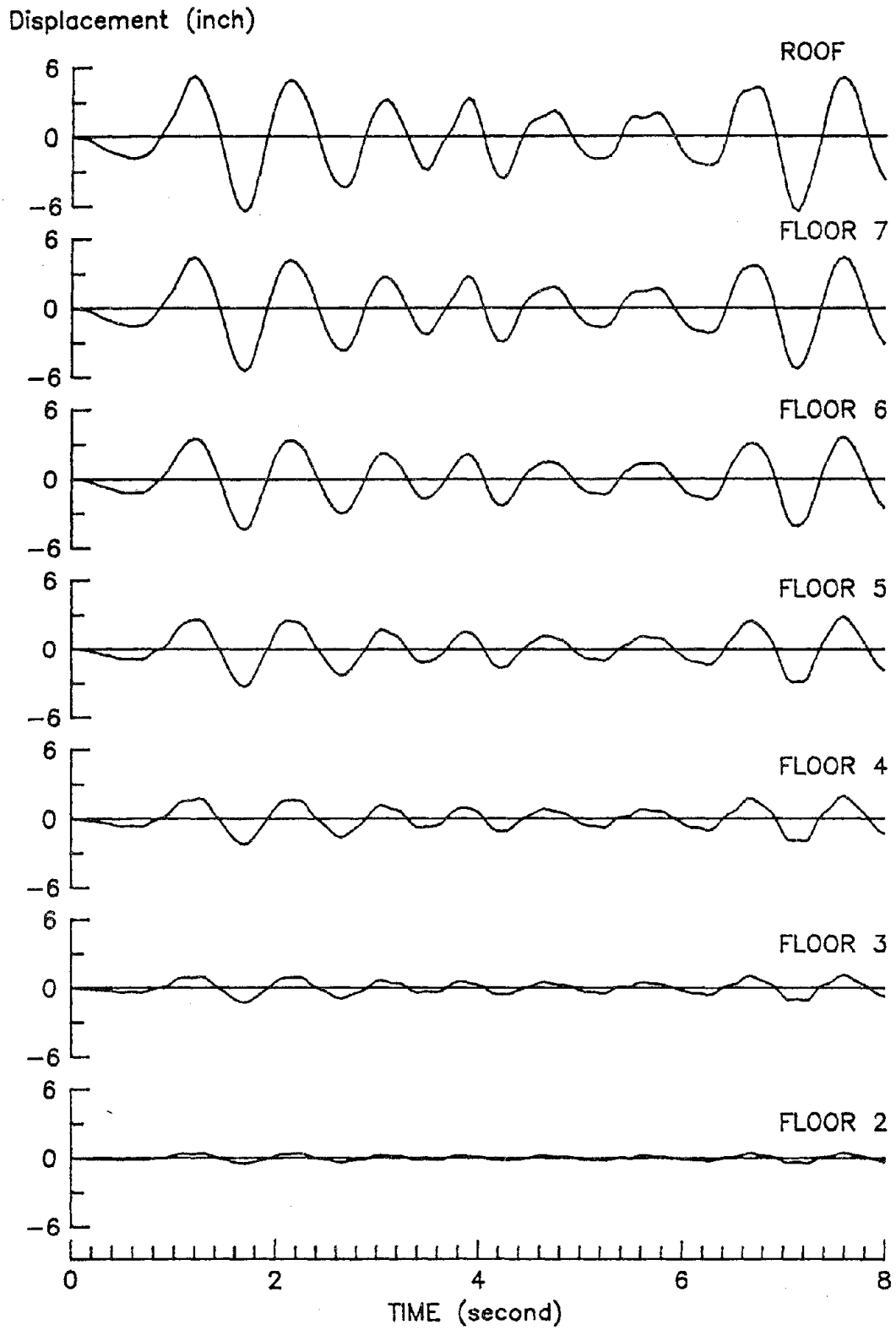

Figure 5.11: LINEAR-ELASTIC DISPLACEMENT TIME-HISTORIES OF WALL G DUE TO TAFT-40 (e/D = 0.25)

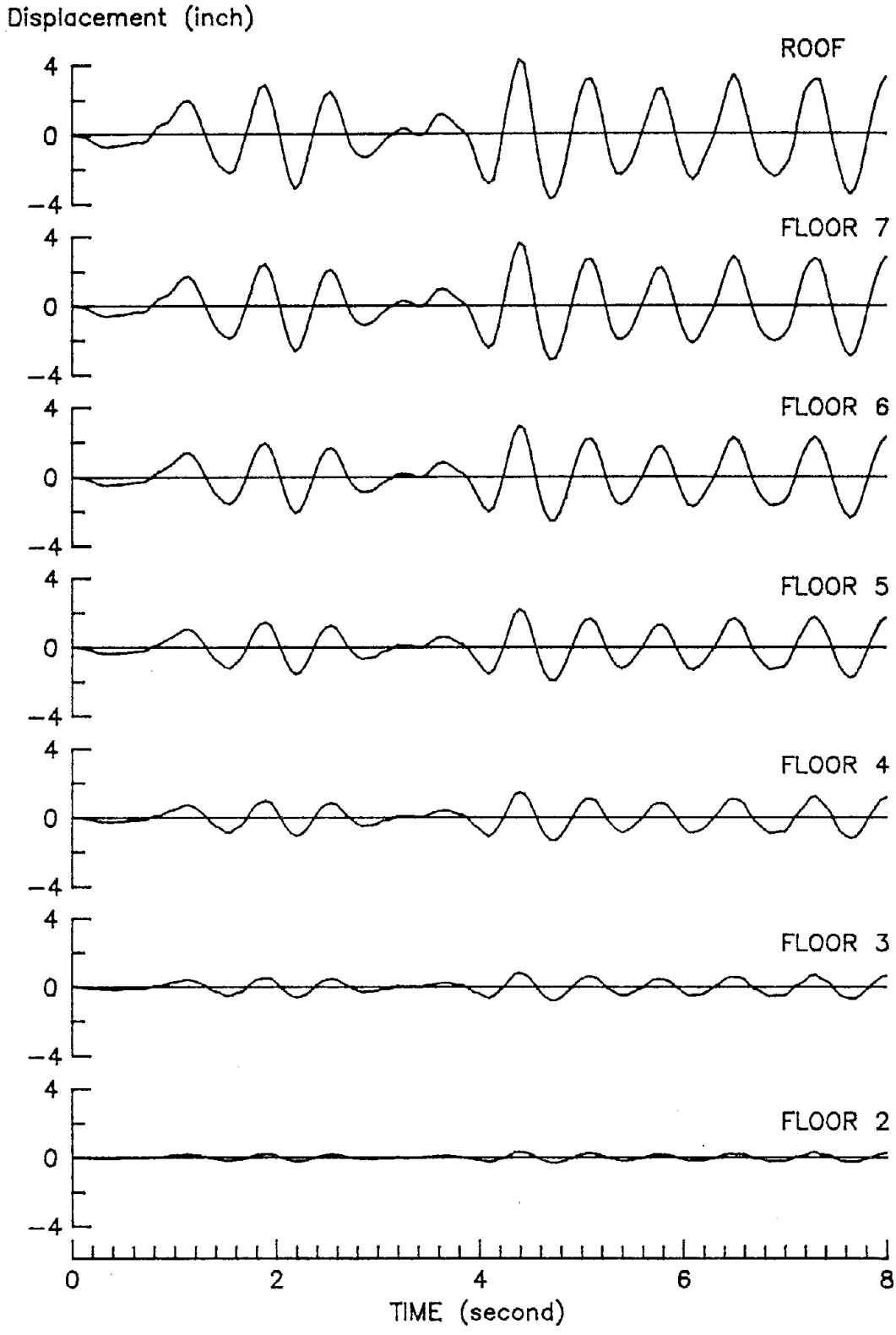

Figure 5.12: LINEAR-ELASTIC DISPLACEMENT TIME-HISTORIES OF WALL B DUE TO TAFT-40 (e/D = 0.05)

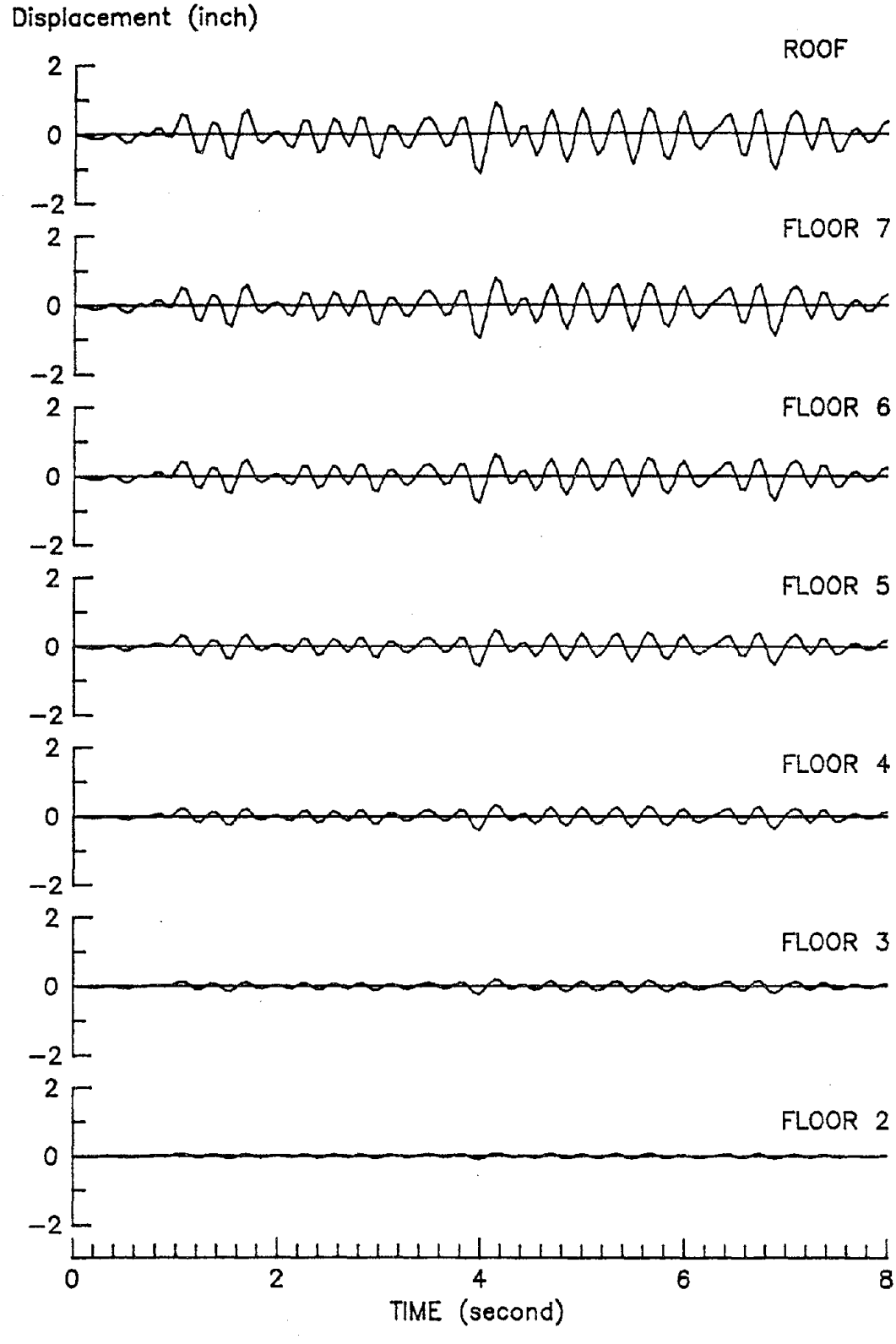

Figure 5.13: LINEAR-ELASTIC DISPLACEMENT TIME-HISTORIES OF WALL B DUE TO TAFT-40 (e/D = 0.25)

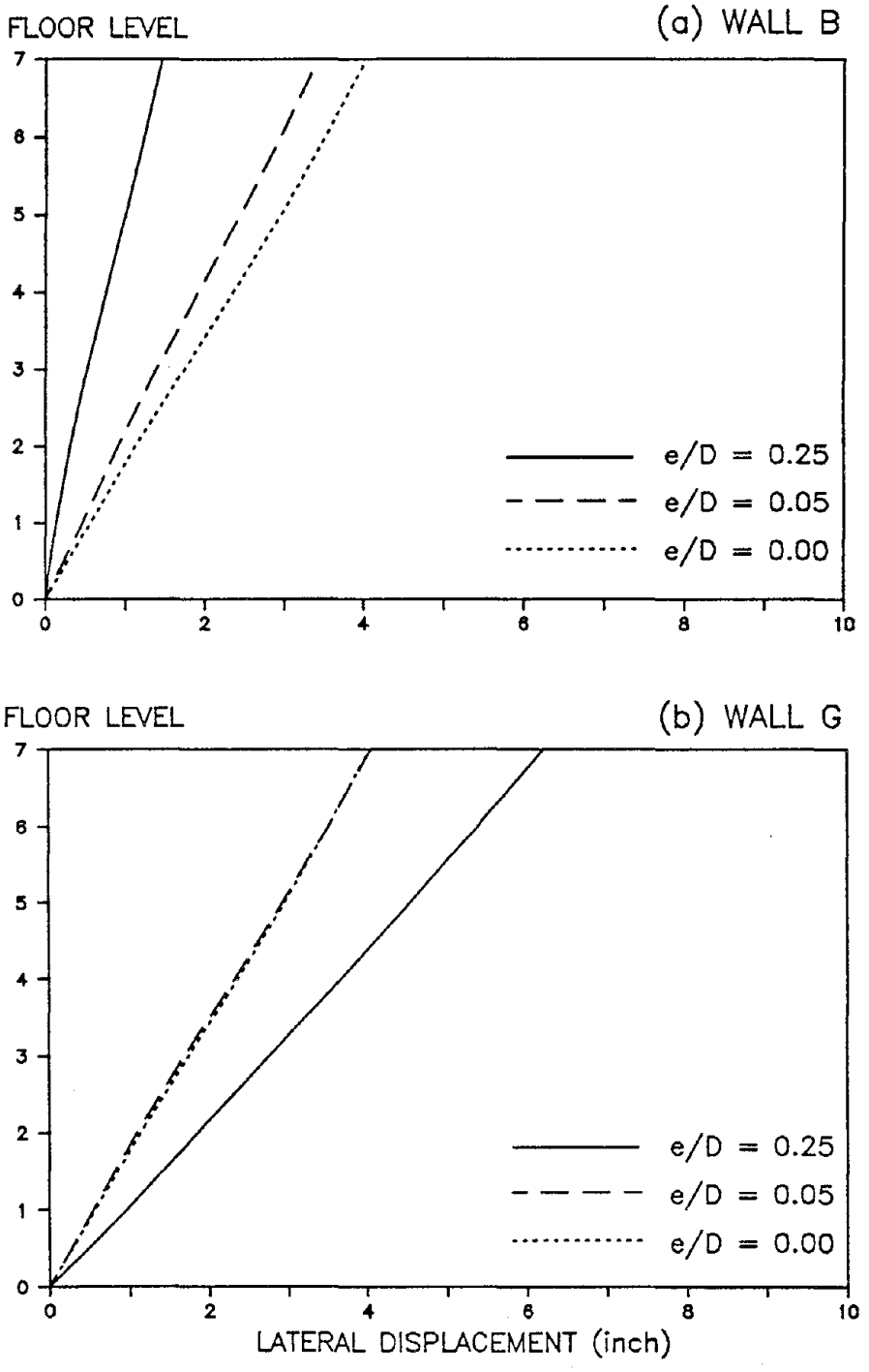

Figure 5.14: DISPLACEMENT ENVELOPES (TAFT-40 , 0-8 SECONDS)

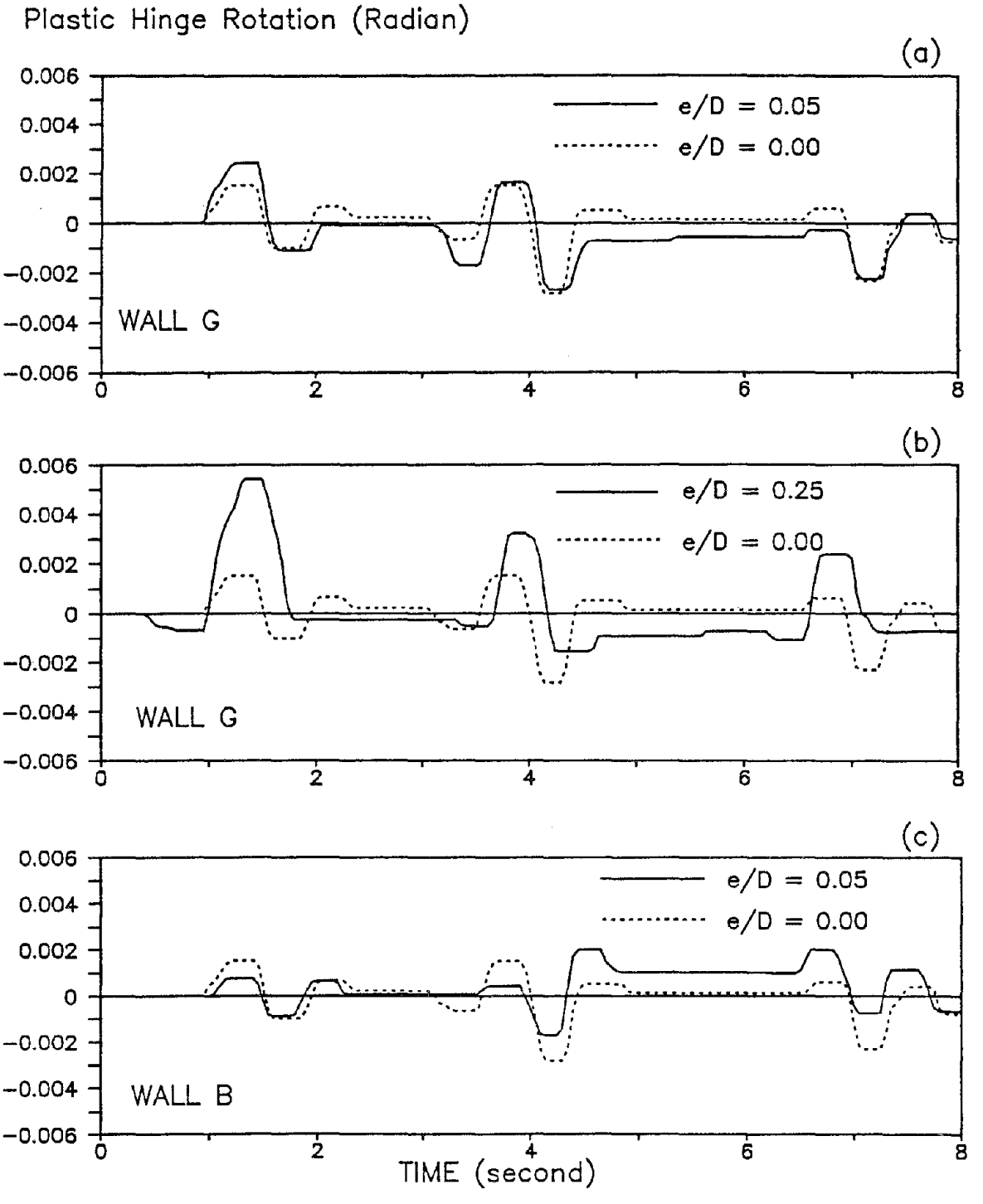

Figure 5.15: PLASTIC HINGE ROTATION AT THE BASE OF WALLS DUE TO TAFT-40 FOR 0-8 SECONDS

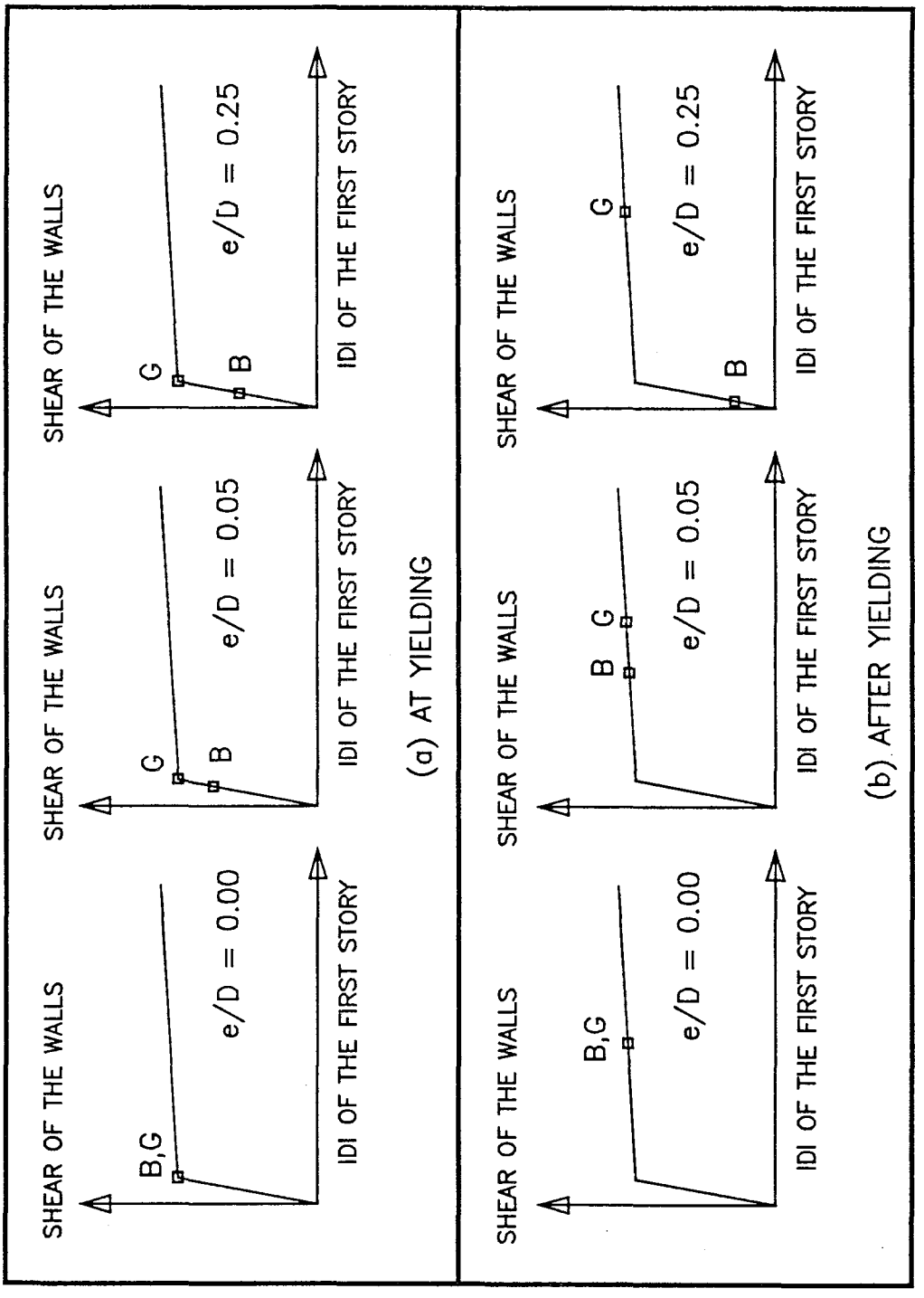

Figure 5.16: SHEAR VERSUS INTER-STORY DRIFT INDEX OF WALLS B AND G

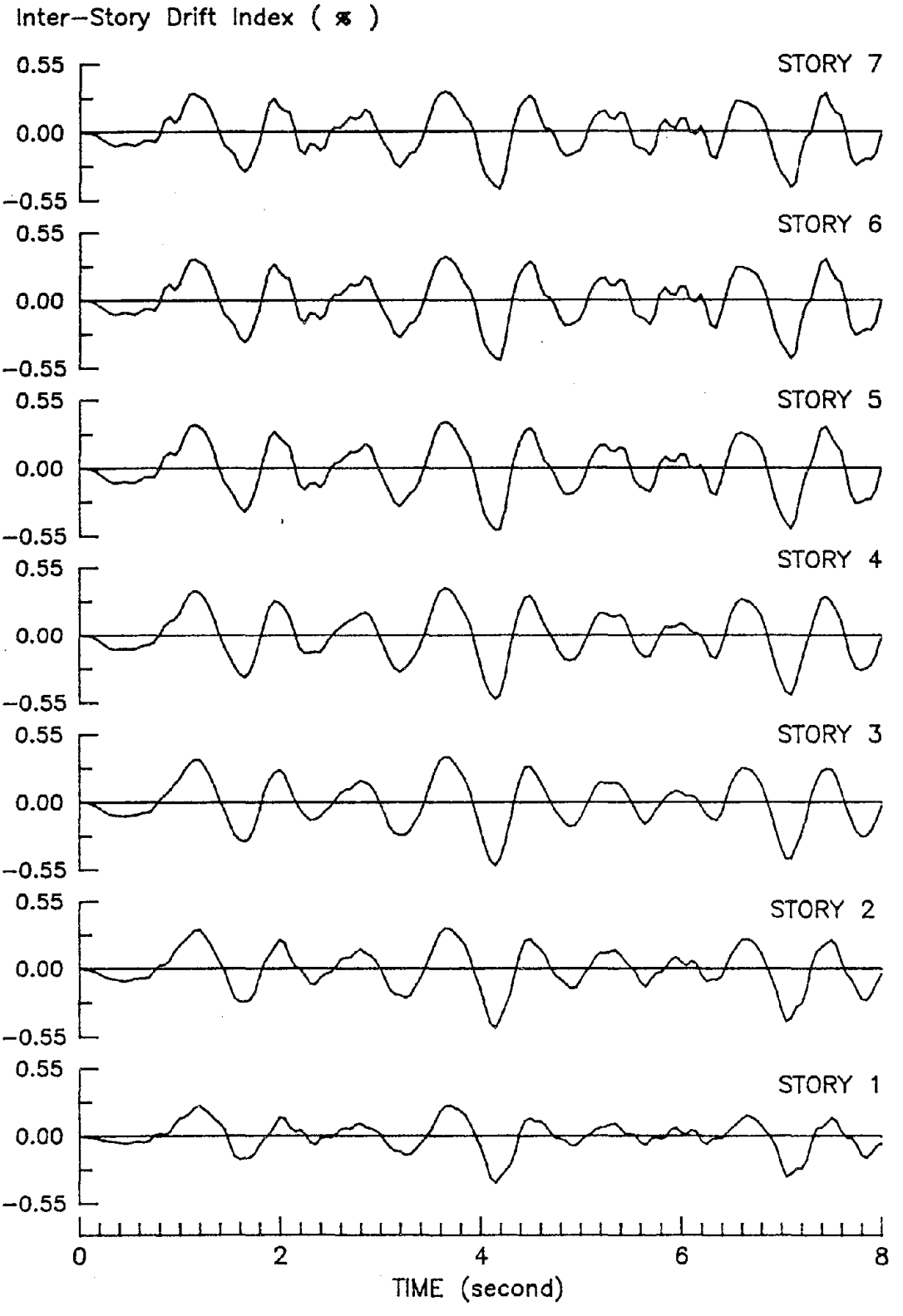

Figure 5.17: INTER-STORY DRIFT INDEX TIME-HISTORIES OF THE CONCENTRIC STRUCTURE DUE TO TAFT-40

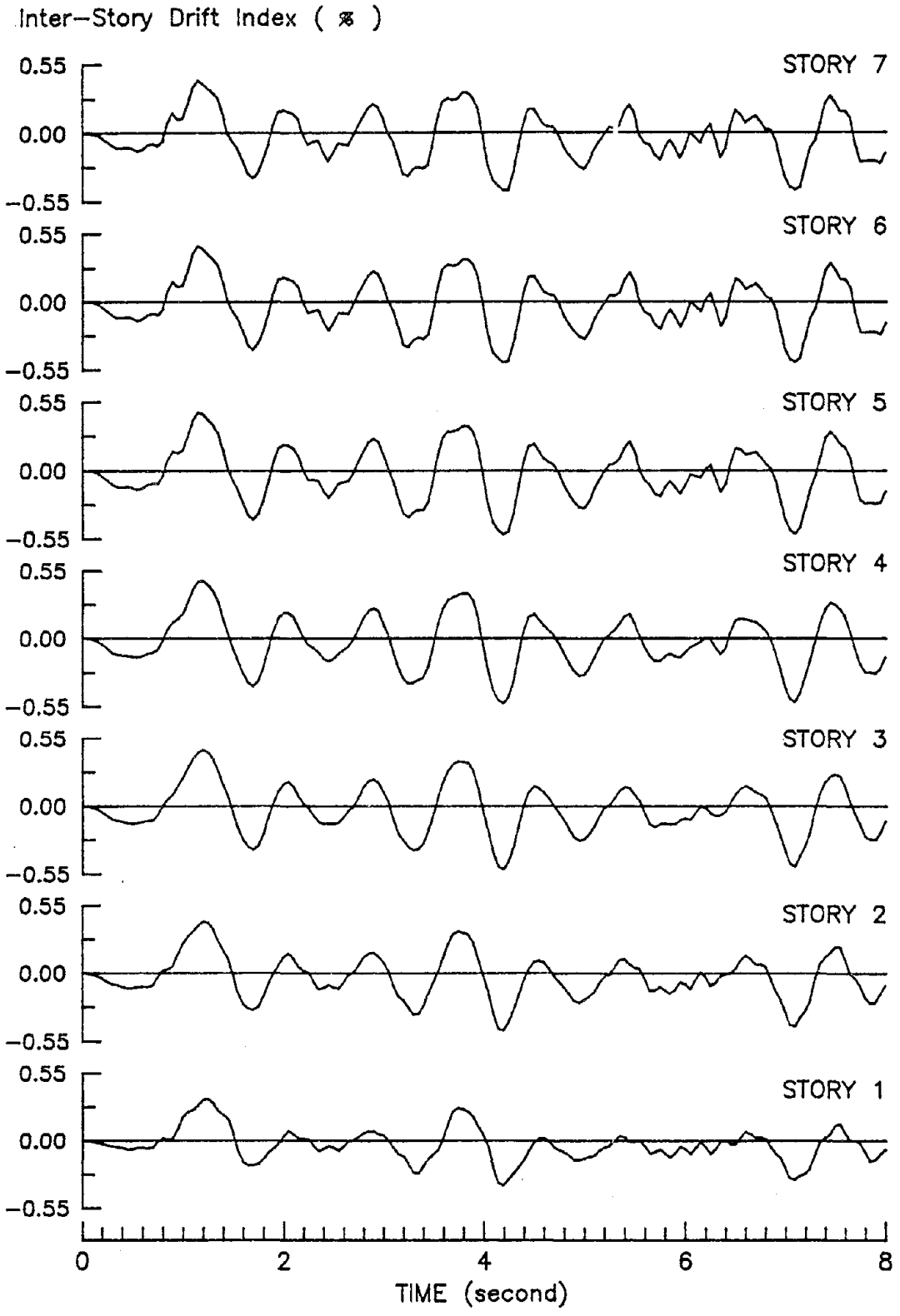

Figure 5.18: INTER-STORY DRIFT INDEX TIME-HISTORIES OF WALL G DUE TO TAFT-40 (e/D = 0.05)

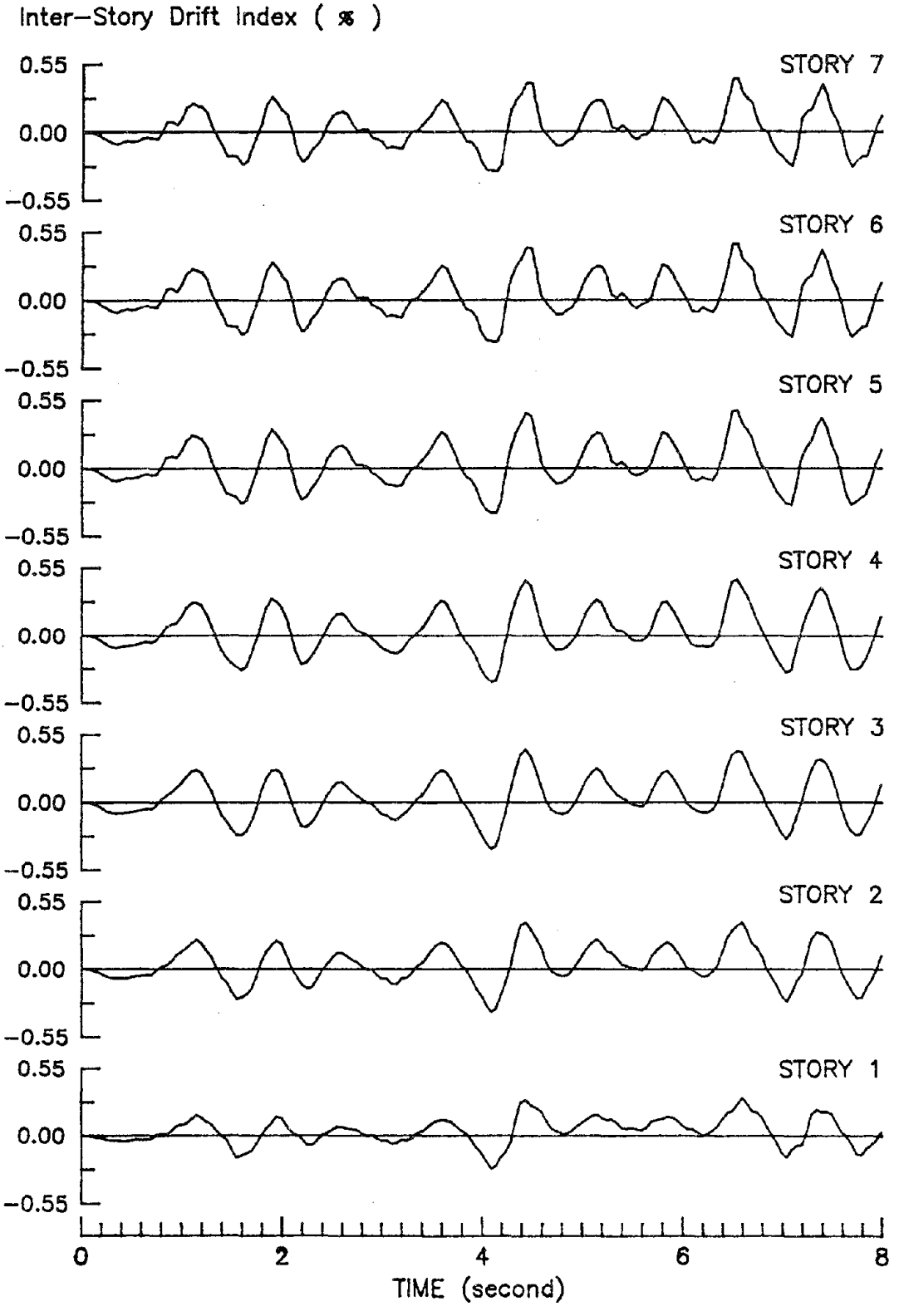

Figure 5.19: INTER-STORY DRIFT INDEX TIME-HISTORIES OF WALL B DUE TO TAFT-40 (e/D = 0.05)

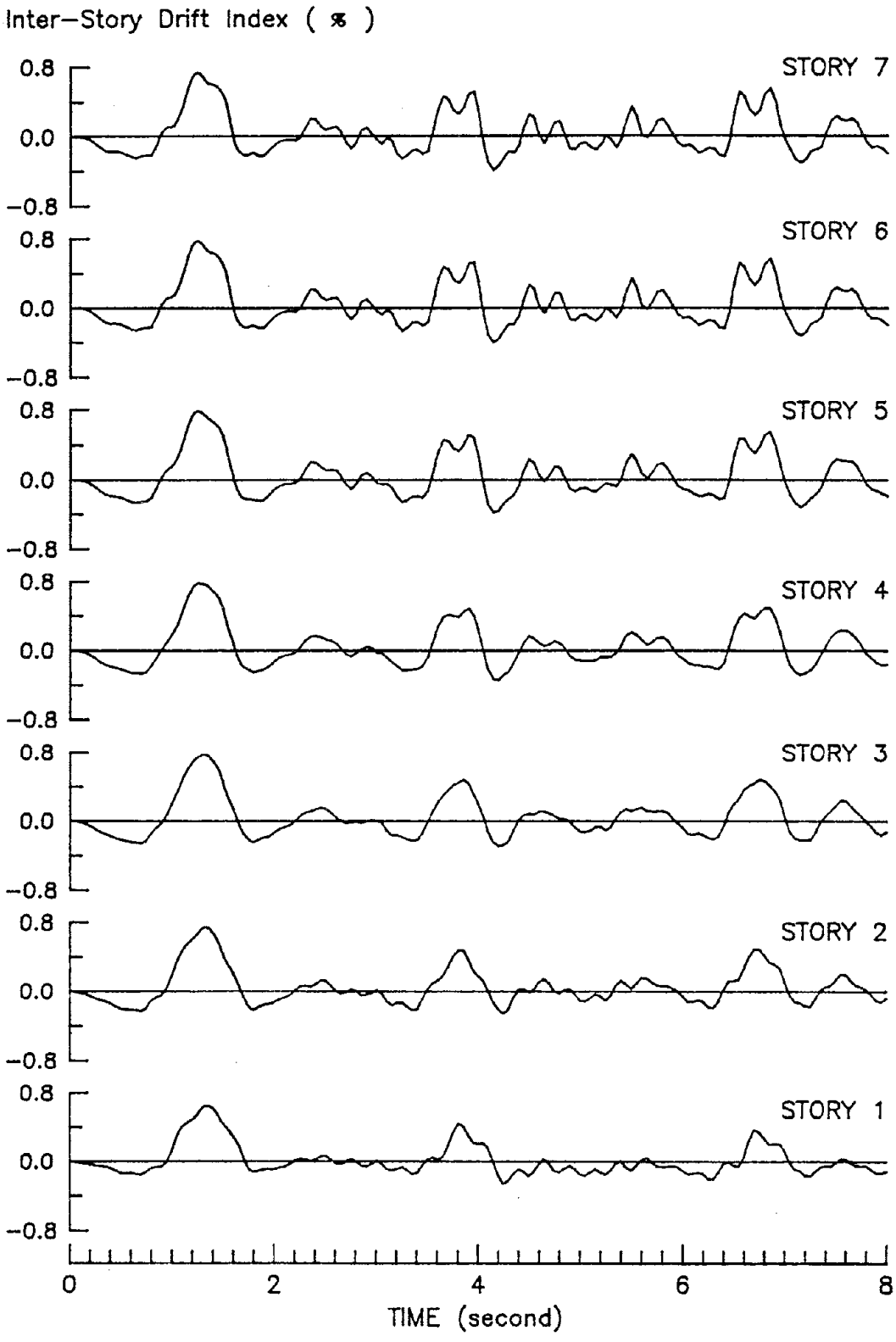

Figure 5.20: INTER-STORY DRIFT INDEX TIME-HISTORIES OF WALL G DUE TO TAFT-40 (e/D = 0.25)

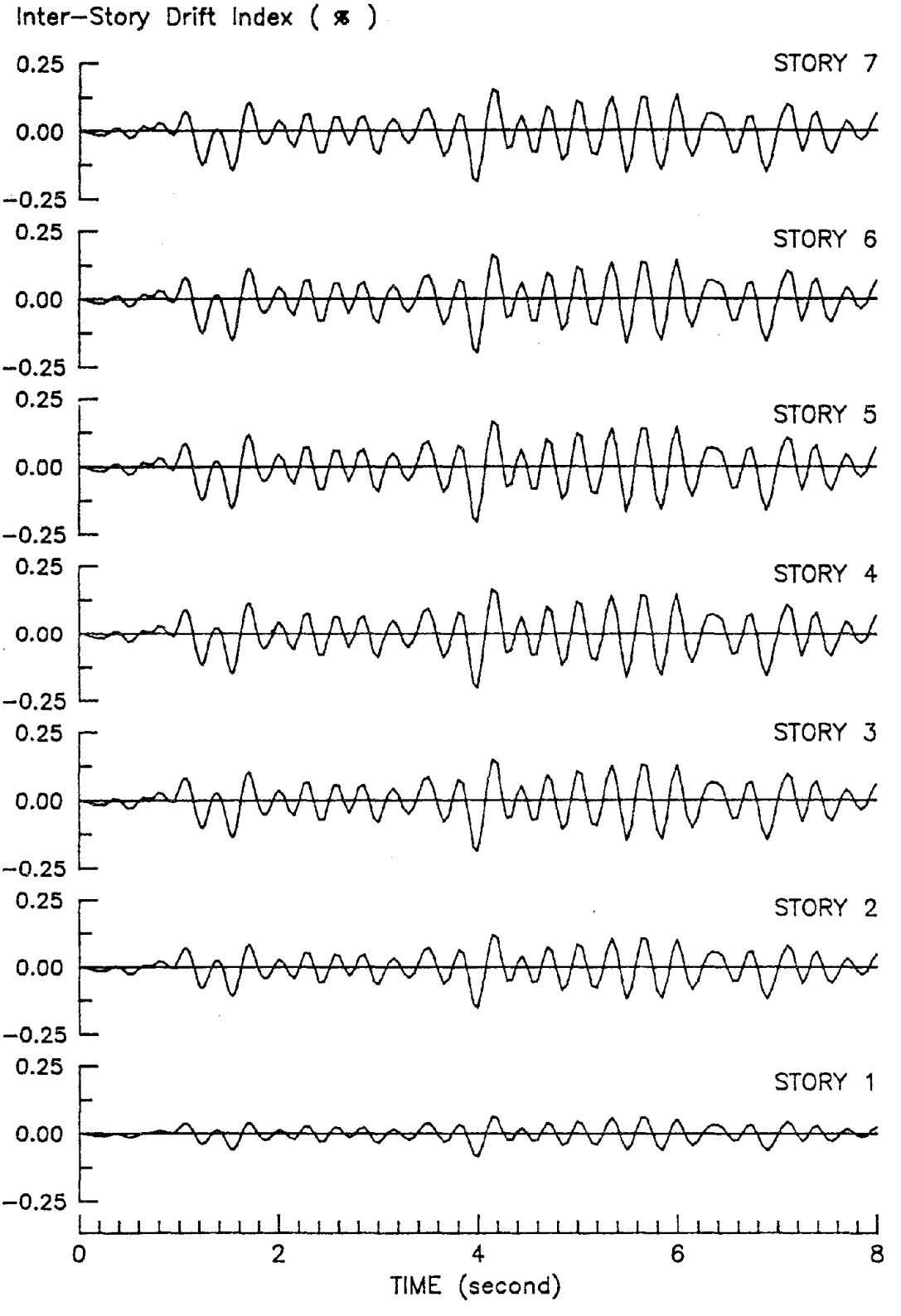

Figure 5.21: INTER-STORY DRIFT INDEX TIME-HISTORIES OF WALL B DUE TO TAFT-40 (e/D = 0.25)

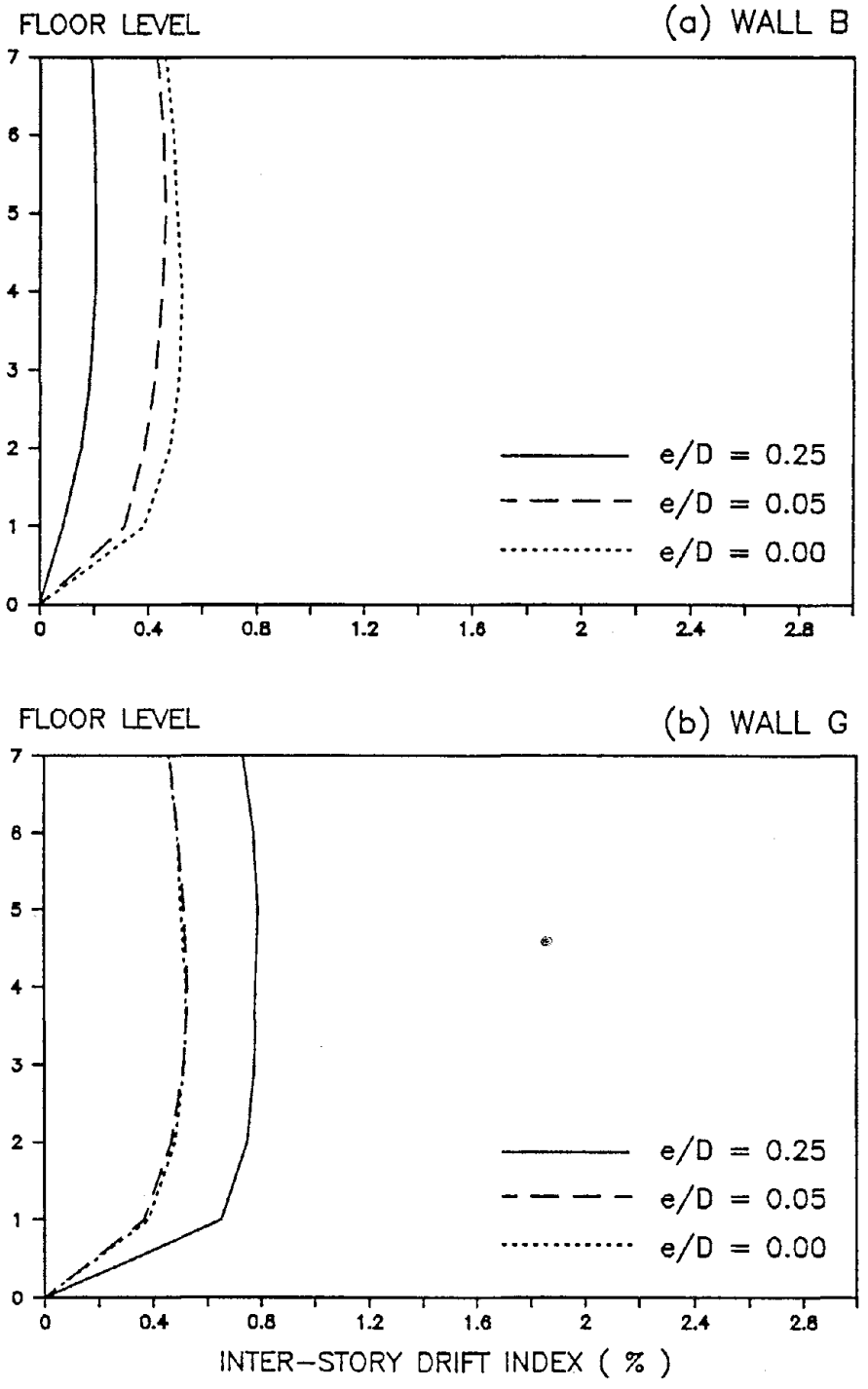

Figure 5.22: INTER-STORY DRIFT INDEX ENVELOPES (TAFT-40 , 0-8 SECONDS)

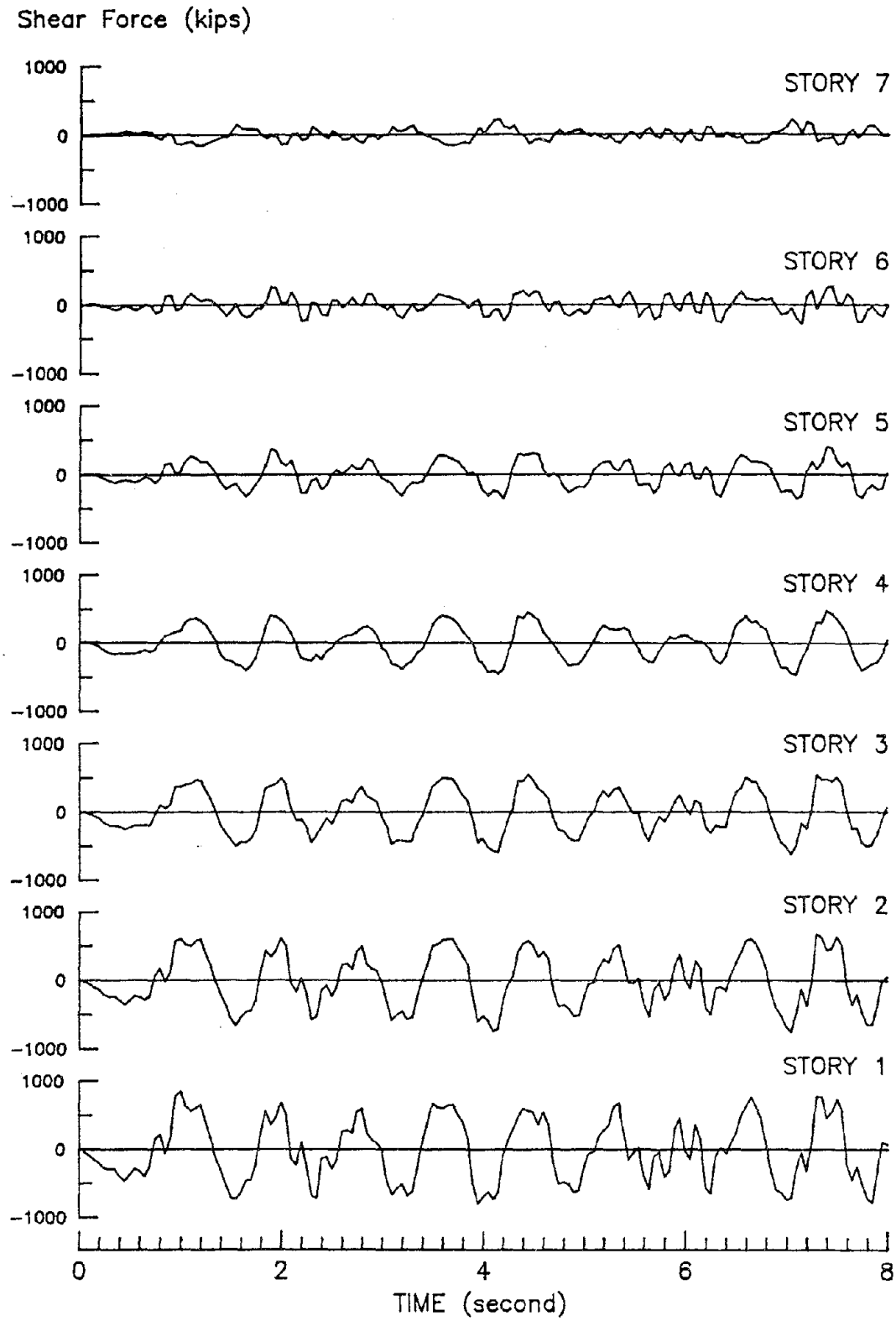

Figure 5.23: STORY SHEAR TIME-HISTORIES OF WALL B (OR G) FOR THE CONCENTRIC STRUCTURE DUE TO TAFT-40

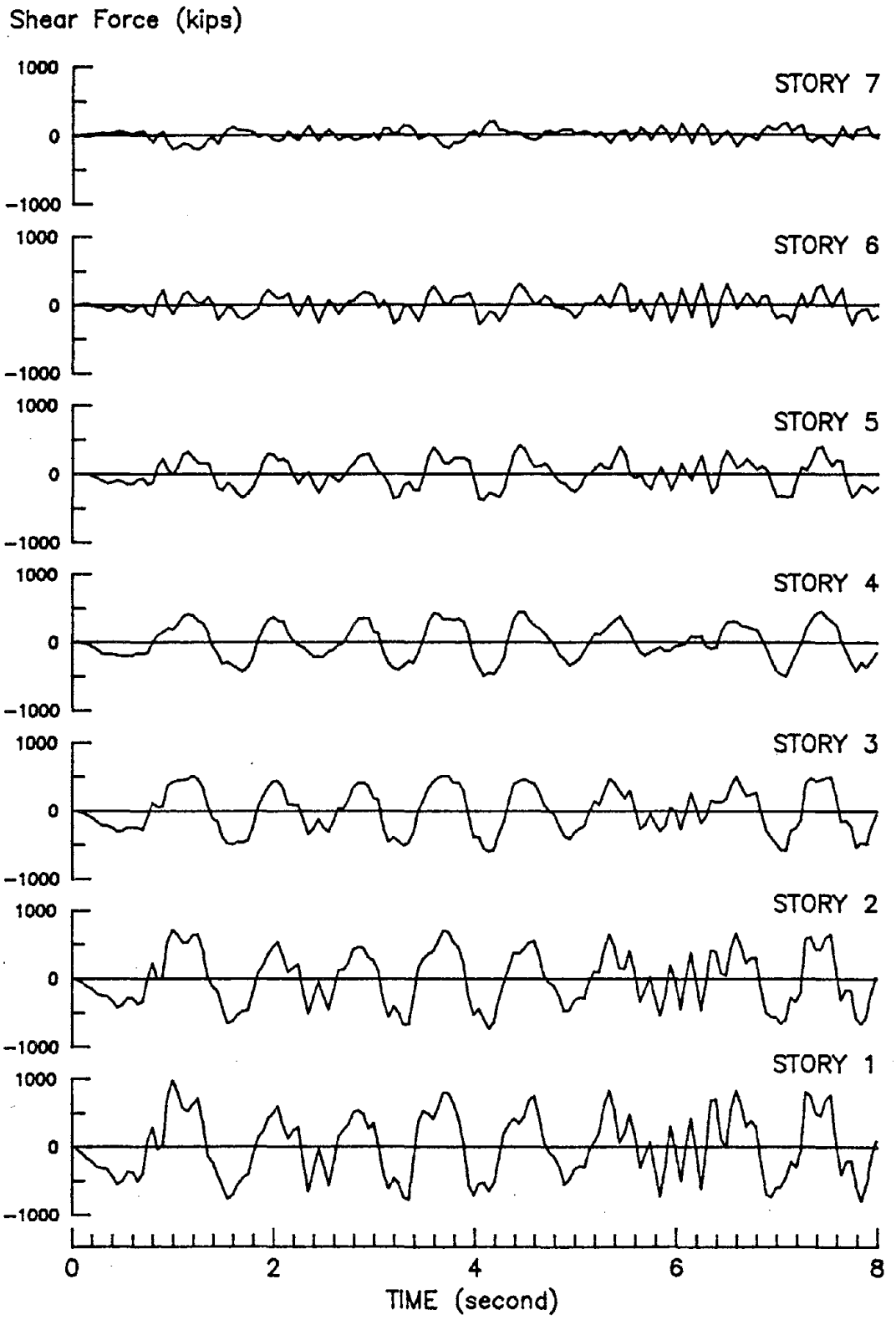

Figure 5.24: STORY SHEAR TIME-HISTORIES OF WALL G DUE TO TAFT-40 (e/D = 0.05)

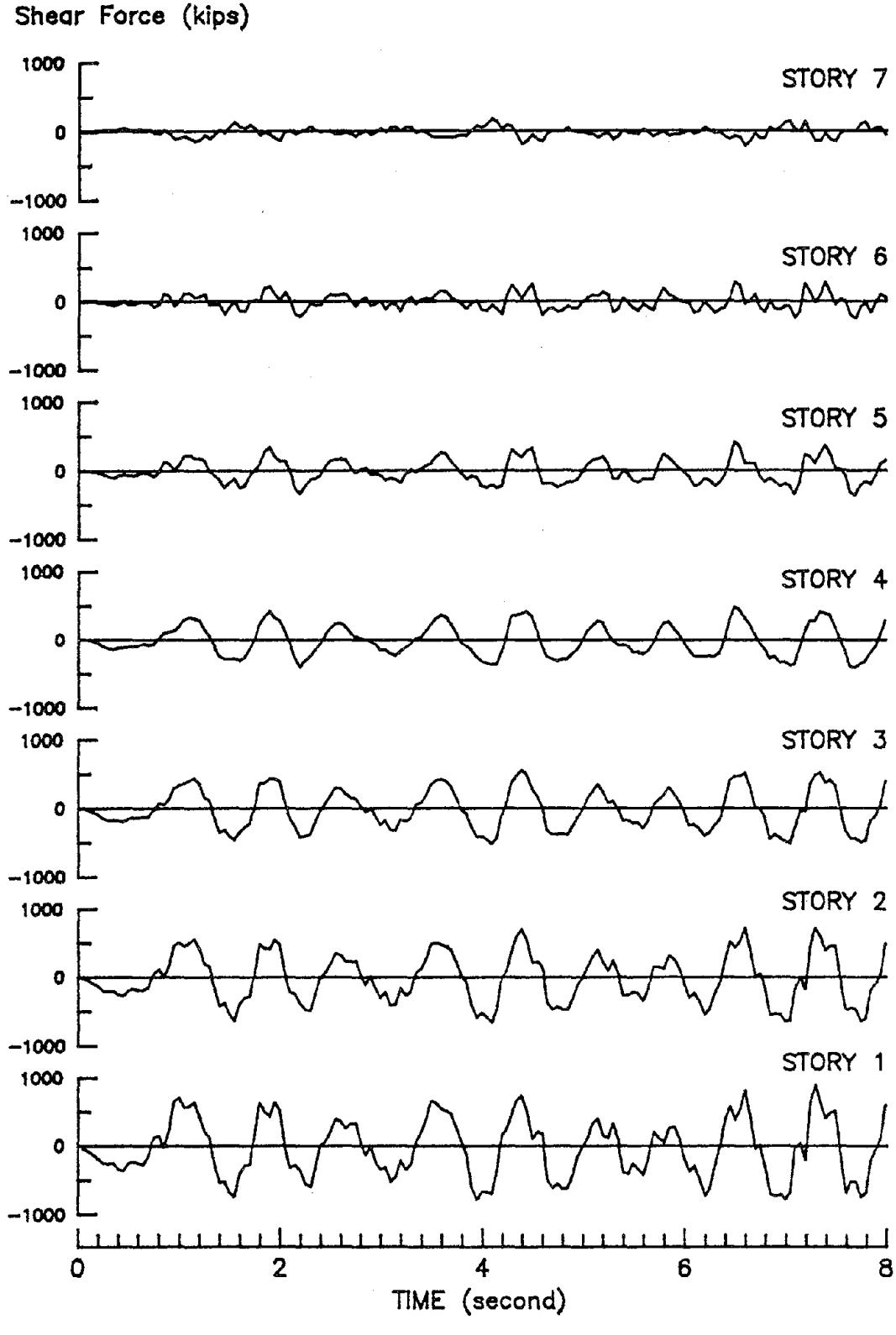

Figure 5.25: STORY SHEAR TIME-HISTORIES OF WALL B DUE TO TAFT-40 (e/D = 0.05)

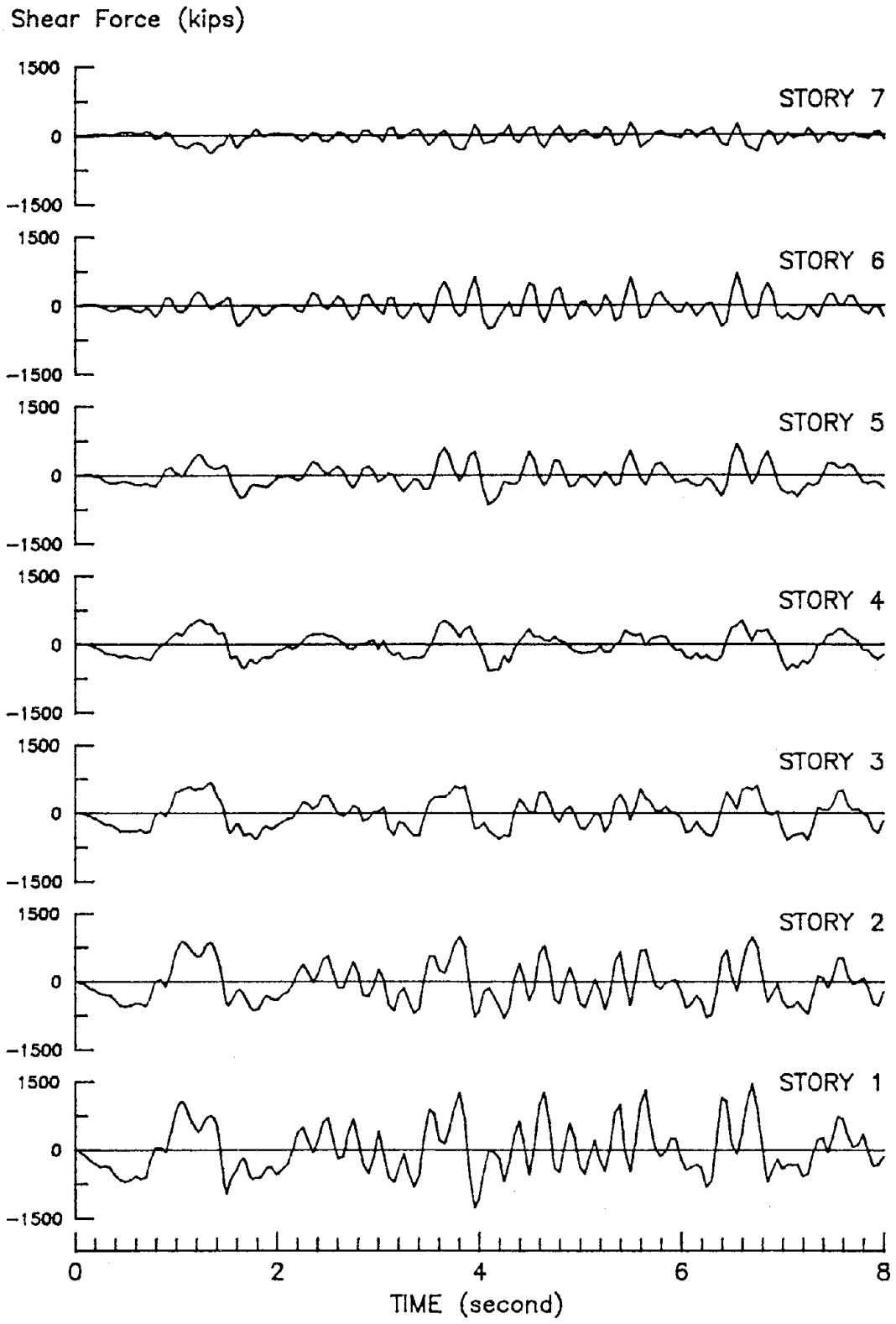

Figure 5.26: STORY SHEAR TIME-HISTORIES OF WALL G DUE TO TAFT-40 (e/D = 0.25)

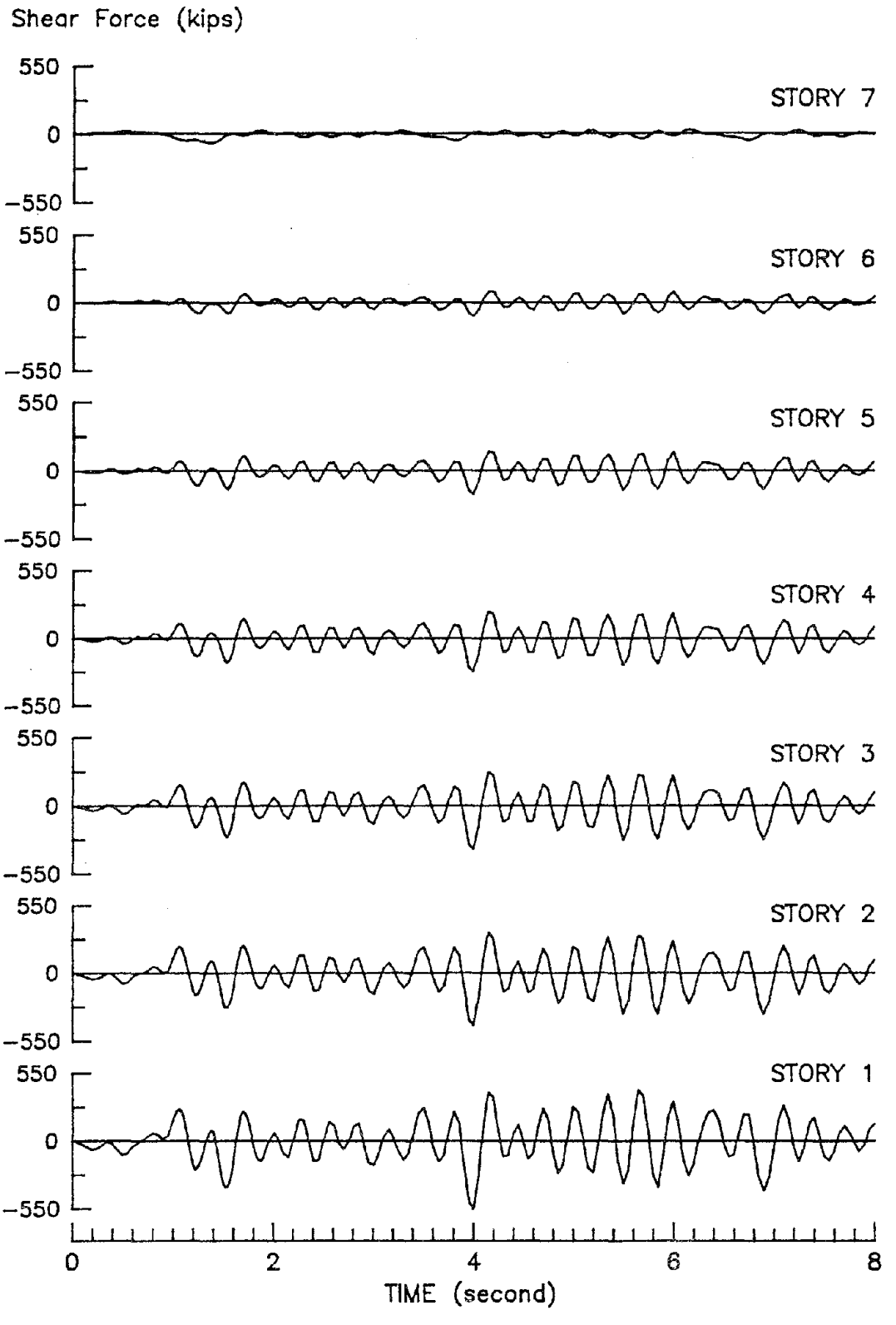

Figure 5.27: STORY SHEAR TIME-HISTORIES OF WALL B DUE TO TAFT-40 (e/D = 0.25)

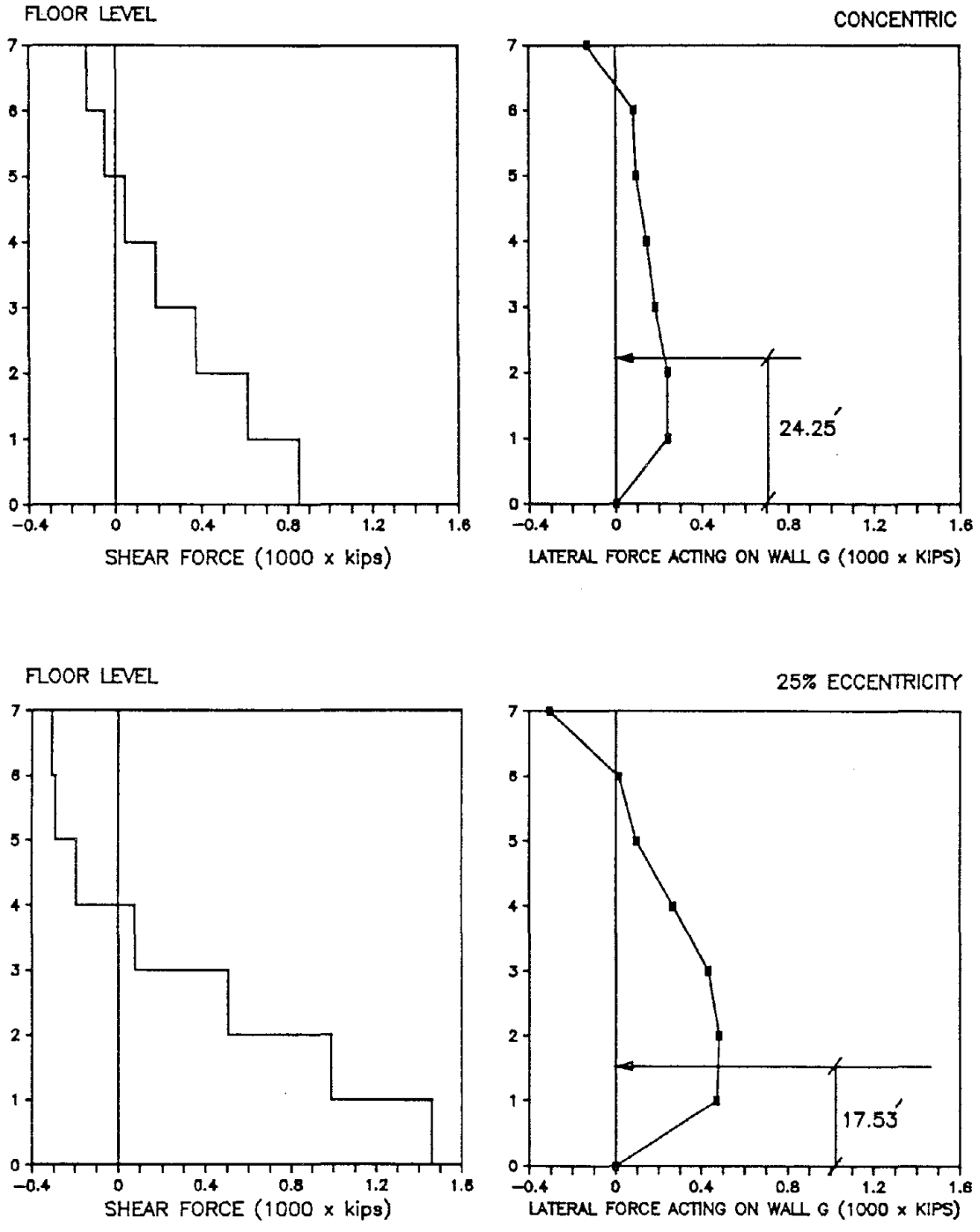

Figure 5.28(a): SHEAR FORCE AND LATERAL FORCE DISTRIBUTION PROFILES OF WALL G AT THE TIME OF MAXIMUM WALL G BASE SHEAR (TAFT-40, 0-8 SECONDS)

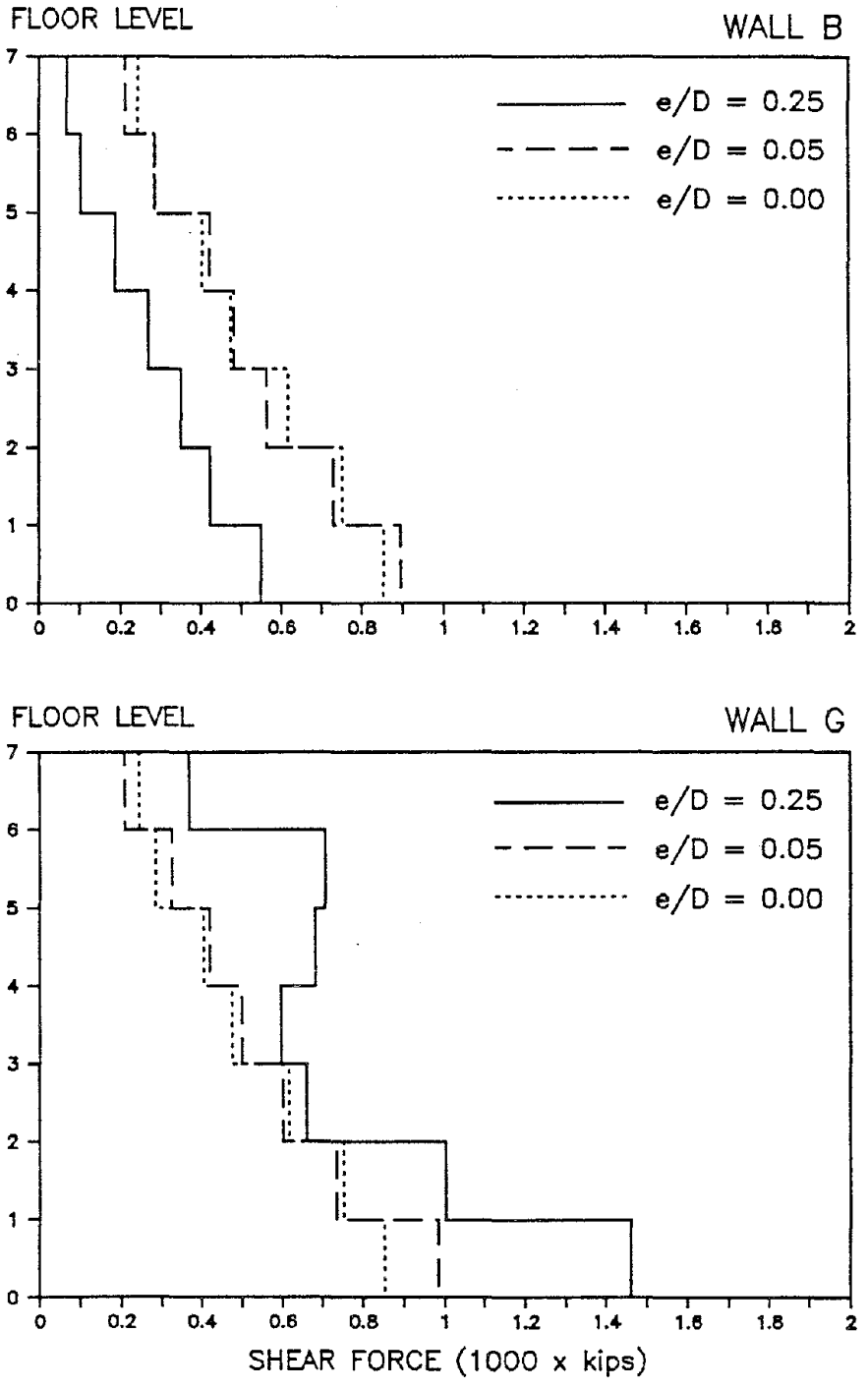

Figure 5.28(b): SHEAR FORCES ENVELOPES (TAFT-40 , 0-8 SECONDS)

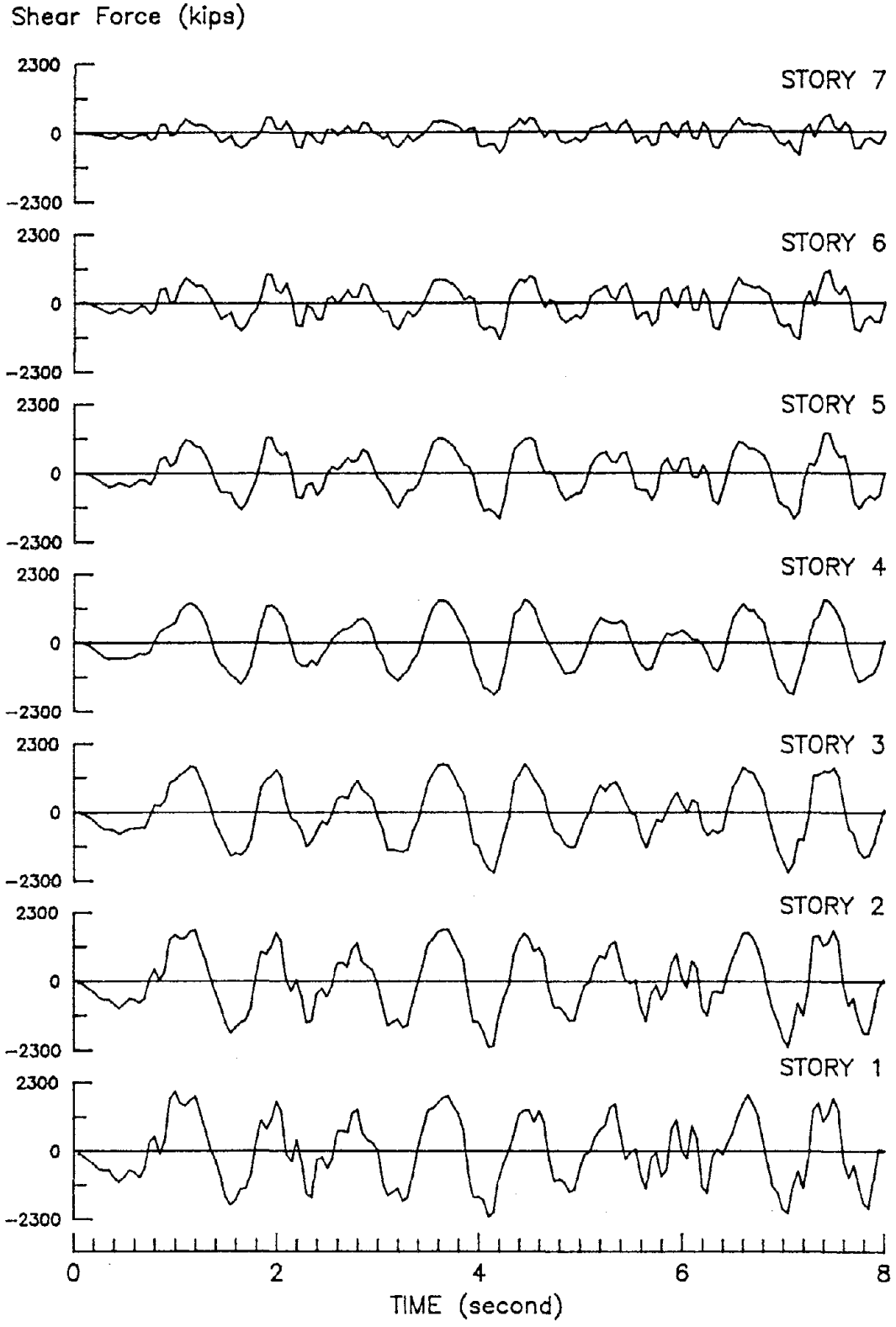

Figure 5.29: TOTAL STORY SHEAR TIME-HISTORIES OF THE CONCENTRIC STRUCTURE DUE TO TAFT-40

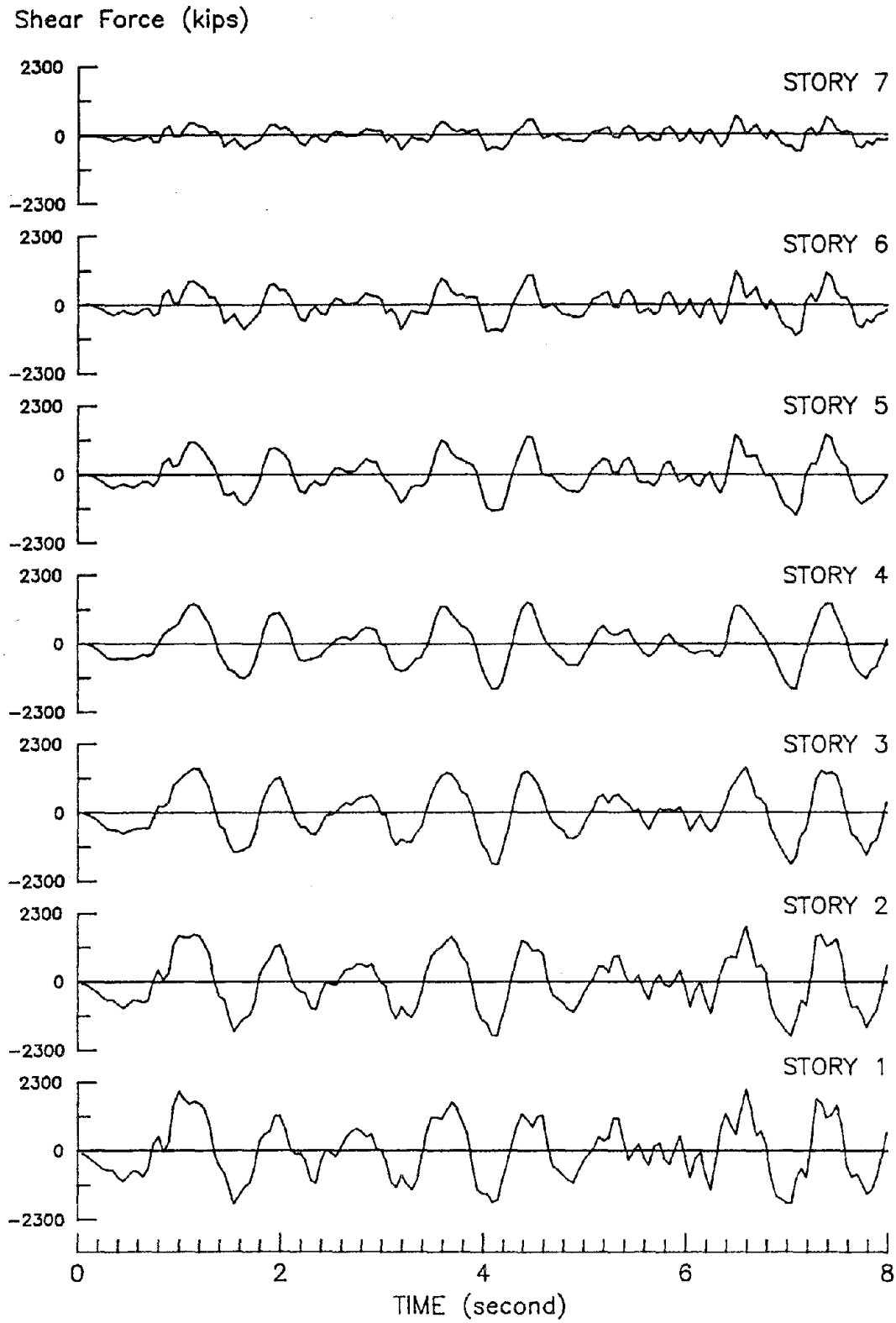

Figure 5.30: TOTAL STORY SHEAR TIME-HISTORIES DUE TO TAFT-40 (e/D = 0.05)

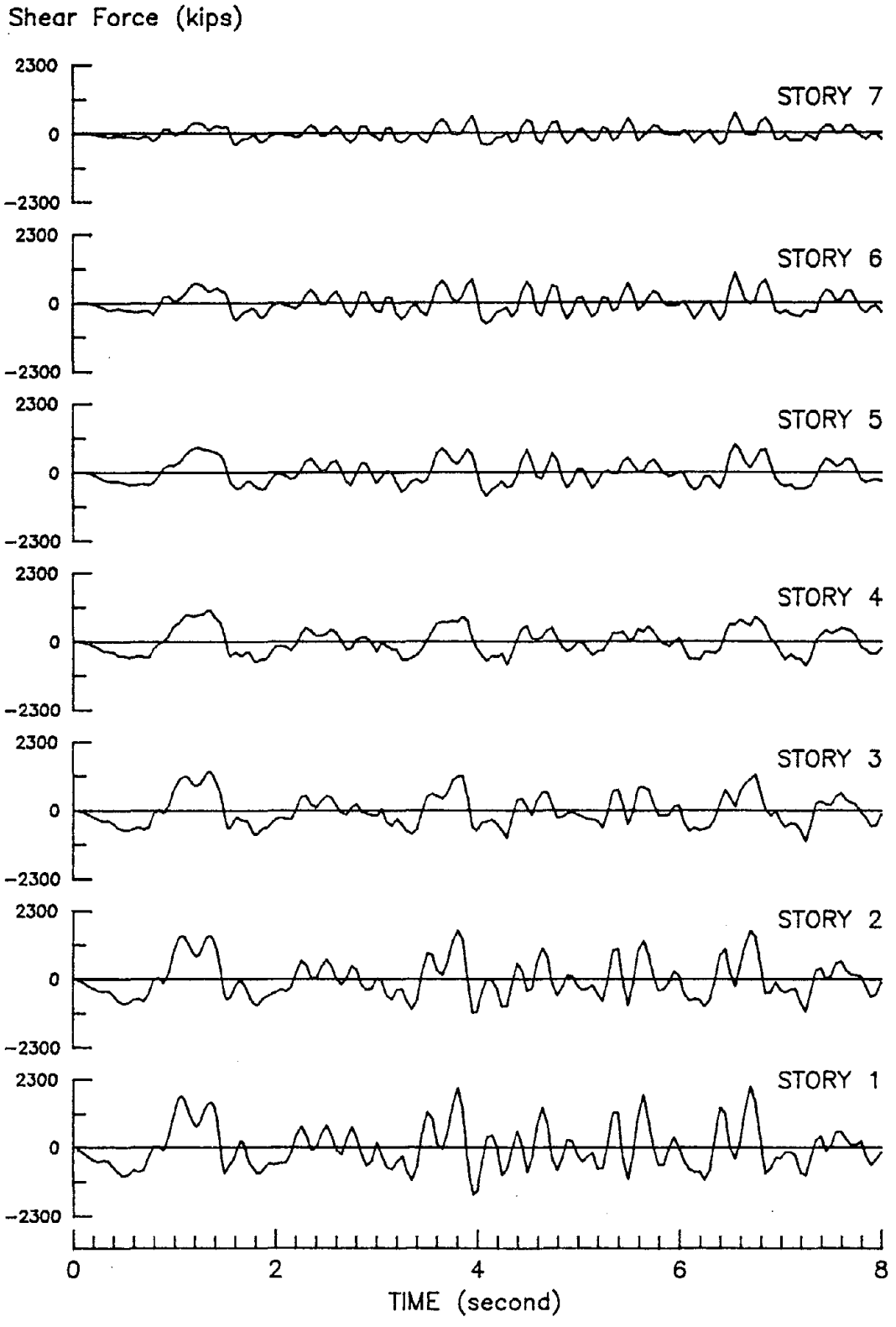

Figure 5.31: TOTAL STORY SHEAR TIME-HISTORIES DUE TO TAFT-40 (e/D = 0.25)

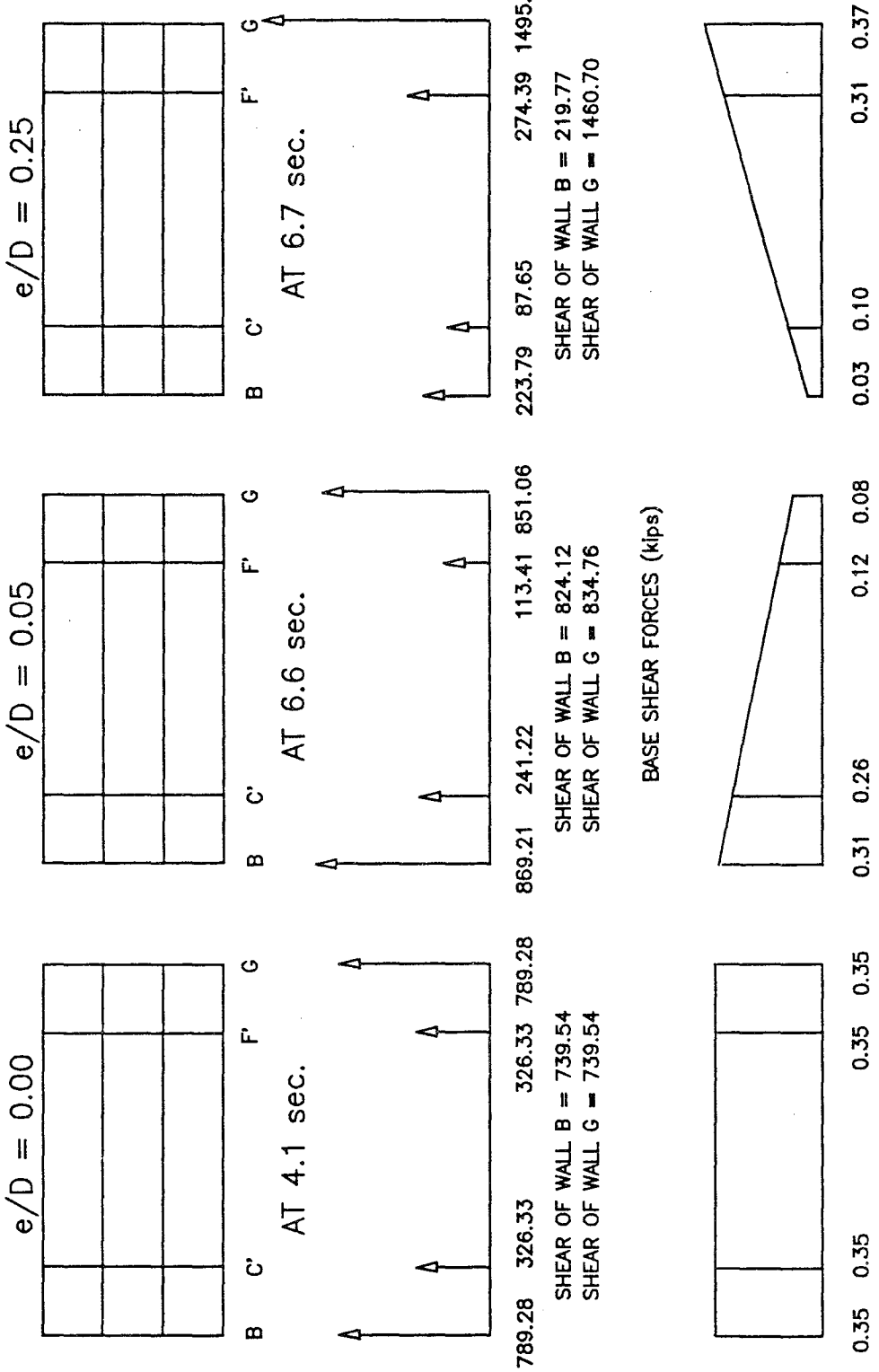

Figure 5.32: BASE SHEAR AND INTER-STORY DRIFT INDEX AT TIME OF MAXIMUM TOTAL BASE SHEAR (TAFT-40)

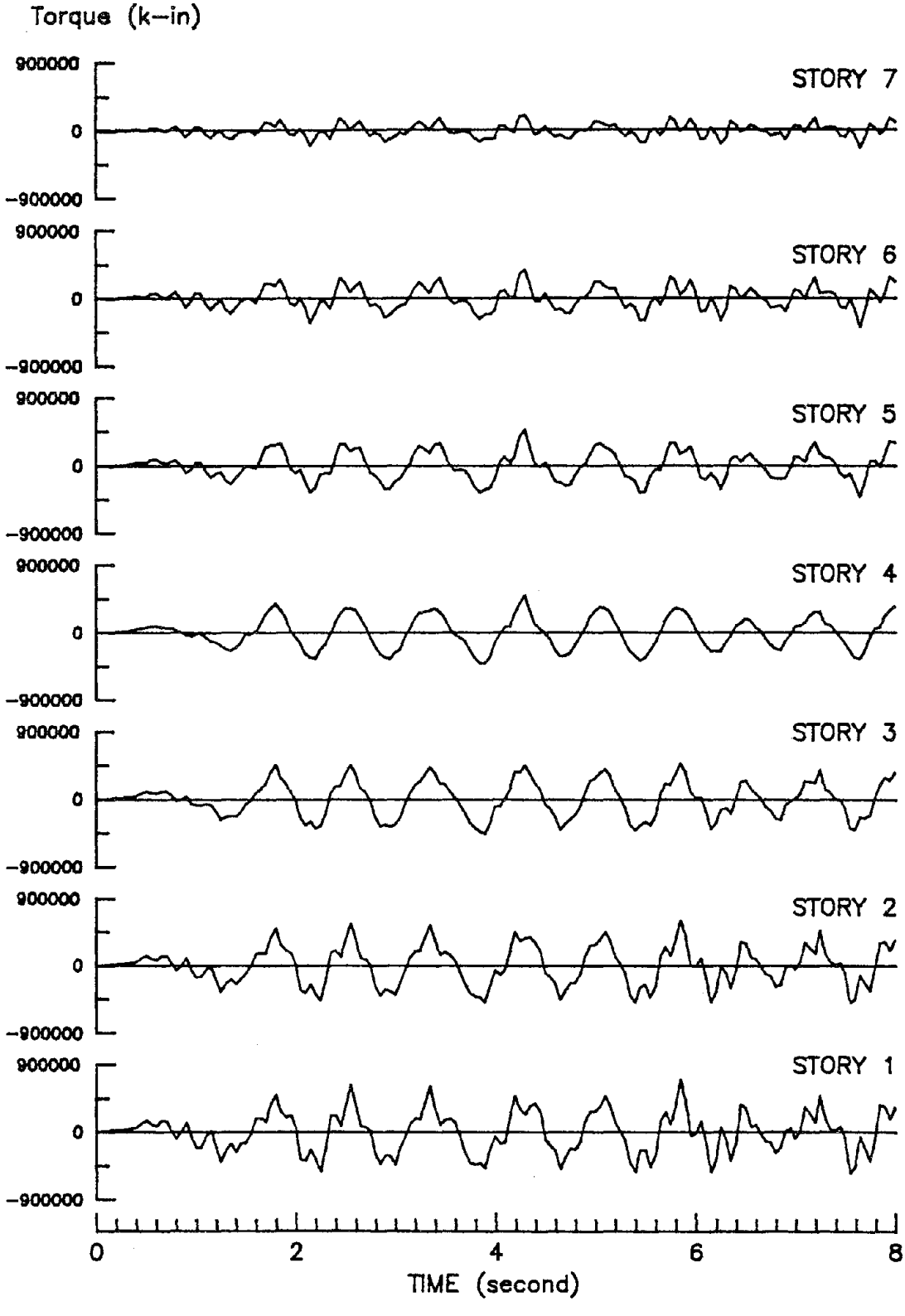

Figure 5.33: TOTAL STORY TORQUE TIME-HISTORIES DUE TO TAFT-40 (e/D = 0.05)

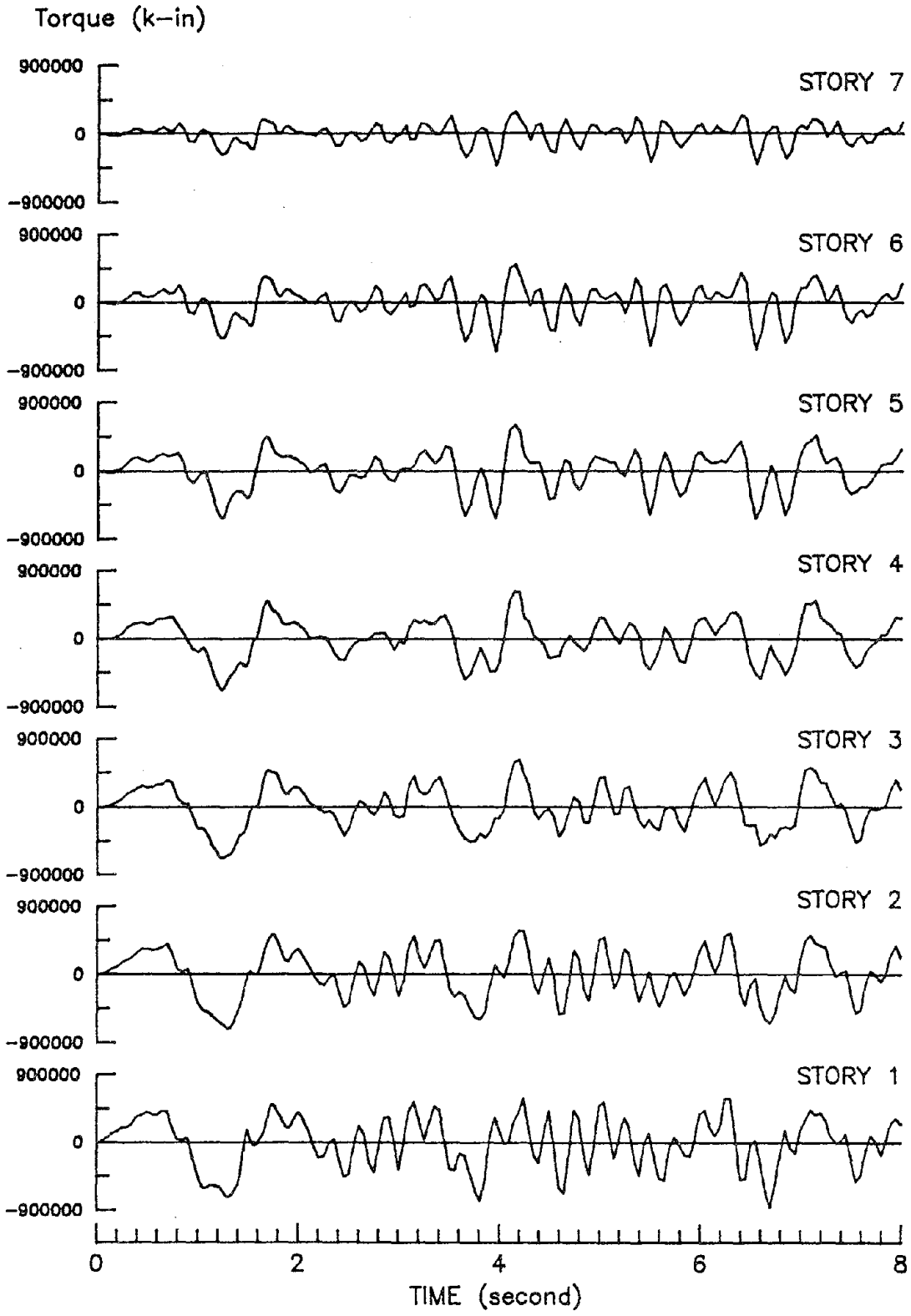

Figure 5.34: TOTAL STORY TORQUE TIME-HISTORIES DUE TO TAFT-40 (e/D = 0.25)

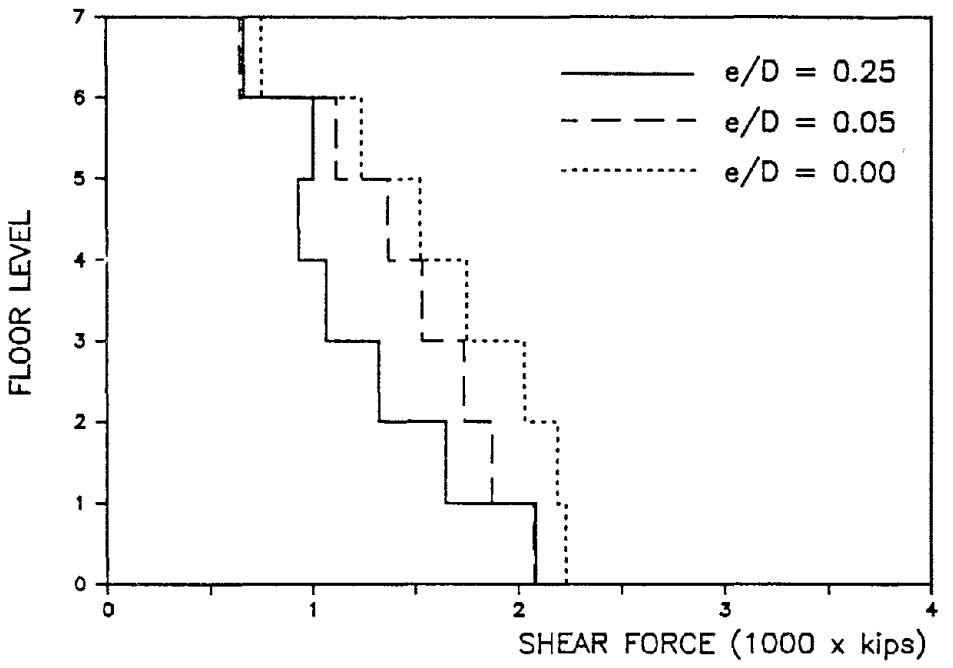

Figure 5.35: TOTAL STORY SHEAR ENVELOPES (TAFT-40 , 0-8 SECONDS)

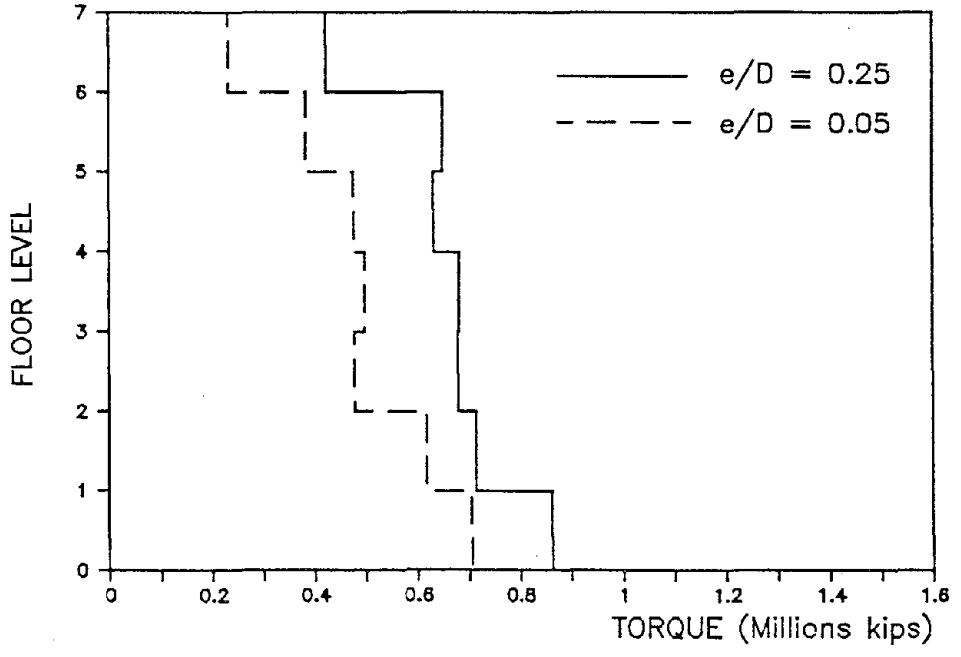

Figure 5.36: STORY TORQUE ENVELOPES (TAFT-40 , 0-8 SECONDS)

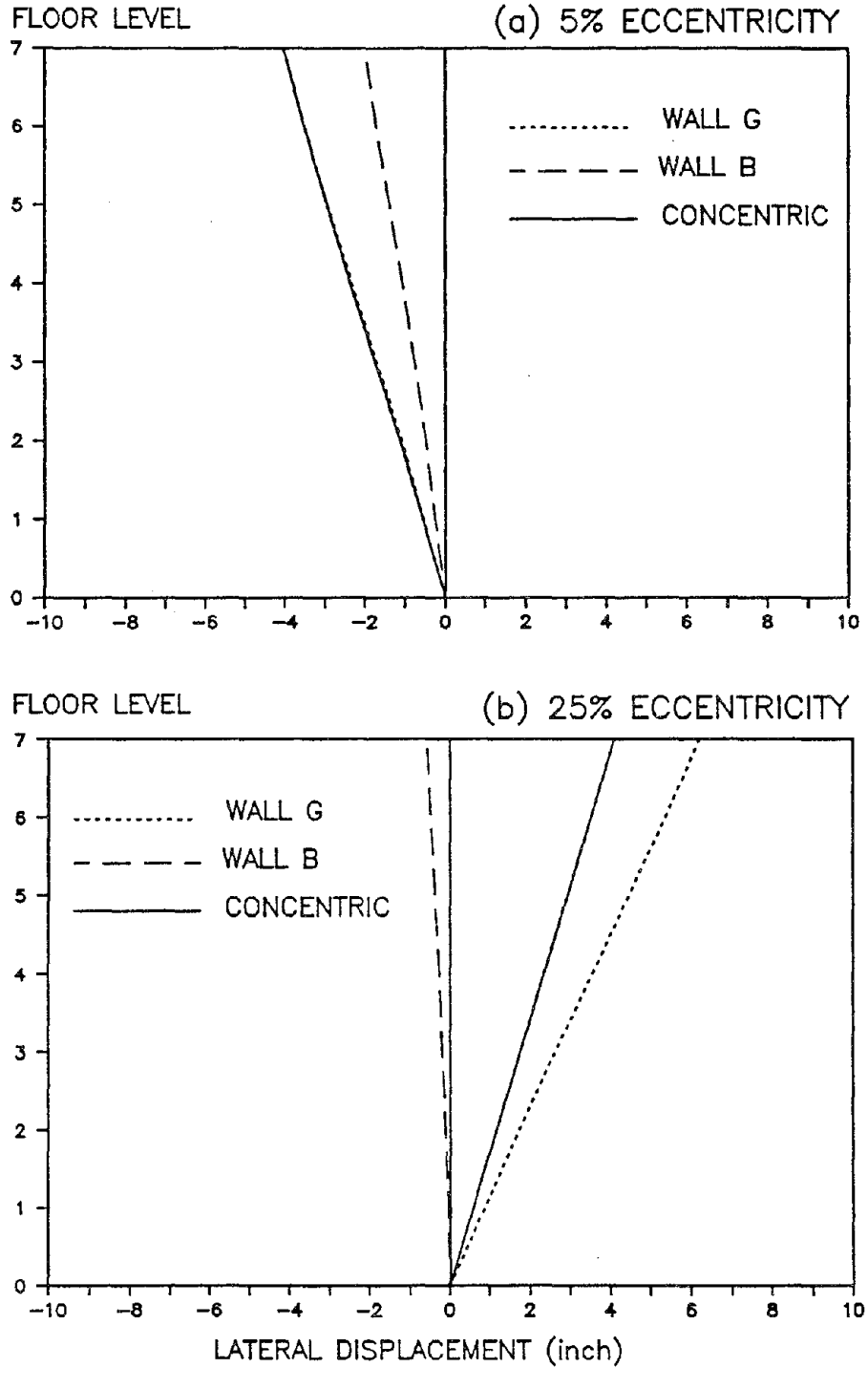

Figure 5.37: DISPLACEMENT PROFILES AT TIME OF MAXIMUM ROOF DISPLACEMENT

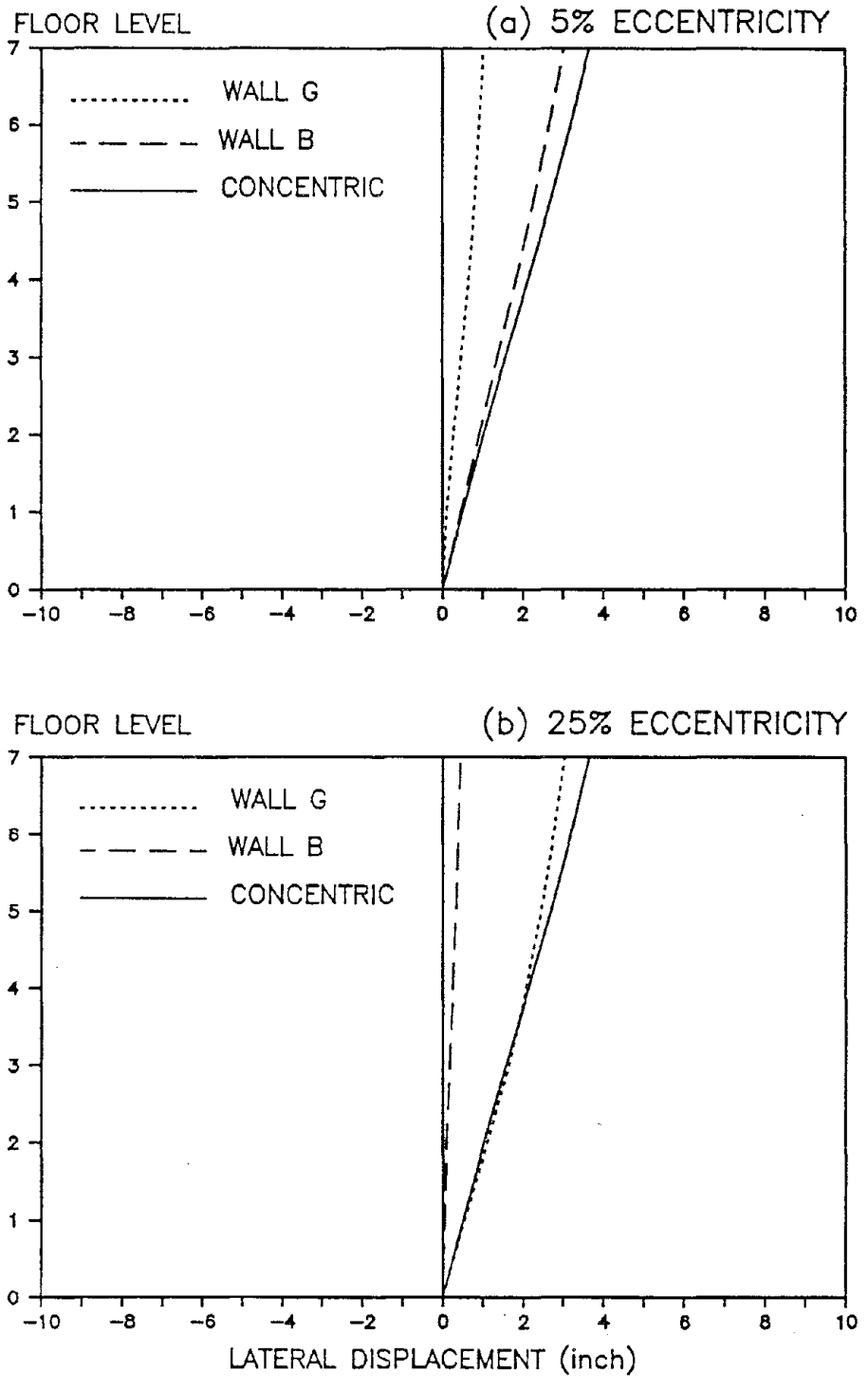

Figure 5.38: DISPLACEMENT PROFILES AT TIME OF MAXIMUM BASE SHEAR

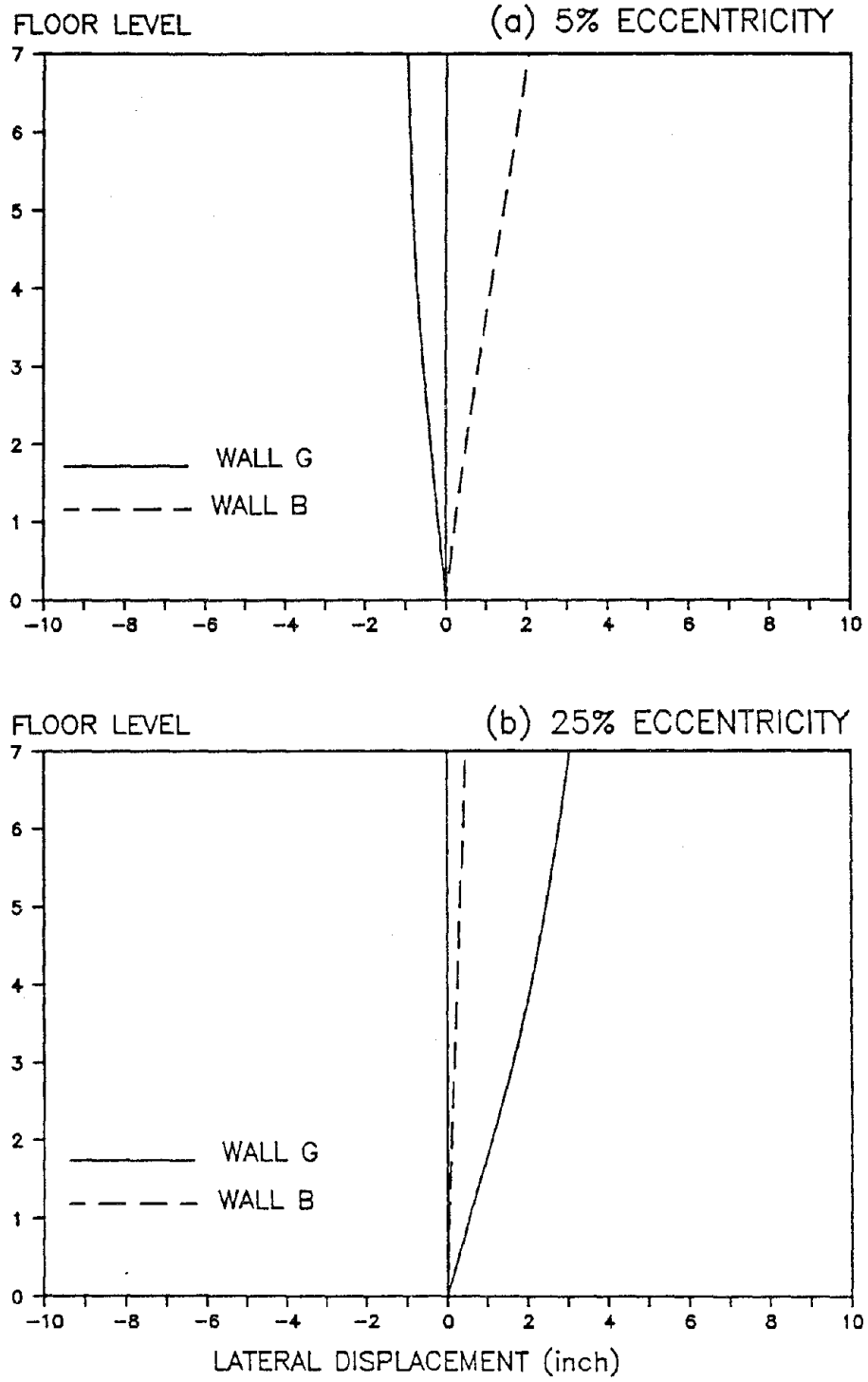

Figure 5.39: DISPLACEMENT PROFILES AT TIME OF MAXIMUM BASE TORQUE

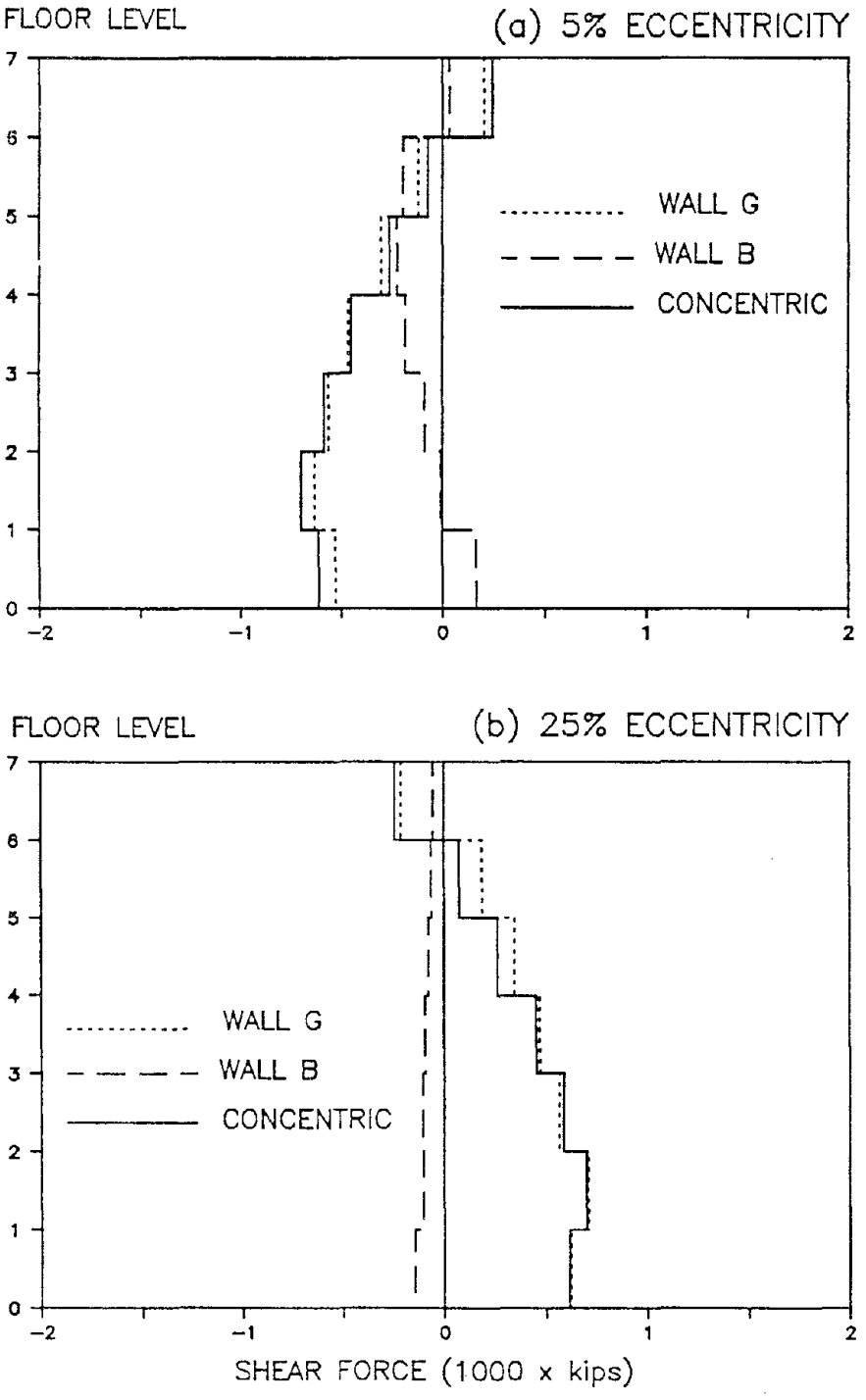

Figure 5.40: SHEAR FORCE PROFILES AT TIME OF MAXIMUM ROOF DISPLACEMENT

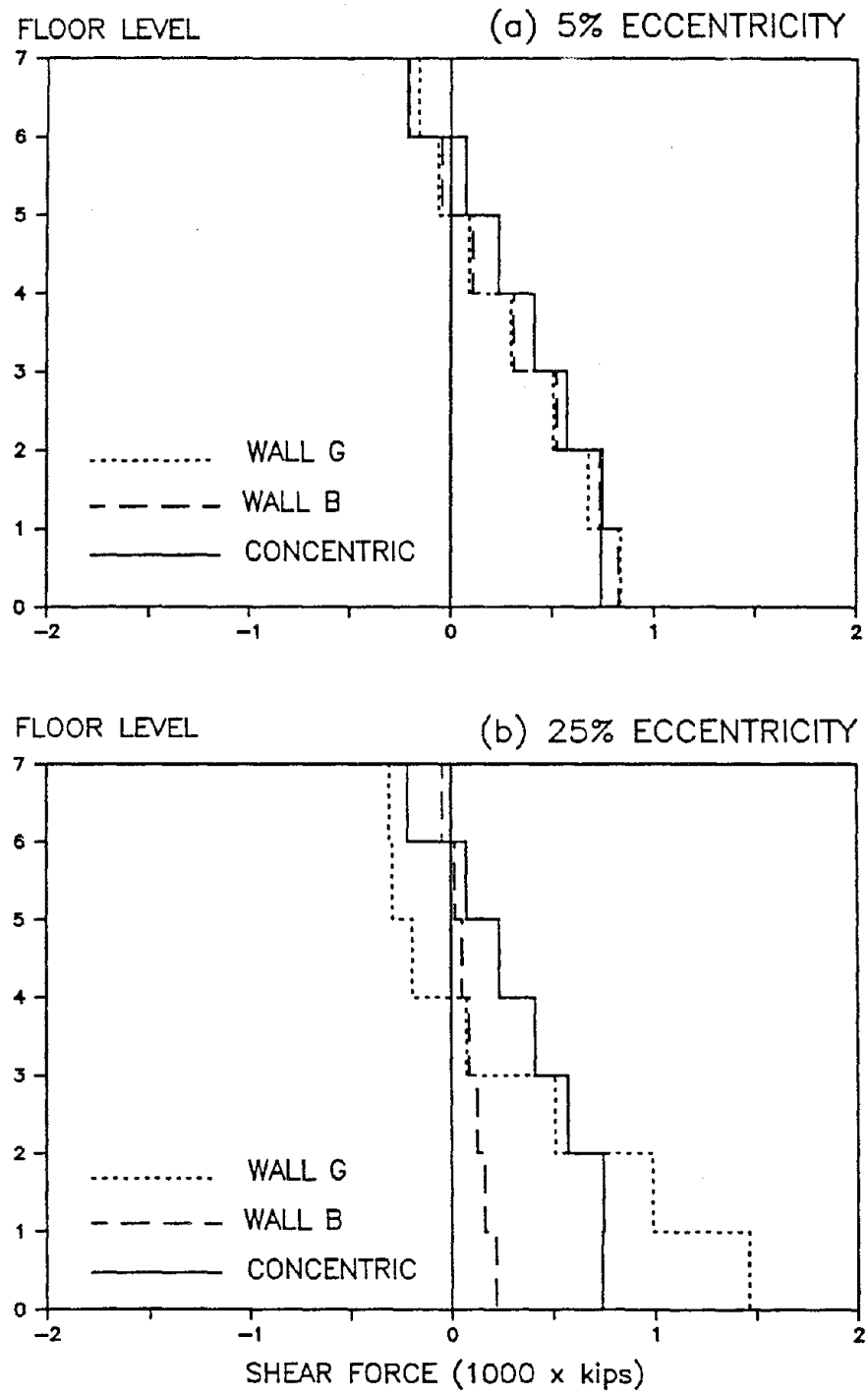

Figure 5.41: SHEAR FORCE PROFILES AT TIME OF MAXIMUM TOTAL BASE SHEAR

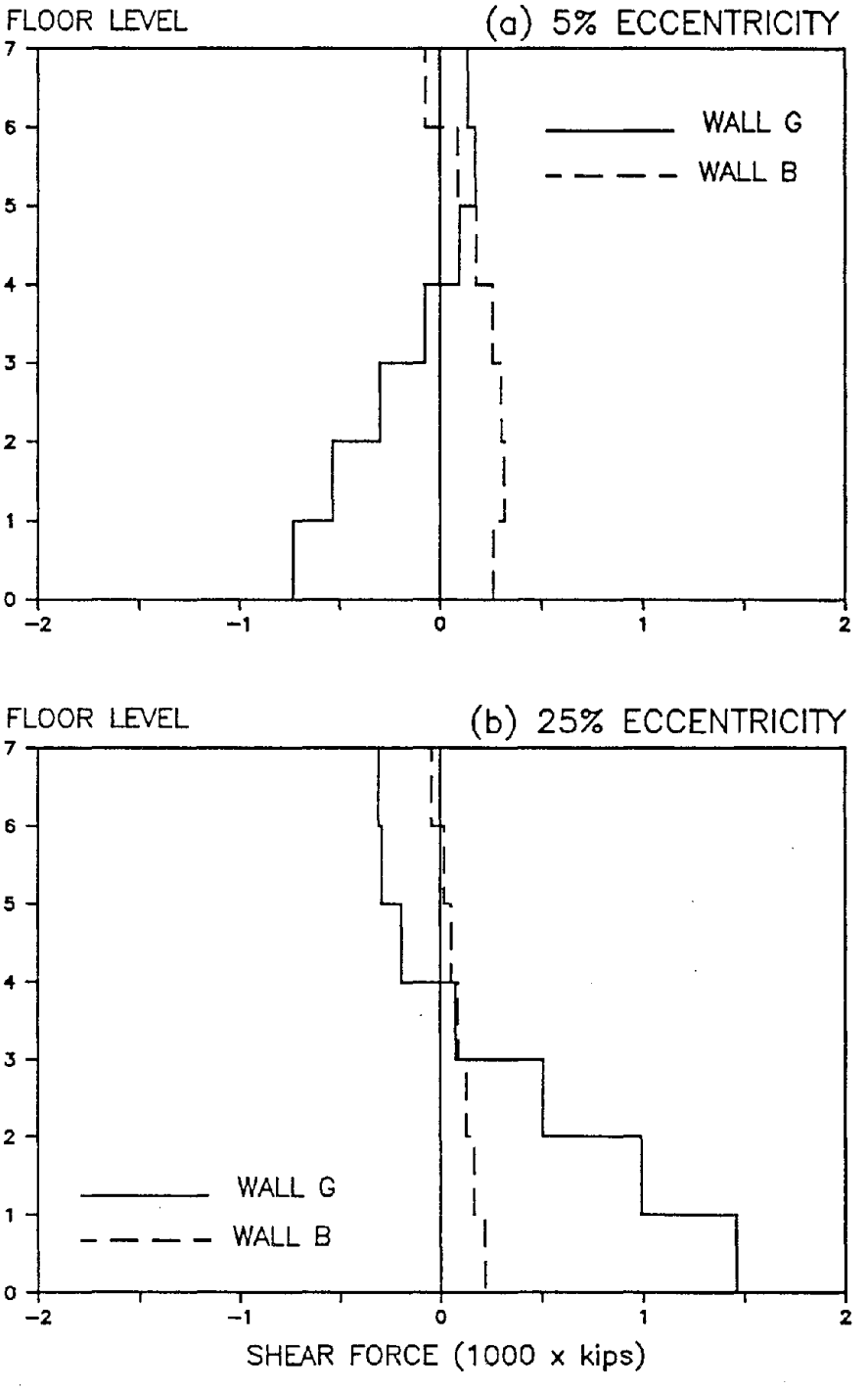

Figure 5.42: SHEAR FORCE PROFILES AT TIME OF MAXIMUM BASE TORQUE

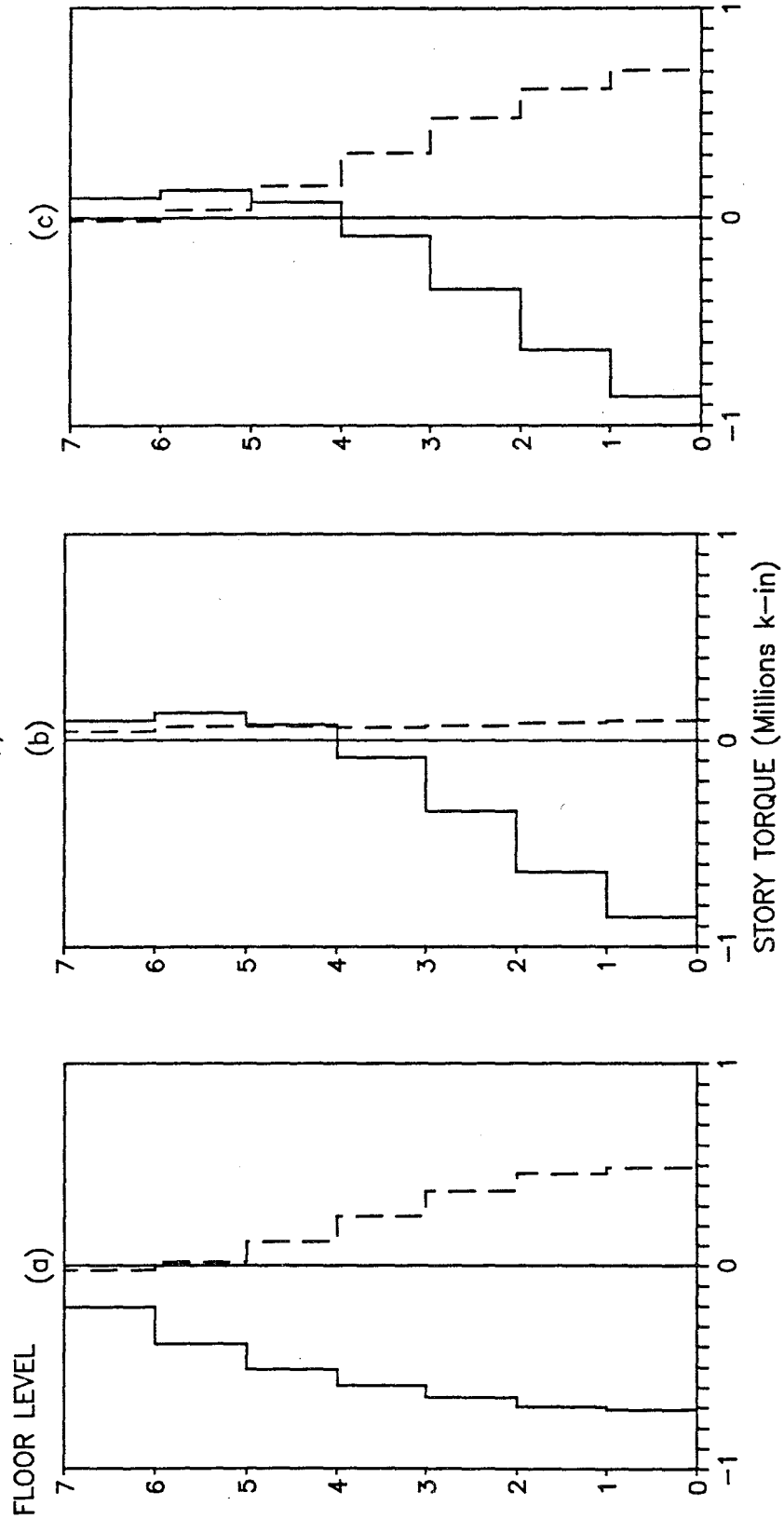

Figure 5.43: TORQUE PROFILES AT TIME OF MAXIMUM (a) ROOF DISPLACEMENT, (b) TOTAL BASE SHEAR, (c) BASE TORQUE

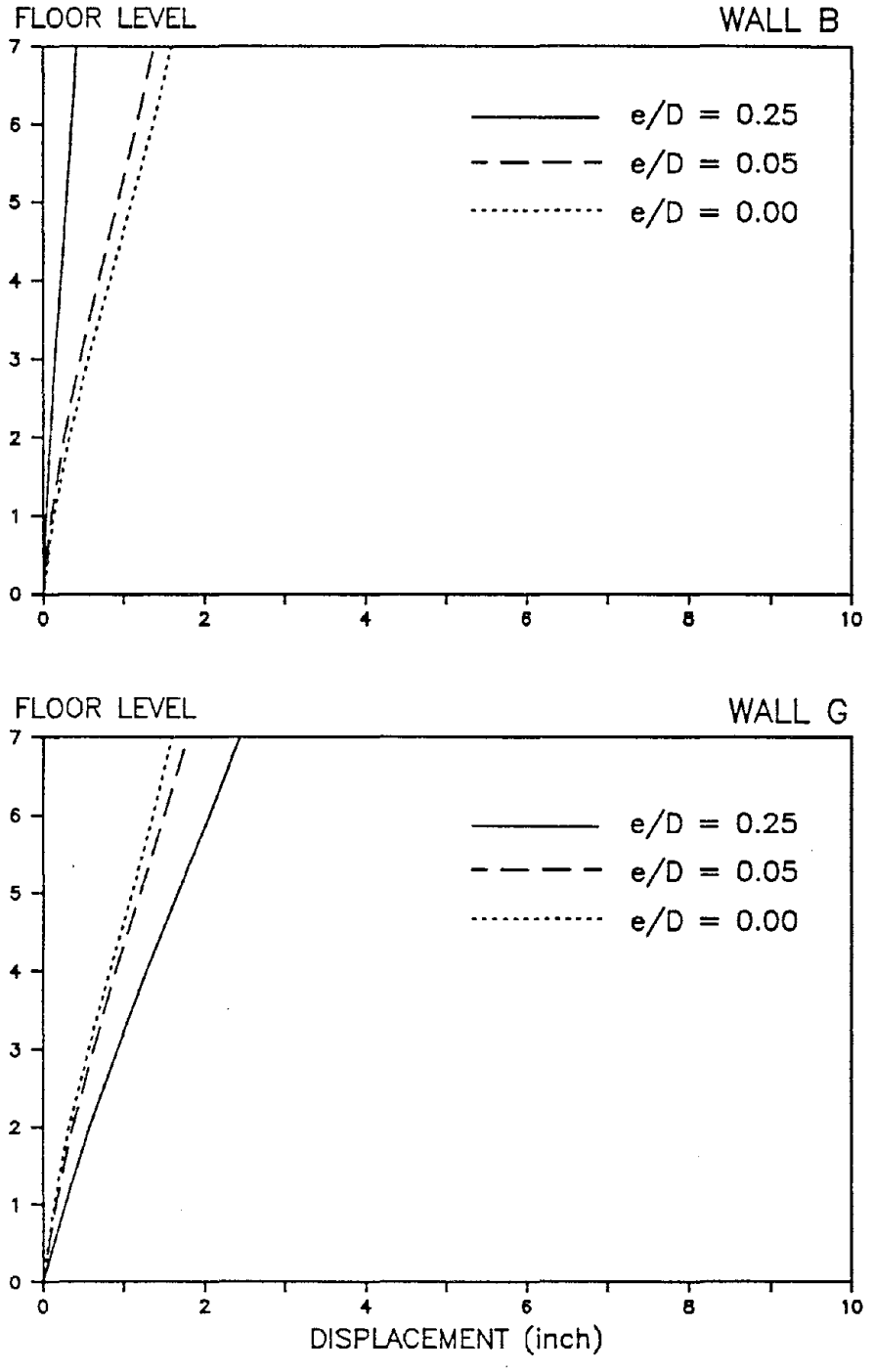

Figure 5.44: DISPLACEMENT ENVELOPES (TAFT-18 , 0-2 SECONDS)

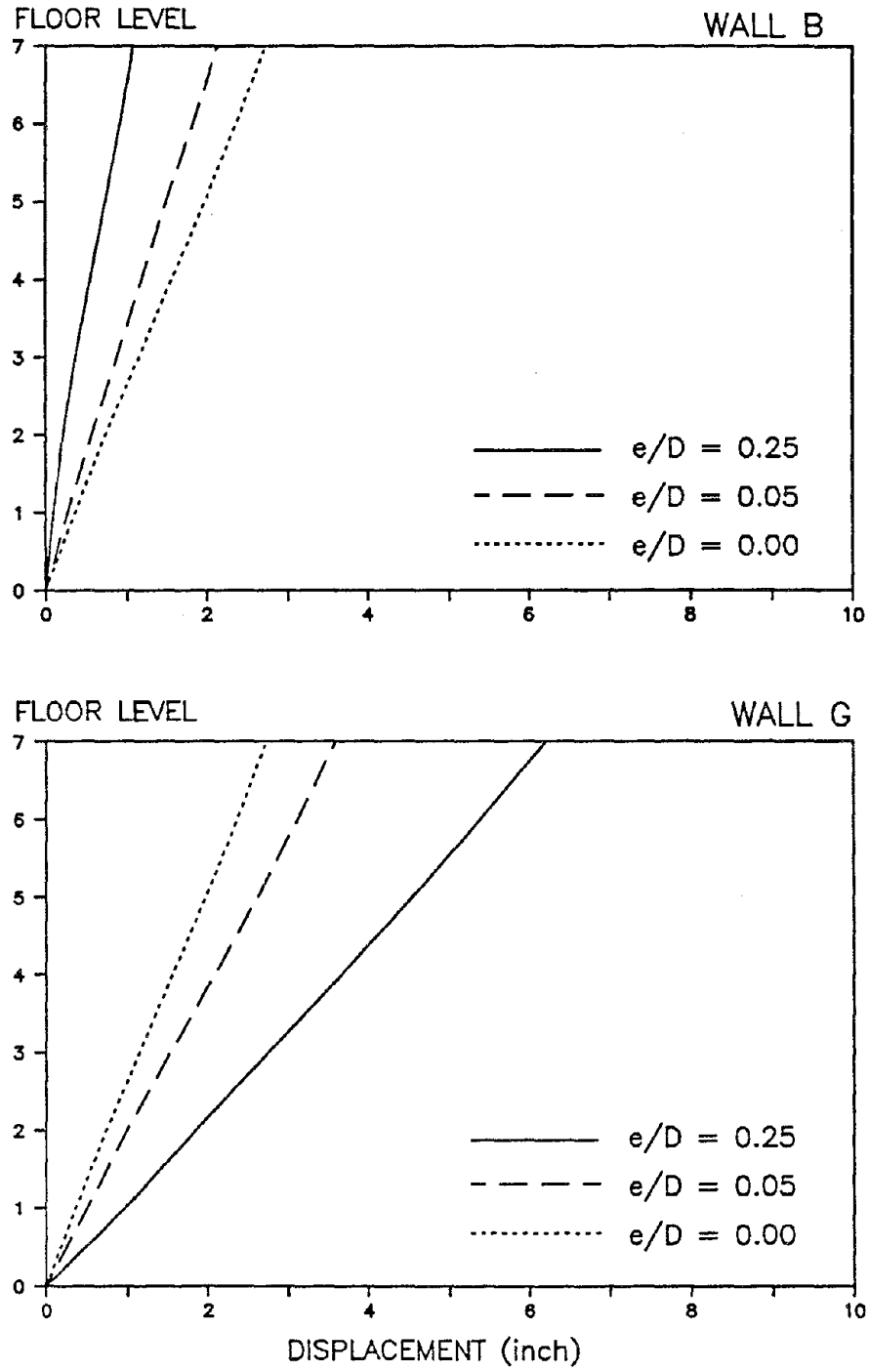

Figure 5.45: DISPLACEMENT ENVELOPES (TAFT-40 , 0-2 SECONDS)

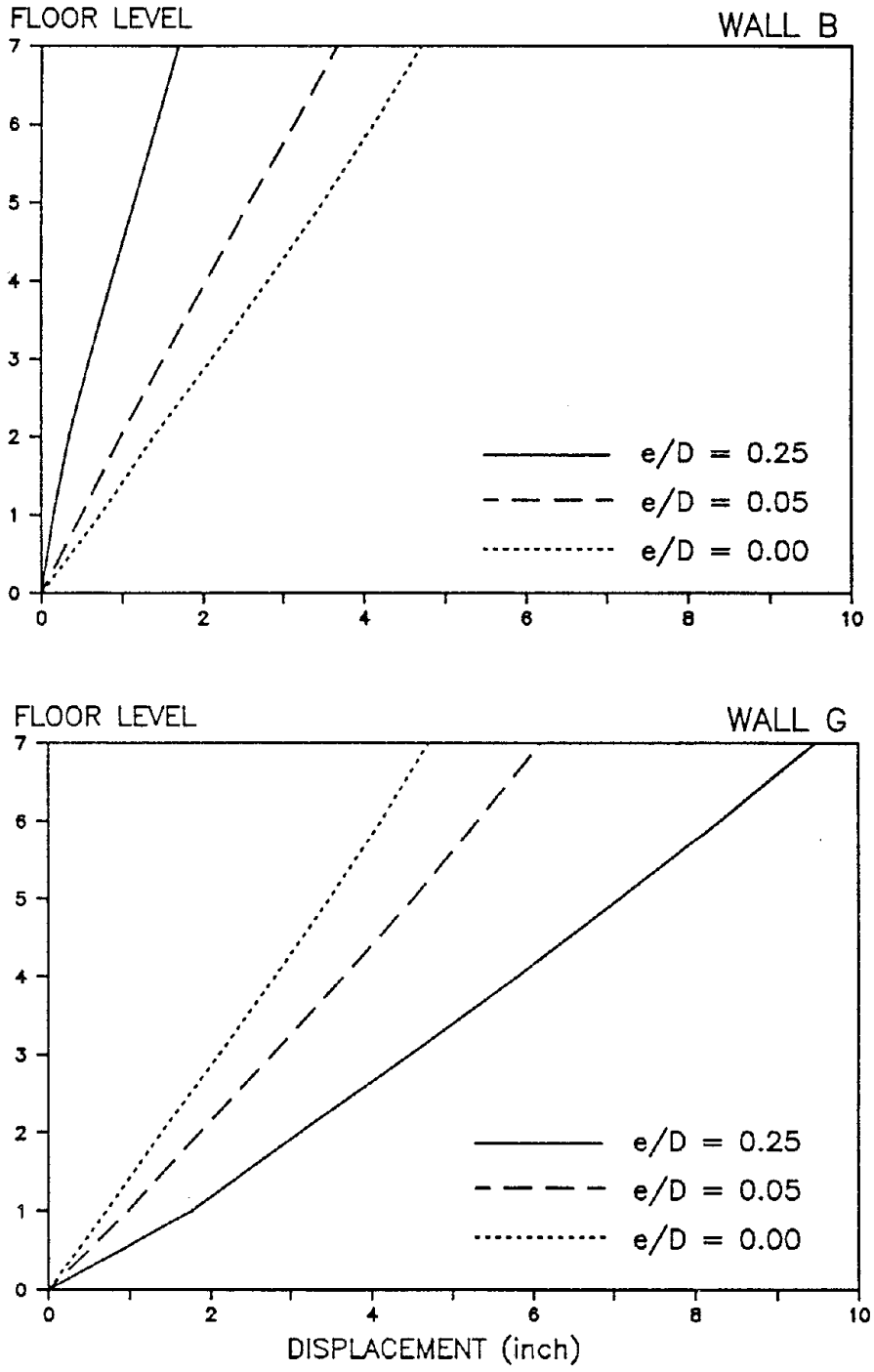

Figure 5.46: DISPLACEMENT ENVELOPES (TAFT-60 , 0-2 SECONDS)

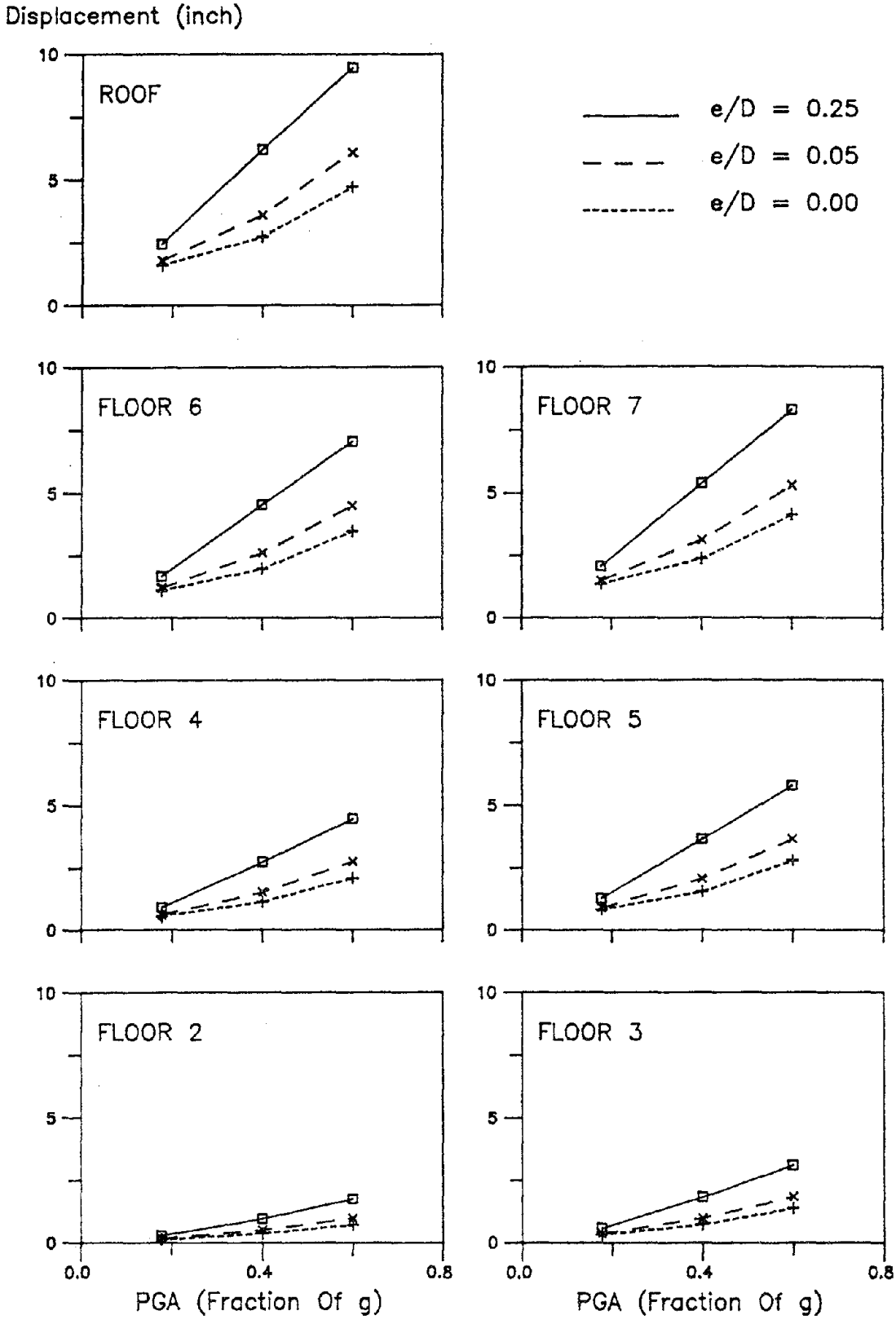

Figure 5.47: DISPLACEMENTS OF WALL G VERSUS PEAK GROUND ACCELERATION

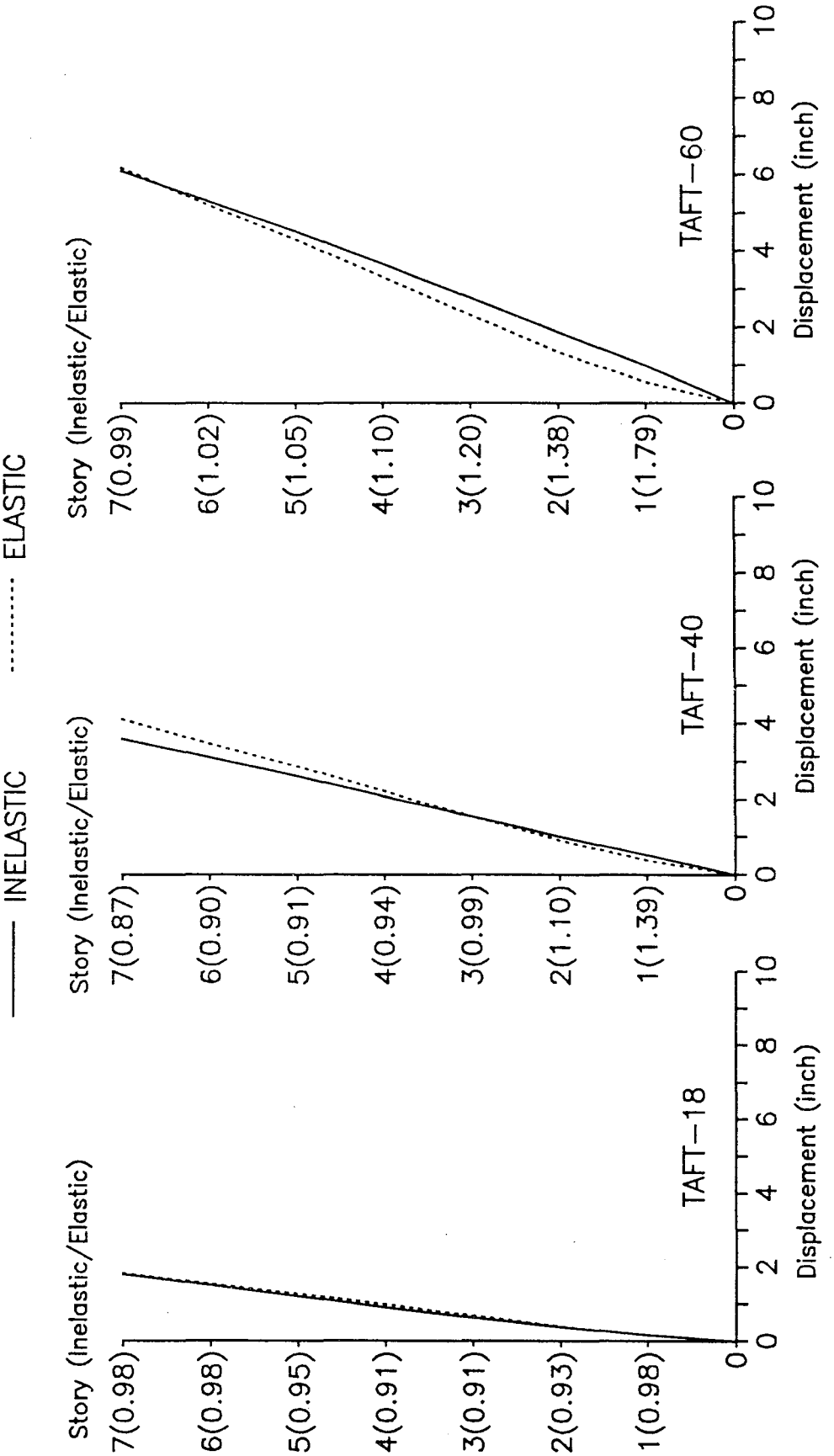

Figure 5.48: DISPLACEMENT ENVELOPES OF WALL G (5% STATIC ECCENTRICITY)

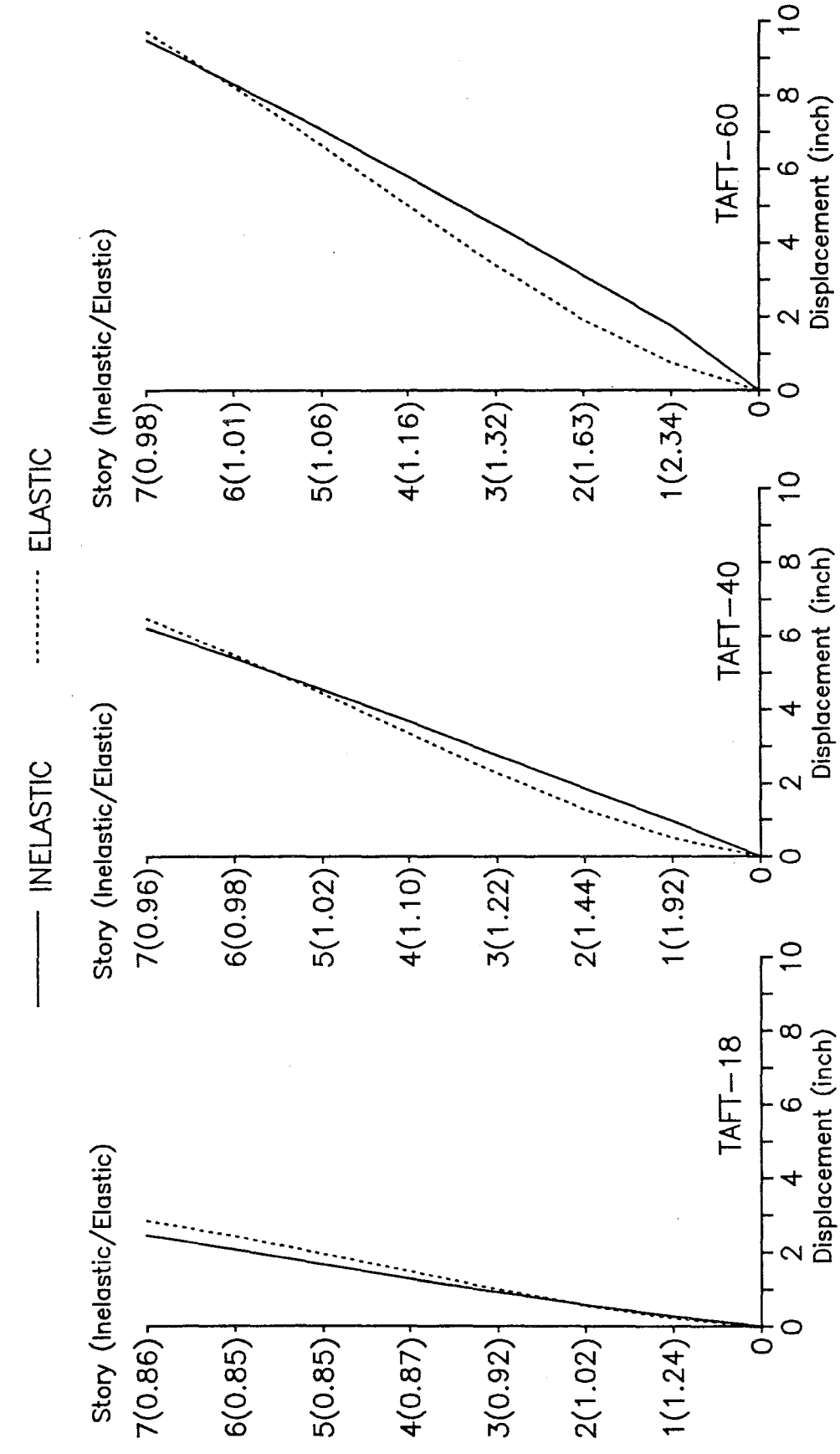

Figure 5.49: DISPLACEMENT ENVELOPES OF WALL G (25% STATIC ECCENTRICITY)

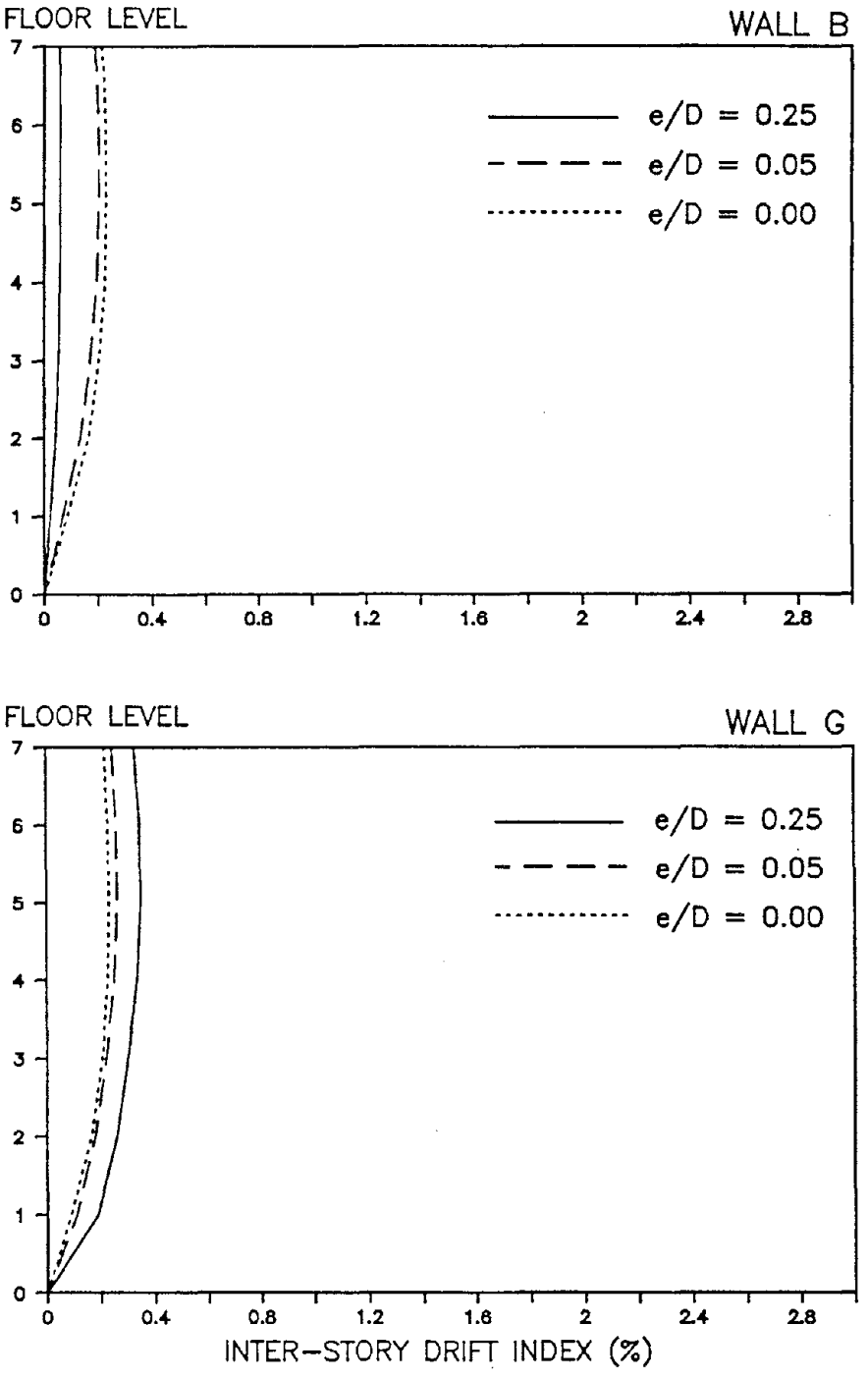

Figure 5.50: INTER-STORY DRIFT INDEX ENVELOPES (TAFT-18 , 0-2 SECONDS)

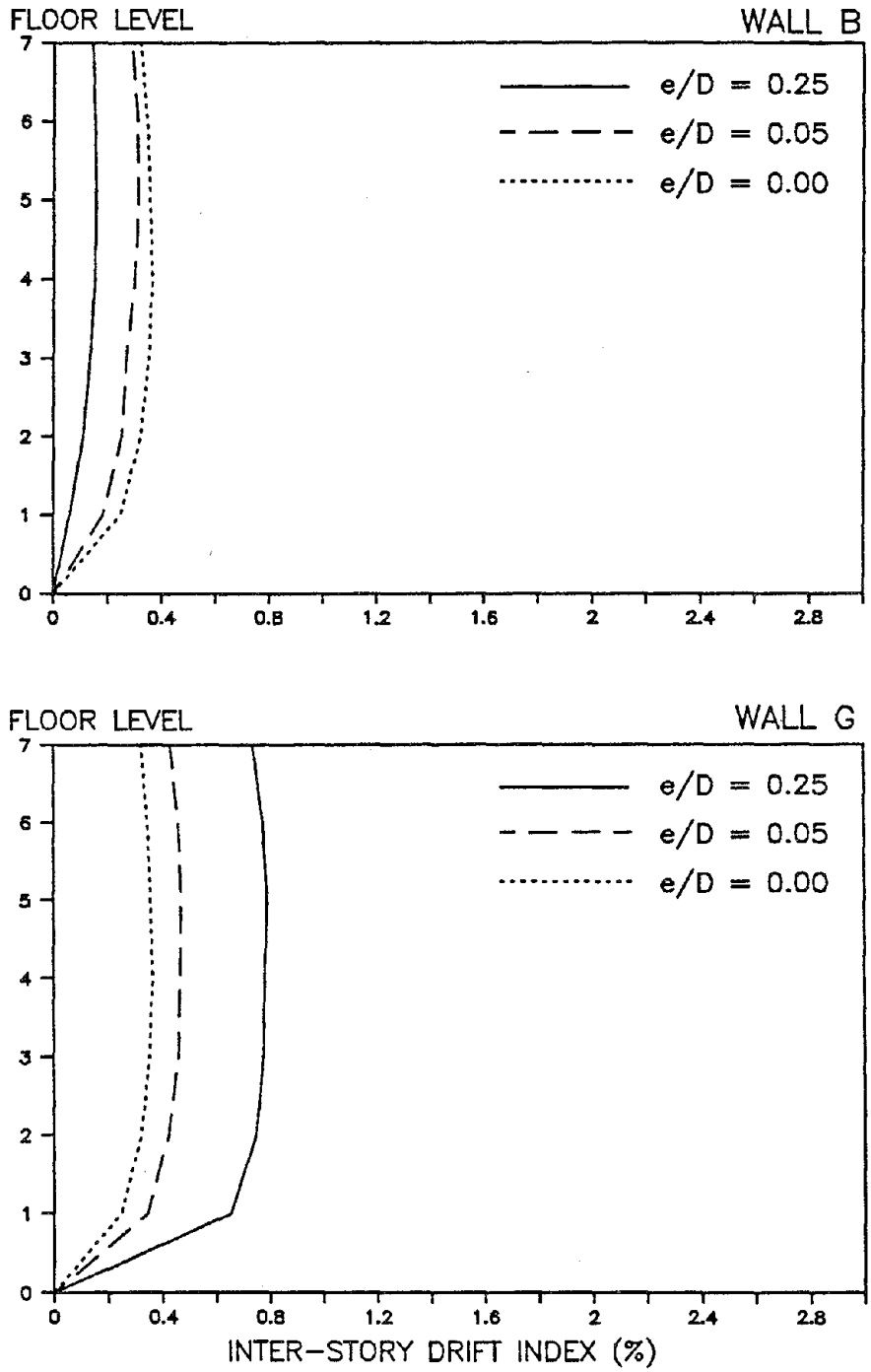

Figure 5.51: INTER-STORY DRIFT INDEX ENVELOPES (TAFT-40 , 0-2 SECONDS)

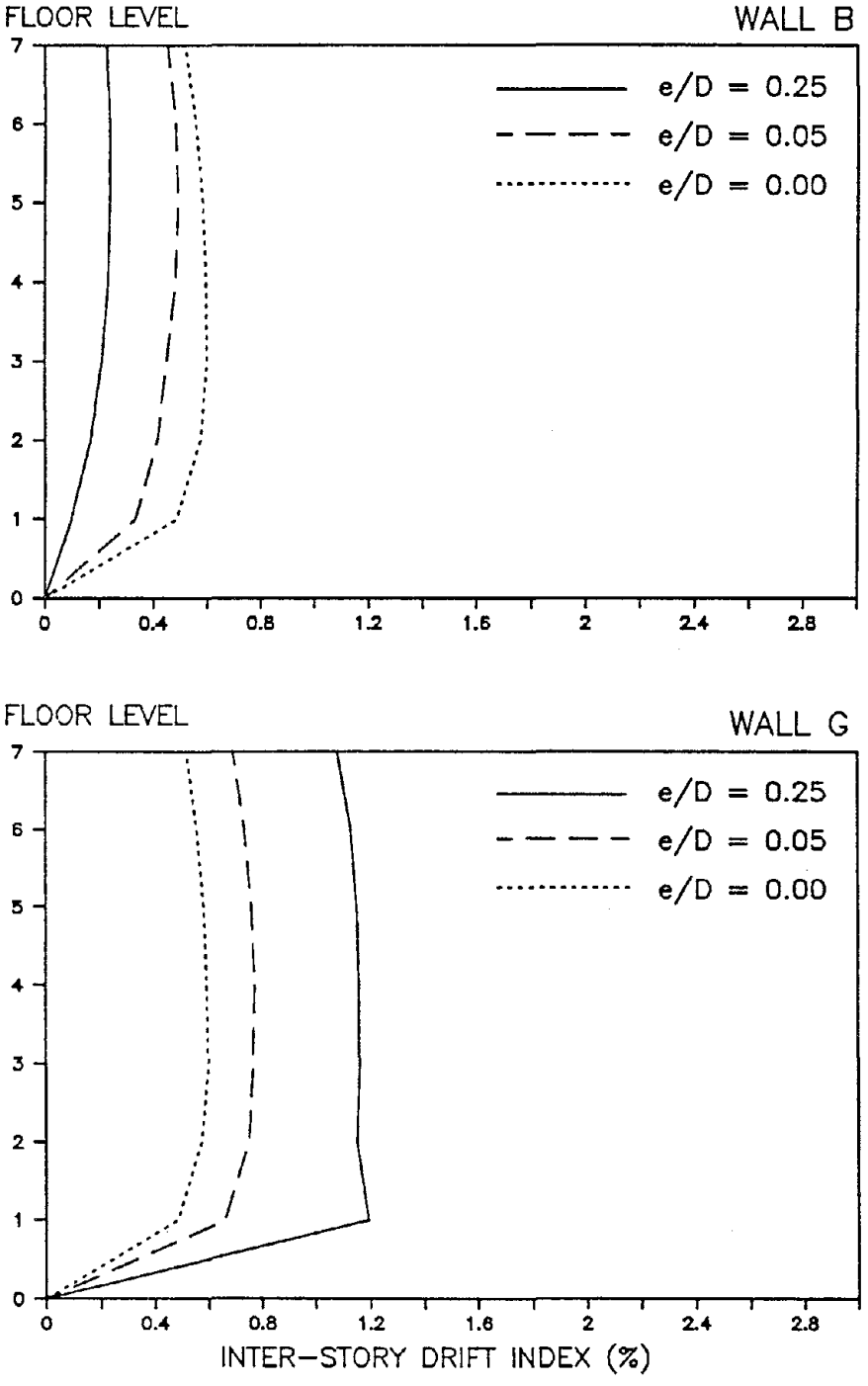

Figure 5.52: INTER-STORY DRIFT INDEX ENVELOPES (TAFT-60 , 0-2 SECONDS)

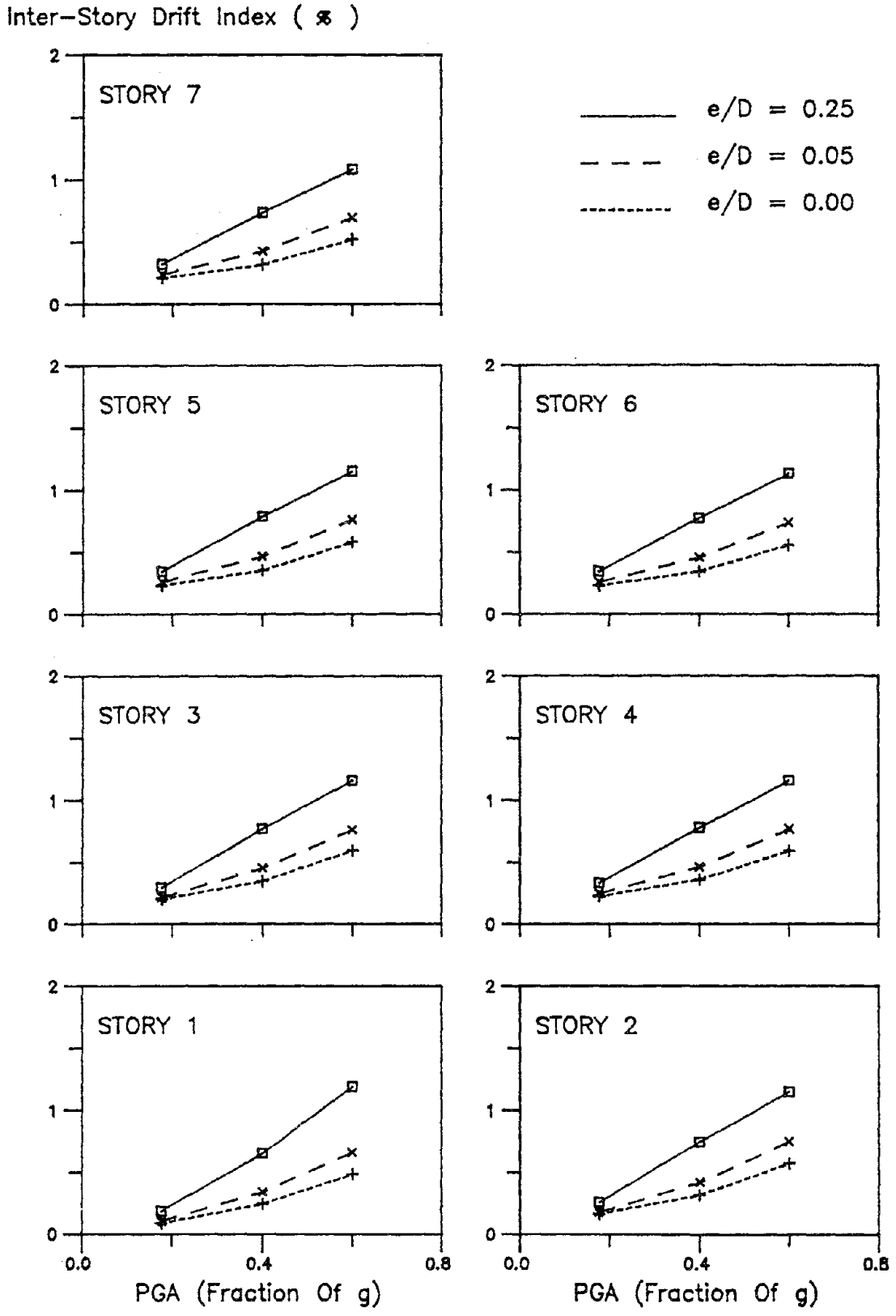

Figure 5.53: INTER-STORY DRIFT INDICES OF WALL G VERSUS PEAK GROUND ACCELERATION

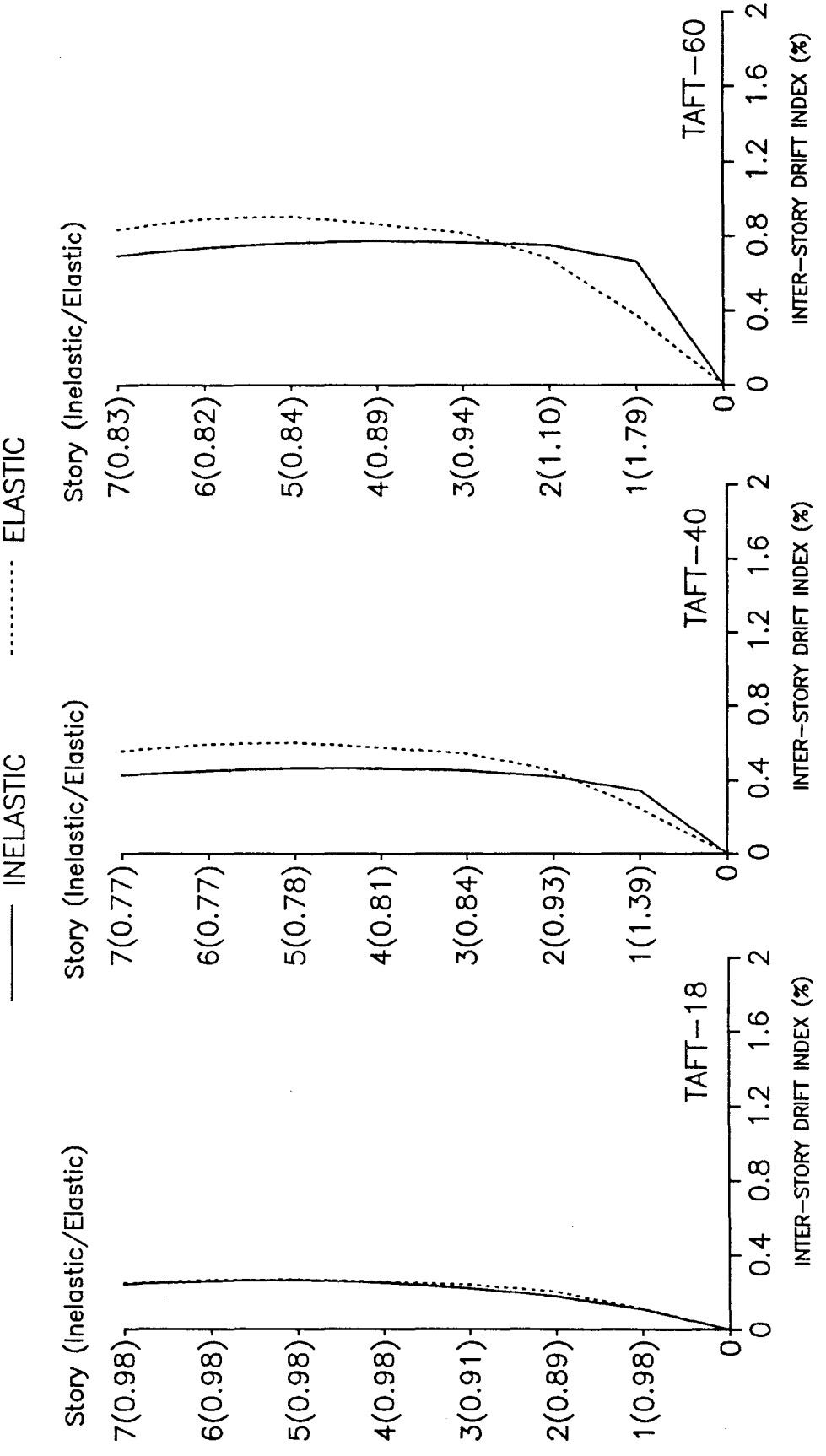

Figure 5.54: INTER-STORY DRIFT INDEX ENVELOPES OF WALL G (5% STATIC ECCENTRICITY)

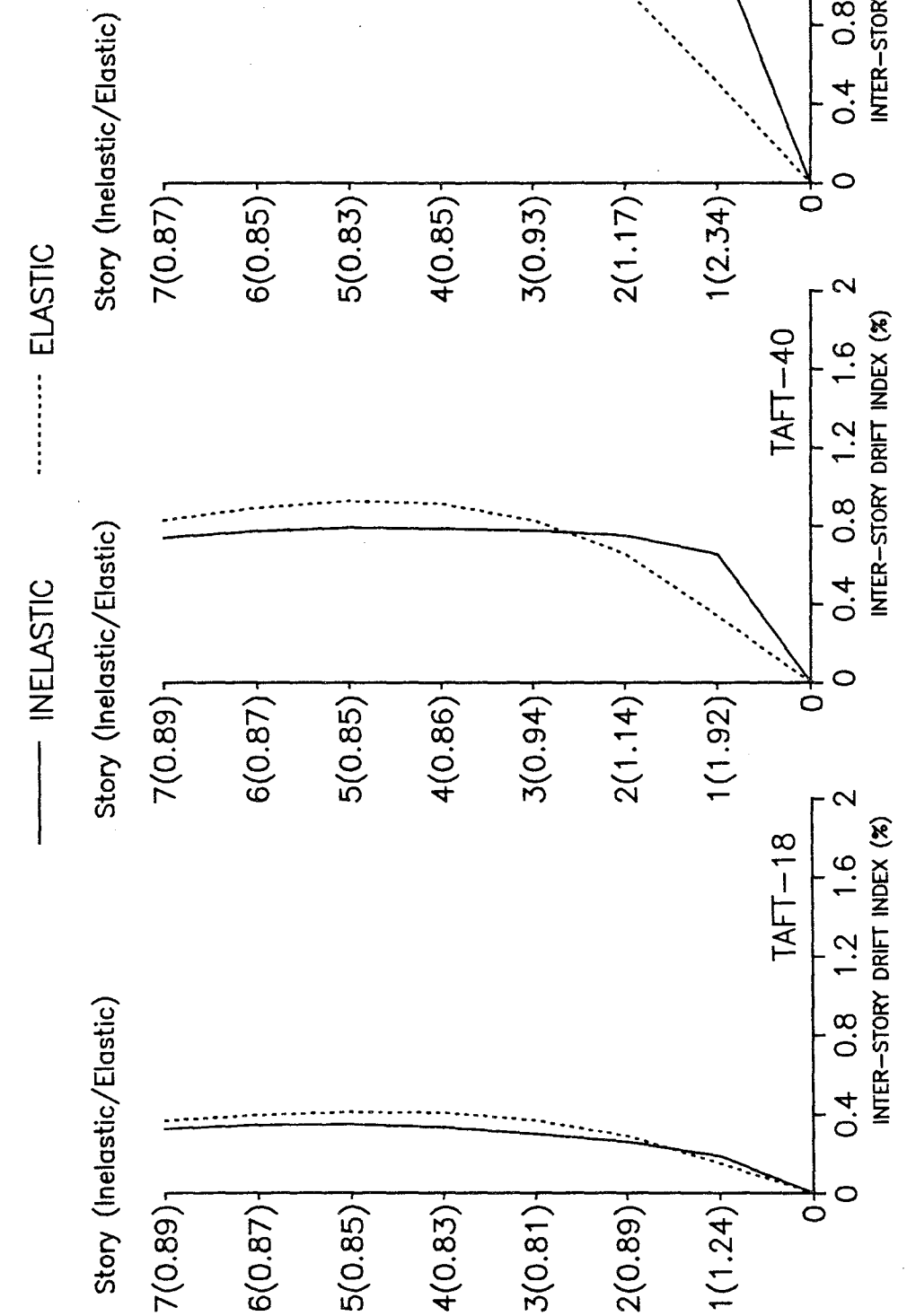

Figure 5.55: INTER-STORY DRIFT INDEX ENVELOPES OF WALL G (25% STATIC ECCENTRICITY)

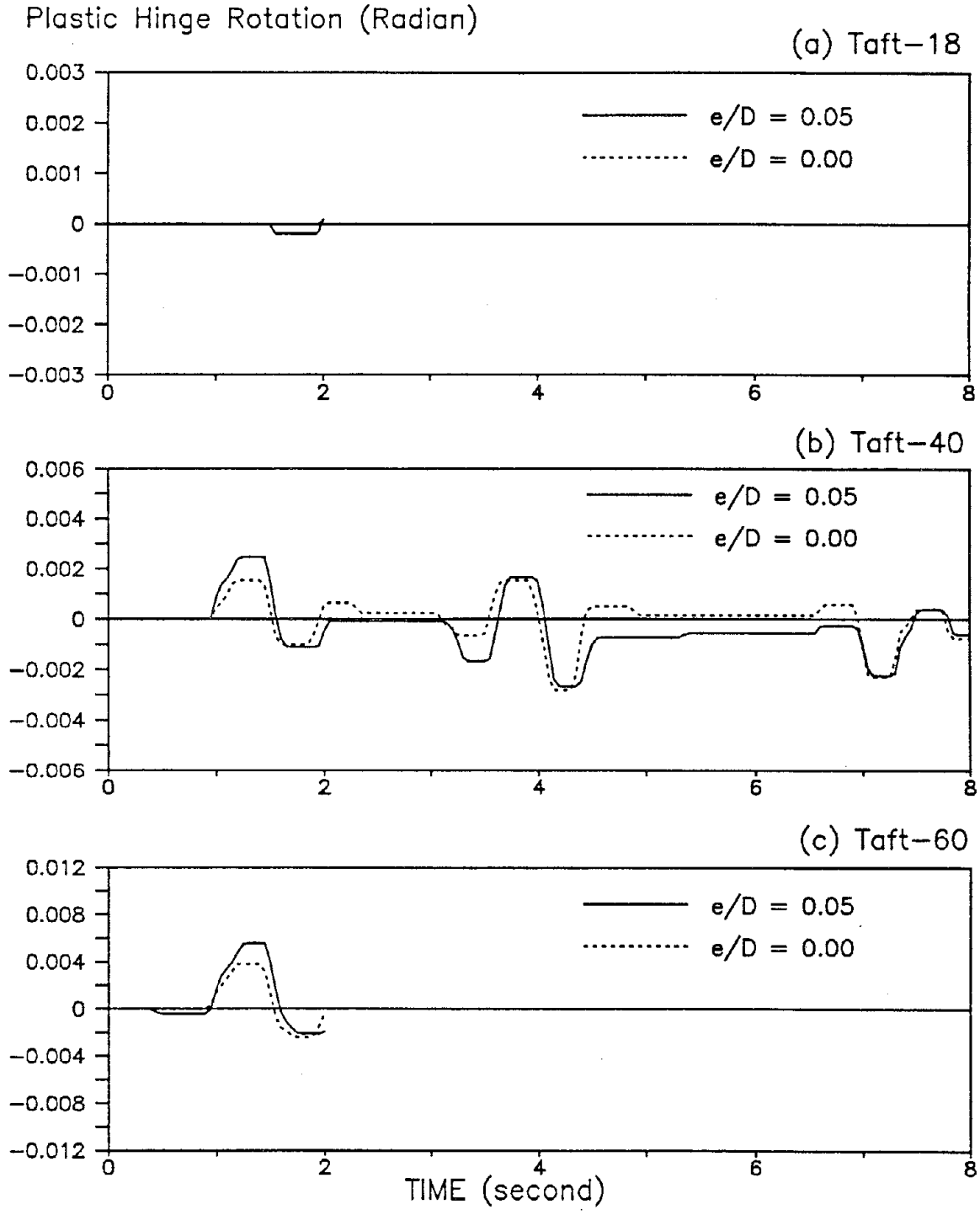

Figure 5.56: TIME-HISTORY OF PLASTIC ROTATION AT THE BASE OF WALL G (0% VERSUS 5% STATIC ECCENTRICITY)

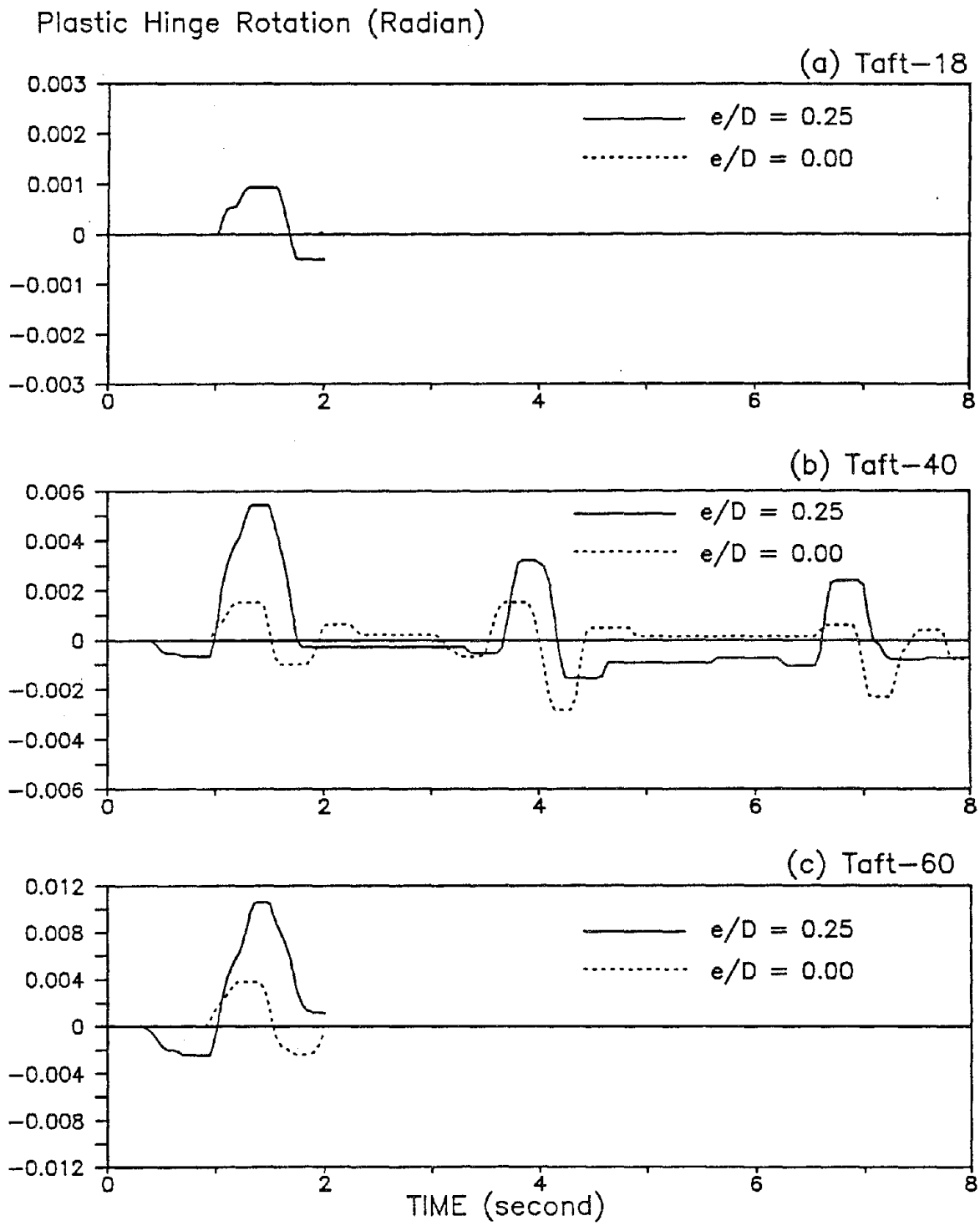

Figure 5.57: TIME-HISTORY OF PLASTIC ROTATION AT THE BASE OF WALL G (0% VERSUS 25% STATIC ECCENTRICITY)

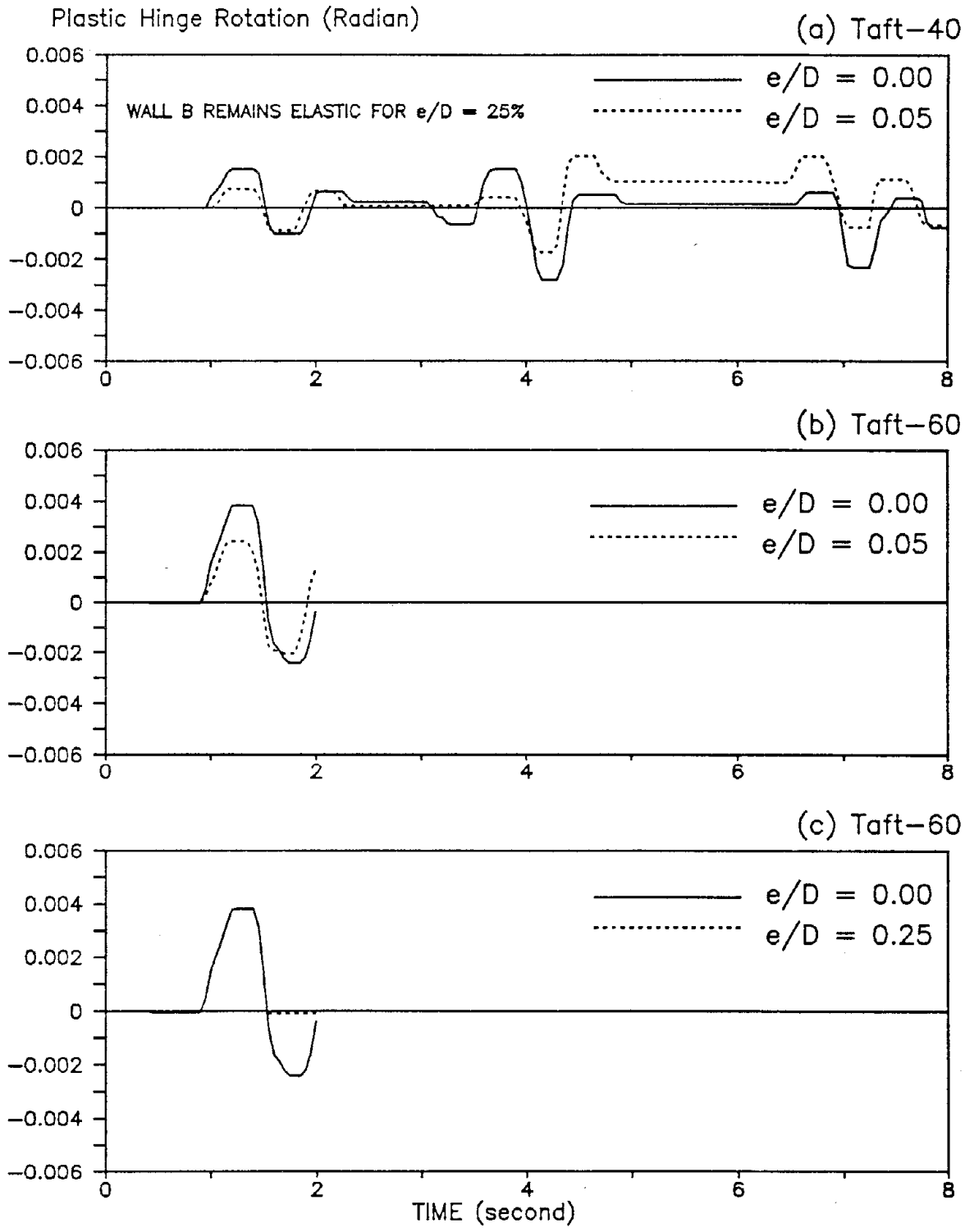

Figure 5.58: TIME-HISTORY OF PLASTIC ROTATION AT THE BASE OF WALL B

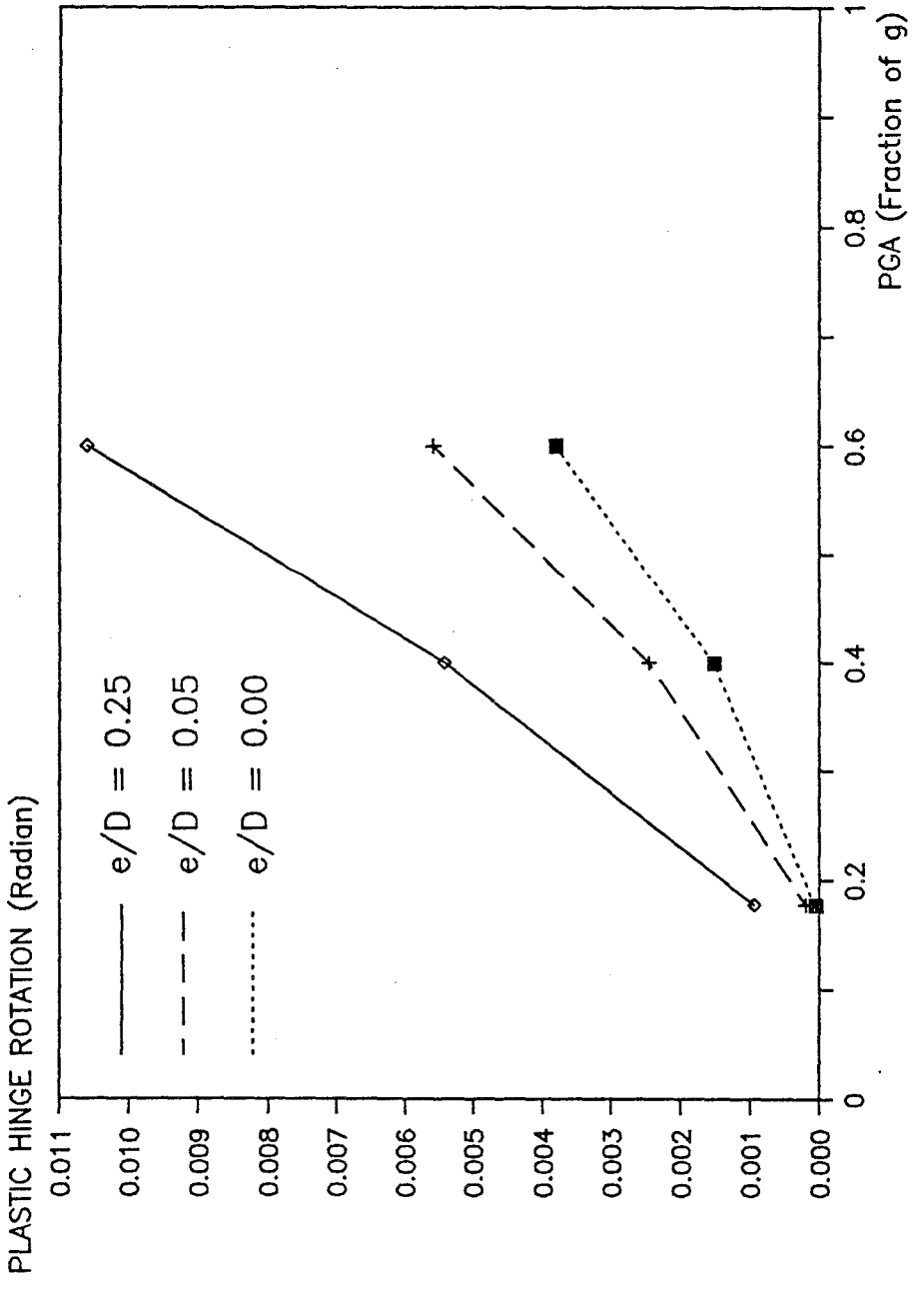

Figure 5.59: MAXIMUM PLASTIC HINGE ROTATIONS AT THE BASE OF WALL G VERSUS PEAK GROUND ACCELERATION

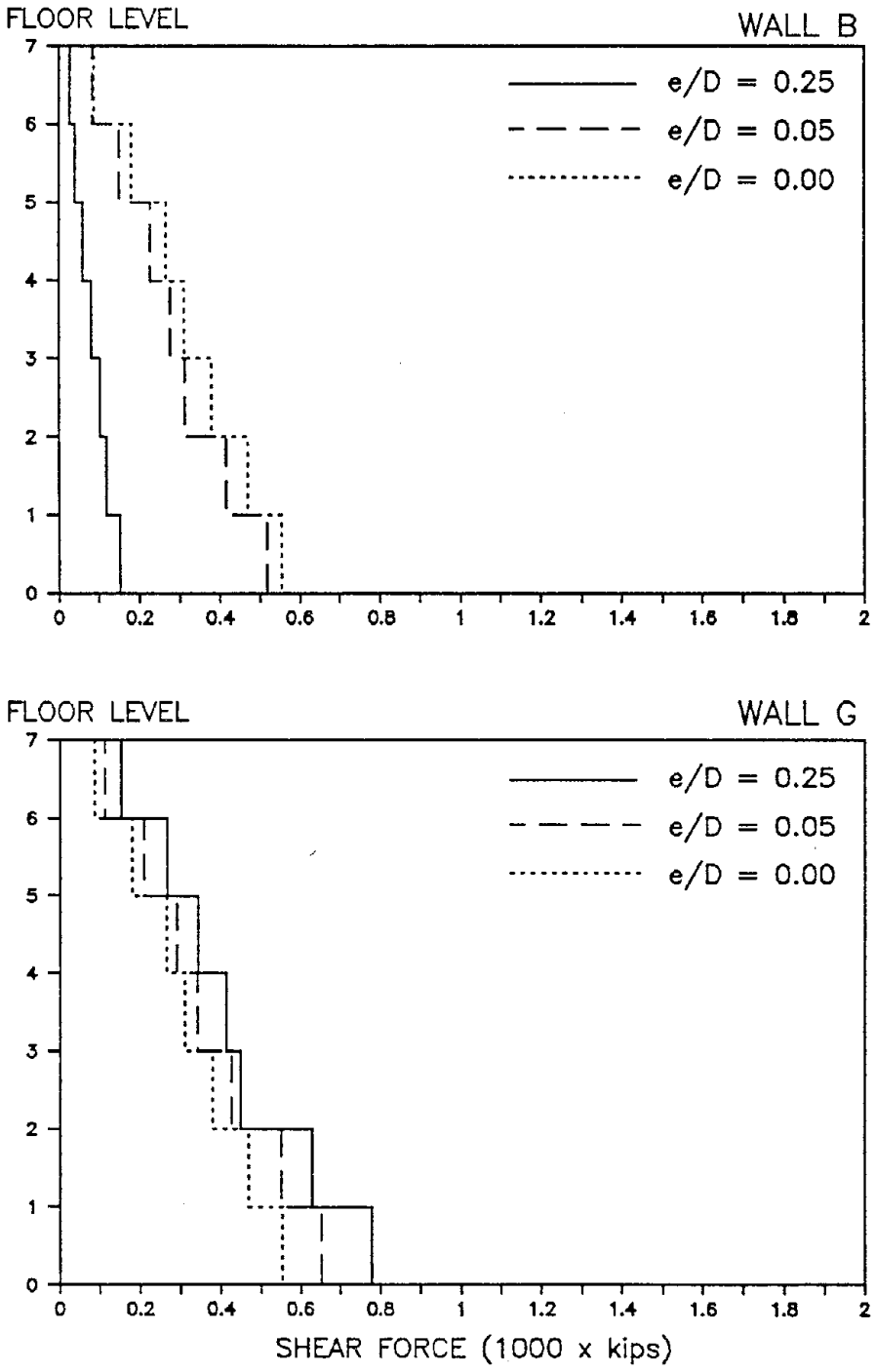

Figure 5.60: SHEAR PROFILE ENVELOPES OF WALLS (TAFT-18 , 0-2 SECONDS)

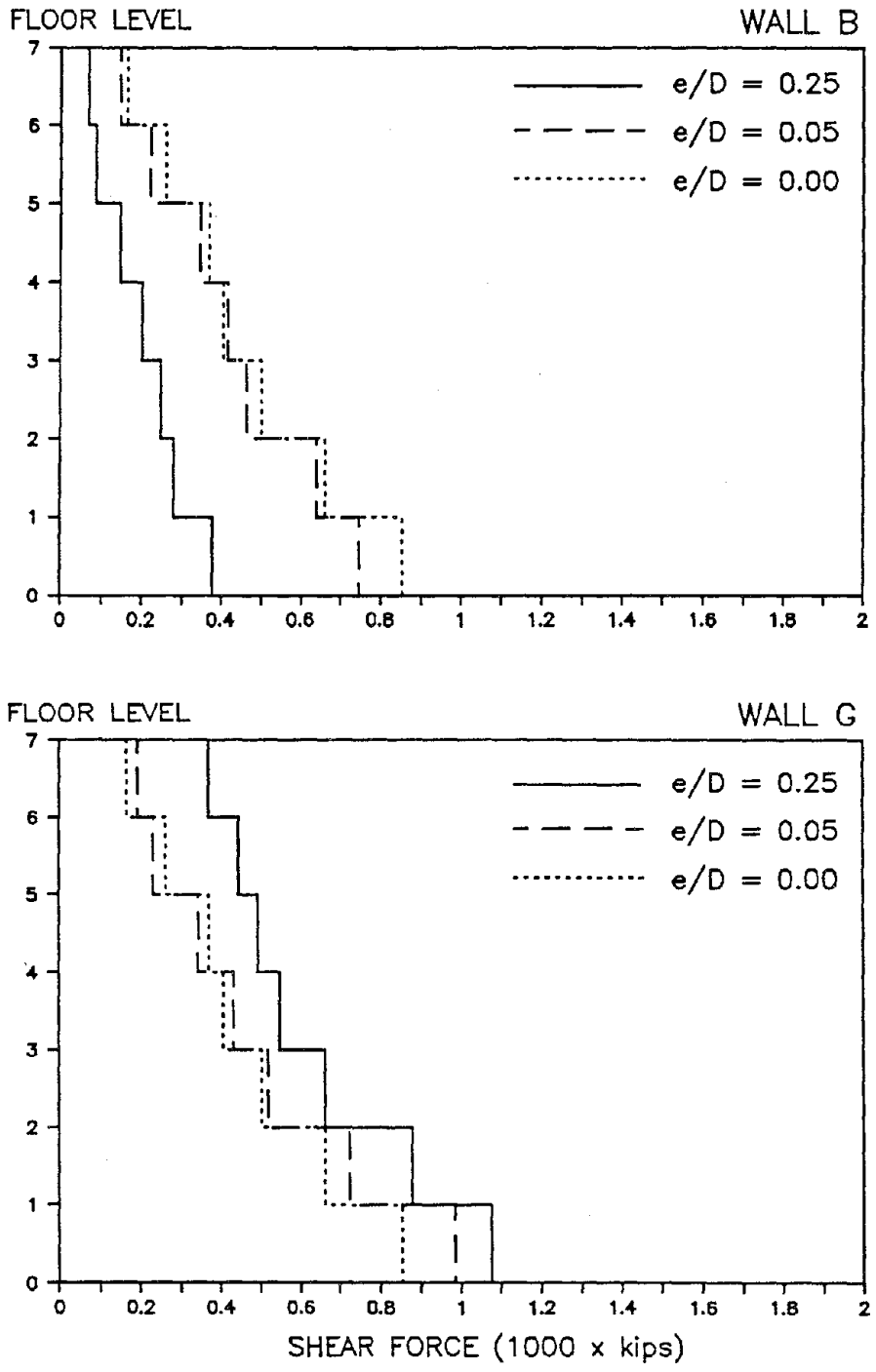

Figure 5.61: SHEAR PROFILE ENVELOPES OF WALLS (TAFT-40 , 0-2 SECONDS)

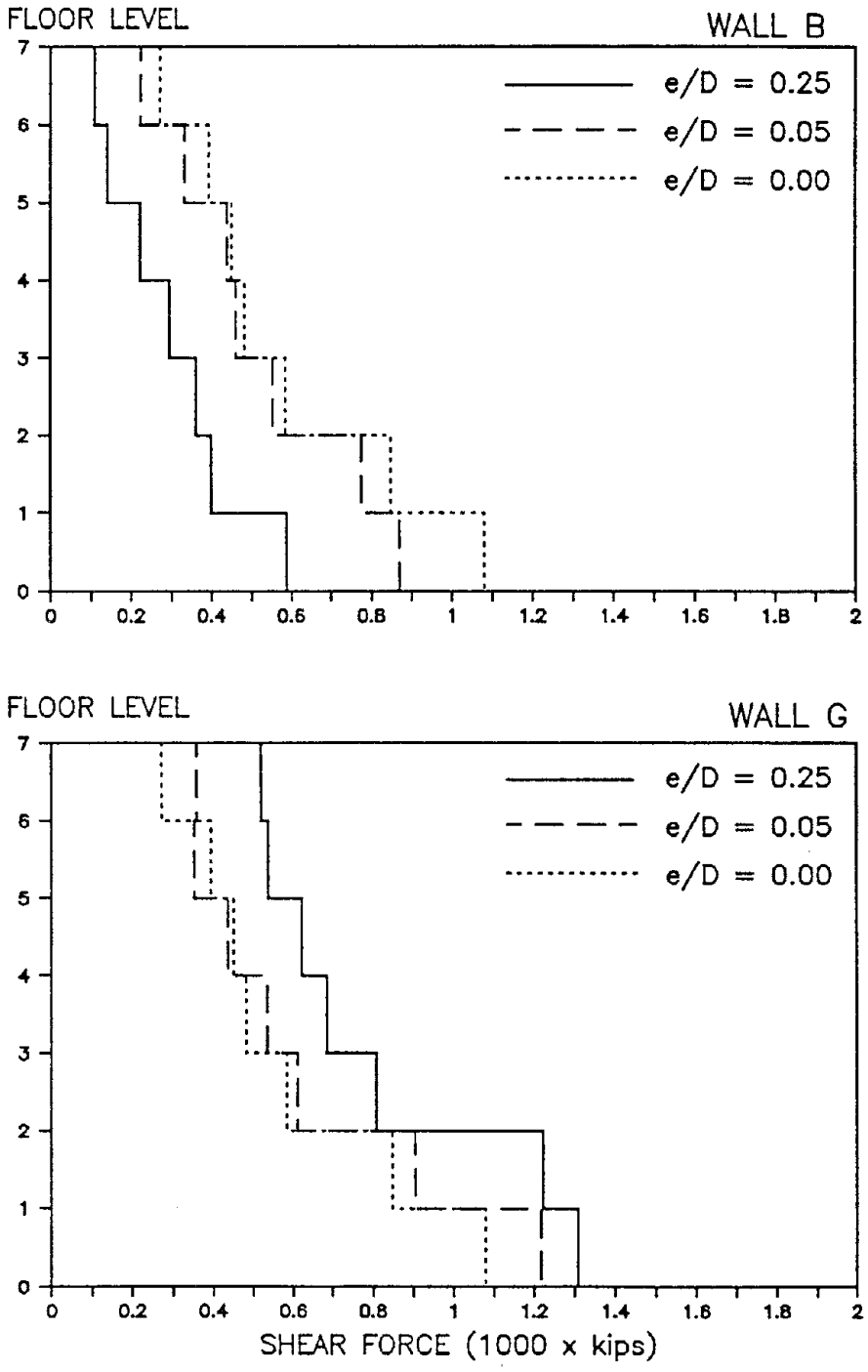

Figure 5.62: SHEAR PROFILE ENVELOPES OF WALLS (TAFT-60 , 0-2 SECONDS)

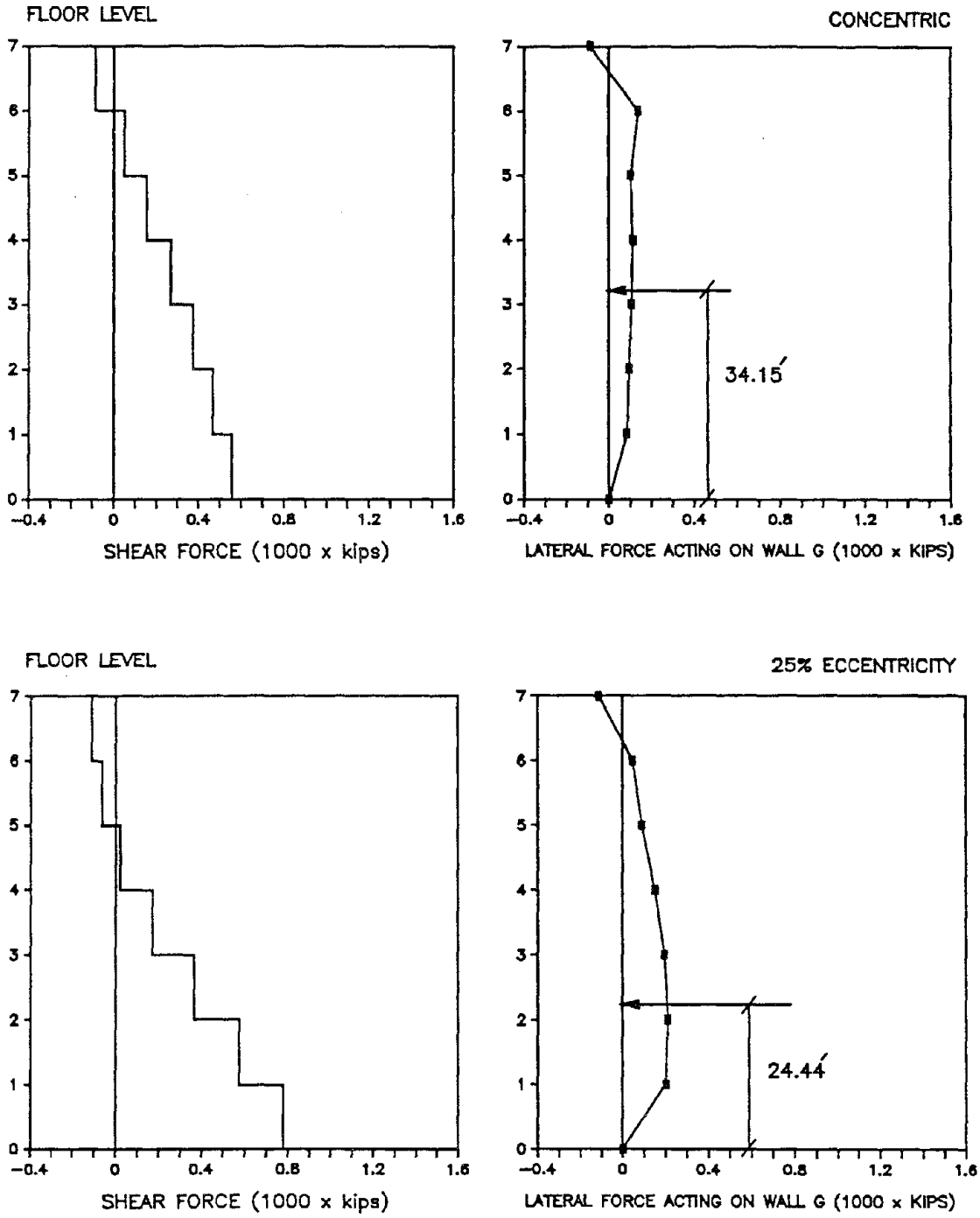

Figure 5.63: SHEAR FORCE AND LATERAL FORCE DISTRIBUTION PROFILES OF WALL G AT THE TIME OF MAXIMUM WALL G BASE SHEAR (TAFT-18, 0-2 SECONDS)

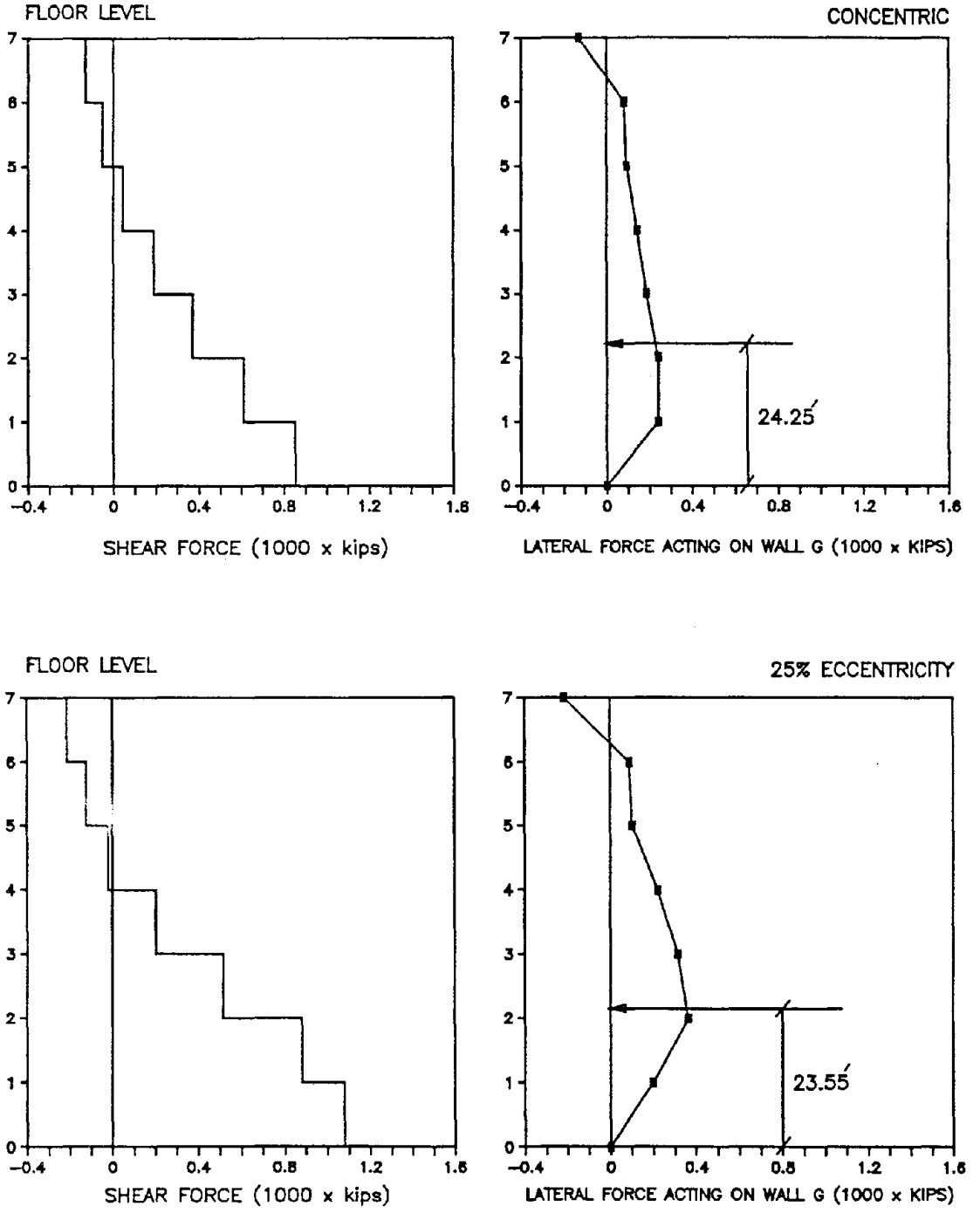

Figure 5.64: SHEAR FORCE AND LATERAL FORCE DISTRIBUTION PROFILES OF WALL G AT THE TIME OF MAXIMUM WALL G BASE SHEAR (TAFT-40, 0-2 SECONDS)

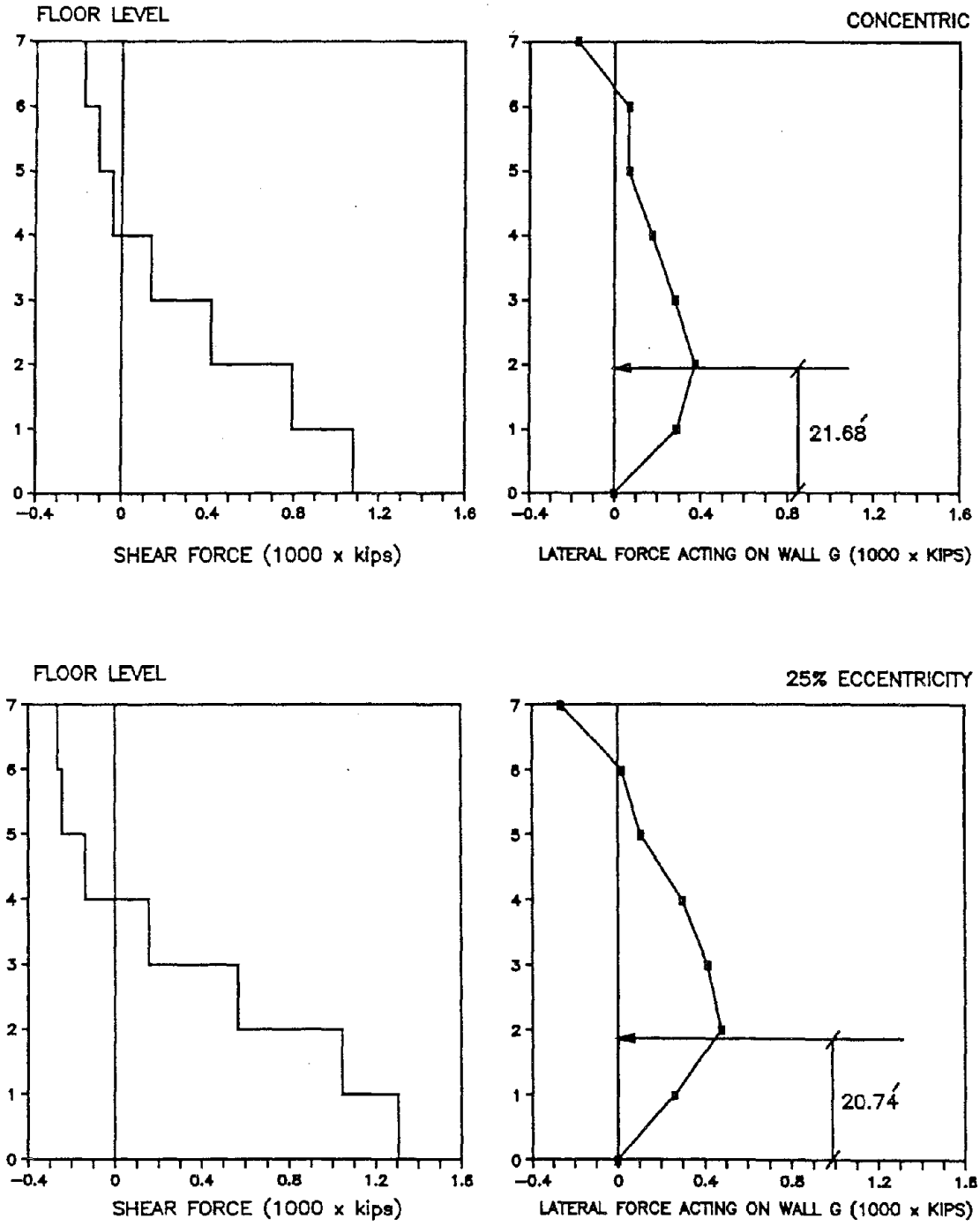

Figure 5.65: SHEAR FORCE AND LATERAL FORCE DISTRIBUTION PROFILES OF WALL G AT THE TIME OF MAXIMUM WALL G BASE SHEAR (TAFT-60, 0-2 SECONDS)

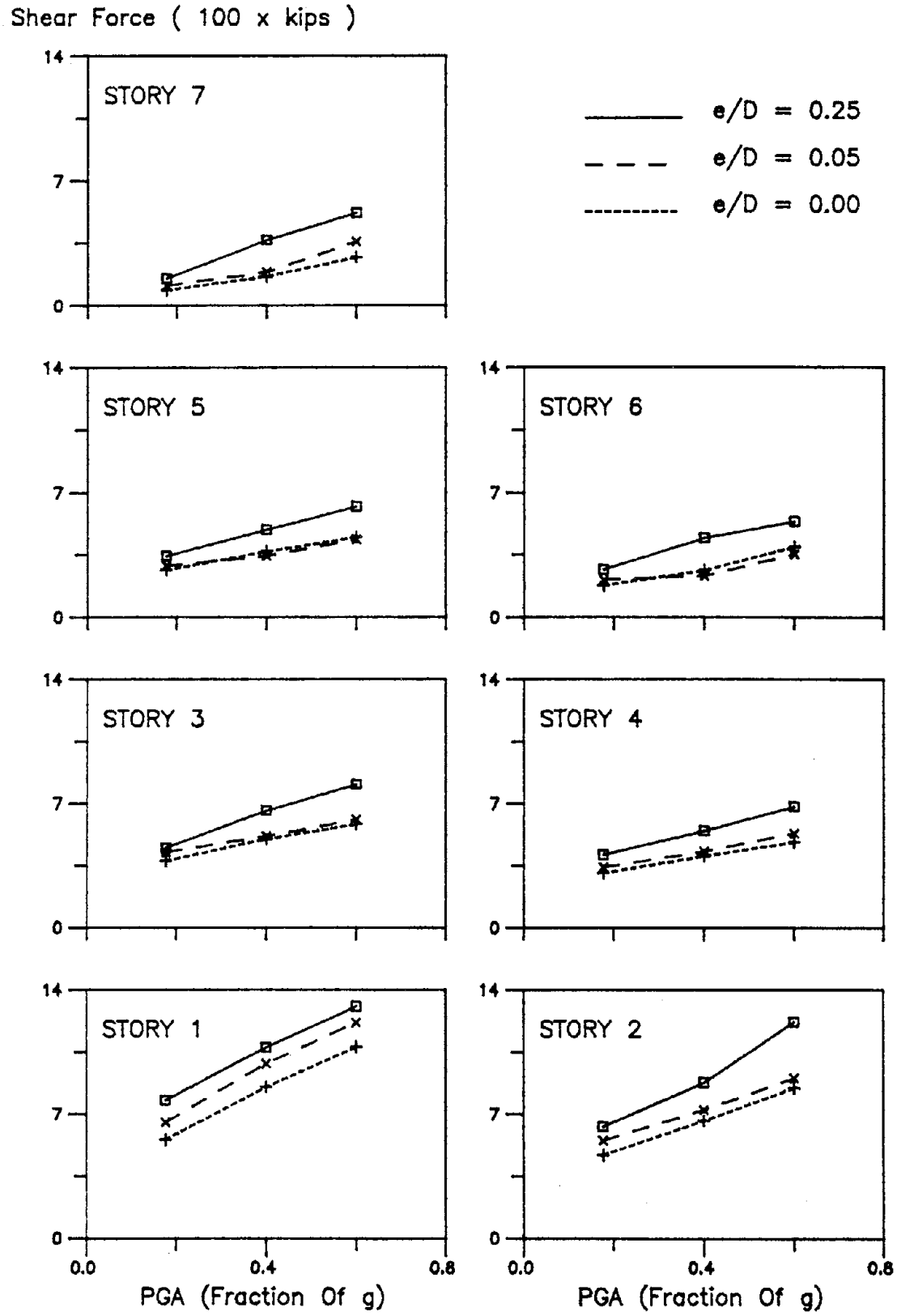

Figure 5.66: MAXIMUM SHEAR OF WALL G VERSUS PEAK GROUND ACCELERATION

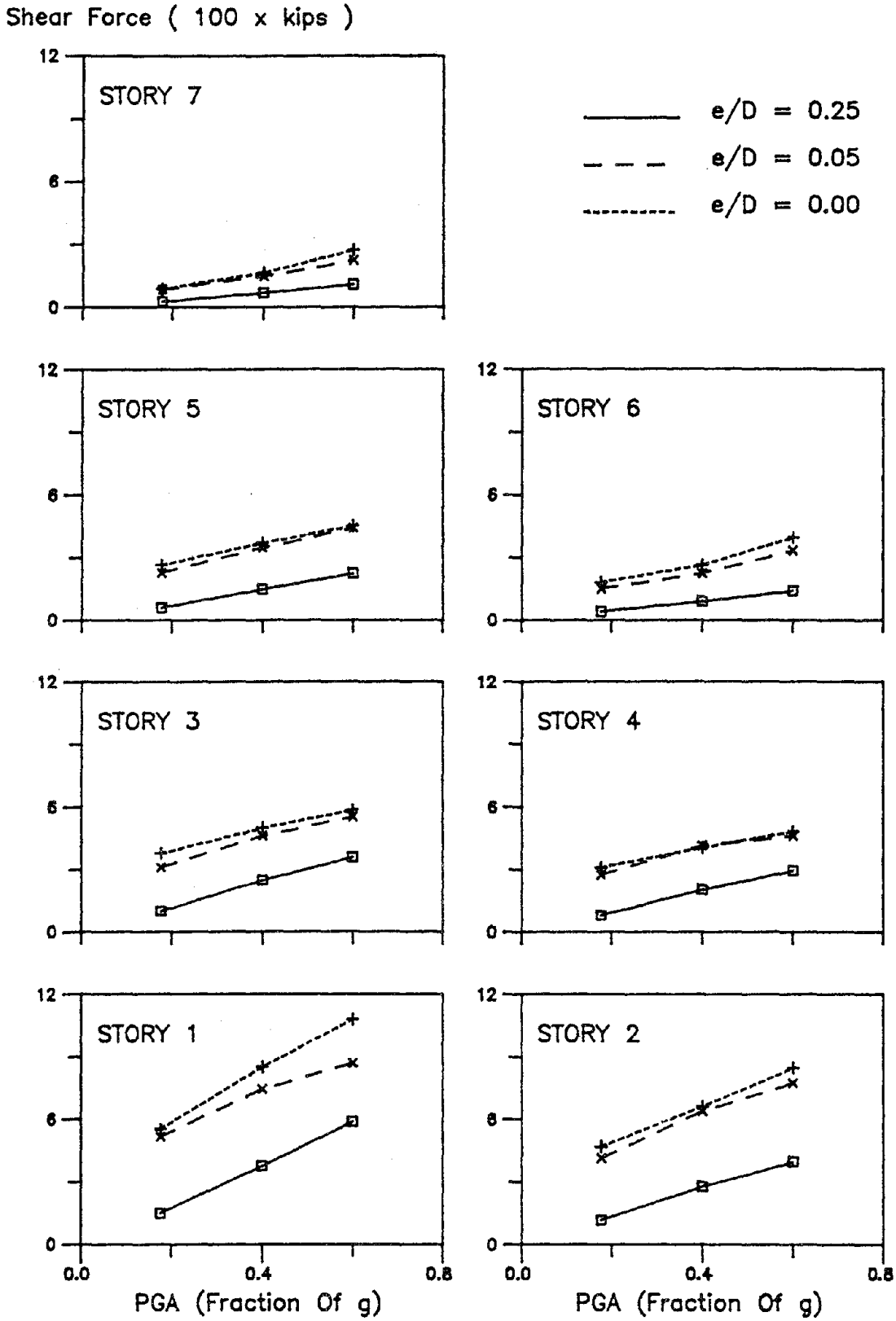

Figure 5.67: MAXIMUM SHEAR OF WALL B VERSUS PEAK GROUND ACCELERATION

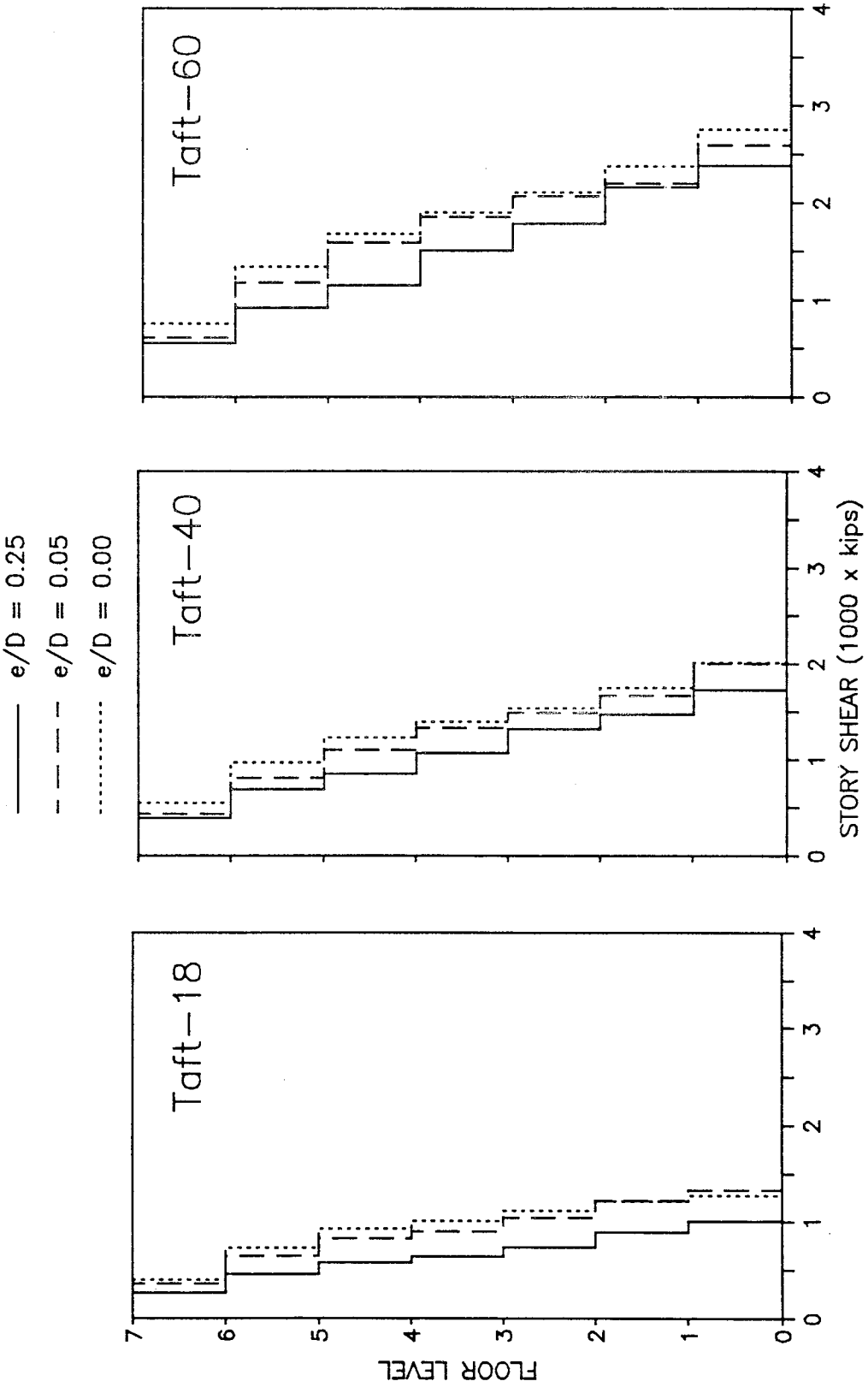

Figure 5.68: TOTAL STORY SHEAR PROFILE ENVELOPES

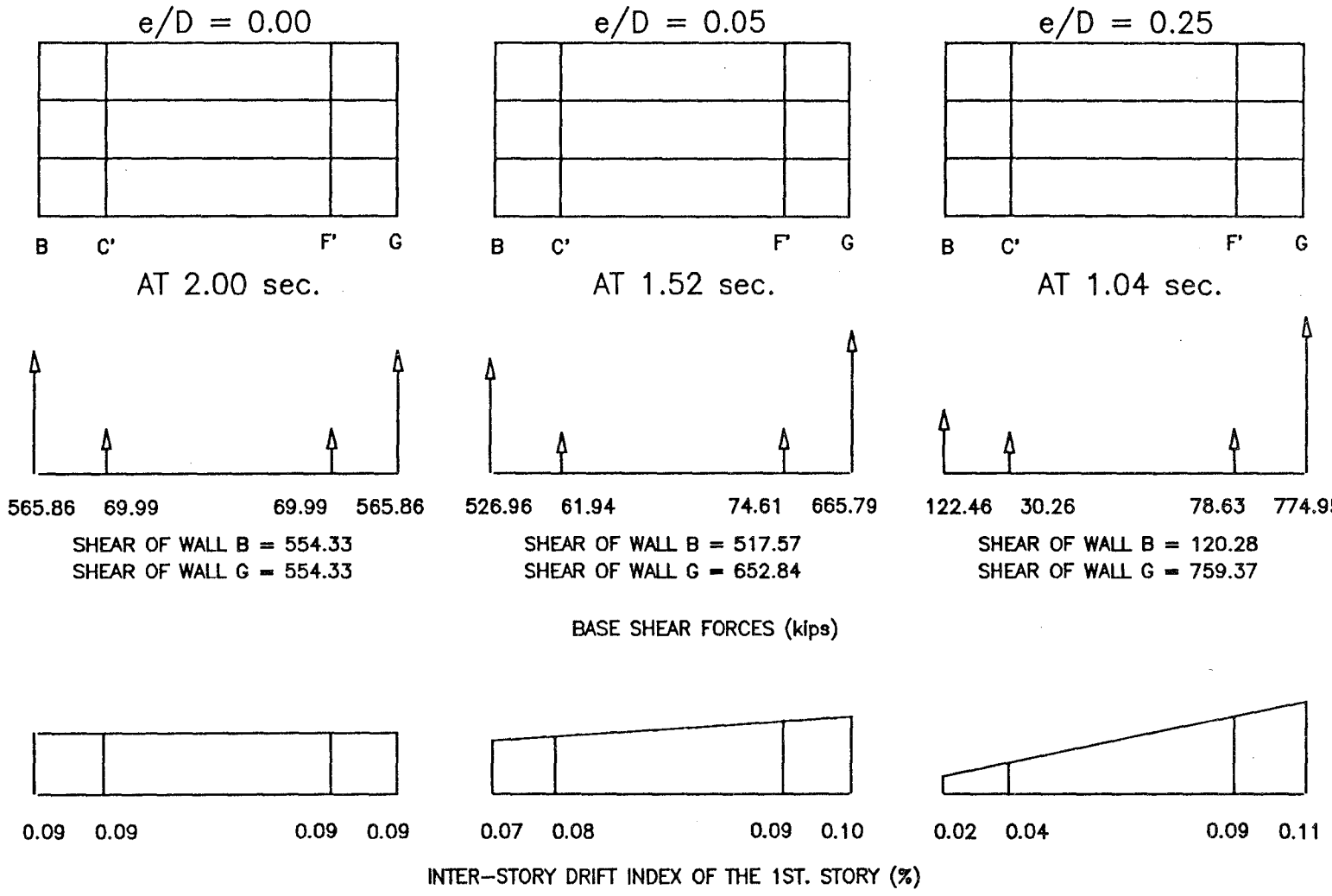

Figure 5.69: BASE SHEAR AND INTER-STORY DRIFT INDEX AT TIME OF MAXIMUM TOTAL BASE SHEAR (TAFT-18)

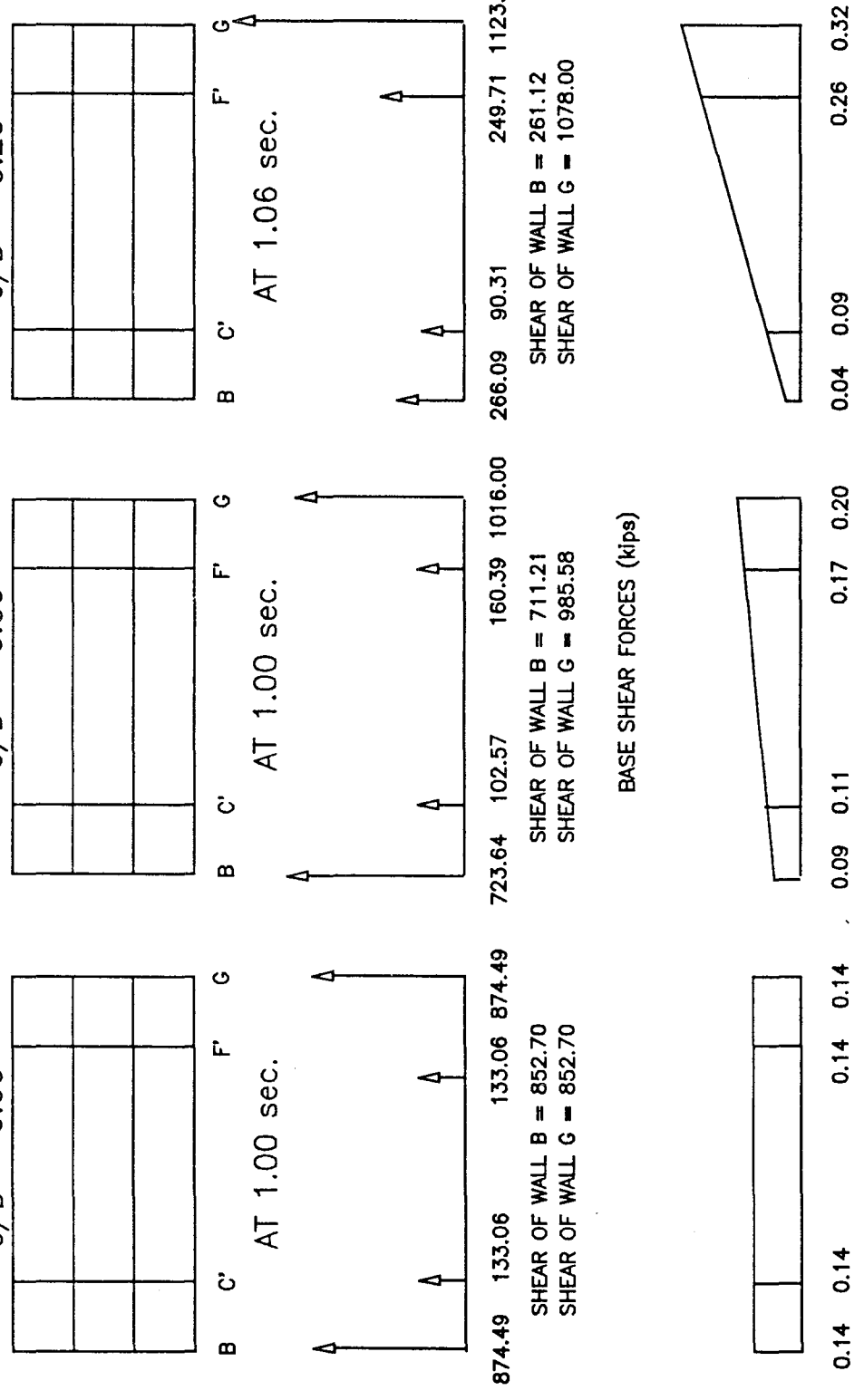

Figure 5.70: BASE SHEAR AND INTER-STORY DRIFT INDEX AT TIME OF MAXIMUM TOTAL BASE SHEAR (TAFT-40)

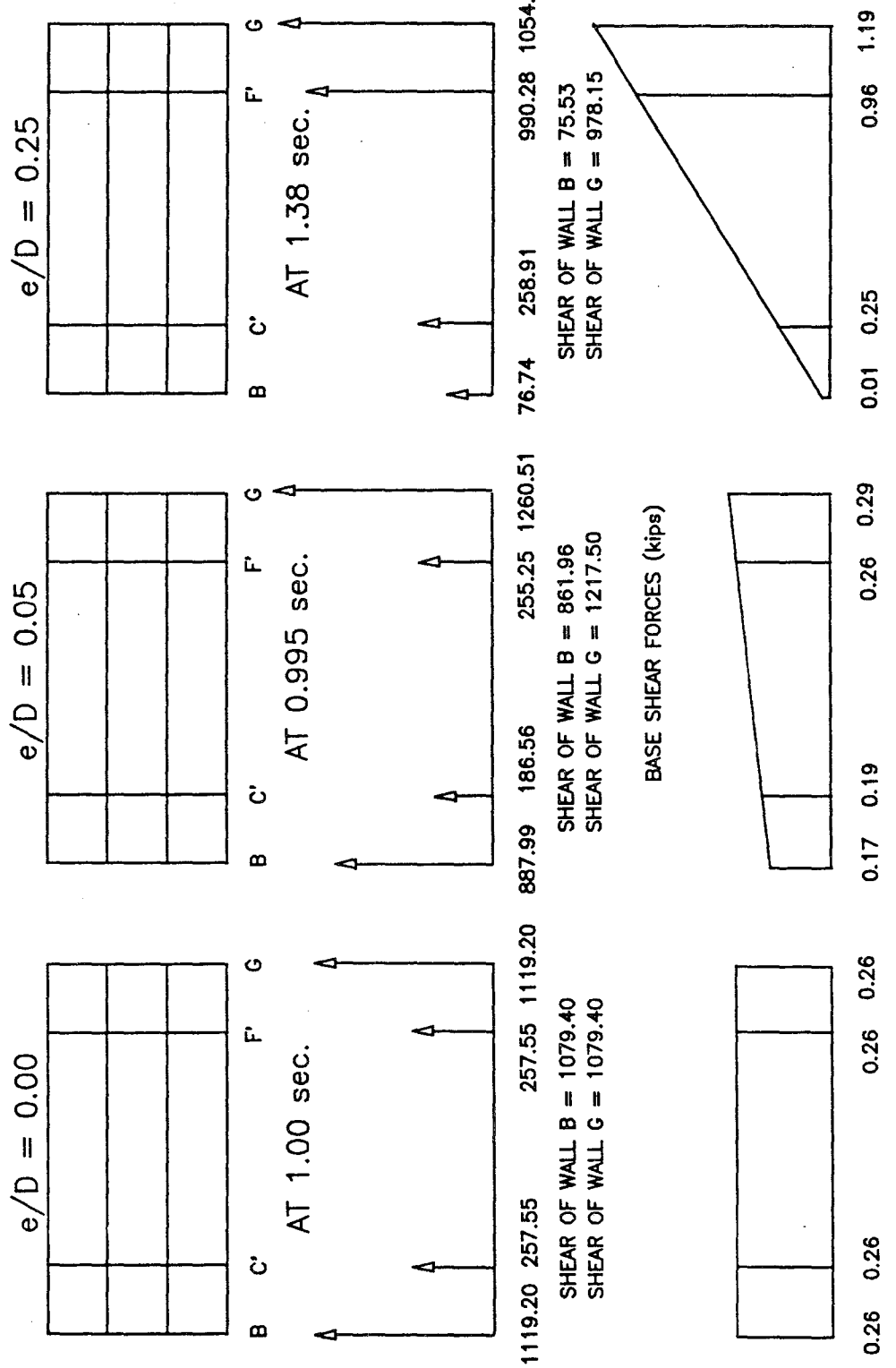

Figure 5.71: BASE SHEAR AND INTER-STORY DRIFT INDEX AT TIME OF MAXIMUM TOTAL BASE SHEAR (TAFT-60)

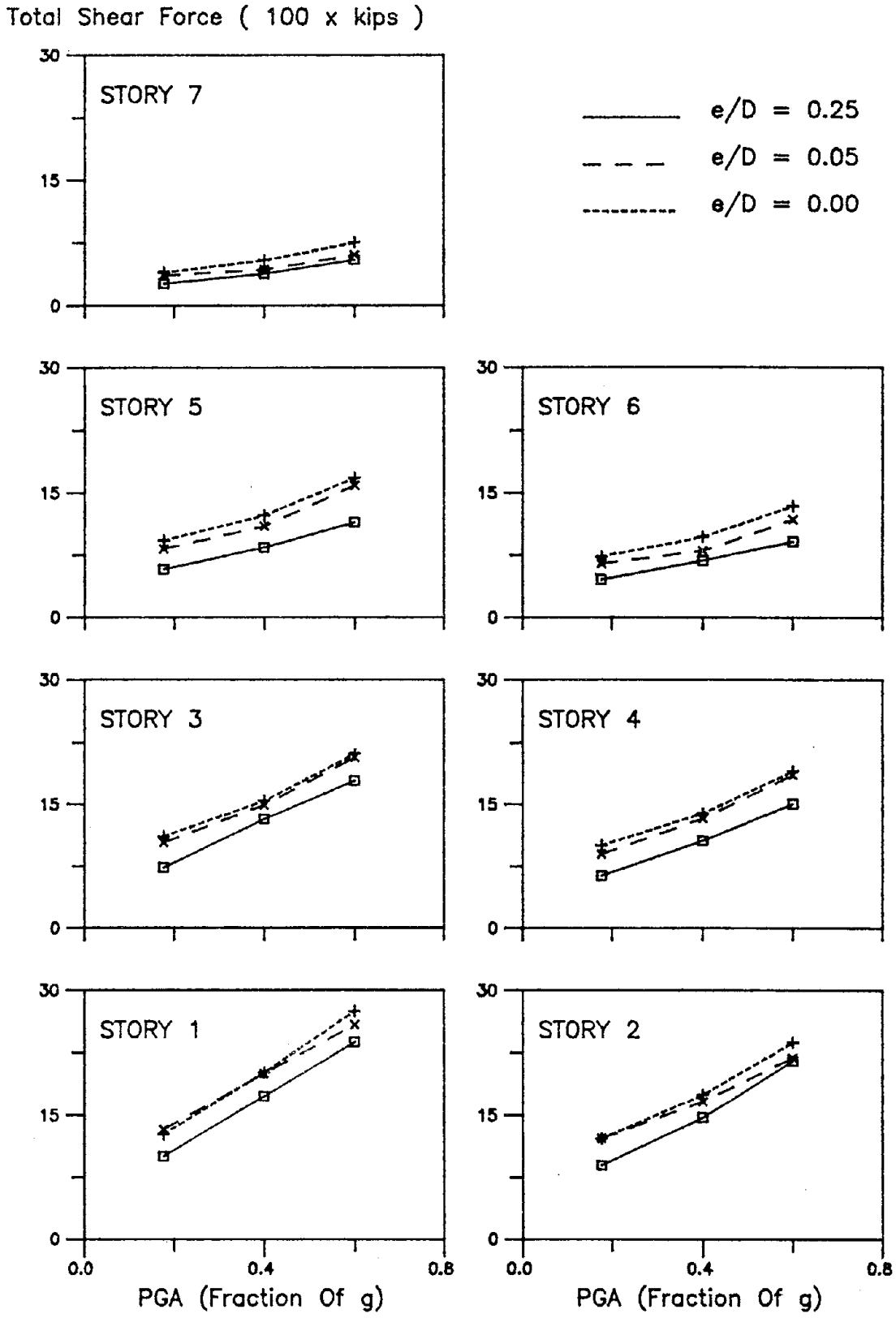

Figure 5.72: MAXIMUM TOTAL STORY SHEAR VERSUS PEAK GROUND ACCELERATION

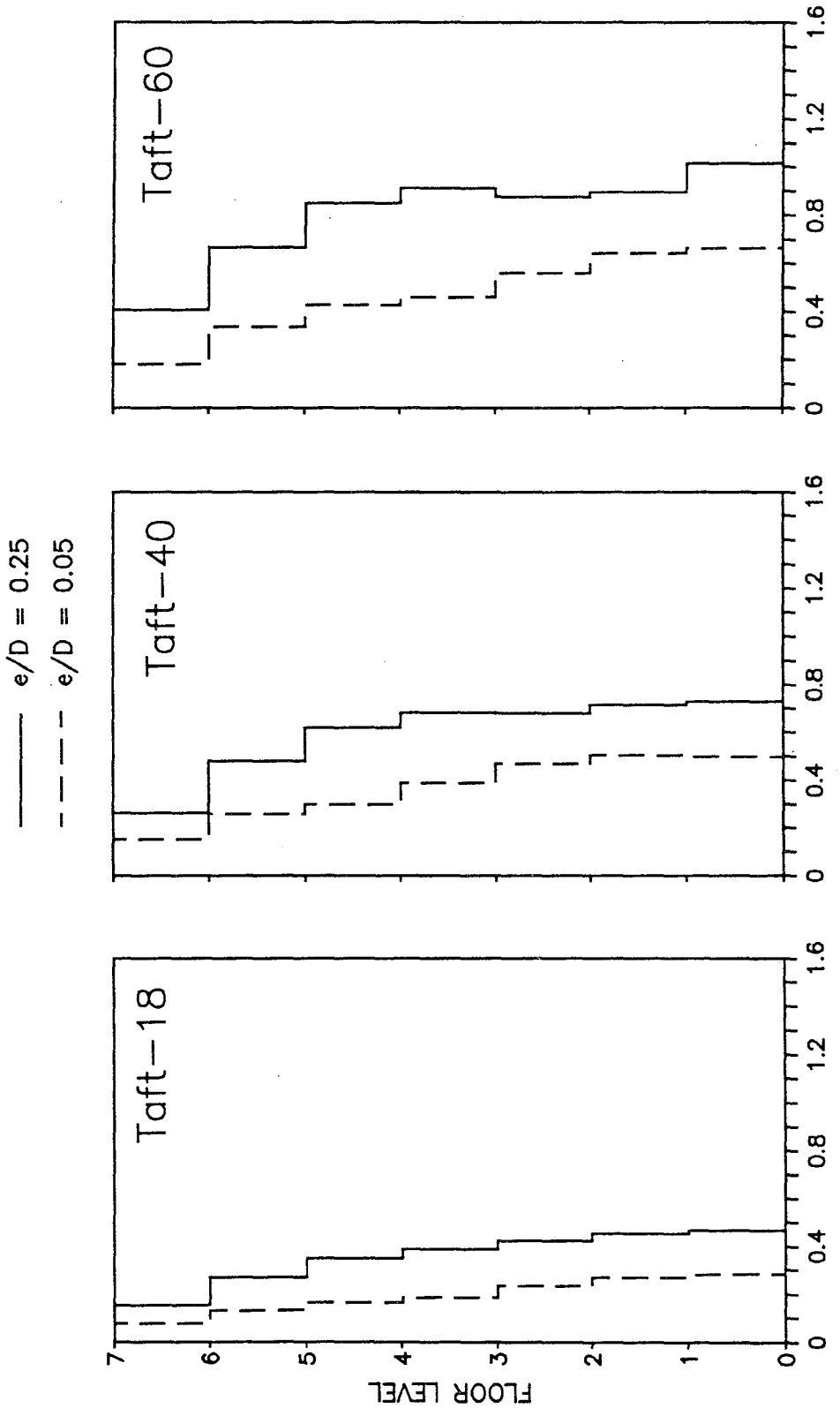

Figure 5.73: STORY TORQUE PROFILE ENVELOPES

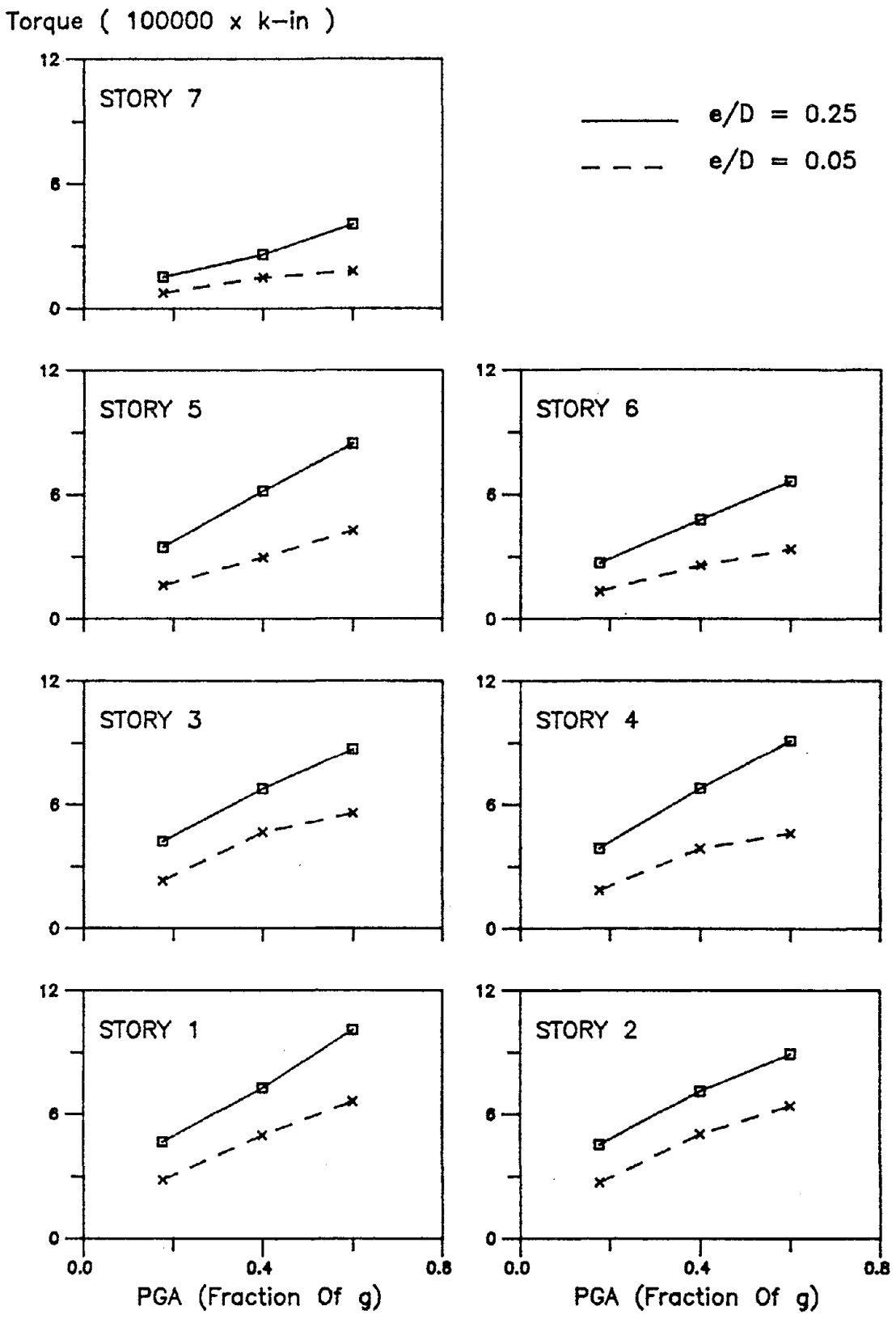

Figure 5.74: MAXIMUM STORY TORQUE VERSUS PEAK GROUND ACCELERATION

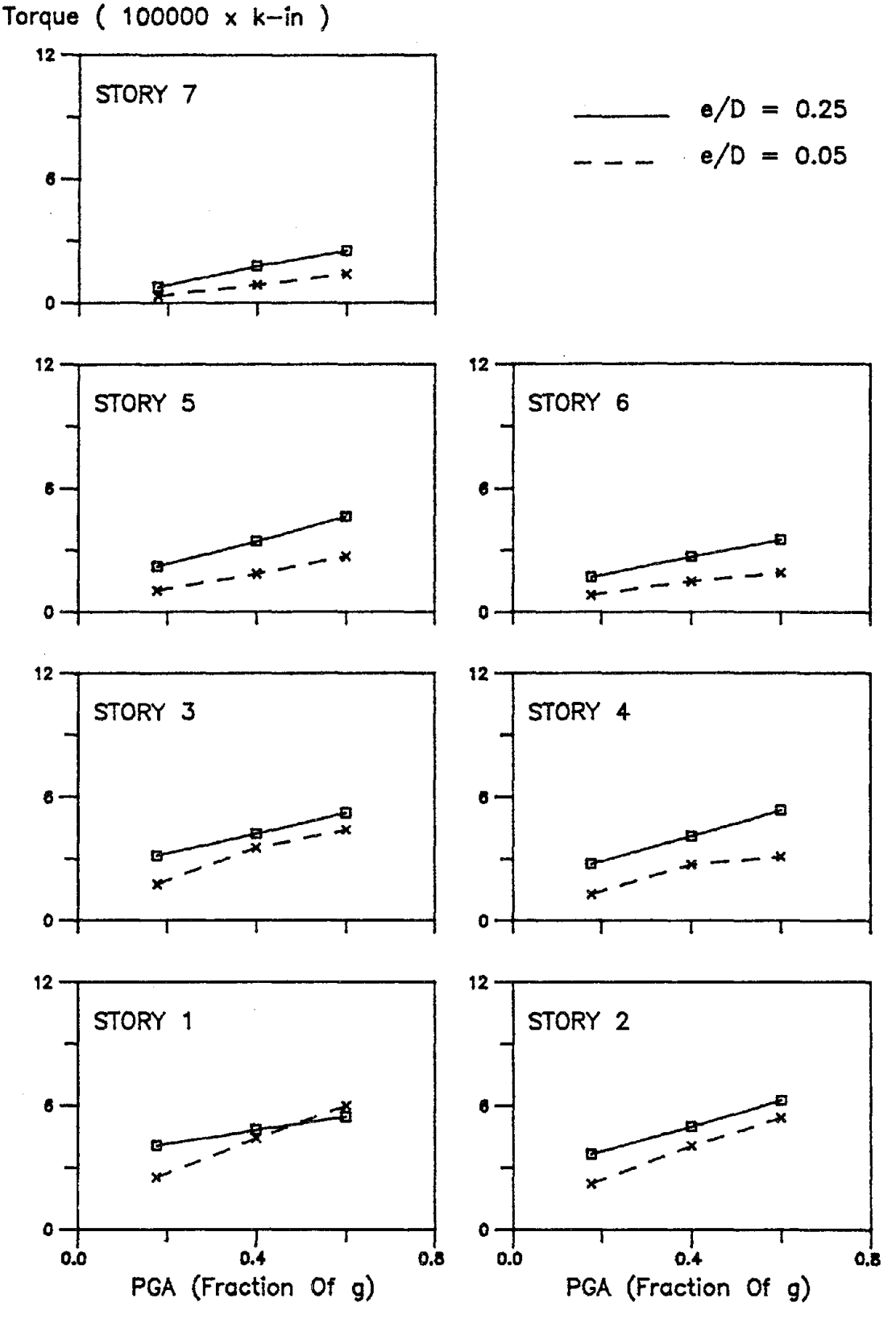

Figure 5.75: MAXIMUM STORY TORQUE RESISTED BY WALLS VERSUS PEAK GROUND ACCELERATION

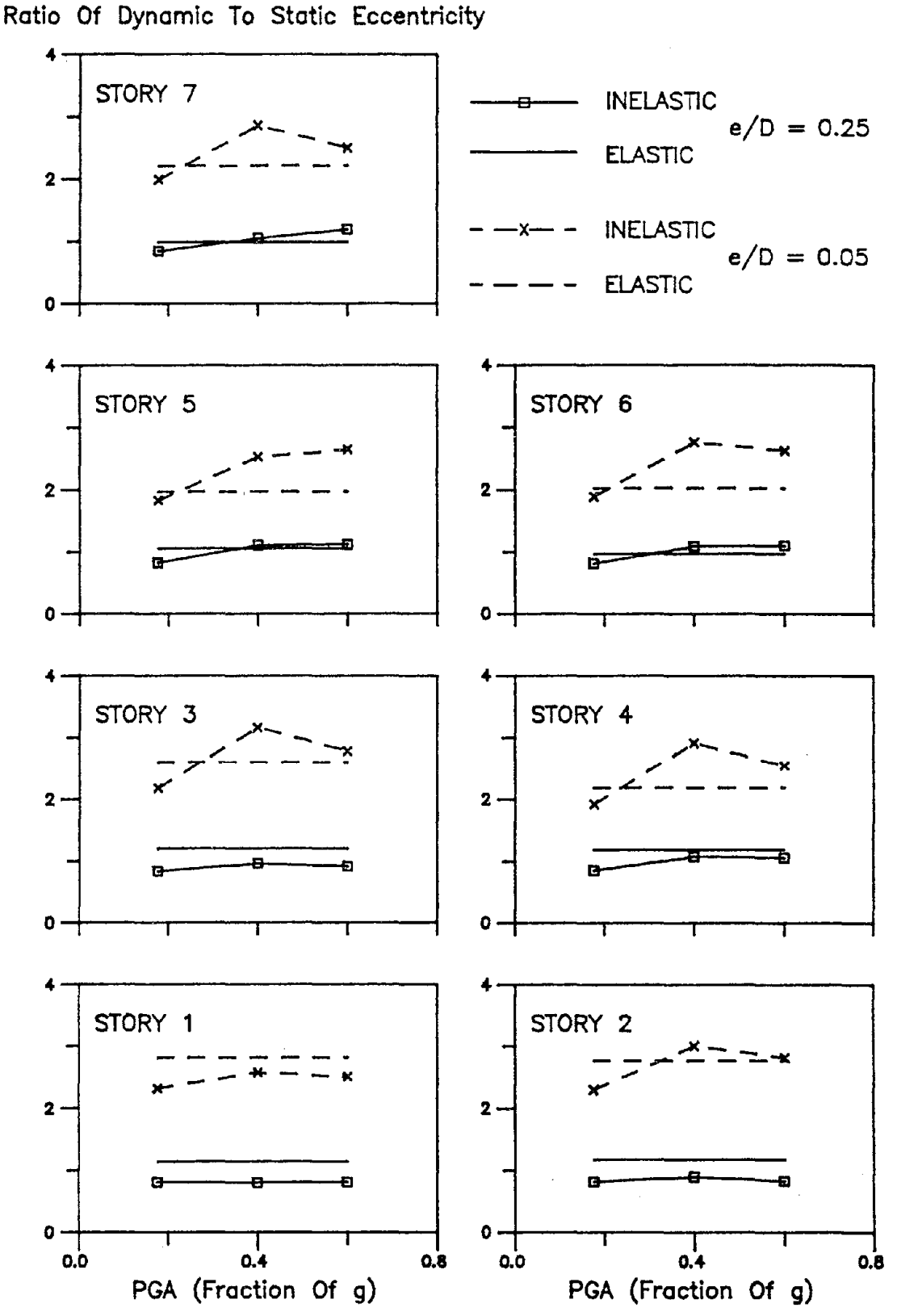

Figure 5.76: ECCENTRICITY AMPLIFICATION VERSUS PEAK GROUND ACCELERATION

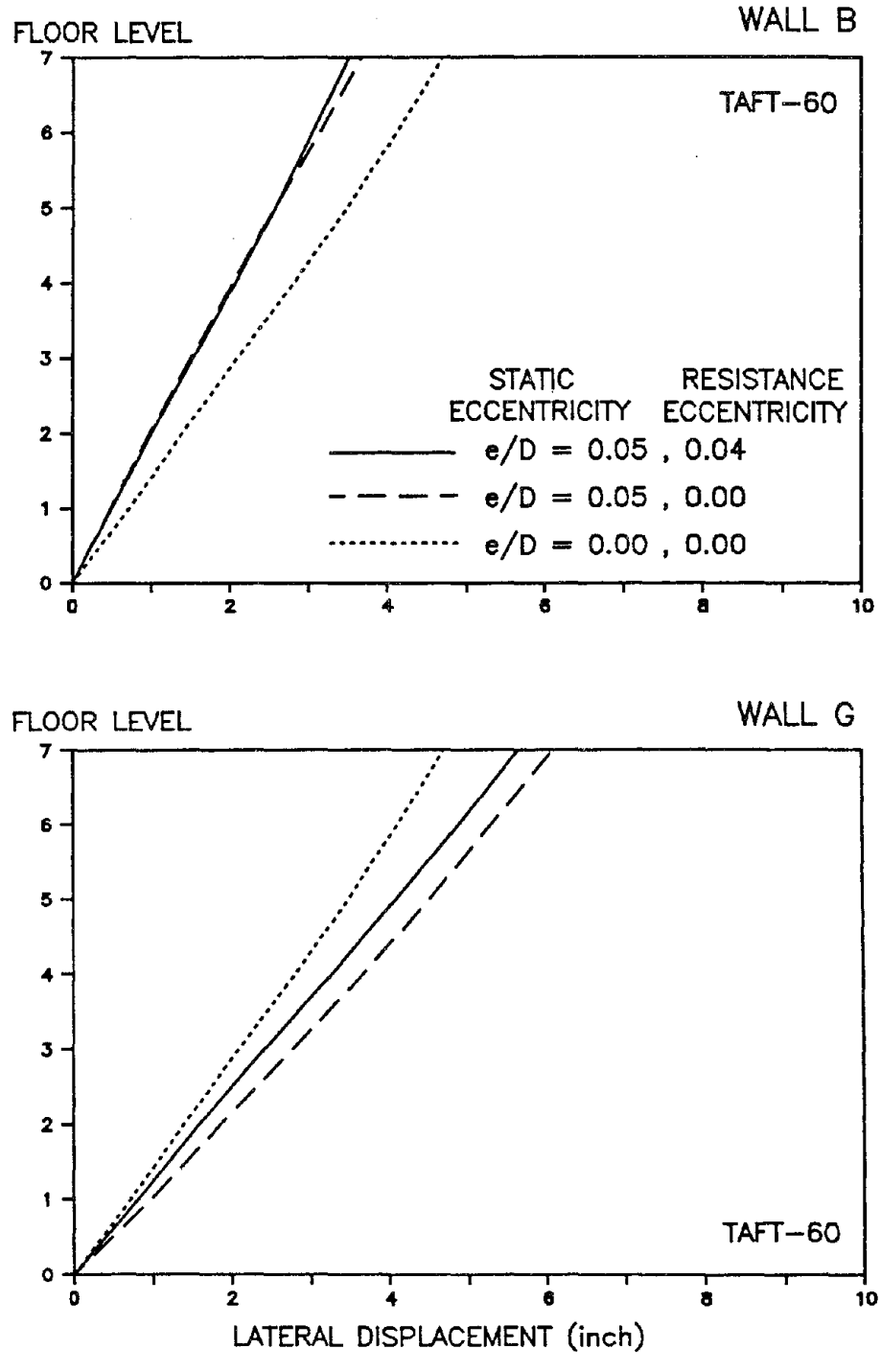

Figure 5.77: DISPLACEMENT ENVELOPES OF WALLS MASS ECCENTRICITY VERSUS RESISTANCE/MASS ECCENTRICITY DUE TO TAFT-60, 0-2 SECONDS

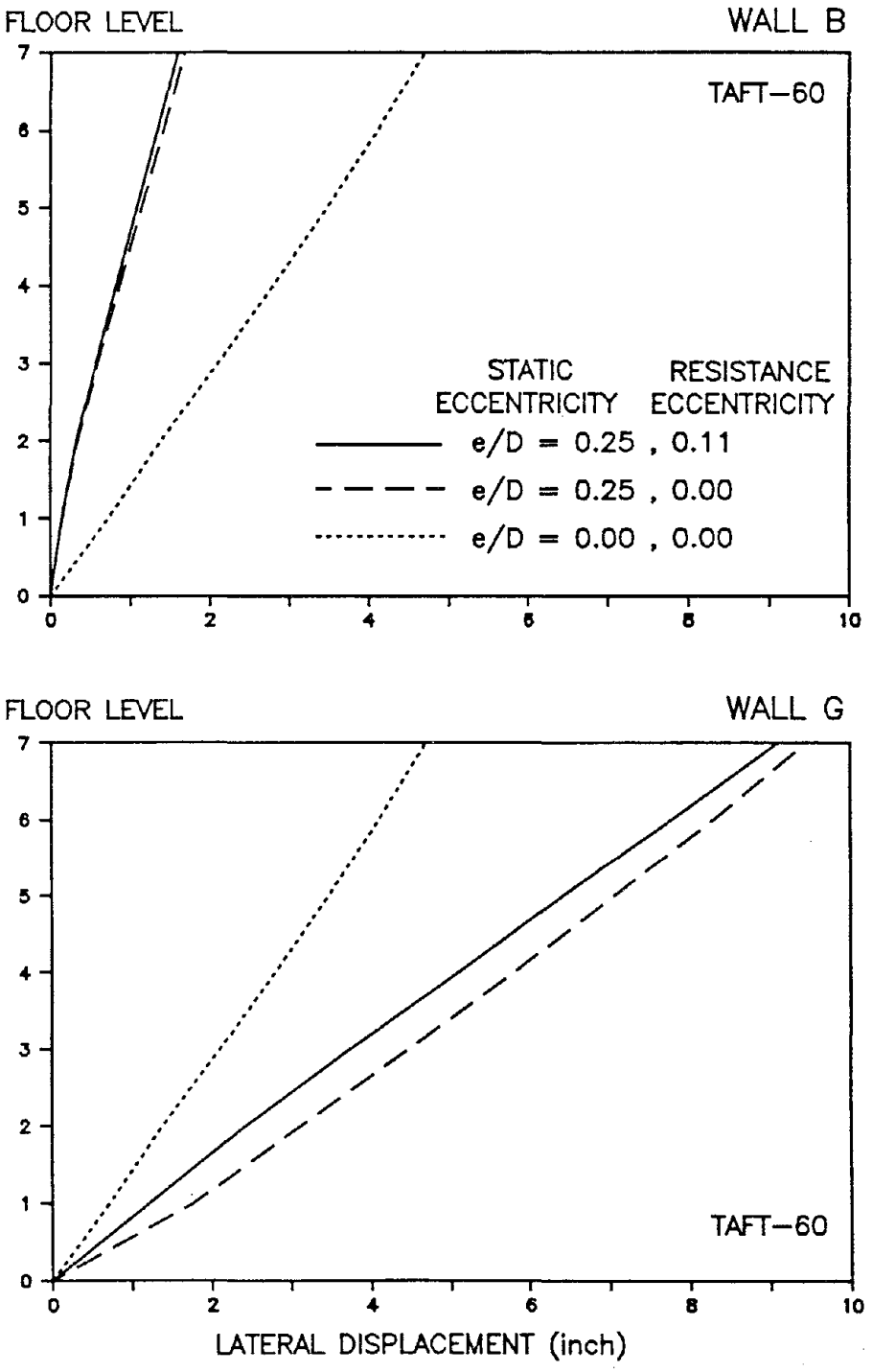

Figure 5.78: DISPLACEMENT ENVELOPES OF WALLS MASS ECCENTRICITY VERSUS RESISTANCE/MASS ECCENTRICITY DUE TO TAFT-60, 0-2 SECONDS

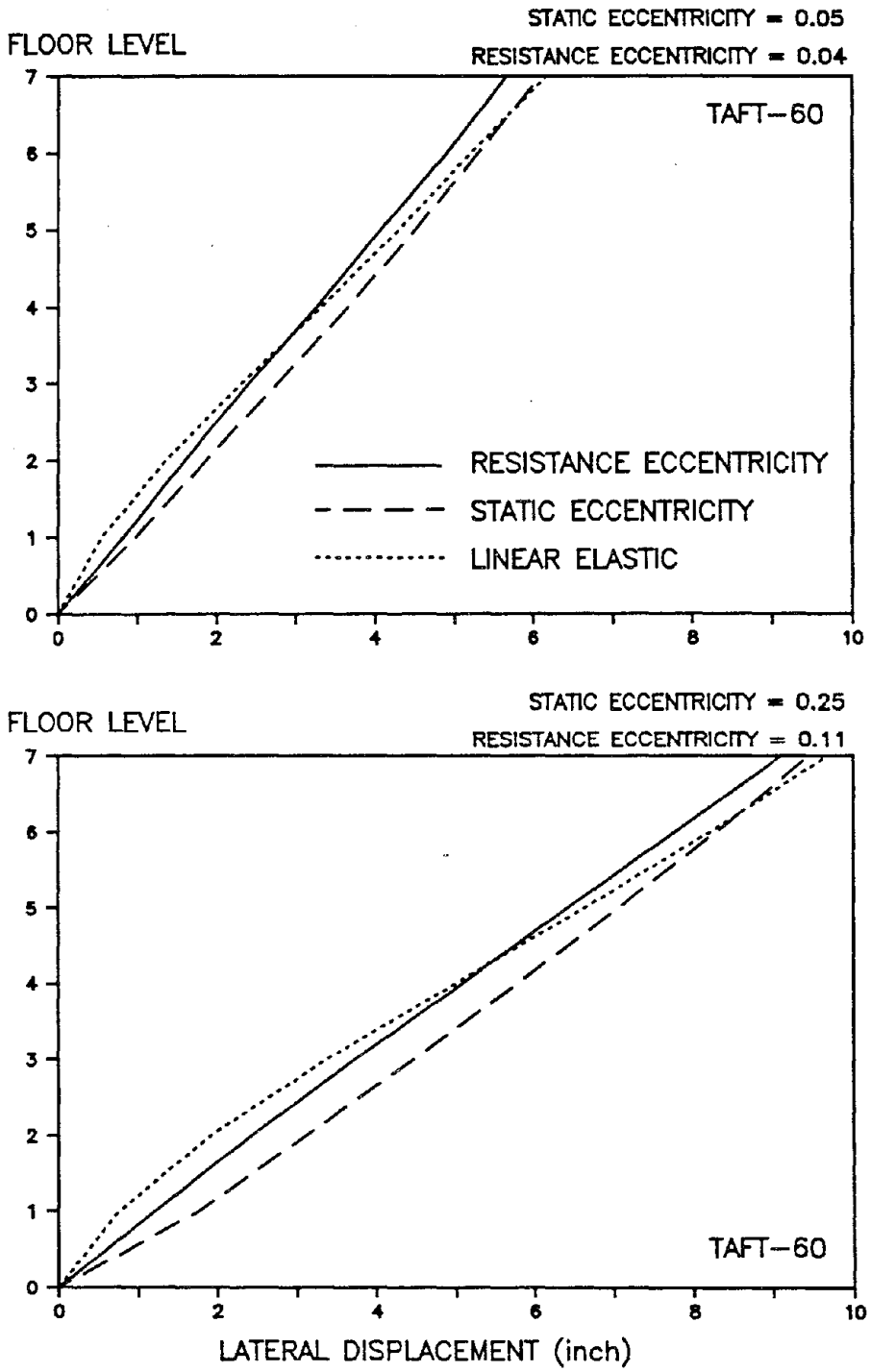

Figure 5.79: DISPLACEMENT ENVELOPES OF WALL G LINEAR-ELASTIC VERSUS NON-LINEAR INELASTIC DUE TO TAFT-60, 0-2 SECONDS

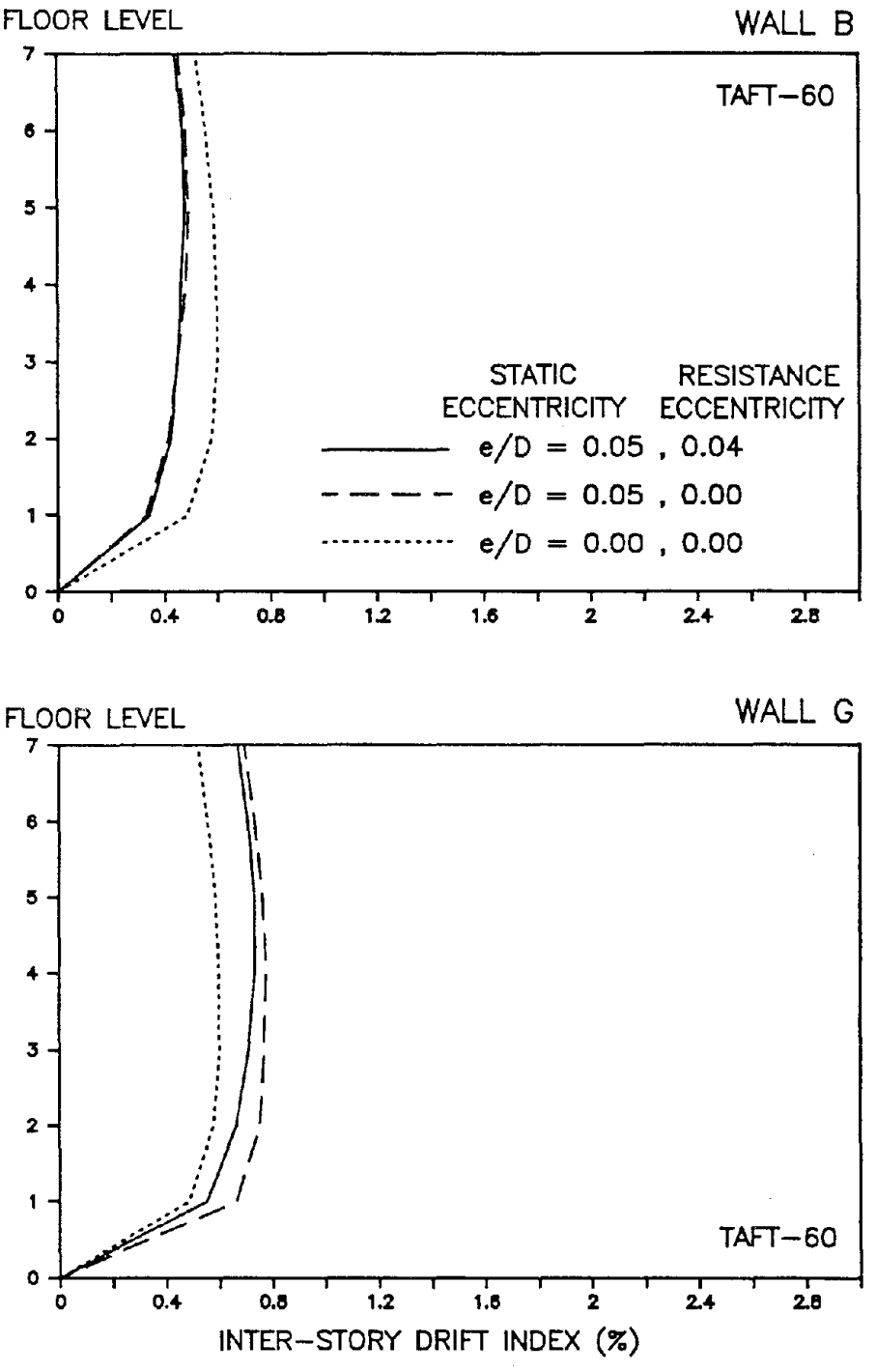

Figure 5.80: INTER-STORY DRIFT INDEX ENVELOPES OF WALLS MASS ECCENTRICITY VERSUS RESISTANCE/MASS ECCENTRICITY DUE TO TAFT-60, 0-2 SECONDS

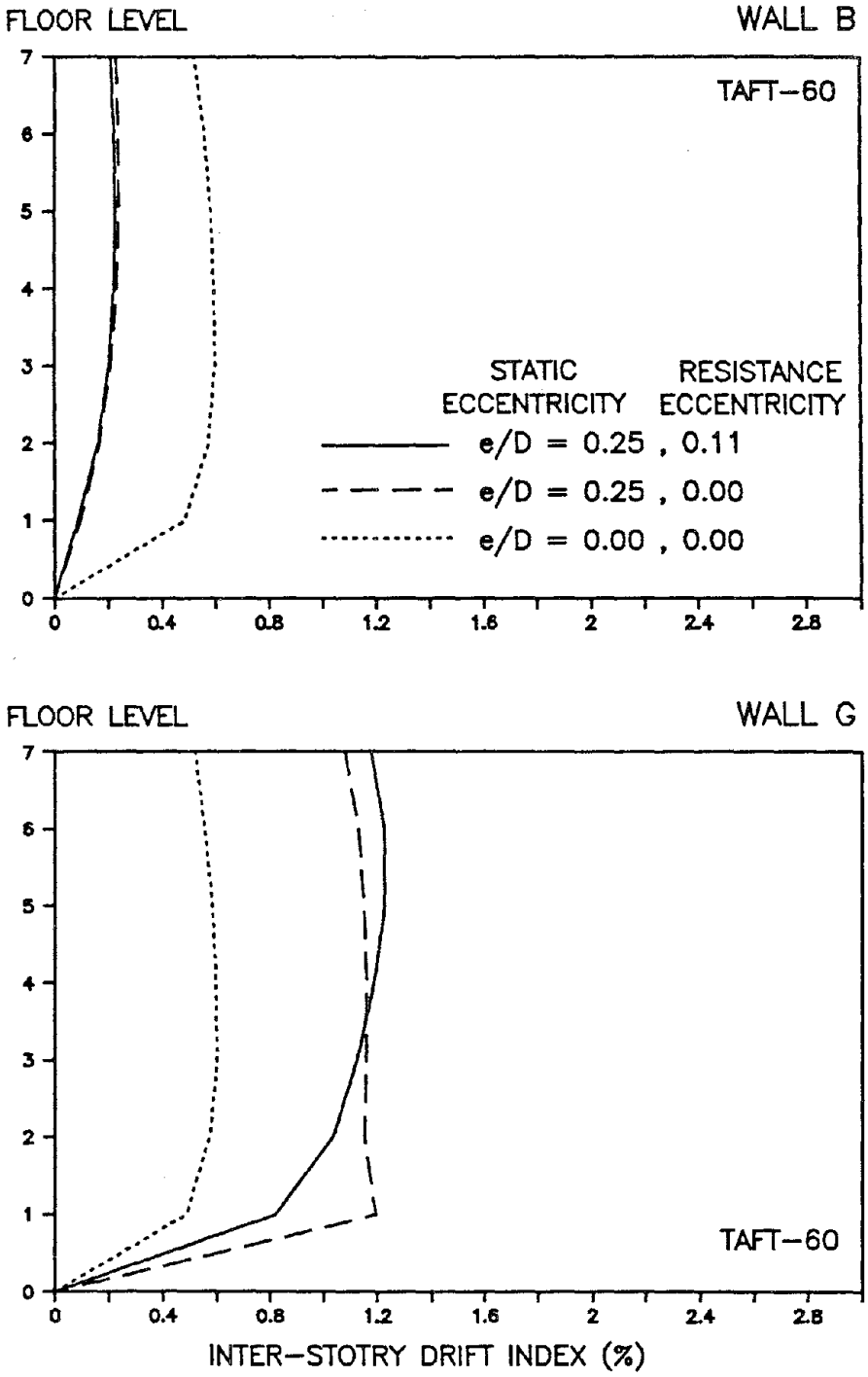

Figure 5.81: INTER-STORY DRIFT INDEX ENVELOPES OF WALLS MASS ECCENTRICITY VERSUS RESISTANCE/MASS ECCENTRICITY DUE TO TAFT-60, 0-2 SECONDS

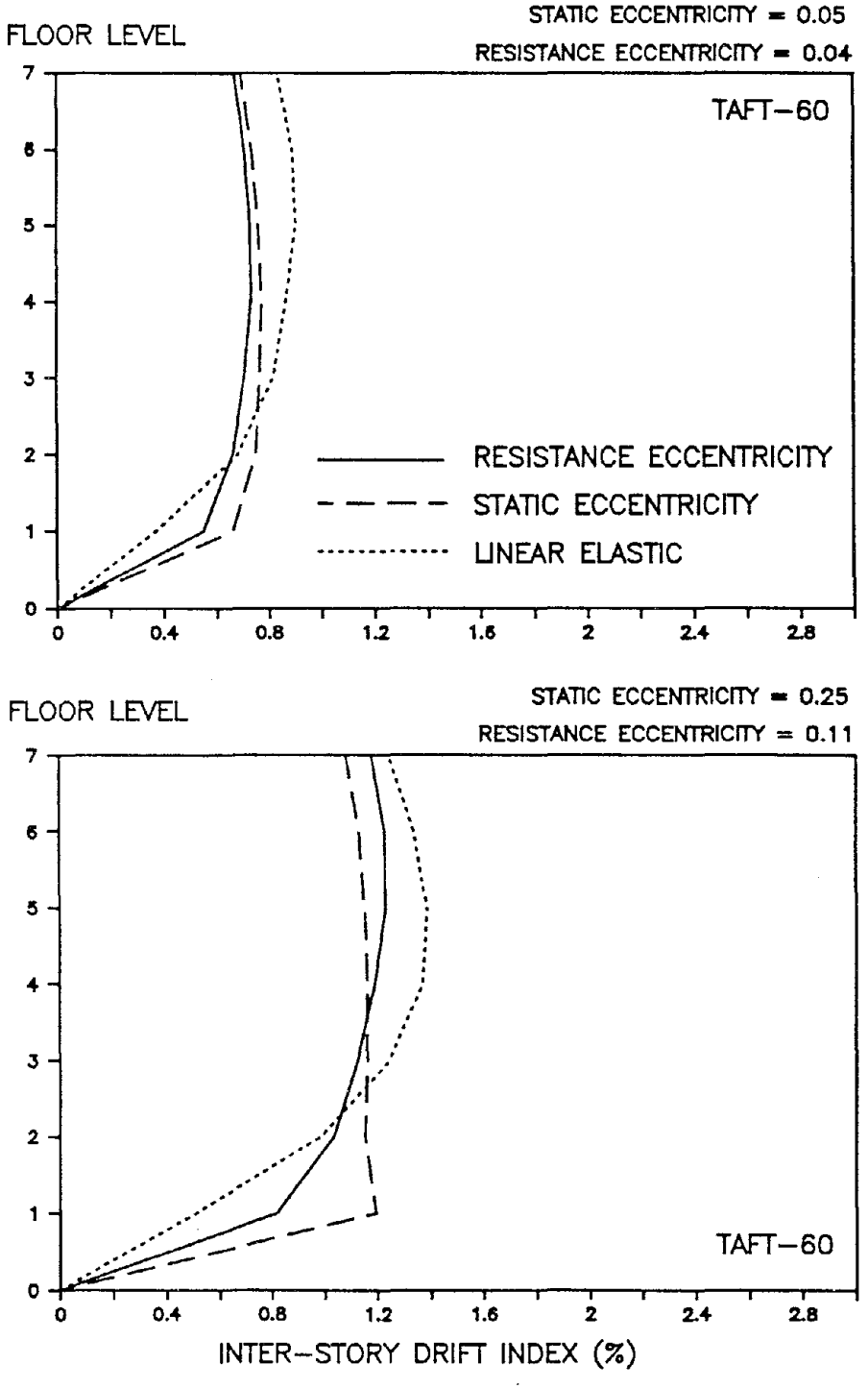

Figure 5.82: WALL G INTER-STORY DRIFT INDEX ENVELOPES LINEAR-ELASTIC VERSUS NON-LINEAR INELASTIC DUE TO TAFT-60, 0-2 SECONDS

EARTHQUAKE ENGINEERING RESEARCH CENTER REPORT SERIES

EERC reports are available from the National Information Service for Earthquake Engineering(NISEE) and from the National Technical Information Service(NTIS). Numbers in parentheses are Accession Numbers assigned by the National Technical Information Service; these are followed by a price code. Contact NTIS, 5285 Port Royal Road, Springfield Virginia, 22161 for more information. Reports without Accession Numbers were not available from NTIS at the time of printing. For a current complete list of EERC reports (from EERC 67-1) and availablity information, please contact University of California, EERC, NISEE, 1301 South 46th Street, Richmond, California 94804.

UCB/EERC-80/01 "Earthquake Response of Concrete Gravity Dams Including Hydrodynamic and Foundation Interaction Effects," by Chopra, A.K., Chakrabarti, P. and Gupta, S., January 1980, (AD-A087297)A10.

UCB/EERC-80/02 "Rocking Response of Rigid Blocks to Earthquakes," by Yim, C.S., Chopra, A.K. and Penzien, J., January 1980, (PB80 166 002)A04.

UCB/EERC-80/03 "Optimum Inelastic Design of Seismic-Resistant Reinforced Concrete Frame Structures," by Zagajeski, S.W. and Bertero, V.V., January 1980, (PB80 164 635)A06.

UCB/EERC-80/04 "Effects of Amount and Arrangement of Wall-Panel Reinforcement on Hysteretic Behavior of Reinforced Concrete Walls," by Iliya, R. and Bertero, V.V., February 1980, (PB81 122 525)A09.

UCB/EERC-80/05 "Shaking Table Research on Concrete Dam Models," by Niwa, A. and Clough, R.W., September 1980, (PB81 122 368)A06.

UCB/EERC-80/06 "The Design of Steel Energy-Absorbing Restrainers and their Incorporation into Nuclear Power Plants for Enhanced Safety (Vol 1a): Piping with Energy Absorbing Restrainers: Parameter Study on Small Systems," by Powell, G.H., Oughourlian, C. and Simons, J., June 1980.

UCB/EERC-80/07 "Inelastic Torsional Response of Structures Subjected to Earthquake Ground Motions," by Yamazaki, Y., April 1980, (PB81 122 327)A08.

UCB/EERC-80/08 "Study of X-Braced Steel Frame Structures under Earthquake Simulation," by Ghanaat, Y., April 1980, (PB81 122 335)A11.

UCB/EERC-80/09 "Hybrid Modelling of Soil-Structure Interaction," by Gupta, S., Lin, T.W. and Penzien, J., May 1980, (PB81 122 319)A07.

UCB/EERC-80/10 "General Applicability of a Nonlinear Model of a One Story Steel Frame," by Sveinsson, B.I. and McNiven, H.D., May 1980, (PB81 124 877)A06.

UCB/EERC-80/11 "A Green-Function Method for Wave Interaction with a Submerged Body," by Kioka, W., April 1980, (PB81 122 269)A07.

UCB/EERC-80/12 "Hydrodynamic Pressure and Added Mass for Axisymmetric Bodies.," by Nilrat, F., May 1980, (PB81 122 343)A08.

UCB/EERC-80/13 "Treatment of Non-Linear Drag Forces Acting on Offshore Platforms," by Dao, B.V. and Penzien, J., May 1980, (PB81 153 413)A07.

UCB/EERC-80/14 "2D Plane/Axisymmetric Solid Element (Type 3-Elastic or Elastic-Perfectly Plastic)for the ANSR-II Program," by Mondkar, D.P. and Powell, G.H., July 1980, (PB81 122 350)A03.

UCB/EERC-80/15 "A Response Spectrum Method for Random Vibrations," by Der Kiureghian, A., June 1981, (PB81 122 301)A03.

UCB/EERC-80/16 "Cyclic Inelastic Buckling of Tubular Steel Braces," by Zayas, V.A., Popov, E.P. and Mahin, S.A., June 1981, (PB81 124 885)A10.

UCB/EERC-80/17 "Dynamic Response of Simple Arch Dams Including Hydrodynamic Interaction," by Porter, C.S. and Chopra, A.K., July 1981, (PB81 124 000)A13.

UCB/EERC-80/18 "Experimental Testing of a Friction Damped Aseismic Base Isolation System with Fail-Safe Characteristics," by Kelly, J.M., Beucke, K.E. and Skinner, M.S., July 1980, (PB81 148 595)A04.

UCB/EERC-80/19 "The Design of Steel Energy-Absorbing Restrainers and their Incorporation into Nuclear Power Plants for Enhanced Safety (Vol.1B): Stochastic Seismic Analyses of Nuclear Power Plant Structures and Piping Systems Subjected to Multiple Supported Excitations," by Lee, M.C. and Penzien, J., June 1980, (PB82 201 872)A08.

UCB/EERC-80/20 "The Design of Steel Energy-Absorbing Restrainers and their Incorporation into Nuclear Power Plants for Enhanced Safety (Vol 1C): Numerical Method for Dynamic Substructure Analysis," by Dickens, J.M. and Wilson, E.L., June 1980.

UCB/EERC-80/21 "The Design of Steel Energy-Absorbing Restrainers and their Incorporation into Nuclear Power Plants for Enhanced Safety (Vol 2): Development and Testing of Restraints for Nuclear Piping Systems," by Kelly, J.M. and Skinner, M.S., June 1980.

UCB/EERC-80/22 "3D Solid Element (Type 4-Elastic or Elastic-Perfectly-Plastic) for the ANSR-II Program," by Mondkar, D.P. and Powell, G.H., July 1980, (PB81 123 242)A03.

UCB/EERC-80/23 "Gap-Friction Element (Type 5) for the Ansr-II Program," by Mondkar, D.P. and Powell, G.H., July 1980, (PB81 122 285)A03.

UCB/EERC-80/24 "U-Bar Restraint Element (Type 11) for the ANSR-II Program," by Oughourlian, C. and Powell, G.H., July 1980, (PB81 122 293)A03.

UCB/EERC-80/25 "Testing of a Natural Rubber Base Isolation System by an Explosively Simulated Earthquake," by Kelly, J.M., August 1980, (PB81 201 360)A04.

UCB/EERC-80/26 "Input Identification from Structural Vibrational Response," by Hu, Y., August 1980, (PB81 152 308)A05.

UCB/EERC-80/27 "Cyclic Inelastic Behavior of Steel Offshore Structures," by Zayas, V.A., Mahin, S.A. and Popov, E.P., August 1980, (PB81 196 180)A15.

UCB/EERC-80/28 "Shaking Table Testing of a Reinforced Concrete Frame with Biaxial Response," by Oliva, M.G., October 1980, (PB81 154 304)A10.

UCB/EERC-80/29 "Dynamic Properties of a Twelve-Story Prefabricated Panel Building," by Bouwkamp, J.G., Kollegger, J.P. and Stephen, R.M., October 1980, (PB82 138 777)A07.

UCB/EERC-80/30 "Dynamic Properties of an Eight-Story Prefabricated Panel Building," by Bouwkamp, J.G., Kollegger, J.P. and Stephen, R.M., October 1980, (PB81 200 313)A05.

UCB/EERC-80/31 "Predictive Dynamic Response of Panel Type Structures under Earthquakes," by Kollegger, J.P. and Bouwkamp, J.G., October 1980, (PB81 152 316)A04.

UCB/EERC-80/32 "The Design of Steel Energy-Absorbing Restrainers and their Incorporation into Nuclear Power Plants for Enhanced Safety (Vol 3): Testing of Commercial Steels in Low-Cycle Torsional Fatigue," by Spanner, P., Parker, E.R., Jongewaard, E. and Dory, M., 1980.

UCB/EERC-80/33 "The Design of Steel Energy-Absorbing Restrainers and their Incorporation into Nuclear Power Plants for Enhanced Safety (Vol 4): Shaking Table Tests of Piping Systems with Energy-Absorbing Restrainers," by Stiemer, S.F. and Godden, W.G., September 1980, (PB82 201 880)A05.

UCB/EERC-80/34 "The Design of Steel Energy-Absorbing Restrainers and their Incorporation into Nuclear Power Plants for Enhanced Safety (Vol 5): Summary Report," by Spencer, P., 1980.

UCB/EERC-80/35 "Experimental Testing of an Energy-Absorbing Base Isolation System," by Kelly, J.M., Skinner, M.S. and Beucke, K.E., October 1980, (PB81 154 072)A04.

UCB/EERC-80/36 "Simulating and Analyzing Artificial Non-Stationary Earth Ground Motions," by Nau, R.F., Oliver, R.M. and Pister, K.S., October 1980, (PB81 153 397)A04.

UCB/EERC-80/37 "Earthquake Engineering at Berkeley - 1980," by , September 1980, (PB81 205 674)A09.

UCB/EERC-80/38 "Inelastic Seismic Analysis of Large Panel Buildings," by Schricker, V. and Powell, G.H., September 1980, (PB81 154 338)A13.

UCB/EERC-80/39 "Dynamic Response of Embankment, Concrete-Gavity and Arch Dams Including Hydrodynamic Interation," by Hall, J.F. and Chopra, A.K., October 1980, (PB81 152 324)A11.

UCB/EERC-80/40 "Inelastic Buckling of Steel Struts under Cyclic Load Reversal.," by Black, R.G., Wenger, W.A. and Popov, E.P., October 1980, (PB81 154 312)A08.

UCB/EERC-80/41 "Influence of Site Characteristics on Buildings Damage during the October 3,1974 Lima Earthquake," by Repetto, P., Arango, I. and Seed, H.B., September 1980, (PB81 161 739)A05.

UCB/EERC-80/42 "Evaluation of a Shaking Table Test Program on Response Behavior of a Two Story Reinforced Concrete Frame," by Blondet, J.M., Clough, R.W. and Mahin, S.A., December 1980, (PB82 196 544)A11.

UCB/EERC-80/43 "Modelling of Soil-Structure Interaction by Finite and Infinite Elements," by Medina, F., December 1980, (PB81 229 270)A04.

UCB/EERC-81/01 "Control of Seismic Response of Piping Systems and Other Structures by Base Isolation," by Kelly, J.M., January 1981, (PB81 200 735)A05.

UCB/EERC-81/02 "OPTNSR- An Interactive Software System for Optimal Design of Statically and Dynamically Loaded Structures with Nonlinear Response," by Bhatti, M.A., Ciampi, V. and Pister, K.S., January 1981, (PB81 218 851)A09.

UCB/EERC-81/03 "Analysis of Local Variations in Free Field Seismic Ground Motions," by Chen, J.-C., Lysmer, J. and Seed, H.B., January 1981, (AD-A099508)A13.

UCB/EERC-81/04 "Inelastic Structural Modeling of Braced Offshore Platforms for Seismic Loading," by Zayas, V.A., Shing, P.-S.B., Mahin, S.A. and Popov, E.P., January 1981, (PB82 138 777)A07.

UCB/EERC-81/05 "Dynamic Response of Light Equipment in Structures," by Der Kiureghian, A., Sackman, J.L. and Nour-Omid, B., April 1981, (PB81 218 497)A04.

UCB/EERC-81/06 "Preliminary Experimental Investigation of a Broad Base Liquid Storage Tank," by Bouwkamp, J.G., Kollegger, J.P. and Stephen, R.M., May 1981, (PB82 140 385)A03.

UCB/EERC-81/07 "The Seismic Resistant Design of Reinforced Concrete Coupled Structural Walls," by Aktan, A.E. and Bertero, V.V., June 1981, (PB82 113 358)A11.

UCB/EERC-81/08 "Unassigned," by Unassigned, 1981.

UCB/EERC-81/09 "Experimental Behavior of a Spatial Piping System with Steel Energy Absorbers Subjected to a Simulated Differential Seismic Input," by Stiemer, S.F., Godden, W.G. and Kelly, J.M., July 1981, (PB82 201 898)A04.

UCB/EERC-81/10 "Evaluation of Seismic Design Provisions for Masonry in the United States," by Sveinsson, B.I., Mayes, R.L. and McNiven, H.D., August 1981, (PB82 166 075)A08.

UCB/EERC-81/11 "Two-Dimensional Hybrid Modelling of Soil-Structure Interaction," by Tzong, T.-J., Gupta, S. and Penzien, J., August 1981, (PB82 142 118)A04.

UCB/EERC-81/12 "Studies on Effects of Infills in Seismic Resistant R/C Construction," by Brokken, S. and Bertero, V.V., October 1981, (PB82 166 190)A09.

UCB/EERC-81/13 "Linear Models to Predict the Nonlinear Seismic Behavior of a One-Story Steel Frame," by Valdimarsson, H., Shah, A.H. and McNiven, H.D., September 1981, (PB82 138 793)A07.

UCB/EERC-81/14 "TLUSH: A Computer Program for the Three-Dimensional Dynamic Analysis of Earth Dams," by Kagawa, T., Mejia, L.H., Seed, H.B. and Lysmer, J., September 1981, (PB82 139 940)A06.

UCB/EERC-81/15 "Three Dimensional Dynamic Response Analysis of Earth Dams," by Mejia, L.H. and Seed, H.B., September 1981, (PB82 137 274)A12.

UCB/EERC-81/16 "Experimental Study of Lead and Elastomeric Dampers for Base Isolation Systems," by Kelly, J.M. and Hodder, S.B., October 1981, (PB82 166 182)A05.

UCB/EERC-81/17 "The Influence of Base Isolation on the Seismic Response of Light Secondary Equipment," by Kelly, J.M., April 1981, (PB82 255 266)A04.

UCB/EERC-81/18 "Studies on Evaluation of Shaking Table Response Analysis Procedures," by Blondet, J. M., November 1981, (PB82 197 278)A10.

UCB/EERC-81/19 "DELIGHT.STRUCT: A Computer-Aided Design Environment for Structural Engineering," by Balling, R.J., Pister, K.S. and Polak, E., December 1981, (PB82 218 496)A07.

UCB/EERC-81/20 "Optimal Design of Seismic-Resistant Planar Steel Frames," by Balling, R.J., Ciampi, V. and Pister, K.S., December 1981, (PB82 220 179)A07.

UCB/EERC-82/01 "Dynamic Behavior of Ground for Seismic Analysis of Lifeline Systems," by Sato, T. and Der Kiureghian, A., January 1982, (PB82 218 926)A05.

UCB/EERC-82/02 "Shaking Table Tests of a Tubular Steel Frame Model," by Ghanaat, Y. and Clough, R.W., January 1982, (PB82 220 161)A07.

UCB/EERC-82/03 "Behavior of a Piping System under Seismic Excitation: Experimental Investigations of a Spatial Piping System supported by Mechanical Shock Arrestors," by Schneider, S., Lee, H.-M. and Godden, W. G., May 1982, (PB83 172 544)A09.

UCB/EERC-82/04 "New Approaches for the Dynamic Analysis of Large Structural Systems," by Wilson, E.L., June 1982, (PB83 148 080)A05.

UCB/EERC-82/05 "Model Study of Effects of Damage on the Vibration Properties of Steel Offshore Platforms," by Shahrivar, F. and Bouwkamp, J.G., June 1982, (PB83 148 742)A10.

UCB/EERC-82/06 "States of the Art and Pratice in the Optimum Seismic Design and Analytical Response Prediction of R/C Frame Wall Structures," by Aktan, A.E. and Bertero, V.V., July 1982, (PB83 147 736)A05.

UCB/EERC-82/07 "Further Study of the Earthquake Response of a Broad Cylindrical Liquid-Storage Tank Model," by Manos, G.C. and Clough, R.W., July 1982, (PB83 147 744)A11.

UCB/EERC-82/08 "An Evaluation of the Design and Analytical Seismic Response of a Seven Story Reinforced Concrete Frame," by Charney, F.A. and Bertero, V.V., July 1982, (PB83 157 628)A09.

UCB/EERC-82/09 "Fluid-Structure Interactions: Added Mass Computations for Incompressible Fluid," by Kuo, J.S.-H., August 1982, (PB83 156 281)A07.

UCB/EERC-82/10 "Joint-Opening Nonlinear Mechanism: Interface Smeared Crack Model," by Kuo, J.S.-H., August 1982, (PB83 149 195)A05.

UCB/EERC-82/11 "Dynamic Response Analysis of Techi Dam," by Clough, R.W., Stephen, R.M. and Kuo, J.S.-H., August 1982, (PB83 147 496)A06.

UCB/EERC-82/12 "Prediction of the Seismic Response of R/C Frame-Coupled Wall Structures," by Aktan, A.E., Bertero, V.V. and Piazzo, M., August 1982, (PB83 149 203)A09.

UCB/EERC-82/13 "Preliminary Report on the Smart 1 Strong Motion Array in Taiwan," by Bolt, B.A., Loh, C.H., Penzien, J. and Tsai, Y.B., August 1982, (PB83 159 400)A10.

UCB/EERC-82/14 "Shaking-Table Studies of an Eccentrically X-Braced Steel Structure," by Yang, M.S., September 1982, (PB83 260 778)A12.

UCB/EERC-82/15 "The Performance of Stairways in Earthquakes," by Roha, C., Axley, J.W. and Bertero, V.V., September 1982, (PB83 157 693)A07.

UCB/EERC-82/16 "The Behavior of Submerged Multiple Bodies in Earthquakes," by Liao, W.-G., September 1982, (PB83 158 709)A07.

UCB/EERC-82/17 "Effects of Concrete Types and Loading Conditions on Local Bond-Slip Relationships," by Cowell, A.D., Popov, E.P. and Bertero, V.V., September 1982, (PB83 153 577)A04.

UCB/EERC-82/18 "Mechanical Behavior of Shear Wall Vertical Boundary Members: An Experimental Investigation," by Wagner, M.T. and Bertero, V.V., October 1982, (PB83 159 764)A05.

UCB/EERC-82/19 "Experimental Studies of Multi-support Seismic Loading on Piping Systems," by Kelly, J.M. and Cowell, A.D., November 1982.

UCB/EERC-82/20 "Generalized Plastic Hinge Concepts for 3D Beam-Column Elements," by Chen, P. F.-S. and Powell, G.H., November 1982, (PB83 247 981)A13.

UCB/EERC-82/21 "ANSR-II: General Computer Program for Nonlinear Structural Analysis," by Oughourlian, C.V. and Powell, G.H., November 1982, (PB83 251 330)A12.

UCB/EERC-82/22 "Solution Strategies for Statically Loaded Nonlinear Structures," by Simons, J.W. and Powell, G.H., November 1982, (PB83 197 970)A06.

UCB/EERC-82/23 "Analytical Model of Deformed Bar Anchorages under Generalized Excitations," by Ciampi, V., Eligehausen, R., Bertero, V.V. and Popov, E.P., November 1982, (PB83 169 532)A06.

UCB/EERC-82/24 "A Mathematical Model for the Response of Masonry Walls to Dynamic Excitations," by Sucuoglu, H., Mengi, Y. and McNiven, H.D., November 1982, (PB83 169 011)A07.

UCB/EERC-82/25 "Earthquake Response Considerations of Broad Liquid Storage Tanks," by Cambra, F.J., November 1982, (PB83 251 215)A09.

UCB/EERC-82/26 "Computational Models for Cyclic Plasticity, Rate Dependence and Creep," by Mosaddad, B. and Powell, G.H., November 1982, (PB83 245 829)A08.

UCB/EERC-82/27 "Inelastic Analysis of Piping and Tubular Structures," by Mahasuverachai, M. and Powell, G.H., November 1982, (PB83 249 987)A07.

UCB/EERC-83/01 "The Economic Feasibility of Seismic Rehabilitation of Buildings by Base Isolation," by Kelly, J.M., January 1983, (PB83 197 988)A05.

UCB/EERC-83/02 "Seismic Moment Connections for Moment-Resisting Steel Frames.," by Popov, E.P., January 1983, (PB83 195 412)A04.

UCB/EERC-83/03 "Design of Links and Beam-to-Column Connections for Eccentrically Braced Steel Frames," by Popov, E.P. and Malley, J.O., January 1983, (PB83 194 811)A04.

UCB/EERC-83/04 "Numerical Techniques for the Evaluation of Soil-Structure Interaction Effects in the Time Domain," by Bayo, E. and Wilson, E.L., February 1983, (PB83 245 605)A09.

UCB/EERC-83/05 "A Transducer for Measuring the Internal Forces in the Columns of a Frame-Wall Reinforced Concrete Structure," by Sause, R. and Bertero, V.V., May 1983, (PB84 119 494)A06.

UCB/EERC-83/06 "Dynamic Interactions Between Floating Ice and Offshore Structures," by Croteau, P., May 1983, (PB84 119 486)A16.

UCB/EERC-83/07 "Dynamic Analysis of Multiply Tuned and Arbitrarily Supported Secondary Systems," by Igusa, T. and Der Kiureghian, A., July 1983, (PB84 118 272)A11.

UCB/EERC-83/08 "A Laboratory Study of Submerged Multi-body Systems in Earthquakes," by Ansari, G.R., June 1983, (PB83 261 842)A17.

UCB/EERC-83/09 "Effects of Transient Foundation Uplift on Earthquake Response of Structures," by Yim, C.-S. and Chopra, A.K., June 1983, (PB83 261 396)A07.

UCB/EERC-83/10 "Optimal Design of Friction-Braced Frames under Seismic Loading," by Austin, M.A. and Pister, K.S., June 1983, (PB84 119 288)A06.

UCB/EERC-83/11 "Shaking Table Study of Single-Story Masonry Houses: Dynamic Performance under Three Component Seismic Input and Recommendations," by Manos, G.C., Clough, R.W. and Mayes, R.L., July 1983, (UCB/EERC-83/11)A08.

UCB/EERC-83/12 "Experimental Error Propagation in Pseudodynamic Testing," by Shiing, P.B. and Mahin, S.A., June 1983, (PB84 119 270)A09.

UCB/EERC-83/13 "Experimental and Analytical Predictions of the Mechanical Characteristics of a 1/5-scale Model of a 7-story R/C Frame-Wall Building Structure," by Aktan, A.E., Bertero, V.V., Chowdhury, A.A. and Nagashima, T., June 1983, (PB84 119 213)A07.

UCB/EERC-83/14 "Shaking Table Tests of Large-Panel Precast Concrete Building System Assemblages," by Oliva, M.G. and Clough, R.W., June 1983, (PB86 110 210/AS)A11.

UCB/EERC-83/15 "Seismic Behavior of Active Beam Links in Eccentrically Braced Frames," by Hjelmstad, K.D. and Popov, E.P., July 1983, (PB84 119 676)A09.

UCB/EERC-83/16 "System Identification of Structures with Joint Rotation," by Dimsdale, J.S., July 1983, (PB84 192 210)A06.

UCB/EERC-83/17 "Construction of Inelastic Response Spectra for Single-Degree-of-Freedom Systems," by Mahin, S. and Lin, J., June 1983, (PB84 208 834)A05.

UCB/EERC-83/18 "Interactive Computer Analysis Methods for Predicting the Inelastic Cyclic Behaviour of Structural Sections," by Kaba, S. and Mahin, S., July 1983, (PB84 192 012)A06.

UCB/EERC-83/19 "Effects of Bond Deterioration on Hysteretic Behavior of Reinforced Concrete Joints," by Filippou, F.C., Popov, E.P. and Bertero, V.V., August 1983, (PB84 192 020)A10.

UCB/EERC-83/20 "Correlation of Analytical and Experimental Responses of Large-Panel Precast Building Systems," by Oliva, M.G., Clough, R.W., Velkov, M. and Gavrilovic, P., May 1988.

UCB/EERC-83/21 "Mechanical Characteristics of Materials Used in a 1/5 Scale Model of a 7-Story Reinforced Concrete Test Structure," by Bertero, V.V., Aktan, A.E., Harris, H.G. and Chowdhury, A.A., October 1983, (PB84 193 697)A05.

UCB/EERC-83/22 "Hybrid Modelling of Soil-Structure Interaction in Layered Media," by Tzong, T.-J. and Penzien, J., October 1983, (PB84 192 178)A08.

UCB/EERC-83/23 "Local Bond Stress-Slip Relationships of Deformed Bars under Generalized Excitations," by Eligehausen, R., Popov, E.P. and Bertero, V.V., October 1983, (PB84 192 848)A09.

UCB/EERC-83/24 "Design Considerations for Shear Links in Eccentrically Braced Frames," by Malley, J.O. and Popov, E.P., November 1983, (PB84 192 186)A07.

UCB/EERC-84/01 "Pseudodynamic Test Method for Seismic Performance Evaluation: Theory and Implementation," by Shing, P.-S.B. and Mahin, S.A., January 1984, (PB84 190 644)A08.

UCB/EERC-84/02 "Dynamic Response Behavior of Kiang Hong Dian Dam," by Clough, R.W., Chang, K.-T., Chen, H.-Q. and Stephen, R.M., April 1984, (PB84 209 402)A08.

UCB/EERC-84/03 "Refined Modelling of Reinforced Concrete Columns for Seismic Analysis," by Kaba, S.A. and Mahin, S.A., April 1984, (PB84 234 384)A06.

UCB/EERC-84/04 "A New Floor Response Spectrum Method for Seismic Analysis of Multiply Supported Secondary Systems," by Asfura, A. and Der Kiureghian, A., June 1984, (PB84 239 417)A06.

UCB/EERC-84/05 "Earthquake Simulation Tests and Associated Studies of a 1/5th-scale Model of a 7-Story R/C Frame-Wall Test Structure," by Bertero, V.V., Aktan, A.E., Charney, F.A. and Sause, R., June 1984, (PB84 239 409)A09.

UCB/EERC-84/06 "R/C Structural Walls: Seismic Design for Shear," by Aktan, A.E. and Bertero, V.V., 1984.

UCB/EERC-84/07 "Behavior of Interior and Exterior Flat-Plate Connections subjected to Inelastic Load Reversals," by Zee, H.L. and Moehle, J.P., August 1984, (PB86 117 629/AS)A07.

UCB/EERC-84/08 "Experimental Study of the Seismic Behavior of a Two-Story Flat-Plate Structure," by Moehle, J.P. and Diebold, J.W., August 1984, (PB86 122 553/AS)A12.

UCB/EERC-84/09 "Phenomenological Modeling of Steel Braces under Cyclic Loading," by Ikeda, K., Mahin, S.A. and Dermitzakis, S.N., May 1984, (PB86 132 198/AS)A08.

UCB/EERC-84/10 "Earthquake Analysis and Response of Concrete Gravity Dams," by Fenves, G. and Chopra, A.K., August 1984, (PB85 193 902/AS)A11.

UCB/EERC-84/11 "EAGD-84: A Computer Program for Earthquake Analysis of Concrete Gravity Dams," by Fenves, G. and Chopra, A.K., August 1984, (PB85 193 613/AS)A05.

UCB/EERC-84/12 "A Refined Physical Theory Model for Predicting the Seismic Behavior of Braced Steel Frames," by Ikeda, K. and Mahin, S.A., July 1984, (PB85 191 450/AS)A09.

UCB/EERC-84/13 "Earthquake Engineering Research at Berkeley - 1984," by , August 1984, (PB85 197 341/AS)A10.

UCB/EERC-84/14 "Moduli and Damping Factors for Dynamic Analyses of Cohesionless Soils," by Seed, H.B., Wong, R.T., Idriss, I.M. and Tokimatsu, K., September 1984, (PB85 191 468/AS)A04.

UCB/EERC-84/15 "The Influence of SPT Procedures in Soil Liquefaction Resistance Evaluations," by Seed, H.B., Tokimatsu, K., Harder, L.F. and Chung, R.M., October 1984, (PB85 191 732/AS)A04.

UCB/EERC-84/16 "Simplified Procedures for the Evaluation of Settlements in Sands Due to Earthquake Shaking," by Tokimatsu, K. and Seed, H.B., October 1984, (PB85 197 887/AS)A03.

UCB/EERC-84/17 "Evaluation of Energy Absorption Characteristics of Highway Bridges Under Seismic Conditions - Volume I and Volume II (Appendices)," by Imbsen, R.A. and Penzien, J., September 1986.

UCB/EERC-84/18 "Structure-Foundation Interactions under Dynamic Loads," by Liu, W.D. and Penzien, J., November 1984, (PB87 124 889/AS)A11.

UCB/EERC-84/19 "Seismic Modelling of Deep Foundations," by Chen, C.-H. and Penzien, J., November 1984, (PB87 124 798/AS)A07.

UCB/EERC-84/20 "Dynamic Response Behavior of Quan Shui Dam," by Clough, R.W., Chang, K.-T., Chen, H.-Q., Stephen, R.M., Ghanaat, Y. and Qi, J.-H., November 1984, (PB86 115177/AS)A07.

UCB/EERC-85/01 "Simplified Methods of Analysis for Earthquake Resistant Design of Buildings," by Cruz, E.F. and Chopra, A.K., February 1985, (PB86 112299/AS)A12.

UCB/EERC-85/02 "Estimation of Seismic Wave Coherency and Rupture Velocity using the SMART 1 Strong-Motion Array Recordings," by Abrahamson, N.A., March 1985, (PB86 214 343)A07.

UCB/EERC-85/03 "Dynamic Properties of a Thirty Story Condominium Tower Building," by Stephen, R.M., Wilson, E.L. and Stander, N., April 1985, (PB86 118965/AS)A06.

UCB/EERC-85/04 "Development of Substructuring Techniques for On-Line Computer Controlled Seismic Performance Testing," by Dermitzakis, S. and Mahin, S., February 1985, (PB86 132941/AS)A08.

UCB/EERC-85/05 "A Simple Model for Reinforcing Bar Anchorages under Cyclic Excitations," by Filippou, F.C., March 1985, (PB86 112 919/AS)A05.

UCB/EERC-85/06 "Racking Behavior of Wood-framed Gypsum Panels under Dynamic Load," by Oliva, M.G., June 1985.

UCB/EERC-85/07 "Earthquake Analysis and Response of Concrete Arch Dams," by Fok, K.-L. and Chopra, A.K., June 1985, (PB86 139672/AS)A10.

UCB/EERC-85/08 "Effect of Inelastic Behavior on the Analysis and Design of Earthquake Resistant Structures," by Lin, J.P. and Mahin, S.A., June 1985, (PB86 135340/AS)A08.

UCB/EERC-85/09 "Earthquake Simulator Testing of a Base-Isolated Bridge Deck," by Kelly, J.M., Buckle, I.G. and Tsai, H.-C., January 1986, (PB87 124 152/AS)A06.

UCB/EERC-85/10 "Simplified Analysis for Earthquake Resistant Design of Concrete Gravity Dams," by Fenves, G. and Chopra, A.K., June 1986, (PB87 124 160/AS)A08.

UCB/EERC-85/11 "Dynamic Interaction Effects in Arch Dams," by Clough, R.W., Chang, K.-T., Chen, H.-Q. and Ghanaat, Y., October 1985, (PB86 135027/AS)A05.

UCB/EERC-85/12 "Dynamic Response of Long Valley Dam in the Mammoth Lake Earthquake Series of May 25-27, 1980," by Lai, S. and Seed, H.B., November 1985, (PB86 142304/AS)A05.

UCB/EERC-85/13 "A Methodology for Computer-Aided Design of Earthquake-Resistant Steel Structures," by Austin, M.A., Pister, K.S. and Mahin, S.A., December 1985, (PB86 159480/AS)A10 .

UCB/EERC-85/14 "Response of Tension-Leg Platforms to Vertical Seismic Excitations," by Liou, G.-S., Penzien, J. and Yeung, R.W., December 1985, (PB87 124 871/AS)A08.

UCB/EERC-85/15 "Cyclic Loading Tests of Masonry Single Piers: Volume 4 - Additional Tests with Height to Width Ratio of 1," by Sveinsson, B., McNiven, H.D. and Sucuoglu, H., December 1985.

UCB/EERC-85/16 "An Experimental Program for Studying the Dynamic Response of a Steel Frame with a Variety of Infill Partitions," by Yanev, B. and McNiven, H.D., December 1985.

UCB/EERC-86/01 "A Study of Seismically Resistant Eccentrically Braced Steel Frame Systems," by Kasai, K. and Popov, E.P., January 1986, (PB87 124 178/AS)A14.

UCB/EERC-86/02 "Design Problems in Soil Liquefaction," by Seed, H.B., February 1986, (PB87 124 186/AS)A03.

UCB/EERC-86/03 "Implications of Recent Earthquakes and Research on Earthquake-Resistant Design and Construction of Buildings," by Bertero, V.V., March 1986, (PB87 124 194/AS)A05.

UCB/EERC-86/04 "The Use of Load Dependent Vectors for Dynamic and Earthquake Analyses," by Leger, P., Wilson, E.L. and Clough, R.W., March 1986, (PB87 124 202/AS)A12.

UCB/EERC-86/05 "Two Beam-To-Column Web Connections," by Tsai, K.-C. and Popov, E.P., April 1986, (PB87 124 301/AS)A04.

UCB/EERC-86/06 "Determination of Penetration Resistance for Coarse-Grained Soils using the Becker Hammer Drill," by Harder, L.F. and Seed, H.B., May 1986, (PB87 124 210/AS)A07.

UCB/EERC-86/07 "A Mathematical Model for Predicting the Nonlinear Response of Unreinforced Masonry Walls to In-Plane Earthquake Excitations," by Mengi, Y. and McNiven, H.D., May 1986, (PB87 124 780/AS)A06.

UCB/EERC-86/08 "The 19 September 1985 Mexico Earthquake: Building Behavior," by Bertero, V.V., July 1986.

UCB/EERC-86/09 "EACD-3D: A Computer Program for Three-Dimensional Earthquake Analysis of Concrete Dams," by Fok, K.-L., Hall, J.F. and Chopra, A.K., July 1986, (PB87 124 228/AS)A08.

UCB/EERC-86/10 "Earthquake Simulation Tests and Associated Studies of a 0.3-Scale Model of a Six-Story Concentrically Braced Steel Structure," by Uang, C.-M. and Bertero, V.V., December 1986, (PB87 163 564/AS)A17.

UCB/EERC-86/11 "Mechanical Characteristics of Base Isolation Bearings for a Bridge Deck Model Test," by Kelly, J.M., Buckle, I.G. and Koh, C.-G., November 1987.

UCB/EERC-86/12 "Effects of Axial Load on Elastomeric Isolation Bearings," by Koh, C.-G. and Kelly, J.M., November 1987.

UCB/EERC-87/01 "The FPS Earthquake Resisting System: Experimental Report," by Zayas, V.A., Low, S.S. and Mahin, S.A., June 1987.

UCB/EERC-87/02 "Earthquake Simulator Tests and Associated Studies of a 0.3-Scale Model of a Six-Story Eccentrically Braced Steel Structure," by Whittaker, A., Uang, C.-M. and Bertero, V.V., July 1987.

UCB/EERC-87/03 "A Displacement Control and Uplift Restraint Device for Base-Isolated Structures," by Kelly, J.M., Griffith, M.C. and Aiken, I.D., April 1987.

UCB/EERC-87/04 "Earthquake Simulator Testing of a Combined Sliding Bearing and Rubber Bearing Isolation System," by Kelly, J.M. and Chalhoub, M.S., 1987.

UCB/EERC-87/05 "Three-Dimensional Inelastic Analysis of Reinforced Concrete Frame-Wall Structures," by Moazzami, S. and Bertero, V.V., May 1987.

UCB/EERC-87/06 "Experiments on Eccentrically Braced Frames with Composite Floors," by Ricles, J. and Popov, E., June 1987.

UCB/EERC-87/07 "Dynamic Analysis of Seismically Resistant Eccentrically Braced Frames," by Ricles, J. and Popov, E., June 1987.

UCB/EERC-87/08 "Undrained Cyclic Triaxial Testing of Gravels-The Effect of Membrane Compliance," by Evans, M.D. and Seed, H.B., July 1987.

UCB/EERC-87/09 "Hybrid Solution Techniques for Generalized Pseudo-Dynamic Testing," by Thewalt, C. and Mahin, S.A., July 1987.

UCB/EERC-87/10 "Ultimate Behavior of Butt Welded Splices in Heavy Rolled Steel Sections," by Bruneau, M., Mahin, S.A. and Popov, E.P., July 1987.

UCB/EERC-87/11 "Residual Strength of Sand from Dam Failures in the Chilean Earthquake of March 3, 1985," by De Alba, P., Seed, H.B., Retamal, E. and Seed, R.B., September 1987.

UCB/EERC-87/12 "Inelastic Seismic Response of Structures with Mass or Stiffness Eccentricities in Plan," by Bruneau, M. and Mahin, S.A., September 1987.

UCB/EERC-87/13 "CSTRUCT: An Interactive Computer Environment for the Design and Analysis of Earthquake Resistant Steel Structures," by Austin, M.A., Mahin, S.A. and Pister, K.S., September 1987.

UCB/EERC-87/14 "Experimental Study of Reinforced Concrete Columns Subjected to Multi-Axial Loading," by Low, S.S. and Moehle, J.P., September 1987.

UCB/EERC-87/15 "Relationships between Soil Conditions and Earthquake Ground Motions in Mexico City in the Earthquake of Sept. 19, 1985," by Seed, H.B., Romo, M.P., Sun, J., Jaime, A. and Lysmer, J., October 1987.

UCB/EERC-87/16 "Experimental Study of Seismic Response of R. C. Setback Buildings," by Shahrooz, B.M. and Moehle, J.P., October 1987.

UCB/EERC-87/17 "The Effect of Slabs on the Flexural Behavior of Beams," by Pantazopoulou, S.J. and Moehle, J.P., October 1987.

UCB/EERC-87/18 "Design Procedure for R-FBI Bearings," by Mostaghel, N. and Kelly, J.M., November 1987.

UCB/EERC-87/19 "Analytical Models for Predicting the Lateral Response of R C Shear Walls: Evaluation of their Reliability," by Vulcano, A. and Bertero, V.V., November 1987.

UCB/EERC-87/20 "Earthquake Response of Torsionally-Coupled Buildings," by Hejal, R. and Chopra, A.K., December 1987.

UCB/EERC-87/21 "Dynamic Reservoir Interaction with Monticello Dam," by Clough, R.W., Ghanaat, Y. and Qiu, X-F., December 1987.

UCB/EERC-87/22 "Strength Evaluation of Coarse-Grained Soils," by Siddiqi, F.H., Seed, R.B., Chan, C.K., Seed, H.B. and Pyke, R.M., December 1987.

UCB/EERC-88/01 "Seismic Behavior of Concentrically Braced Steel Frames," by Khatib, I., Mahin, S.A. and Pister, K.S., January 1988.

UCB/EERC-88/02 "Experimental Evaluation of Seismic Isolation of Medium-Rise Structures Subject to Uplift," by Griffith, M.C., Kelly, J.M., Coveney, V.A. and Koh, C.G., January 1988.

UCB/EERC-88/03 "Cyclic Behavior of Steel Double Angle Connections," by Astaneh-Asl, A. and Nader, M.N., January 1988.

UCB/EERC-88/04 "Re-evaluation of the Slide in the Lower San Fernando Dam in the Earthquake of Feb. 9, 1971," by Seed, H.B., Seed, R.B., Harder, L.F. and Jong, H.-L., April 1988.

UCB/EERC-88/05 "Experimental Evaluation of Seismic Isolation of a Nine-Story Braced Steel Frame Subject to Uplift," by Griffith, M.C., Kelly, J.M. and Aiken, I.D., May 1988.

UCB/EERC-88/06 "DRAIN-2DX User Guide.," by Allahabadi, R. and Powell, G.H., March 1988.

UCB/EERC-88/07 "Cylindrical Fluid Containers in Base-Isolated Structures," by Chalhoub, M.S. and Kelly, J.M. , April 1988.

UCB/EERC-88/08 "Analysis of Near-Source Waves: Separation of Wave Types using Strong Motion Array Recordings," by Darragh, R.B., June 1988.

UCB/EERC-88/09 "Alternatives to Standard Mode Superposition for Analysis of Non-Classically Damped Systems," by Kusainov, A.A. and Clough, R.W., June 1988.

UCB/EERC-88/10 "The Landslide at the Port of Nice on October 16, 1979," by Seed, H.B., Seed, R.B., Schlosser, F., Blondeau, F. and Juran, I., June 1988.

UCB/EERC-88/11 "Liquefaction Potential of Sand Deposits Under Low Levels of Excitation," by Carter, D.P. and Seed, H.B., August 1988.

UCB/EERC-88/12 "Nonlinear Analysis of Reinforced Concrete Frames Under Cyclic Load Reversals," by Filippou, F.C. and Issa, A., September 1988.

UCB/EERC-88/13 "Implications of Recorded Earthquake Ground Motions on Seismic Design of Building Structures," by Uang, C.-M. and Bertero, V.V., November 1988.

UCB/EERC-88/14 "An Experimental Study of the Behavior of Dual Steel Systems," by Whittaker, A.S. , Uang, C.-M. and Bertero, V.V., September 1988.

UCB/EERC-88/15 "Dynamic Moduli and Damping Ratios for Cohesive Soils," by Sun, J.I., Golesorkhi, R. and Seed, H.B., August 1988.

UCB/EERC-88/16 "Reinforced Concrete Flat Plates Under Lateral Load: An Experimental Study Including Biaxial Effects," by Pan, A. and Moehle, J., October 1988.

UCB/EERC-88/17 "Earthquake Engineering Research at Berkeley - 1988," by EERC, November 1988.

UCB/EERC-88/18 "Use of Energy as a Design Criterion in Earthquake-Resistant Design," by Uang, C.-M. and Bertero, V.V., November 1988.

UCB/EERC-88/19 "Steel Beam-Column Joints in Seismic Moment Resisting Frames," by Tsai, K.-C. and Popov, E.P., November 1988.

UCB/EERC-88/20 "Base Isolation in Japan, 1988," by Kelly, J.M., December 1988.

UCB/EERC-89/01 "Behavior of Long Links in Eccentrically Braced Frames," by Engelhardt, M.D. and Popov, E.P., January 1989.

UCB/EERC-89/02 "Earthquake Simulator Testing of Steel Plate Added Damping and Stiffness Elements," by Whittaker, A., Bertero, V.V., Alonso, J. and Thompson, C., January 1989.

UCB/EERC-89/03 "Implications of Site Effects in the Mexico City Earthquake of Sept. 19, 1985 for Earthquake-Resistant Design Criteria in the San Francisco Bay Area of California," by Seed, H.B. and Sun, J.I., March 1989.

UCB/EERC-89/04 "Earthquake Analysis and Response of Intake-Outlet Towers," by Goyal, A. and Chopra, A.K., July 1989.

UCB/EERC-89/05 "The 1985 Chile Earthquake: An Evaluation of Structural Requirements for Bearing Wall Buildings," by Wallace, J.W. and Moehle, J.P., July 1989.

UCB/EERC-89/06 "Effects of Spatial Variation of Ground Motions on Large Multiply-Supported Structures," by Hao, H., July 1989.

UCB/EERC-89/07 "EADAP - Enhanced Arch Dam Analysis Program: User's Manual," by Ghanaat, Y. and Clough, R.W., August 1989.

UCB/EERC-89/08 "Seismic Performance of Steel Moment Frames Plastically Designed by Least Squares Stress Fields," by Ohi, K. and Mahin, S.A., August 1989.

UCB/EERC-89/09 "Feasibility and Performance Studies on Improving the Earthquake Resistance of New and Existing Buildings Using the Friction Pendulum System," by Zayas, V., Low, S., Mahin, S.A. and Bozzo, L., July 1989.

UCB/EERC-89/10 "Measurement and Elimination of Membrane Compliance Effects in Undrained Triaxial Testing," by Nicholson, P.G., Seed, R.B. and Anwar, H., September 1989.

UCB/EERC-89/11 "Static Tilt Behavior of Unanchored Cylindrical Tanks," by Lau, D.T. and Clough, R.W., September 1989.

UCB/EERC-89/12 "ADAP-88: A Computer Program for Nonlinear Earthquake Analysis of Concrete Arch Dams," by Fenves, G.L., Mojtahedi, S. and Reimer, R.B., September 1989.

UCB/EERC-89/13 "Mechanics of Low Shape Factor Elastomeric Seismic Isolation Bearings," by Aiken, I.D., Kelly, J.M. and Tajirian, F., December 1989.

UCB/EERC-89/14 "Preliminary Report on the Seismological and Engineering Aspects of the October 17, 1989 Santa Cruz (Loma Prieta) Earthquake," by EERC, October 1989.

UCB/EERC-89/15 "Experimental Studies of a Single Story Steel Structure Tested with Fixed, Semi-Rigid and Flexible Connections," by Nader, M.N. and Astaneh-Asl, A., August 1989.

UCB/EERC-89/16 "Collapse of the Cypress Street Viaduct as a Result of the Loma Prieta Earthquake," by Nims, D.K., Miranda, E., Aiken, I.D., Whittaker, A.S. and Bertero, V.V., November 1989.

UCB/EERC-90/01 "Mechanics of High-Shape Factor Elastomeric Seismic Isolation Bearings," by Kelly, J.M., Aiken, I.D. and Tajirian, F.F., March 1990.

UCB/EERC-90/02 "Javid's Paradox: The Influence of Preform on the Modes of Vibrating Beams," by Kelly, J.M., Sackman, J.L. and Javid, A., May 1990.

UCB/EERC-90/03 "Earthquake Simulator Tests of Viscoelastic Dampers for Medium Rise Structures," by Kelly, J.M. and Aiken, I.D., May 1990.

UCB/EERC-90/04 "Damage to the San Francisco-Oakland Bay Bridge During the October 17, 1989 Earthquake," by Astaneh, A., June 1990.

UCB/EERC-90/05 "Preliminary Report on the Principal Geotechnical Aspects of the October 17, 1989 Loma Prieta Earthquake," by Seed, R.B., Dickenson, S.E., Riemer, M.F., Bray, J.D., Sitar, N., Mitchell, J.K., Idriss, I.M., Kayen, R.E., Kropp, A., Harder, L.F., Jr. and Power, M.S., April 1990.

UCB/EERC-90/06 "Models of Critical Regions in Reinforced Concrete Frames Under Seismic Excitations," by Zulfiqar, N. and Filippou, F., May 1990.

UCB/EERC-90/07 "A Unified Earthquake-Resistant Design Method for Steel Frames Using ARMA Models," by Takewaki, I., Conte, J.P., Mahin, S.A. and Pister, K.S., June 1990.

UCB/EERC-90/08 "Soil Conditions and Earthquake Hazard Mitigation in the Marina District of San Francisco," by Mitchell, J.K., Masood, T., Kayen, R.E. and Seed, R.B., May 1990.

UCB/EERC-90/09 "Influence of the Earthquake Ground Motion Process and Structural Properties on Response Characteristics of Simple Structures," by Conte, J.P., Pister, K.S. and Mahin, S.A., July 1990.

UCB/EERC-90/10 "Experimental Testing of the Resilient-Friction Base Isolation Sytsem," by Clark, P.W. and Kelly, J.M., July 1990.

UCB/EERC-90/11 "Seismic Hazard Analysis: Improved Models, Uncertainties and Sensitivities," by Araya, R. and Der Kiureghian, A., March 1988.

UCB/EERC-90/12 "Effects of Torsion on the Linear and Nonlinear Seismic Response of Structures," by Sedarat, H. and Bertero, V.V., September 1989.